Michela Chiappalone
Valentina Pasquale
Monica Frega   *Editors*

In Vitro Neuronal Networks

From Culturing Methods to Neuro-Technological Applications

Springer

Advances in Neurobiology

Volume 22

More information about this series at http://www.springer.com/series/8787

Michela Chiappalone • Valentina Pasquale
Monica Frega

Editors

In Vitro Neuronal Networks

From Culturing Methods to
Neuro-Technological Applications

Editors
Michela Chiappalone
Rehab Technologies IIT-INAIL Joint Lab
Istituto Italiano di Tecnologia
Genova, Italy

Valentina Pasquale
Neuroscience and Brain Technologies
Istituto Italiano di Tecnologia
Genova, Italy

Monica Frega
Department of Clinical Neurophysiology
University of Twente
Enschede, The Netherlands

This book is dedicated to our mentors

Preface

In vitro cultures of dissociated neurons coming from different brain areas retain important functional properties of the tissue of origin, thus representing a perfect trade-off between more realistic (but complex) experimental models and theoretical (but limited) modeling approaches. Moreover, the possibilities offered by the latest technologies allow the simultaneous monitoring of several units at high spatiotemporal resolution and for very long time periods, from hours to days and even months. These technological developments are giving new opportunities in terms of experimental design, but also posing new problems in terms of data management and interpretation.

In this book, the authors provide an overview of the incredible developments achieved in the study of in vitro neuronal networks to make the scientific community aware of the enormous potential of this experimental model but also of its limitations. We will start from culturing methodologies, including the use of innovative nanotechnologies and nanomaterials. The establishment of stem cell-derived neuronal cultures will be also discussed, as well as the description of in vitro experimental models exhibiting pathological behaviors. We will review the techniques used for measuring networks' activity from many channels, mostly focusing on planar microelectrode arrays. Then, we will present recent improvements in large-scale data analysis and interpretation. Finally, we will introduce a set of applications for novel experimental designs, including neurotoxicology, stem cell technology, closed-loop electrophysiology, and hybrid systems.

The book has four major parts:

Part I: In Vitro Neuronal Cultures: Experimental Models and Nanomaterials
Part II: Recording Techniques
Part III: Data Analysis Methods
Part IV: Applications

This book is designed for professionals from both academic and non-academic fields working, or starting to work, with cultures of neurons in vitro. Target specialists among academics could be professors, technicians, postdocs, and graduate and

undergraduate students. Outside academia, managers in business development/sales could be interested in knowing the latest state-of-the-art achievements. It is also designed for teaching undergraduate and graduate students and researchers.

Genova, Italy   Michela Chiappalone
Genova, Italy   Valentina Pasquale
Enschede, The Netherlands   Monica Frega

Acknowledgments

Contents

About the Editors

Michela Chiappalone's research interests are in the field of neuroengineering. She obtained a PhD in Electronic Engineering and Computer Science from the University of Genova (Italy) in 2003. In 2002, she has been visiting scholar in the Department of Physiology, Northwestern University (Chicago, IL, USA). After a postdoc at the University of Genova, in 2007, she joined the Neuroscience and Brain Technologies Department at the Istituto Italiano di Tecnologia (IIT) as a postdoc. In 2013, she got a group leader position ("researcher") in the same institution. In 2015, she has been visiting professor at KUMED (Kansas City, KS, USA), hosted by Prof. R.J. Nudo. From 2012 to 2015, M. Chiappalone has been coordinator of the FET Open European Project BrainBow, judged excellent. In 2017, M. Chiappalone joined the Rehab Technologies IIT-INAIL joint lab of IIT to lead a group aimed at interfacing robotic devices with the nervous system for applications in neuroprosthetics, neuromodulation, and neurorehabilitation. In 2018, she got the National Scientific Habilitation as Full Professor of Bioengineering. She authored 60 papers published in international journals, 50 peer-reviewed contributions to international conferences, and 8 book chapters, and she gave more than 60 scientific talks at international/national conferences and research institutions.

Valentina Pasquale got the PhD in "Humanoid Technologies" from the University of Genova and Istituto Italiano di Tecnologia in 2010. During her PhD, she focused on developing analysis tools to characterize the spontaneous and evoked activity of cortical and hippocampal networks cultured on microelectrode arrays, seen as a reduced biological model for the generation of coordinated neuronal activity. During postdoc, she was involved in neuro-robotics and neuro-prosthetics studies, aimed at understanding how to interface artificial devices (as a small robot or a simulated neural network) and neuronal systems, with the final goal of advancing the design of future brain-machine interfaces and brain prostheses. Currently, she has been working as senior postdoc in Dr. Tommaso Fellin's lab (Optical Approaches to Brain Function). Her interests include in vivo studies combining optogenetics and electrophysiology for a deeper understanding of inhibitory interneurons' contribution to the generation and control of sleep waves. She is also involved in the design and development of technological tools for patterned optical stimulation through light phase modulation.

Monica Frega received her PhD in Bioengineering from the University of Genova in 2014. During her PhD, she developed a novel 3D neuronal model, and she demonstrated the possibility of coupling cultured 3D networks to microelectrode array devices and functionally monitoring their electrophysiological activity. Her thesis "Neuronal network dynamics in 2D and 3D in vitro neuro-engineered systems," carried out under the supervision of Prof. Dr. Sergio Martinoia, was judged "excellent" by the PhD committee and recognized as "outstanding PhD research" from Springer. Between 2014 and 2018, she worked as a postdoctoral researcher in the group of Prof. Dr. Nael Nadif Kasri at Radboudumc (Nijmegen, the Netherlands), where she applied her expertise in bioengineering to state-of-the-art stem cell biology to study neurodevelopmental disorders. While her academic path and PhD allowed her to develop engineering and technical capabilities, during the postdoc, she acquired expertise in stem cell biology. Through

these working experiences, Monica Frega became a truly interdisciplinary researcher. In 2018, Monica Frega started her job at the University of Twente as assistant professor in the Clinical Neurophysiology group. Her research mainly focuses on neurological disorders, with the aim to bridge the gap between research and clinic. She makes use of human in vitro models (neuronal cells derived from human-induced pluripotent stem cell from healthy subject and patients grown on microelectrode arrays) in combination with EEG data recordings from patients to study basic physiological processes involved in neurological disorders.

Part I
In Vitro Neuronal Cultures: Experimental Models and Nanomaterials

Past, Present, and Future of Neuronal Models In Vitro

Jason M. Keller and Monica Frega

Abstract Over the past century, robust methods were developed that enable the isolation, culture, and dynamic observation of mammalian neuronal networks in vitro. But even if neuronal culture cannot yet fully recapitulate the normal brain, the knowledge that has been acquired from these surrogate in vitro models is invaluable. Indeed, neuronal culture has continued to propel basic neuroscience research, proving that in vitro systems have legitimacy when it comes to studying either the healthy or diseased human brain. Furthermore, scientific advancement typically parallels technical refinements in the field. A pertinent example is that a collective drive in the field of neuroscience to better understand the development, organization, and emergent properties of neuronal networks is being facilitated by progressive advances in micro-electrode array (MEA) technology. In this chapter, we briefly review the emergence of neuronal cell culture as a technique, the current trends in human stem cell-based modeling, and the technologies used to monitor neuronal communication. We conclude by highlighting future prospects that are evolving specifically out of the combination of human neuronal models and MEA technology.

Keywords In vitro models · Neuronal cell culture techniques · Microelectrode arrays

J. M. Keller
Department of Human Genetics, Radboudumc, Donders Institute for Brain, Cognition, and Behaviour, Nijmegen, The Netherlands

M. Frega (✉)
Department of Clinical Neurophysiology, University of Twente, Enschede, The Netherlands

Department of Human Genetics, Radboudumc, Donders Institute for Brain, Cognition, and Behaviour, Nijmegen, The Netherlands
e-mail: m.frega@utwente.nl

1 Introduction

Neuronal cell culture as an experimental technique has existed in the field of neurobiological research for more than a century and refinement of the technology has progressed steadily since its inception. Deeper explorations into the fundamental cellular and molecular underpinnings of brain function have undoubtedly propelled the continued use of neuronal cultures as an accessible and economical surrogate model system. It is argued that the questions scientists can ultimately ask, or even answer, may depend exclusively on the tools available to them (Dyson 2012). This is almost certainly true when trying to unravel the complexities of the mammalian nervous system and, by extension, the molecular pathophysiology of human neurological diseases. Presently, and in many cases, those asking the questions might only find answers with high fidelity in a reduced, ex vivo preparation of tissue or cells. And despite several shortcomings, the advantages offered by in vitro models are incentive enough to promote further development of the technology, especially as an adjunct to other paradigms commonly used for neurobiological research.

Notably, there are two broader technological trends moving in parallel that we will emphasize. They will both have a profound impact on how in vitro systems are routinely used in the near future and what new information can be gained from them. This is especially true with regard to modeling disease. One advancement has been the ability to observe, measure, and manipulate large ensembles of neurons simultaneously. The commercialization of multi-channel electrophysiological recording has allowed researchers to examine not only single neurons but populations of cells in ways that were not feasible for most labs a decade ago. This ability to capture and analyze high-content dynamic data from cultured neuronal networks allows researchers to explore complex emergent properties that more closely mimic human brain physiology. When applied, these powerful and accessible tools can add a fresh perspective to many standard in vitro models. But until relatively recently, another major hurdle has severely limited the translatability between in vitro models and human pathobiology. The second major advancement is stem cell technology, which will allow us to study human neurons directly. Classically, the field has relied on sourcing neural cells from non-human species, mostly rodents, or from a sparse number of human biopsies. It is becoming progressively more feasible to generate, quickly and efficiently, different types of human neurons in a dish from stem cells. More importantly, when derived from a patient, stem cells retain the specific genetic profile of the donor, which opens the door to personalized medicine. Progress in stem cell technology is poised to overcome a persistent obstacle and revolutionize our mechanistic understanding of human neurobiology and disease.

In the following introductory chapter, our prognosis on the future state of the art is intentionally biased towards the use of in vitro models built from human stem cells because contemporary advancements in this field are fueling a renaissance in culture-based disease modeling. We will spotlight some of the paramount reasons for adopting stem cell-based models as the new standard in basic and clinical neuroscience. But to begin, we will briefly summarize the development of neuronal cell culture as an exploratory technique early last century since it directly foreshadowed the advent of neural stem cell biology today.

2 Neuronal Cell Culture: Brief History, Technological Improvements, and Protocol Standardization

In the first decade of the twentieth century, the American developmental biologist and experimental embryologist Ross Granville Harrison ushered in a new era for the field of neuroscience by developing the first known cell culture of neurons. This was done on the heels of the work by the venerated Spanish pathologist Santiago Ramón y Cajal during the 1890s. But to appreciate his achievement, and to understand Harrison's motivation, it helps to recount the contentious scientific debate that evolved out of the second half of the nineteenth century, a historical context that is well known to modern neuroscientists.

Several renowned neuroanatomists were studying the complex cytoarchitecture of the nervous system by using what were at the time cutting-edge histological techniques. The techniques allowed the first observations of such structural features as neuronal perikarya and neurite fibers. Out of their pioneering explorations arose two competing schools of thought to explain what they saw and hence the developmental architecture of the brain: reticular theory and the neuron doctrine. The earlier one, reticular theory, was based on the work of several notable histologists, initially proposed by the German anatomist Josef von Gerlach in 1871, and later fervently adopted by the Italian physician and pathologist Camillo Golgi (López-Muñoz et al. 2006). Reticular theory held that the nervous system was not comprised of discrete cells but instead its fibrous ("reticular") structure was syncytial. Alternatively, the neuron doctrine, which was founded on the experimental observations made by the Swiss anatomist and embryologist Wilhelm His and later also by Cajal, contended that the brain, like other organs, was composed of individual cells, that nerve fibers grew out from those cells, and importantly, that they were discontinuous (Louis and Stapf 2001).

Although in hindsight it may seem the neuron doctrine should have quickly prevailed, the basis for both theories, that of fixed-tissue analysis, had its limitations. For example, only static and relatively gross observations were possible. The general limitations of the technology, such as the inability to resolve individual synapses microscopically, which would not happen until the 1950s with the electron microscope (Gray 1959; Yuste 2015), made either interpretation seem plausible to each theory's respective proponents. Golgi is famous for his 1873 discovery of the silver impregnation technique bearing his name, a histological stain that could clearly resolve neuronal soma and their processes (Golgi 1873), but he became a strong proponent of reticular theory. Cajal immediately adopted and even further refined Golgi's technique, allowing him to produce immersive, detailed renderings of the fine structure of the brain for which he is recognized. Cajal adeptly inferred from his analyses (ca. 1888–1892) that the brain is also composed of cells, the cells are not continuous but contiguous (i.e., via synapses), and the nerve fibers are outgrowths of the neuronal soma. He was able to go so far as to describe the growth

cone in detail and proposed that its function relates to chemotaxis (Ramón y Cajal 1890). Nevertheless, the matter was at an impasse, particularly because the staining techniques and specimens used by neuroanatomists at the time were so similar, but it was instead their interpretations that diverged (Harrison 1910). The scientific debate lingered, particularly between the most outspoken proponents, such as Golgi and Cajal, and spilled over into the turn of the century. Reticular theory even regained traction, despite Cajal's brilliant work and the wide acceptance of the neuron doctrine (Harrison 1910; Louis and Stapf 2001).

Harrison was a contemporary of Cajal, having earned his Ph.D. in 1894 from Johns Hopkins University in the United States (Hamburger 1980). He acutely understood the limitations of nineteenth century histological techniques and seized the opportunity to apply his own creative tactic to answer the neurite outgrowth question, a solution that would become a major technological advancement in the field (Hamburger 1980; Banker and Goslin 1988; Millet and Gillette 2012). It was, as Harrison himself implied, a synergy between methods in bacteriology and embryology (Harrison 1910). He reasoned that if one could observe the formation of neurites from a neuronal soma, this would support Cajal's hypothesis that neuronal processes develop as outgrowths from the cell. To accomplish this experimentally, he devised a "hanging drop" chamber that would allow long-term cultivation of embryonic tissue while allowing repeated observation of the cells using a standard light microscope, without the need to directly interfere with the cells (Harrison 1910). He isolated neural tube from the embryonic frog and grew pieces of it in a drop of lymph (coagulated blood serum), essentially a predecessor to modern cell culture media. This allowed Harrison to dynamically observe the elongation of the axon from the cell soma and to see the growth cone in action, thereby experimentally confirming Cajal's hypothesis. Consequently, this also represented the first reported in vitro model to study neuronal development, and the utility of this new technique was not lost on Harrison:

> "This method, which obviously has many possibilities in the study of the growth and differentiation of tissues, has two very distinct advantages over the methods of investigation usually employed. It not only enables one to study the behavior of cells and tissues in an unorganized medium free from the influences that surround them in the body of the organism, but it also renders it possible to keep them under direct continuous observation, so that all such developmental processes as involve movement and change of form may be seen directly instead of having to be inferred from series of preserved specimens taken at different stages." (Harrison 1910)

Harrison's initial methodology was quickly seized upon and adopted for other types of mammalian cells and especially for disease research (Millet and Gillette 2012). Throughout the twentieth century, techniques have been continuously refined in order to enhance the long-term viability of cultured mammalian neurons (reviewed by Millet and Gillette 2012). In particular, advancements in the 1970s and 1980s made neuronal cell culture more accessible and useful to a multitude of researchers (Banker and Goslin 1988). Protocols to isolate and culture brain tissue from rodents were progressively optimized and standardized (Banker and Cowan 1977; McCarthy and de Vellis 1980; Thomas 1985; Brewer and Cotman

1989), and then chemically defined, serum-free media formulations were developed and made commercially available (Brewer et al. 1993; Bardy et al. 2015), thereby providing accessibility to the technique for a larger number of laboratories. The technical refinements led to better growth, differentiation, and long-term survival of cells under controlled conditions, particularly allowing for better consistency and reproducibility.

But neurons are not mitotically active, and therefore primary rodent cells must be continuously harvested from fresh animals. On the other hand, a major obstacle for creating primary human neuronal models is obtaining adequate amounts of viable material to begin with, and it is especially not feasible to access nervous tissue in patients for biopsy, except under very rare circumstances. Attempts were made to circumvent some of these issues, and beginning in the 1970s, cell lines were derived from rodent and human tumors, typically from surgical biopsies or resected tissue. Some of the classic cell lines include SH-SY5Y, NT2, or PC-12 cells, which can be propagated in culture indefinitely but then coaxed on demand to differentiate into neuronal-like cells with neuronal properties (Gordon et al. 2013). But the utility of these cell lines for modeling human disease is, for the most part, extremely limited considering they are derived from a few parent sources and, when differentiated, only represent approximations of mature neurons with some generic neuronal properties and no control over cell subtype specificity. In comparison, primary rodent neurons grown in culture are a much more accurate proxy for mature neurons in vivo.

Thus, for many decades, rodents have proven to be invaluable as an economical and stalwart source of primary mammalian brain tissue and neuronal cells for most laboratories. From the embryonic or early postnatal brains of mice and rats, one can isolate brain slices (Yamamoto 1972) or large numbers of viable dissociated neurons from specific brain regions that retain the ability to develop and mature in culture. One of the key advantages of using rodents is a facile ability to directly link and validate phenotypes in a dish to in vivo brain physiology and behavior in the laboratory. Therefore, rodents continue to be an acceptable source of neuronal and non-neuronal cells for certain purposes, such as for investigating the basic mechanisms of neuronal communication, for testing the neurotoxicity of drugs and chemicals (see Chapter "Application of Microelectrode Array Approaches to Neurotoxicity Testing and Screening"), and for modeling neurological disorders in vitro (e.g., stroke, epilepsy and memory disorders; see Chapter "In Vitro Models of Brain Disorders"). Additionally, especially with mice, a multitude of transgenic disease models exist and generating new ones is an efficient and relatively straightforward process, especially for monogenic disorders.

Despite the feasibility of using rodent-based in vitro models, it has become apparent that translatability will be influenced by species differences. Due to their genomic divergence, shortened developmental timing and reduced complexity, among many other differences (Ardhanareeswaran et al. 2017), rodent brains can at best only approximate the normal or pathological processes found in the human CNS, and at worst some diseases cannot be replicated in rodents at all. The many diverging aspects imply that rodent models necessarily and generally cannot fully

recapitulate human disease. For example, at the cellular level there are notable differences with respect to a specific subtype of glial cell called astrocytes. The much larger size and complexity of human astrocytes clearly denotes a wide evolutionary gap, and they have become fundamentally different from rodent astrocytes (Oberheim et al. 2009). Rodent neurons also show functional divergence, such as a faster rate of network maturation (Napoli and Obeid 2016), making it questionable if they can accurately represent human neuronal networks. It is generally understood that rodent-based disease models are problematic, for such reasons as the difficulty in extrapolating from rodent to human phenotypes and that sporadic human diseases generally cannot be replicated in laboratory animals (Han et al. 2011). In response, there has been a consensual push in the biomedical community to gravitate away from non-human models in the hopes that human cell-based test systems for diagnostics, drug discovery, or other applications will prove to be much more predictive and accurate. Therefore, moving beyond the reliance on non-human sources of neuronal cells has been a longstanding goal in medical neurobiology.

3 Human Pluripotent Stem Cells

Human pluripotent stem cells are believed to be capable of fulfilling this goal. One variety with appealing characteristics that has been studied for many years are embryonic stem (ES) cells (see Chapter "Advances in Human Stem Cell-Derived Neuronal Cell Culturing and Analysis"). ES cells are derived from embryonic blastocysts, can self-renew in culture, and retain almost unlimited potential to differentiate into any somatic cell from all three germ layers (Thomson et al. 1998). At first, there was much anticipation over using ES cells for regenerative medicine, but using them for in vitro disease modeling has proved trickier. Although this is a renewable source of human cells that can be differentiated into neurons, there are several major limitations (Han et al. 2011; Ardhanareeswaran et al. 2017). For example, ES cells are typically collected from donor fetuses, creating substantial ethical concerns. A related problem is therefore limited availability, and since human samples are typically scarce, it creates a small bank derived from only a few subjects, similar to the tumor-derived cell lines mentioned earlier. Another important caveat is that since ES cells are isolated from very early stage fetuses, there is of course no clinical characterization to accompany the cells, thereby severely constraining their usefulness in disease research.

Alternatively, using the breakthrough technology initially reported in 2006, stem cells can be generated directly from somatic cells (e.g., blood or skin fibroblasts) (see Chapter "Advances in Human Stem Cell-Derived Neuronal Cell Culturing and Analysis"). In this case, the differentiated cells are reverted, or reprogrammed, back into pluripotent stem cells through ectopic expression of four transcription factors.

The process for creating "induced" pluripotent stem (iPS) cells was first described by Shinya Yamanaka's group (Takahashi and Yamanaka 2006) using mouse fibroblasts as the starting point, and they subsequently applied their methodology to human fibroblasts (Takahashi et al. 2007). The four transcription factors that induce pluripotency, now commonly referred to as "Yamanaka factors," consist of c-Myc, Klf4, Oct3/4, and Sox2, which are normally expressed in undifferentiated ES cells at high levels. An enormous advantage over ES cells is that iPS cells can be made postnatally, thereby creating cultures on a patient's own genetic background, and neurons derived from those stem cells should therefore more closely reflect each patient's personal physiology. For this reason, iPS cell technology is frequently touted for its potential as an indicative and predictive platform for personalized medicine. But although the potential is understood by many, application of this technology is in its infancy, plus culturing iPS cells, differentiating them into neurons and using them to model disease is still problematic (Engle et al. 2018). Notably, it requires expensive materials and a dedicated effort above and beyond what was required for primary rodent neurons (Engle et al. 2018).

A first generation of methodologies have been developed for converting human stem cells into neuronal cells, and some protocols are described for lineage-specific subtypes of neurons (Mertens et al. 2016). A significant improvement was the discovery that neuronal differentiation can be directed via forced expression of single pro-neurogenic transcription factors, resulting in a more rapid conversion to a uniform population of cells to study (Thoma et al. 2012; Zhang et al. 2013; Chanda et al. 2014; Mertens et al. 2016). The process of protocol optimization is ongoing, where one goal is to improve efficiency by boosting the production of functionally mature neurons as quickly as possible (e.g., see Nehme et al. 2018). Many investigators are actively searching for the right, and minimal, combinations of either small molecules, mitogen or morphogen signaling, and/or transcription factor expression to efficiently generate subtypes of neurons (Mertens et al. 2016). But some cell types are more challenging than others. For example, parvalbumin-expressing interneurons have thus far proven difficult, particularly due to their protracted maturation rate in culture and a general lack of knowledge of what instructs their maturation (Marín 2013; Maroof et al. 2013; Nicholas et al. 2013). They constitute a disease-relevant population of neurons (Ogiwara et al. 2007; Vogt et al. 2018) yet up to now their direct study is still hampered by the inability to make them efficiently from human cells.

Nevertheless, many groups have begun to explore neurological disease modeling in iPS cell-derived neurons under current differentiation protocols. The first iPS cell disease model described was for amyotrophic lateral sclerosis (ALS) (Dimos et al. 2008). Several more disease models are in development, such as for epilepsy (Tidball and Parent 2016; Odawara et al. 2016), neurodevelopmental disorders, neurodegenerative diseases, polygenic psychiatric diseases, and others (Park et al. 2008). The study of early human brain development and neurodevelopmental disorders (NDDs) will potentially benefit greatly from iPS cell technology. Several

NDD models generated from patient-derived neurons are already described, including for Rett syndrome (Marchetto et al. 2010), fragile X syndrome (Halevy et al. 2015), Down syndrome (Park et al. 2008), and Timothy syndrome (Paşca et al. 2011). Alterations in the molecular, cellular, and neuronal network developmental trajectory can be captured at very early stages by monitoring the dynamic steps going from stem cells to neurons (Ardhanareeswaran et al. 2017). It is also now possible to build a large cohort of diverse iPS cell-derived disease models, allowing researchers to make direct comparisons between NDDs that share certain clinical features, all on the same cell-based platform. For example, many NDDs are comorbid with autism spectrum disorder (ASD). By comparing the in vitro neuronal models of NDDs with and without ASD, this may give further insight into the pertinent, overlapping molecular and genetic networks involved, especially in idiopathic cases of disease. Furthermore, by incorporating modern genome editing technologies like CRISPR-Cas9 (reviewed by Komor et al. 2017), one can create isogenic control cells on each patient's genetic background, where a mutation is specifically corrected and compared back to the diseased cells (Soldner and Jaenisch 2018). Conversely, genome editing allows investigators to validate gene-to-phenotype relationships by inducing a similar mutation in cells collected from healthy subjects.

Until this point, our discussion has been focused on monolayer cultures of neurons. But the future direction of in vitro models is heading towards increased complexity, most particularly by using three-dimensional (3D) culture techniques. The need for more accurate ex vivo human models has led to the development of brain organoids, a stem cell-based 3D approach that better recapitulates the cellular composition, architecture, and functionality observed in vivo (reviewed by Amin and Paşca 2018). The capacity of brain organoids to spontaneously self-organize and form structures (e.g., like cortex) resembling their in vivo counterparts makes them an ideal in vitro model to study either normal developmental processes or disease pathogenesis (Di Lullo and Kriegstein 2017). With regard to drug discovery, it is generally accepted that cellular models who mimic the in vivo environment are better predictors of drug efficacy (Engle et al. 2018), and therefore organoid-based platforms could become essential for pre-clinical drug screening. Moreover, organoids may allow for clearer patient stratification based on more defined endophenotypes. Many predict that organoids will sufficiently bridge the gap between traditional 2D cultures and in vivo disease models or patients, as they are more physiologically relevant than monolayer cultures and far more amenable to manipulation of niche components, signaling pathways, and genome editing than in vivo models. For example, organoids have been used to study neural progenitor dysfunctions during brain development, which were found in microcephaly, caused by specific mutations or Zika virus (Lancaster et al. 2013; Garcez et al. 2016), and in ASD (Mariani et al. 2015). This highlights their potential for modeling very early developmental aspects of neurological diseases that are otherwise experimentally inaccessible.

4 Techniques for Monitoring and Manipulating Neural Network Activity

As described in the previous section, over the past century researchers have made great progress in developing protocols to create neuronal models that have relevance for the study of healthy and diseased human brain. At the same time, the growing interest of neuroscientists to explore the dynamics of neuronal systems and the increasing need to observe, measure, and manipulate not only single neurons but populations of cells also required technological advancement (Yuste 2015).

Different techniques exist for measuring and evoking the electrophysiological activity of in vitro neuronal networks. An initial broad distinction, however, can be made between intracellular and extracellular techniques. The intracellular technique allows the direct measurement of changes in electrical potential across the cell membrane by using electrodes positioned directly on the target cell (e.g., patch-clamp electrophysiology) (Hubel 1957; Neher and Sakmann 1976). With this technique, it is possible to measure and record large-amplitude, single-neuron action potentials and also sub-threshold synaptic and ion-channel signals. However, conventional patch-clamp electrophysiology is time consuming because electrodes need to be individually micro-positioned at the target cell. Also, electrical activity cannot be repeatedly monitored in the same neurons during development due to the loss of cell viability after only a few hours. Alternatively, extracellular field potentials induced by neuronal activity can be measured with extracellular microelectrodes positioned near to the cell soma, with respect to a reference electrode. The extracellular technique allows non-invasive, long-term recordings of activity exhibited by a population of neurons growing in close proximity to the electrode, but at the cost of a smaller signal amplitude and lack of sensitivity for sub-threshold signals.

In the 1970s, the advantages of the extracellular technique together with the advent of thin-film fabrication processes promoted the development of substrate-integrated micro-electrode arrays (MEAs). Thomas et al. described the first MEA in 1972, a device with 30 platinized gold microelectrodes (two rows of 15 electrodes each, spaced 100 μm apart) embedded into a glass substrate and passivated with a photoresistor (Thomas Jr. et al. 1972). This device allowed the recording of field potentials from spontaneously contracting sheets of cultured chick cardiomyocytes. Five years later, Guenter Gross and his collaborators recorded activity from an isolated snail ganglion laid over the electrodes (Gross et al. 1977). In 1980, Pine succeeded in recording activity from a 3-week-old neuronal network (i.e., superior cervical ganglion neurons dissociated from rat), using a MEA with 32 gold electrodes (two rows of 16 electrodes each, spaced 250 μm apart), platinized and insulated with silicon dioxide (Pine 1980). Essentially, these three hallmark studies laid the foundations for and marked the beginnings of in vitro network electrophysiology using MEAs.

MEAs afford end users the unique opportunity to record and stimulate groups of neurons, simultaneously and non-invasively, across spatially separated regions in a

network. Network activity can also be monitored over time, and this allows detailed investigations of the dynamics of in vitro neuronal models. Hence, this technology has garnered the interest of and contributions from a very broad cross-disciplinary research community. Indeed, over the last decades dissociated neuronal networks (or brain slices) harvested from rodents and then coupled to MEAs have been used as a standard model system to investigate the basic mechanisms of neuronal communication, to evaluate the neurotoxicity of drugs and chemicals (see Chapter "Application of Microelectrode Array Approaches to Neurotoxicity Testing and Screening"), and to study human disease in vitro (see Chapter "In Vitro Models of Brain Disorders"). Furthermore, the possibility to perform genetic manipulations (e.g., RNA interference) or to use dissociated neuronal cultures from transgenic mice allows researchers to link the effects of genetic disruption to neuronal network activity, to monitor the effects on network development, and to perform drug testing on disease models. In particular, neuronal cultures coupled to MEAs have been used to study neurological diseases like epilepsy (Colombi et al. 2013; Gullo et al. 2014; Hales et al. 2012), Alzheimer disease (Charkhkar et al. 2015; Gortz et al. 2013; Varghese et al. 2010), and intellectual disability (Martens et al. 2016). Finally, the possibility to combine MEA recordings with other physiological techniques, like calcium imaging and single-cell patch-clamp electrophysiology (Vardi et al. 2016; Herzog et al. 2011), has increased the general scientific interest towards this technology.

As alluded to above, the main advantage of MEA technology is the ability to simultaneously record the neuronal network activity from different electrodes. However, the extracellular activity is composed of the collective contribution of many cells rather than a single neuron. This is due to the low number of microelectrodes embedded in the substrate (few tens of microelectrodes) and to their relatively large spatial separation (hundreds of micrometers). Until the early 2000s, little improvement was made to increase the spatial resolution of these devices, mostly because thin-film technology limited the number and density of substrate-integrated electrode sites. However, during the past decade, neuroscientists began to require systems with higher resolution to study other types of impaired phenomena in neurological disorders (e.g., the propagation of signals from the axon, neuronal network connectivity), and to evaluate functional alterations in neurons and the effects of chemical manipulations with unprecedented statistical significance and sensitivity.

To fill this need for high-resolution investigation of neuronal network activity, MEAs with closely spaced electrodes, possibly down to cellular and sub-cellular scales, were developed by exploiting CMOS technology and by adopting concepts that were previously established for light imaging sensors (see Chaps. 11 and 14). With the advent of CMOS-MEAs, the electrophysiological activity of neuronal networks could be monitored and manipulated (i.e., electrically) with thousands of electrodes simultaneously, thereby providing a very high level of sensitivity (Frey et al. 2010; Hierlemann et al. 2011; Berdondini et al. 2005, 2009). In particular, Tsai and coworkers recently developed a novel CMOS-MEA that contains 65,536 simultaneously recording and stimulating microelectrodes (Tsai et al. 2017). Thus,

MEA technology has started to move in the direction of very high-density arrays, which consequently offers an unprecedented spatiotemporal resolution for large-area electrophysiological recordings of neuronal networks in vitro.

Human stem cell technology has opened up many new possibilities in the neuroscience field (see previous section of this chapter and Chapter "Advances in Human Stem Cell-Derived Neuronal Cell Culturing and Analysis"). Indeed, the ability to use human material, to study patient phenotypes in cultured neuronal networks, and to perform drug screening on patient-specific neurons has paved the way for precision medicine. However, stem cell biology presents many new challenges to the MEA field that require careful consideration. For example, the network activity of neurons derived from healthy subjects and patients (e.g., with different mutations, isogenic lines) should be compared in order to validate any observed phenotypes. Furthermore, a large number of recordings is generally required to reduce iPS cell line-to-line variability and to obtain robust endpoint measures. Finally, drug screening should be performed on neuronal networks derived from several different iPS cell parent lines to prove any rescue of an observed in vitro phenotype. With regard to these issues, during the past decade a need has been growing in the neuroscience community for new devices, especially for multi-well MEA platforms. To answer this call, companies such as Multi Channel Systems (www.multichannelsystems.com), Alpha MED Scientific (www.med64.com) and Axion Biosystems (www.axionbiosystems.com) have developed multi-well systems allowing recordings from 6 to 96 independent culture wells simultaneously on a single plate. The downside in the current technology, however, is that the number of electrodes per well decreases with the increase in the number of wells (i.e., Multi Channel Systems: 12 electrodes for 24-well plate and 3 electrodes for 96-well plate; Axiol Biosystems: 64 electrodes for both 6- and 12-well plates, 16 electrodes for both 24- and 48-well plate and 8 electrodes for 96-well plate).

5 Future Perspectives

The neuroscience field is asking for a combination of two types of approach. On the one hand, the possibility to simultaneously record electrophysiological activity from many independent cultures is strongly needed. On the other, a more detailed examination of the electrophysiological activity of human neuronal networks is very important when modeling neurological disease. Indeed, a high-resolution system might be sensitive to phenotypes that cannot be detected on low-density arrays, and those phenotypes might be relevant for a proper understanding of disease pathology or as an endpoint for drug screening. Thus, the field needs a system that can run many experiments in parallel but also with the resolution of a high-density array. At present, no commercially available system like this exists. However, companies that already produce high-density electrode arrays are developing systems in a multi-well format, and we foresee that a multi-well/high-density system will be very advantageous in future neuroscience research.

As previously discussed (see Sect. 3 of this chapter), the rapid advancement in stem cell technology and the need for more accurate human models has led to the development of 3D brain organoids. Indeed, despite their utility for studying basal neurophysiological processes, 2D human iPS cell-based models are limited in their ability to recapitulate complex in vivo-like cell–cell interactions, tissue architecture, or physiological functions. Because 3D brain organoids are presumed to better mimic the in vivo environment, many research groups are using this model system to study disease. Circuit functionality is known to be disrupted in many neurological disorders, and an ability to recreate complex neuronal circuitry is required to obtain novel insight into the pathobiology and to open up new prospects for treatment (Yuste 2015). Unfortunately, monitoring the electrophysiological activity in deep layers of brain organoids is still a challenge, and there is an urgent need to develop novel techniques and devices for 3D network recording.

By combining advancements in human stem cell biology and MEA technology, neuroscientists are taking the tools into sometimes unpredictable directions. However, we foresee that, in the near future, bioengineers and neurobiologists will need to cooperate even more closely to create and characterize in vitro neuronal models that have relevance for the study of the human brain.

References

Amin, N. D., & Paşca, S. P. (2018). Building models of brain disorders with three-dimensional Organoids. *Neuron, 100*(2), 389–405.

Ardhanareeswaran, K., Mariani, J., Coppola, G., Abyzov, A., & Vaccarino, F. M. (2017). Human induced pluripotent stem cells for modelling neurodevelopmental disorders. *Nature Reviews. Neurology, 13*(5), 265–278.

Banker, G., & Goslin, K. (1988). Developments in neuronal cell culture. *Nature, 336*(6195), 185–186.

Banker, G. A., & Cowan, W. M. (1977). Rat hippocampal neurons in dispersed cell culture. *Brain Research, 126*(3), 397–342.

Bardy, C., van den Hurk, M., Eames, T., Marchand, C., Hernandez, R., Kellogg, M., et al. (2015). Neuronal medium that supports basic synaptic functions and activity of human neurons in vitro. *Proceedings of the National Academy of Sciences of the United States of America, 112*(20), E2725–E2734.

Berdondini, L., Imfeld, K., Maccione, A., Tedesco, M., Neukom, S., Koudelka-Hep, M., et al. (2009). Active pixel sensor array for high spatio-temporal resolution electrophysiological recordings from single cell to large scale neuronal networks. *Lab on a Chip, 9*, 2644–2651.

Berdondini, L., van der Wal, P. D., Guenat, O., de Rooij, M. F., Koudelka-Hep, M., Seitz, P., et al. (2005). High-density electrode array for imaging in vitro electrophysiological activity. *Biosensors and Bioelectronics, 21*, 167–174.

Brewer, G. J., & Cotman, C. W. (1989). Survival and growth of hippocampal neurons in defined medium at low density: Advantages of a sandwich culture technique or low oxygen. *Brain Research, 494*(1), 65–74.

Brewer, G. J., Torricelli, J. R., Evege, K., & Price, P. J. (1993). Optimized survival of hippocampal neurons in B27-supplemented Neurobasal, a new serum-free medium combination. *Journal of Neuroscience Research, 35*(5), 567–576.

Chanda, S., Ang, C. E., Davila, J., Pak, C., Mall, M., Lee, Q. Y., et al. (2014). Generation of induced neuronal cells by the single reprogramming factor ASCL1. *Stem Cell Reports, 3*(2), 282–296.

Charkhkar, H., Meyyappan, S., Matveeva, E., Moll, J. R., McHail, D. G., Peixoto, N., et al. (2015). Amyloid beta modulation of neuronal network activity in vitro. *Brain Research, 1629*, 1–9.

Colombi, I., Mahajani, S., Frega, M., Gasparini, L., & Chiappalone, M. (2013). Effects of antiepileptic drugs on hippocampal neurons coupled to micro-electrode arrays. *Frontiers in Neuroengineering, 6*, 10.

Di Lullo, E., & Kriegstein, A. R. (2017). The use of brain organoids to investigate neural development and disease. *Nature Reviews. Neuroscience, 18*(10), 573–584.

Dimos, J. T., Rodolfa, K. T., Niakan, K. K., Weisenthal, L. M., Mitsumoto, H., Chung, W., et al. (2008). Induced pluripotent stem cells generated from patients with ALS can be differentiated into motor neurons. *Science, 321*, 1218–1221.

Dyson, F. J. (2012). History of science. Is science mostly driven by ideas or by tools? *Science, 338*(6113), 1426–1427.

Engle, S. J., Blaha, L., & Kleiman, R. J. (2018). Best practices for translational disease modeling using human iPSC-derived neurons. *Neuron, 100*(4), 783–797.

Frey, U., Sedivy, J., Heer, F., Pedron, R., Ballini, M., Mueller, J., et al. (2010). Switch-matrix-based high-density microelectrode Array in CMOS technology. *IEEE Journal of Solid-State Circuits, 45*, 467–482.

Garcez, P. P., Loiola, E. C., da Costa, R. M., Higa, L. M., Trindade, P., Delvecchio, R., et al. (2016). Zika virus impairs growth in human neurospheres and brain organoids. *Science, 352*, 816–818.

Golgi, C. (1873). Sulla struttura della sostanza grigia del cervello. *Gazzetta Medica Italiana (Lombardia), 33*, 244–246 (in Italian).

Gordon, J., Amini, S., & White, M. K. (2013). General overview of neuronal cell culture. *Methods in Molecular Biology, 1078*, 1–8.

Gortz, P., Siebler, M., Ihl, R., Henning, U., Luckhaus, C., Supprian, T., et al. (2013). Multielectrode array analysis of cerebrospinal fluid in Alzheimer's disease versus mild cognitive impairment: A potential diagnostic and treatment biomarker. *Biochemical and Biophysical Research Communications, 434*(2), 293–297.

Gray, E. G. (1959). Axo-somatic and axo-dendritic synapses of the cerebral cortex: An electron microscope study. *Journal of Anatomy, 93*, 420–433.

Gross, G. W., Rieske, E., Kreutzberg, G. W., & Meyer, A. (1977). A new fixed-array multi-microelectrode system designed for long-term monitoring of extracellular single unit neuronal activity in vitro. *Neuroscience Letters, 6*(2–3), 101–105.

Gullo, F., Manfredi, I., Lecchi, M., Casari, G., Wanke, E., & Becchetti, A. (2014). Multi-electrode array study of neuronal cultures expressing nicotinic beta2-V287L subunits, linked to autosomal dominant nocturnal frontal lobe epilepsy. An in vitro model of spontaneous epilepsy. *Frontiers in Neural Circuits, 8*, 87.

Hales, C. M., Zeller-Townson, R., Newman, J. P., Shoemaker, J. T., Killian, N. J., & Potter, S. M. (2012). Stimulus-evoked high frequency oscillations are present in neuronal networks on microelectrode arrays. *Frontiers in Neural Circuits, 6*, 29.

Halevy, T., Czech, C., & Benvenisty, N. (2015). Molecular mechanisms regulating the defects in fragile X syndrome neurons derived from human pluripotent stem cells. *Stem Cell Reports, 4*(1), 37–46.

Hamburger, V. (1980). S. Ramón y Cajal, R. G. Harrison, and the beginnings of neuroembryology. *Perspectives in Biology and Medicine, 23*(4), 600–616.

Han, S. S., Williams, L. A., & Eggan, K. C. (2011). Constructing and deconstructing stem cell models of neurological disease. *Neuron, 70*(4), 626–644.

Harrison, R. G. (1910). The outgrowth of the nerve fiber as a mode of protoplasmic movement. *The Journal of Experimental Zoology, 9*(4), 787–846.

Herzog, N., Shein-Idelson, M., & Hanein, Y. (2011). Optical validation of in vitro extra-cellular neuronal recordings. *Journal of Neural Engineering, 8*(5), 056008.

Hierlemann, A., Frey, U., Hafizovic, S., & Heer, F. (2011). Growing cells atop microelectronic chips: Interfacing electrogenic cells in vitro with CMOS-based microelectrode arrays. *Proceedings of the IEEE, 99*, 252–284.

Hubel, D. H. (1957). Tungsten microelectrode for recording from single units. *Science, 125*, 549–550.

Komor, A. C., Badran, A. H., & Liu, D. R. (2017). CRISPR-based technologies for the manipulation of eukaryotic genomes. *Cell, 168*(1–2), 20–36.

Lancaster, M. A., Renner, M., Martin, C.-A., Wenzel, D., Bicknell, L. S., Hurles, M. E., et al. (2013). Cerebral organoids model human brain development and microcephaly. *Nature, 501*, 373–379.

López-Muñoz, F., Boya, J., & Alamo, C. (2006). Neuron theory, the cornerstone of neuroscience, on the centenary of the Nobel prize award to Santiago Ramón y Cajal. *Brain Research Bulletin, 70*(4–6), 391–405.

Louis, E. D., & Stapf, C. (2001). Unraveling the neuron jungle: The 1879-1886 publications by Wilhelm his on the embryological development of the human brain. *Archives of Neurology, 58*(11), 1932–1935.

Marchetto, M. C., Carromeu, C., Acab, A., Yu, D., Yeo, G. W., Mu, Y., et al. (2010). A model for neural development and treatment of Rett syndrome using human induced pluripotent stem cells. *Cell, 143*(4), 527–539.

Mariani, J., Coppola, G., Zhang, P., Abyzov, A., Provini, L., Tomasini, L., et al. (2015). FOXG1-dependent dysregulation of GABA/glutamate neuron differentiation in autism spectrum disorders. *Cell, 162*, 375–390.

Marín, O. (2013). Human cortical interneurons take their time. *Cell Stem Cell, 12*(5), 497–499.

Maroof, A. M., Keros, S., Tyson, J. A., Ying, S. W., Ganat, Y. M., Merkle, F. T., et al. (2013). Directed differentiation and functional maturation of cortical interneurons from human embryonic stem cells. *Cell Stem Cell, 12*(5), 559–572.

Martens, M. B., Frega, M., Classen, J., Epping, L., Bijvank, E., Benevento, M., et al. (2016). Euchromatin histone methyltransferase 1 regulates cortical neuronal network development. *Scientific Reports, 6*, 35756.

McCarthy, K. D., & de Vellis, J. (1980). Preparation of separate astroglial and oligodendroglial cell cultures from rat cerebral tissue. *The Journal of Cell Biology, 85*(3), 890–902.

Mertens, J., Marchetto, M. C., Bardy, C., & Gage, F. H. (2016). Evaluating cell reprogramming, differentiation and conversion technologies in neuroscience. *Nature Reviews. Neuroscience, 17*(7), 424–437.

Millet, L. J., & Gillette, M. U. (2012). Over a century of neuron culture: From the hanging drop to microfluidic devices. *Yale Journal of Biology and Medicine, 85*, 501–521.

Napoli, A., & Obeid, I. (2016). Comparative analysis of human and rodent brain primary neuronal culture spontaneous activity using micro-electrode Array technology. *Journal of Cellular Biochemistry, 117*(3), 559–565.

Neher, E., & Sakmann, B. (1976). Single-channel currents recorded from membrane of denervated frog muscle fibres. *Nature, 260*(5554), 799–802.

Nehme, R., Zuccaro, E., Ghosh, S. D., Li, C., Sherwood, J. L., Pietilainen, O., et al. (2018). Combining NGN2 programming with developmental patterning generates human excitatory neurons with NMDAR-mediated synaptic transmission. *Cell Reports, 23*(8), 2509–2523.

Nicholas, C. R., Chen, J., Tang, Y., Southwell, D. G., Chalmers, N., Vogt, D., et al. (2013). Functional maturation of hPSC-derived forebrain interneurons requires an extended timeline and mimics human neural development. *Cell Stem Cell, 12*(5), 573–586.

Oberheim, N. A., Takano, T., Han, X., He, W., Lin, J. H. C., Wang, F., et al. (2009). Uniquely hominid features of adult human astrocytes. *Journal of Neuroscience, 29*(10), 3276–3287.

Odawara, A., Katoh, H., Matsuda, N., & Suzuki, I. (2016). Physiological maturation and drug responses of human induced pluripotent stem cell-derived cortical neuronal networks in long-term culture. *Scientific Reports, 6*, 26181.

Ogiwara, I., Miyamoto, H., Morita, N., Atapour, N., Mazaki, E., Inoue, I., et al. (2007). Nav1.1 localizes to axons of parvalbumin-positive inhibitory interneurons: A circuit basis for epileptic seizures in mice carrying an Scn1a gene mutation. *The Journal of Neuroscience, 27*, 5903–5914.

Park, I. H., Arora, N., Huo, H., Maherali, N., Ahfeldt, T., Shimamura, A., et al. (2008). Disease-specific induced pluripotent stem cells. *Cell, 134*(5), 877–886.

Paşca, S. P., Portmann, T., Voineagu, I., Yazawa, M., Shcheglovitov, A., Paşca, A. M., et al. (2011). Using iPSC-derived neurons to uncover cellular phenotypes associated with Timothy syndrome. *Nature Medicine, 17*(12), 1657–1662.

Pine, J. (1980). Recording action potentials from cultured neurons with extracellular microcircuit electrodes. *Journal of Neuroscience Methods, 2*(1), 19–31.

Ramón y Cajal, S. (1890). A quelle epoque apparaissent les expansions des cellule nerveuses de la moelle epinere du poulet. *Anatomischer Anzeiger, 5*, 609–613.

Soldner, F., & Jaenisch, R. (2018). Stem cells, genome editing, and the path to translational medicine. *Cell, 175*(3), 615–632.

Takahashi, K., Tanabe, K., Ohnuki, M., Narita, M., Ichisaka, T., Tomoda, K., et al. (2007). Induction of pluripotent stem cells from adult human fibroblasts by defined factors. *Cell, 131*, 861–872.

Takahashi, K., & Yamanaka, S. (2006). Induction of pluripotent stem cells from mouse embryonic and adult fibroblast cultures by defined factors. *Cell, 126*, 663–676.

Thoma, E. C., Wischmeyer, E., Offen, N., Maurus, K., Sirén, A. L., Schartl, M., et al. (2012). Ectopic expression of neurogenin 2 alone is sufficient to induce differentiation of embryonic stem cells into mature neurons. *PLoS One, 7*(6), e38651.

Thomas Jr., C. A., Springer, P. A., Loeb, G. E., Berwald-Netter, Y., & Okun, L. M. (1972). A miniature microelectrode array to monitor the bioelectric activity of cultured cells. *Experimental Cell Research, 74*(1), 61–66.

Thomas, W. E. (1985). Synthesis of acetylcholine and gamma-aminobutyric acid by dissociated cerebral cortical cells in vitro. *Brain Research, 332*(1), 79–89.

Thomson, J. A., Itskovitz-Eldor, J., Shapiro, S. S., Waknitz, M. A., Swiergiel, J. J., Marshall, V. S., et al. (1998). Embryonic stem cell lines derived from human blastocysts. *Science, 282*, 1145–1147.

Tidball, A. M., & Parent, J. M. (2016). Exciting cells: Modeling genetic epilepsies with patient-derived induced pluripotent stem cells. *Stem Cells, 34*(1), 27–33.

Tsai, D., Sawyer, D., Bradd, A., Yuste, R., & Shepard, K. L. (2017). A very large-scale microelectrode array for cellular-resolution electrophysiology. *Nature Communications, 8*, 1802.

Vardi, R., Goldental, A., Sardi, S., Sheinin, A., & Kanter, I. (2016). Simultaneous multi-patch-clamp and extracellular-array recordings: Single neuron reflects network activity. *Scientific Reports, 6*, 36228.

Varghese, K., Molnar, P., Das, M., Bhargava, N., Lambert, S., Kindy, M. S., et al. (2010). A new target for amyloid beta toxicity validated by standard and high-throughput electrophysiology. *PLoS One, 5*(1), e8643.

Vogt, D., Cho, K. K. A., Shelton, S. M., Paul, A., Huang, Z. J., Sohal, V. S., et al. (2018). Mouse Cntnap2 and human CNTNAP2 ASD alleles cell autonomously regulate PV+ cortical interneurons. *Cerebral Cortex, 28*(11), 3868–3879.

Yamamoto, C. (1972). Activation of hippocampal neurons by mossy fiber stimulation in thin brain sections in vitro. *Experimental Brain Research, 14*(4), 423–435.

Yuste, R. (2015). From the neuron doctrine to neural networks. *Nature Reviews. Neuroscience, 16*(8), 487–497.

Zhang, Y., Pak, C., Han, Y., Ahlenius, H., Zhang, Z., Chanda, S., et al. (2013). Rapid single-step induction of functional neurons from human pluripotent stem cells. *Neuron, 78*(5), 785–798.

In Vitro Models of Brain Disorders

Joost le Feber

Abstract The brain is the most complex organ of the body, and many pathological processes underlying various brain disorders are poorly understood. Limited accessibility hinders observation of such processes in the in vivo brain, and experimental freedom is often insufficient to enable informative manipulations. In vitro preparations (brain slices or cultures of dissociated neurons) offer much better accessibility and reduced complexity and have yielded valuable new insights into various brain disorders. Both types of preparations have their advantages and limitations with regard to lifespan, preservation of in vivo brain structure, composition of cell types, and the link to behavioral outcome is often unclear in in vitro models. While these limitations hamper general usage of in vitro preparations to study, e.g., brain development, in vitro preparations are very useful to study neuronal and synaptic functioning under pathologic conditions. This chapter addresses several brain disorders, focusing on neuronal and synaptic functioning, as well as network aspects. Recent progress in the fields of brain circulation disorders, excitability disorders, and memory disorders will be discussed, as well as limitations of current in vitro models.

Keywords Brain disorders · In vitro model · Micro Electrode Array · Hypoxia · Excitability · Memory

1 Introduction

The brain is by far the most complex organ of the human body, and our understanding of brain physiology and pathology remains limited. Given the highly complex combination of physiological processes, various pathologies may result in a wide range of brain disorders. Due to the lack of understanding of the underlying

J. le Feber (✉)

Clinical Neurophysiology, MIRA Institute for Biomedical Technology and Technical Medicine, University of Twente, Enschede, The Netherlands
e-mail: j.lefeber@utwente.nl

mechanisms and difficulties to measure many of the relevant processes in patients, brain disorders are generally diagnosed and classified by the occurrence of clinical symptoms. Because different pathologies may result in similar symptoms, some brain disorders lead to spectrum diagnoses with no clear definition of the underlying pathology. Epilepsy, for example, is such a spectrum diagnosis that may have causes that range from channelopathies to traumatic brain injury or stroke (Bhalla et al. 2011; Shorvon 2011). On the other hand, different diagnoses may exist for disorders that to a certain extent share pathology. For example, the formation of Lewy bodies is strongly associated with Parkinson's Disease, but also with Dementia with Lewy bodies. Discrimination between these diagnoses is often based on the temporal evolution of clinical symptoms (Emre et al. 2007; McKeith et al. 2005).

Practical and ethical limitations severely hamper the investigation of brain disorders in situ, and new insights are obtained mainly from animal models. The poor correlation between clinical diagnosis of brain disorders and the underlying pathological mechanisms complicates the design of animal models to investigate brain disorders and to develop treatment. A primary criterion for animal models is often the ability to mimic clinical symptoms. However, these symptoms may arise from mechanisms that differ from that leading to the patient's disorder. Consequently, many approaches that seemed very promising in animal studies could not, or only partially, be translated to the clinic (van der Worp et al. 2010).

A possible improvement lies in the use of in vitro models of brain disorders. In vitro models can target a specific mechanism and investigate possible treatment. Adversely, in vitro models usually do not exhibit all symptoms that are clinically associated with the disorder. Whereas it may be difficult to distill a specific mechanism underlying a disorder for detailed investigation in an in vitro model, the translation of results to the clinic may also be obscured. Moreover, the high experimental freedom of in vitro models may lead to solutions that cannot be translated to treatment because clinical practice shows far less freedom. For example, drugs that worked well in in vitro models may not be able to pass the blood–brain barrier, or may appear to cause problems in systems that were not included in the in vitro model (de Lange et al. 2017). Still, in vitro models can be very useful to study brain disorders and for development of treatment, provided that relevant underlying mechanisms can be isolated in an in vitro model and care is taken that treatment may also be applicable in patients. Accordingly, currently available in vitro models concentrate on dysfunction at the cellular or synaptic level, or, more recently, at the level of small networks.

2   In Vitro Models

In vitro models exist for a range of brain disorders. The most prominent include stroke, epilepsy, and memory-related disorders. The main objectives to pursue through the model are investigation of disease pathophysiology, identification of novel biomarkers, options for mechanism-based treatment, or high-throughput drug

screening. In vitro models may be based on acute or organotypic brain slices, or on cultures of dissociated neurons. Acute slices are more frequently used than organotypic slices, and, after preparation, can typically be used for several hours, although recently methods have been developed that facilitate longer slice viability (Buskila et al. 2014). Animals are anaesthetized and decapitated. Then, the brain is removed and stored in cold artificial cerebrospinal fluid. After dissection of the relevant areas, usually hippocampus or cortex, $\sim$300–500 μm thick slices are cut on a microtome and put in a dish with carbogen (a mixture of 95% O_2 and 5% CO_2) bubbled medium.

The use of brain slices allows the electrophysiological study of neurons, synapses, or neural circuits under controlled conditions, in isolation from the rest of the brain and body. It facilitates stimulating and/or recording from single or multiple neurons or axons and provides large experimental freedom. Brain slice experiments are faster and cheaper than in vivo studies and do not require anesthesia after the initial decapitation. Separation of the brain tissue from the body avoids muscle artifacts, as well as possible limitations imposed by the blood–brain barrier. Finally, brain slices maintain some of the structural connections that are present in vivo, but are lost in dissociated cell cultures. Drawbacks include the limited time window for experiments, the missing input and output connections as present in the whole brain, and, in particular, the high oxygen fraction in the gas mixture needed for perfusion. Maintaining brain slices in 95% O_2 may produce hyperoxia, oxidative stress, and increased cell death (D'Agostino et al. 2007). Furthermore, decapitation and extraction of the brain before the slice is placed in the recording solution may have effects on the tissue, and slicing of the brain damages the edges of preparations.

Organotypic slices combine an in vivo-like structure with a long time window for experimenting. However, this approach is technically more challenging because it generally requires thinner slices and sterility must be maintained throughout their life in vitro (Hutter-Schmid et al. 2015). Furthermore, organotypic slices are preferably obtained from a young donor, and undergo further development during their life in vitro. In vitro development may differ from regular in vivo development, which limits the usability of organotypic brain slices to model brain disorders that typically occur with aging (Humpel 2015).

An alternative approach uses neurons, usually obtained from embryonic or newborn rats or mice, which are dissociated, and plated on micro electrode arrays (MEAs). Also, the differentiation of induced pluripotent stem cells has become a compelling technique to acquire cells for plating on MEAs. After plating, neurons grow out dendrites and axons, and form new synapses. Newly formed synapses include glutamatergic, excitatory synapses as well as GABAergic ones, which are in principle inhibitory. During early development (up to $\sim$10 days), however, GABAergic synapses exert a net excitatory effect (Ben-Ari 2002). After a maturation period of $\sim$3 weeks, cultures show quasi stable firing patterns and are ready for experimenting. Cultures of dissociated neurons on MEAs offer easy access to many neurons, while cultures remain vital for up to several months. Whereas dissociated cultures lack typical in vivo brain structure, these models are

mainly applied to study basic physiological functioning of various types of neurons, synapses, and astrocytes. Relevant brain disorders include circulation disorders (Patel 2008), excitability disorders (Badawy et al. 2012; Holmes and Ben-Ari 2001), and memory disorders (Ashford 2008; Kopelman 2002), which will be addressed in the following sections.

3 Brain Circulation Disorders

3.1 Stroke

The most prominent disorder related to interrupted brain circulation is (ischemic) stroke. Taking into consideration that about 13 million people per year suffer a stroke worldwide, which is lethal in 30% of all patients and another third is left permanently disabled (Mackay and Mensah 2004), stroke poses a serious health problem, particularly to an aging population. The only effective treatment to improve outcome is acute recanalization by intravenous thrombolysis (Grond et al. 1998; Wardlaw et al. 1997) or intra-arterial thrombectomy (Goyal et al. 2016; Rodrigues et al. 2016). Treatment to promote recovery of ischemic cerebral damage is not available. Moreover, secondary damage of brain tissue occurs in approximately one third of patients during the first days after the infarct and leads to additional neurological impairment. For these patients, no therapy is available (Roger et al. 2011).

Occlusion of a brain artery typically results in an infarct core, with loss of neuronal functioning followed by irreversible brain damage and cell death within minutes. The core is often surrounded by a penumbral region, with some remaining, but significantly reduced perfusion through collateral arteries (Fig. 1). The ischemic penumbra is defined as an area of brain tissue with insufficient blood flow to maintain neuronal activity but adequate blood flow to preserve neuronal viability (Symon et al. 1977). Here, neuronal function is severely compromised although damage is initially reversible. During the first days, the penumbra may further deteriorate or recover. The underlying processes that determine either outcome remain ill understood. Whereas the infarct core must be regarded as lost, the penumbra offers opportunities for the development of treatment to promote recovery.

The restricted availability of oxygen and glucose in the penumbra significantly limits the mitochondrial production of adenosine tri phosphate (ATP), the major energy source in the brain. One of the early consequences of ATP depletion in the ischemic penumbra is large-scale synaptic failure (Bolay et al. 2002; Hofmeijer et al. 2014; Khazipov et al. 1995; le Feber et al. 2017). However, synapses initially remain intact, and if oxygen is restored in time, synaptic failure appears to be reversible (Somjen 1990). Impeded synaptic trafficking generally leads to strongly reduced neuronal activity in the penumbra. In stroke patients, a reduction in cerebral blood flow below 15–18 ml/100 g/min was found to cause immediate electrical silence,

Fig. 1 The ischemic penumbra. In the core of a stroke (indicate as a light gray area), all perfusion is impeded and neurons rapidly progress to cell death. Often an area with some remaining collateral perfusion, the penumbra, lies around the core (indicated by the dark area). In the ischemic penumbra cells initially remain viable but silent, due to large-scale synaptic failure occurring in this area
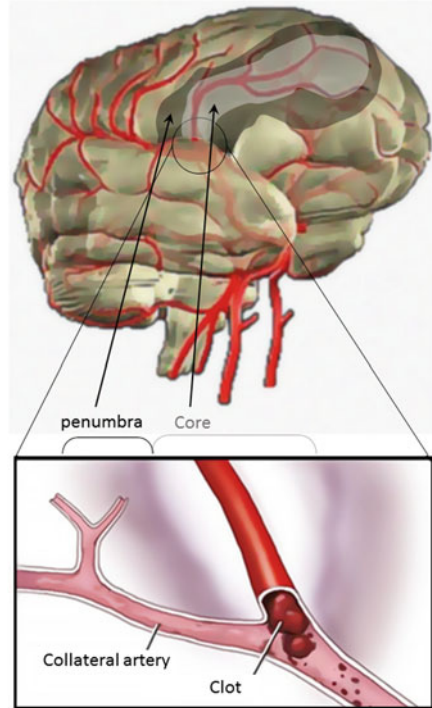
as observed by flattening of the EEG (Yang et al. 2014). Although functionally silent, the penumbra is considered structurally intact and viable (Hofmeijer and van Putten 2012). Electrophysiological dysfunction is regarded as a key event in the pathogenesis of ischemic brain injury, but the following sequence of events is not well known. Further steps following the initial, reversible silence are difficult to determine in patients. This is where in vitro models can be exploited.

3.2 Postanoxic Encephalopathy

Another common disorder associated with failure of brain circulation is postanoxic encephalopathy (PAE), resulting from a period of low or absent cerebral perfusion after cardiac arrest or shock, severe respiratory distress, suffocation or near-drowning. In contrast to stroke, impeded circulation in PAE is transient. The duration, as well as the depth of ischemia, the "hypoxic burden", differs widely between patients, and is a key determinant of the neurological outcome. PAE after cardiac arrest has been widely studied. Annually, around 1 out of 1000 people in the western world experience a cardiac arrest (Berdowski et al. 2010; Rea et al. 2004). Around 80% of these patients remain comatose after restoration of

spontaneous circulation (Madl and Holzer 2004). Although on average 20–30% of these patients survive and regain consciousness (Zandbergen et al. 2003), most remain unconscious and evolve towards brain death or a persistent vegetative state (Kaye 2005). It is critical to restore circulation as soon as possible. While earlier reports suggested that mild therapeutic hypothermia may limit further brain damage (Arrich et al. 2010; Bernard et al. 2002; Hypothermia after Cardiac Arrest Study Group 2002), more recently it has been shown that prevention of fever is probably more relevant, motivating most centers to treat these patients accordingly (Nielsen et al. 2013). Other treatments have not shown substantial benefit (Moragas Garrido and Gascón Bayarri 2012).

Given the complexity and expenses of treatment, and the emotional burden for relatives, in combination with the relatively small fraction of patients with neurological recovery, early stage reliable prognosis for individual patients is invaluable. Studies on outcome prediction have focused mostly on neurological examination, clinical neurophysiological tests and biochemical parameters. Results for biochemical parameters and neuroimaging are inconclusive (Zandbergen 2008). Timing and development of abnormalities in continuous EEG recording reportedly provide better prognostic tools (Hofmeijer et al. 2015; Oh et al. 2015; Ruijter et al. 2017; Tjepkema-Cloostermans et al. 2015). While continuous EEG has been shown to allow reliable prognostication, underlying pathophysiological mechanisms remain unclear. Although the EEG reflects synaptic activity (Buzsaki et al. 2012), it is far from trivial, if not impossible, to deduce detailed characteristics of synaptic and neuronal functioning under postanoxic conditions in situ. In vitro models provide better accessibility to neurons and synapses and have been used to study mechanisms underlying PAE.

3.3   In Vitro Models of Oxygen/Glucose Deprivation

Regular cellular functioning requires ATP, which is normally produced by oxidizing glucose. Impeded blood circulation in the brain means that less glucose and oxygen, and therefore less ATP, become available to cells in the brain.

3.3.1   Brain Slices

Slices can be obtained from animals with induced stroke, but mostly hypoxia or transient anoxia are applied after preparation of the slices. For transient anoxia, carbogen perfusion is temporarily replaced by a 95% N_2/5% CO_2 mixture. For hypoxia, oxygen and nitrogen can be mixed in any ratio, and supplemented with 5% CO_2. Most slice models restrict oxygen, but not glucose. Reduction of glucose from the perfusion medium had similar effects as oxygen restriction although recovery of synaptic function occurred after longer periods of glucose lack than of oxygen lack (Schurr et al. 1989).

Brain slices have long been used to study the relationship between metabolism and activity (Lipton and Whittingham 1984). Neurons in acute brain slices usually survive periods of anoxia of several minutes, and they remain able to generate action potentials (Fujiwara et al. 1987). On this time scale, much stronger alterations were seen in synaptic functioning (Lipton and Whittingham 1982). Evoked inhibitory postsynaptic potentials (IPSPs) were abolished within a few minutes after the onset of hypoxia, while evoked excitatory postsynaptic potentials (EPSPs) were maintained five times longer (Fujiwara et al. 1987; Krnjević et al. 1991). This seemingly higher vulnerability of inhibitory hippocampal synapses, however, has been contradicted in later work that showed that inhibitory synaptic transmission is quite resistant to short (3 min or 4–6 min) lasting anoxia (Khazipov et al. 1993; Zhu and Krnjević 1994). Recordings from cortical slices did not reveal any differences in susceptibility for hypoxia between interneurons and pyramidal cells (Luhmann et al. 1993). Work by Khazipov et al. (1993) revealed that particularly excitatory synapses to inhibitory postsynaptic neurons appeared vulnerable to hypoxia. Administration of exogenous receptor agonists suggested that the suppression of EPSCs is due to presynaptic mechanisms (Khazipov et al. 1993, 1995; Sun et al. 2002). Suppression of IPSPs may also depend on presynaptic mechanisms (Khazipov et al. 1993; Krnjević et al. 1991) although later work suggested that evoked transmitter release from GABAergic terminals was not affected by anoxia (Khazipov et al. 1995).

Synaptic depression is in principle reversible, provided that the hypoxic burden, determined by depth and duration of hypoxia, is sufficiently mild. Lower oxygen levels during hypoxia, and longer duration were associated with a lower recovery rate of synaptic function upon restoration of oxygenation (Schurr et al. 1989). Excitatory synaptic transmission recovered immediately as oxygenation was reinitiated (Sun et al. 2002). After reoxygenation, inhibitory synaptic transmission (to pyramidal cells) recovered slowly, and not always completely (Krnjević et al. 1991). The hypoxia-induced reduction in excitatory and inhibitory synaptic transmission was significantly smaller in immature than in adult neocortical slices (Luhmann et al. 1993).

3.3.2   Cultures of Dissociated Neurons

While the use of acute brain slices has enabled the discovery of several consequences of exposure to hypoxia, one of the major limitations laid in the restricted duration of experiments. Recovery or further deterioration in the ischemic penumbra, as well as decisive development in postanoxic encephalopathy occurs at longer timescales. Therefore, other models have been developed, in particular based on cultures of dissociated neurons. Such cultures, plated on micro electrode arrays (MEAs), have been exposed to transient anoxia (Hofmeijer et al. 2014; Stoyanova et al. 2016) as an in vitro model of postanoxic encephalopathy, or to hypoxia of varying depth and duration (le Feber et al. 2016, 2017, 2018) to model the ischemic penumbra.

Hypoxia was achieved by regulation of the gas mixture above the culture medium bath, which contained air and N_2 in any desired ratio, supplemented with 5% CO_2. This resulted in partial oxygen pressures between 1% and 19% of atmospheric pressure, and facilitated variable duration of hypoxia. Although the composition of gas mixtures could be changed quite rapidly, slow diffusion in the medium bath significantly slowed down imposed changes. Consequently, the timing of changes observed under hypoxic conditions in dissociated cultures and acute slices cannot be directly compared.

Exposure to hypoxia rapidly decreased recorded spontaneous activity (Fig. 2), probably related to suppressed excitatory synaptic transmission (Hofmeijer et al. 2014; Segura et al. 2016). The extracellular recording technique enables the detection of action potentials, but does not show subthreshold fluctuations of the membrane potential. Traditional techniques, based on intracellular recordings, determine (changes in) synaptic efficacy by the observed changes in excitatory (inhibitory) postsynaptic potentials (EPSPs and IPSPs) or currents.
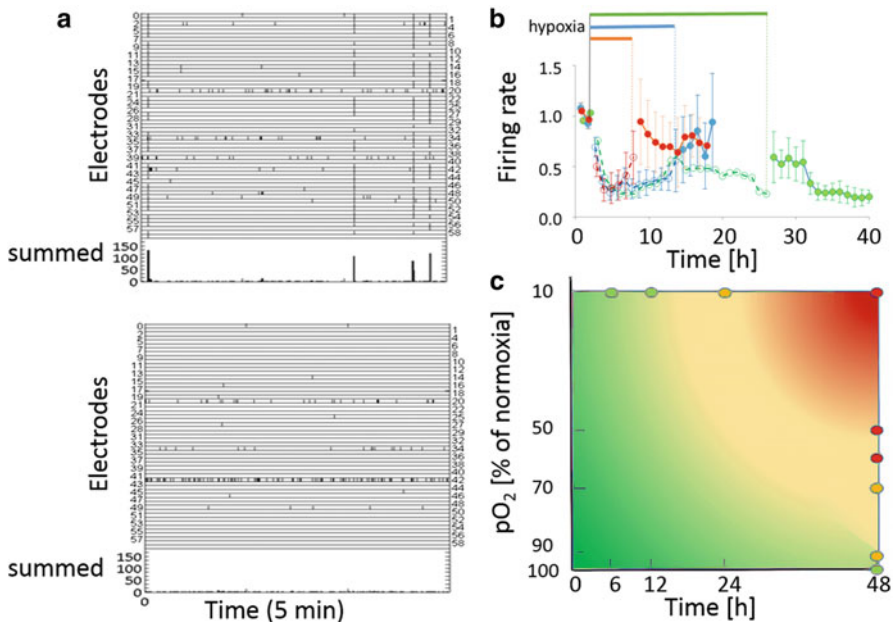
Fig. 2 Hypoxia affects network activity in cultures of dissociated cortical neurons. (**a**) shows the effect of severe hypoxia (10% of normoxia) on firing rate and pattern. During normoxic recording (upper panel), there is more activity and patterns show more frequent synchronized bursting than during hypoxia (lower panel). (**b**) quantifies network wide activity as recorded before, during, and after hypoxia at this depth (expressed as a fraction of baseline activity). Partial recovery of activity during hypoxia suggests the presence of activity homeostatic mechanisms that aim to compensate for the low activity. Further recovery of activity occurs if the culture is reoxygenated after 6 or 12 h. Upon reoxygenation after 24 h only partial recovery occurred. Recovery depended not only on the duration, but also on hypoxic depth (**c**). Figures based on le Feber et al. (2016, 2017, 2018)
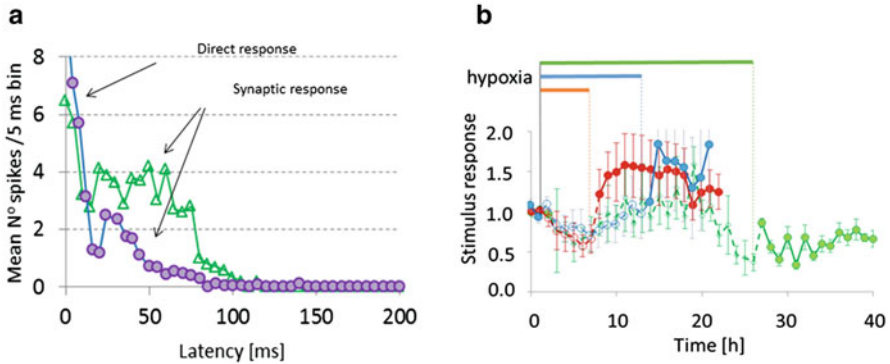
Fig. 3 Hypoxia affects stimulus responses. Responses to electrical stimulation through one of the electrodes typically contain a direct response dominated by directly induced action potentials with latencies up to 10–15 ms, followed by a synaptically mediated network response. (**a**) shows two examples of average responses to stimulation at two different electrodes in one culture when stimulated at $t = 0$. (**b**) quantifies the synaptic phase of stimulus responses before, during, and after hypoxia (10% of normoxia), and shows that stimulus responses become strongly potentiated if the culture is reoxygenated after 6 or 12 h, but not after 24 h (le Feber et al. 2015, 2018)

In MEA-based hypoxia models, synaptic functioning was assessed by the synaptically mediated phase of responses to electrical stimulation. These responses typically consist of two phases: a direct response and a synaptically mediated response (Fig. 3a). The direct response, with latencies up to ∼15 ms is dominated by action potentials that are directly induced by the stimulation current. Consequently, this phase of the stimulus response reproduces relatively well, has low jitter, and persists during excitatory synaptic blockade (Marom and Shahaf 2002; Wagenaar et al. 2004), indicating that a substantial part of the response in this phase does not depend on synaptic transmission. The group of neurons that is synchronously activated in the first phase, in turn, often generates sufficient input to the rest of the network to induce a network response. This indirect response is abolished after synaptic blockade (Fedorovich et al. 2017) and represents the synaptically mediated network response.

Experimental results confirmed that synaptic failure occurs rapidly after the induction of hypoxia (Hofmeijer et al. 2014; le Feber et al. 2016), while neurons remain viable, and able to generate action potentials (le Feber et al. 2016; Segura et al. 2016). This is at least in part due to presynaptic mechanisms, including adenosine-mediated mechanisms (Khazipov et al. 1995; Sun et al. 2002), impeded phosphorylation of presynaptic proteins (Bolay et al. 2002), and impeded endocytosis and exocytosis of synaptic vesicles (Fedorovich et al. 2017). Synaptic failure leads to significant reduction of ongoing network activity (Hofmeijer et al. 2014; le Feber et al. 2016; Segura et al. 2016).

Low activity may jeopardize network viability because neuronal survival depends on regular calcium influx, which is promoted by electrical activity (Ghosh et al. 1994; Mao et al. 1999). Low activity has been shown to trigger compensatory

mechanisms aiming to maintain the total network activity within a certain (healthy) working range. Such homeostatic activity regulation can be achieved by up-regulation of excitatory synapses (Turrigiano 2008), and down-regulation inhibitory synapses (Kilman et al. 2002). At longer time scales, activity homeostasis may also be achieved by growth of axons (Schmitz et al. 2009) and dendrites (Wong and Ghosh 2002), and the formation of spines and boutons (Florence et al. 1998). Partial recovery of activity during hypoxia and potentiated stimulus responses upon return to normoxia (Fig. 3b), as well as a relative increase of the excitatory synapse density (le Feber et al. 2016, 2017, 2018) support the idea of activity homeostasis. As synaptic scaling has been shown to take place postsynaptically (Turrigiano et al. 1998), it may reflect postsynaptic compensation of presynaptic failure. This process requires ATP, which is scarce under hypoxic conditions, and the effectiveness is questionable. Furthermore, activity homeostatic processes may lead to network hyperexcitability, a phenomenon that is frequently observed in patients after stroke (Liepert et al. 2000; Manganotti et al. 2002; Swayne et al. 2008).

3.3.3 Limitations

For models of brain circulation disorders, it is important that the fraction of astrocytes in the cell population mirrors that in vivo. Astrocytes occupy a substantial amount of space in the in vivo brain (Azevedo et al. 2009; Magistretti and Pellerin 1999) and provide essential metabolic support to neurons during transient ischemia (Rossi et al. 2007; Takano et al. 2009). Experiments in hippocampus showed that during hypoxia astrocytes may reduce presynaptic transmitter release (Martín et al. 2007). Conversely, astrocytes are able to restore neuronal activity under conditions of glucose deprivation due to lactate provided by the astrocytes (Rouach et al. 2008).

A general limitation of slices as well as dissociated cultures lies in the interpretation of hypoxia/normoxia. Partial oxygen pressure during normoxia in the in vivo rat brain averages around $pO_2 \approx 30$–35 mmHg (Grote et al. 1996; Nair et al. 1987), much lower than normoxia as normally applied to slices or dissociated cultures. Neurons obtained from the striatum have been cultured under low oxygen conditions and were shown to survive. They showed larger mitochondrial networks, greater cytoplasmic fractions of mitochondria, and larger mitochondrial perimeters than those cultured at atmospheric oxygen levels (Tiede et al. 2011), illustrating that cells adapted to low oxygen, and that culturing under lower oxygen conditions from the time of plating may improve the resemblance between in vivo and in vitro.

4   Excitability Disorders/Epilepsy

Neuronal excitability at the cellular level can be described as the propensity of a neuron to generate an action potential in response to receiving a defined input signal. Excitability is a critical parameter for brain functioning and should not increase or

decrease beyond the boundaries of a certain healthy working range. Subthreshold excitability, for instance, may occur during anesthesia (Palmieri et al. 1999) or in disorders of consciousness (Lapitskaya et al. 2013), whereas the most prominent disorder associated with excessive excitability is epilepsy.

Epilepsy is a chronic condition, and the fourth most common neurological disorder in the USA (England et al. 2012). Affecting people of all ages, an estimated 70 million people suffer from epilepsy worldwide (Singh and Trevick 2016). Recurrent, unprovoked seizures form the hallmark of epilepsy, which can severely affect patients' safety, relationships, work, driving, and quality of life. Epilepsy is a spectrum condition with a wide range of seizure types, varying from person to person (Jensen 2011). For about one third of all patients with epilepsy, no adequate treatment is available. Despite significant efforts to develop new antiepileptic medications over the past decade, this percentage has remained relatively stable, possibly related to the unknown cause in ~60% of epilepsy cases (Epilepsy Foundation). Partial or focal seizures originate in a part of one hemisphere, whereas primary generalized seizures start in both hemispheres simultaneously. Further subdivision of seizures is based solely on clinical and electroencephalographic (EEG) descriptive data (Berg and Millichap 2013; Fisher et al. 2017), acknowledging that the events and mechanisms underlying different seizures remain largely unknown. Classification of epilepsy, on the other hand, is not solely based on clinical data, but also involves pathophysiologic mechanisms, anatomic substrates, and etiology.

Various models are available to study the underlying mechanisms of epilepsy and possible treatment. In vivo models are most suited to capture the behavioral outcome of epilepsy, however, underlying mechanisms often remain uncertain, as these are difficult to assess in vivo (although recent advances in optogenetics have facilitated such work (Paz et al. 2013)). As the underlying pathology may substantially determine the effectiveness of certain therapies, it is difficult to evaluate treatment in models that mimic behavioral outcome, but may build on different underlying mechanisms.

4.1   In Vitro Models of Epilepsy

As an alternative, in vitro models enable a more mechanistic approach of epilepsy. However, these models may not cover the behavioral aspects of epilepsy, which may complicate translation of results to clinical patient care. To provide a structure for in vitro research, different facets of epileptic disorders may be defined and modeled separately (Engel and Schwartzkroin 2006).

Epileptogenesis Acquired epilepsies often begin with an epileptogenic insult, which can occur at any stage in life. Alternatively, disrupting events like brain trauma or stroke may trigger epileptogenesis. Acquired epilepsies depend on plasticity-induced changes and require time to develop (Lopes da Silva and Gorter 2009).

The Interictal State Even if the brain is characterized by an epileptic condition, seizures are absent most of the time. In many patients with epilepsy, interictal activity may appear in the EEG, like spikes or spike-waves, or pathological high-frequency oscillations (HFOs). Results of numerous studies suggest that interictal spikes and HFOs reflect pathological network activity that leads to seizure generation (Levesque et al. 2017). The interictal state is particularly interesting to study the natural mechanisms that prevent or promote ictus generation (Avoli 2001).

Ictal Onset Alotaiby et al. reviewed electrophysiological techniques to detect and predict seizure onset minutes to hours before they occurred. In some conditions, the transition from the interictal state to ictal onset takes considerable time. Preictal EEG findings may reflect pathological development that slowly builds up to the ictus (Alotaiby et al. 2014; Engel and Schwartzkroin 2006).

Ictus and Ictus Termination Seizures can last from ~10 s (Hughes 2009) to more than 5 min, from which point it is defined as status epilepticus (Trinka et al. 2012). Seizure-like events lasting more than 10s have also been observed in vitro in most cortical and limbic structures (Armand et al. 1998; Dreier and Heinemann 1991). The vast majority of ictal events display an evolutional pattern which reflects a sequence of pathophysiologic disturbances (Antonio et al. 2016; Dietzel and Heinemann 1986; Lux et al. 1986). As a result, adjacent and distant anatomic structures are recruited in the epileptic process (Dreier and Heinemann 1991). Excessive synchrony is the feature that defines most seizure states. Mechanisms underlying this synchrony can be analyzed, potentially yielding insights into how to interfere with ongoing seizure activity (Uhlhaas and Singer 2006).

The Postictal Period Most seizures are followed by a period of neurologic deficit, often as a consequence of the natural mechanisms that act to terminate the seizure. Postictal deficits recover over time to a variable extent (Fisher and Engel 2010). Postictal disturbances can be more disabling than the seizures themselves (Sutula and Pitkänen 2002).

Long-Term Consequences Many studies have found that the occurrence of seizures may induce alteration in subsequent seizure manifestations, such as increased frequency and severity (Kadam et al. 2010; Williams et al. 2009)

4.1.1 Brain Slices

Acute slices combine preservation of certain circuitry with large experimental freedom and relative ease of preparation and have been used widely as in vitro models of epilepsy. They have yielded a wealth of new insights on neurobiological mechanisms responsible for the onset and termination of seizures (Librizzi et al. 2017; Motamedi et al. 2006; Weissinger et al. 2005), seizure control and prevention (Hongo et al. 2015), propagation of seizure activity (Losi et al. 2016; Weissinger et al. 2005), and seizure-induced cell death (Frantseva et al. 2000), as well as well-developed protocols to induce seizure-like activity (Harrison et al. 2004; Pal et al.

2001; Rutecki et al. 1987; Schwartzkroin and Prince 1978; Srinivas et al. 2007; Tancredi and Avoli 1987; Tancredi et al. 1990). However, acute slices can only be maintained healthy for several hours, and, as research in the epilepsy field is moving from a primary focus on controlling seizures to addressing disease pathophysiology (Pacico and Mingorance-Le Meur 2014), processes that occur on time scales beyond the lifespan of acute cultures become more relevant. Organotypic slices and cultures of dissociated neurons offer a much longer time span and may be preferred for pathophysiology studies. Organotypic slices generally require relatively thin slicing and a high degree of sterility, making this approach technically challenging. Furthermore, organotypic slices appear most viable when obtained from a young donor. However, many neural circuits relevant for epilepsy have not yet been fully developed in newborn animals. Consequently, not many papers have been published on intact functional adult organotypic slices (Humpel 2015). Cultures of dissociated cultures lack typical structure as found in vivo. However, certain processes that affect excitability at the cellular or network level may still be studied.

4.1.2 Cultures of Dissociated Neurons

In pioneering work, Furshpan and Potter showed that cultures of dissociated hippocampal neurons of neonatal rats that were chronically exposed to high Mg^{2+} and a glutamate receptor antagonist generated intense seizure-like activity, suggesting that such models allow seizure-related cellular mechanisms to be studied in long-term cell culture (Furshpan and Potter 1989). The observation that networks of dissociated cortical or hippocampal neurons develop activity patterns that are dominated by synchronous bursts that show remarkable resemblance to interictal spikes (Ramakers et al. 1990) has been confirmed in numerous later studies, see, e.g., (Chiappalone et al. 2007; Eckmann et al. 2008; Pasquale et al. 2008; van Pelt et al. 2004). In dissociated hippocampal cultures, AMPA antagonists were more effective to block synchronized bursts than NMDA antagonists, which agrees with reports involving comparison of AMPA and NMDA receptor antagonists in anticonvulsant therapy (Rogawski 2011). This indicates that developing network models may be useful for the study of mechanisms that govern pathological network activity in diseases such as epilepsy (Suresh et al. 2016).

Thus, without pharmacological manipulation, cultures of dissociated cortical or hippocampal neurons display characteristics of hyperexcitable networks. This increased excitability has been related to the absence of afferent input to these networks. It has been suggested that insufficient activity within neural networks leads to a very low average level of synaptic/neuronal depression (Eytan and Marom 2006; Steriade and Amzica 1999). Assuming that networks need a certain degree of synaptic depression to maintain homeostatic conditions, insufficient synaptic depression enhances recurrent excitation in strongly recurrent excitatory networks like cortex, and creates a hyperexcitable network (Fig. 4). Enhanced recurrent excitation has been described as one of the major causes of hyperexcitability (Paz and Huguenard 2015). Moreover, sustained activity deficiency induces homeostatic
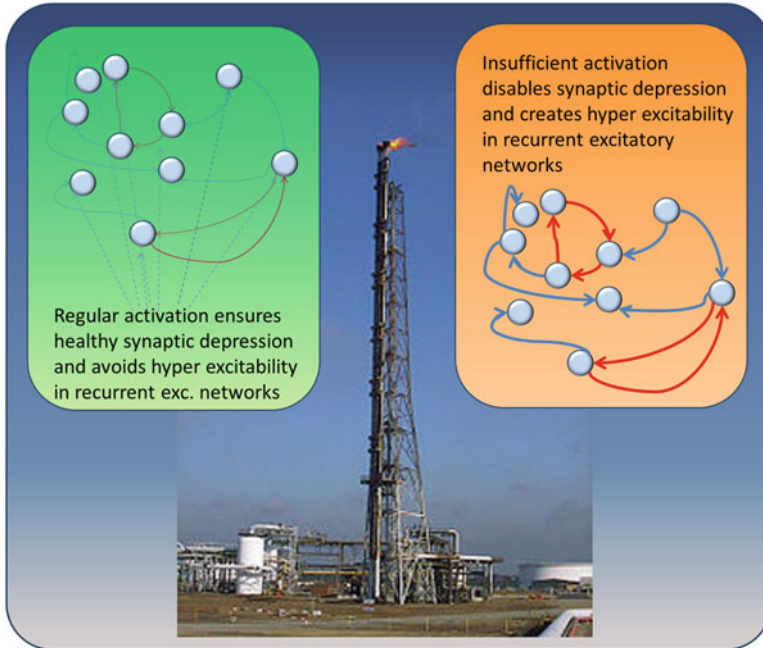
Fig. 4 The principle that regular firing may be necessary to avoid an "explosive" situation is not exclusive to neuronal networks, but also occurs in, e.g., a gas flare, used for burning off flammable gas released by plant equipment. Frequent burning off prevents the formation of dangerously explosive gas mixtures. However, a dangerously explosive gas mixture may develop during an extended period without burning off, and the same spark that was necessary for frequent burning off may trigger an explosion instead

up-regulation of excitability (Kilman et al. 2002; Turrigiano 2008; Turrigiano et al. 1998), thus reinforcing the hyperexcitability of networks.

Wagenaar et al. showed that providing input to cortical cultures by random electrical stimulation facilitated dispersed firing and impeded synchronized network bursts (Wagenaar et al. 2005). Also pharmacologically achieved mild excitation decreased network excitability (le Feber et al. 2014).

The transition to seizure-like activity in networks of dissociated neurons generally requires additional manipulation and may be achieved pharmacologically, e.g. using glutamate agonists (Kiese et al. 2017), or GABA antagonists like bicuculine (Colombi et al. 2013) or picrotoxin (Jewett et al. 2016). Also interference with the extracellular matrix formation early in development affects the establishment of balance between excitation and inhibition. A recent study suggested that decreasing expression of Hyaluronic acid (the backbone of the neural extracellular matrix) can be epileptogenic (Vedunova et al. 2013). Enzymatic removal of the ECM in mature cultures led to transient enhancement of neuronal activity, but prevented further disinhibition-induced hyperexcitability (Bikbaev et al. 2015).

Alternatively, directed genetic modifications that lead to lethal seizures in mice (i.e., mature microRNA-128 deficiency) can be reproduced in dissociated cultures and lead to significantly increased neuronal activity, burst rate, and burst duration, reflecting the increased excitability of these networks (McSweeney et al. 2016). Also cultures with mutant neuronal nicotinic acetylcholine receptors, which may cause a partial sleep-related epilepsy (autosomal dominant nocturnal frontal lobe epilepsy), were shown to become hyperexcitable and to represent an in vitro chronic model of spontaneous epileptiform activity, i.e., not requiring pre-treatment with convulsants (Gullo et al. 2014). These results support the utility of MEAs in developing in vitro models of neuroexcitability disorders, such as epilepsy.

In summary, cultures of dissociated neurons may be used to model the interictal period without any further manipulation. The transition to seizures and paroxysmal activity may be achieved by additional manipulations that affect the excitation—inhibition ratio, or genetic modifications. The development of such models facilitates the investigation of ictal onset, ictus and ictus termination, and is invaluable for pharmacological studies searching for anticonvulsant drugs. Recent advances in the differentiation of induced pluripotent stem cells provide the appealing opportunity to grow cultures that replicate patient-specific genetic deficits that may be crucial for the development of epilepsy.

4.1.3 Limitations

The link to behavioral outcome is not always clear in in vitro models. Different species may develop different "epilepsy" mechanisms and the in vitro spatiotemporal scale may differ from in vivo. It is important that in vitro models must survive long enough to observe processes of interest, which is especially true for slower biological processes, such as changes in gene expression and translation into proteins. This limits the use of acute brain slices in particular.

Seizure propagation cannot be studied as possibly relevant structures may not be included in slices. Schevon et al. (2012) showed that seizures may contain a core, showing intense hypersynchronous firing indicative of recruitment to the seizure, and adjacent territories where there is only low-level, unstructured firing (the "ictal penumbra"). Such processes, although possibly mechanistically crucial and useful, for example, for seizure prediction, may not be captured by slice models, and most likely not by dissociated neurons-based models. Cultures of dissociated neurons are relatively small, typically 1–2 mm in diameter, which does not facilitate investigation of seizure propagation.

In coupled networks, bursts were shown to propagate from one network to the other (Baruchi et al. 2008; Bisio et al. 2014). However, one of two connected cultures usually became dominant, initiating substantially more bursts than the other (Baruchi et al. 2008). This dominance was generally maintained during the entire monitored developmental frame, thus suggesting that the implementation of this hierarchy arose from early network development (Bisio et al. 2014). Dominance of one culture appeared more or less randomly, which hampered the construction

of engineered circuitry to mimic seizure propagation. Recent developments in patterned culturing based on surface micro patterning (Roth et al. 2012; Scott et al. 2012) or physical constraints (le Feber et al. 2015a; Pan et al. 2011; Renault et al. 2015) provide tools to incorporate certain circuitry in cultures of dissociated neurons, which may further facilitate the investigation of spreading seizures.

5   Memory Disorders

With aging, the risk of developing memory loss increases. Age-associated memory impairment is the mildest form, characterized by self-perception of memory loss and lower scores on a standardized memory test (Larrabee and Crook 1994). About 40% of people aged 65 or older have age-associated memory impairment, around 1% of these people develop dementia (Small 2002). In the Western world, prevalence doubles every 5 years beyond the age of 65 (Jorm and Jolley 1998), and averages 5–10% for people above that age (Hugo and Ganguli 2014). Globally, dementia affected about 46 million people in 2015 (Vos et al. 2016). About 10% of people develop the disorder at some point in their lives (Loy et al. 2014). Alzheimer's disease (AD) is the most common cause of late life dementia (Small 2002), followed by other causes like Dementia with Lewy Bodies (DLB), vascular disease, and Parkinson's Disease (PDD).

Patients diagnosed with dementia may be treated with cholinesterase inhibitors, but the benefit is generally small (Schneider et al. 2014). For milder forms of memory loss, no drug treatments is available (Small 2002). Despite tremendous efforts taken to investigate dementia, the underlying mechanisms are only partially understood, and may involve misfolded proteins, apoptosis, inflammatory responses, vascular deficiencies, mitochondrial impairment or synaptic damage, depending on the type of dementia. Whereas ischemia-induced malfunction seems a key aspect in vascular dementia, misfolding of specific proteins aggregation may be crucial in AD, DLB, or PDD. These different pathological etiologies, however, may share substantial common pathways (Raz et al. 2016).

5.1   Alzheimer's Disease

AD is characterized by the combined presence of extracellular amyloid-β (Aβ) plaques and intraneuronal neurofibrillary (tau) tangles (Bloom 2014). AD is associated with neurodegeneration, characterized by initial synaptic injury followed by neuronal loss, but the precise mechanisms leading to neurodegeneration are not completely clear (Crews and Masliah 2010). Animal models have relied on the utilization of genetic mutations associated with familial AD. The aggregation of both Aβ and tau has been faithfully reproduced in animal models, including aspects of memory impairment (Götz and Götz 2009), with cognitive deficits

appearing to occur earlier than extracellular plaques (LaFerla and Green 2012). Mechanisms, as determined from animal models, may involve impaired axonal transport, conceptually linked to oxidative stress, mitochondrial dysfunction, and widespread synaptic loss, in addition to inflammation and neuronal death (Götz and Götz 2009). A number of recent in vitro studies have investigated the interference of Aβ oligomers with synaptic function, for a review see (Crews and Masliah 2010).

5.1.1 Brain Slices

Aging organotypic brain slices have been shown to express beta-amyloid (Marksteiner and Humpel 2008). However, brain slices are usually obtained from neonatal brains, which may be inappropriate for studies on brain ageing and many age-related neuropsychiatric disorders (Jang et al. 2018). Furthermore, Aβ affects synaptic plasticity in the picomolar concentration range, and with aging the extracellular Aβ concentration decreases from the high picomolar to the low picomolar values. Some of the effects of Aβ may therefore be lost or altered after slice preparation (Waters 2010). Although the effect of Aβ exposure on synaptic functioning has been confirmed in hippocampal slice cultures (Ahuja et al. 2007), but differed between regions (Chong et al. 2011). Young age of the donor and limited duration of experiments remain restricting factors in the use of brain slice Alzheimer models.

5.1.2 Cultures of Dissociated Neurons

Aβ added to cultures of dissociated mouse hippocampal neurons on MEAs rapidly reduced their firing rate (Kuperstein et al. 2010), without significant cell death at low concentrations (Varghese et al. 2010). Reduced activity resulted from synaptic dysfunction, which could be reversed through use of curcumin, an inhibitor of Aβ oligomerization (Varghese et al. 2010). Recent work suggests that the sensitivity to detect early changes occurring after the addition of amyloid oligomers to the medium of in vitro electrophysiological recordings may be further enhanced by the use of high density electrode arrays (Amin et al. 2017). In vitro neuronal models using patient-derived stem cells are currently being developed, for a review see (Chinchalongporn et al. 2015)

5.2 Dementia with Lewy Bodies

Spherical inclusions of abnormal aggregates of (alpha-synuclein) protein in the somata (Lewy bodies) and elongated structures in the processes (Lewy neurites) are the neuropathological hallmark of Dementia with Lewy Bodies (DLB) (Goedert et al. 2013). It is not well understood whether and how these inclusions lead to cognitive impairment or dementia. Neurotoxin-based animal models are available,

as well as *disease gene-based* models (Bezard et al. 2013). Experimental results show that abnormal accumulation of α-synuclein in the hippocampus correlated with memory impairment and structural synaptic deficits (Lim et al. 2011). Power et al. (2017) showed mitochondrial and nuclear degradation in neurons with developing Lewy bodies. Lost integrity of mitochondria reduces the availability of ATP production and may thus form a link to mechanisms involved in vascular dementia. Accumulating evidence suggests that not cell death but rather α-synuclein aggregate-related synaptic dysfunction triggers DLB pathology (Calo et al. 2016; Colom-Cadena et al. 2017; Kramer and Schulz-Schaeffer 2007; Schulz-Schaeffer 2010; Sommer et al. 2000). More recently proposed models involve differentiation from human-induced pluripotent stem cells. Thus far, focus has mainly been on the differentiation of relevant cell types and the appearance of protein clusters, and not yet on the mechanisms of disease initiation and progression (Livesey 2014).

While animal models have been able to reproduce the most important clinical observations of misfolded proteins in combination with memory deficits, detailed insights into the mechanisms linking protein aggregation to memory loss remain hard to acquire, partly related to limitations in experimental control and accessibility of individual neurons and synapses. In vitro models have been developed to obtain detailed mechanistic insights.

5.2.1 Brain Slices

Excessive alpha synuclein was shown to affect cell morphology and synaptic plasticity. Viral overexpression of alpha-synuclein triggered the formation of distorted neurites, intraneuritic swellings, and granular perikaryal deposits in organotypic midbrain slice cultures (Zach et al. 2007). Hippocampal slices exposed to alpha-synuclein oligomers showed enhanced excitatory synaptic transmission within a few hours, driven by a receptor-mediated mechanism (Ferreira et al. 2017), which prevented further potentiation by physiological stimuli. (Diogenes et al. 2012). Fibrils or monomer did not disrupt long-term potentiation (Froula et al. 2018). The relatively short lifespan of these preparations impeded the investigation of changes on longer time scales.

5.2.2 Cultures of Dissociated Neurons

Volpicelli-Daley et al. (2011) showed that preformed alpha-synuclein fibrils added to the medium bath, enter primary neurons, leading to the formation of Lewy body-like inclusions, selective decreases in synaptic proteins, progressive impairments in neuronal excitability and connectivity, and, eventually, neuron death. Extracellular added monomers with or without low concentration fibril seeds, or rotenone also triggered the formation of intracellular alpha-synuclein inclusion bodies, with induction-dependent differences in morphology, location, and function (toxicity) (Raiss et al. 2016). Alpha-synuclein fibrils or oligomers added to the medium bath

of dissociated cortical cultures significantly reduced the mean firing rate and synchronicity (Peelaerts et al. 2015). Recent evidence shows that high concentrations of extracellularly added alpha-synuclein monomers may interfere with synaptic function, significantly preceding the formation of intracellular inclusion bodies, suggesting that these inclusions, although characterized as a pathological hallmark, may not be key in the pathology (Hassink et al. 2018). Rather, impeded activity may be an essential step as neuronal survival depends on regular calcium influx, which is promoted by electrical activity (Ghosh et al. 1994; Mao et al. 1999). This view is supported by the finding that alpha-synuclein was found mainly in excitatory neurons and synapses (Taguchi et al. 2014).

5.3 Memory In Vitro

Whereas animal models have been developed that provide quantification of memory performance in relation to pathologic protein clustering, this has been problematic in in vitro models. Recent progress, however, enables the evaluation of a kind of memory in networks of dissociated cortical neurons (le Feber et al. 2015b). The basic idea is that activity patterns are determined by connectivity and that connectivity, in turn, is affected by certain activity patterns through plasticity mechanisms like spike timing-dependent plasticity. The finding that input-deprived networks develop quasi stable activity patterns (Stegenga et al. 2008; van Pelt et al. 2004) and connectivity (le Feber et al. 2007) suggests that activity and connectivity are in equilibrium in these networks (le Feber et al. 2010). External input, in the form of electrical stimulation through one of the electrodes, may induce a new pattern, trigger connectivity changes, and drive the network out of the activity $\Longleftrightarrow$ connectivity equilibrium. Responses to electrical stimulation have been shown to rapidly activate "major burst leader" neurons (Eckmann et al. 2008) and to share great similarity beyond activation of a major leader neuron (Pasquale et al. 2017), suggesting that the driving forces behind connectivity changes occur in particular before activation of the major leader. Connectivity continues to change until a new balance between activity and connectivity has been established. The new equilibrium includes the response to the stimulus (le Feber et al. 2015b), and consequently, repeated application of this input induces no further connectivity changes. Thus, inability of a stimulus to alter network connectivity suggests that the network already memorized that stimulus. Stimulation at a different electrode was shown to still induce connectivity changes upon first application, but not when repeated multiple times. Switching back to the first electrode, electrical stimulation did not induce connectivity changes, indicating that the memory trace persisted (illustrated in Fig. 5). This work shows that (random) cortical networks are able to form memory traces of experienced inputs and shows that there is no direct relationship between the input and the memory trace. Rather, the formed memory trace depends on the input and the connectivity at the time of receiving the input. Memory retrieval might occur through stimuli that trigger the replay of the whole
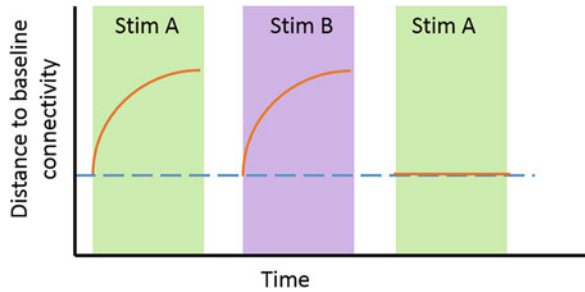
Fig. 5 Illustration of connectivity changes in random cortical networks upon stimulation (solid red lines), compared to unstimulated (dashed blue line), based on experimental data and modeling in (le Feber et al. 2015b). Vertical scale indicates connectivity differences with respect to connectivity before the first stimulus of that specific type (A or B). Without stimulation, connectivity fluctuates and the distance to the initial connectivity is not zero, but it does not increase. Stimulation through electrode A initially induces large connectivity changes, which rapidly decrease when the stimulation is repeated. Repeated stimulation at another electrode (B) yields a very similar pattern of connectivity changes. Return to stimulus A induces no connectivity changes that exceed random fluctuations. Green background indicates repeated stimulation at electrode A, purple: electrode B

trace. Recent work by Pasquale et al. (2017) showed strong similarity between spontaneous and induced activity patterns, but activity patterns evoked by the same stimulus were more similar to each other than to patterns evoked by other stimuli or spontaneous patterns.

In sum, cultures of dissociated neurons provide a platform that enables the induction of protein aggregates, evaluation of synaptic functioning and cell viability during and after the formation of aggregates, and associated memory performance. Thus, cultured neuronal networks seem very well suited to study the mechanisms underlying memory disorders, as well as possible therapeutic treatment.

6   Conclusions

Several models of brain disorders have been described in this section, which are exemplary to illustrate the power of MEA-based models of brain disorders. Depending on the research question, the cellular composition (fraction of inhibitory/excitatory neurons; ratio astrocytes: neurons, etc.) may be crucial, but this is not yet fully controlled in primary neuronal cultures. Recent techniques using forced differentiation of induced stem cells may help to solve this problem (Zhang et al. 2013). This provides a very strong platform for the development of new models of brain disorders, particularly in combination with newly developed tools to engineer-specific structures.

All presented models have their merits, but also drawbacks that should be solved to facilitate wider use. For example, it is not clear how hypoxia in cultures translates to in vivo oxygen levels, as physiological oxygen concentrations are

much lower than those commonly used to culture cells. Culturing cells under physiological oxygen pressure from the day of plating has been shown feasible and may solve future problems in the interpretation of normoxia and hypoxia. Also the interpretation of spontaneously occurring network bursts remains debated. They may reflect hyperexcitability of input-deprived networks, but may also play a role in information processing (Kepecs and Lisman 2003; Singer 1993), or to increase the reliability of communication between neurons and to avoid synaptic transmission failure (Chen et al. 2009). A crucial step, that still remains unclear in MEA-based memory disorder models, is memory retrieval. Discovery of this mechanism would not only be a major breakthrough in memory research, but would certainly facilitate widespread use of MEA-based models for memory disorders.

Whereas brain slices should be used when the in vivo connectivity is crucial, models based on cultures of dissociated neurons are well suited to investigate general functioning of neurons and synapses under pathological conditions. A major advantage of this approach is the longer lifespan, which allows for the investigation of processes that occur at time scales of days or weeks. Important new insights provided by MEA-based models include the finding that synaptic failure, and consequently neuronal silence, often precedes neuronal death under hypoxic conditions, or after exposure to excessive alpha-synuclein or beta-amyloid. This has brought forward that insufficient activity may be an important step in the evolution towards cell death. Regular activity appeared also crucial to maintain network excitability within boundaries. These are important new insights that could be obtained using the advantages of dissociated cultures, that emphasize the importance of activity homeostasis, and may open up new possibilities for treatment.

References

Ahuja, T. K., Mielke, J. G., Comas, T., Chakravarthy, B., & Mealing, G. A. R. (2007). Hippocampal slice cultures integrated with multi-electrode arrays: A model for study of long-term drug effects on synaptic activity. *Drug Development Research, 68*, 84–93.

Alotaiby, T. N., Alshebeili, S. A., Alshawi, T., Ahmad, I., & Abd El-Samie, F. E. (2014). EEG seizure detection and prediction algorithms: A survey. *EURASIP Journal on Advances in Signal Processing, 2014*, 183.

Amin, H., Nieus, T., Lonardoni, D., Maccione, A., & Berdondini, L. (2017). High-resolution bio-electrical imaging of Abeta-induced network dysfunction on CMOS-MEAs for neurotoxicity and rescue studies. *Scientific Reports, 7*, 2460.

Antonio, L. L., Anderson, M. L., Angamo, E. A., Gabriel, S., Klaft, Z. J., Liotta, A., et al. (2016). In vitro seizure like events and changes in ionic concentration. *Journal of Neuroscience Methods, 260*, 33–44.

Armand, V., Gabriel, S., Hoffmann, P., Heinemann, U., & Vergnes, M. (1998). Epileptiform activity and changes in field potential responses induced by low [Mg2+]0 in a genetic rat model of absence epilepsy. *Brain Research, 803*, 19–26.

Arrich, J., Holzer, M., Herkner, H., & Mullner, M. (2010). Cochrane corner: Hypothermia for neuroprotection in adults after cardiopulmonary resuscitation. *Anesthesia and Analgesia, 110*, 1239.

Ashford, J. W. (2008). Screening for memory disorders, dementia and Alzheimer's disease. *Aging Health, 4*, 399–432.

Avoli, M. (2001). Do interictal discharges promote or control seizures? Experimental evidence from an in vitro model of epileptiform discharge. *Epilepsia, 42*(Suppl 3), 2–4.

Azevedo, F. A. C., Ludmila, R. B., Carvalho, L. T., Gribergb, J. M., Farfel, R. E. L., Ferretti, R. E. P., et al. (2009). Equal numbers of neuronal and nonneuronal cells make the human brain an isometrically scaled-up primate brain. *The Journal of Comparative Neurology, 513*, 532–541.

Badawy, R. A. B., Loetscher, T., Macdonell, R. A. L., & Brodtmann, A. (2012). Cortical excitability and neurology: Insights into the pathophysiology. *Functional Neurology, 27*, 131–145.

Baruchi, I., Volman, V., Raichman, N., Shein, M., & Ben-Jacob, E. (2008). The emergence and properties of mutual synchronization in in vitro coupled cortical networks. *The European Journal of Neuroscience, 28*, 1825–1835.

Ben-Ari, Y. (2002). Excitatory actions of gaba during development: The nature of the nurture. *Nature Reviews Neuroscience, 3*, 728.

Berdowski, J., Berg, R. A., Tijssen, J. G. P., & Koster, R. W. (2010). Global incidences of out-of-hospital cardiac arrest and survival rates: Systematic review of 67 prospective studies. *Resuscitation, 81*, 1479–1487.

Berg, A. T., & Millichap, J. J. (2013). The 2010 revised classification of seizures and epilepsy. *Continuum: Lifelong Learning in Neurology, 19*, 571–597.

Bernard, S. A., Gray, T. W., Buist, M. D., Jones, B. M., Silvester, W., Gutteridge, G., et al. (2002). Treatment of comatose survivors of out-of-hospital cardiac arrest with induced hypothermia. *The New England Journal of Medicine, 346*, 557–563.

Bezard, E., Yue, Z., Kirik, D., & Spillantini, M. G. (2013). Animal models of Parkinson's disease: Limits and relevance to neuroprotection studies. *Movement Disorders, 28*, 61–70.

Bhalla, D., Godet, B., Druet-Cabanac, M., & Preux, P. M. (2011). Etiologies of epilepsy: A comprehensive review. *Expert Review of Neurotherapeutics, 11*, 861–876.

Bikbaev, A., Frischknecht, R., & Heine, M. (2015). Brain extracellular matrix retains connectivity in neuronal networks. *Scientific Reports, 5*, 14527.

Bisio, M., Bosca, A., Pasquale, V., Berdondini, L., & Chiappalone, M. (2014). Emergence of bursting activity in connected neuronal sub-populations. *PLoS One, 9*, e107400.

Bloom, G. S. (2014). Amyloid-beta and tau: The trigger and bullet in Alzheimer disease pathogenesis. *JAMA Neurology, 71*, 505–508.

Bolay, H., Gürsoy-Özdemir, Y., Sara, Y., Onur, R., Can, A., & Dalkara, T. (2002). Persistent defect in transmitter release and synapsin phosphorylation in cerebral cortex after transient moderate ischemic injury. *Stroke, 33*, 1369–1375.

Buskila, Y., Breen, P. P., Tapson, J., van Schaik, A., Barton, M., & Morley, J. W. (2014). Extending the viability of acute brain slices. *Scientific Reports, 4*, 5309.

Buzsaki, G., Anastassiou, C. A., & Koch, C. (2012). The origin of extracellular fields and currents–EEG, ECoG, LFP and spikes. *Nature Reviews Neuroscience, 13*, 407–420.

Calo, L., Wegrzynowicz, M., Santivanez-Perez, J., & Grazia Spillantini, M. (2016). Synaptic failure and alpha-synuclein. *Movement Disorders, 31*, 169–177.

Chen, L., Deng, Y., Luo, W., Wang, Z., & Zeng, S. (2009). Detection of bursts in neuronal spike trains by the mean inter-spike interval method. *Progress in Natural Science, 19*, 229–235.

Chiappalone, M., Vato, A., & Berdondini, L. (2007). Koudelka-hep, and Martinoia S. Network dynamics and synchronous activity in cultured cortical neurons. *International Journal of Neural Systems, 17*, 87–103.

Chinchalongporn, V., Koppensteiner, P., Prè, D., Thangnipon, W., Bilo, L., & Arancio, O. (2015). Connectivity and circuitry in a dish versus in a brain. *Alzheimer's Research & Therapy, 7*, 44.

Chong, S. A., Benilova, I., Shaban, H., De Strooper, B., Devijver, H., Moechars, D., et al. (2011). Synaptic dysfunction in hippocampus of transgenic mouse models of Alzheimer's disease: A multi-electrode array study. *Neurobiology of Disease, 44*, 284–291.

Colombi, I., Mahajani, S., Frega, M., Gasparini, L., & Chiappalone, M. (2013). Effects of antiepileptic drugs on hippocampal neurons coupled to micro-electrode arrays. *Frontiers in Neuroengineering, 6*, 10.

Colom-Cadena, M., Pegueroles, J., Herrmann, A. G., Henstridge, C. M., Munoz, L., Querol-Vilaseca, M., et al. (2017). Synaptic phosphorylated alpha-synuclein in dementia with Lewy bodies. *Brain, 140*, 3204–3214.

Crews, L., & Masliah, E. (2010). Molecular mechanisms of neurodegeneration in Alzheimer's disease. *Human Molecular Genetics, 19*, R12–R20.

D'Agostino, D. P., Putnam, R. W., & Dean, J. B. (2007). Superoxide (*O2-) production in CA1 neurons of rat hippocampal slices exposed to graded levels of oxygen. *Journal of Neurophysiology, 98*, 1030–1041.

de Lange, E. C. M., van den Brink, W., Yamamoto, Y., de Witte, W. E. A., & Wong, Y. C. (2017). Novel CNS drug discovery and development approach: Model-based integration to predict neuro-pharmacokinetics and pharmacodynamics. *Expert Opinion on Drug Discovery, 12*, 1207–1218.

Dietzel, I., & Heinemann, U. (1986). Dynamic variations of the brain cell microenvironment in relation to neuronal hyperactivity. *Annals of the New York Academy of Sciences, 481*, 72–86.

Diogenes, M. J., Dias, R. B., Rombo, D. M., Vicente Miranda, H., Maiolino, F., Guerreiro, P., et al. (2012). Extracellular alpha-synuclein oligomers modulate synaptic transmission and impair LTP via NMDA-receptor activation. *The Journal of Neuroscience, 32*, 11750–11762.

Dreier, J. P., & Heinemann, U. (1991). Regional and time dependent variations of low Mg2+ induced epileptiform activity in rat temporal cortex slices. *Experimental Brain Research, 87*, 581–596.

Eckmann, J. P., Jacobi, S., Marom, S., Moses, E., & Zbinden, C. (2008). Leader neurons in population bursts of 2d living neural networks. *New Journal of Physics, 10*, 015011.

Emre, M., Aarsland, D., Brown, R., Burn, D. J., Duyckaerts, C., Mizuno, Y., et al. (2007). Clinical diagnostic criteria for dementia associated with Parkinson's disease. *Movement Disorders, 22*, 1689–1707; quiz 1837.

Engel, J. J., & Schwartzkroin, P. A. (2006). What should be modeled? In A. Pitkänen, P. A. Schwartzkroin, & S. L. Moshé (Eds.), *Models of seizures and epilepsy* (pp. 1–14). New York: Elsevier.

England, M. J., Liverman, C. T., Schultz, A. M., & Strawbridge, L. M. (2012). Summary: A reprint from epilepsy across the spectrum: Promoting health and understanding. *Epilepsy Currents, 12*, 245–253.

Eytan, D., & Marom, S. (2006). Dynamics and effective topology underlying synchronization in networks of cortical neurons. *The Journal of Neuroscience, 26*, 8465–8476.

Fedorovich, S., Hofmeijer, J., van Putten, M. J. A. M., & le Feber, J. (2017). Reduced synaptic vesicle recycling during hypoxia in cultured cortical neurons. *Frontiers in Cellular Neuroscience, 11*, 32.

Ferreira, D. G., Temido-Ferreira, M., Vicente Miranda, H., Batalha, V. L., Coelho, J. E., Szego, E. M., et al. (2017). Alpha-synuclein interacts with PrP(C) to induce cognitive impairment through mGluR5 and NMDAR2B. *Nature Neuroscience, 20*, 1569–1579.

Fisher, R. S., & Engel Jr., J. J. (2010). Definition of the postictal state: When does it start and end? *Epilepsy & Behavior: E&B, 19*, 100–104.

Fisher, R. S., Cross, J. H., D'Souza, C., French, J. A., Haut, S. R., Higurashi, N., et al. (2017). Instruction manual for the ILAE 2017 operational classification of seizure types. *Epilepsia, 58*, 531–542.

Florence, S. L., Taub, H. B., & Kaas, J. H. (1998). Large-scale sprouting of cortical connections after peripheral injury in adult macaque monkeys. *Science, 282*, 1117–1121.

Frantseva, M. V., Velazquez, J. L., Hwang, P. A., & Carlen, P. L. (2000). Free radical production correlates with cell death in an in vitro model of epilepsy. *The European Journal of Neuroscience, 12*, 1431–1439.

Froula, J. M., Henderson, B. W., Gonzalez, J. C., Vaden, J. H., McLean, J. W., Wu, Y., et al. (2018). α-Synuclein fibril-induced paradoxical structural and functional defects in hippocampal neurons. *Acta Neuropathologica Communications, 6*, 35.

Fujiwara, N., Higashi, H., Shimoji, K., & Yoshimura, M. (1987). Effects of hypoxia on rat hippocampal neurones in vitro. *The Journal of Physiology, 384*, 131–151.

Furshpan, E. J., & Potter, D. D. (1989). Seizure-like activity and cellular damage in rat hippocampal neurons in cell culture. *Neuron, 3*, 199–207.

Ghosh, A., Carnahan, J., & Greenberg, M. (1994). Requirement for BDNF in activity-dependent survival of cortical neurons. *Science, 263*, 1618–1623.

Goedert, M., Spillantini, M. G., Del Tredici, K., & Braak, H. (2013). 100 years of Lewy pathology. *Nature Reviews Neurology, 9*, 13–24.

Götz, J., & Götz, N. N. (2009). Animal models for Alzheimer's disease and frontotemporal dementia: A perspective. *ASN Neuro, 1*, e00019.

Goyal, M., Menon, B. K., van Zwam, W. H., Dippel, D. W. J., Mitchell, P. J., Demchuk, A. M., et al. (2016). Endovascular thrombectomy after large-vessel ischaemic stroke: A meta-analysis of individual patient data from five randomised trials. *The Lancet, 387*, 1723–1731.

Grond, M., Stenzel, C., Schmülling, S., Rudolf, J., Neveling, M., Lechleuthner, A., et al. (1998). Early intravenous thrombolysis for acute ischemic stroke in a community-based approach. *Stroke, 29*, 1544–1549.

Grote, J., Laue, O., Eiring, P., & Wehler, M. (1996). Evaluation of brain tissue O2 supply based on results of PO2 measurements with needle and surface microelectrodes. *Journal of the Autonomic Nervous System, 57*, 168–172.

Gullo, F., Manfredi, I., Lecchi, M., Casari, G., Wanke, E., & Becchetti, A. (2014). Multi-electrode array study of neuronal cultures expressing nicotinic beta2-V287L subunits, linked to autosomal dominant nocturnal frontal lobe epilepsy. An in vitro model of spontaneous epilepsy. *Frontiers in Neural Circuits, 8*, 87.

Harrison, P. K., Sheridan, R. D., Green, A. C., Scott, I. R., & Tattersall, J. E. H. (2004). A guinea pig hippocampal slice model of organophosphate-induced seizure activity. *Journal of Pharmacology and Experimental Therapeutics, 310*, 678.

Hassink, G. C., Raiss, C. C., Segers-Nolten, I. M. J., van Wezel, R. J. A., Subramaniam, V., le Feber, J., et al. (2018). Exogenous α-synuclein hinders synaptic communication in cultured cortical primary rat neurons. *PLoS One, 13*, e0193763.

Hofmeijer, J., & van Putten, M. J. A. M. (2012). Ischemic cerebral damage. *Stroke, 43*, 607–615.

Hofmeijer, J., Mulder, A. T. B., Farinha, A. C., van Putten, M. J. A. M., & le Feber, J. (2014). Mild hypoxia affects synaptic connectivity incultured neuronal networks. *Brain Research, 1557*, 180–189.

Hofmeijer, J., Beernink, T. M. J., Bosch, F. H., Beishuizen, A., Tjepkema-Cloostermans, M. C., & van Putten, M. J. A. M. (2015). Early EEG contributes to multimodal outcome prediction of postanoxic coma. *Neurology, 85*, 137–143.

Holmes, G. L., & Ben-Ari, Y. (2001). The neurobiology and consequences of epilepsy in the developing brain. *Pediatric Research, 49*, 320–325.

Hongo, Y., Takasu, K., Ikegaya, Y., Hasegawa, M., Sakaguchi, G., & Ogawa, K. (2015). Heterogeneous effects of antiepileptic drugs in an in vitro epilepsy model – A functional multineuron calcium imaging study. *European Journal of Neuroscience, 42*, 1818–1829.

Hughes, J. R. (2009). Absence seizures: A review of recent reports with new concepts. *Epilepsy & Behavior: E&B, 15*, 404–412.

Hugo, J., & Ganguli, M. (2014). Dementia and cognitive impairment: Epidemiology, diagnosis, and treatment. *Clinics in Geriatric Medicine, 30*, 421–442.

Humpel, C. (2015). Organotypic brain slice cultures: A review. *Neuroscience, 305*, 86–98.

Hutter-Schmid, B., Kniewallner, K., & Humpel, C. (2015). Organotypic brain slice cultures as a model to study angiogenesis of brain vessels. *Frontiers in Cell and Developmental Biology, 3*, 52.

Hypothermia after Cardiac Arrest Study Group. (2002). Mild therapeutic hypothermia to improve the neurologic outcome after cardiac arrest. *The New England Journal of Medicine, 346*, 549–556.

Jang, S., Kim, H., Kim, H. J., Lee, S. K., Kim, E. W., Namkoong, K., et al. (2018). Long-term culture of organotypic hippocampal slice from old 3xTg-AD mouse: An ex vivo model of Alzheimer's disease. *Psychiatry Investigation, 15*, 205–213.

Jensen, F. E. (2011). Epilepsy as a spectrum disorder: Implications from novel clinical and basic neuroscience. *Epilepsia, 52*, 1–6.

Jewett, K. A., Christian, C. A., Bacos, J. T., Lee, K. Y., Zhu, J., & Tsai, N.-P. (2016). Feedback modulation of neural network synchrony and seizure susceptibility by Mdm2-p53-Nedd4-2 signaling. *Molecular Brain, 9*, 32.

Jorm, A. F., & Jolley, D. (1998). The incidence of dementia: A meta-analysis. *Neurology, 51*, 728–733.

Kadam, S. D., White, A. M., Staley, K. J., & Dudek, F. E. (2010). Continuous electroencephalographic monitoring with radio-telemetry in a rat model of perinatal hypoxia-ischemia reveals progressive post-stroke epilepsy. *The Journal of Neuroscience, 30*, 404–415.

Kaye, P. (2005). Early prediction of individual outcome following cardiopulmonary resuscitation: Systematic review. *Emergency Medicine Journal: EMJ, 22*, 700–705.

Kepecs, A., & Lisman, J. (2003). Information encoding and computation with spikes and bursts. *Network (Bristol, England), 14*, 103–118.

Khazipov, R., Bregestovski, P., & Ben-Ari, Y. (1993). Hippocampal inhibitory interneurons are functionally disconnected from excitatory inputs by anoxia. *Journal of Neurophysiology, 70*, 2251–2259.

Khazipov, R., Congar, P., & Ben-Ari, Y. (1995). Hippocampal CA1 lacunosum-moleculare interneurons: Comparison of effects of annoxia on excitatory and inhibitory postsynaptic currents. *Journal of Neurophysiology, 74*, 2138–2149.

Kiese, K., Jablonski, J., Hackenbracht, J., Wrosch, J. K., Groemer, T. W., Kornhuber, J., et al. (2017). Epigenetic control of epilepsy target genes contributes to a cellular memory of epileptogenesis in cultured rat hippocampal neurons. *Acta Neuropathologica Communications, 5*, 79.

Kilman, V., van Rossum, M., & Turrigiano, G. (2002). Activity deprivation reduces miniature IPSC amplitude by decreasing the number of postsynaptic GABAa receptors clusterd at neocortical synapses. *The Journal of Neuroscience, 22*, 1328–1337.

Kopelman, M. D. (2002). Disorders of memory. *Brain, 125*, 2152–2190.

Kramer, M. L., & Schulz-Schaeffer, W. J. (2007). Presynaptic α-synuclein aggregates, not lewy bodies, cause neurodegeneration in dementia with lewy bodies. *The Journal of Neuroscience, 27*, 1405–1410.

Krnjević, K., Xu, Y. Z., & Zhang, L. (1991). Anoxic block of GABAergic IPSPs. *Neurochemical Research, 16*, 279–284.

Kuperstein, I., Broersen, K., Benilova, I., Rozenski, J., Jonckheere, W., Debulpaep, M., et al. (2010). Neurotoxicity of Alzheimer's disease Aβ peptides is induced by small changes in the Aβ(42) to Aβ(40) ratio. *The EMBO Journal, 29*, 3408–3420.

LaFerla, F. M., & Green, K. N. (2012). Animal models of Alzheimer disease. *Cold Spring Harbor Perspectives in Medicine, 2*, a006320.

Lapitskaya, N., Gosseries, O., De Pasqua, V., Pedersen, A. R., Nielsen, J. F., de Noordhout, A. M., et al. (2013). Abnormal corticospinal excitability in patients with disorders of consciousness. *Brain Stimulation, 6*, 590–597.

Larrabee, G. J., & Crook 3rd, T. H. (1994). Estimated prevalence of age-associated memory impairment derived from standardized tests of memory function. *International Psychogeriatrics, 6*, 95–104.

le Feber, J., Rutten, W. L. C., Stegenga, J., Wolters, P. S., Ramakers, G. J., & Van Pelt, J. (2007). Conditional firing probabilities in cultured neuronal networks: A stable underlying structure in widely varying spontaneous activity patterns. *Journal of Neural Engineering, 4*, 54–67.

le Feber, J., Stegenga, J., & Rutten, W. L. C. (2010). The effect of slow electrical stimuli to achieve learning in cultured networks of rat cortical neurons. *PLoS One, 5*, e8871.

le Feber, J., Stoyanova, I. I., & Chiappalone, M. (2014). Connectivity, excitability and activity patterns in neuronal networks. *Physical Biology, 11*, 036005.

le Feber, J., Postma, W., de Weerd, E., Weusthof, M., & Rutten, W. L. C. (2015a). Barbed channels enhance unidirectional connectivity between neuronal networks cultured on multi electrode arrays. *Frontiers in Neuroscience, 9*, 412.

le Feber, J., Witteveen, T., van Veenendaal, T. M., & Dijkstra, J. (2015b). Repeated stimulation of cultured networks of rat cortical neurons induces parallel memory traces. *Learning & Memory, 22*, 594–603.

le Feber, J., Tzafi Pavlidou, S., Erkamp, N., van Putten, M. J. A. M., & Hofmeijer, J. (2016). Progression of neuronal damage in an in vitro model of the ischemic penumbra. *PLoS One, 11*, e0147231.

le Feber, J., Erkamp, N., Van Putten, M. J. A. M., & Hofmeijer, J. (2017). Loss and recovery of functional connectivity in cultured cortical networks exposed to hypoxia. *Journal of Neurophysiology, 118*, 394–403.

le Feber, J., Dummer, A., Hassink, G. C., van Putten, M. J. A. M., & Hofmeijer, J. (2018). Evolution of excitation-inhibition ratio in cortical cultures exposed to hypoxia. *Frontiers in Cellular Neuroscience, 12*, 183.

Levesque, M., Salami, P., Shiri, Z., & Avoli, M. (2017). Interictal oscillations and focal epileptic disorders. *The European Journal of Neuroscience, 48*, 2915–2927.

Librizzi, L., Losi, G., Marcon, I., Sessolo, M., Scalmani, P., Carmignoto, G., et al. (2017). Interneuronal network activity at the onset of seizure-like events in entorhinal cortex slices. *The Journal of Neuroscience, 37*, 10398–10407.

Liepert, J., Storch, P., Fritsch, A., & Weiller, C. (2000). Motor cortex disinhibition in acute stroke. *Clinical Neurophysiology, 111*, 671–676.

Lim, Y., Kehm, V. M., Lee, E. B., Soper, J. H., Li, C., Trojanowski, J. Q., et al. (2011). α-Syn suppression reverses synaptic and memory defects in a mouse model of dementia with lewy bodies. *The Journal of Neuroscience: The Official Journal of the Society for Neuroscience, 31*, 10076–10087.

Lipton, P., & Whittingham, T. S. (1982). Reduced ATP concentration as a basis for synaptic transmission failure during hypoxia in the in vitro guinea-pig hippocampus. *The Journal of Physiology, 325*, 51–65.

Lipton, P., & Whittingham, T. S. (1984). Energy metabolism and brain slice function. In R. Dingledine (Ed.), *Brain slices*. Boston: Springer.

Livesey, F. J. (2014). Human stem cell models of dementia. *Human Molecular Genetics, 23*, R35–R39.

Lopes da Silva FH, and Gorter JA EPILEPTOGENESIS | Epileptogenesis and plasticity A2 - Schwartzkroin, Philip A. In: Encyclopedia of basic epilepsy research. Oxford: Academic, 2009, p. 221–227.

Losi, G., Marcon, I., Mariotti, L., Sessolo, M., Chiavegato, A., & Carmignoto, G. (2016). A brain slice experimental model to study the generation and the propagation of focally-induced epileptiform activity. *Journal of Neuroscience Methods, 260*, 125–131.

Loy, C. T., Schofield, P. R., Turner, A. M., & Kwok, J. B. (2014). Genetics of dementia. *Lancet (London, England), 383*, 828–840.

Luhmann, H. J., Kral, T., & Heinemann, U. (1993). Influence of hypoxia on excitation and GABAergic inhibition in mature and developing rat neocortex. *Experimental Brain Research, 97*, 209–224.

Lux, H. D., Heinemann, U., & Dietzel, I. (1986). Ionic changes and alterations in the size of the extracellular space during epileptic activity. *Advances in Neurology, 44*, 619–639.

Mackay, J., & Mensah, G. (2004). *The atlas of heart disease and stroke* (p. 112). Geneva: WHO.

Madl, C., & Holzer, M. (2004). Brain function after resuscitation from cardiac arrest. *Current Opinion in Critical Care, 10*, 213–217.

Magistretti, P. J., & Pellerin, L. (1999). Astrocytes couple synaptic activity to glucose utilization in the brain. *News in Physiological Sciences: An International Journal of Physiology Produced Jointly by the International Union of Physiological Sciences and the American Physiological Society, 14*, 177–182.

Manganotti, P., Patuzzo, S., Cortese, F., Palermo, A., Smania, N., & Fiaschi, A. (2002). Motor disinhibition in affected and unaffected hemisphere in the early period of recovery after stroke. *Clinical Neurophysiology, 113*, 936–943.

Mao, Z., Bonni, A., Xia, F., Nadal-Vicens, M., & Greenberg, M. E. (1999). Neuronal activity-dependent cell survival mediated by transcription factor MEF2. *Science, 286*, 785–790.

Marksteiner, J., & Humpel, C. (2008). Beta-amyloid expression, release and extracellular deposition in aged rat brain slices. *Molecular Psychiatry, 13*, 939–952.

Marom, S., & Shahaf, G. (2002). Development, learning and memory in large random networks of cortical neurons: Lessons beyond anatomy. *Quarterly Reviews of Biophysics, 35*, 63–87.

Martín, E. D., Fernández, M., Perea, G., Pascual, O., Haydon, P. G., Araque, A., et al. (2007). Adenosine released by astrocytes contributes to hypoxia-induced modulation of synaptic transmission. *Glia, 55*, 36–45.

McKeith, I. G., Dickson, D. W., Lowe, J., Emre, M., O'Brien, J. T., Feldman, H., et al. (2005). Diagnosis and management of dementia with Lewy bodies: Third report of the DLB Consortium. *Neurology, 65*, 1863–1872.

McSweeney, K. M., Gussow, A. B., Bradrick, S. S., Dugger, S. A., Gelfman, S., Wang, Q., et al. (2016). Inhibition of microRNA 128 promotes excitability of cultured cortical neuronal networks. *Genome Research, 26*, 1411–1416.

Moragas Garrido, M., & Gascón Bayarri, J. (2012). Chapter 7: Hypoxic encephalopathy. In R. Tanasescu (Ed.), *Miscellanea on encephalopathies – A second look*. London: InTech.

Motamedi, G. K., Salazar, P., Smith, E. L., Lesser, R. P., Webber, W. R. S., Ortinski, P. I., et al. (2006). Termination of epileptiform activity by cooling in rat hippocampal slice epilepsy models. *Epilepsy Research, 70*, 200–210.

Nair, P. K., Buerk, D. G., & Halsey, J. H. J. (1987). Comparisons of oxygen metabolism and tissue pO_2 in cortex and hippocampus of gerbil brain. *Stroke, 18*, 616–622.

Nielsen, N., Wetterslev, J., Cronberg, T., Erlinge, D., Gasche, Y., Hassager, C., et al. (2013). Targeted temperature management at 33 degrees C versus 36 degrees C after cardiac arrest. *The New England Journal of Medicine, 369*, 2197–2206.

Oh, S. H., Park, K. N., Shon, Y. M., Kim, Y. M., Kim, H. J., Youn, C. S., et al. (2015). Continuous amplitude-integrated electroencephalographic monitoring is a useful prognostic tool for hypothermia-treated cardiac arrest patients. *Circulation, 132*, 1094–1103.

Pacico, N., & Mingorance-Le Meur, A. (2014). New in vitro phenotypic assay for epilepsy: Fluorescent measurement of synchronized neuronal calcium oscillations. *PLoS One, 9*, e84755.

Pal, S., Sun, D., Limbrick, D., Rafiq, A., & DeLorenzo, R. J. (2001). Epileptogenesis induces long-term alterations in intracellular calcium release and sequestration mechanisms in the hippocampal neuronal culture model of epilepsy. *Cell Calcium, 30*, 285–296.

Palmieri, M. G., Iani, C., Scalise, A., Desiato, M. T., Loberti, M., Telera, S., et al. (1999). The effect of benzodiazepines and flumazenil on motor cortical excitability in the human brain. *Brain Research, 815*, 192–199.

Pan, L., Alagapan, S. F., Franca, E., Brewer, G. J., & Wheeler, B. C. (2011). Propagation of action potential activity in a predefined microtunnel neural network. *Journal of Neural Engineering, 8*, 1–12.

Pasquale, V., Massobrio, P., Bologna, L. L., Chiappalone, M., & Martinoia, S. (2008). Self-organization and neuronal avalanches in networks of dissociated cortical neurons. *Neuroscience, 153*, 1354–1369.

Pasquale, V., Martinoia, S., & Chiappalone, M. (2017). Stimulation triggers endogenous activity patterns in cultured cortical networks. *Scientific Reports, 7*, 9080.

Patel, P. M. (2008). Chapter 6 - Cerebral ischemia. In A. K. Gupta & A. W. Gelb (Eds.), *Essentials of neuroanesthesia and neurointensive care* (pp. 36–42). Philadelphia: W.B. Saunders.

Paz, J. T., & Huguenard, J. R. (2015). Microcircuits and their interactions in epilepsy: Is the focus out of focus? *Nature Neuroscience, 18*, 351–359.

Paz, J. T., Davidson, T. J., Frechette, E. S., Delord, B., Parada, I., Peng, K., et al. (2013). Closed-loop optogenetic control of thalamus as a tool for interrupting seizures after cortical injury. *Nature Neuroscience, 16*, 64–70.

Peelaerts, W., Bousset, L., Van der Perren, A., Moskalyuk, A., Pulizzi, R., Giugliano, M., et al. (2015). Alpha-Synuclein strains cause distinct synucleinopathies after local and systemic administration. *Nature, 522*, 340–344.

Power, J. H., Barnes, O. L., & Chegini, F. (2017). Lewy bodies and the mechanisms of neuronal cell death in Parkinson's disease and dementia with lewy bodies. *Brain Pathology (Zurich, Switzerland), 27*, 3–12.

Raiss, C. C., Braun, T. S., Konings, I. B. M., Grabmayr, H., Hassink, G. C., Sidhu, A., et al. (2016). Functionally different α-synuclein inclusions yield insight into Parkinson's disease pathology. *Scientific Reports, 6*, 23116.

Ramakers, G. J., Corner, M. A., & Habets, A. M. (1990). Development in the absence of spontaneous bioelectric activity results in increased stereotyped burst firing in cultures of dissociated cerebral cortex. *Experimental Brain Research, 79*, 157–166.

Raz, L., Knoefel, J., & Bhaskar, K. (2016). The neuropathology and cerebrovascular mechanisms of dementia. *Journal of Cerebral Blood Flow & Metabolism, 36*, 172–186.

Rea, T. D., Pearce, R. M., Raghunathan, T. E., Lemaitre, R. N., Sotoodehnia, N., Jouven, X., et al. (2004). Incidence of out-of-hospital cardiac arrest. *The American Journal of Cardiology, 93*, 1455–1460.

Renault, R., Sukenik, N., Descroix, S., Malaquin, L., Viovy, J.-L., Peyrin, J.-M., et al. (2015). Combining microfluidics, optogenetics and calcium imaging to study neuronal communication in vitro. *PLoS One, 10*, e0120680.

Rodrigues, F. B., Neves, J. B., Caldeira, D., Ferro, J. M., Ferreira, J. J., & Costa, J. (2016). Endovascular treatment versus medical care alone for ischaemic stroke: Systematic review and meta-analysis. *The BMJ, 353*, i1754.

Rogawski, M. A. (2011). Revisiting AMPA receptors as an antiepileptic drug target. *Epilepsy Curr, 11*, 56–63.

Roger, V. L., Go, A. S., Lloyd-Jones, D. M., Adams, R. J., Berry, J. D., Brown, T. M., et al. (2011). Heart disease and stroke statistics–2011 update: A report from the American Heart Association. *Circulation, 123*, e18–e209.

Rossi, D. J., Brady, J. D., & Mohr, C. (2007). Astrocyte metabolism and signaling during brain ischemia. *Nature Neuroscience, 10*, 1377–1386.

Roth, S., Bugnicourt, G., Bisbal, M., Gory-Fauré, S., Brocard, J., & Villard, C. (2012). Neuronal architectures with axo-dendritic polarity above silicon nanowires. *Small, 8*, 671–675.

Rouach, N., Koulakoff, A., Abudara, V., Willecke, K., & Giaume, C. (2008). Astroglial metabolic networks sustain hippocampal synaptic transmission. *Science, 322*, 1551–1555.

Ruijter, B. J., Hofmeijer, J., Meijer, H. G. E., & van Putten, M. J. A. M. (2017). Synaptic damage underlies EEG abnormalities in postanoxic encephalopathy: A computational study. *Clinical Neurophysiology, 128*, 1682–1695.

Rutecki, P. A., Lebeda, F. J., & Johnston, D. (1987). 4-Aminopyridine produces epileptiform activity in hippocampus and enhances synaptic excitation and inhibition. *Journal of Neurophysiology, 57*, 1911–1924.

Schevon, C. A., Weiss, S. A., McKhann Jr., G., Goodman, R. R., Yuste, R., Emerson, R. G., et al. (2012). Evidence of an inhibitory restraint of seizure activity in humans. *Nature Communications, 3*, 1060.

Schmitz, Y., Luccarelli, J., Kim, M., Wang, M., & Sulzer, D. (2009). Glutamate controls growth rate and branching of dopaminergic axons. *The Journal of Neuroscience, 29*, 11973–11981.

Schneider, L. S., Mangialasche, F., Andreasen, N., Feldman, H., Giacobini, E., Jones, R., et al. (2014). Clinical trials and late-stage drug development for Alzheimer's disease: An appraisal from 1984 to 2014. *Journal of Internal Medicine, 275*, 251–283.

Schulz-Schaeffer, W. J. (2010). The synaptic pathology of α-synuclein aggregation in dementia with Lewy bodies, Parkinson's disease and Parkinson's disease dementia. *Acta Neuropathologica, 120*, 131–143.

Schurr, A., West, C. A., & Rigor, B. M. (1989). Electrophysiology of energy metabolism and neuronal function in the hippocampal slice preparation. *Journal of Neuroscience Methods, 28*, 7–13.

Schwartzkroin, P. A., & Prince, D. A. (1978). Cellular and field potential properties of epileptogenic hippocampal slices. *Brain Research, 147*, 117–130.

Scott, M. A., Wissner-Gross, Z. D., & Yanik, M. F. (2012). Ultra-rapid laser protein micropatterning: Screening for directed polarization of single neurons. *Lab on a Chip, 12*, 2265–2276.

Segura, I., Lange, C., Knevels, E., Moskalyuk, A., Pulizzi, R., Eelen, G., et al. (2016). The oxygen sensor PHD2 controls dendritic spines and synapses via modification of Filamin A. *Cell Reports, 14*, 2653–2667.

Shorvon, S. D. (2011). The etiologic classification of epilepsy. *Epilepsia, 52*, 1052–1057.

Singer, W. (1993). Synchronization of cortical activity and its putative role in information processing and learning. *Annual Review of Physiology, 55*, 349–374.

Singh, A., & Trevick, S. (2016). The epidemiology of global epilepsy. *Neurologic Clinics, 34*, 837–847.

Small, G. W. (2002). What we need to know about age related memory loss. *BMJ: British Medical Journal, 324*, 1502–1505.

Somjen, G. (1990). Mechanism of the reversible arrest of function during transient cerebral hypoxia and ischemia. In B. Schurr & M. Rigor (Eds.), *Cerebral ischemia and resuscitation* (pp. 301–319). Boston/Boca Raton, FL: CRC Press.

Sommer, B., Barbieri, S., Hofele, K., Wiederhold, K., Probst, A., Mistl, C., et al. (2000). Mouse models of alpha-synucleinopathy and Lewy pathology. *Experimental Gerontology, 35*, 1389–1403.

Srinivas, K. V., Jain, R., Saurav, S., & Sikdar, S. K. (2007). Small-world network topology of hippocampal neuronal network is lost, in an in vitro glutamate injury model of epilepsy. *The European Journal of Neuroscience, 25*, 3276–3286.

Stegenga, J., le Feber, J., Marani, E., & Rutten, W. L. C. (2008). Analysis of cultured neuronal networks using intra-burst firing characteristics. *IEEE Transactions on Biomedical Engineering, 55*, 1382–1390.

Steriade, M., & Amzica, F. (1999). Intracellular study of ecxcitability in the seizure-prone neocortex in vivo. *Journal of Neurophysiology, 82*, 3108–3122.

Stoyanova, I., Hofmeijer, J., van Putten, M. A. M., & le Feber, J. (2016). Acyl ghrelin improves synapse recovery in an in vitro model of postanoxic encephalopathy. *Molecular Neurobiology, 53*, 1–8.

Sun, M.-K., Xu, H., & Alkon, D. L. (2002). Pharmacological protection of synaptic function, spatial learning, and memory from transient hypoxia in rats. *The Journal of Pharmacology and Experimental Therapeutics, 300*, 408–416.

Suresh, J., Radojicic, M., Pesce, L. L., Bhansali, A., Wang, J., Tryba, A. K., et al. (2016). Network burst activity in hippocampal neuronal cultures: The role of synaptic and intrinsic currents. *Journal of Neurophysiology, 115*, 3073–3089.

Sutula, T., & Pitkänen, A. (2002). Summary: Seizure-induced damage in experimental models. In *Progress in Brain Research* (pp. 133–135). New York: Elsevier.

Swayne, O. B. C., Rothwell, J. C., Ward, N. S., & Greenwood, R. J. (2008). Stages of motor output reorganization after hemispheric stroke suggested by longitudinal studies of cortical physiology. *Cerebral Cortex, 18*, 1909–1922.

Symon, L., Branston, N. M., Strong, A. J., & Hope, T. D. (1977). The concepts of thresholds of ischaemia in relation to brain structure and function. *Journal of Clinical Pathology. Supplement (Royal College of Pathologists), 11*, 149–154.

Taguchi, K., Watanabe, Y., Tsujimura, A., Tatebe, H., Miyata, S., Tokuda, T., et al. (2014). Differential expression of alpha-synuclein in hippocampal neurons. *PLoS One, 9*, e89327.

Takano, T., Oberheim, N., Cotrina, M. L., & Nedergaard, M. (2009). Astrocytes and ischemic injury. *Stroke, 40*, S8–S12.

Tancredi, V., & Avoli, M. (1987). Control of spontaneous epileptiform discharges by extracellular potassium: An "in vitro" study in the CA1 subfield of the hippocampal slice. *Experimental Brain Research, 67*, 363–372.

Tancredi, V., Hwa, G. G., Zona, C., Brancati, A., & Avoli, M. (1990). Low magnesium epileptogenesis in the rat hippocampal slice: Electrophysiological and pharmacological features. *Brain Research, 511*, 280–290.

Tiede, L. M., Cook, E. A., Morsey, B., & Fox, H. S. (2011). Oxygen matters: Tissue culture oxygen levels affect mitochondrial function and structure as well as responses to HIV viroproteins. *Cell Death & Disease, 2*, e246.

Tjepkema-Cloostermans, M. C., Hofmeijer, J., Trof, R. J., Blans, M. J., Beishuizen, A., & van Putten, M. J. A. M. (2015). Electroencephalogram predicts outcome in patients with postanoxic coma during mild therapeutic hypothermia. *Critical Care Medicine, 43*, 159–167.

Trinka, E., Hofler, J., & Zerbs, A. (2012). Causes of status epilepticus. *Epilepsia, 53*(Suppl 4), 127–138.

Turrigiano, G. (2008). The self-tuning neuron: Synaptic scaling of excitatory synapses. *Cell, 135*, 422–435.

Turrigiano, G. G., Leslie, K. R., Desai, N. S., Rutherford, L. C., & Nelson, S. B. (1998). Activity-dependent scaling of quantal amplitude in neocortical neurons. *Nature, 391*, 892–896.

Uhlhaas, P. J., & Singer, W. (2006). Neural synchrony in brain disorders: Relevance for cognitive dysfunctions and pathophysiology. *Neuron, 52*, 155–168.

van der Worp, H. B., Howells, D. W., Sena, E. S., Porritt, M. J., Rewell, S., O'Collins, V., et al. (2010). Can animal models of disease reliably inform human studies? *PLoS Medicine, 7*, e1000245.

van Pelt, J., Wolters, P. S., Corner, M. A., Rutten, W. L. C., & Ramakers, G. J. (2004). Long-term characterization of firing dynamics of spontaneous bursts in cultured neural networks. *IEEE Transactions on Biomedical Engineering, 51*, 2051–2062.

Varghese, K., Molnar, P., Das, M., Bhargava, N., Lambert, S., Kindy, M. S., et al. (2010). A new target for amyloid beta toxicity validated by standard and high-throughput electrophysiology. *PLoS One, 5*, e8643.

Vedunova, M., Sakharnova, T., Mitroshina, E., Perminova, M., Pimashkin, A., Zakharov, Y., et al. (2013). Seizure-like activity in hyaluronidase-treated dissociated hippocampal cultures. *Frontiers in Cellular Neuroscience, 7*, 149.

Volpicelli-Daley, L. A., Luk, K. C., Patel, T. P., Tanik, S. A., Riddle, D. M., Stieber, A., et al. (2011). Exogenous alpha-synuclein fibrils induce Lewy body pathology leading to synaptic dysfunction and neuron death. *Neuron, 72*, 57–71.

Vos, T., Allen, C., Arora, M., Barber, R. M., Bhutta, Z. A., Brown, A., et al. (2016). Global, regional, and national incidence, prevalence, and years lived with disability for 310 diseases and injuries, 1990–2015: A systematic analysis for the Global Burden of Disease Study 2015. *The Lancet, 388*, 1545–1602.

Wagenaar, D. A., Madhavan, R., Pine, J., & Potter, S. M. (2005). Controlling bursting in cortical cultures with closed-loop multi-electrode stimulation. *The Journal of Neuroscience, 25*, 680–688.

Wagenaar, D. A., Pine, J., & Potter, S. M. (2004). Effective parameters for stimulation of dissociated cultures using multi-electrode arrays. *Journal of Neuroscience Methods, 138*, 27–37.

Wardlaw, J. M., Warlow, C. P., & Counsell, C. (1997). Systematic review of evidence on thrombolytic therapy for acute ischaemic stroke. *The Lancet, 350*, 607–614.

Waters, J. (2010). The concentration of soluble extracellular amyloid-β protein in acute brain slices from CRND8 mice. *PLoS One, 5*, e15709.

Weissinger, F., Buchheim, K., Siegmund, H., & Meierkord, H. (2005). Seizure spread through the life cycle: Optical imaging in combined brain slices from immature, adult, and senile rats in vitro. *Neurobiology of Disease, 19*, 84–95.

Williams, P. A., White, A. M., Clark, S., Ferraro, D. J., Swiercz, W., Staley, K. J., et al. (2009). Development of spontaneous recurrent seizures after kainate-induced status epilepticus. *The Journal of Neuroscience, 29*, 2103–2112.

Wong, R. O. L., & Ghosh, A. (2002). Activity-dependent regulation of dendritic growth and patterning. *Nature Reviews. Neuroscience, 3*, 803–812.

Yang, D., Nakajo, Y., Iihara, K., Kataoka, H., Nakagawara, J., Zhao, Q., et al. (2014). An integrated stroke model with a consistent penumbra for the assessment of neuroprotective interventions. *European Neurology, 71*, 4–18.

Zach, S., Bueler, H., Hengerer, B., & Gillardon, F. (2007). Predominant neuritic pathology induced by viral overexpression of alpha-synuclein in cell culture. *Cellular and Molecular Neurobiology, 27*, 505–515.

Zandbergen, E. G. (2008). Postanoxic coma: How (long) should we treat? *European Journal of Anaesthesiology Supplement, 42*, 39–42.

Zandbergen, E. G., de Haan, R. J., Reitsma, J. B., & Hijdra, A. (2003). Survival and recovery of consciousness in anoxic-ischemic coma after cardiopulmonary resuscitation. *Intensive Care Medicine, 29*, 1911–1915.

Zhang, Y., Pak, C., Han, Y., Ahlenius, H., Zhang, Z., Chanda, S., et al. (2013). Rapid single-step induction of functional neurons from human pluripotent stem cells. *Neuron, 78*, 785–798.

Zhu, P. J., & Krnjević, K. (1994). Anoxia selectively depresses excitatory synaptic transmission in hippocampal slices. *Neuroscience Letters, 166*, 27–30.

Neuronal Cultures and Nanomaterials

Mattia Bramini, Anna Rocchi, Fabio Benfenati, and Fabrizia Cesca

Abstract In recent years, the scientific community has witnessed an exponential increase in the use of nanomaterials for biomedical applications. In particular, the interest of graphene and graphene-based materials has rapidly risen in the neuroscience field due to the properties of this material, such as high conductivity, transparency and flexibility. As for any new material that aims to play a role in the biomedical area, a fundamental aspect is the evaluation of its toxicity, which strongly depends on material composition, chemical functionalization and dimensions. Furthermore, a wide variety of three-dimensional scaffolds have also started to be exploited as a substrate for tissue engineering. In this application, the topography is probably the most relevant amongst the various properties of the different materials, as it may allow to instruct and interrogate neural networks, as well as to drive neural growth and differentiation.

This chapter discusses the in vitro approaches, ranging from microscopy analysis to physiology measurements, to investigate the interaction of graphene with the central nervous system. Moreover, the in vitro use of three-dimensional scaffolds is described and commented.

Fabio Benfenati and Fabrizia Cesca are the senior authors

M. Bramini (✉) · F. Cesca (✉)
Center for Synaptic Neuroscience and Technology (NSYN@UniGe), Istituto Italiano di Tecnologia, Genova, Italy

Graphene Labs, Istituto Italiano di Tecnologia, Genova, Italy
e-mail: mattia.bramini@iit.it; fabrizia.cesca@iit.it

A. Rocchi
Center for Synaptic Neuroscience and Technology (NSYN@UniGe), Istituto Italiano di Tecnologia, Genova, Italy

F. Benfenati
Center for Synaptic Neuroscience and Technology (NSYN@UniGe), Istituto Italiano di Tecnologia, Genova, Italy

Graphene Labs, Istituto Italiano di Tecnologia, Genova, Italy

Department of Experimental Medicine, University of Genova, Genova, Italy

1 Introduction

Injuries to the central (CNS) and peripheral (PNS) nervous systems most often lead to death or permanent disabilities, causing a loss of quality of life. These life-threatening injuries can be caused by physical trauma, like stroke or traumatic nerve injuries, degenerative diseases, infection and cancer. Numerous cellular mechanisms mediate the response to neuronal injury, including the apoptotic death of neurons, axonal degeneration, demyelination, excitotoxicity, oxidative stress and inflammation (Fitch and Silver 2008). Thus, neuronal damage is a multifaceted process involving the simultaneous alteration of the morphology, activity and connectivity within the network. Despite the intense research effort addressing several aspects of neurodegeneration, many aspects of the pathological events leading to neuronal death have not yet been fully described and this, coupled with the intrinsic poor regenerative properties of the brain, has a strong impact on the ability of clinicians to modify the natural history of diseases. Accordingly, there is an urgent need to combine the pharmacological treatment of the symptoms with new therapeutic strategies to fully restore the lost function(s).

Nanotechnologies have the potential to make a very significant impact on society. The ability of nanomaterials to interact with and enter into cells, affecting their biochemical functions, makes them extremely interesting tools in the field of nanomedicine (European Commission PH 2006). Amongst the numerous potential biomedical applications, neuroscience offers some of the most exciting opportunities for bio-nanomaterials. Broadly speaking, neuroscience research employs materials for three main purposes, i.e. (1) nanomaterials for drug delivery and live-imaging applications, (2) 2D/3D scaffolds to drive neuronal (re)growth upon injury, and (3) recording/stimulating electrodes for network analysis and interrogation. While the latter point is comprehensively addressed in other sections of this book, in this chapter we summarize the main findings related to the use of nanomaterials, in particular graphene flakes, and 2D/3D biocompatible scaffolds, with nerve tissue in vitro by reporting few significant case studies.

2 Interaction Between Graphene and Graphene-Related Materials with Neural Cells In Vitro

The biological effects elicited by exposure of various cell types to G flakes (including G flakes) have been thoroughly described and include the physical interaction with cell membranes (Seabra et al. 2014), disruption of cell cytoskeleton (Tian et al. 2017), oxidative stress (Mittal et al. 2016), mitochondrial and DNA

damage (Pelin et al. 2017; Fahmi et al. 2017), autophagy (Chen et al. 2014) and apoptosis (Lim et al. 2016). At the same time and in contrast with the above reported studies, other investigations highlighted the promising properties of graphene (G) materials for biomedical applications, banking on the fact that graphene oxide (GO) shows good biocompatibility, especially if opportunely functionalized (Cheng et al. 2016). Thus, the use of G flakes for biological purposes is to be planned with adequate precautions.

According to the EU Graphene Flagship guidelines, graphene-related materials (GRMs) include single- and few-layered G (1–10 layers; GR), G oxide (single layer, 1:1 C/O ratio; GO), reduced G oxide (rGO), graphite nano- and micro-platelets (more than 10 layers, but <100 nm thickness and average lateral size in the order of the nm and μm, respectively), G and G oxide quantum dots (GQDs and GOQDs, respectively) and a variety of hybridized G nanocomposites (Wick et al. 2014). The physical-chemical features of the various G materials influence their behaviour in the biological environment. Nanomaterials can have different biological impacts depending on many features such as dimension, surface chemistry, contact area and material purity. Thickness, determined by the number of layers, is directly related to the flexibility of the material, while the lateral dimension is linked to the degree of deformability, and both parameters influence G interactions with cells, in particular with the plasma membrane. In addition, higher oxygen content will render the material less hydrophobic, improving its stability when dispersed in aqueous media and biological fluids (Wick et al. 2014). Interestingly, published data suggest that GO is less toxic than bare G, rGO and hydrogenated-G (Akhavan et al. 2012; Bianco 2013; Ou et al. 2016; Bramini et al. 2018). Additionally, smaller flakes are less toxic than large flakes, and highly dispersible G solutions are safer than aggregating ones. G is characterized by very little degradation in cells and tissues, although carboxylated and oxidated derivatives may form under some conditions (Donaldson et al. 2006; Kurapati et al. 2016). As mentioned above, an increasing research effort is devoted to design novel G-based technologies for the treatment of neural disorders, including neuro-oncology, neuro-imaging, neuroregeneration, functional neuro-surgery and peripheral nerve surgery. The mechanisms of interaction of GRMs with neurons and astrocytes have been investigated, depicting a situation where the physiological effects of G exposure are strongly dependent on the intrinsic characteristics of the various materials, as detailed in the next sections (Bramini et al. 2016; Defterali et al. 2016; Rauti et al. 2016). However, material biocompatibility is still a major concern, and all the above-mentioned points have to be clearly assessed when investigating material biosafety.

In the next paragraphs, we will focus on recent works describing the biological and physiological effects elicited when primary neural cells (neurons, astrocytes) in vitro are exposed to non-functionalized G flakes (pristine G, GR, and graphene oxide, GO) in solution. This experimental system represents a realistic scenario, and its study is of fundamental importance to establish guidelines for the safe handling of G nanomaterials. In this context, we also address the problem of studying the interaction of GRMs with the blood–brain barrier (BBB), especially in view of the potential use of this material for drug delivery applications. By adopting an in vitro

approach, the detailed molecular mechanisms underlying the interaction between GRMs and the BBB can be fully investigated and understood, helping the design of future G-based medical devices.

2.1 Interaction Between Graphene Flakes and Primary Neurons In Vitro

Primary rat cortical (Bramini et al. 2016) and hippocampal (Rauti et al. 2016) neurons were exposed to GR/GO flakes at two different concentrations (1 and 10 µg/ml) and for different times. When large G micro-flakes (lateral dimension of few micrometres) were used, a clear cytotoxicity was observed after 6–8 days of material exposure (Rauti et al. 2016). Interestingly, when cells were treated with the same concentration of small G nano-flakes (lateral dimension of few hundreds of nanometres), no reduction in cell density or viability was observed, thus demonstrating a clear lateral size-related cytotoxicity (Bramini et al. 2016; Rauti et al. 2016; Tu et al. 2014). However, the absence of cell death does not rule out the possibility that the exposure to the various materials causes more subtle alterations to network physiology and functionality. Thus, a combination of cell biology, electrophysiology, microscopy and 'omics' techniques was employed to perform a detailed analysis of the physiology of GR/GO-treated cultures.

Large aggregates were found in contact with the cell membrane (Fig. 1a), while smaller, nano-sized particles were actively internalized. As for many other nanomaterials (Mu et al. 2012; Sandin et al. 2012), GR/GO flakes were internalized mainly through the endo-lysosomal pathway. Of note, electron microscopy analysis revealed a number of particles apparently free in the cytoplasm, which had likely pierced the membrane or escaped intracellular organelle routes. The amount of internalized material was relatively low, never exceeding 15% of the total amount of material present in the dish; however, even this low amount of internalization induced a strong autophagy reaction, probably due to the high sensitivity of neurons to any perturbation of their physiological environment (Bramini et al. 2016).

A closer analysis of Ca^{2+} dynamics revealed marked alterations in nano-flakes-exposed neurons, consisting in reduced number of spontaneously oscillating cells, reduced basal cytoplasmic Ca^{2+} concentration and altered responses to external stimuli such as the pro-convulsant drug bicuculline. Interestingly, these effects were elicited only by chronic GO exposure, while GR/GO acute exposure did not cause any functional alteration (Bramini et al. 2016; Rauti et al. 2016). GO-exposed neurons were characterized by impaired excitatory synaptic transmission (Fig. 1b–d), with reduced miniature excitatory post-synaptic current (mEPSC) frequency and amplitude, accompanied by a decrease in the number of excitatory synapses (Bramini et al. 2016; Rauti et al. 2016), and by increased miniature inhibitory post-synaptic current (mIPSC) frequency (Bramini et al. 2016). The resulting imbalance between synaptic excitation and inhibition is likely at the basis of the reduced network activity detected by Ca^{2+} imaging, which mostly reflects the activity of
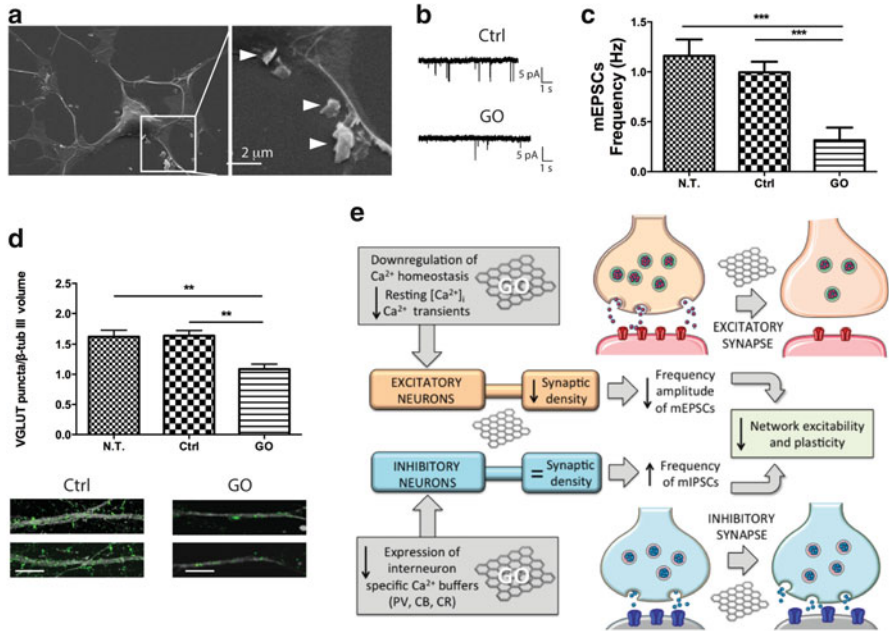
Fig. 1 Interaction of graphene with primary neurons. (**a**) SEM images showing the interaction of GR flakes with primary neuronal cells. A large number of flakes (white arrowheads) were found in contact with the cell membrane. (**b**) Representative recordings of miniature excitatory post-synaptic currents (mEPSCs) in cortical neurons exposed to GO or vehicle. (**c**) Mean ($\pm$SEM) frequency of mEPSCs in control and GO-treated neurons. (**d**) Density of VGLUT1-positive excitatory synapses (scale bars, 5 μm; ** p <0.01, one-way ANOVA and Bonferroni's multiple comparison test). (**e**) Schematic representation of the mechanisms of the effects of chronic exposure of GO on the activity of neuronal networks [**a**–**e** modified with permission from Bramini et al. (2016)]

excitatory neurons (Fig. 1e) (Murphy et al. 1998). Thus, GO nano-flakes specifically interfered with presynaptic vesicle recycling mechanisms (Rauti et al. 2016). The mechanisms by which GO elicits such effects are at present unknown and can be only speculated upon to include changes in plasma- and intracellular membrane lipid composition, alterations of cytoskeleton and/or changes in the membrane targeting and functionality of ion channels. Surprisingly, passive cell properties, neuronal network organization and overall network activity of neurons interfaced with GR did not differ from control cultures, exposed only to vehicle. This could be explained by the lower hydrophilicity of GR flakes and by their poorer dispersibility in cell culture media (Chong et al. 2015), which would favour the formation of larger aggregates with modest ability to interact with the cell membrane (Bussy and Kostarelos 2017).

Proteomic and lipidomic analyses were conducted to better understand the molecular and cellular processes affected by the exposure to GO (Bramini et al. 2016). In agreement with the previously described experimental results, the clear-

est output of the proteomic screen was the impairment of Ca^{2+} signalling, of vital importance in almost every aspect of neural cell physiology. Several Ca^{2+}-binding and buffering proteins were markedly up- or downregulated in nano-flakes-exposed cultures. Moreover, the expression of several proteins involved in intracellular trafficking was also altered, which likely mediated the observed endocytotic and/or phagocytic response. For what concerns the lipidomic analysis, instead, nano-flakes-exposed neurons were characterized by the upregulation of phosphatidylethanolamines (PEs) and downregulation of phosphatidylserines (PSs). PEs are one of the major components of the plasma- and synaptic vesicle (SV) membrane phospholipids (Nelson and Freeman 1960; Manzoli et al. 1969; Morita et al. 2012), and play important roles in SV fusion and fission (Gaffaney et al. 2008). On the other hand, PSs contribute to the negative charge of the cytosolic face of the membranes, thus regulating their fusion propensity. While the upregulation of PE could reflect the intense membrane trafficking activated by G exposure, the change in the PE/PS ratio may participate in the above-described alterations of synaptic transmission.

In summary, these studies have highlighted the crucial factors that determine the cellular and molecular pathways activated in response to nanomaterials, i.e. (1) the exposure time (acute vs chronic), (2) material size, shape, and (3) surface properties.

2.2 Interaction Between Graphene Flakes and Primary Glial Cells In Vitro

By adopting the same material used for neuronal studies, primary astrocytes were exposed to GR and GO micro and nano-flakes for up to 7 days in vitro. Similarly to neurons, exposure to GR/GO flakes did not cause cell death (Rauti et al. 2016) neither at short-time treatments (24 and 72 h) nor upon long-term exposure (7 days) (Chiacchiaretta et al. 2018). However, G-exposed astrocytes displayed marked morphological alterations already after 72 h, changing from a regular and flat shape to an irregular morphology characterized by multiple protrusions resembling that of in vitro activated/mature glia (Chiacchiaretta et al. 2018), and similar to changes induced by carbon nanotubes (Gottipati et al. 2014). Such morphological changes were associated with, and likely due to, the flake-mediated disruption of the actin and tubulin cytoskeleton, in line with recent literature (Tian et al. 2017). Similar to neurons, astrocytes internalized nanomaterials through the endo-lysosomal pathway. However, due to their higher endocytic activity, they internalized a much higher amount of the material (up to 30–40%), in the absence of autophagy reaction, coherent with their primary function of defending neurons from stressing insults.

Following a similar approach to the one applied for neurons, proteomics and lipidomics studies were performed on GR/GO-exposed astrocyte cultures. Extended lipidomics analysis revealed that cholesterol was one of the most altered lipids in

GO-exposed astrocytes. Cholesterol is a structural component of lipid rafts, which mediate the signalling between endoplasmic reticulum and plasma membrane also in astroglial cells (Weerth et al. 2007). Changes in the levels of this particular lipid can therefore underlie some of the observed physiological changes. Furthermore, similar to the data obtained in neurons, proteomics suggested that Ca^{2+} homeostasis is also impaired in astrocytes. Indeed, experimental results revealed the very same alterations described in GO-exposed neurons, i.e. a reduced number of spontaneously oscillating cells, reduced basal cytoplasmic Ca^{2+} concentration and altered responses to external stimuli, in this case ATP. Once again, these effects were elicited only by GO, while GR exposure did not cause any functional alteration (Chiacchiaretta et al. 2018). Interestingly, the proteomic and lipidomic profiles of astrocyte cultures treated with GR were very different from the ones obtained upon GO treatment, underlying once more that the response of cells to nanomaterials is strictly determined by their different physical-chemical properties (Chiacchiaretta et al. 2018).

For what concerns the electrophysiological properties of astrocytes, a marked alteration of K^+ currents was selectively triggered by GO, more specifically, an increase in outward rectifying currents was observed, together with a hyperpolarized membrane potential, decreased input resistance and increase in specific conductance. The observed phenotypes were ascribed to the increased membrane targeting of Kir4.1 channels, functionally linked to extracellular K^+ buffering and enhanced Na^+-dependent glutamate uptake. Very interestingly, blocking endocytosis by incubating astrocytes with low doses of Na^+ azide rescued the morphology and Kir4.1 targeting, indicating that the effects were caused by the actively internalized material (Chiacchiaretta et al. 2018). A marked increase in astrocyte-released 'synaptic-like' microvesicles (MVs) was also described in GO-treated cultures (Rauti et al. 2016). MVs are released into the extracellular space by direct budding from the plasma membrane of astrocytes and have important roles in astrocyte–astrocyte and astrocyte–neuron communication. Once again, this effect was selective for GO, as GR treatment did not promote MV release.

Ca^{2+} dynamics, glutamate uptake and MV release are all fundamental processes in the astrocyte-to-neuron communication. Thus, a step forward was taken, and an astrocyte-neuron co-culture system was employed to analyse if and how G-exposed astrocytes influence the activity of the overlying neuronal network. Primary neurons were grown together with primary astrocytes pre-treated with GR/GO or left untreated (control samples). After 2 weeks of co-cultures, the physiology and functionality of primary neuronal cells were monitored by electrophysiological measurements and fluorescence microscopy analysis. This experimental approach gave very interesting results, showing that GO-treated astrocytes influenced spontaneous synaptic activity and accelerated the maturation of the intrinsic excitability of co-cultured neurons. Neurons were altogether more excitable, but unexpectedly, excitatory transmission was preserved, while a significant increase in miniature inhibitory post-synaptic currents (mIPSCs) was observed, paralleled by an increase in the number of inhibitory synapses. Also in this case, similar to previous findings, this effect was specific for GO flakes (Chiacchiaretta et al. 2018).

Finally, to complete the CNS picture, microglia cells were also analysed; however, less data are presently available about the impact of G flakes on the physiology of this cell population. Chronic treatment of mixed neuronal-glial cultures with G material did not cause an increase in the number of microglial cells (Bramini et al. 2016; Rauti et al. 2016). A different picture instead emerged from the analysis of pure glial cultures, i.e. composed mainly of astrocytes and microglial cells. In this case, the vast majority of material was endocytosed by microglia. Surprisingly, chronic exposure to GR flakes caused a marked reduction in the number of microglial cells, while the opposite effect was caused by chronic GO exposure, which resulted in an increased number of microglia (Bramini et al. unpublished observations). While these consequences might be due to a toxic effect of GR versus a pro-inflammatory effect of GO, more studies are needed to address the molecular pathways that are specifically involved. In general, we believe that the selective effects of GO over GR can be explained by the different chemical reactivity of the two substances, directly related to the presence of oxygen species on the surface of GO flakes, which determines their surface charge and protein binding capability, although additional effects of roughness and morphology cannot be excluded.

2.3   Graphene Flakes as Cargoes for Drug Delivery to the CNS: Modelling the BBB In Vitro

Extremely relevant in neurology is the possibility of using G flakes for controlled delivery and release of drugs and small molecules to the brain. Lamentably, one of the limitations of G is its very low accumulation in the brain parenchyma upon intravenous injection (Zhang et al. 2011). Once injected intravenously, G will engage with ions, lipids and proteins, resulting in the formation of a biomolecular corona that might affect the distribution of G and trigger inflammatory responses (Dell'Orco et al. 2010). In addition, nanosheets can be phagocytosed by macrophages, releasing pro-inflammatory cytokines (Zhou et al. 2012), and interact with several blood components inducing hemolysis (Liao et al. 2011). Finally, G could accumulate in the endothelium of the blood–brain barrier (BBB) system rather than in the CNS to which they are targeted (McCallion et al. 2016), as it has already been reported for other types of nanoparticles (Ye et al. 2013; Bramini et al. 2014).

As a matter of fact, the passage through the BBB is particularly challenging, as this barrier significantly limits the delivery of drugs, blocking roughly the 100% of large molecules, including neuro-therapeutics, and more than 98% of all small-molecule drugs (Upadhyay 2014). According to Mendonca et al., systemically injected rGO nanosheets cross the BBB through a transitory decrease in the BBB paracellular tightness and accumulate in the thalamus and hippocampus of rats (Mendonca et al. 2016a). Functionalizing the G surface could bypass the BBB blockage and foster the entry of G-based nanocarriers into the CNS. In fact,

molecules can be loaded onto G substrates via π–π stacking interactions, hydrogen bonding or hydrophobic interactions (Georgakilas et al. 2016; Chen et al. 2013; Reina et al. 2017). Surface functionalization has the double advantage of loading high quantity of biomolecules and specifically delivering them to target cells, while allowing a more homogenous dispersion of the material, since pure G is highly hydrophobic and tends to aggregate in aqueous solution, including biological fluids (John et al. 2015; Mattei and Rehman 2014). The G surface was functionalized with specific biomolecules that enabled the material to cross the BBB, i.e. transferrin and apolipoprotein E (John et al. 2015; Allen and Cullis 2004; Goenka et al. 2014). More recently, the functionalization of GO nanocomposites with lactoferrin has been described (Liu et al. 2013), and of PEG-GO with the Tat protein of the Human Immunodeficiency Virus (HIV), which allowed the drug-loaded PEG-GO system to cross the BBB by transcytosis, while leaving the barrier endothelium fully preserved (Yang et al. 2015). rGO-PEG particles were also able to cross the endothelial layer of the BBB without disrupting the tight junctions, in both in vitro and in vivo studies (Mendonca et al. 2016a, b).

Thus, several attempts have been made to modify GRMs to facilitate BBB crossing, however so far such approaches encountered limited success. To better tackle this issue, a deeper understanding is needed of the cellular and molecular mechanisms controlling the interaction between nanomaterials and the vascular endothelium. This kind of information is difficult to obtain from in vivo experiments, which are intrinsically complex and whose results are determined by a high number of variables. Because of this, in vitro models of BBB have been developed, which we describe in the following paragraphs.

2.3.1   In Vitro Blood–Brain Barrier Models

Similarly to other complex tissue structures such as the renal, the intestinal or the pulmonary barrier, the BBB is primarily made of endothelial cells that regulate the transport of solutes, ions and water using both transcellular and tight-junction-mediated paracellular routes. A big effort is presently devoted to the investigation of the effects of GRM exposure to the BBB by using in vitro models, and following experimental and computational modelling approaches. The development of a reliable in vitro BBB model has been for a long time a goal for all those research lines aimed at developing brain-penetrating drugs. Indeed, in vitro barrier models have been intensively used and have shown many advantages over in vivo systems (Silliman and Wang 2006; Polli 2008; Ogunshola 2011; Wolff et al. 2015). Moreover, such models are undoubtedly an appropriate complement to in vivo studies, especially when employed as an efficient and reliable screening platform to assess the efficiency of nanomaterial targeting to the brain, and the associated risks. To date, only few validated in vitro models of BBB are available. Of note, as the isolation of primary brain capillary endothelial cells is very laborious and time-consuming (Navone et al. 2013), they are often replaced by a number of immortalized rat or mouse cell lines, such as RBE4 (Roux et al. 1994), GPNT

(Regina et al. 1999) and bEnd.3 (Omidi et al. 2003). However, the physiology of these rodent cell lines is in some respects different from the human BBB, thus, three human immortalized cell lines have been developed: BB19 (Prudhomme et al. 1996; Kusch-Poddar et al. 2005), NKIM-6 (Ketabi-Kiyanvash et al. 2007) and hCMEC/D3 (Weksler et al. 2005).

The most common device that mimics the in vivo situation and enables the growth of specialized cell types is the transwell system (Corning Inc., Corning, NY) (Ye et al. 2013; Ragnaill et al. 2011). BBB models can be developed using one, two, or more cell types (Fig. 2a). The endothelial cells are usually seeded onto an upper porous filter membrane, which is then placed into a lower acceptor plate. The cells are submersed in cell culture medium and grown into a monolayer until they become polarized. The upper and lower compartments are in this case called 'apical' and 'basolateral', respectively (Fig. 2b). Comparing the system to the in vivo structure, the apical side mimics the blood, while the basolateral side mimics the brain. So far, a great number of biomolecules and nanomaterials have been studied in transwell systems (Ye et al. 2013; Weksler et al. 2005; Ragnaill et al. 2011; Poller et al. 2008). Transport studies are normally carried out by loading molecules into the apical chamber and detecting the molecules that cross cell monolayers and reach the basolateral chamber according to fluorescent or radioactive signals labelling the sample (Hubatsch et al. 2007; Vu et al. 2009). Moreover, efforts have been also directed at co-culturing various brain capillary endothelial cells with astrocytes and/or pericytes and neurons to better mimic the in vivo situation. In the most common co-culture models, endothelial cells are grown on the apical side of the transwell membrane, whereas astrocytes, pericytes or neurons are grown either on the bottom of the well [non-contact (Raghnaill et al. 2014)] or directly on the abluminal side of the membrane [contact (Nakagawa et al. 2009)]. The 'contact' models allow the non-endothelial cells to affect the endothelial layer solely by close-range association (Takeshita et al. 2014), and better mimic the in vivo scenario. Astrocytes are the most common cell type that endothelial cells are co-cultured with, and typically these more advanced models exhibit high electrical resistances, low permeability to low molecular weight compounds and functional expression of the most important drug transporters (Nakagawa et al. 2009).

The most commonly used techniques to determine the quality of the in vitro models evaluate the trans-endothelial electrical resistance (TEER), and measure the permeability of specific paracellular markers. The TEER measures the permeability of the cell layer to ions; a defined low voltage is applied between two electrodes, one placed in the apical compartment and the other one in the basolateral compartment, the resulting current is measured and the resistance calculated from Ohm's law '$R = V/I$', where R is the resistance, V the voltage and I the current. Thus, a high resistance indicates low passage of ions (conductivity) and the formation of a tight barrier. In vivo values of resistance across the BBB are in the range of 1500–8000 Ω cm^2 (Crone and Olesen 1982; Smith and Rapoport 1986; Butt and Jones 1992), and a value of 40–200 Ω cm^2 is considered the lowest functional limit for in vitro models, depending on the cell line used (Wolff et al. 2015; Reichel et al. 2003). Although TEER is a relatively simple way of measuring barrier tightness,
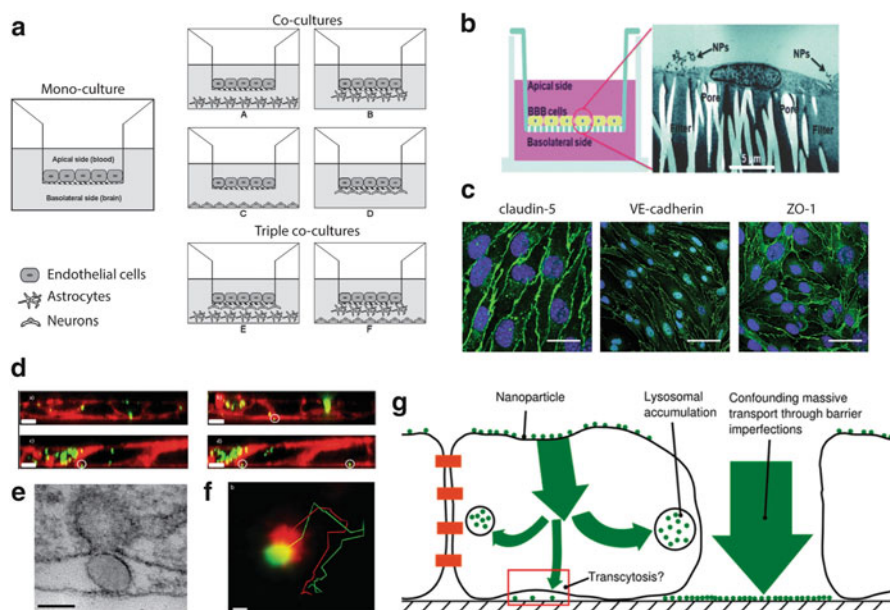
Fig. 2 In vitro blood–brain barrier models for studying the interaction with nanomaterials. (**a**) The different kinds of in vitro BBB transwell models are presented: monoculture of endothelial cells; non-contact (A, C) and contact (B, D) co-cultures of endothelial cells and either astrocytes (A, B) or neurons (C, D) and triple co-cultures of endothelial cells with neurons in contact and astrocytes in non-contact position (E) or vice versa (F) [modified with permission from Bicker et al. (2014)]. (**b**) Schematic cartoon and electron microscopy image of the transwell system used to set up the in vitro BBB model (scale bar, 5 μm). Cells were seeded on a micro-porous membrane onto a transwell insert and grown until forming a monolayer. The apical compartment of the system mimics the blood, while the basolateral compartment mimics the brain side. In the EM image, cells were exposed to SiO_2 nanoparticles [modified with permission from Ragnaill et al. (2011)]. (**c**) A confluent monolayer of bEnd.3 cells was imaged by confocal microscopy showing the expression and localization of claudin-5 (scale bar, 10 μm), vascular endothelial (VE)-cadherin (scale bar, 30 μm) and ZO-1 (scale bar, 20 μm) in the green channel, and nuclei stained by Hoechst in the blue channel. (**d**) Translocation of 100 nm PS-COOH nanoparticles (green) across the in vitro BBB model. Cell membrane was stained with CellMask (red) and imaged in three dimension by confocal microscopy (scale bar, 3 μm). The panel shows cross-sections of barrier 24 h after a 10 min nanoparticle exposure. Nanoparticles can be seen in the white circles on the basolateral side of the barrier. (**e**) A nanoparticle being exported out of the cell on the lower, basolateral side of the barrier (scale bar, 100 nm). (**f**) A single nanoparticle (green) co-localized with a lysosome (red), and the two moved together over time (scale bar, 500 nm). (**g**) Schematic cartoon summarizing the possible scenario of nanomaterial interaction with the BBB. High lysosomal accumulation has to be expected, as well as low transcytosis; moreover, BBB disruption needs to be checked and addressed [**d**–**g**, modified with permission from Bramini et al. (2014)]

it is not enough to judge the selectivity of the barrier. For this reason, TEER measurements should be accompanied by size selectivity of passively diffusing molecules, as well as by evaluation of tight-junction (TJ) and adherens junction (AJ) protein expressions. Tight junctions form a network of linear fibrils fusing the

apical ends of the lateral membrane of adjacent cells at 'kissing points' at a depth of 0.1–0.6 µm (Aijaz et al. 2006). The most studied is claudin-5, a small (∼23 kDa) trans-membrane protein that contributes to give high resistance to tight junctions (Abbott et al. 2006; Krause et al. 2008), together with zona occludens-1 (ZO-1) and occludins. These markers can be targeted by immunostaining to confirm the presence of the correct cell phenotype (Fig. 2c). Furthermore, since tight junctions prevent the passage of molecules and ions between cells (paracellular pathway), materials must enter the cells by diffusion or active transport in order to pass through the cell barrier. One assay used to measure the 'tightness' of the in vitro BBB transwell model is in fact the apparent permeability of molecules of known molecular weight across the barrier, from apical to the basolateral chamber. The 4 kDa fluorescein isothiocyanate-dextran (FD4), as well as sucrose and mannitol, are often used as markers of paracellular permeability, and tight junction formation can be in this way indirectly confirmed (Ragnaill et al. 2011; Ohno et al. 1978).

Finally, apolipoprotein E and/or transferrin are usually exploited as markers for receptor-mediated transcytosis through the BBB, as they are known to access the brain through a receptor-mediated, ATP-dependent mechanism (Bramini et al. 2014; Ragnaill et al. 2011). To study energy-dependent active processes, such as the receptor-mediated pathways used by these proteins, temperature-dependent studies are performed. The rationale behind this methodology is that temperature reduction from 37 to 4 °C decreases ATP supply of the cell and leads to a decreased rate of uptake and intracellular transport. As an example, the transported mass of apolipoprotein E across the in vitro BBB transwell was assessed and the percentage of the transported mass after 4 h was ∼25% of the original exposure dose, suggesting that a substantial amount of the protein is able to pass across the barrier over the period of time monitored in the assay (Ragnaill et al. 2011). The rate of apolipoprotein E transport in hCMEC/D3 was higher at 37 °C compared to the rate of protein transport at 4 °C (Zensi et al. 2009), indicating a temperature-dependent transport across the barrier.

2.3.2   Nanomaterials Transport Across In Vitro Blood–Brain Barrier Models

Once a confluent monolayer is formed onto the micro-porous membrane of the transwell system, the transport across the barrier and the apparent permeability of different nanomaterials can be measured, comparing the transport over time through the porous filter alone and with the cell monolayer. As expected, the transport of nanoparticles across the in vitro BBB model is significantly reduced compared to the transport through the filter alone in the absence of cells, suggesting that the cell monolayer is acting as a barrier to prevent the nanoparticles from crossing the barrier (Ye et al. 2013; Bramini et al. 2014; Ragnaill et al. 2011). In addition, these studies suggest that active transport of nanoparticles across the cell monolayer is occurring to some extent. A limited transport of nanomaterials across the barrier was also observed using the murine cell line bEnd.3 exposed to GR and GO flakes

(Bramini et al. unpublished observations), suggesting that the barrier is actually acting like a barricade towards the flakes, being able to block the majority of them from reaching the basolateral chamber. Temperature-dependent transport assays can also be performed to investigate possible energy-dependent mechanisms through which nanoparticles are led through the barrier (Ye et al. 2013; Bramini et al. 2014; Ragnaill et al. 2011). A reduction of transport at low temperature would be indicative of an energy-dependent mechanism of translocation, even taking into account that the diffusion in liquids at 37 °C is roughly 2.5 times higher than at 4 °C. Thus, transwell models are indeed good tools to mimic BBB physiology, to be employed as a first method for screening nanoparticle transport through biological barriers. However, further investigations to understand the mechanisms of interaction of nanoparticles with cells are needed, especially at the cellular and molecular level.

2.3.3   Innovative In Vitro Approaches to Study the Interactions of Nanomaterials with the BBB

When working with in vitro transwell systems, one should be aware of the intrinsic limitations of the model, including the osmotic gradient, which is due to the vertical diffusion design of the system, and which might play a role in the transport of biomolecules from the apical to the basolateral compartments. Moreover, detailed and high-resolution cellular and molecular analysis of the transport mechanisms of the materials applied to the apparatus are not possible because of the physical features of the system (Beuckmann and Galla 1998). In addition, several technical issues that arise specifically for nanoparticles need to be carefully considered. Indeed, both technical limitations and barrier imperfections can originate unreliable results (Bramini et al. 2014), such as: (1) dye leakage from fluorescently labelled material (Salvati et al. 2011; Tenuta et al. 2011); (2) big fluorescent agglomerates in the basolateral compartment, which could impair the quantification of the nanomaterial crossing the cell monolayer, if such quantification is only based on fluorescence detection; (3) non-specific 'stickiness' of nanomaterials to the porous membrane, which may lead to an underestimation of the nanoparticle transport through the barrier; and (4) imperfections of the cell monolayer, such as regions not covered by cells, and/or and multi-layer areas.

To achieve a better understanding of the mechanisms of interactions between nanomaterials and cells, electron microscopy and confocal microscopy approaches are also carried out (Fig. 2d–f). The primary advantage of electron microscopy imaging is its powerful magnification, which can reach 50 pm [1 nm is the limit for biological samples; (Erni et al. 2009)]. However, these techniques can capture only snapshots of events that had been fixed in time, and what happened before or what will occur after that specific moment cannot be analysed. In this context, using fixed samples represents a limitation, especially when the kinetics of the events is of interest. This aspect can nowadays be approached by live cell imaging techniques such as spinning disc confocal microscopy and total internal reflection fluorescence

microscopy (TIRFM), which are usually applied in order to assess and visualize the capability of nanomaterials to cross the in vitro BBB, and to follow their localization in time and space in a qualitative and quantitative manner (Bramini et al. 2014). TIRFM allows observation of the localization and dynamics of molecules and processes in an optical section near the plasma membrane, usually between 20 and 300 nm (Toomre et al. 2000). This is advantageous for many biological events that take place in or close to the plasma membrane, such as nanoparticle translocation to the basolateral membrane of the BBB. Moreover, live-imaging approaches can be applied to microfluidic chip devices (Booth and Kim 2012) that combine porous membranes, similar to transwells, and shear stress, which plays an important role in BBB physiology (Cucullo et al. 2011). Thus, by using these techniques it is possible to combine kinetic studies with spatial information in live samples. 3D imaging reconstruction of the cell monolayer and nanoparticle identification, as well as nanoparticle trajectory identification, can be evaluated with advanced imaging processing software, ultimately giving a quantitative and qualitative overview of the interaction of nanoparticles with the BBB (Fig. 2g).

2.4   Graphene Flakes and the Brain: Safe or Unsafe?

The in vitro studies on primary neurons and glial cells described in this chapter have been fundamental to understand the physiological consequences of G flake exposure to CNS cell populations, showing that, albeit chronic exposure to GR/GO in solution does not cause cell death, it has a strong impact on a number of fundamental physiological processes, thus potentially leading to toxicity when administered for prolonged amounts of time. However, some characteristics of GO nano-flakes could be harnessed to restore pathological alterations in chronic neurodegenerative diseases or upon acute insults, for example, their ability to modulate astrocyte K^+ buffering, glutamate uptake and MV release, or their specific modulation of neuronal Ca^{2+} dynamics and synaptic activity. Based on the results described in this chapter, we can conclude that the lateral dimensions of G flakes are critical in defining the extent of material cytotoxicity. Moreover, its oxidative state determines the ability of flakes to perturb the normal homeostasis and network activity. Important aspects that still need to be addressed include the correlation between dimensionality, oxidative state and, unquestionably, G flake concentration. Given the heterogeneity of the GRMs on the market, such analysis will be challenging but nevertheless necessary to draw the complete picture of GRM biocompatibility.

For what concerns the interaction of GRMs with the BBB, research is still in its infancy and a lot of work is required to understand the short- and long-term effects of GRM exposure on the physiology of the barrier. Our unpublished observations suggest that GO and GR flakes in solution do not have overt toxic effects on the BBB structure, as the endothelium layer remains intact and functional up to 48 h of G exposure (Bramini et al. unpublished observations), while in vitro and in vivo studies indicate that rGO flakes are toxic to the barrier (Mendonca et al. 2016a, b).

Thus, once more, the intrinsic properties of the materials are crucial to determine their biocompatibility. In our opinion, the effects of nanomaterial accumulation into the BBB endothelium itself, rather than into the brain, have to be addressed, in particular for what concern the possible consequences of lysosomal accumulation. An aspect that is relatively unexplored is in fact the indirect mechanism(s) of nanomaterial-induced signalling across barriers, a topic that was pioneered by Dr. Case and colleagues at University of Bristol (Bhabra et al. 2009; Sood et al. 2011). By employing a variety of experimental systems including human corneal cells in vitro, human placenta ex vivo and mice in vivo, they showed that even if nanoparticles do not cross a barrier, they may still induce a signal that is transduced across the barrier and causes damage or metabolic changes to the cells on the other side. This mechanism could have significant repercussions for the nanosafety field at large, in particular as the rate of nanoparticle passage across the BBB is low, and it has been already demonstrated for polystyrene nanoparticles (Raghnaill et al. 2014). Hence, standard toxicity investigations are not enough to explore all the effects stemming from exposure of nanoparticles to cell barriers, and the possibility of nanoparticle-induced long-term and long-range paracrine signalling needs to be taken into consideration in future studies.

3 Two- and Three-Dimensional Biocompatible Scaffolds for Neuroregeneration

In the last years, neural tissue engineering has greatly progressed thanks to the advancements in biomaterial science research. In fact, the combination of different material forms and states, diverse chemical functionalization and the possible association with other biomaterials to form composites have greatly expanded the possibilities to engineer tissue-mimetic scaffolds. Two main approaches have been adopted in the field of regenerative medicine, i.e. (1) cell-based approaches based on cell transplantation and (2) endogenous cell stimulation. In the former case, the aim is to replace or induce the survival of injured cells, for example with the transplantation of embryonic stem cells (ESCs), induced pluripotent stem cell (iPSCs) and mesenchymal stem cells (MSCs) into the damaged area of the brain (Bang et al. 2005; Lerou and Daley 2005; Willerth 2011). Transplanted cells can directly repair the affected tissues, and also act indirectly by releasing soluble factors such as neurotrophins for neuronal growth and anti-inflammatory molecules. However, the efficacy of cell-based therapies has been hampered by poor cell survival and integration in the host tissue, largely due to the unfavourable environment around the damaged area (Halberstadt et al. 2006; Silva 2005). In the latter case, the delivery of bioactive molecules is used to promote neuroprotection. A long history of investigation has shown the beneficial effect of growth factors, including neurotrophins and anti-inflammatory agents, in preclinical studies for neurological diseases (Zhang et al. 2009; Victorio et al. 2010; Nagahara and

Tuszynski 2011). However, poor results have been obtained in clinical trials. The delivery of compounds to the brain has always been the main obstacle to the development of successful therapies. As discussed in the previous paragraphs, almost 98% of small molecules do not cross the BBB and therefore the systemic delivery of drugs (i.e. oral and intravenous) requires high range dosages to reach a therapeutic concentration in the central nervous system, which may lead to systemic side effects. Consequently, the systemic routes of administration have encountered limited applications.

In this scenario, natural or synthetic polymers in different formulations (gels, porous scaffolds and fibres) have been adapted for medical purposes to overcome these limitations. Biopolymer-based scaffolds provide an attractive approach for brain protection because of the multiplicity of materials and techniques available to make them suitable for specific uses. Biomaterials can be used to provide trophic support to damaged tissue, to deliver transplanted cells and neuroprotective compounds, including proteins and oligonucleotides (Srikanth and Kessler 2012). Extensive research efforts are currently devoted to the development of devices able to optimize several properties including the biocompatibility, biodegradability, bioactivity and the physical and mechanical features of the substrate. In this section, we discuss the importance of the topographical cues for scaffold design and highlight our recent studies about two- (2D) and three- (3D) dimensional scaffolds for in vitro applications with neuronal cultures.

3.1 Topographical Cues for Scaffold Design

Brain wiring is a complex process that begins during the development of the central nervous system and allows the formation of mature neuronal network. Neurons send out cell protrusions in response to orchestrated signals from the extracellular compartment and establish connections with neighbouring cells. The tight regulation of attractive and repulsive cues is necessary to guarantee the accuracy of circuit formation (Tessier-Lavigne and Goodman 1996). Amongst several players, the extracellular matrix (ECM) has crucial role in this process. All cells in solid tissues are in fact anchorage-dependent and sense cues residing in the ECM. ECM provides structural support as well as bioactive molecules to regulate cellular activity, and represent a highly regulated environment required for neuronal migration, polarization, differentiation and homeostasis (Barros et al. 2011). Studies have shown that the aberrant interaction between ECM and specific cellular receptors contributes to the onset and development of neurological diseases, including mental retardation, epilepsy and Alzheimer's disease (Dityatev and Schachner 2003; Dityatev et al. 2010; Gall and Lynch 2004). Thus, the engineering of scaffolds that mimic the native state of the ECM is a promising approach towards the treatment of these and other pathologies.

Cellular responses to the ECM are dictated by the biochemical and physical properties of the matrix, and in turn the composition of the ECM determines

the interaction with neuronal populations and subsequent cellular behaviour. To take advantage of specific cell–ECM interaction, ECM components have been incorporated in the engineered scaffolds. For instance, the adhesive peptide PHSRN found in fibronectin has been largely exploited for its ability to increase cell adhesion (Aota et al. 1994; Potter et al. 2008). Other investigators have used RGD (Arg-Gly-Asp), IKVAV (Ile-Lys-Val-Ala-Val) and YIGSR (Tyr-Ile-Gly-Ser-Arg) peptides to induce the differentiation of neural stem cells and neural cells in culture (Salinas and Anseth 2008; Sawyer et al. 2005; Kubinova et al. 2010; Callahan et al. 2013; Li et al. 2014).

In addition to the biochemical composition of ECM, the physical properties of the extracellular space regulate neuronal response (Hynes 2009). The ECM is endowed with both micro- and nano-scale features that are sensed by growth cone filopodia and influence cell adhesion, spreading, morphology and differentiation. Thus, modifying the scaffold topography may substantially affect neuronal behaviours. Over the past 15–20 years, a variety of topographical features (e.g. grooves, ridges, holes and pillars) have been largely investigated (Lietz et al. 2006; Schnell et al. 2007). Topographical effects are always strictly connected with the chemical properties of the materials and the origin of the neuronal cells under study; however, key concepts have been identified for the design of planar and three-dimensional devices.

3.2   Effect of Topography on Cell Adhesion and Morphology

A number of studies have shown a profound influence of micron-scale topography on the ability of cells to adhere and develop onto specific substrates. Micron-sized grooves and fibres have been incorporated into scaffolds made of different materials, including silicon (Khan et al. 2005), poly(lactic-co-glycolic acid) (PLGA) (Li et al. 2018) and poly(methyl methacrylate) (PMMA) (Johansson et al. 2006), and are amongst the most common continuous topographical features that have been employed to control cell attachment and shape. Grooved surfaces are typically manufactured according to a repeated pattern with equal groove and ridge widths and a set groove depth. Several observations have shown that primary neurons are able to interact with these surfaces and induce a response in terms of alignment and outgrowth. The majority of the cells show a parallel alignment along the major axis of the substrate, with their alignment and orientation enhanced when grating depth increases, suggesting the ability of growing neurites to perceive the geometry of the surrounding space (Chua et al. 2014; Miller et al. 2002).

At the 2D level, the influence of nanotopography on neuronal growth and development has been extensively studied. We have developed a nanopatterned biocompatible poly-ε-caprolactone (PCL) film, engineered through a novel fast-prototyping method involving a single-step plasma treatment (Cesca et al. 2014) (Fig. 3a). To evaluate the biocompatibility of this device, primary cortical neurons were grown on flat and nanopatterned substrates for 7 days, and the rate of cell death was lower for nanopatterned devices compared to flat surfaces (Fig. 3b). In
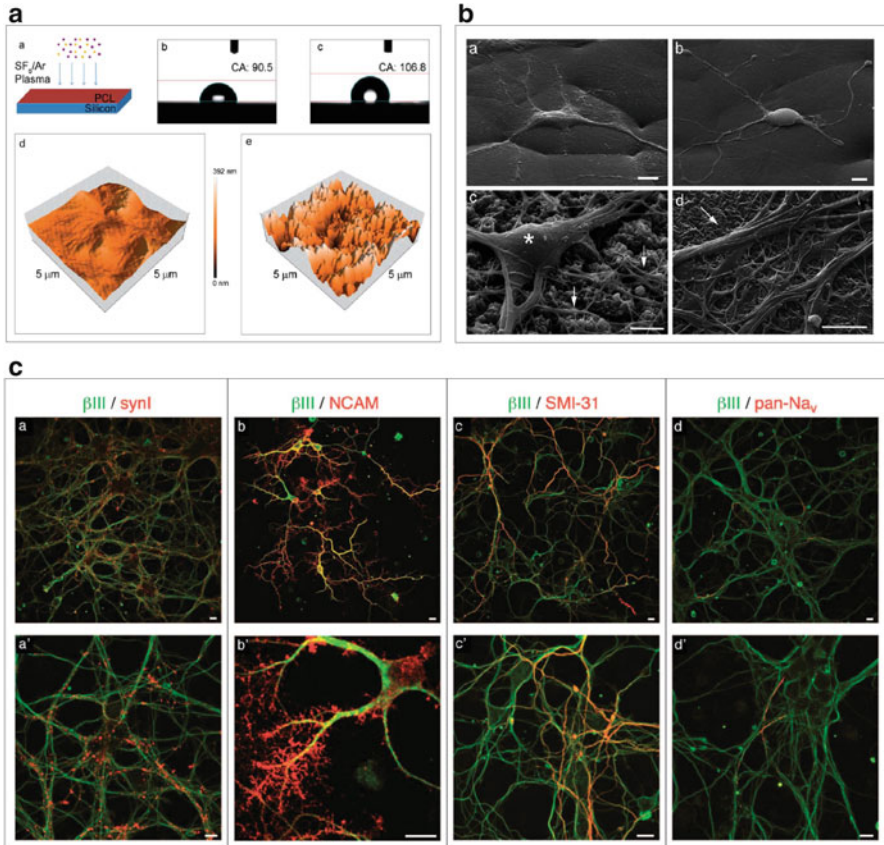
Fig. 3 (**a**) PCL nanopatterned surface fabrication and characterization. (*a*) Schematic view of the fast single-step plasma etching for the nano-texturing of PCL films. Surface water contact angle (*b*, *c*) and AFM measurements (*d*, *e*) of merely spin-coated (*b*, *d*) and nanopatterned (*c*, *e*) surfaces. (**b**) SEM images of primary hippocampal cultures plated on flat (*a*, *b*) and nanopatterned (*c*, *d*) PCL substrates. Cells were grown for 7 days, fixed and processed for SEM. Only few cells grew on flat films, forming a sparse network. On nanopatterned substrates, instead, neurons were healthy, as indicated by the smooth surface of cell bodies (asterisk) and by the dense network of neurites (arrows), which grew in tight adhesion with the substrate. Scale bars: 5 μm. (**c**) Confocal images of primary hippocampal cultures plated on nanopatterned PCL substrates at two magnifications (upper and lower rows). Neurons were grown for 7 days on the substrates, fixed and processed for confocal microscopy. A range of markers typically expressed in mature neuronal cultures were analysed, as indicated. βIII, neuronal class III β-tubulin (green channel in all panels); in the red channel: synI, synapsin I (*a*, *a′*); NCAM, neural cell adhesion molecule (*b*, *b′*); SMI-31, phosphorylated neurofilament heavy chain (*c*, *c′*); pan-Na_v. pan-voltage-gated Na^+ channels (*d*, *d′*). Neurons formed a rich network, characterized by a dense pattern of synaptic contacts (*a*, *a′*). Na_v localization was restricted to the axonal initial segment (*d*, *d′*), and neurons displayed differentiated axons (*c*, *c′*). NCAM-immunoreactivity (*b*, *b′*) was highly expressed all around the cell bodies and neurites, indicating a very strong adhesion of the cells to the substrates. Scale bars: 10 μm. All images are taken, with permission, from Cesca et al. (2014)

addition, the morphology of the cells was evaluated by immunostaining for the synaptic marker synapsin I, for the neural adhesion molecule NCAM and for the axonal marker SMI-31, showing that nanopatterned surfaces are effective to enhance the expression of neuronal markers and support the development and maturation of the neuronal network (Fig. 3c).

3.3 Effect of Topography on Migration

Efficient migration requires an asymmetric cell morphology consisting of a leading and a trailing edge, and specific molecular mechanisms are in place to guide cells along the desired direction. Neurons are able to integrate biochemical and biophysical signals, including soluble signals, adhesion molecules and substrate stiffness, to reach their final destination and correctly integrate into the appropriate morphological and functional circuit. In this context, surface topography contributes to the orientation of cell migration, mainly reducing sites of adhesion. Nano- and micro-fabricated devices with unique features have been developed to recapitulate or modify neuronal migration. For example, nano-patterning of polymethyl methacrylate (PMMA) silicon wafers, consisting of parallel grooves with a depth of 300 nm, widths of 100–400 nm and spacing of 100–1600 nm, was used to drive dorsal root ganglia (DRG) neuron growth. On these substrates, most axons displayed contact guidance on all patterns down to 100 nm, and preferred to grow on the ridge edges (Johansson et al. 2006). Moreover, nanofibres were used to tailor neuronal outgrowth. Corey and colleagues provided the first example of aligned outgrowth of neuronal processes from DRG and primary motor neurons grown onto poly-L-lactate (PLLA) nanofibres (Corey et al. 2007, 2008).

Micro-pillar-based topographies have also been exploited to provide insight into mechanisms of cell migration; in this case, the spatial distribution and size of pillars have been shown to affect the migrational behaviour of cells (Micholt et al. 2013; Repic et al. 2016). For instance, we have applied a combination of 3D topography and nanostructured surfaces to develop super-hydrophobic (SH) scaffolds made of teflon-like (C4F8) polymers (Limongi et al. 2013) (Fig. 4a). Surface wettability is considered one of the most important surface properties affecting the biocompatibility of an implanted material. Super-hydrophobicity is a largely studied and characterized phenomenon in which a drop placed on a surface adopts quasi-spherical shape with a contact angle greater than 150°. In the case of materials for biomedical applications, super-hydrophobicity minimizes the interaction between cells and substrate and promotes cell–cell interactions. Our SH devices presented a periodic hexagonal lattice of cylindrical pillars, whose sidewalls were nano-sculptured with a regular pattern of grooves. Primary neurons grown under SH conditions displayed a lower mortality rate at early stages in vitro, compared to neurons grown onto standard glass substrates. Both neuronal somas and their processes were suspended between adjacent nanopatterned pillars, likely due to the tension developed at the adhesion sites between neurons and the top
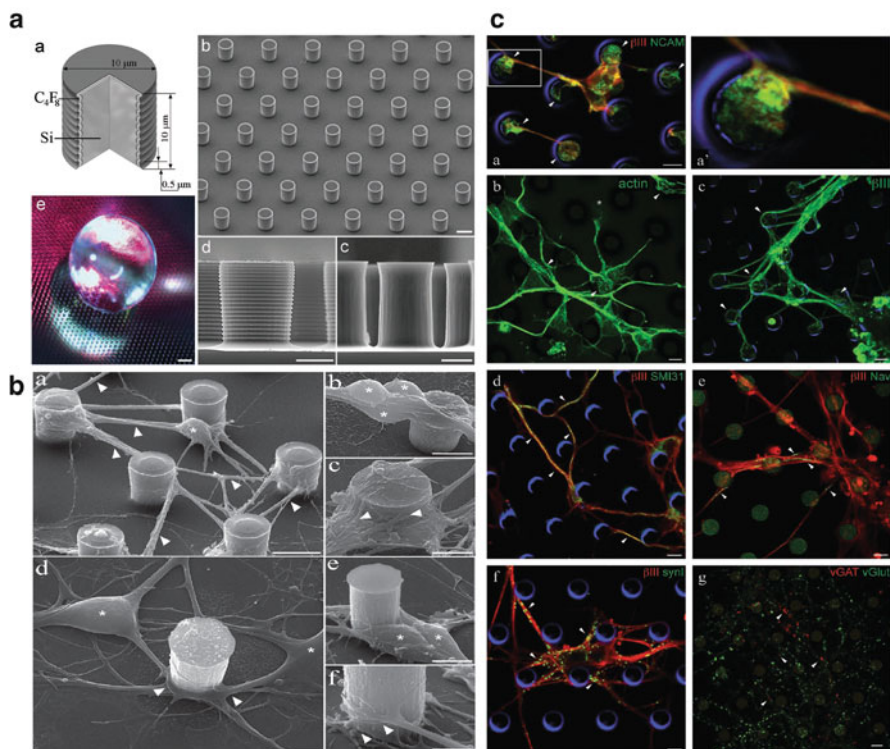
Fig. 4 (**a**) Construction details and high contact angle of the SH devices. (*a*) Compositional 3D section of a single nanopatterned pillar with technical drawings. SEM micrographs: (*b*) low magnification of the device surface (scale bar, 10 μm) and high magnification of the smooth (*c*) and nanopatterned (*d*) pillar sidewalls (scale bar, 5 μm). (*e*) Stereo microscope image of a drop that remains on the NSH surface keeping its shape and the contact angle constant. (**b**) Scanning electron micrographs of 3 DIV hippocampal neurons drop-plated on SH nanostructured (*a–c*) and smooth (*d–f*) pillared substrates. (*a*) Low magnification: both the neuronal somas (asterisk) and their processes, often organized in bundles (arrowheads), are suspended between adjacent nanostructured pillars. (*b*) Higher magnification of a small group of suspended neuronal cell bodies (asterisks) close to a pillar. (*c*) Neuronal projections from 3 DIV neurons densely wrap the pillar nanopatterned sidewall (arrowheads). (*d*) Low magnification of neuronal cell bodies (asterisks) and their processes (arrowheads) lying at the base of the smooth pillars. (*e*) A small group of neuronal cell bodies (asterisks) at the base of a pillar. (*f*) High magnification of neuronal processes attached to the base and the lower part of a smooth pillar (arrowheads). Scale bars: 10 μm (*a, d*), 5 μm (*b, c, e*) and 3 μm (*f*). (**c**) Immunocytochemical characterization of primary hippocampal cultures grown on nanostructured SH (NSH) substrates. Neurons were grown on NSH substrates for 3 (*a, a'*), 7 (*b, c*) or 10 (*d–g*) DIV, fixed and stained using the indicated antibodies. (*a*) A strong expression of the adhesion molecule NCAM (green) is detected in the regions of contact between the neurons and the pillars (arrowheads). (*a'*) Higher magnification of the boxed image in (*a*), showing the area of contact between a neurite and the pillar top. (*b, c*) Actin and βIII-tubulin cytoskeleton develops around the pillars (arrowheads). The asterisk in (*b*) indicates a growth cone. (*d, e*) SMI-31 staining indicated the presence of normally developed axons [arrowheads in (d)] bearing Na$^+$-channels correctly localized at the axonal initial segment [arrowheads in (e)]. (*f, g*) Cultures grown on NSH substrates develop synaptic connections labelled by the synaptic vesicle protein synapsin I [synI, arrowheads in (*f*)], and differentiate excitatory (vGlut-positive; green) and inhibitory (vGAT-positive; red) neurons. Arrowheads in (*g*) point to the synaptic terminals of inhibitory neurons. Scale bars, 10 μm. In the images where the patterned substrate was not clearly visible, the outline of the pillars was rendered in the blue channel. All images are taken, with permission, from Limongi et al. (2013)

surface of pillars, thus creating a true 3D network (Fig. 4b) characterized by the expression of several markers of mature neurons (Fig. 4c). The engineered devices also supported the growth of mixed-cell populations including neuronal and glial co-cultures. Hence, this 3D culture system represents a valuable tool to support the long-term growth and maintenance of neuronal cells. Compared to fibrous matrices, rigid 3D open scaffolds possess adequate stability to support neuronal growth and maturation, being able to face the mechanical forces that are typically experienced at the scaffold–cell interface. In addition, the restricted areas of adhesion on the pillared devices allow neurons to develop a 3D pattern of synaptic connections, free from the constraints imposed by the standard 2D substrates.

3.4 Effect of Topography on Neuronal Differentiation

Topographical stimuli play a critical role to guide neuronal differentiation. Therefore, an environment that mimics native interactions is required to study and modulate the differentiation process. A number of studies have shown that when employing nano-fibrous scaffolds, fibre diameter has a strong impact on adult neural stem/progenitor cell (NSC) differentiation and proliferation (Christopherson et al. 2009). As shown by Pan and colleagues, the size of grooves affects the ability of differentiation of hiPSCs towards the neuronal lineage (Pan et al. 2013). In another study, NSCs were grown on substrates with different topographies, in order to understand their influence on the differentiation of the overlying cultures. Interestingly, NSCs cultured on flat surfaces predominantly yielded astrocytes, whereas those cultured on multi-tubule conduit structures (30–90 μm in diameter) showed a dramatic increase in the expression of neuronal marker β-III tubulin compared to the conventional substrates, indicating a higher level of neuronal differentiation (Wang et al. 2010).

3.5 Effect of Topography on Drug Delivery

As described above, delivering molecules to the CNS is a challenging problem due to the presence of BBB and blood–spinal cord barrier (BSCB). Current research involves the development of natural and synthetic polymers to deliver therapeutic compounds directly into the brain and spinal cord. The manipulation of micro- and nanotopography represents a new tool in the field, with the potential to improve delivery techniques. According to this view, micro-fabricated polycaprolactone (PCL) devices have been optimized for the in vitro controlled release of brain-derived neurotrophic factor (BDNF) (Limongi et al. 2018). BDNF belongs to the family of neurotrophins and plays a critical role in neuronal survival, differentiation and synapse formation during development and throughout adulthood. Authors have developed 3D hydrophobic micropillared PCL (MP-PCL) scaffolds characterized

by micro- and nano-structured topography. The MP-PCL surface was designed as an array of cylindrical pillars of 10 μm in height and in diameter, arranged in a hexagonal lattice with periodicity of 30 μm with nano-thread sidewalls. The designed morphology promoted cell viability compared to control conditions, and importantly, it was characterized by enhanced drug delivery capability with respect to the monolithic unstructured supports. After incubation with BDNF, MP-PCL patterned devices progressively released the neurotrophin and increased neuronal survival. The ability of the described devices to influence all processes listed above makes them promising candidates for drug delivery, and to assist neural repair after mechanical or pathological injuries.

4   Conclusions

In this chapter, we have discussed some of the research lines currently under investigation to employ smart materials for biomedical applications, concentrating on the most promising approaches to target the central nervous system. For reasons of space, several issues have not been comprehensively addressed, including the possibility to functionalize nanoparticles and 2D/3D substrates with chemical cues, to facilitate the interaction with the biological matter and improve the biocompatibility minimizing toxic, non-wanted reactions and side effects. Smart materials, including GRMs, have the potential to play a crucial role for both neural tissue engineering and treatment and diagnosis of neurological diseases. However, before GRMs are routinely used to engineer sophisticated bio-sensing interfaces adaptable to the CNS, a detailed comprehension of the behaviour of such materials in a biological context is mandatory. To address this point, reliable in vitro models are fundamental before moving to in vivo applications. We have underlined which in our view are crucial prerequisites for in vitro neuroscience research on GRMs and nanomaterials in general, i.e. (1) the use of primary cells, as neural-like cell lines lack most of the mechanisms underlying neural excitability and synaptic transmission; (2) the use of fully characterized materials, to facilitate the reproducibility of experiments and data; (3) the accurate interpretation of the molecular and cellular mechanisms underlying the interaction between materials and cells, before in vivo experiments are designed and performed.

We have underlined the notion that topographical cues are extremely powerful tools to influence cell behaviour in terms of adhesion, morphology, migration and differentiation. In fact, geometrical features of scaffolds and supports cooperate with biochemical compounds to synergistically ameliorate the biological response. The recent development of micro-fabrication technologies has provided a range of robust techniques to modulate the cell–material interaction; however, several aspects related to the ability of cells—of neural cells in particular—to respond to topographical stimuli have not been yet elucidated. Amongst the most compelling issues to address, it will be crucial to identify the signal transduction pathways induced in the cell by the interaction with the surface of the material, and which

are the initial triggers of several biological effects. Second, the study of the interaction of neuronal cells with scaffolds will greatly benefit of the possibility to perform high-throughput analysis for the transcriptome (microarray analysis, RNAseq) and proteome (proteomic analysis). Last but not least, the influence of topographical cues on cell fate in vivo is still completely unexplored. A crucial point that future research will have to address is \pagebreak to transfer the large body of knowledge obtained from in vitro evidence to the in vivo context. A detailed elucidation of all these aspects will greatly improve our ability to engineer and select suitable materials and platforms for tissue engineering and regenerative medicine applications.

References

Abbott, N. J., Ronnback, L., & Hansson, E. (2006). Astrocyte-endothelial interactions at the blood-brain barrier. *Nature Reviews. Neuroscience, 7*(1), 41–53.

Aijaz, S., Balda, M. S., & Matter, K. (2006). Tight junctions: Molecular architecture and function. *International Review of Cytology, 248*, 261–298.

Akhavan, O., Ghaderi, E., & Akhavan, A. (2012). Size-dependent genotoxicity of graphene nanoplatelets in human stem cells. *Biomaterials, 33*(32), 8017–8025.

Allen, T. M., & Cullis, P. R. (2004). Drug delivery systems: Entering the mainstream. *Science, 303*(5665), 1818–1822.

Aota, S., Nomizu, M., & Yamada, K. M. (1994). The short amino acid sequence Pro-His-Ser-Arg-Asn in human fibronectin enhances cell-adhesive function. *The Journal of Biological Chemistry, 269*(40), 24756–24761.

Bang, O. Y., Lee, J. S., Lee, P. H., & Lee, G. (2005). Autologous mesenchymal stem cell transplantation in stroke patients. *Annals of Neurology, 57*(6), 874–882.

Barros, C. S., Franco, S. J., & Muller, U. (2011). Extracellular matrix: Functions in the nervous system. *Cold Spring Harbor Perspectives in Biology, 3*(1), a005108.

Beuckmann, C. T., & Galla, H.-J. (1998). Tissue culture of brain endothelial cells—induction of blood-brain barrier properties by brain factors. In W. M. Pardridge (Ed.), *Introduction to the blood-brain barrier*. Cambridge: Cambridge University Press.

Bhabra, G., Sood, A., Fisher, B., Cartwright, L., Saunders, M., Evans, W. H., et al. (2009). Nanoparticles can cause DNA damage across a cellular barrier. *Nature Nanotechnology, 4*(12), 876–883.

Bianco, A. (2013). Graphene: Safe or toxic? The two faces of the medal. *Angewandte Chemie, 52*(19), 4986–4997.

Bicker, J., Alves, G., Fortuna, A., & Falcao, A. (2014). Blood-brain barrier models and their relevance for a successful development of CNS drug delivery systems: A review. *European Journal of Pharmaceutics and Biopharmaceutics, 87*(3), 409–432.

Booth, R., & Kim, H. (2012). Characterization of a microfluidic in vitro model of the blood-brain barrier (muBBB). *Lab on a Chip, 12*(10), 1784–1792.

Bramini, M., Alberini, G., Colombo, E., Chiacchiaretta, M., DiFrancesco, M. L., Maya-Vetencourt, J. F., et al. (2018). Interfacing graphene-based materials with neural cells. *Frontiers in Systems Neuroscience, 12*, 12.

Bramini, M., Sacchetti, S., Armirotti, A., Rocchi, A., Vazquez, E., Leon Castellanos, V., et al. (2016). Graphene oxide nanosheets disrupt lipid composition, Ca(2+) homeostasis, and synaptic transmission in primary cortical neurons. *ACS Nano, 10*(7), 7154–7171.

Bramini, M., Ye, D., Hallerbach, A., Nic Raghnaill, M., Salvati, A., Aberg, C., et al. (2014). Imaging approach to mechanistic study of nanoparticle interactions with the blood-brain barrier. *ACS Nano, 8*(5), 4304–4312.

Bussy, C., & Kostarelos, K. (2017). Culture media critically influence graphene oxide effects on plasma membranes. *Chem, 2*(3), 322–323.

Butt, A. M., & Jones, H. C. (1992). Effect of histamine and antagonists on electrical resistance across the blood-brain barrier in rat brain-surface microvessels. *Brain Research, 569*(1), 100–105.

Callahan, L. A., Xie, S., Barker, I. A., Zheng, J., Reneker, D. H., Dove, A. P., et al. (2013). Directed differentiation and neurite extension of mouse embryonic stem cell on aligned poly(lactide) nanofibers functionalized with YIGSR peptide. *Biomaterials, 34*(36), 9089–9095.

Cesca, F., Limongi, T., Accardo, A., Rocchi, A., Orlando, M., Shalabaeva, V., et al. (2014). Fabrication of biocompatible free-standing nanopatterned films for primary neuronal cultures. *RSC Advances, 4*(86), 45696–45702.

Chen, G. Y., Chen, C. L., Tuan, H. Y., Yuan, P. X., Li, K. C., Yang, H. J., et al. (2014). Graphene oxide triggers toll-like receptors/autophagy responses in vitro and inhibits tumor growth in vivo. *Advanced Healthcare Materials, 3*(9), 1486–1495.

Chen, Y., Star, A., & Vidal, S. (2013). Sweet carbon nanostructures: Carbohydrate conjugates with carbon nanotubes and graphene and their applications. *Chemical Society Reviews, 42*(11), 4532–4542.

Cheng, C. L., Li, S., Thomas, A., Kotov, A. N., & Haag, R. (2016). Functional graphene nanomaterials based architectures: Biointeractions, fabrications, and emerging biological applications. *Chemical Reviews, 117*(3), 1826–1914.

Chiacchiaretta, M., Bramini, M., Rocchi, A., Armirotti, A., Giordano, E., Vázquez, E., et al. (2018, Aug 15). Graphene oxide upregulates the homeostatic functions of primary astrocytes and modulates astrocyte-to-neuron communication. *Nano Letters*. https://doi.org/10.1021/acs.nanolett.8b02487

Chong, Y., Ge, C., Yang, Z., Garate, J. A., Gu, Z., Weber, J. K., et al. (2015). Reduced cytotoxicity of graphene nanosheets mediated by blood-protein coating. *ACS Nano, 9*(6), 5713–5724.

Christopherson, G. T., Song, H., & Mao, H. Q. (2009). The influence of fiber diameter of electrospun substrates on neural stem cell differentiation and proliferation. *Biomaterials, 30*(4), 556–564.

Chua, J. S., Chng, C. P., Moe, A. A., Tann, J. Y., Goh, E. L., Chiam, K. H., et al. (2014). Extending neurites sense the depth of the underlying topography during neuronal differentiation and contact guidance. *Biomaterials, 35*(27), 7750–7761.

Corey, J. M., Gertz, C. C., Wang, B. S., Birrell, L. K., Johnson, S. L., Martin, D. C., et al. (2008). The design of electrospun PLLA nanofiber scaffolds compatible with serum-free growth of primary motor and sensory neurons. *Acta Biomaterialia, 4*(4), 863–875.

Corey, J. M., Lin, D. Y., Mycek, K. B., Chen, Q., Samuel, S., Feldman, E. L., et al. (2007). Aligned electrospun nanofibers specify the direction of dorsal root ganglia neurite growth. *Journal of Biomedical Materials Research. Part A, 83*(3), 636–645.

Crone, C., & Olesen, S. P. (1982). Electrical resistance of brain microvascular endothelium. *Brain Research, 241*(1), 49–55.

Cucullo, L., Hossain, M., Puvenna, V., Marchi, N., & Janigro, D. (2011). The role of shear stress in blood-brain barrier endothelial physiology. *BMC Neuroscience, 12*, 40.

Defterali, C., Verdejo, R., Majeed, S., Boschetti-de-Fierro, A., Mendez-Gomez, H. R., Diaz-Guerra, E., et al. (2016). In vitro evaluation of biocompatibility of uncoated thermally reduced graphene and carbon nanotube-loaded PVDF membranes with adult neural stem cell-derived neurons and glia. *Frontiers in Bioengineering and Biotechnology, 4*, 94.

Dell'Orco, D., Lundqvist, M., Oslakovic, C., Cedervall, T., & Linse, S. (2010). Modeling the time evolution of the nanoparticle-protein corona in a body fluid. *PLoS One, 5*(6), e10949.

Dityatev, A., & Schachner, M. (2003). Extracellular matrix molecules and synaptic plasticity. *Nature Reviews. Neuroscience, 4*(6), 456–468.

Dityatev, A., Seidenbecher, C. I., & Schachner, M. (2010). Compartmentalization from the outside: The extracellular matrix and functional microdomains in the brain. *Trends in Neurosciences, 33*(11), 503–512.

Donaldson, K., Aitken, R., Tran, L., Stone, V., Duffin, R., Forrest, G., et al. (2006). Carbon nanotubes: A review of their properties in relation to pulmonary toxicology and workplace safety. *Toxicological Sciences, 92*(1), 5–22.

Erni, R., Rossell, M. D., Kisielowski, C., & Dahmen, U. (2009). Atomic-resolution imaging with a sub-50-pm electron probe. *Physical Review Letters, 102*(9), 096101.

European Commission PH. (2006). *Nanotechnologies*. http://ec.europa.eu/health/scientific_committees/opinions_layman/fr/nanotechnologies/l-3/1-introduction.htm

Fahmi, T., Branch, D., Nima, Z. A., Jang, D. S., Savenka, A. V., Biris, A. S., et al. (2017). Mechanism of graphene-induced cytotoxicity: Role of endonucleases. *Journal of Applied Toxicology, 37*(11), 1325–1332.

Fitch, M. T., & Silver, J. (2008). CNS injury, glial scars, and inflammation: Inhibitory extracellular matrices and regeneration failure. *Experimental Neurology, 209*(2), 294–301.

Gaffaney, J. D., Dunning, F. M., Wang, Z., Hui, E., & Chapman, E. R. (2008). Synaptotagmin C2B domain regulates Ca2+-triggered fusion in vitro: Critical residues revealed by scanning alanine mutagenesis. *The Journal of Biological Chemistry, 283*(46), 31763–31775.

Gall, C. M., & Lynch, G. (2004). Integrins, synaptic plasticity and epileptogenesis. *Advances in Experimental Medicine and Biology, 548*, 12–33.

Georgakilas, V., Tiwari, J. N., Kemp, K. C., Perman, J. A., Bourlinos, A. B., Kim, K. S., et al. (2016). Noncovalent functionalization of graphene and graphene oxide for energy materials, biosensing, catalytic, and biomedical applications. *Chemical Reviews, 116*(9), 5464–5519.

Goenka, S., Sant, V., & Sant, S. (2014). Graphene-based nanomaterials for drug delivery and tissue engineering. *Journal of Controlled Release, 173*, 75–88.

Gottipati, M. K., Bekyarova, E., Brenner, M., Haddon, R. C., & Parpura, V. (2014). Changes in the morphology and proliferation of astrocytes induced by two modalities of chemically functionalized single-walled carbon nanotubes are differentially mediated by glial fibrillary acidic protein. *Nano Letters, 14*(7), 3720–3727.

Halberstadt, C., Emerich, D. F., & Gonsalves, K. (2006). Combining cell therapy and nanotechnology. *Expert Opinion on Biological Therapy, 6*(10), 971–981.

Hubatsch, I., Ragnarsson, E. G., & Artursson, P. (2007). Determination of drug permeability and prediction of drug absorption in Caco-2 monolayers. *Nature Protocols, 2*(9), 2111–2119.

Hynes, R. O. (2009). The extracellular matrix: Not just pretty fibrils. *Science, 326*(5957), 1216–1219.

Johansson, F., Carlberg, P., Danielsen, N., Montelius, L., & Kanje, M. (2006). Axonal outgrowth on nano-imprinted patterns. *Biomaterials, 27*(8), 1251–1258.

John, A. A., Subramanian, A. P., Vellayappan, M. V., Balaji, A., Mohandas, H., & Jaganathan, S. K. (2015). Carbon nanotubes and graphene as emerging candidates in neuroregeneration and neurodrug delivery. *International Journal of Nanomedicine, 10*, 4267–4277.

Ketabi-Kiyanvash, N., Herold-Mende, C., Kashfi, F., Caldeira, S., Tommasino, M., Haefeli, W. E., et al. (2007). NKIM-6, a new immortalized human brain capillary endothelial cell line with conserved endothelial characteristics. *Cell and Tissue Research, 328*(1), 19–29.

Khan, S. P., Auner, G. G., & Newaz, G. M. (2005). Influence of nanoscale surface roughness on neural cell attachment on silicon. *Nanomedicine, 1*(2), 125–129.

Krause, G., Winkler, L., Mueller, S. L., Haseloff, R. F., Piontek, J., & Blasig, I. E. (2008). Structure and function of claudins. *Biochimica et Biophysica Acta, 1778*(3), 631–645.

Kubinova, S., Horak, D., Kozubenko, N., Vanecek, V., Proks, V., Price, J., et al. (2010). The use of superporous Ac-CGGASIKVAVS-OH-modified PHEMA scaffolds to promote cell adhesion and the differentiation of human fetal neural precursors. *Biomaterials, 31*(23), 5966–5975.

Kurapati, R., Backes, C., Menard-Moyon, C., Coleman, J. N., & Bianco, A. (2016). White graphene undergoes peroxidase degradation. *Angewandte Chemie, 55*(18), 5506–5511.

Kusch-Poddar, M., Drewe, J., Fux, I., & Gutmann, H. (2005). Evaluation of the immortalized human brain capillary endothelial cell line BB19 as a human cell culture model for the blood-brain barrier. *Brain Research, 1064*(1-2), 21–31.

Lerou, P. H., & Daley, G. Q. (2005). Therapeutic potential of embryonic stem cells. *Blood Reviews, 19*(6), 321–331.

Li, C. W., Davis, B., Shea, J., Sant, H., Gale, B. K., & Agarwal, J. (2018). Optimization of micropatterned poly(lactic-co-glycolic acid) films for enhancing dorsal root ganglion cell orientation and extension. *Neural Regeneration Research, 13*(1), 105–111.

Li, X., Liu, X., Josey, B., Chou, C. J., Tan, Y., Zhang, N., et al. (2014). Short laminin peptide for improved neural stem cell growth. *Stem Cells Translational Medicine, 3*(5), 662–670.

Liao, K. H., Lin, Y. S., Macosko, C. W., & Haynes, C. L. (2011). Cytotoxicity of graphene oxide and graphene in human erythrocytes and skin fibroblasts. *ACS Applied Materials and Interfaces, 3*(7), 2607–2615.

Lietz, M., Dreesmann, L., Hoss, M., Oberhoffner, S., & Schlosshauer, B. (2006). Neuro tissue engineering of glial nerve guides and the impact of different cell types. *Biomaterials, 27*(8), 1425–1436.

Lim, M. H., Jeung, I. C., Jeong, J., Yoon, S. J., Lee, S. H., Park, J., et al. (2016). Graphene oxide induces apoptotic cell death in endothelial cells by activating autophagy via calcium-dependent phosphorylation of c-Jun N-terminal kinases. *Acta Biomaterialia, 46*, 191–203.

Limongi, T., Cesca, F., Gentile, F., Marotta, R., Ruffilli, R., Barberis, A., et al. (2013). Nanostructured superhydrophobic substrates trigger the development of 3D neuronal networks. *Small, 9*(3), 402–412.

Limongi, T., Rocchi, A., Cesca, F., Tan, H., Miele, E., Giugni, A., et al. (2018). Delivery of brain-derived neurotrophic factor by 3D biocompatible polymeric scaffolds for neural tissue engineering and neuronal regeneration. *Molecular Neurobiology, 55*(12), 8788–8798.

Liu, G., Shen, H., Mao, J., Zhang, L., Jiang, Z., Sun, T., et al. (2013). Transferrin modified graphene oxide for glioma-targeted drug delivery: In vitro and in vivo evaluations. *ACS Applied Materials and Interfaces, 5*(15), 6909–6914.

Manzoli, F. A., Barbieri, M., & Carinci, P. (1969). Lipid composition of brain synaptic vesicle fraction. *Acta Anatomica Supplementum (Basel)*, (56), 283–292.

Mattei, T. A., & Rehman, A. A. (2014). Technological developments and future perspectives on graphene-based metamaterials: A primer for neurosurgeons. *Neurosurgery, 74*(5), 499–516. Discussion.

McCallion, C., Burthem, J., Rees-Unwin, K., Golovanov, A., & Pluen, A. (2016). Graphene in therapeutics delivery: Problems, solutions and future opportunities. *European Journal of Pharmaceutics and Biopharmaceutics, 104*, 235–250.

Mendonca, M. C., Soares, E. S., de Jesus, M. B., Ceragioli, H. J., Batista, A. G., Nyul-Toth, A., et al. (2016b). PEGylation of reduced graphene oxide induces toxicity in cells of the blood-brain barrier: An in vitro and in vivo study. *Molecular Pharmaceutics, 13*(11), 3913–3924.

Mendonca, M. C., Soares, E. S., de Jesus, M. B., Ceragioli, H. J., Irazusta, S. P., Batista, A. G., et al. (2016a). Reduced graphene oxide: Nanotoxicological profile in rats. *J Nanobiotechnology., 14*(1), 53.

Micholt, L., Gartner, A., Prodanov, D., Braeken, D., Dotti, C. G., & Bartic, C. (2013). Substrate topography determines neuronal polarization and growth in vitro. *PLoS One, 8*(6), e66170.

Miller, C., Jeftinija, S., & Mallapragada, S. (2002). Synergistic effects of physical and chemical guidance cues on neurite alignment and outgrowth on biodegradable polymer substrates. *Tissue Engineering, 8*(3), 367–378.

Mittal, S., Kumar, V., Dhiman, N., Chauhan, L. K., Pasricha, R., & Pandey, A. K. (2016). Physico-chemical properties based differential toxicity of graphene oxide/reduced graphene oxide in human lung cells mediated through oxidative stress. *Scientific Reports, 6*, 39548.

Morita, S. Y., Shirakawa, S., Kobayashi, Y., Nakamura, K., Teraoka, R., Kitagawa, S., et al. (2012). Enzymatic measurement of phosphatidylserine in cultured cells. *Journal of Lipid Research, 53*(2), 325–330.

Mu, Q., Su, G., Li, L., Gilbertson, B. O., Yu, L. H., Zhang, Q., et al. (2012). Size-dependent cell uptake of protein-coated graphene oxide nanosheets. *ACS Applied Materials and Interfaces, 4*(4), 2259–2266.

Murphy, D. D., Cole, N. B., Greenberger, V., & Segal, M. (1998). Estradiol increases dendritic spine density by reducing GABA neurotransmission in hippocampal neurons. *The Journal of Neuroscience, 18*(7), 2550–2559.

Nagahara, A. H., & Tuszynski, M. H. (2011). Potential therapeutic uses of BDNF in neurological and psychiatric disorders. *Nature Reviews. Drug Discovery, 10*(3), 209–219.

Nakagawa, S., Deli, M. A., Kawaguchi, H., Shimizudani, T., Shimono, T., Kittel, A., et al. (2009). A new blood-brain barrier model using primary rat brain endothelial cells, pericytes and astrocytes. *Neurochemistry International, 54*(3-4), 253–263.

Navone, S. E., Marfia, G., Invernici, G., Cristini, S., Nava, S., Balbi, S., et al. (2013). Isolation and expansion of human and mouse brain microvascular endothelial cells. *Nature Protocols, 8*(9), 1680–1693.

Nelson, G. J., & Freeman, N. K. (1960). The phospholipid and phospholipid fatty acid composition of human serum lipoprotein fractions. *The Journal of Biological Chemistry, 235*, 578–583.

Ogunshola, O. O. (2011). In vitro modeling of the blood-brain barrier: Simplicity versus complexity. *Current Pharmaceutical Design, 17*(26), 2755–2761.

Ohno, K., Pettigrew, K. D., & Rapoport, S. I. (1978). Lower limits of cerebrovascular permeability to nonelectrolytes in the conscious rat. *The American Journal of Physiology, 235*(3), H299–H307.

Omidi, Y., Campbell, L., Barar, J., Connell, D., Akhtar, S., & Gumbleton, M. (2003). Evaluation of the immortalised mouse brain capillary endothelial cell line, b.End3, as an in vitro blood-brain barrier model for drug uptake and transport studies. *Brain Research, 990*(1-2), 95–112.

Ou, L., Song, B., Liang, H., Liu, J., Feng, X., Deng, B., et al. (2016). Toxicity of graphene-family nanoparticles: A general review of the origins and mechanisms. *Particle and Fibre Toxicology, 13*(1), 57.

Pan, F., Zhang, M., Wu, G., Lai, Y., Greber, B., Scholer, H. R., et al. (2013). Topographic effect on human induced pluripotent stem cells differentiation towards neuronal lineage. *Biomaterials, 34*(33), 8131–8139.

Pelin, M., Fusco, L., Leon, V., Martin, C., Criado, A., Sosa, S., et al. (2017). Differential cytotoxic effects of graphene and graphene oxide on skin keratinocytes. *Scientific Reports, 7*, 40572.

Poller, B., Gutmann, H., Krahenbuhl, S., Weksler, B., Romero, I., Couraud, P. O., et al. (2008). The human brain endothelial cell line hCMEC/D3 as a human blood-brain barrier model for drug transport studies. *Journal of Neurochemistry, 107*(5), 1358–1368.

Polli, J. E. (2008). In vitro studies are sometimes better than conventional human pharmacokinetic in vivo studies in assessing bioequivalence of immediate-release solid oral dosage forms. *The AAPS Journal, 10*(2), 289–299.

Potter, W., Kalil, R. E., & Kao, W. J. (2008). Biomimetic material systems for neural progenitor cell-based therapy. *Frontiers in Bioscience, 13*, 806–821.

Prudhomme, J. G., Sherman, I. W., Land, K. M., Moses, A. V., Stenglein, S., & Nelson, J. A. (1996). Studies of plasmodium falciparum cytoadherence using immortalized human brain capillary endothelial cells. *International Journal for Parasitology, 26*(6), 647–655.

Raghnaill, M. N., Bramini, M., Ye, D., Couraud, P. O., Romero, I. A., Weksler, B., et al. (2014). Paracrine signalling of inflammatory cytokines from an in vitro blood brain barrier model upon exposure to polymeric nanoparticles. *The Analyst., 139*(5), 923–930.

Ragnaill, M. N., Brown, M., Ye, D., Bramini, M., Callanan, S., Lynch, I., et al. (2011). Internal benchmarking of a human blood-brain barrier cell model for screening of nanoparticle uptake and transcytosis. *European Journal of Pharmaceutics and Biopharmaceutics, 77*(3), 360–367.

Rauti, R., Lozano, N., Leon, V., Scaini, D., Musto, M., Rago, I., et al. (2016). Graphene oxide nanosheets reshape synaptic function in cultured brain networks. *ACS Nano, 10*(4), 4459–4471.

Regina, A., Romero, I. A., Greenwood, J., Adamson, P., Bourre, J. M., Couraud, P. O., et al. (1999). Dexamethasone regulation of P-glycoprotein activity in an immortalized rat brain endothelial cell line, GPNT. *Journal of Neurochemistry, 73*(5), 1954–1963.

Reichel, A., Begley, D. J., & Abbott, N. J. (2003). An overview of in vitro techniques for blood-brain barrier studies. *Methods in Molecular Medicine, 89*, 307–324.

Reina, G., Gonzalez-Dominguez, J. M., Criado, A., Vazquez, E., Bianco, A., & Prato, M. (2017). Promises, facts and challenges for graphene in biomedical applications. *Chemical Society Reviews, 46*(15), 4400–4416.

Repic, T., Madirazza, K., Bektur, E., & Sapunar, D. (2016). Characterization of dorsal root ganglion neurons cultured on silicon micro-pillar substrates. *Scientific Reports, 6*, 39560.

Roux, F., Durieu-Trautmann, O., Chaverot, N., Claire, M., Mailly, P., Bourre, J. M., et al. (1994). Regulation of gamma-glutamyl transpeptidase and alkaline phosphatase activities in immortalized rat brain microvessel endothelial cells. *Journal of Cellular Physiology, 159*(1), 101–113.

Salinas, C. N., & Anseth, K. S. (2008). The influence of the RGD peptide motif and its contextual presentation in PEG gels on human mesenchymal stem cell viability. *Journal of Tissue Engineering and Regenerative Medicine, 2*(5), 296–304.

Salvati, A., Aberg, C., dos Santos, T., Varela, J., Pinto, P., Lynch, I., et al. (2011). Experimental and theoretical comparison of intracellular import of polymeric nanoparticles and small molecules: Toward models of uptake kinetics. *Nanomedicine, 7*(6), 818–826.

Sandin, P., Fitzpatrick, L. W., Simpson, J. C., & Dawson, K. A. (2012). High-speed imaging of Rab family small GTPases reveals rare events in nanoparticle trafficking in living cells. *ACS Nano, 6*(2), 1513–1521.

Sawyer, A. A., Hennessy, K. M., & Bellis, S. L. (2005). Regulation of mesenchymal stem cell attachment and spreading on hydroxyapatite by RGD peptides and adsorbed serum proteins. *Biomaterials, 26*(13), 1467–1475.

Schnell, E., Klinkhammer, K., Balzer, S., Brook, G., Klee, D., Dalton, P., et al. (2007). Guidance of glial cell migration and axonal growth on electrospun nanofibers of poly-epsilon-caprolactone and a collagen/poly-epsilon-caprolactone blend. *Biomaterials, 28*(19), 3012–3025.

Seabra, A. B., Paula, A. J., de Lima, R., Alves, O. L., & Duran, N. (2014). Nanotoxicity of graphene and graphene oxide. *Chemical Research in Toxicology, 27*(2), 159–168.

Silliman, C. C., & Wang, M. (2006). The merits of in vitro versus in vivo modeling in investigation of the immune system. *Environmental Toxicology and Pharmacology, 21*(2), 123–134.

Silva, G. A. (2005). Nanotechnology approaches for the regeneration and neuroprotection of the central nervous system. *Surgical Neurology, 63*(4), 301–306.

Smith, Q. R., & Rapoport, S. I. (1986). Cerebrovascular permeability coefficients to sodium, potassium, and chloride. *Journal of Neurochemistry, 46*(6), 1732–1742.

Sood, A., Salih, S., Roh, D., Lacharme-Lora, L., Parry, M., Hardiman, B., et al. (2011). Signalling of DNA damage and cytokines across cell barriers exposed to nanoparticles depends on barrier thickness. *Nature Nanotechnology, 6*(12), 824–833.

Srikanth, M., & Kessler, J. A. (2012). Nanotechnology-novel therapeutics for CNS disorders. *Nature Reviews. Neurology, 8*(6), 307–318.

Takeshita, Y., Obermeier, B., Cotleur, A., Sano, Y., Kanda, T., & Ransohoff, R. M. (2014). An in vitro blood-brain barrier model combining shear stress and endothelial cell/astrocyte co-culture. *Journal of Neuroscience Methods, 232*, 165–172.

Tenuta, T., Monopoli, M. P., Kim, J., Salvati, A., Dawson, K. A., Sandin, P., et al. (2011). Elution of labile fluorescent dye from nanoparticles during biological use. *PLoS One, 6*(10), e25556.

Tessier-Lavigne, M., & Goodman, C. S. (1996). The molecular biology of axon guidance. *Science, 274*(5290), 1123–1133.

Tian, X., Yang, Z., Duan, G., Wu, A., Gu, Z., Zhang, L., et al. (2017). Graphene oxide nanosheets retard cellular migration via disruption of actin cytoskeleton. *Small, 13*(3). https://doi.org/10.1002/smll.201602133

Toomre, D., Steyer, J. A., Keller, P., Almers, W., & Simons, K. (2000). Fusion of constitutive membrane traffic with the cell surface observed by evanescent wave microscopy. *The Journal of Cell Biology, 149*(1), 33–40.

Tu, Q., Pang, L., Chen, Y., Zhang, Y., Zhang, R., Lu, B., et al. (2014). Effects of surface charges of graphene oxide on neuronal outgrowth and branching. *The Analyst., 139*(1), 105–115.

Upadhyay, R. K. (2014). Drug delivery systems, CNS protection, and the blood brain barrier. *BioMed Research International, 2014*, 869269.

Victorio, S. C., Havton, L. A., & Oliveira, A. L. (2010). Absence of IFNgamma expression induces neuronal degeneration in the spinal cord of adult mice. *Journal of Neuroinflammation, 7*, 77.

Vu, K., Weksler, B., Romero, I., Couraud, P. O., & Gelli, A. (2009). Immortalized human brain endothelial cell line HCMEC/D3 as a model of the blood-brain barrier facilitates in vitro studies of central nervous system infection by Cryptococcus neoformans. *Eukaryotic Cell, 8*(11), 1803–1807.

Wang, G., Ao, Q., Gong, K., Wang, A., Zheng, L., Gong, Y., et al. (2010). The effect of topology of chitosan biomaterials on the differentiation and proliferation of neural stem cells. *Acta Biomaterialia, 6*(9), 3630–3639.

Weerth, S. H., Holtzclaw, L. A., & Russell, J. T. (2007). Signaling proteins in raft-like microdomains are essential for Ca2+ wave propagation in glial cells. *Cell Calcium, 41*(2), 155–167.

Weksler, B. B., Subileau, E. A., Perriere, N., Charneau, P., Holloway, K., Leveque, M., et al. (2005). Blood-brain barrier-specific properties of a human adult brain endothelial cell line. *The FASEB Journal, 19*(13), 1872–1874.

Wick, P., Louw-Gaume, A. E., Kucki, M., Krug, H. F., Kostarelos, K., Fadeel, B., et al. (2014). Classification framework for graphene-based materials. *Angewandte Chemie, 53*(30), 7714–7718.

Willerth, S. M. (2011). Neural tissue engineering using embryonic and induced pluripotent stem cells. *Stem Cell Research and Therapy, 2*(2), 17.

Wolff, A., Antfolk, M., Brodin, B., & Tenje, M. (2015). In vitro blood-brain barrier models—an overview of established models and new microfluidic approaches. *Journal of Pharmaceutical Sciences, 104*(9), 2727–2746.

Yang, L., Wang, F., Han, H., Yang, L., Zhang, G., & Fan, Z. (2015). Functionalized graphene oxide as a drug carrier for loading pirfenidone in treatment of subarachnoid hemorrhage. *Colloids and Surfaces. B, Biointerfaces, 129*, 21–29.

Ye, D., Raghnaill, M. N., Bramini, M., Mahon, E., Aberg, C., Salvati, A., et al. (2013). Nanoparticle accumulation and transcytosis in brain endothelial cell layers. *Nanoscale, 5*(22), 11153–11165.

Zensi, A., Begley, D., Pontikis, C., Legros, C., Mihoreanu, L., Wagner, S., et al. (2009). Albumin nanoparticles targeted with Apo E enter the CNS by transcytosis and are delivered to neurones. *Journal of Controlled Release, 137*(1), 78–86.

Zhang, L., Ma, Z., Smith, G. M., Wen, X., Pressman, Y., Wood, P. M., et al. (2009). GDNF-enhanced axonal regeneration and myelination following spinal cord injury is mediated by primary effects on neurons. *Glia, 57*(11), 1178–1191.

Zhang, X., Yin, J., Peng, C., Hu, W., Zhu, Z., Li, W., et al. (2011). Distribution and biocompatibility studies of graphene oxide in mice after intravenous administration. *Carbon, 49*, 986–995.

Zhou, H., Zhao, K., Li, W., Yang, N., Liu, Y., Chen, C., et al. (2012). The interactions between pristine graphene and macrophages and the production of cytokines/chemokines via TLR- and NF-kappaB-related signaling pathways. *Biomaterials, 33*(29), 6933–6942.

Part II
Recording Techniques

Large-Scale, High-Resolution Microelectrode Arrays for Interrogation of Neurons and Networks

Marie Engelene J. Obien and Urs Frey

Abstract High-density microelectrode arrays (HD-MEAs) are increasingly being used for the observation and manipulation of neurons and networks in vitro. Large-scale electrode arrays allow for long-term extracellular recording of the electrical activity from thousands of neurons simultaneously. Beyond population activity, it has also become possible to extract information of single neurons at subcellular level (e.g., the propagation of action potentials along axons). In effect, HD-MEAs have become an electrical imaging platform for label-free extraction of the structure and activation of cells in cultures and tissues. The quality of HD-MEA data depends on the resolution of the electrode array and the signal-to-noise ratio. In this chapter, we begin with an introduction to HD-MEA signals. We provide an overview of the developments on complementary metal-oxide-semiconductor or CMOS-based HD-MEA technology. We also discuss the factors affecting the performance of HD-MEAs and the trending application requirements that drive the efforts for future devices. We conclude with an outlook on the potential of HD-MEAs for advancing basic neuroscience and drug discovery.

Keywords Action potential · Electrical imaging · Electrical stimulation · Extracellular recording · High-density microelectrode arrays

1 Introduction

The next frontier in neuroscience is to map the whole brain and to understand how the networks of neurons within the brain function (Alivisatos et al. 2013; Marblestone et al. 2013). This requires developing techniques for simultaneous

M. E. J. Obien (✉) · U. Frey
Bio Engineering Laboratory, Department of Biosystems Science and Engineering, ETH Zürich, Basel, Switzerland

MaxWell Biosystems, Basel, Switzerland
e-mail: marie.obien@mxwbio.com

recording of neuronal activity at multiple spatial and temporal scales and for manipulating the activity of neurons of interest. At the in vitro level, realizing a high-resolution recording method enables to study neuronal mechanisms and to characterize brain disease models that can be used for drug discovery. Complementary metal-oxide-semiconductor or CMOS-based high-density microelectrode arrays (HD-MEAs) offer a promising platform for high-resolution acquisition of neuronal data. Thousands of neurons can be simultaneously *recorded* and/or electrically stimulated over time scales of microseconds to months. Owing to the high-density feature, a single neuron can be recorded by hundreds of electrodes. This facilitates assigning recorded spikes to their source neurons, termed *spike-sorting*, and allows for the subcellular mapping of a neuron's axonal arbor.

Electrical recording of neuronal activity has been popularly used for analyzing single neurons and neuronal networks (Contreras 2004; Llinas 1988). Electrical signals produced by neurons can be detected at a distance from the source. Several recording tools apply to different spatial scales. At the mesoscale, where local neuronal populations can be analyzed, a popular method is extracellular recording using metal electrodes. An electrode placed inside a brain slice in vitro or inserted in the brain in vivo detects electrical signals produced by the surrounding cells. A wide range of neural phenomena can be observed, from the spiking activity of individual neurons (extracellular action potentials or EAPs; bandwidth: 300–3000 Hz) to the slower network activity of small populations (local field potentials or LFPs; bandwidth: 1–300 Hz), shown in Fig. 1. Additionally, the same electrode can be used to deliver electrical stimulation to a local area in the brain. While this method for brain recording and stimulation is relatively easy, the challenge lies in making sense of the recorded data. With hundreds of possible signal sources surrounding an electrode, the specificity and selectivity of such technique is poor. Thus, *extracellular recording* has been widely used for analyzing population activity. In contrast, *intracellular recording* by patch clamp has been the gold standard for analyzing single neurons and synaptic connectivity of a few cells. However, patch

Fig. 1 Extracellular and intracellular recording. Left: Illustration of cells across cortical layers modified with permission from Buzsáki et al. (2012). Right: Signals of simultaneous extracellular recording and intracellular whole-cell patch-clamp recording modified with permission from Henze et al. (2000)
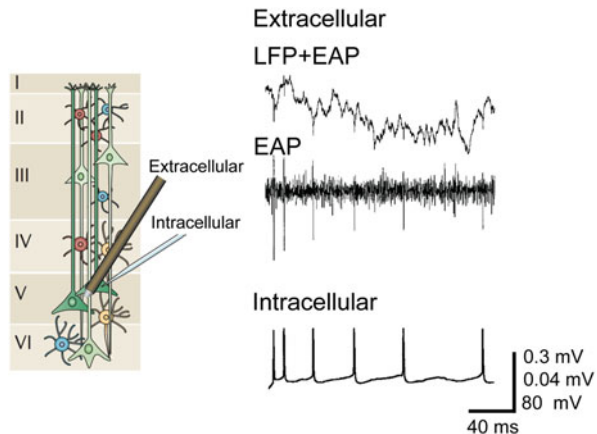
clamp necessitates intricate skill to perform. The viability of patched neurons lasts only up to a few hours. Moreover, current implementations of the experimental setup are bulky. All these limit the capability of the patch-clamp technique to scale for studying networks of neurons (Wood et al. 2004).

To achieve high-resolution activity mapping of neuronal networks, multiple electrical sensors tightly spaced in an array can be utilized. Microelectrode arrays (MEAs, also termed multielectrode arrays) allow for simultaneous long-term recording of LFPs and EAPs from a population of neurons at submillisecond time scale. In order to increase spatial resolution, that is, to place thousands of electrodes per square millimeter, the area taken up by wiring between electrodes-to-readout circuitry has to be reduced. This has been made possible by using industrial CMOS technology to create high-density MEAs (HD-MEAs). As an added benefit, readout circuitry, such as amplifiers and analog-to-digital converters, can be included on the same substrate as the electrodes in order to improve signal quality. The design of the on-chip signal conditioning circuitry should consider the electrode impedance and the possible sources of noise to ensure high quality signals. HD-MEAs with good signal-to-noise ratio (SNR) can be used to map single neuronal activity at subcellular resolution and to observe network activity at the same time (Ballini et al. 2014; Dragas et al. 2017; Frey et al. 2010), illustrated in Fig. 2.

1.1 Terminology

Over the years, a wide repertoire of terms has been used to refer to and distinguish between all the different forms of MEAs, for example emphasizing the type of transducers used (multitransistor array, microelectrode array, multielectrode array, micronail array, capacitive-coupled array, 3D MEA), the type of substrate (active array, passive array, silicon array, CMOS array), the shape of the device (needle-type probe, polytrode, neuro dish), the channel count (multichannel array), the electrode density (HD-MEA) or the application (implantable array, in vivo MEA, in vitro MEA), and more. We would therefore like to briefly explain the terminology used in the context of this chapter.

We generalize the term MEA to cover both substrate-integrated planar MEAs and implantable neural probes. We also include capacitive-coupled devices, such as multitransistor arrays in the definition of MEAs. We then distinguish between implantable, in vivo MEAs, such as polytrodes and neural probes, and in vitro MEAs that generally include a cell culture dish or other types of medium chamber. We use the term "array" to refer to the actual area that encompasses the transducer elements only, and we use device or MEA to refer to the entire device. With system, we refer to the MEA and all required components to operate it, such as the data acquisition hardware and software. We use the terms "active" and "passive" to distinguish between devices with active circuit elements, such as transistors, and devices without such elements.
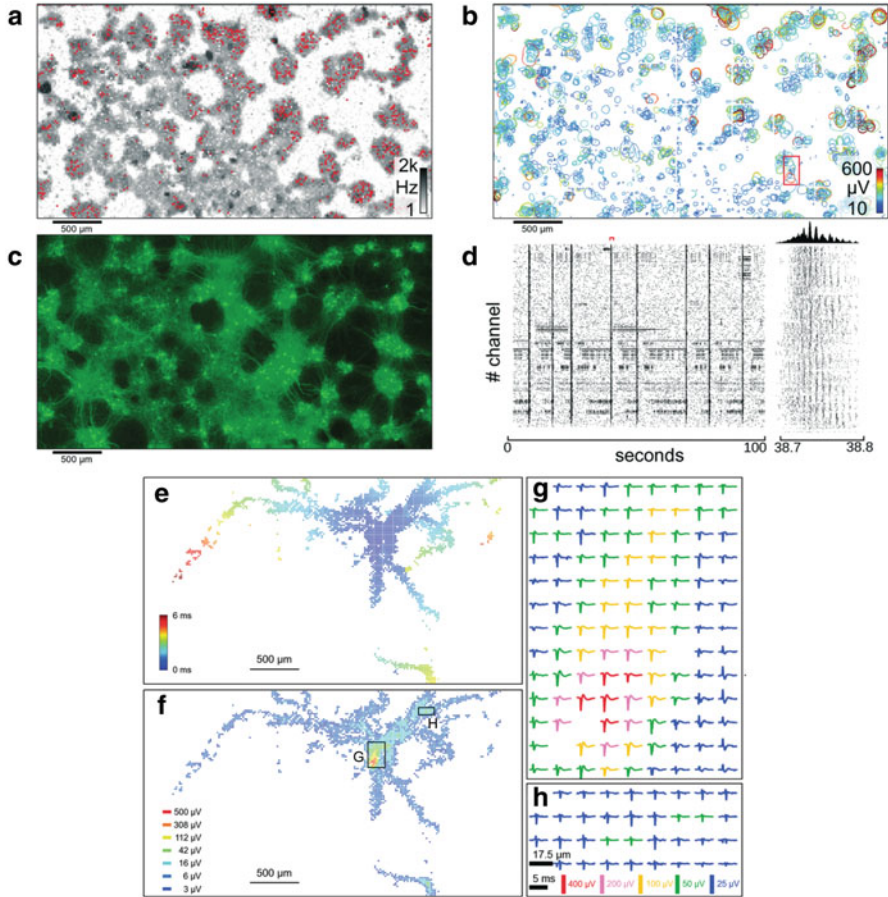
Fig. 2 Obtaining network-wide and single-neuron activity maps using CMOS-based HD-MEAs. (A-D) Networks. (**a**) Average EAP firing rate as measured by each electrode (26,400 electrodes in total) shown as pixels colored with a logarithmic gray-scale between 1 and 2 kHz. Red dots correspond to the electrodes selected for the raster plot in (**d**). (**b**) Representation of all 2000 individual neurons identified through spike-sorting the signals. A circle represents each detectable cell; the edges indicate where the amplitude of the measured signals exceeds −4.5 standard deviations of the electrode noise. The colors correspond to the amplitude of the most negative peak detected by the electrodes within the circle. (**c**) Fluorescence image of transfected cells (around 5% of all cells in the culture). (**d**) Raster plot of 100 s of activity for 1024 electrodes recorded simultaneously. Red marker shows the time period in close up view (bursting activity) on the right. Histogram at the upper right shows the number of spikes per time bin of the burst close up. (**e**–**h**) Single neuron electrical footprint. (**e**) All electrodes that captured activity attributed to a single neuron are colored according to the time of arrival of the AP at the electrode locations. (**f**) The same electrodes in (**e**) are colored according to the amplitude of the most negative peak detected. (**g**–**h**) Spike-triggered averages (30–50 averages) of the EAP electrical footprint from the two areas of the array as indicated by black boxes in (**f**). All figures modified with permission from Müller et al. (2015)

2 CMOS-Based HD-MEA Technology

Since the single extracellular microelectrodes used in the middle of the last century (Gesteland et al. 1959; Weale 1951), development quickly proceeded to MEAs with multiple transducers for the purpose of increasing the number of neurons observed (Csicsvari et al. 2003; Gross et al. 1977; Pine 1980; Thomas et al. 1972) and to increase reliability of spike sorting (Gray et al. 1918; Harris et al. 2000). Passive transducer devices based on electrodes embedded in glass or silicon substrates with fixed wiring to amplifiers for in vitro and also in vivo applications became commercially available in the late 90s and early years of this century.

A wave of fabrication and semiconductor technological advances paved the way towards the miniaturization of modern biosensor devices. Microelectrode arrays have thus been improved by integrating active electronic components in the same substrate, together with the electrodes. A technology for constructing integrated circuits is called complementary metal-oxide-semiconductor (CMOS), hence the term CMOS-based MEAs. Already early on, silicon-based biosensors for interfacing cells with microelectronics were developed (Bergveld 1970; Parce et al. 1989). Active devices, employing FETs were fabricated and 2D arrays demonstrated (Besl and Fromherz 2002). Devices using CMOS technology were fabricated in academic facilities (DeBusschere and Kovacs 2001) and industrial foundries, usually in conjunction with additional processing steps for biocompatibility reasons (Berdondini et al. 2002; Eversmann et al. 2003; Franks et al. 2003). Later on, similar to CMOS cameras, MEAs have been developed with thousands of electrodes, producing high-density microelectrode arrays (HD-MEAs) while also improving the signal quality of recordings (Hierlemann et al. 2011; Obien et al. 2015). Tapping into the large and established CMOS production industry provides an economy of scale for HD-MEA production.

The key advantage of integrating active electronic components on the same substrate as the actual electrodes is the possibility of a much higher electrode number and density. Due to the possibility of using active switches to time multiplex signals, integrated circuits make it feasible to transfer data from such high channel counts off chip and to overcome the connectivity limitation of passive devices. Additionally, such cointegration allows for amplifying the signals with optimal quality, due to minimal parasitic capacitances and resistances (Hierlemann et al. 2011). The monolithic cointegration also allows for including additional functionality, for example, on-chip spike detection, closed-loop capabilities, electrical stimulation, electronic chip identification, device calibration, and other types of sensing modalities, such as temperature, pH, and optical or neurotransmitter sensing (Baumann et al. 1999; Dragas et al. 2017; Johnson et al. 2013b; Park et al. 2017; Tokuda et al. 2006).

2.1 MEA Types

MEA architectures have evolved throughout the years. In general, the electrode-to-readout routing scheme can be divided into two types: fixed wiring, that is, each electrode is directly wired to outside of the array, connecting to the signal conditioning circuit; and multiplexed array, that is, routing from electrodes traverses switches before reaching the signal conditioning circuit. We further classify the MEA device types, shown in Fig. 3.

Passive Conventional MEAs have fixed wiring and are passive (i.e., no active circuit elements, such as amplifiers). Each electrode connects directly to a signal pad outside the array through a wire. The pads are then connected to external equipment for signal conditioning. Passive MEAs are typically easier to fabricate and many different substrates and electrode materials can be used. The user has direct access to all electrodes simultaneously, however, wiring and electrode geometry limit the total number of electrodes that can fit in a given area. Examples of passive MEAs
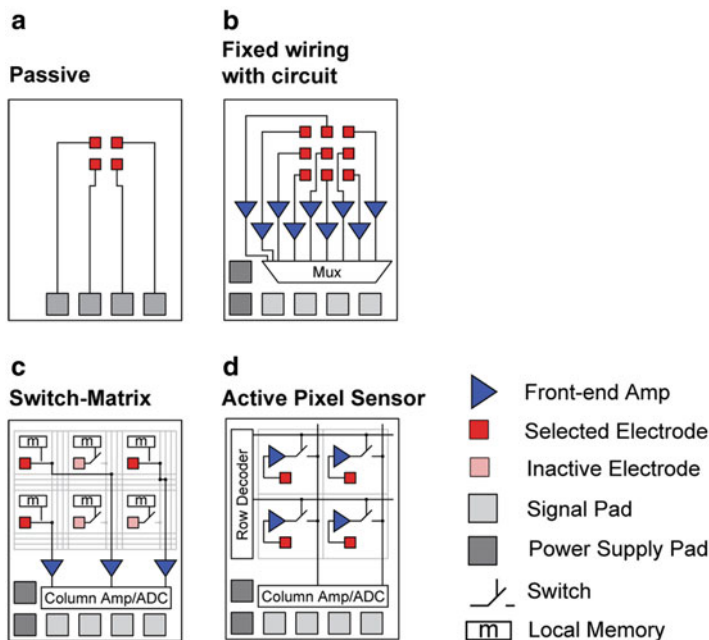
Fig. 3 MEA architectures. This table summarizes the different architectures used for MEAs. (**a**) Passive: Fixed wiring with electrodes directly connected to signal pads and no active circuitry. (**b**) Fixed wiring with electrodes directly connected to on-chip active circuitry for signal conditioning. (**c**) Switch-matrix (SM): Multiplexed array with flexible addressing achieved by adding more routing resources within the array. (**d**) Active pixel sensor (APS): Multiplexed array with all electrodes sampled at fast speeds for a full-frame readout. Modified with permission from (Obien et al. 2015)

were developed and used by Alpha MED n.d., Multi Channel Systems GmbH n.d., Greschner et al. (2014), Gross et al. (1977), Litke et al. (2004), Nisch et al. (1994), Oka et al. (1999), Pine (1980), Regehr et al. (1989), Segev et al. (2004), and Thomas et al. (1972).

Fixed Wiring with On-Chip Circuitry These types of MEAs have electrodes directly wired to on-chip active circuit elements that are used for signal conditioning, such as amplification and filtering. One variation employs multiplexers to allow readout of more electrodes despite a limited number of signal output pads. Multiplexing can be done only if the amplifiers and filters are before the multiplexer. Although this architecture allows for increased electrode count, the electrode density cannot be maximized (i.e., direct wiring of each electrode to signal conditioning circuitry limits how close electrodes can be packed together). Selected fixed wiring with on-chip circuitry MEA references are (DeBusschere and Kovacs 2001; Greve et al. 2007; Offenhäusser et al. 1997).

For in vivo MEAs, the connectivity limitation is even more severe, as connections cannot be wired out on all four sides of the array, but only on one of the narrow sides. Examples of in vivo passive and fixed wiring devices are (Berényi et al. 2014; Blanche et al. 2005; Csicsvari et al. 2003; Du et al. 2011; Fujisawa et al. 2008; Gray et al. 1918; Herwik et al. 2009; Jones et al. 1992; Kipke et al. 2003; Montgomery et al. 2008; O'Keefe and Recce 1993; Olsson and Wise 2005; Wise et al. 1970)

Switch-Matrix (SM) The switch-matrix (SM) concept uses transistors to implement switches within the array to route signals from electrodes to readout circuitry placed outside the actual electrode array.

In the SM concept, these routing means is operated in static mode, meaning that some electrodes are selected by opening or closing the switches and a recording is then started without changing the electrode selection. Typically, not all electrodes detect activity during an MEA experiment, thus choosing a subset of "interesting" electrodes is possible. A common protocol is to first scan all the electrodes in successive recordings to determine which electrodes to later continuously record during an experiment. The advantage of this concept is that large, low-noise amplifiers can be implemented outside the actual electrode array, allowing to optimize amplifiers for best possible SNR. SM MEAs have been implemented and various degree of flexibility that the routing means provide. Very simply row, column-based selectability has been implemented (Huys et al. 2012). Increased degree of freedom in selecting subsets of electrodes was achieved for the following in vivo probes (Lopez et al. 2014, 2016, 2018; Seidl et al. 2011). The availability of a large set of wires, switches, and local memory allows for even more complex routing paths that connect a subset of electrodes to the readout and stimulation channels in a flexible manner. Frey et al. (2010) use 1.2 memory cells on average per electrode, allowing already fairly complex routing. Ballini et al. (2014) use 2.2 memory cells per electrode, drastically increasing the possibilities in selecting subsets. Viswam et al. (2016) increased the number of bits per electrode to more then 3, virtually allowing arbitrarily subset selections. Switch-matrix MEAs were

developed by Ballini et al. (2014), Dragas et al. (2017), Frey et al. (2010), Huys et al. (2012), Lopez et al. (2014, 2016, 2018), Seidl et al. (2011) and Yuan et al. (2018).

Full-Frame Readout (Active Pixel Sensor or APS) Similar to image sensors used in cameras, all electrodes in active pixel sensor (APS) MEAs can be sampled at fast speeds in full-frame readout. Typically, rectangular subarrays can be chosen as regions of interest and sampled at faster rates than full-frame readout. For full-frame readout, the front-end amplification and filtering have to be before the multiplexing, meaning that the front-end amplifier has to be located within the pixel itself. This is because the electrode exhibits high impedance and therefore, without an amplifier, cannot drive multiplexed readout lines at sufficient speed. The small pixel area (i.e., available area near each electrode) serves as a limitation to designing very low noise circuitry for APS MEAs, since small-sized amplifiers inherently generate larger noise levels. Thus, while all electrodes can be recorded at the same time, only relatively large signals are detectable from noise. Examples of APS MEAs are Angotzi (2018), Aziz et al. (2009), Berdondini et al. (2009), Bertotti et al. (2014), Eversmann et al. (2003, 2011), Heer et al. (2006), Johnson et al. (2013a, b), Maccione et al. (2013), Ogi (2017), Park et al. (2017), Shahrokhi et al. (2009), Tsai et al. (2017), and Yuan et al. (2018).

2.2 Developments in MEA Technology

The evolution of MEAs with respect to overall sensing area and electrode densities is illustrated in Fig. 4a. A variety of historical and current MEA devices are included. The electrode count is shown with solid lines. The devices are categorized into "passive" (including both passive and fixed wiring MEAs) and "active" (multiplexed arrays such as SM and APS HD-MEAs). Recent HD-MEAs (SM and APS) aim to increase the total number of electrodes and the spatial resolution to allow for ever more demanding applications to be executed. One parameter used to characterize the density of MEAs is *single-cell separability*. Here, we used a threshold of 1000 electrodes per mm^2 as the minimum requirement to effectively assign spikes to a neuron.

The design of on-chip signal conditioning is crucial to achieve high quality signals. However, due to area availability and power consumption limitations, there remains a compromise between the quality of recorded signals and the number of parallel electrodes readout. SM HD-MEAs prioritize signal quality, while APS HD-MEAs target a high number of parallel readout channels, see Fig. 4b. We consider 10 μVrms as the minimum noise requirement for effective *spike detectability*. Figure 4b illustrates the tradeoff between the number of parallel (or quasi parallel) readout channels and the total input referred noise of the amplification chain. It shows the fundamental fact that a low-noise front-end amplifier requires both area and power. Limiting either will inherently increase the noise levels. The power
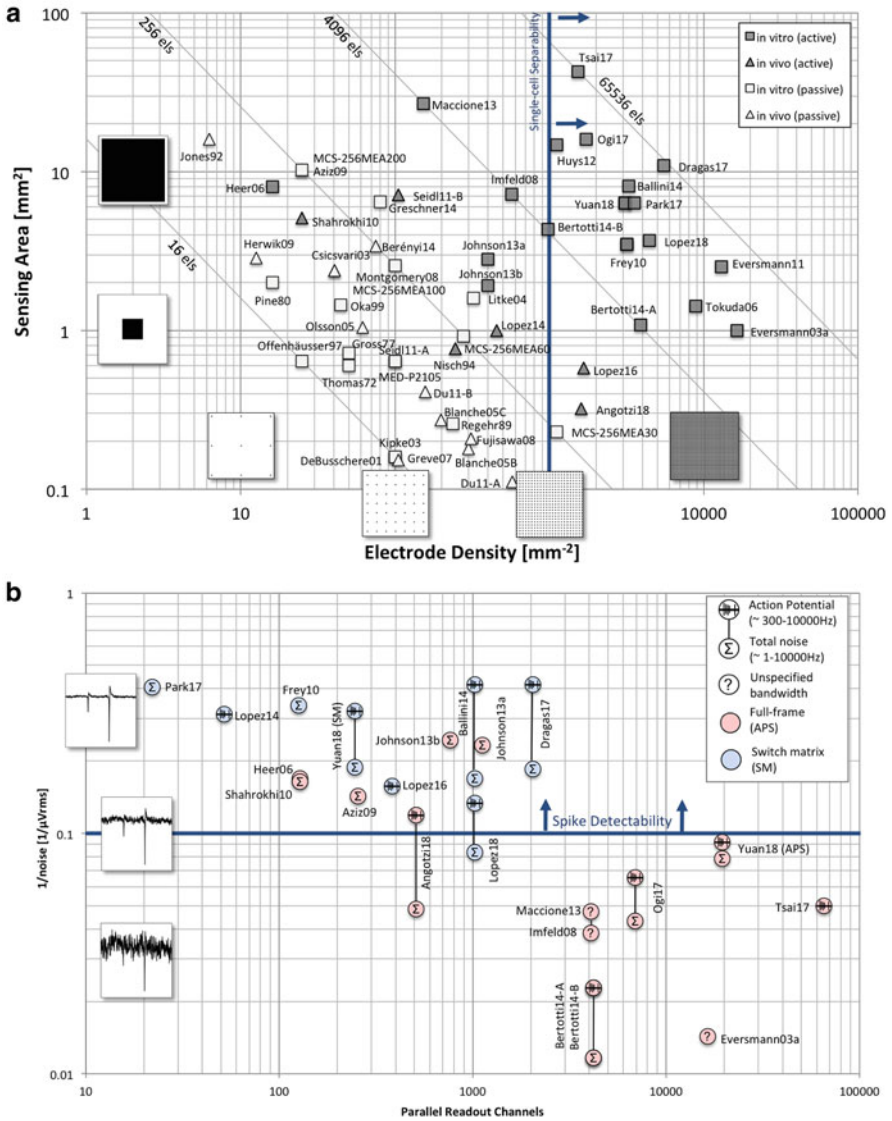
Fig. 4 Device comparison. (**a**) HD-MEA in vivo and in vitro implementations are shown according to the sensing area size and electrode density. For devices with a regular sensor pitch, such as most in vitro MEA devices, the total area is calculated as number of electrodes times the pixel area. For all devices, the number of electrode times the inverse of the electrode density matches the total area. The light gray lines illustrate the number of electrodes. (**b**) CMOS-based MEAs are compared with respect to parallel recording channel count and noise level. The noise values shown are approximated root-mean-square values stated in the respective citations. Note that the conditions under which these measurements were taken usually differ significantly (noise bandwidth, inclusion or exclusion of electrode noise, inclusion of ADC quantization noise, etc.). This graph only serves as a rough comparison, indicating noise values under both known and unknown conditions. The waveforms to illustrate the noise levels are simulated and have a spectrum

budget for the entire device, including all circuitry within the array and surrounding it, is limited by the amount of produced heat that one can tolerate. For the area constraints, one has to separately consider the area within the array and surrounding it. Within the array, the electrode density dictates the available area per pixel. Outside the array, the area is limited mostly by the fabrication cost.

2.2.1 Electrodes and Transducers

Choosing the materials for the insulator, conductor, microelectrode, and substrate is crucial, in particular with respect to biocompatibility. Various techniques for fabricating microelectrodes have been reviewed in Huang et al. (2009), Li et al. (2003), and Park and Shuler (2003). All materials that will be in contact with or near cells and tissue need to be tested for toxicity in prolonged periods of time (Hassler et al. 2011). It is also important to consider the biological experiments for which the microelectrodes will be used, whether in vivo or in vitro, chronic or acute recording. Moreover, deciding the type of MEA to use is highly dependent on the type of recorded signals needed, whether EAPs and/or LFPs or intracellular action potentials (IAPs), single cell resolution or not. If the MEA is to be used for stimulation, the charge capacity of electrodes is an important aspect. The electrode needs to be able to mediate reactions at the electrode–electrolyte interface to allow electron flow in the electrode to transition into ion flow in the electrolyte towards stimulating nearby cells (Cogan 2008).

Generally, an important goal of electrode fabrication is to achieve low impedance. Low electrode impedance results in higher signal-to-noise ratio (SNR), with a typical target SNR of 5:1 or higher (Cogan 2008). Oppositely, high electrode impedance combined with a large parasitic capacitance and amplifier input capacitance (see Sect. 2.3) will negatively affect recordings, especially at higher frequencies (Cogan 2008; Robinson 1968). In addition, uniformity of the electrode impedance across an array of electrodes may be important to obtain consistent data.

Typically, electrodes are made with metallic conductors such as gold (Au), titanium nitride (TiN), platinum (Pt), stainless steel, aluminum (Al), and alloys like iridium oxide (IrOx). Since the electrodes used in MEAs are on the micrometer scale, it is a challenge to achieve low electrode impedance with plain conductors only. Increasing the effective surface area of electrodes can be achieved by modification with porous conductive materials such as Pt-black, Au nanostructures, carbon nanotubes (CNTs), TiN, and conductive polymers like poly(3,4-

Fig. 4 (continued) typical for MEA recordings. The simulated spikes in the boxes (left) are typical spikes for acute brain slice measurements recorded with microelectrodes. The recorded amplitudes may vary significantly depending on preparation and sensor characteristics. Modified with permission from Obien et al. (2015)

ethylenedioxythiophene) (PEDOT). Emerging materials aside from PEDOT and CNTs include doped diamond and graphene. By modifying the surface, the electrode impedance can be decreased drastically and neuronal recording can be improved (Cui et al. 2001; Franks et al. 2005; Keefer et al. 2008; Ludwig et al. 2006; Viswam et al. 2014). See Kim et al. (2014) and Nam and Wheeler (2011) for a review of electrode materials and surface modification.

Nonmetallic electrodes have been mostly used in conjunction with field-effect transistor (FET)-based transducers (Bergveld 1970; Fromherz et al. 1991). An OGFET can, for example, be obtained if the fabrication process of an FET is stopped before depositing the gate material (Jenkner et al. 2004). Easier to fabricate is the so-called extended-gate FET (EGFET), in which the FET is fabricated without modification from a standard CMOS process. Metal and via interconnections are used to extend the gate to the surface of the chip, where an insulated electrode implements the "extended gate." Such insulation ensures that no faradaic currents occur. However, as Hierlemann et al. pointed out, devices with metal electrodes also usually connect to an FET directly (Imfeld et al. 2008) or through a filter capacitor (Heer et al. 2006), resulting in a largely capacitive recording situation (Hierlemann et al. 2011). OGFET, EGFET, and devices that directly connect the electrode to the first FET usually need to include some measures to properly bias the gate or some calibration mechanism, which may cause transient currents to flow at the electrode. Whereas for devices with a capacitively coupled front-end stage, controlling the electrode input node is generally not needed. Devices with an FET-based transducer, but using a metalized gate exposed to the liquid, have also been developed (Jobling et al. 1981).

Recently, ultrasmall electrodes are being developed to record intracellular activity, including subthreshold signals, as reviewed in (Spira and Hai 2013). This is achieved by 3D structured electrodes such as silicon nanowires (Robinson et al. 2013), plasmonic antennas (Dipalo et al. 2018), and Au mushrooms (Hai et al. 2009) penetrating the cell membrane. Electroporation was shown to facilitate measurement of intracellular activity (Hai and Spira 2012; Koester et al. 2010).

2.2.2 MEA Recording Hardware

Apart from the electrode array, CMOS devices also require the design of neuronal amplifiers and some sort of data transmitter, either of the amplified analog signals or, more typically, of the already digitized data. Generally, a neural amplifier needs to have high input impedance, which is significantly higher than the electrode impedance, to ensure signal integrity. The amplifier should be of low power to prevent substrate heating that could damage cells or tissue. For in vitro MEA devices, a variety of target applications have to be considered. Therefore, gain and dynamic range requirements can be quite demanding and should be adjustable, such as to cover applications with maximal amplitudes of a few hundred microvolts in acute slice preparations and, on the other hand, up to 10 mV in measurements from cardiomyocytes. The same also holds true for the flexibility in the recording

bandwidth. Some applications may require either lower frequency signals or spikes in the EAP band only, while some experiments target both bands with different gain requirements at the same time. The circuits need to implement some sort of high-pass filter to block the large *1/f* noise of the electrode–liquid interface typically observed.

MEA systems can also include digital-to-analog conversion (DAC) and stimulation circuitry (discussed in the next subsection). MEA systems need to include an interface to transmit the data and receive commands for controlling the system's operation. The requirements are different for implantable devices, where usually the target application is much more defined, but also the power, reliability, and safety requirements are more stringent. These systems often implement spike detection or classification and wireless transmission in the system, either as a monolithic implementation or hybrid approach using multiple ICs. They may also be powered wirelessly. On the other hand, in vitro MEA systems do not require wireless power or data transmission, as they can generally be directly wired to the data-receiving device. In this case, often common interface standards are employed, such as USB (Multi Channel Systems GmbH), Ethernet (Frey et al. 2010), National Instrument's DAQ card (Alpha MED n.d.), CameraLink (Imfeld et al. 2008), or others. Most of these systems support online storage of the full raw data to hard disks, sometimes including some form of lossless data compression (Sedivy et al. 2007).

2.2.3 Electrical Stimulation

MEAs allow observation of neural activity, but can also influence and control activity. Metal electrodes can deliver electrical stimuli directly. CMOS fabrication allows including electrical stimulation circuitry directly on-chip, in turn allowing a high degree of flexibility in generating spatiotemporal patterns of stimulation owing to dense and flexible wiring, higher spatial resolution for stimulation owing to densely packed electrodes and room for on-chip circuitry to blank or suppress stimulation artifacts.

Electrical stimulation has been typically applied as a "trigger" for the so-called stimulus-triggered averaging (Cheney and Fetz 1985). By delivering electrical pulses through the microelectrode, action potentials (APs) can be triggered from nearby neurons, with an effective stimulation range depending on the neuron's distance from the stimulation site and the amplitude of the pulse. With HD-MEAs, stimulus-triggered averaging reveals the electrical activity footprint of a single neuron, that is, signals detected at the electrode sites corresponding to the EAPs from a single neuron, where negative spikes correspond to the AP initiated at the axonal initial segment and the positive spikes represent return current, including the propagation of APs in axons (Bakkum et al. 2013). The stimulation amplitude has to be sufficient to consistently evoke an AP with small temporal jitter (e.g., a jitter of 160 µs) (Bakkum et al. 2008). Figure 5a shows how small axonal signals, typically undetectable from noise, become observable by increasing the number of
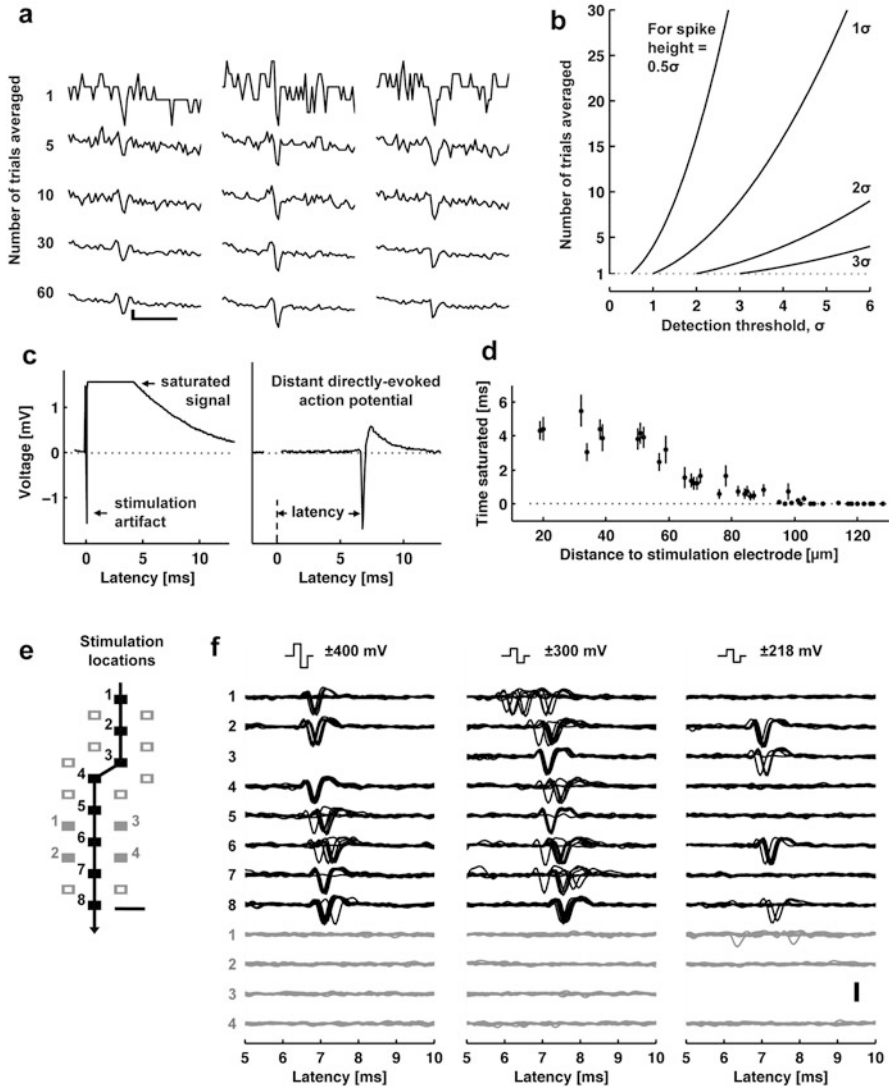
Fig. 5 Stimulation capability of HD-MEAs. (**a**, **b**) Stimulus-triggered averaging improves detection of axonal signals. (**a**) Evoked spikes detected at three chosen sites (columns) along the same axon. Each row shows individual traces obtained by increasing the number of averaged trials, from 1 to 60. Scale bars, 1 ms horizontal, 10 μV vertical. (**b**) The number of averaged trials necessary to detect a spike with a given height (0.5–3 times the standard deviation of the noise, σ) with respect to the detection threshold. (**c**, **d**) Electrical stimulation affects recorded signals of electrodes <100 μm away from the stimulation site. (**c**) Left: A raw trace recorded at an electrode neighboring a stimulation electrode (18 μm away) saturated for about 4 ms (flat line). Right: A raw trace recorded at an electrode located 1.46 mm away from a stimulation electrode did not saturate. (**d**) The duration of a saturated signal occurring after stimuli decreases with increasing distance from the stimulation electrode (mean ± s.e.m.; $N = 18$ stimulation electrodes from five HD-MEAs). Stimuli consisted of biphasic voltage pulses between 100 and 200 ms duration per

trials averaged. The number of trials that must be averaged depends on the spike amplitude as shown in Fig. 5b.

One issue of electrical stimulation is the occurrence of artifacts in the recording channels. Stimulation pulses are typically three to four orders of magnitude larger than the recorded EAPs; the recording channels can pick up the artifacts through the wiring in the circuitry or through the media to neighboring electrodes. If the artifact amplitude is large, the amplification circuits may saturate and this prevents recording neuronal activity until the offset settles back to normal. Figure 5c provides an example of signal saturation due to stimulation in a SM HD-MEA (Frey et al. 2010). A recording electrode near the stimulation electrode (18 μm away) saturated for around 5 ms; another electrode located far from the stimulation site (1.5 mm away) did not saturate. Figure 5d presents the relationship between the distance from stimulation to recording electrode and the duration of saturation for a 11,011-electrode MEA (Frey et al. 2010), without employing any artifact suppression measures. As long as the amplifiers do not fully saturate, artifacts can be suppressed via software by subtracting the estimated artifact (based on templates, filters or local curve fitting) from the data (Hashimoto et al. 2002; Wagenaar and Potter 2002). To also allow recording from electrodes on which saturation would occur, counter measures in hardware have to be employed. One solution is to use a "reset" switch that can bring back the saturated amplifier into normal operation quickly, by resetting the high-pass filter of the front-end amplifier (Frey et al. 2010; Heer et al. 2006).

Local delivery of stimulation pulses can be achieved by HD-MEAs. Figure 5e, f show stimuli activated neuronal responses with high spatiotemporal precision. In a study to track axonal APs (Bakkum et al. 2013; Radivojevic et al. 2016) several ten thousands of stimuli used for stimulus-triggered averaging did not damage the electrodes or the cells. Voltage-mode stimulation was used, although the stimulation hardware supported both current and voltage modes (Livi et al. 2010).

Combined recording and stimulation capabilities allow for performing closed-loop experiments, whereby recorded signals are programmed to control the application of electrical stimuli. In such experiments, spike detection is performed online, typically through a dedicated hardware, for example, a desktop with a real-time operating system or a field-programmable gate array (FPGA) (Hafizovic et al. 2007; Müller et al. 2013).
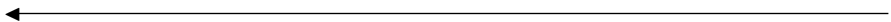
Fig. 5 (continued) phase and between ±400 and 800 mV amplitude. (**e**, **f**) Electrical stimulation can be delivered locally to axons and evoke action potentials. (**e**) Locations of stimulation electrodes that directly evoked (black boxes) or did not evoke (empty or filled gray boxes) APs detected at a soma located ∼890 μm away. The line arrow indicates the orthodromic propagation direction. Scale bar, 20 μm. (**f**) Voltage traces of somatic APs elicited by biphasic voltage stimuli. Traces in response to eight stimuli are overlaid for each of three stimulation magnitudes (indicated at the top), plotted for all effective (black) and four ineffective stimulation sites (gray at the bottom). Stimulation electrode locations are represented as numbered boxes in (**e**). Scale bar, 200 μV. All panels and description adapted with permission from Bakkum et al. (2013)

2.3   Performance of HD-MEAs

Here we discuss the main factors affecting the recording performance of MEAs: (a) neuron–electrode interface; (b) noise; (c) electrode size and density; and (d) recording hardware. Figure 6 illustrates the components of the MEA signal flow (Fejtl et al. 2006; Stett et al. 2003).

2.3.1   Effect of the Neuron–Electrode Interface

The early MEA neuron–electrode interface model assumed a tight seal between the neuron and the electrode (Weis and Fromherz 1997). However, extracellular microelectrodes can record EAPs and LFPs at a distance from active neurons, as observed in acute tissue and in vivo experiments. Likewise, for 2D neuronal networks grown on a MEA, EAPs can be detected from electrodes distant from the neuronal source. Thus, the neuron–electrode interface model can be separated into two parts (see Fig. 7): (1) the fluid side, which considers the effect of the volume conductor to the extracellular potential at the electrodes and (2) the metal side, which models the transformation of the extracellular potential through the electrode to the input of the front-end amplifier.

The distance and orientation of neurons with respect to measuring electrodes affect the amplitude and shape of the detected signals. The characteristics of the extracellular space, such as conductivity, anisotropy, and inhomogeneity, influence the spread of neuronal signals towards the electrodes. These effects can be estimated using the volume conductor theory illustrated in Fig. 7a. As a first order approximation, the MEA surface can be considered as an infinite insulating plane, while the tissue and/or fluid in the MEA dish can be assumed to be infinite, homogeneous, and isotropic. A neuron's membrane current can be decomposed into several point current sources. The method of images can then be applied to Coulomb's law to solve the potential V_e at any given electrode e in a volume conductor with conductivity σ (Ness et al. 2015; Obien et al. 2015):
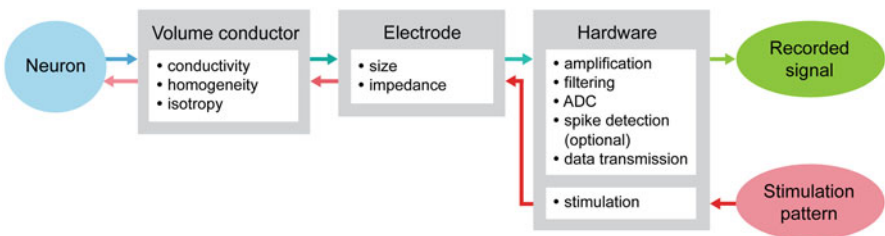

Fig. 6 MEA recording and stimulation system diagram. A neuron's signal, typically an action potential, is transduced through different components of the signal path into a digitally recorded trace. Similarly, a digital pattern generated from a computer or the MEA hardware applies current or voltage at the electrode during stimulation. Adapted with permission from Obien et al. (2015)
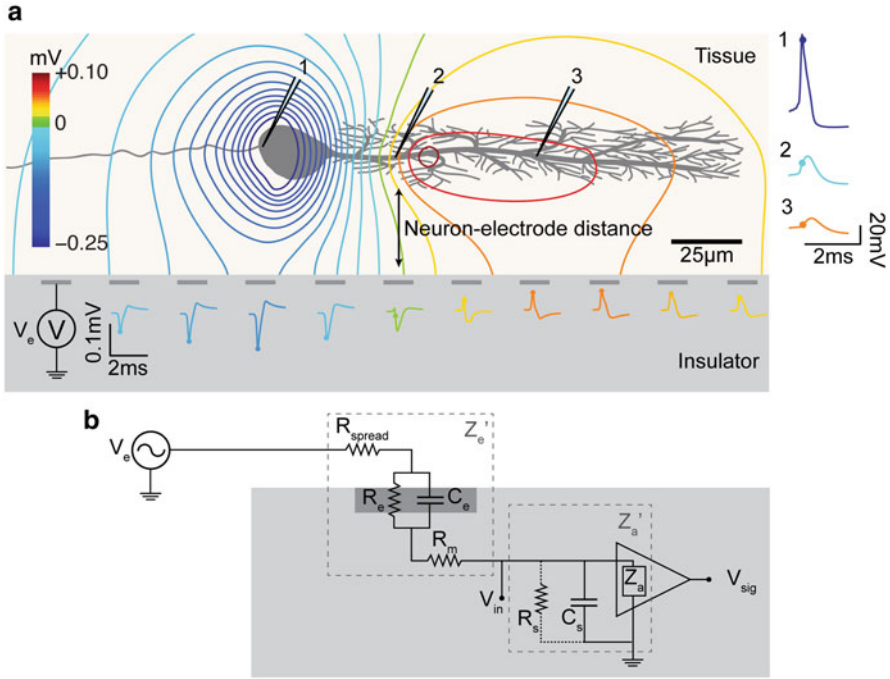
Fig. 7 MEA neuron–electrode interface divided into (**a**) fluid side and (**b**) metal side. (**a**) The potential at the electrode sites can be solved using the volume conductor theory. The MEA surface can be assumed as an insulator such that the method of images applies and can be used to solve the potential at any point on the MEA surface. The neuron–electrode distance and neuron orientation influences the signal amplitude and shape detected at the electrodes. High spatial resolution allows for recording EAPs at several locations of a single neuron, with large negative spikes at the perisomatic area and positive spikes at the dendritic area (i.e., return current). (**b**) The voltage measured at the electrode is transformed by the electrical parameters of the electrode–electrolyte interface, represented by Z_e' as the effective electrode impedance and Z_a' as the effective input impedance. This model is derived from Hierlemann et al. (2011), Nelson et al. (2008), and Robinson (1968). R_{spread}—spreading resistance; R_e and C_e—resistance and capacitance of the electric double layer at the electrode–electrolyte interface; R_m—resistance of the metallic part of the electrode; R_s and C_s—shunt resistance and capacitance. Adapted with permission from Obien et al. (2015)

$$V_e = \frac{1}{2\pi\sigma} \sum \frac{I_n}{r_n}.$$

I_n represents the nth point current source and r_n represents the distance between the point source and the recording electrode e, with $n = 1 \ldots N$, where N is the number of individual point sources. For electrodes larger than an ideal point electrode, V_e can be solved at multiple locations of the electrode's surface area and then averaged. This equation can be extended to include the anisotropy and inhomogeneity of brain

tissue, the saline layer above the tissue, and to use line sources instead of point sources to represent neuronal membrane currents (Ness et al. 2015).

2.3.2   Noise and SNR

One crucial aspect of the MEA signal flow is how noise is fed into the amplification chain and how it affects the signal-to-noise ratio (SNR) of the recorded data. SNR is the key specification for the amplifier design, regardless of the actual amplification (Jochum et al. 2009). There are several noise sources to consider in analyzing MEA recordings. It is important to consider where the noise, or interference, is injected in the signal chain, as the implications on SNR will differ.

Biological Noise   A major source of noise comes from the electrical activity of other cells around the recording electrode (e.g., APs of distant cells) but also ionic activity (e.g., subthreshold events in neurites of nearby cells) and synaptic noise due to the stochastic nature of synaptic transmission. Several models of biological noise, or sometimes also called background noise, have been developed by simulating uncorrelated single-unit spiking activities or examining multicompartmental neuron models located at distances far enough away from the electrodes such that the spikes cannot be resolved (Camuñas-Mesa and Quiroga 2013; Eaton and Henriquez 2005; Jäckel et al. 2012; Lempka et al. 2011; Martinez et al. 2009). Although such models replicate the average biological noise in experiments, it is possible that the cell type, size, and morphology along with the firing rates and correlated activity can affect the shape of the background signal. For spike analysis, LFP is also considered biological noise and is filtered out.

Electrode–Electrolyte Interface Noise   On top of biological noise, the liquid–metal interface also adds to noise. At low frequencies, such as below 10 Hz, processes at the electrode generate noise with a steep roll-off of *1/f* or even *1/f²* (Hassibi et al. 2004; Heer 2005). More relevant for electrophysiology are the frequencies above that, where thermal noise is the main contributor (Gesteland et al. 1959; Liu et al. 2007). The equivalent thermal noise can be calculated as follows:

$$v_n = \sqrt{4 \cdot k \cdot T \cdot \text{Re}\left(Z_e'\right) \cdot \Delta f},$$

where k is the Boltzmann constant, T is the absolute temperature, $Re(Z_e')$ is the real part of the effective electrode impedance, and Δf is the noise bandwidth. Another source of noise is the 50–60 Hz hum from power lines. This noise is largely picked up between the microelectrode and the connection to the input of the preamplifier, due to its high impedance at that frequency. Hence, minimizing the distance between the electrode and the amplifier is a major design requirement for MEA circuits (Harrison 2008). Proper grounding and shielding of the MEA setup can minimize interference.

Device Noise The device or the system that amplifies and digitizes the signals further adds to noise. Usually, the front-end amplifier is the most important factor to consider. A general design objective for such amplifiers is to ensure that the signal acquisition system does not limit the system performance with regard to noise. As discussed above, this is a design trade-off in which also power and circuit area may play a role. For example, if the maximal allowed contribution to noise from the circuitry is set to 10%, the amplifier noise needs to be 45% or less as compared to the noise of the electrode. A commonly used figure of merit that captures the trade-off between noise and amplifiers' supply current is the noise efficiency factor (NEF) proposed in Steyaert and Sansen 1987. This figure has also been adapted to capture the different supply voltages used to allow for a better comparison with respect to power consumption, coining the term power efficiency factor PEF (Muller et al. 2012). For in vitro MEAs, area is also of critical importance, as it usually impacts electrode density and total channel count. The efficient use of the overall area is reflected in the ratio of the actual array area divided by the overall chip area (see Fig. 4). Quantization noise is another noise contributor of the hardware. It originates from the discretization error made at the ADC part of the MEA system. As an approximation for the quantization noise, typically a value of $\frac{1}{\sqrt{12}}$ times the magnitude of the least significant bit (LSB) is used. Typical ADCs used for MEA systems have a minimum of 8-bit resolution; systems that employ off-chip ADCs generally use 16-bit resolution. Finally, the transmission of data may also affect the quality of the recorded signal (e.g., if a lossy compression has to be used due to bandwidth constraints).

2.3.3 Effect of Electrode Size and Density

Sizes of published microelectrodes range from 5–50 μm in diameter (Kim et al. 2014) and even >50 μm. The most evident contribution of electrode size to SNR is the electrode impedance $Z_e{}'$, which in turn determines electrode noise. Large electrodes (>50 μm) have a positive effect on the SNR due to low impedance. Moreover, large electrodes have a higher possibility of getting physically near the neurons and of picking up higher amplitude spikes (Camuñas-Mesa and Quiroga 2013); for example, studies by Andersen et al. (2010), Moxon (1999), Paik et al. (2003), and Ward et al. (2009) claim that larger recording electrodes can record from more neurons simultaneously. However, the detected amplitude of a large EAP signal from a neuron is reduced as it is averaged out by nearby smaller amplitude signals, thus resulting in a lower SNR. Sorting all the signals detected by a single large electrode to their respective individual sources can also be daunting when many neurons are nearby.

For recording EAPs, especially for dissociated cell culture experiments, the use of small electrodes (<15 μm diameter) minimizes averaging. Small electrodes are inferior against large electrodes in terms of impedance, but this can be improved by surface modification. For example, the influence of electrode size (<10 μm
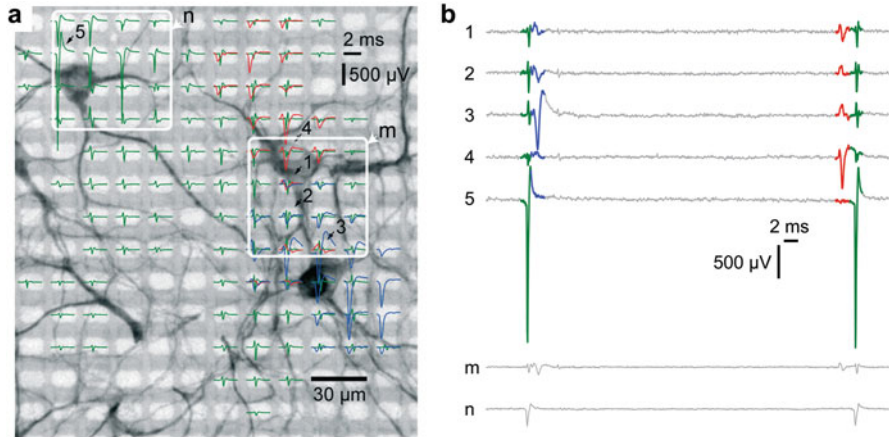
Fig. 8 Comparison of the recording capability of small electrodes at high-density and large electrodes. (**a**) The EAPs of three identified neurons (green, red, and blue) detected from each electrode site (light gray rectangles) are superimposed to a fluorescence image (MAP 2 staining) of a cell culture on a HD-MEA. Each spike represents the spike-triggered average over 50 trials. Spikes with amplitude below 50 µV are not shown. White squares represent the location of hypothetical large electrodes (60 × 60 µm) used for comparison of signals. (**b**) Raw traces from small electrodes (1–5) and large electrodes (m, n) indicated in (**a**). Signals for the large electrodes (m, n) are estimated by averaging the traces of the small electrodes within the area covered by the white squares. Estimated signals from (m, n) show reduced amplitudes due to the averaging effect only. The impedance effect due to electrode size differences may be neglected due to high input impedance at the first-end amplifier of the HD-MEA, and is thus not considered. Modified with permission from Müller et al. (2015)

diameter) on recorded signal amplitude significantly decreases by depositing Pt-black on platinum microelectrodes (Viswam et al. 2014). HD-MEAs have small electrodes to allow the integration of a large number of sensors in an array. The dense grid of electrodes in HD-MEAs, shown in Fig. 8, increases the possibility of having an electrode "at the right spot" while also allowing a single neuron to be recorded from multiple electrodes. Also, the effective input capacitance can be significantly smaller in HD-MEAs as compared to passive devices, due to a small C_s, which in turn allows for a smaller C_e (see Fig. 7b and the next subsection for more information). As a result, small electrodes are much more preferable in this situation, with only electrode noise being the limiting factor.

For LFP recording, Nelson and Pouget (Nelson and Pouget 2010) discussed that the electrode impedance and recording site geometry are not crucial. This is because LFPs only vary in a spatial scale much larger than the size of electrodes used for extracellular recordings, for example, by a few hundred micrometers (Katzner et al. 2009) or even by 1 mm (Destexhe et al. 1999). In addition, LFPs are of lower temporal frequency, making electrode noise a more important factor as in that range, it is dominated by $1/f^2$ noise, which makes larger electrodes more favorable.

Novel 3D microstructure and nanostructure electrodes aim to detect subthreshold neuronal signals (e.g., synaptic potentials, membrane oscillations) and membrane potentials (Spira and Hai 2013). These subthreshold signals cannot be detected by MEAs; these signals are conventionally measured using patch clamp. The 3D electrodes seek to achieve either a tight seal with the neuronal membrane or to temporarily puncture into the membrane and access the intracellular space of a neuron. With advancements in fabrication techniques, large-scale integration of 3D microelctrodes and nanoelectrodes is feasible on HD-MEAs (Dipalo et al. 2018).

It is therefore important to choose optimal electrode sizes depending on the targeted application. In addition, a high density of electrodes will inherently limit the electrode size.

2.3.4 Effect of the Recording Hardware

HD-MEA circuitry includes amplifiers, filters, and some sort of data transmitter of either the amplified analog signals or, more typically, of the already digitized data. The front-end amplifier has a major effect in the performance of the HD-MEA. It needs high input impedance to ensure signal quality.

A neuronal signal is transduced by an electrode into a current, and this process depends on the parameters of the effective electrode impedance $Z_e{}'$ and effective input impedance $Z_a{}'$. We discuss this using the equivalent circuit of the electrode–electrolyte interface shown in Fig. 7b. Noise (e.g., thermal noise and power line hum) can be injected into the recorded signal at the liquid–metal interface. $Z_e{}'$ is the total impedance due to R_{spread}, R_e, C_e, and R_m. R_{spread} represents the effect of the electrode geometry and liquid conductivity. R_e and C_e are the resistance and capacitance of the electrode double layer formed at the electrode–electrolyte interface. R_m is the resistance of the metallic part of the electrode. Connected in series to $Z_e{}'$ is $Z_a{}'$, which is mostly influenced by the input impedance of the front-end amplifier Z_a and the shunt capacitance C_s. C_s includes the capacitances from connectors and wires from the liquid to the amplifier. The shunt resistance R_s is usually negligible. All these represent the metal side of the neuron–electrode interface. For more details on the circuit model, see Hierlemann et al. (2011), Nelson et al. (2008), and Robinson (1968).

Front-end amplifiers are designed to have large $Z_a{}'$ in order to preserve signal quality. The ratio between $Z_e{}'$ and $Z_a{}'$ shows how to derive the voltage at the input of the amplifier as (Nelson et al. 2008):

$$V_{\text{in}}(\omega) = \frac{V_e(\omega)}{1 + \left(Z'_e(\omega) / Z'_a(\omega)\right)},$$

where $V_e(\omega)$ is the total extracellular potential at the electrode, $V_{\text{in}}(\omega)$ is the voltage at the input of the front-end amplifier. V_{in} will be smaller than V_e, that is, the signal will be attenuated if $Z_a{}'$ is not substantially larger than $Z_e{}'$.
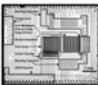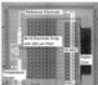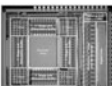
In addition to the effect of the input impedance, the circuitry near the cells must be low powered in order to prevent heating that could damage the cells. Appropriate settings for gain and dynamic range of the readout depend on the preparation (e.g., maximum amplitudes of a few hundred microvolts in acute slice preparations and up to 10 mV in cardiomyocyte experiments). The recording bandwidth needs to be flexible to cover both LFP and EAP frequency ranges, depending on the experiment, in order to avoid filtering out signals of interest.

Many of the circuit requirements can be traded against each other; for example, one can easily lower the noise by increasing the area or power consumption. The key challenge therefore is to set the target specifications for the given application accurately and optimize the systems for it, without overdesigning specific requirements.

3   Applications of HD-MEAs

In this section, we discuss specific neuroscience studies from selected experiments. Measurements done using passive MEAs can also be done using CMOS-based HD-MEAs. However, the high spatiotemporal resolution of HD-MEAs leads to novel types of data that were not possible to collect using conventional MEA devices.

In recent years, CMOS-based MEAs have been increasingly used for neuroscience and biomedical research. Figure 9 lists the currently available CMOS-based in vitro MEAs, their key specifications, and some experimental preparations for which they have been applied so far. The two most prominent preparations investigated using these devices are dissociated cell cultures from snails (Eversmann et al. 2003), rats (Bakkum et al. 2013; Gandolfo et al. 2010; Hafizovic et al. 2007; Heer et al. 2007; Lambacher et al. 2010; Lewandowska et al. 2015, 2016; Müller et al. 2015) and chicken (Hafizovic et al. 2007) and acute retina from mice (Fiscella et al. 2012, 2015; Franke et al. 2016; Maccione et al. 2014; Menzler and Zeck 2011; Yonehara et al. 2016), rats (Eickenscheidt et al. 2012; Lloyd et al. 2014; Stutzki et al. 2014), rabbits (Ballini et al. 2014; Fiscella et al. 2014; Zeck et al. 2011), hamsters (Jones et al. 2015), guinea pigs (Bertotti et al. 2014; Velychko et al. 2014), and humans (Reinhard et al. 2014). Additionally, data from acute slices of cerebellum (Frey et al. 2009a; Obien et al. 2014), cortex (Ferrea et al. 2012; Medrihan et al. 2014), and olfactory bulb (Johnson et al. 2013a) have been presented. Cultured cardiomyocytes were also studied (DeBusschere and Kovacs 2001; Heer et al. 2004; Huys et al. 2012; Imfeld et al. 2008; Sanchez-Bustamante et al. 2008), and first results from mice organotypic hippocampal slices were presented (Gong et al. 2016). This section reviews recent neuroscience applications of HD-MEAs.

Ref	Micrograph	Key Specs	Published Recordings	Published Stimulation
APS (Eversmann et al., 2003) Other versions: (Eversmann et al., 2011)		• Technology: 0.5µm • Chip area: 35mm² • Array area: 1.0mm² (2.9%) • Rec. sites: 16384 (OSFET) • Stim. sites: 0 • Channels: 16384 • Trans. density: 16384mm⁻² • Power: 656mW	• Acute (Rr, Mr, Lr): (Menzler and Zeck, 2011; Stutzki et al., 2014; Zeck et al., 2011) • Cultures (S, Rc): (Eversmann et al., 2003; Lambacher et al., 2010)	• Acute (Lr): (Eickenscheidt et al., 2012)
APS (Heer et al., 2006) Other versions: (Heer et al., 2004)		• Technology: 0.6µm • Chip area: 42mm² • Array area: 8.0mm² (19%) • Rec. sites: 128 (Pt) • Stim. sites: 128 (Pt) • Channels: 128 • Trans. density: 16mm⁻² • Power: 120mW	• Cultures (Cch, Rc): (Hafizovic et al., 2007; Heer et al., 2007, 2004)	• Cultures (Rc): (Hafizovic et al., 2007)
APS (Imfeld et al., 2008) Other versions: (Berdondini et al., 2005;		• Technology: 0.35µm • Chip area: 29mm² • Array area: 7.2mm² (25%) • Rec. sites: 4096 • Stim. sites: 16 (newer versions) • Channels: 4096 • Trans. density: 567mm⁻² • Power: 132mW	• Acute (Mcr): (Ferrea et al., 2012; Maccione et al., 2014; Medrihan et al., 2014) • Cultures (Rch): (Gandolfo et al., 2010; Imfeld et al., 2008)	• Cultures (Rc): (Maccione et al., 2013)
SM (Frey et al., 2009)		• Technology: 0.6µm • Chip area: 46mm² • Array area: 3.5mm² (7.6%) • Rec. sites: 11011 (Pt) • Stim. sites: 11011 (Pt) • Channels: 126 • Trans. density: 3150mm⁻² • Power: 135mW	• Acute (Rpr, Lr, Hr, Mpr): (Frey et al., 2009; Fiscella et al., 2012, 2014, 2015; Jones et al., 2014, 2015; Obien et al., 2014; Reinhard et al., 2014; Franke et al., 2016) • Cultures (Rh, Rc): (Sanchez-Bustamante et al., 2008; Bakkum et al., 2013; Lewandowska et al., 2015, 2016) • Organotypic (Mc): (Gong et al., 2014)	• Acute (Rr): (Lloyd et al., 2014) • Cultures (Rc): (Bakkum et al., 2013)
SM (Huys et al., 2012)		• Technology: 0.18µm • Chip area: 64mm² • Array area: 14.7mm² (23%) • Rec. sites: 16384 (W) • Stim. sites: 16384 (W) • Channels: 1 • Trans. density: 1111mm⁻² • Power: 35mW	• Cultures (Rh): (Huys et al., 2012)	• Cultures (Rh): (Huys et al., 2012)
APS (Johnson et al., 2013a) Other versions: (Johnson et al., 2013b)		• Technology: 0.18µm • Chip area: 4mm² • Array area: 2.8mm² (70%) • Rec. sites: 1120 (Al/Pt) • Stim. sites: 0 • Channels: 1120 • Trans. density: 400mm⁻² • Power: 14.1mW	• Acute (Mo): (Johnson et al., 2013a)	
SM (Ballini et al., 2013)		• Technology: 0.35µm • Chip area: 77mm² • Array area: 8.1mm² (11%) • Rec. sites: 26400 (Pt) • Stim. sites: 26400 (Pt) • Channels: 1024 • Trans. density: 3265mm⁻² • Power: 75mW	• Cultures (Rc): (Ballini et al., 2014; Müller et al., 2015) • Acute (Mr): (Yonehara et al., 2016)	• Cultures (Rc): (Ballini et al., 2014; Müller et al., 2015)
APS (Bertotti et al., 2014)	Not available	• Technology: 0.18µm • Array area: 4.3; 1.1mm² • Rec. sites: 4225 (OSFET) • Stim. sites: 1024 (CAP) • Channels: 4225 • Trans. density: 977; 3906mm⁻²	• Acute (Gr): (Bertotti et al., 2014)	• Acute (Gr): (Bertotti et al., 2014)
SM (Viswam et al., 2016)		• Technology: 0.18µm • Chip area: 106.8mm² • Array area: 10.9mm² • Rec. sites: 59760 (Pt) • Stim. sites: 59760 (Pt) • Channels: 2048 (AP)+32(LFP) • Trans. density: 5487mm⁻²	• Cultures (Rc): (Viswam et al., 2016)	• Cultures (Rc): (Viswam et al., 2016)

M: Mouse, R: Rat, H: Human, L: Rabbit, C: Chicken, G: Guinea pig, S: Snail
r: Retina, p: Cerebellum, o: Olfactory bulb, c: Cerebral cortex/hippocampus, h: Cardiomyocytes

Fig. 9 CMOS-based in vitro MEAs, their key specifications and references to biological applications for recording and stimulation. The specifications may differ for other device versions. Modified with permission from (Obien et al. 2015)

3.1 Electrical Imaging

HD-MEAs can be used to monitor the electrical activity of neurons in a cell culture or tissue preparation at high-resolution, thus termed here as *electrical imaging*. Examples of electrical imaging of a cell culture are shown in Fig. 2. The whole sample can be electrically imaged to create activity or amplitude maps of active neurons. Moreover, HD-MEAs with low noise can reveal subcellular resolution maps of single neurons.

Similarly, electrical imaging can be performed for 3D samples, such as acute brain slices. Two types of electrical images can be obtained: (a) based on EAPs shown in Fig. 10 and (b) based on LFPs presented in Fig. 11. The neurons and network structure in slices are physiologically and biochemically similar to the in vivo situation.

Depth recording of EAPs from neurons up to 100 μm distance from the MEA surface has been shown (Egert et al. 2002; Frey et al. 2009b). In Fig. 10 we show a demonstration of subcellular resolution electrical imaging of single Purkinje cells (PCs) in acute cerebellar slices (Frey et al. 2009a). To ensure the quality of recorded signals, proper tissue adhesion on the MEA surface has to be maintained throughout the experiment (Egert et al. 2002). EAPs were observed along the PC layer, and, after spike sorting, the EAP footprint of a single PC was analyzed. The negative spikes were recorded around the perisomatic area of the neuron, while positive spikes were obtained along the molecular layer corresponding to the dendrites of the PC.

Large LFPs and oscillations inherent in different states of the brain can also be imaged at longer time scales. Such recordings have been done for different brain areas (e.g., hippocampus and suprachiasmatic nucleus). HD-MEAs can easily capture electrical images of neuronal network activity in slices. For instance, functional imaging of the dentate gyrus has been demonstrated using HD-MEAs (Ferrea et al. 2012). Field excitatory postsynaptic potentials (fEPSPs) evoked by electrical stimulation were detected across different layers of the acute slice, as shown in Fig. 11.

3.2 Axonal Studies

HD-MEAs with high SNR, such as SM HD-MEAs (Frey et al. 2010; Müller et al. 2015), allowed for detection and tracking of APs propagating along a neuron's axon for the first time (Bakkum et al. 2013), and more recent studies continue to be performed (Radivojevic et al. 2016, 2017). Axonal signals are difficult to measure using conventional methods—thin axons are challenging to patch, and extracellular signal amplitudes are low compared to those from the soma and axon initial segment. In this work, the propagation of APs along the full arbor of a neuron has been electrically imaged, shown in Fig. 12a–c. Subsequently, axonal AP velocity
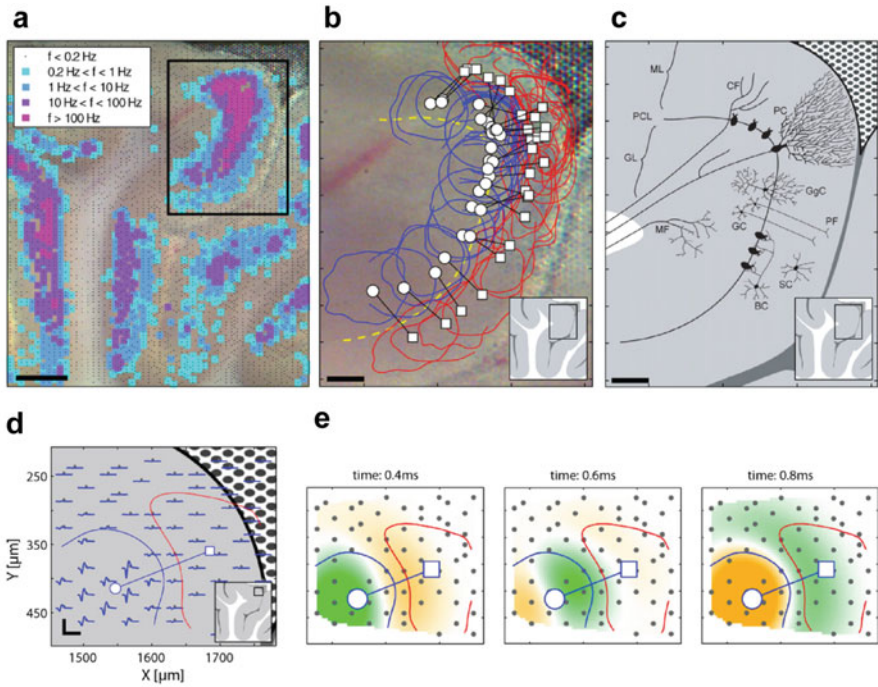
Fig. 10 High-resolution electrical imaging of spontaneous cerebellar Purkinje cell activity using HD-MEAs. (**a**) Activity map of the detectable spike activity in the recording area. Small dots correspond to the electrodes used for recording (∼30% of the available electrodes). Events exceeding a threshold of ±36 µV were used to calculate the color-coded event rate. Scale bar: 0.3 mm. (**b**) Close-up of a region with high activity delimited in (**a**). All units identified by spike sorting are marked, that is, the somatic region is blue and the dendritic region is red. Scale bar: 0.1 mm. (**c**) Schematic of the basic cellular structures in the cerebellar slice (Gray et al. 1918). Scale bar: 0.1 mm. *ML* molecular layer, *PCL* Purkinje cell layer, *GL* granular layer, *CF* climbing fiber, *MF* mossy fiber, *PF* parallel fiber, *PC* Purkinje cell, *GgC* Golgi cell, *SC* stellate cell, *BC* basket cell. (**d**) Footprint of a PC selected from the region shown in (**b**). Scale bar: vertical is 200 µV, horizontal is 1.9 ms. (**e**) Current source density (CSD) analysis for the cell shown in (**d**) at several points in time (green: sink; yellow: source). The sink moves from the soma at 0.4 ms to the proximal dendrites at 0.6 ms and covers the dendritic area, while the soma repolarizes. Frequency band: 180–3.5 kHz. (**f–h**) Matching simulated and measured EAP footprints. All panels and descriptions adapted with permission from Frey et al. (2009a)

was found to vary within single axons, hinting that axon velocity might contribute to temporal coding schemes of neuronal information. This capability can help expand new fields of research, such as axonal information processing and neuronal computation. Tracking the velocity of axonal signals also provides a new and promising parameter that can be used for analyzing the effect of different therapies (e.g., drugs and prolonged electrical stimulation) on the information transfer and signaling between neurons.
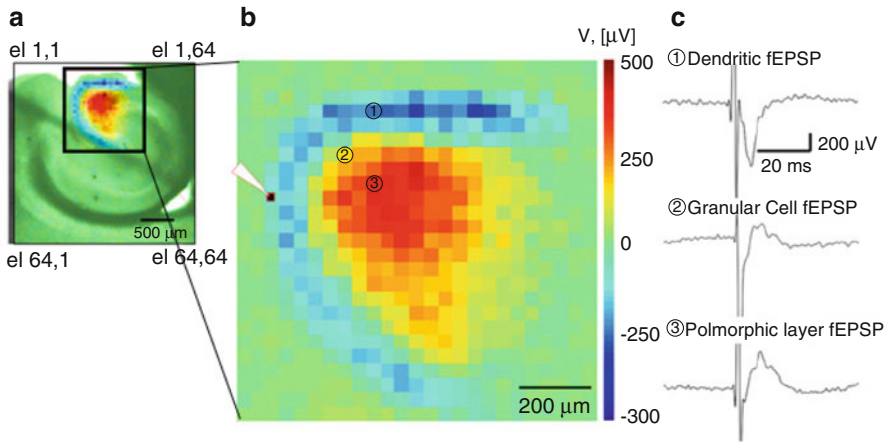
Fig. 11 Imaging network waves in acute hippocampal slices. (**a–c**) Functional imaging of the dentate gyrus, adapted with permission from Ferrea et al. (2012). (**a**) A corticohippocampal slice placed atop an APS HD-MEA, with superimposed color-coded fEPSP activity. (**b**) Close-up on the activated area in (**a**). The white tip indicates the site of stimulation using a patch pipette. (**d**) Recorded traces of fEPSPs from three chosen electrodes indicated in (**b**). Electrode 1 is located in the dendritic layer of the dentate gyrus, electrode 2 in the granular cell layer, and electrode 3 in the polymorphic layer

HD-MEAs have also been used for precise microstimulation. By taking advantage of the high electrode density, the responses of neurons to different stimulation patterns and intensity can be investigated, including how best to selectively stimulate single neurons (Radivojevic et al. 2016), as shown in Fig. 12d–f. Characterization of how stimulation affects neurons can benefit the design of stimulation therapies for clinical use.

Other studies amplify the axonal signals by growing the axons through polydimethylsiloxane (PDMS) microtunnels (Habibey et al. 2017; Lewandowska et al. 2015, 2016). PDMS tunnels were attached on top of an HD-MEA and cultured cortical neurons on each side of the tunnels. In time, many axons naturally enter and grow through the tunnels. While axonal signals outside of tunnels were also detectable, tunnels amplify the signals enough to avoid the need to average across trials and single axonal APs can be observed. By recording the spontaneous activities of the neurons, axonal signals were significantly amplified by a factor of 20–150.

3.3 Characterization of Novel Cell Types

Emerging breakthroughs in cell biology aim to provide in vitro platforms for preclinical drug screening and therapy diagnostics. In particular, human induced
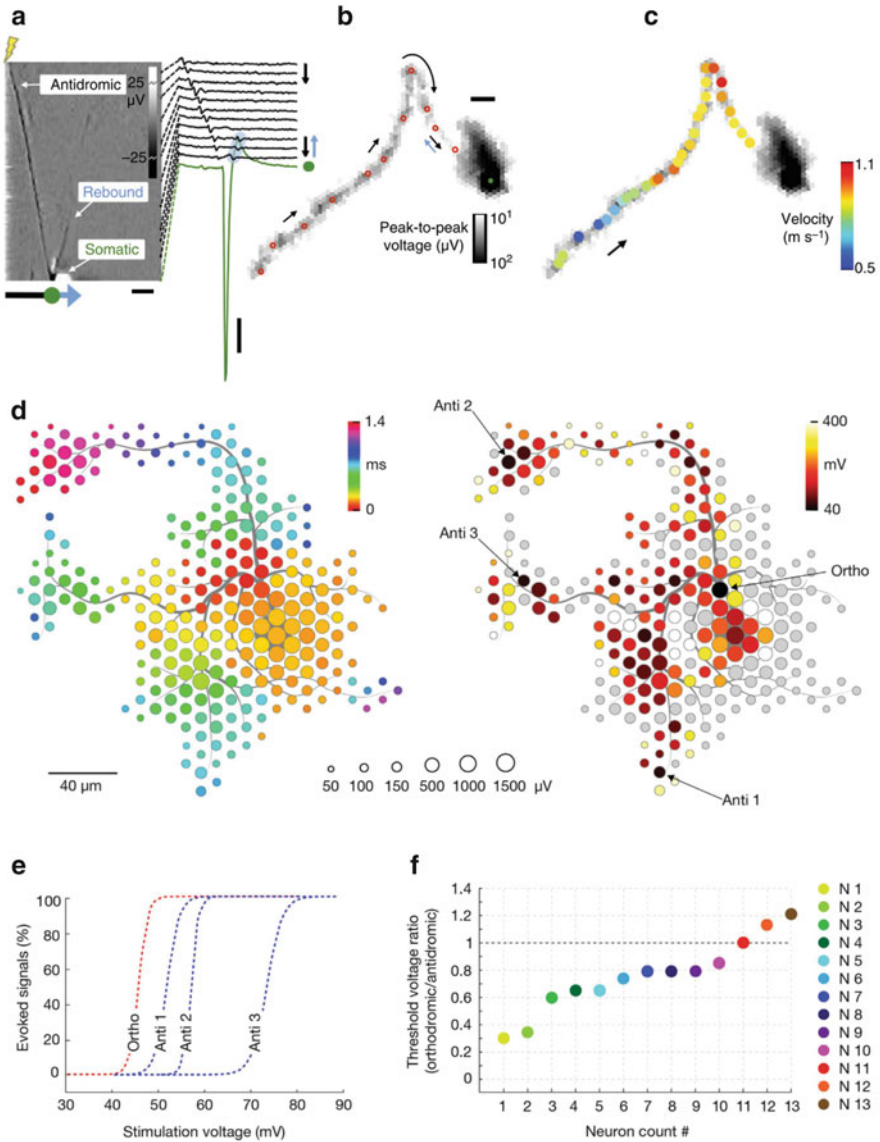
Fig. 12 Triggering and tracking axonal signals with HD-MEAs. (**a–c**) Adapted with permission from Bakkum et al. (2013). (**a**) Antidromic action potential triggered by electrical stimulation at the axon. Left: Heat map shows stimulation-triggered averages of 60 traces from 95 electrodes. Dark colored line from top to bottom indicates the antidromic propagation of an AP from the stimulation site. A subsequent rebound from the soma is also visible. Right: A subset of averaged raw traces. Scale bars, 1 ms horizontal; 100 μV vertical (**b**) The electrical footprint of the stimulated neuron recorded in (**a**). The gray scale pixels indicate the maximum peak-to-peak amplitude of the APs detected at each electrode. The red circles denote the locations of the subset of traces in A. The black arrows show the direction of the AP propagation along the axon, while the blue arrow indicates the subsequent rebound. The green dot is the location where the green trace in (**a**) was

pluripotent stem cell or hiPSC technology enabled to access human cells for in vitro investigation and to model diseases. HD-MEAs allow for efficient readout of hiPSC-derived neurons and cardiomyocytes for functional analysis. Culturing hiPSC derived neurons on HD-MEAs has been proven feasible and the cells remained viable up to 3 months (Amin et al. 2016). Spontaneous activity and responses to electrical stimulation were characterized. The authors found that spontaneous spiking activity of hiPSC derived neurons peaked around 81 DIV and that hiPSC derived neurons responded to electrical stimulation only at 90 DIV. Low-frequency electrical stimulations (0.2 Hz, biphasic current with peak-to-peak amplitude of 300 μA) led to an increase in the number of active electrodes (i.e., from 564 $\pm$ 28 to 688 $\pm$ 21) but decreased the mean firing rate (i.e., 0.66 $\pm$ 0.03 to 0.58 $\pm$ 0.03 spikes/s). Figure 13 summarizes these results.

The recent advent of CRISPR/Cas9-mediated genome editing has paved the way for fast development of disease models (Doudna and Charpentier 2014). Mice models of human diseases can be used to characterize the functional differences of cells from different parts of the body compared to their healthy counterparts. HD-MEAs can provide high-throughput and high-quality characterization of cells in culture and in acute preparations. One application of such characterization is biomarker identification, which has been done for a human retina disease called congenital nystagmus caused by FRMD7 gene mutation (Yonehara et al. 2016). A mouse model of such disease was developed, and light stimulation-evoked responses of RGCs in the retina were recorded and analyzed in a high-throughput manner. Using HD-MEAs, it was found that FRMD7 mutation leads to selective loss of horizontal selection selectivity of RGCs, as illustrated in Fig. 14.

3.4   Closed-Loop Studies

SM HD-MEAs enable simultaneous stimulation and recording of arbitrarily selected neurons in a network. By changing spike timing between sets of neurons via electrical simulations, the functional network connectivity was also changed (Müller et al. 2013). In this study, a reprogrammable event engine unit was programmed into

---

Fig. 12 (continued) recorded from. Scale bar, 100 μm. (**c**) AP propagation velocity changes, as shown by the colored dots along the electrical image of the axon. (D-F) Adapted with permission from Radivojevic et al. (2016). (**d**) Left: A single neuron's spike-triggered average footprint. Circle sizes correspond to logarithmically scaled amplitudes of APs and colors indicate spike time delay (negative peak) with respect to the spike initiation time of the respective neuron. Right: Stimulation map over the neuron's spike-triggered average footprint. Site-specific stimulation thresholds are color-coded; sites that were stimulated but did not evoke an action potential are colored in gray. Four sites are labeled "Anti 1–3" and "Ortho," indicating antidromic and orthodromic stimulation sites, respectively. (**e**) Excitability profiles of Anti 1–3 and Ortho sites. (**f**) Stimulation thresholds for the most sensitive orthodromic and antidromic sites determined for 13 neurons

Fig. 13 Spontaneous activity of hiPSCs. Recorded extracellular signal traces show changes in firing rates during development. The activity develops from single spikes (8 DIV), tonic firing (28 DIV) to bursting, and synchronized spikes (81, and 90 DIV). Red arrows denote the start of propagating burst. Adapted with permission from Amin et al. (2016)
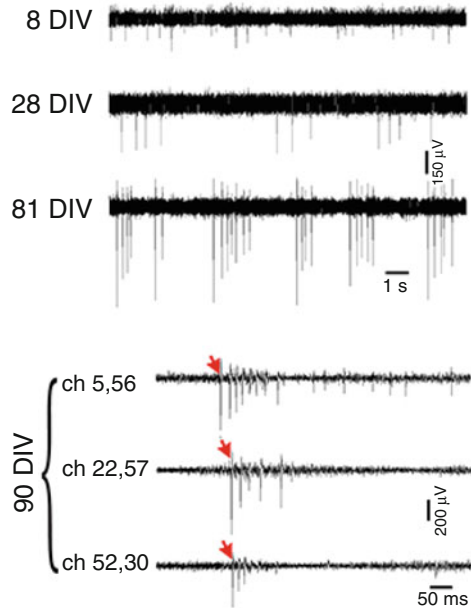
a field-programmable gate array. The system can detect arbitrary action potential patterns and use these to trigger electrical stimulations to arbitrary neurons, providing flexible and submillisecond latency closed-loop feedback. Cross-correlation analysis of spike trains showed the spike timing of the selectively stimulated neurons changed, which indicated that plasticity was induced in the network (Fig. 15).

3.5   Combination with Patch Clamp

The combination of HD-MEA and patch-clamp techniques provides a powerful approach to map monosynaptic connectivity of neurons in vitro. In such a combination, a single neuron or multiple neurons can be patched to detect subthreshold signals, such as postsynaptic potentials (PSPs), while the HD-MEA can be utilized to activate individual neurons by electrical stimulation. This method can be effectively applied to investigate local network mechanisms. First results have been obtained by Jäckel et al., showing contributions of presynaptic neurons, both excitatory and inhibitory, to PSPs (Jäckel et al. 2017), see Fig. 16. This combination technique can also be applied to brain slices; however, as cells are not directly attached on electrodes, higher stimulation amplitudes may be needed to evoke action potentials, which may activate multiple neurons at once. Additionally, the combined methods can enable imaging of a neuron's extracellular potential signature at subcellular resolution while controlling the cell's membrane potential.
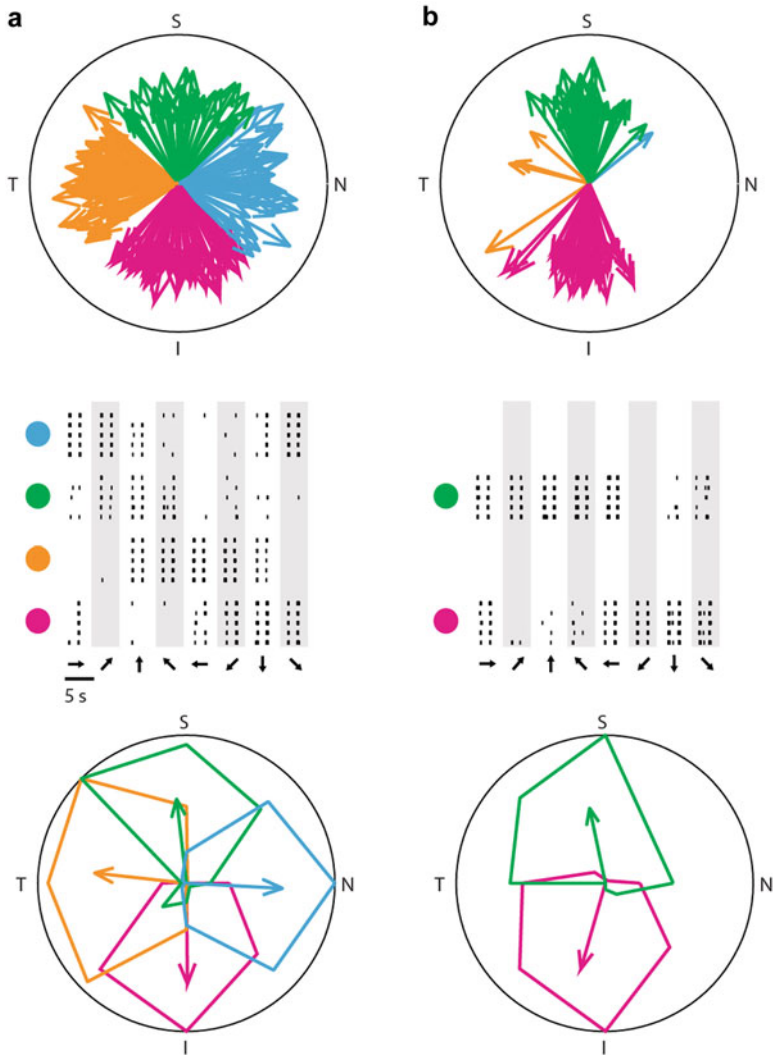
Fig. 14 Screening transgenic mouse models of human eye diseases with HD-MEAs. Top: Polar plots showing the preferred directions (directions of arrows) and direction selectivity index (length of an arrow) of individual direction-selective retinal ganglion cells in (**a**) WT and (**b**) FRMD7[tm] retinas. The color code shows the different preferred directions (green = superior, blue = nasal, purple = inferior, and orange = temporal). (Middle: Raster plots showing the spike responses (each black line is a spike) of example DS cells in WT and FRMD7[tm] retinas in response to motion in eight different directions, indicated by the arrows at the bottom of the plot. Bottom: polar plots of the normalized mean spike numbers of cells shown in middle panes. The preferred direction and DSI of each cell are represented by the direction and length of the corresponding (color-coded) arrow. Adapted with permission from Yonehara et al. (2016)
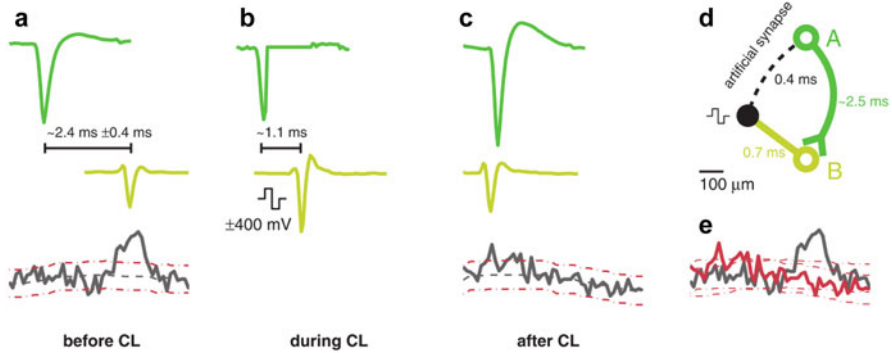
Fig. 15 Effect of closed-loop stimulation. (**a**) Spontaneous activity of two neurons before the application of the closed-loop stimulation. Spike traces are median waveforms of several spikes aligned at the negative peak. Top: In green, spike trace from neuron A, the trigger neuron. Middle: In yellow, spike trance of neuron B, a neuron with correlated spiking activity. Bottom: Cross-correlation curve of spike times of neuron B with respect to neuron A. Red dotted lines denote the 95% confidence intervals. Around 2000–3000 spikes were used to compute the cross-correlation. Elevated correlated activity of neuron B was observed around 2.4 ± 0.4 ms after neuron A fired an AP. (**b**) Same as (**a**), but with closed-loop feedback stimulation applied. The time delay of the spikes between neurons A and B was reduced to around 1.1 ms. Stimulation is applied upon detection of a spike from neuron A. During stimulation, the trace of neuron A was zeroed out. (**c**) Same as (**a**), but after application of the closed-loop stimulation. The cross-correlation plot changed after closed-loop stimulation. (**d**) Schematic of the synaptic connectivity between neurons A and B and the artificial synapse caused by closed-loop stimulation. (**e**) Comparison between the cross-correlation curves before (black) and after (red) the closed-loop stimulation. Adapted with permission from Müller et al. (2013)

Future developments of the technology may lead to electrically guided automated intracellular recordings (Annecchino et al. 2017; Kodandaramaiah et al. 2012, 2014; Suk et al. 2017).

Besides patch clamp, combining HD-MEA recordings with single-cell-targeted methods via a movable micropipette allows for advanced electrophysiology experiments (e.g., local puffing of compounds (Engle et al. 2012; Sasaki 2013; Sasaki et al. 2011), virus-stamping (Schubert et al. 2018), and single-cell electroporation (Boudes et al. 2008; Nevian and Helmchen 2007; Tanaka et al. 2009)). Such combination techniques will enable a detailed analysis of single cells in functional neuronal networks. Moreover, pipette-based dye-loading (Eilers and Konnerth 2009) can be used to obtain morphologies of recorded cells on the HD-MEAs. This enables acquisition of comprehensive information from defined cells towards developing precise and realistic multicompartment models.
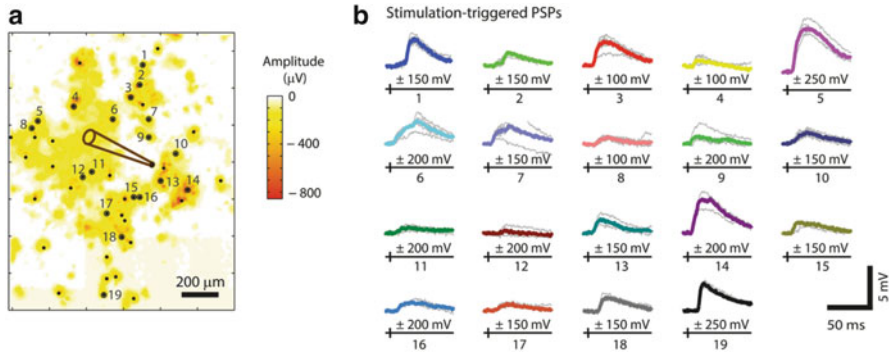
Fig. 16 Mapping synaptic connectivity through a combination of patch clamp and HD-MEA. (**a**) Amplitude map of the spontaneous activity of neurons with selected neurons marked with dots and numbered. The unselected neurons (unnumbered dots) did not evoke any postsynaptic potential (PSP) response. Each selected neuron was stimulated with bipolar voltage pulses ranging from 100 to 250 mV amplitude. The location of a single patched neuron is also shown. (**b**) PSP responses of the patched neuron (gray: individual traces; colored: median traces) to stimulation of individual presynaptic neurons. The minimum voltage values needed to evoke PSPs per presynaptic neuron are shown below the traces. The stimulus timing is also shown below the traces. Adapted with permission from (Jäckel et al. 2017)

4 Outlook

This chapter shows the current state of CMOS-based HD-MEA research in terms of technology and applications. Novel types of data can be obtained, which opens up new waves of possibilities for neuroscience discoveries and medical advancements. Potential future developments include device hardware improvements, advanced experimental methods, and new data analysis techniques.

Next generation HD-MEAs may target increased array area, electrode density, and number of parallel recording/stimulation channels. A larger array area will extend the observable region of a sample, allowing for simultaneous access to more neurons in cell cultures and to more distal brain areas in slices. This also enables opportunities for coculturing different tissues or brain regions. Higher spatial resolution and more recording channels will assist spike-sorting accuracy and will potentially increase the number of detectable neurons per square millimeter. Multiple HD-MEAs can also be combined in a multiwell-plate format, making HD-MEAs compatible to applications in drug discovery and development.

Aside from improving the devices through resolution and scalability, adding new functionalities may also be done. Other readout circuitry may also be integrated in HD-MEA devices (e.g., neurotransmitter and impedance measurement units) (Dragas et al. 2017). Multimodal measurement of neuronal activity will be helpful to understand the overall neuronal network function and the interplay between electrical activity and biochemical release.

Another promising route is the combination of HD-MEA with different tools separate from the device, such as optical methods. Fluorescent calcium and voltage indicators, generic markers, and optogenetics have been used to map and manipulate brain activity. Similar to extracellular recordings, the presence of many molecules and compartments in the brain with different optical properties renders optical recording and analysis challenging. Of interest is to pinpoint the advantages and constraints of electrophysiological versus optical methods to determine how they can complement each other. For example, optogenetic manipulation of specific cellular subpopulations, while measuring the responses of the neurons using HD-MEAs, will allow for studying functional roles of different classes of neurons (El Hady et al. 2013). Additionally, the effect of different optogenetic therapies to compensate for neuronal dysfunction can be tested with HD-MEAs.

Data obtained from next generation HD-MEAs and multimodal experiments require advanced computational analysis and modeling techniques. Fast implementations of spike-sorting algorithms and parallel computing are needed to handle the large amounts of data produced during long-term HD-MEA experiments. Multiscale modeling, a systems biology technique, may be employed to synchronize events recorded at different time and spatial scales. Overall, all data analysis methods need to be optimized to extract meaningful information within a feasible time from the massive amounts of datasets produced.

References

Alivisatos, A. P., Andrews, A. M., Boyden, E. S., Chun, M., Church, G. M., Deisseroth, K., et al. (2013). Nanotools for neuroscience and brain activity mapping. *ACS Nano, 7*, 1850–1866.

Alpha MED. Scientific Inc. http://www.med64.com

Amin, H., Maccione, A., Marinaro, F., Zordan, S., Nieus, T., & Berdondini, L. (2016). Electrical responses and spontaneous activity of human iPS-derived neuronal networks characterized for 3-month culture with 4096-electrode arrays. *Frontiers in Neuroscience, 10*, 121.

Andersen, R. A., Hwang, E. J., & Mulliken, G. H. (2010). Cognitive neural prosthetics. *Annual Review of Psychology, 61*, 169–90, C1–3.

Angotzi, G. N., Malerba, M., Boi, F., Miele, E., Maccione, A., Amin, H., et al. (2018). A synchronous neural recording platform for multiple high-resolution CMOS probes and passive electrode arrays. *IEEE Transactions on Biomedical Circuits and Systems, 12*(3), 532–542.

Annecchino, L. A., Morris, A. R., Copeland, C. S., Agabi, O. E., Chadderton, P., & Schultz, S. R. (2017). Robotic automation of in vivo two-photon targeted whole-cell patch-clamp electrophysiology. *Neuron, 95*, 1048–1055.e3.

Aziz, J. N. Y., Abdelhalim, K., Shulyzki, R., Genov, R., Bardakjian, B. L., Derchansky, M., et al. (2009). 256-channel neural recording and delta compression microsystem with 3D electrodes. *IEEE Journal of Solid-State Circuits, 44*, 995–1005.

Bakkum, D. J., Chao, Z. C., & Potter, S. M. (2008). Long-term activity-dependent plasticity of action potential propagation delay and amplitude in cortical networks. *PLoS One, 3*, e2088.

Bakkum, D. J., Frey, U., Radivojevic, M., Russell, T. L., Müller, J., Fiscella, M., et al. (2013). Tracking axonal action potential propagation on a high-density microelectrode array across hundreds of sites. *Nature Communications, 4*, 2181.

Ballini, M., Muller, J., Livi, P., Chen, Y., Frey, U., Stettler, A., et al. (2014). A 1024-channel CMOS microelectrode array with 26,400 electrodes for recording and stimulation of electrogenic cells in vitro. *IEEE Journal of Solid-State Circuits, 49*, 2705–2719.

Baumann, W., Lehmann, M., Schwinde, A., Ehret, R., Brischwein, M., & Wolf, B. (1999). Microelectronic sensor system for microphysiological application on living cells. *Sensors and Actuators B: Chemical, 55*, 77–89.

Berdondini, L., Massobrio, P., Chiappalone, M., Tedesco, M., Imfeld, K., Maccione, A., et al. (2009). Extracellular recordings from locally dense microelectrode arrays coupled to dissociated cortical cultures. *Journal of Neuroscience Methods, 177*, 386–396.

Berdondini, L., Overstolz, T., de Rooij, N., Koudelka-Hep, M., Martinoia, S., Seitz, P., et al. (2002). High resolution electrophysiological activity imaging of in-vitro neuronal networks. In *Microtechnologies in Medicine & Biology 2nd Annual International IEEE-EMB Special Topic Conference on* (IEEE) (pp. 241–244). Retrieved February 1, 2011, from http://ieeexplore.ieee.org/xpls/abs_all.jsp?arnumber=1002322

Berényi, A., Somogyvári, Z., Nagy, A. J., Roux, L., Long, J. D., Fujisawa, S., et al. (2014). Large-scale, high-density (up to 512 channels) recording of local circuits in behaving animals. *Journal of Neurophysiology, 111*, 1132–1149.

Bergveld, P. (1970). Development of an ion-sensitive solid-state device for neurophysiological measurements. *IEEE Transactions on Biomedical Engineering, 17*, 70–71.

Bertotti, G., Velychko, D., Dodel, N., Keil, S., Wolansky, D., Tillak, B., et al. (2014). A CMOS-based sensor array for in-vitro neural tissue interfacing with 4225 recording sites and 1024 stimulation sites. In *Biomedical Circuits and Systems Conference (BioCAS) (Lausanne, Switzerland)* (pp. 304–307)

Besl, B., & Fromherz, P. (2002). Transistor array with an organotypic brain slice: Field potential records and synaptic currents. *The European Journal of Neuroscience, 15*, 999–1005.

Blanche, T. J., Spacek, M. A., Hetke, J. F., & Swindale, N. V. (2005). Polytrodes: High-density silicon electrode arrays for large-scale multiunit recording. *Journal of Neurophysiology, 93*, 2987–3000.

Boudes, M., Pieraut, S., Valmier, J., Carroll, P., & Scamps, F. (2008). Single-cell electroporation of adult sensory neurons for gene screening with RNA interference mechanism. *Journal of Neuroscience Methods, 170*, 204–211.

Buzsáki, G., Anastassiou, C. A., & Koch, C. (2012). The origin of extracellular fields and currents—EEG, ECoG, LFP and spikes. *Nature Reviews. Neuroscience, 13*, 407–420.

Camuñas-Mesa, L. A., & Quiroga, R. Q. (2013). A detailed and fast model of extracellular recordings. *Neural Computation, 25*, 1191–1212.

Cheney, P. D., & Fetz, E. E. (1985). Comparable patterns of muscle facilitation evoked by individual corticomotoneuronal (CM) cells and by single intracortical microstimuli in primates: Evidence for functional groups of CM cells. *Journal of Neurophysiology, 53*, 786–804.

Cogan, S. F. (2008). Neural stimulation and recording electrodes. *Annual Review of Biomedical Engineering, 10*, 275–309.

Contreras, D. (2004). Electrophysiological classes of neocortical neurons. *Neural Networks, 17*, 633–646.

Csicsvari, J., Henze, D. a., Jamieson, B., Harris, K. D., Sirota, A., Barthó, P., et al. (2003). Massively parallel recording of unit and local field potentials with silicon-based electrodes. *Journal of Neurophysiology, 90*, 1314–1323.

Cui, X., Lee, V. a., Raphael, Y., Wiler, J. a., Hetke, J. F., Anderson, D. J., et al. (2001). Surface modification of neural recording electrodes with conducting polymer/biomolecule blends. *Journal of Biomedical Materials Research, 56*, 261–272.

DeBusschere, B. D., & Kovacs, G. T. (2001). Portable cell-based biosensor system using integrated CMOS cell-cartridges. *Biosensors & Bioelectronics, 16*, 543–556.

Destexhe, A., Contreras, D., & Steriade, M. (1999). Spatiotemporal analysis of local field potentials and unit discharges in cat cerebral cortex during natural wake and sleep states. *The Journal of Neuroscience, 19*, 4595–4608.

Dipalo, M., Melle, G., Lovato, L., Jacassi, A., Santoro, F., Caprettini, V., et al. (2018). Plasmonic meta-electrodes allow intracellular recordings at network level on high-density CMOS-multi-electrode arrays. *Nature Nanotechnology, 13*, 965.

Doudna, J. A., & Charpentier, E. (2014). The new frontier of genome engineering with CRISPR-Cas9. *Science (80), 346*, 1258096–1258096.

Dragas, J., Viswam, V., Shadmani, A., Chen, Y., Bounik, R., Stettler, A., et al. (2017). In vitro multi-functional microelectrode array featuring 59,760 electrodes, 2048 electrophysiology channels, stimulation, impedance measurement, and neurotransmitter detection channels. *IEEE Journal of Solid-State Circuits, 52*, 1–15.

Du, J., Blanche, T. J., Harrison, R. R., Lester, H. A., & Masmanidis, S. C. (2011). Multiplexed, high density electrophysiology with nanofabricated neural probes. *PLoS One, 6*, e26204.

Eaton, K. P., & Henriquez, C. S. (2005). Confounded spikes generated by synchrony within neural tissue models. *Neurocomputing, 65–66*, 851–857.

Egert, U., Heck, D., & Aertsen, A. (2002). Two-dimensional monitoring of spiking networks in acute brain slices. *Experimental Brain Research, 142*, 268–274.

Eickenscheidt, M., Jenkner, M., Thewes, R., Fromherz, P., & Zeck, G. (2012). Electrical stimulation of retinal neurons in epiretinal and subretinal configuration using a multicapacitor array. *Journal of Neurophysiology, 107*, 2742–2755.

Eilers, J., & Konnerth, A. (2009). Dye loading with patch pipettes. *Cold Spring Harbor Protocols, 2009*, pdb.prot5201.

El Hady, A., Afshar, G., Bröking, K., Schlüter, O. M., Geisel, T., Stühmer, W., et al. (2013). Optogenetic stimulation effectively enhances intrinsically generated network synchrony. *Frontiers in Neural Circuits, 7*, 167.

Engle, S. E., Broderick, H. J., & Drenan, R. M. (2012). Local application of drugs to study nicotinic acetylcholine receptor function in mouse brain slices. *Journal of Visualized Experiments, 68*, e50034.

Eversmann, B., Jenkner, M., Hofmann, F., Paulus, C., Brederlow, R., Holzapfl, B., et al. (2003). A 128×128 cmos biosensor array for extracellular recording of neural activity. *IEEE Journal of Solid-State Circuits, 38*, 2306–2317.

Eversmann, B., Lambacher, A., Gerling, T., Kunze, A., Fromherz, P., & Thewes, R. (2011). A neural tissue interfacing chip for in-vitro applications with 32k recording/stimulation channels on an active area of 2.6mm^2. In *2011 Proceedings of the ESSCIRC* (pp. 211–214). Helsinki: IEEE.

Fejtl, M., Stett, A., Nisch, W., Boven, K. H., & Möller, A. (2006). On micro-electrode array revival: Its development, sophistication of recording, and stimulation. In M. Taketani & M. Baudry (Eds.), *Advances in network electrophysiology* (pp. 24–37). New York: Springer.

Ferrea, E., Maccione, A., Medrihan, L., Nieus, T., Ghezzi, D., Baldelli, P., et al. (2012). Large-scale, high-resolution electrophysiological imaging of field potentials in brain slices with microelectronic multielectrode arrays. *Frontiers in Neural Circuits, 6*, 80.

Fiscella, M., Farrow, K., Jones, I. L., Jäckel, D., Müller, J., Frey, U., et al. (2012). Recording from defined populations of retinal ganglion cells using a high-density CMOS-integrated microelectrode array with real-time switchable electrode selection. *Journal of Neuroscience Methods, 211*, 103–113.

Fiscella, M., Franke, F., Farrow, K., Müller, J., Roska, B., Azeredo da Silveira, R., et al. (2015). Visual coding with a population of direction-selective neurons. *Journal of Neurophysiology, 114*, 2485–2499.

Fiscella, M., Franke, F., Müller, J., Jones, I. L., & Hierlemann, A. (2014). *Decoding of motion directions by direction-selective retina cells*. In Proceedings of the 9th International Meeting on Substrate-Integrated Microelectrode Arrays, Reutlingen, Germany, 98–99.

Franke, F., Fiscella, M., Sevelev, M., Roska, B., Hierlemann, A., & Azeredo da Silveira, R. (2016). Structures of neural correlation and how they favor coding. *Neuron, 89*, 409–422.

Franks, W., Heer, F., McKay, I., Taschini, S., Sunier, R., Hagleitner, C., et al. (2003). CMOS monolithic microelectrode array for stimulation and recording of natural neural networks. in *TRANSDUCERS '03. 12th International Conference on Solid-State Sensors, Actuators and Microsystems. Digest of Technical Papers (Cat. No.03TH8664)* (pp. 963–966). Boston: IEEE.

Franks, W., Schenker, I., Schmutz, P., & Hierlemann, A. (2005). Impedance characterization and modeling of electrodes for biomedical applications. *IEEE Transactions on Biomedical Engineering, 52*, 1295–1302.

Frey, U., Egert, U., Heer, F., Hafizovic, S., & Hierlemann, A. (2009a). Microelectronic system for high-resolution mapping of extracellular electric fields applied to brain slices. *Biosensors & Bioelectronics, 24*, 2191–2198.

Frey, U., Egert, U., Jackel, D., Sedivy, J., Ballini, M., Livi, P., et al. (2009b). Depth recording capabilities of planar high-density microelectrode arrays. in *2009 4th International IEEE/EMBS Conference on Neural Engineering* (pp. 207–210). Antalya: IEEE.

Frey, U., Sedivy, J., Heer, F., Pedron, R., Ballini, M., Mueller, J., et al. (2010). Switch-matrix-based high-density microelectrode array in CMOS technology. *IEEE Journal of Solid-State Circuits, 45*, 467–482.

Fromherz, P., Offenhausser, A., Vetter, T., & Weis, J. (1991). A neuron-silicon junction: A Retzius cell of the leech on an insulated-gate field-effect transistor. *Science (80-), 252*, 1290–1293.

Fujisawa, S., Amarasingham, A., Harrison, M. T., & Buzsáki, G. (2008). Behavior-dependent short-term assembly dynamics in the medial prefrontal cortex. *Nature Neuroscience, 11*, 823–833.

Gandolfo, M., Maccione, a., Tedesco, M., Martinoia, S., & Berdondini, L. (2010). Tracking burst patterns in hippocampal cultures with high-density CMOS-MEAs. *Journal of Neural Engineering, 7*, 56001.

Gesteland, R., Howland, B., Lettvin, J., & Pitts, W. (1959). Comments on microelectrodes. *Proceedings of the IRE, 47*, 1856–1862.

Gong, W., Senčar, J., Bakkum, D. J., Jäckel, D., Obien, M. E. J., Radivojevic, M., et al. (2016). Multiple single-unit long-term tracking on organotypic hippocampal slices using high-density microelectrode arrays. *Frontiers in Neuroscience, 10*, 537.

Gray, C. M., Maldonado, P. E., Wilson, M., & McNaughton, B. (1918). Tetrodes markedly improve the reliability and yield of multiple single-unit isolation from multi-unit recordings in cat striate cortex. *Journal of Neuroscience Methods, 63*, 43–54.

Greschner, M., Field, G. D., Li, P. H., Schiff, M. L., Gauthier, J. L., Ahn, D., et al. (2014). A polyaxonal amacrine cell population in the primate retina. *The Journal of Neuroscience, 34*, 3597–3606.

Greve, F., Lichtenberg, J., Kirstein, K.-U. U., Frey, U., Perriard, J.-C., & Hierlemann, A. (2007). A perforated CMOS microchip for immobilization and activity monitoring of electrogenic cells. *Journal of Micromechanics and Microengineering, 17*, 462–471.

Gross, G., Rieske, E., Kreutzberg, G., & Meyer, A. (1977). A new fixed-array multi-microelectrode system designed for long-term monitoring of extracellular single unit neuronal activity in vitro. *Neuroscience Letters, 6*, 101–105.

Habibey, R., Latifi, S., Mousavi, H., Pesce, M., Arab-Tehrany, E., & Blau, A. (2017). A multielectrode array microchannel platform reveals both transient and slow changes in axonal conduction velocity. *Scientific Reports, 7*, 1–14.

Hafizovic, S., Heer, F., Ugniwenko, T., Frey, U., Blau, A., Ziegler, C., et al. (2007). A CMOS-based microelectrode array for interaction with neuronal cultures. *Journal of Neuroscience Methods, 164*, 93–106.

Hai, A., Dormann, A., Shappir, J., Yitzchaik, S., Bartic, C., Borghs, G., et al. (2009). Spine-shaped gold protrusions improve the adherence and electrical coupling of neurons with the surface of micro-electronic devices. *Journal of The Royal Society Interface, 6*, 1153–1165.

Hai, A., & Spira, M. E. (2012). On-chip electroporation, membrane repair dynamics and transient in-cell recordings by arrays of gold mushroom-shaped microelectrodes. *Lab on a Chip, 12*, 2865–2873.

Harris, K. D., Henze, D. A., Csicsvari, J., Hirase, H., & Buzsáki, G. (2000). Accuracy of tetrode spike separation as determined by simultaneous intracellular and extracellular measurements. *Journal of Neurophysiology, 84*, 401–414.

Harrison, R. R. (2008). The design of integrated circuits to observe brain activity. *Proceedings of the IEEE, 96*, 1203–1216.

Hashimoto, T., Elder, C. M., & Vitek, J. L. (2002). A template subtraction method for stimulus artifact removal in high-frequency deep brain stimulation. *Journal of Neuroscience Methods, 113*, 181–186.

Hassibi, A., Navid, R., Dutton, R. W., & Lee, T. H. (2004). Comprehensive study of noise processes in electrode electrolyte interfaces. *Journal of Applied Physics, 96*, 1074.

Hassler, C., Boretius, T., & Stieglitz, T. (2011). Polymers for neural implants. *Journal of Polymer Science Part B: Polymer Physics, 49*, 18–33.

Heer, F. (2005). *CMOS-based microelectrode array for communication with electrogenic cells*. PhD thesis, No. 16330, Zurich: ETH Zurich.

Heer, F., Franks, W., Blau, A., Taschini, S., Ziegler, C., Hierlemann, A., et al. (2004). CMOS microelectrode array for the monitoring of electrogenic cells. *Biosensors & Bioelectronics, 20*, 358–366.

Heer, F., Hafizovic, S., Franks, W., Blau, A., Ziegler, C., & Hierlemann, A. (2006). CMOS microelectrode array for bidirectional interaction with neuronal networks. *IEEE Journal of Solid-State Circuits, 41*, 1620–1629.

Heer, F., Hafizovic, S., Ugniwenko, T., Frey, U., Franks, W., Perriard, E., et al. (2007). Single-chip microelectronic system to interface with living cells. *Biosensors & Bioelectronics, 22*, 2546–2553.

Henze, D. A., Borhegyi, Z., Csicsvari, J., Mamiya, A., Harris, K. D., & Buzsáki, G. (2000). Intracellular features predicted by extracellular recordings in the hippocampus in vivo. *Journal of Neurophysiology, 84*, 390–400.

Herwik, S., Kisban, S., Aarts, A. A. A., Seidl, K., Girardeau, G., Benchenane, K., et al. (2009). Fabrication technology for silicon-based microprobe arrays used in acute and sub-chronic neural recording. *Journal of Micromechanics and Microengineering, 19*, 74008.

Hierlemann, A., Frey, U., Hafizovic, S., & Heer, F. (2011). Growing cells atop microelectronic chips: Interfacing electrogenic cells in vitro with CMOS-based microelectrode arrays. *Proceedings of the IEEE, 99*, 252–284.

Huang, X.-J., O'Mahony, A. M., & Compton, R. G. (2009). Microelectrode arrays for electrochemistry: Approaches to fabrication. *Small, 5*, 776–788.

Huys, R., Braeken, D., Jans, D., Stassen, A., Collaert, N., Wouters, J., et al. (2012). Single-cell recording and stimulation with a 16 k micro-nail electrode array integrated on a 0.18 µm CMOS chip. *Lab on a Chip, 12*, 1274–1280.

Imfeld, K., Neukom, S., Maccione, A., Bornat, Y., Martinoia, S., Farine, P.-A., et al. (2008). Large-scale, high-resolution data acquisition system for extracellular recording of electrophysiological activity. *IEEE Transactions on Biomedical Engineering, 55*, 2064–2073.

Jäckel, D., Bakkum, D. J., Russell, T. L., Müller, J., Radivojevic, M., Frey, U., et al. (2017). Combination of high-density microelectrode array and patch clamp recordings to enable studies of multisynaptic integration. *Scientific Reports, 7*, 978.

Jäckel, D., Frey, U., Fiscella, M., Franke, F., & Hierlemann, A. (2012). Applicability of independent component analysis on high-density microelectrode array recordings. *Journal of Neurophysiology, 108*, 334–348.

Jenkner, M., Tartagni, M., Hierlemann, A., & Thewes, R. (2004). Cell-based CMOS sensor and actuator arrays. *IEEE Journal of Solid-State Circuits, 39*, 2431–2437.

Jobling, D. T., Smith, J. G., & Wheal, H. V. (1981). Active microelectrode array to record from the mammalian central nervous system in vitro. *Medical & Biological Engineering & Computing, 19*, 553–560.

Jochum, T., Denison, T., & Wolf, P. (2009). Integrated circuit amplifiers for multi-electrode intracortical recording. *Journal of Neural Engineering, 6*, 012001–012026.

Johnson, B., Peace, S. T., Cleland, T. A., & Molnar, A. (2013a). A 50 μm pitch, 1120-channel, 20 kHz frame rate microelectrode array for slice recording. In *2013 IEEE Biomedical Circuits and Systems Conference (BioCAS), Rotterdam* (pp. 109–112).

Johnson, B., Peace, S. T., Wang, A., Cleland, T. A., & Molnar, A. (2013b). A 768-channel CMOS microelectrode array with angle sensitive pixels for neuronal recording. *IEEE Sensors Journal, 13*, 3211–3218.

Jones, I. L., Russell, T. L., Farrow, K., Fiscella, M., Franke, F., Müller, J., et al. (2015). A method for electrophysiological characterization of hamster retinal ganglion cells using a high-density CMOS microelectrode array. *Frontiers in Neuroscience, 9*, 1–16.

Jones, K. E., Campbell, P. K., & Normann, R. a. (1992). A glass/silicon composite intracortical electrode array. *Annals of Biomedical Engineering, 20*, 423–437.

Katzner, S., Nauhaus, I., Benucci, A., Bonin, V., Ringach, D. L., & Carandini, M. (2009). Local origin of field potentials in visual cortex. *Neuron, 61*, 35–41.

Keefer, E. W., Botterman, B. R., Romero, M. I., Rossi, A. F., & Gross, G. W. (2008). Carbon nanotube coating improves neuronal recordings. *Nature Nanotechnology, 3*, 434–439.

Kim, R., Joo, S., Jung, H., Hong, N., & Nam, Y. (2014). Recent trends in microelectrode array technology for in vitro neural interface platform. *Biomedical Engineering Letters, 4*, 129–141.

Kipke, D. R., Vetter, R. J., Williams, J. C., & Hetke, J. F. (2003). Silicon-substrate intracortical microelectrode arrays for long-term recording of neuronal spike activity in cerebral cortex. *IEEE Transactions on Neural Systems and Rehabilitation Engineering, 11*, 151–155.

Kodandaramaiah, S. B., Flores, F., Holst, G., Wickersham, I., Brown, E., Forest, C. R., et al. (2014). The multipatcher: a robot for high density measurement of intracellular recordings in vivo. In *Proceedings of the Biomedical Engineering Society (BMES), San Antonio, TX*.

Kodandaramaiah, S. B., Franzesi, G. T., Chow, B. Y., Boyden, E. S., & Forest, C. R. (2012). Automated whole-cell patch-clamp electrophysiology of neurons in vivo. *Nature Methods, 9*, 585–587.

Koester, P. J., Tautorat, C., Beikirch, H., Gimsa, J., & Baumann, W. (2010). Recording electric potentials from single adherent cells with 3D microelectrode arrays after local electroporation. *Biosensors & Bioelectronics, 26*, 1731–1735.

Lambacher, a., Vitzthum, V., Zeitler, R., Eickenscheidt, M., Eversmann, B., Thewes, R., et al. (2010). Identifying firing mammalian neurons in networks with high-resolution multi-transistor array (MTA). *Applied Physics A: Materials Science & Processing, 102*, 1–11.

Lempka, S. F., Johnson, M. D., Moffitt, M. A., Otto, K. J., Kipke, D. R., & McIntyre, C. C. (2011). Theoretical analysis of intracortical microelectrode recordings. *Journal of Neural Engineering, 8*, 45006.

Lewandowska, M. K., Bakkum, D. J., Rompani, S. B., & Hierlemann, A. (2015). Recording large extracellular spikes in microchannels along many axonal sites from individual neurons. *PLoS One, 10*, e0118514.

Lewandowska, M. K., Radivojević, M., Jäckel, D., Müller, J., & Hierlemann, A. R. (2016). Cortical axons, isolated in channels, display activity-dependent signal modulation as a result of targeted stimulation. *Frontiers in Neuroscience, 10*. https://doi.org/10.3389/fnins.2016.00083

Li, N., Tourovskaia, A., & Folch, A. (2003). Biology on a chip: Microfabrication for studying the behavior of cultured cells. *Critical Reviews in Biomedical Engineering, 31*, 423–488.

Litke, A. M., Bezayiff, N., Chichilnisky, E. J., Cunningham, W., Dabrowski, W., Grillo, A. A., et al. (2004). What does the eye tell the brain?: Development of a system for the large-scale recording of retinal output activity. *IEEE Transactions on Nuclear Science, 51*, 1434–1440.

Liu, X., Demosthenous, A., & Donaldson, N. (2007). On the noise performance of pt. electrodes. *Conference Proceedings: Annual International Conference of the IEEE Engineering in Medicine and Biology Society, 2007*, 434–436.

Livi, P., Heer, F., Frey, U., Bakkum, D. J., & Hierlemann, A. (2010). Compact voltage and current stimulation buffer for high-density microelectrode arrays. *IEEE Transactions on Biomedical Circuits and Systems, 4*, 372–378.

Llinas, R. (1988). The intrinsic electrophysiological properties of mammalian neurons: Insights into central nervous system function. *Science (80-), 242*, 1654–1664.

Lloyd, J. I., Thomas, R., Michele, F., Felix, F., Jan, M., Milos, R., et al. (2014). Characterization of mammalian retinal ganglion cell response to voltage stimulus. In *Proceedings of the ninth International Meeting on Substrate-Integrated Microelectrode Arrays, Reutlingen, Germany* (pp. 74–75).

Lopez, C. M., Andrei, A., Mitra, S., Welkenhuysen, M., Eberle, W., Bartic, C., et al. (2014). An implantable 455-active-electrode 52-channel CMOS neural probe. *IEEE Journal of Solid-State Circuits, 49*, 248–261.

Lopez, C. M., Mitra, S., Putzeys, J., Raducanu, B., Ballini, M., Andrei, A., et al. (2016). 22.7 A 966-electrode neural probe with 384 configurable channels in 0.13 µm SOI CMOS. In *2016 IEEE International Solid-State Circuits Conference (ISSCC)* (pp. 392–393). IEEE.

Lopez, C. M., Chun, H. S., Wang, S., Berti, L., Putzeys, J., Van Den Bulcke, C., et al. (2018, Nov). A multimodal CMOS MEA for high-throughput intracellular action potential measurements and impedance spectroscopy in drug-screening applications. *IEEE Journal of Solid-State Circuits, 53*(11), 3076–3086.

Ludwig, K. A., Uram, J. D., Yang, J., Martin, D. C., & Kipke, D. R. (2006). Chronic neural recordings using silicon microelectrode arrays electrochemically deposited with a poly(3,4-ethylenedioxythiophene) (PEDOT) film. *Journal of Neural Engineering, 3*, 59–70.

Maccione, A., Hennig, M. H., Gandolfo, M., Muthmann, O., van Coppenhagen, J., Eglen, S. J., et al. (2014). Following the ontogeny of retinal waves: Pan-retinal recordings of population dynamics in the neonatal mouse. *The Journal of Physiology, 592*, 1545–1563.

Maccione, A., Simi, A., Nieus, T., Gandolfo, M., Imfeld, K., Ferrea, E., et al. (2013). Sensing and actuating electrophysiological activity on brain tissue and neuronal cultures with a high-density CMOS-MEA. In *2013 Transducers & Eurosensors XXVII: The 17th International Conference on Solid-State Sensors, Actuators and Microsystems (TRANSDUCERS & EUROSENSORS XXVII)* (pp. 752–755). Barcelona: IEEE.

Marblestone, A. H., Zamft, B. M., Maguire, Y. G., Shapiro, M. G., Cybulski, T. R., Glaser, J. I., et al. (2013). Physical principles for scalable neural recording. *Frontiers in Computational Neuroscience, 7*, 137.

Martinez, J., Pedreira, C., Ison, M. J., & Quian Quiroga, R. (2009). Realistic simulation of extracellular recordings. *Journal of Neuroscience Methods, 184*, 285–293.

Medrihan, L., Ferrea, E., Greco, B., Baldelli, P., & Benfenati, F. (2014). Asynchronous GABA release is a key determinant of tonic inhibition and controls neuronal excitability: A study in the synapsin II−/− mouse. *Cerebral Cortex, 25*, 3356–3368.

Menzler, J., & Zeck, G. (2011). Network oscillations in rod-degenerated mouse retinas. *The Journal of Neuroscience, 31*, 2280–2291.

Montgomery, S. M., Sirota, A., & Buzsáki, G. (2008). Theta and gamma coordination of hippocampal networks during waking and rapid eye movement sleep. *The Journal of Neuroscience, 28*, 6731–6741.

Moxon, K. A. (1999). Multichannel electrode design: Considerations for different applications. In M. A. L. Nicolelis (Ed.), *Methods for neural ensemble recordings* (pp. 25–45). Boca Raton: CRC Press.

Müller, J., Bakkum, D. J., & Hierlemann, A. (2013). Sub-millisecond closed-loop feedback stimulation between arbitrary sets of individual neurons. *Frontiers in Neural Circuits, 6*, 1–11.

Müller, J., Ballini, M., Livi, P., Chen, Y., Radivojevic, M., Shadmani, A., et al. (2015). High-resolution CMOS MEA platform to study neurons at subcellular, cellular, and network levels. *Lab on a Chip, 15*, 2767–2780.

Muller, R., Gambini, S., & Rabaey, J. M. (2012). A 0.013 mm2, 5uW, DC-coupled neural signal acquisition IC with 0.5 V supply. *IEEE Journal of Solid-State Circuits, 47*, 232–243.

Multi Channel Systems GmbH. http://www.multichannelsystems.com

Nam, Y., & Wheeler, B. C. (2011). In vitro microelectrode array technology and neural recordings. *Critical Reviews in Biomedical Engineering, 39*, 45–61.

Nelson, M. J., & Pouget, P. (2010). Do electrode properties create a problem in interpreting local field potential recordings? *Journal of Neurophysiology, 103*, 2315–2317.

Nelson, M. J., Pouget, P., Nilsen, E. a., Patten, C. D., & Schall, J. D. (2008). Review of signal distortion through metal microelectrode recording circuits and filters. *Journal of Neuroscience Methods, 169*, 141–157.

Ness, T. V., Chintaluri, C., Potworowski, J., Łęski, S., Głąbska, H., Wójcik, D. K., et al. (2015). Modelling and analysis of electrical potentials recorded in microelectrode arrays (MEAs). *Neuroinformatics.* https://doi.org/10.1007/s12021-015-9265-6

Nevian, T., & Helmchen, F. (2007). Calcium indicator loading of neurons using single-cell electroporation. *Pflügers Archiv-European Journal of Physiology, 454*, 675–688.

Nisch, W., Böck, J., Egert, U., Hämmerle, H., & Mohr, A. (1994). A thin film microelectrode array for monitoring extracellular neuronal activity in vitro. *Biosensors & Bioelectronics, 9*, 737–741.

O'Keefe, J., & Recce, M. L. (1993). Phase relationship between hippocampal place units and the EEG theta rhythm. *Hippocampus, 3*, 317–330.

Obien, M. E. J., Deligkaris, K., Bullmann, T., Bakkum, D. J., & Frey, U. (2015). Revealing neuronal function through microelectrode array recordings. *Frontiers in Neuroscience, 8*. https://doi.org/10.3389/fnins.2014.00423

Obien, M. E. J., Hierlemann, A., & Frey, U. (2014). Technique for analysis of purkinje cell subcellular functional dynamics in acute cerebellar slices using a high-density microelectrode array. In *Proceedings of the 9th International Meeting on Substrate-Integrated Microelectrode Arrays, Reutlingen, Germany* (pp. 88–90).

Offenhäusser, A., Sprössler, C., Matsuzawa, M., & Knoll, W. (1997). Field-effect transistor array for monitoring electrical activity from mammalian neurons in culture. *Biosensors & Bioelectronics, 12*, 819–826.

Ogi, J., Kato, Y., Matoba, Y., Yamane, C., Nagahata, K., Nakashima, Y., et al. (2017, Dec). Twenty-four-micrometer-pitch microelectrode array with 6912-channel readout at 12 kHz via highly scalable implementation for high-spatial-resolution mapping of action potentials. *Biointerphases, 12*(5), 05F402.

Oka, H., Shimono, K., Ogawa, R., Sugihara, H., & Taketani, M. (1999). A new planar multielectrode array for extracellular recording: Application to hippocampal acute slice. *Journal of Neuroscience Methods, 93*, 61–67.

Olsson III, R. H., & Wise, D. K. (2005). A three-dimensional neural recording microsystem with implantable data compression circuitry. *IEEE Journal of Solid-State Circuits, 40*, 2796–2804.

Paik, S.-J., Park, Y., & Cho, D. D. (2003). Roughened polysilicon for low impedance microelectrodes in neural probes. *Journal of Micromechanics and Microengineering, 13*, 373–379.

Parce, J. W., Owicki, J. C., Kercso, K. M., Sigal, G. B., Wada, H. G., Muir, V. C., et al. (1989). Detection of cell-affecting agents with a silicon biosensor. *Science, 246*, 243–247.

Park, J., Aziz, M. K., Gonzalez, S., Jung, D., Chi, T., Li, S., et al. (2017). A CMOS 22 k-pixel single-cell resolution multi-modality real-time cellular sensing array. In *Proceedings of the Custom Integrated Circuits Conference* (pp. 5–8).

Park, T. H., & Shuler, M. L. (2003). Integration of cell culture and microfabrication technology. *Biotechnology Progress, 19*, 243–253.

Pine, J. (1980). Recording action potentials from cultured neurons with extracellular microcircuit electrodes. Journal of Neuroscience Methods 2, 19–31. Retrieved February 1, 2011, from http://linkinghub.elsevier.com/retrieve/pii/0165027080900424

Radivojevic, M., Franke, F., Altermatt, M., Müller, J., Hierlemann, A., & Bakkum, D. J. (2017). Tracking individual action potentials throughout mammalian axonal arbors. *eLife, 6*, 1–23.

Radivojevic, M., Jäckel, D., Altermatt, M., Müller, J., Viswam, V., Hierlemann, A., et al. (2016). Electrical identification and selective microstimulation of neuronal compartments based on features of extracellular action potentials. *Scientific Reports, 6*, 31332.

Regehr, W. G., Pine, J., Cohan, C. S., Mischke, M. D., & Tank, D. W. (1989). Sealing cultured invertebrate neurons to embedded dish electrodes facilitates long-term stimulation and recording. *Journal of Neuroscience Methods, 30*, 91–106.

Reinhard, K., Mutter, M., Fiscella, M., Müller, J., Franke, F., Hierlemann, A., et al. (2014). Novel insights into visual information processing of human retina. In *Proceedings of the 9th International Meeting on Substrate-Integrated Microelectrode Arrays, Reutlingen, Germany* (p. 102).

Robinson, D. A. (1968). The electrical properties of metal microelectrodes. *Proceedings of the IEEE, 56*, 1065–1071.

Robinson, J. T., Jorgolli, M., & Park, H. (2013). Nanowire electrodes for high-density stimulation and measurement of neural circuits. *Frontiers in Neural Circuits, 7*, 1–5.

Sanchez-Bustamante, C. D., Frey, U., Kelm, J. M., Hierlemann, A., & Fussenegger, M. (2008). Modulation of cardiomyocyte electrical properties using regulated bone morphogenetic protein-2 expression. *Tissue Engineering. Part A, 14*, 1969–1988.

Sasaki, T. (2013). The axon as a unique computational unit in neurons. *Neuroscience Research, 75*, 83–88.

Sasaki, T., Matsuki, N., & Ikegaya, Y. (2011). Action-potential modulation during axonal conduction. *Science, 331*, 599–601.

Schubert, R., Trenholm, S., Balint, K., Kosche, G., Cowan, C. S., Mohr, M. A., et al. (2018). Virus stamping for targeted single-cell infection in vitro and in vivo. *Nature Biotechnology, 36*, 81.

Sedivy, J., Frey, U., Heer, F., Hafizovic, S., & Hierlemann, A. (2007). Multi-chip high-density microelectrode system for electrogenic-cell recording and stimulation. In *2007 IEEE sensors* (pp. 716–719). Atlanta: IEEE.

Segev, R., Goodhouse, J., Puchalla, J., & Berry, M. J. (2004). Recording spikes from a large fraction of the ganglion cells in a retinal patch. *Nature Neuroscience, 7*, 1154–1161.

Seidl, K., Herwik, S., Torfs, T., Neves, H. P., Paul, O., & Ruther, P. (2011). CMOS-based high-density silicon microprobe arrays for electronic depth control in intracortical neural recording. *Journal of Microelectromechanical Systems, 20*, 1439–1448.

Shahrokhi, F., Abdelhalim, K., & Genov, R. (2009). 128-channel fully differential digital neural recording and stimulation interface. In *2009 IEEE International Symposium on Circuits and Systems (IEEE)* (pp. 1249–1252).

Spira, M. E., & Hai, A. (2013). Multi-electrode array technologies for neuroscience and cardiology. *Nature Nanotechnology, 8*, 83–94.

Stett, A., Egert, U., Guenther, E., Hofmann, F., Meyer, T., Nisch, W., et al. (2003). Biological application of microelectrode arrays in drug discovery and basic research. *Analytical and Bioanalytical Chemistry, 377*, 486–495.

Steyaert, M. S. J., & Sansen, W. M. C. (1987). A micropower low-noise monolithic instrumentation amplifier for medical purposes. *IEEE Journal of Solid-State Circuits, 22*, 1163–1168.

Stutzki, H., Leibig, C., Andreadaki, A., Fischer, D., & Zeck, G. (2014). Inflammatory stimulation preserves physiological properties of retinal ganglion cells after optic nerve injury. *Frontiers in Cellular Neuroscience, 8*, 38.

Suk, H.-J., van Welie, I., Kodandaramaiah, S. B., Allen, B., Forest, C. R., & Boyden, E. S. (2017). Closed-loop real-time imaging enables fully automated cell-targeted patch-clamp neural recording in vivo. *Neuron, 95*, 1037–1047.e11.

Tanaka, M., Yanagawa, Y., & Hirashima, N. (2009). Transfer of small interfering RNA by single-cell electroporation in cerebellar cell cultures. *Journal of Neuroscience Methods, 178*, 80–86.

Thomas, C. A., Springer, P. A., Loeb, G. E., Berwald-Netter, Y., & Okum, L. M. (1972). A miniature microelectrode array to monitor the bioelectric activity of cultured cells. *Experimental Cell Research, 74*, 61–66.

Tokuda, T., Yamamoto, A., Kagawa, K., Nunoshita, M., & Ohta, J. (2006). A CMOS image sensor with optical and potential dual imaging function for on-chip bioscientific applications. *Sensors and Actuators A: Physical, 125*, 273–280.

Tsai, D., Sawyer, D., Bradd, A., Yuste, R., & Shepard, K. L. (2017). A very large-scale microelectrode array for cellular-resolution electrophysiology. *Nature Communications, 8*. https://doi.org/10.1038/s41467-017-02009-x

Velychko, D., Eickenscheidt, M., Thewes, R., & Zeck, G. (2014). Simultaneous stimulation and recording of retinal action potentials using capacitively coupled high- density CMOS-based MEAs. In *Proceedings of the 9th International Meeting on Substrate-Integrated Microelectrode Arrays, Reutlingen, Germany* (pp. 78–79).

Viswam, V., Dragas, J., Shadmani, A., Chen, Y., Stettler, A., Mueller, J., et al. (2016). Multi-functional microelectrode array system featuring 59,760 electrodes, 2048 electrophysiology channels, impedance and neurotransmitter measurement units. In *2016 IEEE International Solid-State Circuits Conference, ISSCC 2016, San Francisco, CA, USA, January 31–February 4, 2016* (pp. 394–396).

Viswam, V., Jäckel, D., Ballini, M., Müller, J., Radivojevic, M., Frey, U., et al. (2014). An automated method for characterizing electrode properties of high-density microelectrode arrays. In *Proceedings of the 9th International Meeting on Substrate-Integrated Microelectrode Arrays, Reutlingen, Germany* (pp. 302–303).

Wagenaar, D. A., & Potter, S. M. (2002). Real-time multi-channel stimulus artifact suppression by local curve fitting. *Journal of Neuroscience Methods, 120*, 113–120.

Ward, M. P., Rajdev, P., Ellison, C., & Irazoqui, P. P. (2009). Toward a comparison of microelectrodes for acute and chronic recordings. *Brain Research, 1282*, 183–200.

Weale, R. A. (1951). A new micro-electrode for electro-physiological work. *Nature, 167*, 529–530.

Weis, R., & Fromherz, P. (1997). Frequency dependent signal transfer in neuron transistors. *Physical Review E, 55*, 877–889.

Wise, K. D., Angell, J. B., & Starr, A. (1970). An integrated-circuit approach to extracellular microelectrodes. *IEEE Transactions on Biomedical Engineering, 3*, 238–247.

Wood, C., Williams, C., & Waldron, G. J. (2004). Patch clamping by numbers. *Drug Discovery Today, 9*, 434–441.

Yonehara, K., Fiscella, M., Drinnenberg, A., Esposti, F., Trenholm, S., Krol, J., et al. (2016). Congenital nystagmus gene FRMD7 is necessary for establishing a neuronal circuit asymmetry for direction selectivity. *Neuron, 89*, 177–193.

Yuan, X., Kim, S., Juyon, J., Urbino, M. D., Bullmann, T., Chen, Y., et al. (2016). A microelectrode array with 8,640 electrodes enabling simultaneous full-frame readout at 6.5 kfps and 112-channel switch-matrix readout at 20 kS/s. In *Symposium on VLSI Circuits Digest of Technical Papers, Honolulu, Hawaii* (pp. 258–259).

Yuan, X., Emmenegger, V., Obien, M. E. J., Hierlemann, A., & Frey, U. (2018). Dual-mode microelectrode array featuring 20k electrodes and high SNR for extracellular recording of neural networks. In *2018 IEEE Biomedical Circuits and Systems Conference (BioCAS)* (pp. 1–4).

Zeck, G., Lambacher, A., & Fromherz, P. (2011). Axonal transmission in the retina introduces a small dispersion of relative timing in the ganglion cell population response. *PLoS One, 6*, e20810.

Multisite Intracellular Recordings by MEA

Micha E. Spira, Shun-Ho Huang, Nava Shmoel, and Hadas Erez

Abstract The enormous advances made over the last 50 years in materials science, microelectronics, and nanoelectronics, together with the acknowledgment that substrate-integrated planar multielectrode arrays (MEA) are limited to recording of extracellular field potentials (FPs) rather than the entire electrophysiological signaling repertoire of the brain, have prompted a number of laboratories to merge the advantages of planar MEA technologies (non-damaging and durable) with those of the classical sharp and patch electrodes for intracellular recordings. Unlike extracellular planar electrode-based MEAs, the new generation of three-dimensional (3D) vertical nanoelectrodes are designed to functionally penetrate the plasma membrane of cultured cells and operate in a similar manner to classical intracellular microelectrodes. Although only approximately 10 years has elapsed since the development of the first vertical 3D nanostructure-based MEAs, this technology has progressed to enable recordings of attenuated intracellular action potentials (APs) and synaptic potentials from individual neurons, cardiomyocytes, and striated myotubes. Furthermore, recently the scaling advantages of nanochip/microchip fabrication technologies enabled simultaneously intracellular recordings of APs from hundreds of cultured cardiomyocytes, thus heralding a new milestone in MEA technology.

In this chapter we present the earliest and today's cutting-edge achievements of this "young vertical nano-sensors MEA technology" at the single-cell and network

M. E. Spira (✉) · S.-H. Huang · N. Shmoel · H. Erez
Department of Neurobiology, The Alexander Silberman Institute of Life Science, The Hebrew University of Jerusalem, Jerusalem, Israel

The Charles E. Smith Family and Prof. Joel Elkes Laboratory for Collaborative Research in Psychobiology, The Hebrew University of Jerusalem, Jerusalem, Israel

The Harvey M. Kruger Family Center for Nanoscience, The Hebrew University of Jerusalem, Jerusalem, Israel
e-mail: Spira@cc.huji.ac.il

levels, explain the biophysical principles and the various configurations used to form functional nanoelectrode/cell hybrids, and describe the quality and characteristic features of the recorded intracellular APs and subthreshold synaptic potentials by the vertical nanoelectrode-based MEA. Basic cell-biological mechanisms that curtail the length of time intracellular access by the nanoelectrodes are discussed, and approaches to overcome this problem are offered.

Recent development of biotechnologies that use induced human pluripotent stem cells taken from healthy subjects and patients, and in vitro drug screening for the development of personalized medicine as well as basic brain research will benefit tremendously from the use of MEAs that record the entire brain electrophysiological signaling repertoire from individual cells within an operational network rather than only extracellular FPs.

1   Introduction

Multielectrode arrays (MEA) are extensively used nowadays to study basic and applied electrophysiological aspects of in vivo and in vitro neuronal and cardiomyocyte circuits (Obien et al. 2014; Fekete 2015; Seymour et al. 2017). The core technology and concepts of contemporary MEA goes back half a century to the pioneering studies of Wise et al. (1970) and Thomas et al. (1972). Whereas great progress has been made over the last 50 years in realizing sophisticated MEA platforms made up of thousands of addressable, high-density, small-diameter low impedance sensors (Berdondini et al. 2005, 2009a, b; Amin et al. 2016; Jackel et al. 2017; Jun et al. 2017; Viswam et al. 2017), the quality of the interfaces formed between the excitable cells (neurons and muscles) and the planar electrodes still remains the weakest constituent of the bioelectronics hybrid. MEA devices based on planar electrodes are "blind" to subthreshold excitatory, inhibitory, and electrotonic synaptic potentials generated by individual neurons. Thus, rather than directly recording and analyzing dynamic changes in synaptic transmission in relation to drugs and toxin screening, different forms of plasticity (learning and memory), or various types of diseases, planar MEA users rely on indirect and complex parameters such as the averages of field potential (FP) frequencies, firing patterns, and others to extract information about the underlying basic biophysical mechanisms. These essentially descriptive FP-related parameters cannot be used to unequivocally analyze and determine diverse synaptic mechanisms or the membrane's excitable properties that underlie the actions of pharmacological reagents, plasticity, or disease pathologies. Crucially, neurons that do not fire action potentials (APs) are not "visible" to planar electrodes and thus go undetected. Since in some

brain areas and possibly in cultures that preserve intact brain properties a fraction of the neurons do not fire or fire at low rates, their proven subthreshold contributions to neuronal computations goes undetected and ignored (Shoham et al. 2006; Epsztein et al. 2011; Barth and Poulet 2012). Ignoring silent neurons due to the technical limitations of cells/planar-electrodes-based MEA goes on despite the documentation that meaningful subthreshold computations play critical roles in neuronal network functions (Lefler et al. 2014).

The enormous advances made over the last 50 years in materials science, microelectronics, and nanoelectronics, together with the acknowledgment of the limitations of substrate-integrated planar MEA, have prompted a number of laboratories to begin merging the advantages of planar MEA technologies (non-damaging and durable) with those of sharp and patch microelectrodes for intracellular recordings of the entire signaling spectrum of neuronal and cardiomyocyte networks. As in the case of research using planar electrode MEAs, the now decade-old generation of nanoelectrode-based MEAs uses passive or active (transistorized) electrodes. However, unlike extracellular planar electrode based MEAs, three-dimensional (3D) vertical nanoelectrodes are designed to perforate or actually penetrate the plasma membrane of cultured cells and thereby form direct Ohmic contact with the cell cytosol. As explained below, when successful, these devices operate in a similar manner to classical sharp-intracellular glass microelectrodes or whole-cell patch electrodes. Because the diameter of 3D vertical nanoelectrodes is in the range of 50–500 nm, penetration of cells by vertical nanoelectrodes was assumed not to damage the plasma membrane or the cells in any significant manner. Although only approximately 10 years has elapsed since the development of the first vertical 3D nanoelectrodes-based MEAs this "young" technology has progressed sufficiently to enable recordings of attenuated intracellular APs and synaptic potentials from neurons, cardiomyocytes, and striated myotubes (Spira et al. 2007; Hai et al. 2010a, b; Tian et al. 2010; Angle and Schaefer 2012; Duan et al. 2012; Fendyur and Spira 2012; Gao et al. 2012; Robinson et al. 2012; Xie et al. 2012; Spira and Hai 2013; Angle et al. 2014; Lin and Cui 2014; Lin et al. 2014; Qing et al. 2014; Rabieh et al. 2016; Shmoel et al. 2016; Abbott et al. 2017, 2018; Dipalo et al. 2017; Liu et al. 2017). Nevertheless, cumulative experience has also pointed to a number of difficulties that require creative solutions. Furthermore, alongside the progress made in intracellular recordings by vertical nanorods, pillars, wires, tubes, and cylinders a recent study emanating from the laboratory of Hongkun Park (Abbott et al. 2017, 2018) confirmed the scaling advantages of nanochip/microchip fabrication technologies by simultaneously recording intracellular APs from hundreds of cultured primary cardiomyocytes, thus heralding a new milestone in MEA technology.

The remainder of this chapter is organized as follows. It begins by familiarizing the reader with the terminology used by briefly describing the cell–electrode interface formed in cultures and presenting a simplified analog electrical circuit depicting the relationships between the two. Next it explains the contribution of the various parameters to the mode of electrical coupling formed between excitable cells and the recording electrode (extracellular or intracellular). This is followed by an examination of the mechanisms that underlie the sealing of the interfacing

junction formed between cultured cells and vertical nanoelectrodes. The next section discusses the mechanisms by which vertical nanoelectrodes make direct Ohmic contact with the cytosol. Multisite, long-term recordings from cultured excitable cells are among the major aims of this novel technology that are yet to be achieved. Thus, it next discusses how conserved cell-biological membrane repair mechanisms that have evolved to protect cells from injury in fact interfere with the presence of nanoelectrodes and curtail the length of time intracellular access can be maintained. Alternative ways of making Ohmic contact between nanoelectrodes and the cell interior that are better able to achieve long-term stability are then considered. The final section presents the earliest and today's cutting-edge achievements of this young technology at the single-cell and network levels. Since different laboratories are currently using different designs, diverse fabrication approaches and materials, the reader is referred to the original publications for technical details. Likewise, different laboratories use different terms to better describe the features of the vertical nanoelectrodes that they have fabricated (pillars, rods, wires, tubes, cylinders, and mushroom-shaped). For the sake of simplicity, we refer in the following to all shapes and forms as vertical nanoelectrodes.

2 The Biophysical Principles that Enable Cell-Noninvasive Extracellular Electrodes to Record Intracellular Potentials

The mode of recordings (i.e., extracellular or intracellular), the quality of the recorded potentials in terms of the signal-to-noise ratio, and electrical coupling (the ratio of the recorded potential to the voltage generated across the plasma membrane V_{elect}/V_{cell}) are defined by three parameters: (a) the electrical properties of the cell's plasma membrane that faces the electrode (the junctional membrane), (b) the seal resistance formed by the gap between the living cell membrane and the electrode surface, and (c) the impedance of the sensing pad and stray capacitance introduced by the conducting lines and the recording amplifier. A simplified analog electrical circuit that depicts these elements superimposed on a schematic drawing of an excitable cell adhering to a 3D microelectrode electrode is illustrated in Fig. 1a. It should be noted that in principle the shown analog circuits represent both 3D and planar electrode–cell interfacings. In this simplified model, the cell's surface area is subdivided into a non-junctional membrane (R_{njm}) that faces the grounded culture medium and a junctional membrane (R_{jm}) that interface with the electrode. Each of these membranes is represented in the circuit by passive electrical elements, a resistor and a capacitor in parallel R_{njm}, C_{njm}, R_{jm}, and C_{jm} respectively. For the sake of simplicity, the circuit and the ensuing analysis ignore the presence of voltage-gated ion channels in the junctional membrane and the anticipated transient changes (increased potassium and decreased sodium and calcium) in the ionic composition of the solution in the restricted volume of the gap between the electrode and the junctional membrane during neuronal activity.
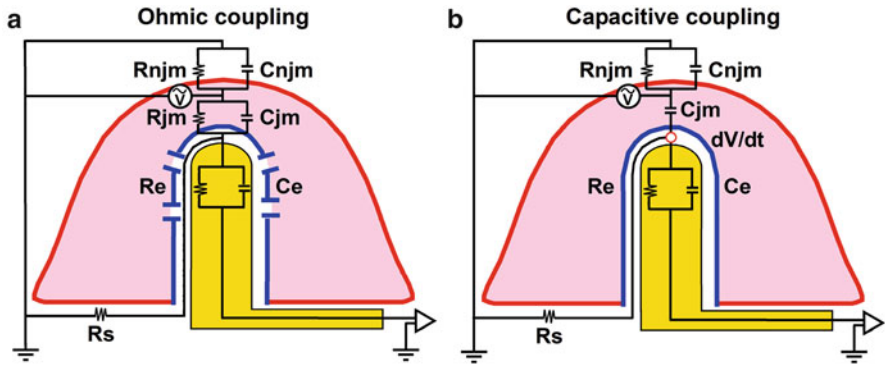
Fig. 1 A schema depicting the basic relationships between a cell (Pink) and a vertical nano-electrode/microelectrode (Yellow) superimposed on a simplified analog electrical circuit. The neuron's plasma membrane is subdivided into a non-junctional membrane (njm, red) that faces the culture medium, and a junctional membrane (jm, blue) that faces the electrode (For details see text). (**a**) When the value of the junctional membrane resistance is low (as indicated by the discontinuous blue line) the electrical coupling coefficient between the cell and the electrode is Ohmic. Under these conditions attenuated spikes and subthreshold synaptic potentials with genuine intracellular features can be recorded. (**b**) When the junctional membrane resistance is high, it can be neglected and the electrical coupling between the neuron and the electrode is capacitive. Under these conditions attenuated signals are recorded as the time derivative of the intracellular electrophysiological signals

The cleft between the cell and the electrode (analogous to the extracellular space between living cells in tissue) is represented by a single resistor (R_s). The value of R_s is defined by the dimensions of the contact area between the cell's membrane and the sensing electrode. The electrode is represented by a resistor and capacitor in parallel (R_e and C_e respectively).

Changing the relationships between the junctional membrane properties, the seal resistance, and the electrode impedance is expected to robustly alter the recording mode from extracellular to intracellular, and change the shape and the amplitude of the recorded potentials from microvolts to tens of millivolts. A quantitative estimate of the expected electrical coupling levels between a given excitable cell and a particular microelectrode configuration can be acquired by the use of various analog electrical circuit simulators (e.g., the open source SPICE). The values of the electrical elements comprising a given analog circuit and the input voltage (spike or synaptic potential) can be experimentally extracted or estimated. Various approaches to obtain and estimate the parameters of a given cell–circuit hybrid and the simulation outcomes will not be described here. For examples the reader is referred to the following publications: Fromherz (2003), Hai et al. (2010a, b), Fendyur et al. (2011), Sileo et al. (2013), Spira and Hai (2013), Angle et al. (2015), Massobrio et al. (2016), Shmoel et al. (2016), Dipalo et al. (2017), Abbott et al. (2018), and Massobrio et al. (2018).

Remarkable experimental manipulations supporting the above suppositions were provided almost 20 years ago by Jenkner and Fromherz (1997) using isolated leech neurons, and later by Cohen et al. (2008) using *Aplysia* neurons. In both studies a sharp recording and stimulating intracellular electrode was inserted into a neuron's somata cultured on a substrate-integrated flat electrode (Fig. 2). In addition, a micromanipulator-driven fire-polished pipette positioned on top of the neuron was used to displace the cell body or its thick axon towards the planar electrode and
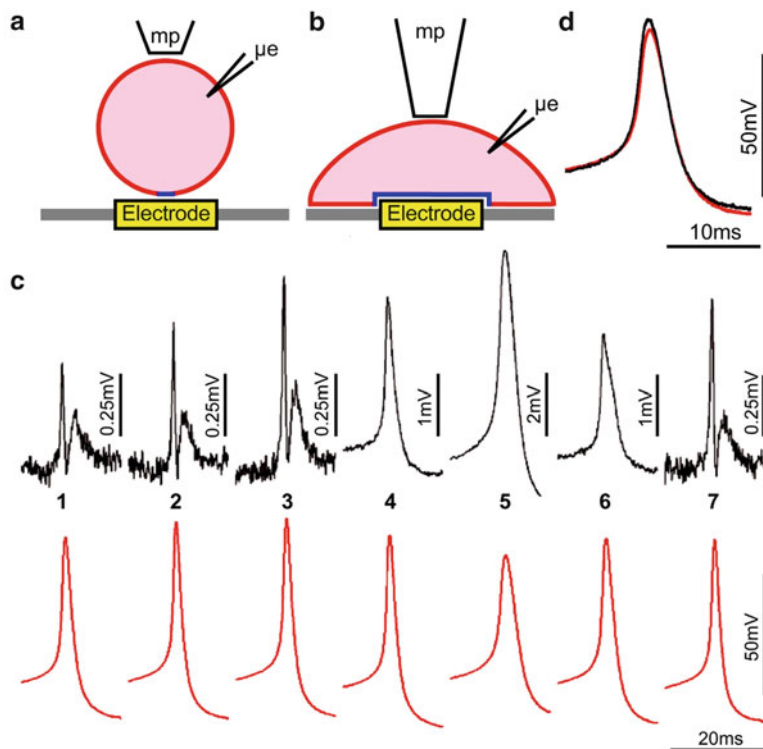
Fig. 2 From extracellular to intracellular recordings by compression of a neuron onto the surface of a substrate-integrated planar electrode. (**a**) A schema depicting a cultured Aplysia neuron cell body residing on the surface of a planar electrode. A fire-polished glass micropipette (mp) compress the cell body downwards towards the flat electrode (yellow) (**b**), while recording the transmembrane potential by an intracellular sharp electrode (μe). (**c**) Intracellular voltage recordings in red and extracellular field potential recordings by the planar electrode in black. Initially as the cell was compressed downwards (*c1* to *c3*) the amplitude of the FP increased while the intracellularly recorded AP maintained its amplitude. Further increase in the applied pressure lead to transition of the recorded action potential from extracellular to intracellular (*c3* to *c4*). This was accompanied by a decrease in the amplitude of the intracellularly recorded AP (red traces *c4* and 5). Releasing the pressure (*c6* and *c7*), lead to reversal of the process. Note the differences in the vertical scale bars along the black traces. (**d**) Overlapping of the normalized potentials recorded by the sharp and flat electrodes (*c5*) (Reprinted with permission from Cohen et al. (2008). Copyright Elsevier Biosensors and Bioelectronics 2008)

its surrounding substrate (Fig. 2). Gentle downward compression of the cell by the fire-polished pipette concomitant with readjustment of the intracellular electrode position was done under visual control. Both Jenkner and Fromherz (1997) and Cohen et al. (2008) reported that when the somata or an axon was mechanically displaced downwards towards the surface of a planar electrode, the contact area between the cell and the substrate increased (Fig. 2). This gradual increase in the contact area was accompanied by an increase in the amplitude of the FP generated by a depolarizing pulse delivered to the neuronal cell by the sharp intracellular electrode. The increased FP amplitude was not associated with a significant change in the FP shape (Fig. 2). Concomitant intracellular recordings of the APs by the sharp glass electrode revealed that the intracellular spike amplitude and shape were not altered. The increased amplitude of the extracellular FP was attributed to increased R_s due to the increased contact area between the neuron and the electrode, and possibly also due to reduction in the cleft width (Fig. 2). Further increase in the mechanical pressure transformed the extracellular FP (recorded by the planar electrode) into positive monophasic attenuated APs with the characteristic shapes of classical intracellular recordings (Fig. 2). It is important to note that the transition between extracellular FP to an attenuated intracellular AP was accompanied by the decreased amplitude of the intracellularly recorded AP by the sharp electrode. This indicated that stretching the neuron's plasma membrane against the substrate led in addition to the increased Rs to a transition of the cell–electrode coupling from capacitive to Ohmic, probably by generating nano-holes along the stretched membrane that faced the planar electrode. Releasing the mechanical pressure led to a reversal of all the parameters, including the contact area, the FP recorded by the planar electrode, and the amplitude of the intracellularly recorded AP (Fig. 2). These experiments thus demonstrated the potential to alter the recording mode from extracellular to intracellular by reducing the junctional membrane resistance and increasing the seal resistance.

3 Formation of Seal Resistance

The formation of high seal resistance between a cultured cell and an electrode requires the optimal positioning of the cells with respect to the electrode. Unfortunately, initial cell–electrode contact is a low-probability event driven by the gravity of the seeded cells. Currently, the most practical way to increase the likelihood of optimally positioning cells in contact with electrode is by increasing the cells' seeding density and/or the density of the electrodes. Once cells form physical contact with the substrate of the device, they adhere to it by chemophysical process and chemical recognition events of molecular entities anchored to the substrate and receptors in the outer leaflet of the plasma membrane (Sackmann and Bruinsma 2002). The value of seal resistance formed under these conditions is defined by the planar dimensions of the cell-sensing pad junction and the width of the cleft formed between the plasma membrane and the electrode surface (Weis and Fromherz

1997). Using optical methods and biophysical analysis, Braun and Fromherz (1998) and Zeck and Fromherz (2003) estimated that the cleft width formed between rat astrocytes cultured on silicon dioxide coated by laminin was approximately 100 nm. Accordingly, the R_s was estimated to be in the range of single MΩs (Weis and Fromherz 1997). Electron microscopic analysis of thin sections prepared from cultured *Aplysia* neurons grown on 2D-polyaniline-coated glass substrate revealed that the cleft width ranged from hundreds of nanometers in some areas to 20–40 nm in others (Oren et al. 2004). There is a general consensus that cleft dimensions of approximately 20 nm correspond to the minimum width that can be formed by cells grown on substrates coated with biocompatible molecules (Sackmann and Bruinsma 2002). Although the seal resistance, which is in the range of a single MΩ, suffices to enable recordings of extracellular FPs, it is insufficient to enable intracellular recordings. Theoretically, increasing the planar dimensions of the gap between the junctional membrane and the electrode surface should increase the seal resistance (as shown in Fig. 2). However, this cannot be applied to small neurons or other cell types and in particular not to cultured cell networks.

Experiments conducted using different forms of 3D vertical nanoelectrodes have revealed that in spite of the small surface area of these nanostructures, the seal resistances formed between cultured cells and the nanostructures have significantly higher values in the range of 50–500 MΩ than those formed by planar electrodes of larger surface areas (single MΩ values) (Hai et al. 2009a; Robinson et al. 2012; Lin et al. 2014; Dipalo et al. 2017). Apparently, independent of the precise geometry of the 3D structure but limited by the dimensions and pitch (Hanson et al. 2012; Ojovan et al. 2015) the seal resistance around vertical nanostructures is generated by cell-biological mechanisms that actively "engulf" 3D vertical nanostructures (Fig. 3a, b) yielding almost an order of magnitude larger seal resistances than that observed for planar electrodes. This process is apparently associated with a reorganization of the submembrane skeleton and membrane proteins along the junctional membrane. For example, using live confocal microscope imaging, Hai et al. (2009b) documented the formation of actin rings around the stalk of gold mushroom-shaped microelectrodes when cultured Aplysia neurons are interfaced with 3D microelectrodes (Fig. 3c).

The structural analysis of chemically fixed junctions formed between cells and nano/micro vertical electrodes by transmission electron microscopy (Spira et al. 2007; Hai et al. 2009a, b, 2010a, b; Hanson et al. 2012) and focused ion beam microscopy (Santoro et al. 2017) revealed that whereas cells tightly engulf the vertical nanostructures, these nanostructures do not spontaneously penetrate the cell's plasma membrane. This structural observation is consistent with electrophysiological observations indicating that in most cases unless the vertical nanoelectrodes are "forced" to perforate or fully penetrate the plasma membrane by electroporating pulses they maintain their extracellular position. Apparently, this conclusion is contradicted by studies demonstrating the transfer of molecules that adhered to the surface of nanopillars to cells residing on them. Nevertheless, it was noted that the probability of spontaneous transfer of optically labeled molecules is low (Xu et al. 2014).
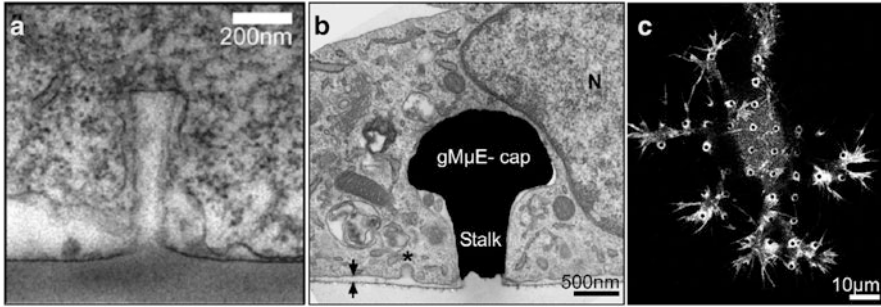
Fig. 3 Electron microscope images of a vertical nanopillar (**a**, Reprinted with permission from Hanson et al. (2012). Copyright American Chemical society Nano Letters 2012) and a gold mushroom-shaped microelectrode (**b**, Reprinted with permission from Hai et al. (2010a) Copyright Nature Publishing Group 2010) engulfed by LH-1 cell and a PC12 cell. Note that the cell's membrane tightly engulfs the vertical nanoelectrode. (**c**) Confocal microscope images of actin rings formed by cultured Aplysia neuron around the stalk of a gold mushroom-shaped microelectrode

Taken together, although the seal resistance formed between cultured cells and vertical nanostructures is (50–500 MΩ) roughly an order of magnitude larger than the one formed between cultured cells and planar electrodes, it is still far from the GΩ seal values formed by classical patch electrodes and plasma membranes.

Because successful intracellular recordings by vertical nanoelectrodes depend on the parallel formation of high seal resistance and low junctional membrane resistance, the next paragraph discusses potential mechanisms to concomitantly increase both parameters.

4 The Reduction of the Junctional Membrane Resistance Is a Critical Parameter to Gain Effective and Durable Intracellular Access

Gaining direct access to the cell cytosol by "piercing" the plasma membrane with a sharp glass microelectrode or by mechanically "breaking" the plasma membrane by suction through a patch electrode along with the formation of a GΩ seal resistance between the glass wall of the electrodes and the plasma membrane (Fig. 4) enables genuine intracellular recordings which can last from minutes to hours (Sakmann and Neher 1984). As the solution contained within the patch electrode gradually perfuses into the cytosol, it alters its ionic content and dilutes diffusible molecular entities of the cytosol. With time, this process interferes with the normal physiology of the cells. To overcome this problem Horn and Marty (1988) developed the perforated patch configuration. Rather than breaking the cell's membrane to gain Ohmic access to the cytosol they introduced ionic channels such as nystatin or gramicidin into the patch electrode solution. These channels then integrate with the plasma membrane
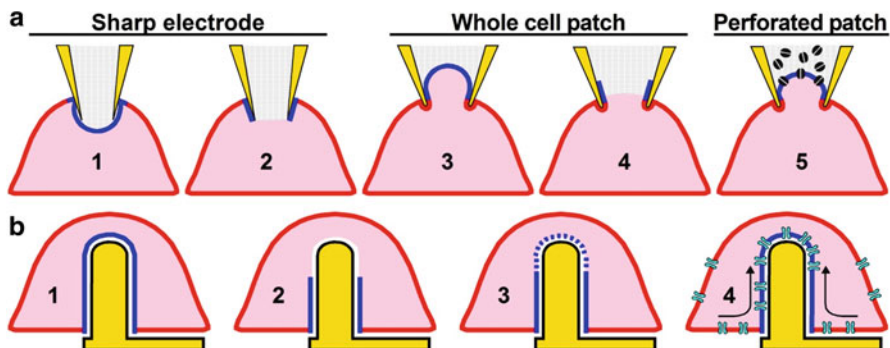
Fig. 4 Schema depicting cell–electrode interfacings formed by classical intracellular electrodes (**a**), and vertical nanoelectrodes (**b**). When a sharp glass microelectrode is mechanically driven against the cell membrane it forms a "membrane dimple" (*a1*, blue). An electroporating pulse breaks open the plasma membrane that faces the electrode tip and a seal is formed between the external side of the glass wall and the cell plasma membrane (*a2*). In the whole-cell patch configuration a membrane patch is sucked into the electrode (*a3* blue). Application of additional suction breaks the membrane open and a GΩ seal is formed between the plasma membrane and the inner surface of the glass wall (*a4*). A similar configuration (to *a1* and *a3*) is formed between a cell that engulfs a vertical nanoelectrode (*b1*). Under these conditions when an electroporating pulse is delivered through the nanoelectrode (*b2* or *b3*), the junctional membrane (blue) is either pierced (*b2*) or porated (*b3*). Another electrode/cell recording configuration is the whole-cell perforated patch (*a5*) in which after GΩ seal formation ion channels within the patch electrode (black) integrate with the plasma membrane to lower the junctional membrane resistance (*a5*). A similar configuration might be formed around an engulfed vertical nanoelectrode by recruiting of ion channels into the junctional membrane around the vertical nanoelectrode (*b4*)

to reduce its resistance (Fig. 4). Together with the formation of high seal resistance between the plasma membrane and the internal wall of the patch pipette, a perforated GΩ patch configuration is formed (Fig. 4a-5). Note that in the perforated patch configuration, the electrode remains outside of the cell but records intracellular potentials, whereas in the case of sharp electrodes and the whole-cell configuration the electrode tips are practically in the cytosol (Fig. 4a-2 and a-4).

Intracellular recordings by vertical nanoelectrodes are based on the same principle of gaining low resistance access to the cytoplasm.

Local membrane poration by current pulses delivered by vertical nanoelectrodes have proven to be the most useful approach to lower the junctional membrane resistance (Braeken et al. 2012; Hai and Spira 2012; Robinson et al. 2012; Xie et al. 2012; Lin et al. 2014; Abbott et al. 2017, 2018). In fact, it still remains unclear whether after electroporation the tip of the nanoelectrodes pierces the plasma membrane (Fig. 4b-2) or generates nanoholes in the junctional membrane (Fig. 4b-3). Whatever the actual mechanism, intracellular access by electroporation is transient and only lasts minutes to approximately 1 h. Thereafter, the electrodes are insulated from the cytosol (Hai and Spira 2012; Xie et al. 2012; Lin et al. 2014; Abbott et al. 2017; Dipalo et al. 2017). The electrode insulation process is

most likely generated by conserved membrane repair mechanisms. A study of the cascades underlying electrical insulation of an electrode after electroporation (Hai and Spira 2012) showed that focal membrane electroporation by gold mushroom-shaped microelectrodes leads to localized increases in the free intracellular calcium concentration ($[Ca^{2+}]_i$) around the electroporating electrode along with a concomitant reduction in the cell's input resistance (R_{in}). This is probably due to reduction in the seal and junctional membrane resistances. Thereafter, within minutes, the input resistance of the cell recovers along with the recovery of the $[Ca^{2+}]_i$. Membrane repair mechanism after injury is a highly conserved cell biological mechanism that serves cells in general and muscle fibers in particular to withstand a variety of physiological and pathological membrane disruptions. Likewise, most cell types, including in particular muscle fibers and neurons, have evolved efficient calcium removal mechanisms. Current concepts suggest that localized membrane repair is triggered by the influx of calcium ions into the cytosol across the large extracellular/intracellular calcium concentration gradient and possibly by the release of calcium ions from intracellular stores. The elevated $[Ca^{2+}]_i$ induces exocytosis of intracellular vesicles such as lysosomes that leads to the formation of "membrane patches" that seal the "punctured" plasma membrane (Fig. 5) (McNeil and Khakee 1992; McNeil and Kirchhausen 2005; Han and Campbell 2007). A complementary mechanism could also be lateral recruitment of membrane into the injured patch (Demonbreun and McNally 2016). The findings of Hai and Spira (2012) were consistent with the "membrane patching model" in that the dynamics of the recovery process from electroporation progressed in discrete steps. It is conceivable that the effective calcium removal mechanisms of cultured neurons and cardiomyocytes enabled the cells to withstand repeated electroporations over a number of days, as reported in a number of studies (Fendyur and Spira 2012; Robinson et al. 2012; Lin et al. 2014; Rabieh et al. 2016; Dipalo et al. 2017). Since there is ample evidence that
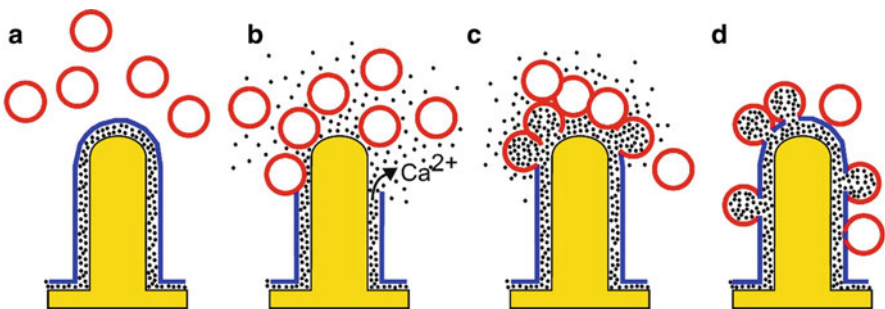
Fig. 5 Schematic representation of the membrane "patch repair" mechanisms. Injury of the plasma membrane (from **a** to **b**) leads to calcium ions influx (black dots) into the cell. The elevated free intracellular calcium ion concentration leads to fusion of intracellular vesicles with the injured patch of the membrane (**c**). (**b**, **c**) Depicts a hypothetical case of membrane piercing by the vertical nanoelectrode. (**d**) Once the membrane is repaired the free intracellular calcium concentration is downregulated to the control level

membrane repair mechanisms are ineffective in patching large diameter holes (Joshi and Schoenbach 2002), it is paradoxically possible that the nanometric dimensions of the electrodes which facilitate their penetration through the plasma membrane underlie the relatively fast process of insulation.

In an attempt to improve the "insertion" of vertical nanoelectrodes into cells, the work by the Francesco De Angelis laboratory (Dipalo et al. 2017) has used plasmonic optoporation to porate the junctional membrane (Messina et al. 2015). They reported that cultured neurons and HL-1 cells can be seamlessly plasmonically optoporated without interrupting ongoing spontaneous action potential activity. Nonetheless, even under these advantageous conditions, intracellular recordings were limited to just over an hour, at which point the electrodes were insulated.

In view of the above observations and the understanding that robust cell biological process underlie it, future approaches to stabilizing nanoelectrode–cytosol contact could attempt to prevent the initiation of membrane repair cascades by limiting the calcium influx (or its release from intracellular stores) or by transiently increasing the calcium buffering capacity of the cells. This is possible by functionalizing vertical nanopillars with molecular entities that effectively fuse and integrate the electrode surface with the plasma membrane (Chernomordik and Kozlov 2008). This approach was developed and tested by the N. Melosh laboratory (Almquist and Melosh 2010, 2011; Verma et al. 2010; Almquist et al. 2011) which was then replicated as proof of concept by a number of laboratories. Recently, VanDersal and Renaud (2016) used cultured DHHC6-depleted HeLa cells (that spread over surface areas better than conventional HeLa cells) to adhere to a planar electrode which resided within a 5 nm thick gold ring decorated by 5 nm thick self-assembled alkanethiol chains. As the HeLa cells spread over the rings, the alkanethiol chains spontaneously fuse with the outer leaflet of the plasma membrane, generating a seal resistance around the planar electrode in the range of 5 GΩ, thus generating a cell attached patch configuration without resorting to suction (Fig. 6). The application of a brief electroporating pulse by the electrode residing within the gold ring transformed the cell attached configuration into a whole-cell patch configuration. Note that under these conditions, the cytosol is not perfused and the whole-cell patch configuration can remain effective for up to 72 h,
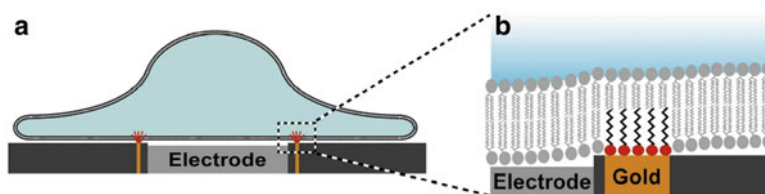
Fig. 6 A schema depicting spontaneous GΩ seal formation when a cultured cell (blue) extends over a substrate-integrated gold ring (yellow) functionalized by alkanethiol (red) encompassing a planar electrode (gray). (**a**) Cross section of a cell adhering to the substrate and the 5 nm thick gold ring functionalized by alkanethiol. (**b**) Enlargement of (**a**) (Reprinted with permission from VanDersal and Renaud (2016). Copyright Sci Rep 2016)

which is significantly longer than any other study attempting to generate a durable low resistance junction between cultured cells and the electrode. As anticipated by the N. Melosh laboratory when adapted to vertical nanopillars, an effective GΩ seal could be formed and therefore reduce, if not prevent, calcium influx after electroporation and hence avoid triggering membrane repair mechanisms and electrode insulation.

Besides electroporation and plasmonic optoporation, increased junctional membrane conductance may be induced by the recruitment of ion channels into the junctional membrane (Fig. 4b-4). Two mechanisms have been considered. Hai et al. (2010a) suggested that culturing *Aplysia* neurons in contact with gold mushroom-shaped microelectrodes functionalized by a multiple Arg-Gly-Asp (RGD) repeat peptide could facilitate the physical contact between the plasma membrane and the electrodes and that the binding of the peptide to receptors on the plasma membrane could lead to structural reorganization of the submembrane skeleton. This in turn might be followed by changes in the density and possibly the type of ionic channels at the junctional membrane. Interestingly, the recruitment of a relatively small number of such channels would suffice to elevate the junctional membrane conductance to support effective electrical coupling. For example, assuming that the junctional membrane conductance (of cultured *Aplysia* neurons) is increased by recruitment of voltage-independent potassium channels with a channel conductance of 10 to 100 pS, 10–100 channels would need to be concentrated within a confined junctional membrane area of 14 μm^2 to reduce the junctional membrane resistance from an estimated value of 100 GΩ to 100 MΩ. This would imply a channel density of 0.5 to 10 channels/μm^2 (Hai et al. 2010a). Interestingly, this type of potassium channel density has been experimentally documented in a number of cell types (Hille 1992).

An alternative mechanism that could lead to accumulation of ion channels within the junctional membrane is the imposed curving of the plasma membrane around the vertical nanoelectrodes. Membrane curvatures have been shown to trigger molecular cascades that could underlie local changes in the expression and density of membrane proteins including ion channels (Epand et al. 2015; Iversen et al. 2015; Lou et al. 2018). In recent studies by the laboratory of B Cui, Zhao et al. (2017) and Lou et al. (2018) documented increased profiles of clathrin-coated pits and the accumulation of clathrin and dynamin at the junctional membrane of SK-MEL-2 cells. This indicated that clathrin-mediated endocytosis is enhanced by the membrane curvature induced by the nanopillar tips. The cytoskeletal element actin was also shown to concentrate around curved membranes (Hai et al. 2009b, and Fig. 3) because actin and its associated proteins are involved in diverse cellular functions; these results may suggest that membrane curvature might affect among other cellular processes the recruitment of ion channels.

5 Reading the Electrophysiological Signaling Repertoire Recorded by Various Types of 3D Nanostructures and Microstructures

The overarching purpose of developing intracellular recording MEA is to produce easy-to-use devices that not only improve the source resolution of AP but can monitor online (without averaging) the entire electrophysiological signaling repertoire of neuronal and cardiomyocyte networks. One characteristic shared by all newly developing technologies is that different investigators experiment with different approaches, designs, materials, and fabrication processes. As a result, identical source signals may be modified in different ways by different recording devices. The quality of electrophysiological recordings may thus range from genuine intracellular recordings of APs and synaptic potentials to complex recordings of integrated extracellular and intracellular potentials or from time derivatives of intracellular recordings as in loose seal configurations (juxtacellular recordings) to classical intracellular APs (Joshi and Hawken 2006; Gold et al. 2009). The next section discusses a few examples and illustrates the relationships between the principles of device and interface designs and the ensuing signal readout. As different laboratories use different fabrication approaches and materials, the reader is referred to the original publications for detailed information on this aspect.

6 Optimal Intracellular Recordings by Scalable Field Effect Transistor Technology

Early in the evolution of scalable 3D nanoelectrodes for intracellular recordings the CM Lieber laboratory pioneered the development and use of a nano-field-effect transistor (FET) located at the tip of a "kinked nanowire" (Tian et al. 2010). Since the performance of FETs does not depend on the impedance between the chemically functionalized nano-FET and the cell, Tian et al. (2010) were able to record endogenously generated APs with amplitudes and shapes identical to intracellular recordings by patch electrodes from single cells.

The initial FET approach that was designed to record from single cells was soon improved by synthetically integrating SiO_2 nanotube on top of the nanoscale FETs. The insertion of lipid-coated SiO_2 FETs nanotube into the cell brought the cytosol into Ohmic contact with the FET and enabled recordings of full-blown transmembrane potentials (Fig. 7a) (Duan et al. 2012). To the best of our knowledge there have been no further applications of the nano-FET located at the tip of a "kinked nanowire" for simultaneous recordings from many individual neurons or cardiomyocytes within a given in vitro network. Recently, the laboratory of H. Park (Abbott et al. 2017) successfully scaled up transistorized vertical nano-MEA device to simultaneously record attenuated intracellular APs from a network of a few hundred cardiomyocytes.

7 Attenuated Intracellular Recordings of Action Potentials by Passive Nanoelectrodes After Membrane Poration

Along with advances in the technology of nanoscale FET electrodes, passive vertical nanowires, pillars, and tubes-based MEA were developed and tested. The Bianxiao Cui laboratory (Xie et al. 2012) fabricated vertical Pt nanowire electrodes (150 nm in diameter and 1–2 μm in height) to simultaneously record endogenous activity from a number of cultured HL-1 cells (Claycomb et al. 1998). Each recording unit was constructed from a common $5 \times 5 \ \mu m^2$ insulated pad from which five vertical nanowires protruded (Fig 7b). Electroporation transformed the extracellularly recorded biphasic FPs by the vertical nanowires to an intracellular recording mode whose shape resembled APs recorded by whole-cell patch electrodes with attenuated amplitude of 1–10 mV (Fig. 7b). Conceivably membrane repair mechanisms caused the porated junctional membrane to gradually recover along with an unavoidable decrease in the AP amplitude and finally the reversal of the recording mode from intracellular to extracellular within 10 min. Electroporation of the same cell could be repeated over a number of days, suggesting that the cells fully recovered from the trauma of electroporation. By using iridium oxide (IrOx) nanotubes rather than solid Pt wires, the Cui laboratory (Lin et al. 2014) caused cultured HL-1 cells and primary rat cardiomyocytes not only to enwrap the vertical tube but also to protrude into its hollow center. The tight interface resulted in recording larger APs (in the range of 1.5–15 mV) for longer durations ranging from minutes to an hour after the delivery of an electroporating pulse. The slow reversal process under these conditions gave sufficient time to examine characteristic pharmacological effects of specific drugs on the frequency and shape of the spontaneous APs. Furthermore, repeated intracellular recording by electroporation could be conducted for 8 days.

In the same year (2012) the Hongkun Park laboratory undertook the challenge to interface scalable vertical nanowires based MEA with cultured mammalian neurons for the first time (Robinson et al. 2012). It should be emphasized that primary cardiomyocytes and in particular the LH-1 cell line cultured on MEA cannot be used as models to predict the recording quality from primary neurons. This is mainly due to the fact that LH-1 cells and cardiomyocytes spread radially over a large surface area, adhere well to the substrate and therefore form high seal resistance around the electrodes. In contrast, cell bodies of mammalian neurons are small, do not spread and adhere as well as cardiomyocytes and thus form lower seal resistances.

Using recording units constructed of nine Ti/Au metallic tips vertical nanowires (150 nm diameter, 3 μm height) the Hongkun Park laboratory (Robinson et al. 2012) recorded intracellular APs of ∼4 mV and were able to stimulate selected cortical neurons to fire action potentials (Fig. 7c). To gain intracellular access for recordings and stimulation, the junctional membrane was electroporated. Although the recordings were of high amplitude, no indications of synaptic communication among the neurons were documented by the vertical nanoelectrodes.
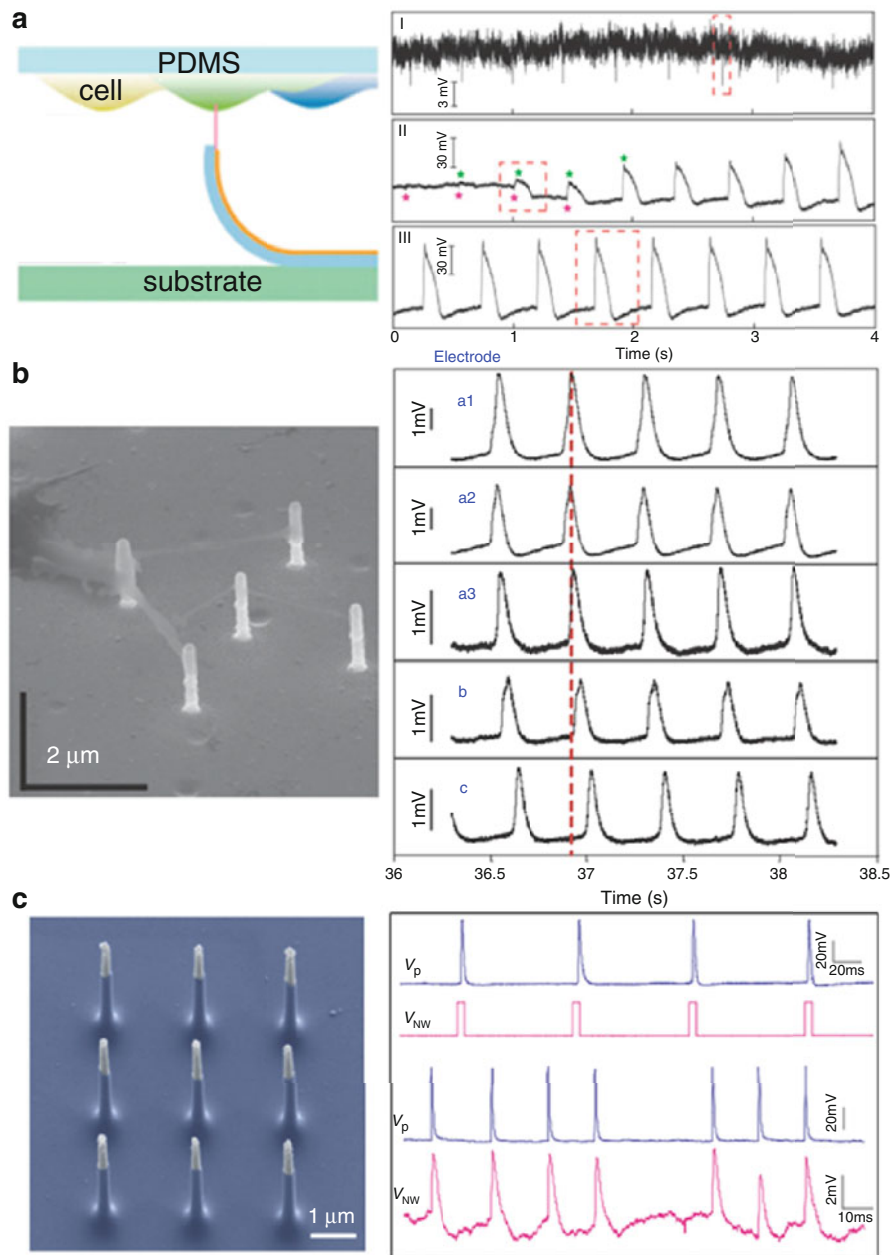
Fig. 7 Examples of the intracellular recording qualities of vertical nanoelectrode arrays. (**a**) Schematics of 3D kinked nanowire FET probe interfaced with an "upside-down" applied sheet of HL-1 cells grown on a PDMS substrate (left). Before insertion of the FET into a cell (I) extracellular FPs are recorded. Insertion of the nanoelectrode through the plasma membrane is associated by a hyperpolarization shift of the recorded potential and transition of the extracellular

In a recent set of experiments the F. De Angelies laboratory (Dipalo et al. 2017) significantly improved the methods to gain direct contact between vertical nano-electrode and the cytosol. Dipalo et al. (2017) fabricated vertical 3D gold plasmonic nanocylinders with a diameter of 150 nm and a height of 1.8 µm on planar electrode (21 × 21 µm) that was electrically in contact with the culturing medium (Fig. 8). The metal coating of the nanocylinders was connected to the planar base (De Angelis et al. 2013; Dipalo et al. 2015). Endogenous APs generated by LH-1 cells that adhere to the flat electrodes and substrate around it were recorded as typical extracellular FPs (inward current, Fig. 8). Instead of electroporation pulses aimed at "piercing" the junctional membrane, they developed the plasmonic optoporation approach in which a short laser pulse "open transiently nanopores exclusively at the tip" of the vertical nanopillar (Messina et al. 2015; Zilio et al. 2017). The ability to precisely control the laser beam was used to optoporate single vertical electrode at a time. This gave the authors the unique opportunity to experimentally determine the contribution of each pillar and the planar electrode to the shape and amplitude of the recorded potential (Fig. 8). Plasmonic optoporation of the cell membrane by one nanopillar changed the recorded extracellular potential to a hybrid extracellular–intracellular potential. When two nanopillars were plasmonically optoporated the weight of the intracellular components was more pronounced. Finally, when all four nanopillars were optoporated, the features of the recorded potentials were comparable to intracellular recordings (Fig. 8). Importantly, the "insertion" of the vertical nanoelectrodes by optoporation did not interfere with the endogenous patterns of AP firing by the cells. This indicates that the optoporation pulse used did not induce a large increase in the cell's membrane resistance, nor did it lead to elevated $[Ca^{2+}]_i$. Nevertheless, since the intracellular recordings configuration did not last for more than an hour, it is conceivable to assume that micrometric motion of the cells in respect to the substrate led to the isolation of the electrodes from the cells. Importantly, this study also documented the presence of spontaneous small amplitude potentials ($\sim$40 µV) with features reminiscent of synaptic potentials. Although the authors did not argue that these potentials were genuine synaptic potentials, it is reasonable to assume that indeed they are. It should be noted, however, that because the cell bodies of the cultured neurons may not adhere and

---

Fig. 7 (continued) FPs to full blown 80 mV intracellular APs (II, III) (Reprinted with permission from Tian et al. (2010) Copyright Science, 2010). (**b**) Passive nanopillar electrode-based MEA constructed of five vertical nanoelectrodes on a common platinum pad. Intracellular recordings were simultaneously obtained from five individual HL-1 cells (right) (Reprinted with permission from Xie et al. (2012). Copyright Nature Publishing Group, 2012). (**c**) Vertical nanowire MEA constructed of nine silicon nanowires on a common pad. Shown are bidirectional recordings and stimulations of cultured primary neurons by the vertical nanoelectrodes concomitantly with recording by patch electrodes. Stimuli applied by the vertical nanoelectrode (2nd trace) evoked action potentials recorded by the patch electrode (1st trace). Stimulations delivered by the patch electrode (3rd trace) evoked action potentials recorded by the nanowire electrode (4th trace) (Reprinted with permission from Robinson et al. (2012). Copyright Nature Publishing Group, 2012)
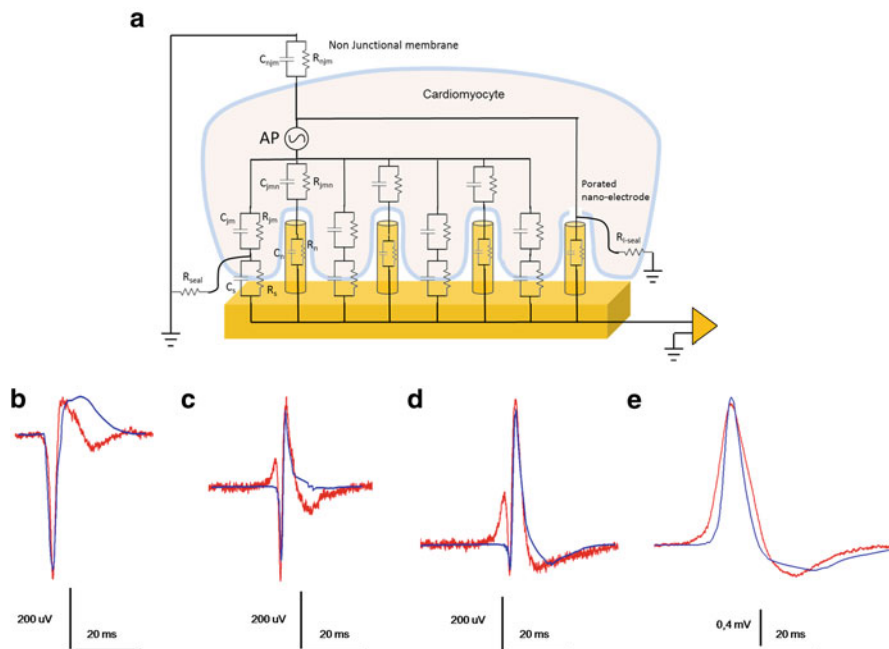
Fig. 8 An analog electrical circuit of a combined planar/vertical nanoelectrodes MEA used to simulate and experimentally study the advantages of plasmonic cell optoporation. (**a**) The analog electrical circuit used to simulate (**b**, blue traces) the actual recordings (**b** red traces). When one or two out of the four vertical nanoelectrodes optoporated the HL-1 cell, the recorded extracellular potential (**b**) transforms to "mixed" extracellular–intracellular recorded potential (**c**, **d**). When all four vertical nanoelectrodes optoporate the cell, the shape of the recorded potentials becomes almost identical to that of genuine attenuated intracellular recordings (**e**) (Reprinted with permission from Dipalo et al. (2017). Copyright ACS https://pubs.acs.org/doi/abs/10.1021%2Facs.nanolett.7b01523. Note: further permissions related to the material excerpted should be directed to the ACS)

cover the entire surface of the flat part of the electrode, it is theoretically possible that these "tentative synaptic potentials" are in fact pickups of FPs generated by remote neurons. If these are genuine synaptic potentials, this together with the report published by the S. Dayeh laboratory (Liu et al. 2017) and work by Shmoel et al. (2016) would be the first to tentatively document recordings of spontaneous synaptic potentials by vertical nanoelectrodes.

Taken together, these results show that at a proof-of-concept level scalable passive vertical nanoelectrodes can be manipulated to form transient contact with the cytosol and have a large enough seal resistance to record attenuated intracellular APs with features similar to whole-cell patch or sharp electrodes. The attenuation of the signals is the outcome of the high impedance of the 3D vertical nanostructures due to their small surface area. Attempts to overcome this limiting factor by the use of multiple vertical nanoelectrodes only partially improve the situation. Another

critical shortcoming of currently used vertical nanoelectrode technology is the limited time (an hour) for intracellular access after membrane electroporation or optoporation. The inhibition or slowdown of the innate membrane repair mechanism which serves to protect cells from damage and isolates the nanoelectrode after membrane poration can be theoretically designed. The issues of high electrode impedance could be overcome by the use of nano-FETs (the CM Lieber solution) and the development of novel materials. The quality of the seal resistance could be substantially improved by developing suitable surface chemistries to effectively fuse the electrodes with the cell membrane (Almquist et al. 2011; Almquist and Melosh 2011; VanDersal and Renaud 2016).

Finally, so far none of the multiple vertical nanoelectrode devices have been effectively applied to monitor the entire electrophysiological repertoire from individual neurons comprising a neuronal network. Nonetheless, the successful scaling of the vertical nano-MEA device by the H. Park laboratory (Abbott et al. 2017) to simultaneously record attenuated intracellular APs from a network of a few hundred cardiomyocytes is a significant achievement marking a new milestone in vertical nanoelectrode array technology.

8   Extracellular Gold Mushroom-Shaped Microelectrode Arrays for Intracellular Recordings

Along with the development of vertical nanoelectrode technologies which in principle operate like classical sharp and whole-cell patch microelectrodes, our laboratory has begun to test a different approach which purposely limited the cell–electrode configuration to a perforated patch electrode arrangement. In contrast to the vertical nanoelectrodes that are designed to penetrate the cells membrane, we used gold mushroom-shaped microelectrodes (gMμEs) with a relatively large cap with a diameter of 1.5–2 μm, a stalk diameter of ∼1 μm, and a height of ∼1.5 μm (Spira et al. 2007, and Fig. 3b). These gMμE record attenuated synaptic and APs from cultured Aplysia neurons with the characteristic features of intracellular recordings by forming a high seal resistance and the induction of low junctional membrane resistance that faces thee electrode (Spira et al. 2007; Hai et al. 2010a, b; Spira and Hai 2013). In these studies, 48–72 h after culturing juvenile *Aplysia* neurons on an RGD repeat functionalized gMμE surface, attenuated APs and subthreshold potentials with characteristic features of intracellular recordings were monitored (Fig. 9). Since the gMμEs are engulfed by the neuron but remain outside of it (Fig. 3b), we referred to this mode of recordings as "IN-CELL recordings" rather than as intracellular recordings. The amplitudes of IN-CELL recorded APs generated by a single *Aplysia* neuron's cell body (∼80 μm in diameter) that adhere to an array of gMμEs ranged from 2 to 30 mV. This range mainly reflected variabilities in the seal resistance formed between individual gMμEs and the cell body. Time-locked, evoked electrotonic EPSPs of up to 5 mV were also recorded from a network
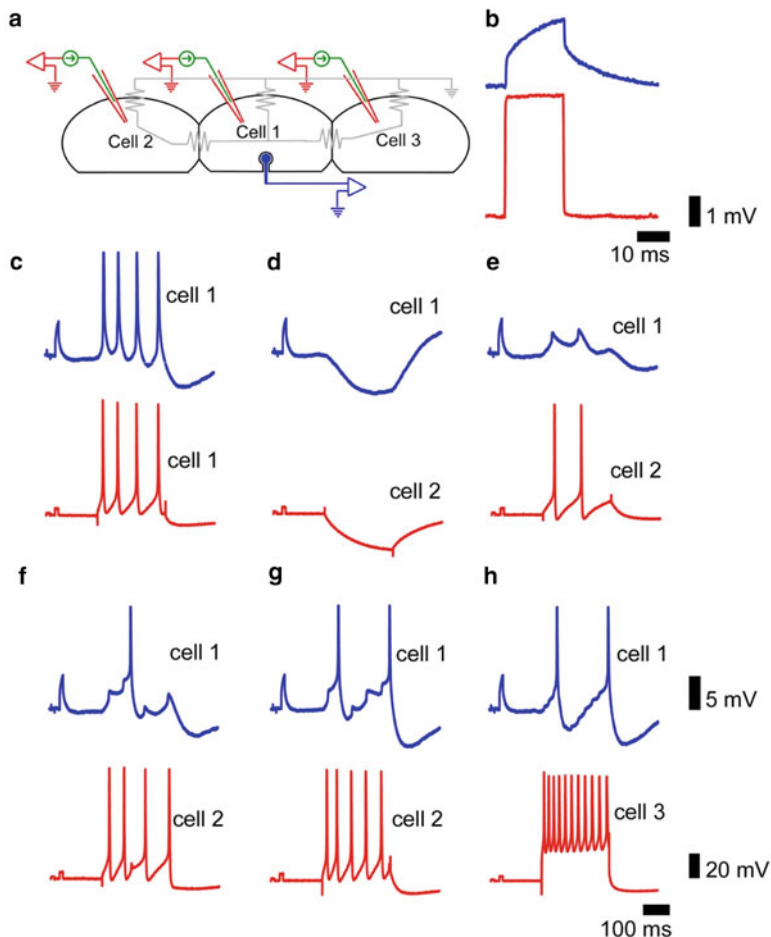
Fig. 9 Synaptic potentials and action potentials (APs) recorded by gold mushroom-shaped microelectrodes. (**a**) Three cells were cultured on a gMμE array. A single sharp intracellular microelectrode was used for both current injection and voltage recordings. (**b**) A calibration pulse of 5 mV, 20 ms as detected by the intracellular microelectrode (red) and a gMμE (blue). (**c**) Depolarization of neuron 1 generated a train of spikes recorded by the intracellular microelectrode (red in cell 1) and the gMμE (blue of cell 1). (**d**) The intracellular electrode was then moved into neuron 2. Hyperpolarization of neuron 2 generated hyperpolarization of neurons 2 and 1. (**e**) Depolarization of neuron 2 to generate two APs elicited two electrical EPSPs riding on the depolarizing pulse (blue) in neuron 1. (**f, g**) Increasing the strength of the intracellular stimulation of neuron 2 generated trains of 4 and 5 spikes in neuron 2 (correspondingly) leading to summation of the EPSPs in neuron 1, to fire one and two APs (**f**) and (**g**), correspondingly) as monitored by the gMμE from neuron 1. In (**h**), the intracellular electrode was moved into neuron 3. Spikes in cell 3 (red) also generate EPSPs which summated to generate action potentials in cell 1. (Reprinted with permission from Hai et al. (2010a). Copyright Nature Publishing Group 2010)

of electrically coupled neurons (Fig. 9 and Hai et al. 2010a, b). The use of an analog electrical circuit model to simulate the experimental results made it clear that the results were only possible if in addition to the increased seal resistance, the junctional membrane conductance was increased with respect to the non-junctional membrane. The mechanisms underlying this junctional membrane conductance increase remained unclear. It is conceivable that the curvature of the gMμE cap and/or the presence of the RGD repeat peptide on the electrode surface may have initiated a molecular cascade leading to recruitment of voltage independent ionic channels to the junctional membrane or to the formation of nanopores within the confined region of the junctional membrane.

The studies conducted using cultured *Aplysia* neurons revealed that the neuron–gMμE junctions were stable for approximately 2 weeks and that the neuron–gMμE hybrid configuration did not alter the passive or active membrane properties of the neurons and their synaptic functions (Hai et al. 2009b, 2010a, b).

The results obtained using gMμE-based MEA to record from primary cultures of rat hippocampal neurons differed in a number of ways from those of *Aplysia* neurons.

In contrast to cultured *Aplysia* neurons, the variability in the shapes and amplitude of the recorded potentials from cultured rat hippocampal neurons was significantly larger (Fig. 10), and ranged from biphasic extracellular FPs with amplitudes of 100 μV to positive monophasic 1–5 mV APs with characteristic features of juxtacellular recordings (Fig 10b) or intracellular recordings
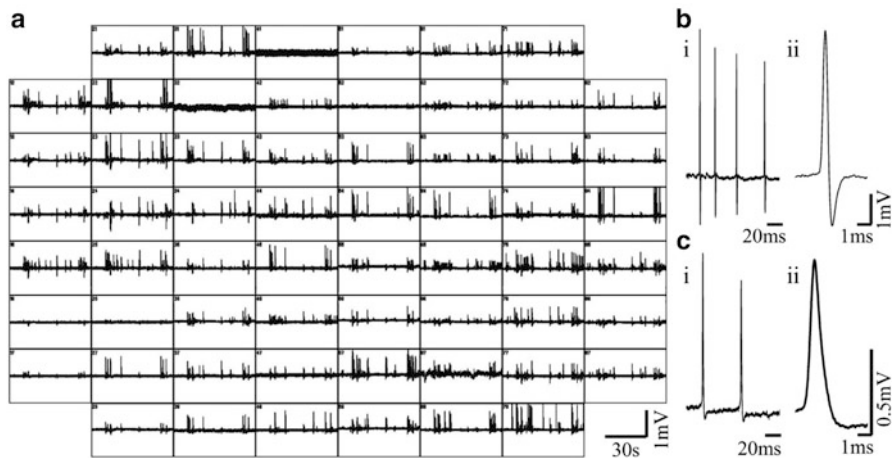
Fig. 10 Spontaneous activity recorded by 60 gMμE-MEA from cultured hippocampal neurons 17 DIV (**a**). Each box represents 30 s of recording from a single gMμE. Note that the majority of the gMμEs recorded monophasic positive action potentials (**b–c**) Enlargement of recorded APs by two gMμEs. Whereas in (**b**) the AP features are of loose seal-like configuration, that of (**c**) is of IN-CELL recordings. (Reprinted with permission from Shmoel et al. (2016). Copyright Nature Publishing Group, 2016)

(Fig. 10c and Shmoel et al. 2016). The large variability can be attributed to two factors. Because of the small diameter of hippocampal neuron cell bodies (15–20 μm), the probability of a neuron to be positioned optimally to engulf a gMμE and form a high seal resistance junction is lower than for the large diameter *Aplysia* neurons. In addition, the short duration of the recorded action potentials (by a fraction of the electrodes Fig. 10) suggest that in these cases the junctional membrane resistance is high. Under these conditions the electrical coupling between the neuron and the gMμE is capacitive rather than Ohmic. Thus, the shapes of the recorded APs resemble the time derivative of the genuine intracellular AP. The range of interfacing modes can be explained by the analog electrical circuits shown in Fig. 1a, b.

The circuits depicted by Fig. 1 illustrate two junctional membrane modes. In Fig. 1b, R_{jm} is large, >100 GΩ. Thus, the resistive component of the junctional membrane could be neglected and the membrane is represented by a capacitor (C_{jm}) with a value that corresponded to its surface area times 1 μF/cm^2. This together with the seal resistance formed by the cleft between the plasma membrane and the gMμE configures a passive electrical differentiator that generated an output potential proportional to the time derivative of the input (Rizzoni 2009). In contrast, if R_{jm} is low ($\sim$1 GΩ) the circuit properties are transformed from a differentiator (Fig. 1b) to an element that does not distort the shape of the wave form (Fig. 1a). These changes corresponded to the transition between a loose seal/juxtacellular recording configuration and an IN-CELL recording. In fact, the changes in the relationships between the R_{jm} and C_{jm} are expected to generate a continuous spectrum of outputs ranging from juxtacellular to IN-CELL recording modes as
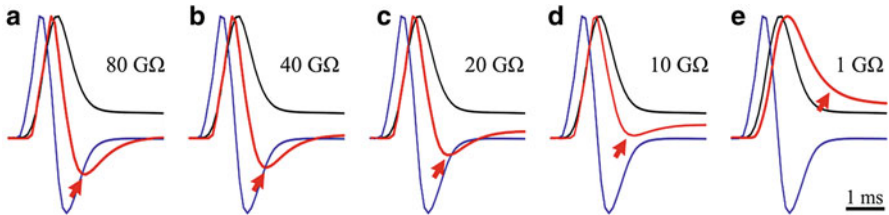
Fig. 11 Simulation of the shapes and amplitudes of action potentials as a function of the junctional membrane resistances using the analog electrical circuits of Fig. 1 and the analog electronic circuit simulator SPICE. The normalized input action-potential (black), its calculated time derivative (blue) and the simulated output (red) for R_{jm} values of 80-1 GΩ (as indicated). The shape of the output action potentials (red) changes (red arrow) from being similar to the time derivative of the input potential (**a**), gradually (**b** and **c**) to an intracellular recording (**d**, **e**). Aside from the dependence of the normalized simulated output shape, the increase in R_{jm} value is associated with a decrease in the amplitude of the simulated output AP, a change in the simulated AP duration, and a shift in the AP peak time with respect to the input AP (not shown for additional details see Shmoel et al. (2016) (Reprinted with permission from Shmoel et al. (2016). Copyright Nature Publishing Group, 2016)

illustrated by simulation of the analog electrical circuits of Fig. 1 (using the general-purpose, analog electronic circuit simulator SPICE) and shown by Fig. 11 (Shmoel et al. 2016).

Interestingly, contrary to what was found in *Aplysia*, the electrical coupling levels and mode of recording formed between hippocampal neurons and gMµEs were not improved by functionalizing the gMµE with the RGD repeat peptide. Ultrastructural observations by our lab and others have revealed that hippocampal neurons (and cardiomyocytes) engulf to tightly interface with gMµEs functionalized by poly-L-lysine or polyethyleneimine/laminin, suggesting that the 3D structure in itself (mushroom, and in fact also vertical nanoelectrodes) is sufficient to facilitate the engulfment (Fendyur et al. 2011; Santoro et al. 2013, 2014a, b; Ojovan et al. 2015; Shmoel et al. 2016; Zhao et al. 2017). Hence, it is conceivable that the expected effects of the RGD repeat peptide on the junctional membrane conductance of hippocampal neurons are not expressed by the time the hippocampal network matures its electrophysiological functions 10–14 days after plating. It is assumed that the peptide layers at the gold electrode surface undergo a degradation process by enzymes secreted by the neurons or by hydrolysis. Attempts to achieve Ohmic contact between gMµEs and the neurons by electroporation were unsuccessful. We observed that the hippocampal neurons–gMµE hybrids remained stable in culture for periods of up to 10 days. We have not yet tested whether gMµEs alter the physiological properties of the neurons or the network.

9 Recordings of Synaptic Potentials by Gold Mushroom-Shaped MEA?

In a number of experiments, we observed the presence of low amplitude ($\sim$100 µV) negative and positive potentials with slower rise and decay times than the APs (Fig. 12). Given that FPs generated by single neurons in culture decay to a third of their amplitude within a distance of approximately 100 µm (Weir et al. 2014), these potentials may reflect the pickup of FPs generated by remote neurons. Alternatively, these potentials could reflect a barrage of genuine excitatory and inhibitory synaptic potentials. Currently we cannot unequivocally differentiate between these possibilities by rigid criteria. Nevertheless, pharmacological experiments support the hypothesis that these are synaptic potentials. Specifically, the application of GABAzine, a GABAergic postsynaptic blocking reagent (1–10 µM), transformed the endogenous FPs firing pattern into typical bursts (Fig. 12a, b, respectively). Concomitantly, it led to the disappearance of the slow negative-going potentials (Fig. 12d, f). Hence, if the slow low-amplitude negative-going potentials had been generated by bursts of APs produced by remote neurons, the frequency and amplitude of the negative potentials would have increased rather than disappeared.
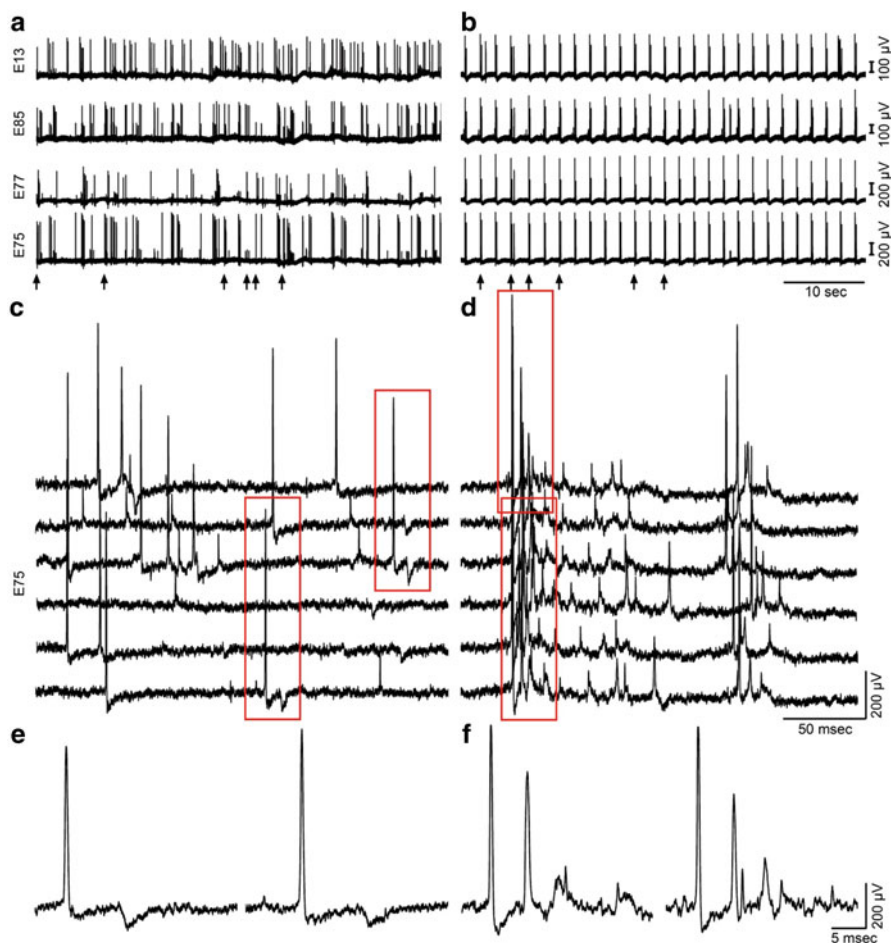
Fig. 12 The effect of GABAzine on recorded spontaneous electrophysiological signaling repertoire. Spontaneous firing as recorded by 4 gMμE before (**a**, **c**) and after the application of 10 μM GABAzine to the culture medium (**b**, **d**). (**c**, **d**) are enlargements of the bursts indicated by arrows in (**a**) and (**b**) respectively. (**e**, **f**) Enlargements of the potentials enclosed by red boxes in (**c**) and (**d**) respectively. GABAzine alters the spike firing pattern to distinct bursts. (**e**) The low-amplitude, long-duration negative potentials recorded before GABAzine application disappear after GABAzine application, and positive, but low-amplitude, long-duration potentials are recorded (**f**). These potentials are tentatively considered to be synaptic. The spikelets are possibly dendritic spikes or the firing of electronically coupled neurons. (Reprinted with permission from Shmoel et al. (2016). Copyright Nature Publishing Group, 2016)

In summary, the electrophysiological and pharmacological observations are consistent with the possibility that the relatively slow low-amplitude potentials recorded by the gMμEs from an in vitro network of hippocampal neurons could represent synaptic potentials.

10 Conclusions

Taken together, the results discussed in this chapter show at a proof-of-concept level that passive and active vertical nanoelectrodes can record attenuated intracellular spikes and subthreshold synaptic potentials from cultured neurons, cardiomyocytes, and skeletal myotubes. The attenuation of the recorded signals is mainly the outcome of the high impedance of the 3D vertical nanoelectrodes due to their small surface area. This could be improved by the use of nano-FETs rather than passive electrodes and the development of novel materials for electrode construction. Another shortcoming of currently used vertical nanoelectrode technology is the low seal resistance formed between the electrode and the cell. This parameter could be substantially improved by developing suitable surface chemistries to effectively fuse the electrodes with the cell's plasma membrane. The limited time, of approximately 1 h, during which intracellular recordings can be obtained after electroporation or optoporation is yet another aspect that should be improved. It is conceivable that slowdown of innate membrane repair mechanism which serves to protect cells from damage after membrane poration can be theoretically designed.

To conclude, the 10-year-old technologies of intracellular electrophysiological recordings from individual cells comprising cellular networks have made tremendous progress. It is foreseen that the use of the novel vertical nanoelectrodes-based MEA technologies that enable to read the entire electrophysiological signaling repertoire from individual cells within an operational network will have a significant impact on the progress of basic and applied brain research.

References

Abbott, J., Ye, T., Ham, D., & Park, H. (2018). Optimizing nanoelectrode arrays for scalable intracellular electrophysiology. *Accounts of Chemical Research, 51*, 600–608.

Abbott, J., Ye, T., Qin, L., Jorgolli, M., Gertner, R. S., Ham, D., et al. (2017). CMOS nanoelectrode array for all-electrical intracellular electrophysiological imaging. *Nature Nanotechnology, 12*, 460–466.

Almquist, B. D., & Melosh, N. A. (2010). Fusion of biomimetic stealth probes into lipid bilayer cores. *Proceedings of the National Academy of Sciences of the United States of America, 107*, 5815–5820.

Almquist, B. D., & Melosh, N. A. (2011). Molecular structure influences the stability of membrane penetrating biointerfaces. *Nano Letters, 11*, 2066–2070.

Almquist, B. D., Verma, P., Cai, W., & Melosh, N. A. (2011). Nanoscale patterning controls inorganic-membrane interface structure. *Nanoscale, 3*, 391–400.

Amin, H., Maccione, A., Marinaro, F., Zordan, S., Nieus, T., & Berdondini, L. (2016). Electrical responses and spontaneous activity of human iPS-derived neuronal networks characterized for 3-month culture with 4096-electrode arrays. *Frontiers in Neuroscience, 10*, 121.

Angle, M. R., Cui, B., & Melosh, N. A. (2015). Nanotechnology and neurophysiology. *Current Opinion in Neurobiology, 32*, 132–140.

Angle, M. R., & Schaefer, A. T. (2012). Neuronal recordings with solid-conductor intracellular nanoelectrodes (SCINEs). *PLoS One, 7*, e43194.

Angle, M. R., Wang, A., Thomas, A., Schaefer, A. T., & Melosh, N. A. (2014). Penetration of cell membranes and synthetic lipid bilayers by nanoprobes. *Biophysical Journal, 107*, 2091–2100.

Barth, A. L., & Poulet, J. F. (2012). Experimental evidence for sparse firing in the neocortex. *Trends in Neurosciences, 35*, 345–355.

Berdondini, L., Imfeld, K., Maccione, A., Tedesco, M., Neukom, S., Koudelka-Hep, M., et al. (2009a). Active pixel sensor array for high spatio-temporal resolution electrophysiological recordings from single cell to large scale neuronal networks. *Lab on a Chip, 9*, 2644–2651.

Berdondini, L., Massobrio, P., Chiappalone, M., Tedesco, M., Imfeld, K., Maccione, A., et al. (2009b). Extracellular recordings from locally dense microelectrode arrays coupled to dissociated cortical cultures. *Journal of Neuroscience Methods, 177*, 386–396.

Berdondini, L., Van Der Wal, P. D., Guenat, O., De Rooij, N. F., Koudelka-Hep, M., Seitz, P., et al. (2005). High-density electrode array for imaging in vitro electrophysiological activity. *Biosensors and Bioelectronics, 21*, 167–174.

Braeken, D., Jans, D., Huys, R., Stassen, A., Collaert, N., Hoffman, L., et al. (2012). Open-cell recording of action potentials using active electrode arrays. *Lab on a Chip, 12*, 4397–4402.

Braun, D., & Fromherz, P. (1998). Fluorescence interferometry of neuronal cell adhesion on microstructured silicon. *Physical Review Letters, 81*, 5241–5244.

Chernomordik, L. V., & Kozlov, M. M. (2008). Mechanics of membrane fusion. *Nature Structural and Molecular Biology, 15*, 675–683.

Claycomb, W. C., Lanson Jr., N. A., Stallworth, B. S., Egeland, D. B., Delcarpio, J. B., Bahinski, A., et al. (1998). HL-1 cells: A cardiac muscle cell line that contracts and retains phenotypic characteristics of the adult cardiomyocyte. *Proceedings of the National Academy of Sciences of the United States of America, 95*, 2979–2984.

Cohen, A., Shappir, J., Yitzchaik, S., & Spira, M. E. (2008). Reversible transition of extracellular field potential recordings to intracellular recordings of action potentials generated by neurons grown on transistors. *Biosensors and Bioelectronics, 23*, 811–819.

De Angelis, F., Malerba, M., Patrini, M., Miele, E., Das, G., Toma, A., et al. (2013). 3D hollow nanostructures as building blocks for multifunctional plasmonics. *Nano Letters, 13*, 3553–3558.

Demonbreun, A. R., & Mcnally, E. M. (2016). Plasma membrane repair in health and disease. *Current Topics in Membranes, 77*, 67–96.

Dipalo, M., Amin, H., Lovato, L., Moia, F., Caprettini, V., Messina, G. C., et al. (2017). Intracellular and extracellular recording of spontaneous action potentials in mammalian neurons and cardiac cells with 3D plasmonic nanoelectrodes. *Nano Letters, 17*, 3932–3939.

Dipalo, M., Messina, G. C., Amin, H., La Rocca, R., Shalabaeva, V., Simi, A., et al. (2015). 3D plasmonic nanoantennas integrated with MEA biosensors. *Nanoscale, 7*, 3703–3711.

Duan, X., Gao, R., Xie, P., Cohen-Karni, T., Qing, Q., Choe, H. S., et al. (2012). Intracellular recordings of action potentials by an extracellular nanoscale field-effect transistor. *Nature Nanotechnology, 7*, 174–179.

Epand, R. M., D'souza, K., Berno, B., & Schlame, M. (2015). Membrane curvature modulation of protein activity determined by NMR. *Biochimica et Biophysica Acta, 1848*, 220–228.

Epsztein, J., Brecht, M., & Lee, A. K. (2011). Intracellular determinants of hippocampal CA1 place and silent cell activity in a novel environment. *Neuron, 70*, 109–120.

Fekete, Z. (2015). Recent advances in silicon-based neural microelectrodes and microsystems: A review. *Sensors and Actuators B: Chemical, 215*, 300–315.

Fendyur, A., Mazurski, N., Shappir, J., & Spira, M. E. (2011). Formation of essential ultrastructural interface between cultured hippocampal cells and gold mushroom-shaped MEA-toward "IN-CELL" recordings from vertebrate neurons. *Frontiers in Neuroengineering, 4*, 14.

Fendyur, A., & Spira, M. E. (2012). Toward on-chip, in-cell recordings from cultured cardiomyocytes by arrays of gold mushroom-shaped microelectrodes. *Frontiers in Neuroengineering, 5*, 21.

Fromherz, P. (2003). *Neuroelectronic interfacing: Semiconductor chips with ion channels, nerve cells, and brain*. Berlin: Wiley-VCH.

Gao, R., Strehle, S., Tian, B., Cohen-Karni, T., Xie, P., Duan, X., et al. (2012). Outside looking in: Nanotube transistor intracellular sensors. *Nano Letters, 12*, 3329–3333.

Gold, C., Girardin, C. C., Martin, K. A., & Koch, C. (2009). High-amplitude positive spikes recorded extracellularly in cat visual cortex. *Journal of Neurophysiology, 102*, 3340–3351.

Hai, A., Dormann, A., Shappir, J., Yitzchaik, S., Bartic, C., Borghs, G., et al. (2009a). Spine-shaped gold protrusions improve the adherence and electrical coupling of neurons with the surface of micro-electronic devices. *Journal of the Royal Society Interface, 6*, 1153–1165.

Hai, A., Kamber, D., Malkinson, G., Erez, H., Mazurski, N., Shappir, J., et al. (2009b). Changing gears from chemical adhesion of cells to flat substrata toward engulfment of micro-protrusions by active mechanisms. *Journal of Neural Engineering, 6*, 066009.

Hai, A., Shappir, J., & Spira, M. E. (2010a). In-cell recordings by extracellular microelectrodes. *Nature Methods, 7*, 200–202.

Hai, A., Shappir, J., & Spira, M. E. (2010b). Long-term, multisite, parallel, in-cell recording and stimulation by an array of extracellular microelectrodes. *Journal of Neurophysiology, 104*, 559–568.

Hai, A., & Spira, M. E. (2012). On-chip electroporation, membrane repair dynamics and transient in-cell recordings by arrays of gold mushroom-shaped microelectrodes. *Lab on a Chip, 12*, 2865–2873.

Han, R., & Campbell, K. P. (2007). Dysferlin and muscle membrane repair. *Current Opinion in Cell Biology, 19*, 409–416.

Hanson, L., Lin, Z. C., Xie, C., Cui, Y., & Cui, B. X. (2012). Characterization of the cell-nanopillar interface by transmission electron microscopy. *Nano Letters, 12*, 5815–5820.

Hille, B. (1992). *Ionic channels of excitable membranes*. Sunderland: Sinauer.

Horn, R., & Marty, A. (1988). Muscarinic activation of ionic currents measured by a new whole-cell recording method. *The Journal of General Physiology, 92*, 145–159.

Iversen, L., Mathiasen, S., Larsen, J. B., & Stamou, D. (2015). Membrane curvature bends the laws of physics and chemistry. *Nature Chemical Biology, 11*, 822–825.

Jackel, D., Bakkum, D. J., Russell, T. L., Muller, J., Radivojevic, M., Frey, U., et al. (2017). Combination of high-density microelectrode array and patch clamp recordings to enable studies of multisynaptic integration. *Scientific Reports, 7*, 978.

Jenkner, M., & Fromherz, P. (1997). Bistability of membrane conductance in cell adhesion observed in a neuron transistor. *Physical Review Letters, 79*, 4705–4708.

Joshi, R. P., & Schoenbach, K. H. (2002). Mechanism for membrane electroporation irreversibility under high-intensity, ultrashort electrical pulse conditions. *Physical Review. E, Statistical, Nonlinear, and Soft Matter Physics, 66*, 052901.

Joshi, S., & Hawken, M. J. (2006). Loose-patch-juxtacellular recording in vivo—a method for functional characterization and labeling of neurons in macaque V1. *Journal of Neuroscience Methods, 156*, 37–49.

Jun, J. J., Steinmetz, N. A., Siegle, J. H., Denman, D. J., Bauza, M., Barbarits, B., et al. (2017). Fully integrated silicon probes for high-density recording of neural activity. *Nature, 551*, 232–236.

Lefler, Y., Yarom, Y., & Uusisaari, M. Y. (2014). Cerebellar inhibitory input to the inferior olive decreases electrical coupling and blocks subthreshold oscillations. *Neuron, 81*, 1389–1400.

Lin, Z. C., & Cui, B. (2014). Nanowire transistors: Room for manoeuvre. *Nature Nanotechnology, 9*, 94–96.

Lin, Z. C., Xie, C., Osakada, Y., Cui, Y., & Cui, B. (2014). Iridium oxide nanotube electrodes for sensitive and prolonged intracellular measurement of action potentials. *Nature Communications, 5*, 3206.

Liu, R., Chen, R., Elthakeb, A. T., Lee, S. H., Hinckley, S., Khraiche, M. L., et al. (2017). High density individually addressable nanowire arrays record intracellular activity from primary rodent and human stem cell derived neurons. *Nano Letters, 17*, 2757–2764.

Lou, H. Y., Zhao, W., Zeng, Y., & Cui, B. (2018). The role of membrane curvature in nanoscale topography-induced intracellular signaling. *Accounts of Chemical Research, 51*, 1046–1053.

Massobrio, G., Martinoia, S., & Massobrio, P. (2018). Equivalent circuit of the neuro-electronic junction for signal recordings from planar and engulfed micro-nano-electrodes. *IEEE Transactions on Biomedical Circuits and Systems, 12*, 3–12.

Massobrio, P., Massobrio, G., & Martinoia, S. (2016). Interfacing cultured neurons to microtransducers arrays: A review of the neuro-electronic junction models. *Frontiers in Neuroscience, 10*, 282.

Mcneil, P. L., & Khakee, R. (1992). Disruptions of muscle fiber plasma membranes. Role in exercise-induced damage. *The American Journal of Pathology, 140*, 1097–1109.

Mcneil, P. L., & Kirchhausen, T. (2005). An emergency response team for membrane repair. *Nature Reviews. Molecular Cell Biology, 6*, 499–505.

Messina, G. C., Dipalo, M., La Rocca, R., Zilio, P., Caprettini, V., Zaccaria, R. P., et al. (2015). Spatially, temporally, and quantitatively controlled delivery of broad range of molecules into selected cells through plasmonic nanotubes. *Advanced Materials, 27*, 7145–7149.

Obien, M. E., Deligkaris, K., Bullmann, T., Bakkum, D. J., & Frey, U. (2014). Revealing neuronal function through microelectrode array recordings. *Frontiers in Neuroscience, 8*, 423.

Ojovan, S. M., Rabieh, N., Shmoel, N., Erez, H., Maydan, E., Cohen, A., et al. (2015). A feasibility study of multi-site, intracellular recordings from mammalian neurons by extracellular gold mushroom-shaped microelectrodes. *Scientific Reports, 5*, 14100.

Oren, R., Sfez, R., Korbakov, N., Shabtai, K., Cohen, A., Erez, H., et al. (2004). Electrically conductive 2D-PAN-containing surfaces as a culturing substrate for neurons. *Journal of Biomaterials Science. Polymer Edition, 15*, 1355–1374.

Qing, Q., Jiang, Z., Xu, L., Gao, R. X., Mai, L. Q., & Lieber, C. M. (2014). Free-standing kinked nanowire transistor probes for targeted intracellular recording in three dimensions. *Nature Nanotechnology, 9*, 142–147.

Rabieh, N., Ojovan, S. M., Shmoel, N., Erez, H., Maydan, E., & Spira, M. E. (2016). On-chip, multisite extracellular and intracellular recordings from primary cultured skeletal myotubes. *Scientific Reports, 6*, 36498.

Rizzoni, G. (2009). *Fundamentals of electrical engineering*. New York: McGraw-Hill.

Robinson, J. T., Jorgolli, M., Shalek, A. K., Yoon, M. H., Gertner, R. S., & Park, H. (2012). Vertical nanowire electrode arrays as a scalable platform for intracellular interfacing to neuronal circuits. *Nature Nanotechnology, 7*, 180–184.

Sackmann, E., & Bruinsma, R. F. (2002). Cell adhesion as wetting transition? *Chemphyschem, 3*, 262–269.

Sakmann, B., & Neher, E. (1984). Patch clamp techniques for studying ionic channels in excitable membranes. *Annual Review of Physiology, 46*, 455–472.

Santoro, F., Dasgupta, S., Schnitker, J., Auth, T., Neumann, E., Panaitov, G., et al. (2014a). Interfacing electrogenic cells with 3D nanoelectrodes: Position, shape, and size matter. *ACS Nano, 8*, 6713–6723.

Santoro, F., Panaitov, G., & Offenhausser, A. (2014b). Defined patterns of neuronal networks on 3D thiol-functionalized microstructures. *Nano Letters, 14*, 6906–6909.

Santoro, F., Schnitker, J., Panaitov, G., & Offenhäusser, A. (2013). On chip guidance and recording of cardiomyocytes with 3D mushroom-shaped electrodes. *Nano Letters, 13*, 5379–5384.

Santoro, F., Zhao, W., Joubert, L. M., Duan, L., Schnitker, J., Van De Burgt, Y., et al. (2017). Revealing the cell-material interface with nanometer resolution by focused ion beam/scanning electron microscopy. *ACS Nano, 11*, 8320–8328.

Seymour, J., Wu, F., Wise, K. D., & Yoon, E. (2017). State-of-the-art MEMS and microsystem tools for brain research. *Microsystems and Nanoengineering, 3*, 1–16.

Shmoel, N., Rabieh, N., Ojovan, S. M., Erez, H., Maydan, E., & Spira, M. E. (2016). Multisite electrophysiological recordings by self-assembled loose-patch-like junctions between cultured hippocampal neurons and mushroom-shaped microelectrodes. *Scientific Reports, 6*, 27110.

Shoham, S., O'connor, D. H., & Segev, R. (2006). How silent is the brain: Is there a "dark matter" problem in neuroscience? *Journal of Comparative Physiology. A, Neuroethology, Sensory, Neural, and Behavioral Physiology, 192*, 777–784.

Sileo, L., Pisanello, F., Quarta, L., Maccione, A., Simi, A., Berdondini, L., et al. (2013). Electrical coupling of mammalian neurons to microelectrodes with 3D nanoprotrusions. *Microelectronic Engineering, 111*, 384–390.

Spira, M. E., & Hai, A. (2013). Multi-electrode array technologies for neuroscience and cardiology. *Nature Nanotechnology, 8*, 83–94.

Spira, M. E., Kamber, D., Dormann, A., Cohen, A., Bartic, C., Borghs, G., et al. (2007). Improved neuronal adhesion to the surface of electronic device by engulfment of protruding micro-nails fabricated on the chip surface. *Transducers and Eurosensors, 1*, 1247–1250.

Thomas Jr., C. A., Springer, P. A., Loeb, G. E., Berwald-Netter, Y., & Okun, L. M. (1972). A miniature microelectrode array to monitor the bioelectric activity of cultured cells. *Experimental Cell Research, 74*, 61–66.

Tian, B., Cohen-Karni, T., Qing, Q., Duan, X., Xie, P., & Lieber, C. M. (2010). Three-dimensional, flexible nanoscale field-effect transistors as localized bioprobes. *Science, 329*, 830–834.

VanDersal, J. J., & Renaud, P. (2016). Biomimetic surface patterning for long-term transmembrane access. *Scientific Reports, 6*, 32485.

Verma, P., Wong, I. Y., & Melosh, N. A. (2010). Continuum model of mechanical interactions between biological cells and artificial nanostructures. *Biointerphases, 5*, 37–44.

Viswam, V., Bounik, R., Shadmani, A., Dragas, J., Obien, M., Muller, J., et al. (2017). High-density mapping of brain slices using a large multi-functional high-density CMOS microelectrode array system. *International Solid State Sensors Actuators and Microsystems Conference, 2017*, 135–138.

Weir, K., Blanquie, O., Kilb, W., Luhmann, H. J., & Sinning, A. (2014). Comparison of spike parameters from optically identified GABAergic and glutamatergic neurons in sparse cortical cultures. *Frontiers in Cellular Neuroscience, 8*, 460.

Weis, R., & Fromherz, P. (1997). Frequency dependent signal-transfer in neuron-transistors. *Physical Review E, 55*, 877–889.

Wise, K. D., Angell, J. B., & Starr, A. (1970). An integrated-circuit approach to extracellular microelectrodes. *IEEE Transactions on Biomedical Engineering, 17*, 238–247.

Xie, C., Lin, Z., Hanson, L., Cui, Y., & Cui, B. (2012). Intracellular recording of action potentials by nanopillar electroporation. *Nature Nanotechnology, 7*, 185–190.

Xu, A. M., Aalipour, A., Leal-Ortiz, S., Mekhdjian, A. H., Xie, X., Dunn, A. R., et al. (2014). Quantification of nanowire penetration into living cells. *Nature Communications, 5*, 3613.

Zeck, G., & Fromherz, P. (2003). Repulsion and attraction by extracellular matrix protein in cell adhesion studied with nerve cells and lipid vesicles on silicon chips. *Langmuir, 19*, 1580–1585.

Zhao, W., Hanson, L., Lou, H. Y., Akamatsu, M., Chowdary, P. D., Santoro, F., et al. (2017). Nanoscale manipulation of membrane curvature for probing endocytosis in live cells. *Nature Nanotechnology, 12*, 750–756.

Zilio, P., Dipalo, M., Tantussi, F., Messina, G. C., & De Angelis, F. (2017). Hot electrons in water: Injection and ponderomotive acceleration by means of plasmonic nanoelectrodes. *Light-Science and Applications, 6*(6), e17002.

From MEAs to MOAs: The Next Generation of Bioelectronic Interfaces for Neuronal Cultures

Andrea Spanu, Mariateresa Tedesco, Sergio Martinoia, and Annalisa Bonfiglio

Abstract Since their introduction in the early 1970s, microelectrode arrays (MEAs) have been dominating the electrophysiology market thanks to their reliability, extreme robustness, and usability. Over the past 40 years, silicon technology has also played a role in the advancement of the field, and CMOS-based in vitro and in vivo systems are now able to achieve unprecedented spatial resolutions, giving the possibility to unveil hidden behavior of cellular aggregates down to the subcellular level. However, both the MEAs and silicon-based electronic devices present unavoidable problems such as their expensiveness, the usual rigidity of the employed materials, and the need of an (usually bulky) external reference electrode. Possible interesting alternatives to these incredibly useful devices unexpectedly lie in the field of organic electronics, thanks to the fast-growing pace of improvement that this discipline has undergone in the last 10–15 years. In this chapter, a particular organic transistor called organic charge-modulated field-effect transistor (OCMFET) will be presented as a promising bio–electronic interface, and a complete description of its employment as a detector of cellular electrical activity and as an ultrasensitive pH sensor will be provided, together with the discussion about the possibility of using such a device as an innovative multisensing tool for both electrophysiology and (neuro)pharmacology.

Keywords OCMFETs · MEAs · Cell electrical activity monitoring · pH sensing · Pharmacology

A. Spanu (✉)
Department of Electrical and Electronic Engineering, University of Cagliari, Cagliari, Italy

Center for Materials and Microsystems, FBK - "Bruno Kessler" Foundation, Trento, Italy
e-mail: andrea.spanu@diee.unica.it

M. Tedesco · S. Martinoia
Department of Bioengineering, Robotics and System Engineering, University of Genoa, Genova, Italy

A. Bonfiglio
Department of Electrical and Electronic Engineering, University of Cagliari, Cagliari, Italy

155

1 Introduction

The beginning of the "microelectrodes array era" can be traced back to the first half of the 1970s, thanks to the seminal paper of Thomas (Thomas et al. 1972), which followed more than two decades of studies on single unit metal electrodes for biological applications (Hubel 1957; Verzeano et al. 1960; Robinson 1968; Wise et al. 1970). This work introduced the idea that it was possible, and somehow convenient, eavesdropping the "cellular chat" from the outside of the cell, instead of being confined by the cell membrane borders, by using a very simple tiny metal electrode. This change of paradigm virtually gave rise to the modern neuroscience field as we know it, allowing for the study of cells aggregates over long periods with a non-destructive approach, and opening up a whole world of new possibilities in the understanding of the central nervous system, and promoting the advent of disciplines such as the brain–machine interface (BMI) field. The seed rapidly spread, and in the following decades an increasing number of MEA-based systems have been designed and implemented, with an escalation of new materials, fabrication techniques, and novel applications (Gross et al. 1977; Rousche et al. 2001; Takeuchi et al. 2004; Blau et al. 2011; Sessolo et al. 2013).

Indeed, the 70s of the twentieth century turned out to be a very important decade for electrophysiology. Besides the advent of MEAs, another important device saw the light in the 1970, namely the ion sensitive FET (ISFET). The very first example of ISFET was introduced by Piet Bergveld as a neurophysiological tool (Bergveld 1970, 1972), and few years later another version of this device, called OSFET, was further optimized for the detection of bioelectrical signals in vitro (Bergveld et al. 1976). The idea of using ISFET-like electronics fascinated the scientific community, and the great effort put in the optimization of the device culminated 20 years later with the work of Fromherz (Fromherz et al. 1991; Weis et al. 1996; Vassanelli and Fromherz 1997; Stett et al. 1997), whose model of neuron–FET interface in vitro is still widely accepted and used in the development of innovative silicon-based systems (Berdondini et al. 2005, 2009; Krause 2000; Ecken et al. 2003; Meyburg et al. 2006; Viswam et al. 2016; Lopez et al. 2018).

Despite their widespread use and the fact that they have definitely conquered the electrophysiological field, the drawbacks associated to the MEA and the ISFET technology are patent, such as the problems associated with the high cost of fabrication, the rigidity (usually) associated to the materials, and the presence of a (again, usually) bulky external reference electrode.

In the last years, the growing need for low-cost and possibly disposable in vitro electrophysiological tools (aiming at the reduction of animal-demanding in vivo experiments) put the organic (bio)electronics field in the limelight. Organic electronics, in fact, represents an interesting alternative in all those applications where inexpensiveness, mechanical compliance, and biocompatibility are required. To date, among the few organic devices that have been employed as bio–electronic interfaces, the organic electrochemical transistor is undoubtedly the more studied. This device can be operated with ultralow voltages and has been able to

reliably detect neuronal activity in vivo, outperforming passive microelectrodes (Khodagholy et al. 2013, 2015). Lately, electrolyte gated organic FETs (EGOFETs) have also been extensively studied and employed as sensor and biosensors (Kergoat et al. 2012; Casalini et al. 2013; Schmoltner et al. 2013), and recently, an attempt to introduce this interesting tool in the cellular domain has been done (Zhang et al. 2017). Although conceptually interesting, the work is at a very early stage, and the actual application of this device in electrophysiology has yet to come. Despite their potentials, OECTs and EGOFETs present drawbacks such as the need of an external reference electrode and the direct exposure of the semiconductor layer to the harsh liquid environment where the sensing takes place, with the former issue not allowing the single device addressability in an array configuration and the latter making these devices not suitable for long-term biological applications.

Besides OECTs and EGOFETs, another interesting organic device, named organic charge-modulated FET (OCMFET), has been recently developed and successfully employed for the detection of electrical activity in vitro. In the following sections, all the different aspects of the OCMFET, from the working principle to future developments, will be presented with the intent of giving an overview of the possible advantages that this versatile organic transistor may bring to electrophysiology and pharmacology.

2   The Organic Charge-Modulated Field-Effect Transistor

The OCMFET is a floating gate organic thin film transistor (OTFT) in a bottom-gate/bottom-contact configuration. The device is gated through an additional contact called control gate, and it can be converted into a high-sensitive charge transducer by exposing the final part of the elongated floating gate to the measurement environment. In fact, the presence of a charge (which is capacitively coupled to the floating gate through an insulating spacer) onto the sensing area induces a shift of the threshold voltage V_{TH} of the device, which can be read out as a modulation of the output current of the transistor. In Fig. 1a, b, the structure and the electrical characteristics of an OCMFET device are shown.

The concept of the device (which was initially developed in CMOS technology) has been proposed by Barbaro et al. in 2006 (Barbaro et al. 2006); its working principle can be explained starting from the expression of the charge Q_{TOT} in the floating gate, which can be estimated taking into account the different voltage contributions in the device according to Gauss equation:

$$Q_{TOT} = C_{CG}\left(V_{FG} - V_{CG}\right) + C_{DF}\left(V_{FG} - V_D\right) + C_{SF}\left(V_{FG} - V_S\right) \qquad (1)$$

where C_{CG}, C_{DF}, and C_{SF} are, respectively, the control capacitance and the parasitic capacitances related to the overlap between drain, source, and the floating gate; V_{CG}, V_D, and V_S are the voltages applied to control capacitor, drain, and source
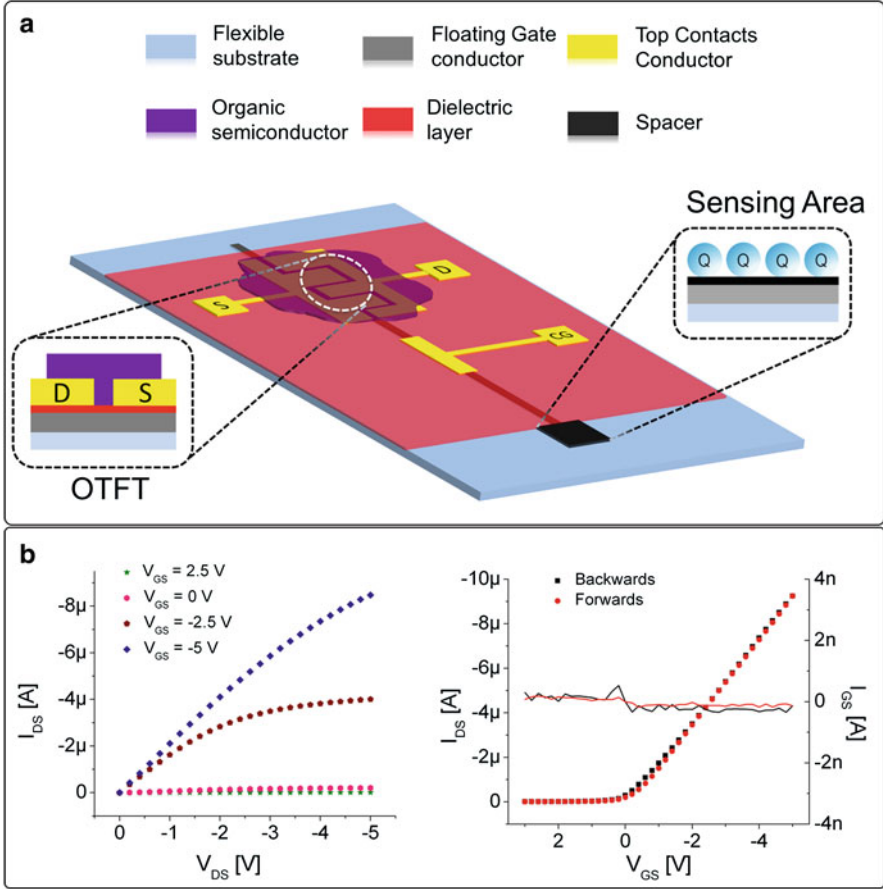
Fig. 1 (**a**) Representation of an OCMFET device. The OCMFET is a floating gate OTFT with a control gate that is needed to set the transistor's working point. The device can be employed as a charge sensor by exposing the final part of the floating gate (called sensing area) to the measurement environment. (**b**) Output and input characteristic of a low-voltage OCMFET biased through the control gate

respectively and V_{FG} is the actual floating gate voltage. This last parameter can be written as:

$$V_{FG} = \frac{C_{CG}}{C_{TOT}} V_G + \frac{C_{DF}}{C_{TOT}} V_D + \frac{C_{SF}}{C_{TOT}} V_S + \frac{Q_{TOT}}{C_{TOT}} \tag{2}$$

where $C_{TOT} = C_{CG} + C_{DF} + C_{SF}$.

If a charge Q_{SENSE} is present on top of the sensing area (and under the hypothesis of perfect charge induction), Q_{TOT} can be written as $Q_0 - Q_{SENSE}$, being Q_0 a constant amount of charge incorporated in the floating gate during the fabrication process, and Q_{SENSE} the charge present onto the sensing area. When the spacer

is thinner than the gate dielectric and Q_0 is negligible, the last equation can be approximated as

$$V_{FG} \approx V_G - \frac{Q_{SENSE}}{C_{TOT}} \qquad (3)$$

Therefore, the floating gate voltage is linearly related to the amount of charge capacitively coupled to the sensing area. The charge variation ΔQ_{SENSE} can be transduced as a corresponding variation of the transistor's threshold voltage:

$$\Delta V_{TH} = -\frac{\Delta Q_{SENSE}}{C_{TOT}} \qquad (4)$$

Unlike the other structures mentioned in this chapter, namely MEAs, OFETs, ISFET-like devices, OECTs, and EGOFETs, the OCMFET does not need any external reference electrode while operated as a sensor; this feature is particularly important when dealing with in vitro (but also in vivo) applications, since such an additional electrical contact usually represents one of the main obstacles to the device portability and miniaturization. Another important feature of the OCMFET is that its sensing mechanism only depends on the nature of the surface of the sensing area, being the organic transistor only used as an amplifier. This physical decoupling of transistor and sensing area brings several advantages in terms of device functionality and stability, allowing for the organic semiconductor to be encapsulated, thus drastically improving the durability of the system. The remarkable versatility of this technological choice has been thoroughly demonstrated during the past years, during which several different sensors have been designed and successfully tested, such as for example DNA hybridization sensors, pressure sensors, and pH sensors (Caboni et al. 2009; Lai et al. 2013a; Spanu et al. 2016).

3 The Micro OCMFET Array: Towards Multisensing Electrophysiological Tools Based on Organic Transistors

As previously highlighted, the OCMFET is a very convenient approach in all those applications where the detection of low charge variations in a liquid environment is involved, such as monitoring the electrical activity of living cells for pharmacology, (neuro)rehabilitation, BMIs, and computational neuroscience. Besides the prementioned features (i.e., the absence of an external reference electrode and the elongated shape of the floating gate, which allows separating the organic semiconductor and the sensing area), other interesting features are its high charge sensitivity, the possibility to be operated at low voltages (Cosseddu et al. 2012), and its relatively high cutoff frequency (up to 100 kHz), due to a high-k–low-k composite dielectric layer (Lai et al. 2013b). Those features make the OCMFET a good candidate for the design of novel electrophysiological/pharmacological tools that can be both
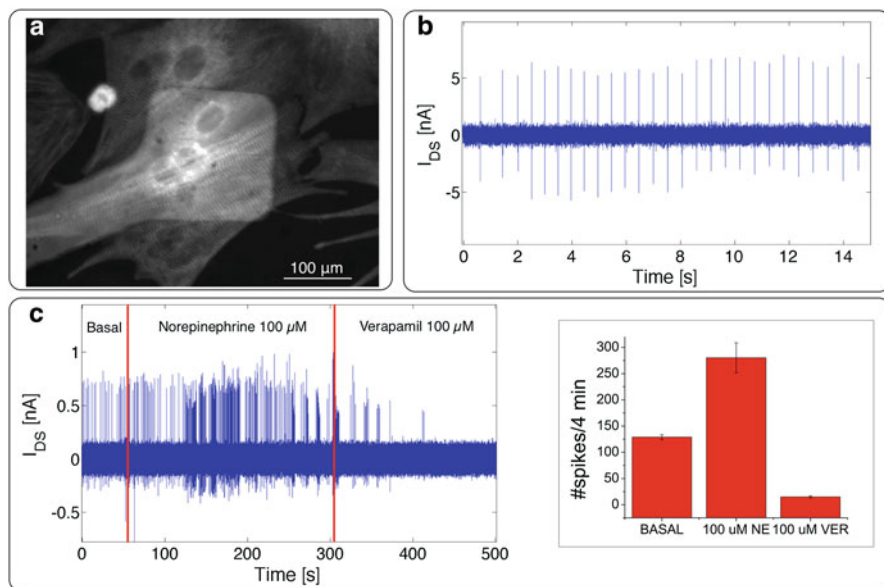
Fig. 2 OCMFET for electrophysiological applications: validation with primary cardiac myocytes from rat embryos. (**a**) Healthy cardiomyocytes onto a sensing area. The culture has been fixed after the recording session and immunostained for the sarcomeric protein Tropomyosin. (**b**) Basal activity of a cardiomyocytes culture maintained 8 days in vitro. (**c**) Chemical modulation of the culture's activity. The basal activity was accelerated using 100 µM of norepinephrine and then suppressed with 100 µM of verapamil. (**c**) (Inset), Beating frequency modulation (statistics on five OCMFETs fabricated within the same MOA) (Spanu et al. 2015; Spanu 2016). Copyright 2015, Nature Publishing Group

referenceless and low cost, thus potentially having the capability to compete with MEA and ISFET technologies. In order to meet the specific requirements of the electrophysiological application, a device called Micro OCMFET Array (MOA) has been recently designed and fabricated, and its capability of transducing bioelectrical signals has been thoroughly investigated (Spanu et al. 2015; Spanu 2016). Primary cardiomyocytes cultures from rat embryos have been chosen as the cellular model for the device sensitivity estimation, due to the optimal covering of the sensing areas that they provide and to their "pace-maker" electrical activity in vitro, which makes the recorded signals highly reproducible and predictable (indeed, very important aspects when dealing with the validation of a new sensor). In Fig. 2a healthy cardiomyocytes cultured onto the sensing area of an OCMFET are shown. The MOA turned out to be capable of reliably monitoring the activity of this kind of culture in both basal conditions and upon chemical stimulation, as reported in Fig. 2b, c.

Using the set of equations previously derived, it is possible to speculate on the sensing capability of the OCMFET. By considering the experimental recordings performed with several devices, the I_{DS} variation associated to a cardiac action potential ranges from hundreds of pA to few nA. By considering an average I_{DS}

variation of 1 nA and representative values of the electronic parameters of the device (a transconductance g_m of 300 pA/mV and the sum of the capacitances C_{TOT} of 100 pF), it is possible to estimate the corresponding charge variation that occurs onto (or in proximity to) the sensing area. For an OCMFET polarized in its saturation region (with $V_{GS} = V_{DS} = -1$ V), it is possible to estimate the relative variation ΔV_{FG} of the floating gate potential induced by the ΔI_{DS}:

$$\Delta V_{FG} = \frac{\Delta I_{DS}}{g_m} \tag{5}$$

As described in Eq. (5), ΔV_{FG} depends linearly on the charge Q_{SENSE}; by considering this charge as being completely associated to the charge displacement occurring on the sensing area during an action potential (Spanu 2016), it is possible to obtain a value of about 0.3 pC. By assuming that this variation is entirely due to the ions crossing the cell membrane during the upstroke of an action potential and by considering a typical membrane capacitance and a cardiac intracellular action potential amplitude ($C_{mem} = 1$ µF/cm^2 and $V_{INTRA} = 120$ mV respectively) it is possible to estimate the corresponding effective area A_{eff} of the cell membrane that faces the sensing area (thus where the charge variation occurs):

$$Q_{SENSE} = C \cdot V_{INTRA} \tag{6}$$

If $C = C_{mem} \cdot A_{eff}$, A_{eff} can be estimated, obtaining a value of 250 µm^2, which is consistent with the adhesion area of a cardiomyocyte soma, thus confirming the plausibility of the proposed transduction principle.

Following this important validation step, the MOA has been preliminary tested with neuronal cultures, a definitely trickier cellular model in terms of signal amplitude and predictability. The stability of the MOA device with neurons was therefore evaluated by using post-natal hippocampal neuronal cultures. In Fig. 3a, a healthy culture of hippocampal neurons cultured onto a MOA device for 21 days is shown (yellow stars indicate some well spread neuronal somata), thus demonstrating the suitability of the system for long-term in vitro neuronal applications. To test the device stability over time (and thus ensuring the feasibility of the device to be used in long term experiments) an OCMFET has been kept inside an incubator (37 °C, 95% of humidity, and 5% of CO_2) for 50 day and the variation of a typical parameter (the charge carriers' mobility) has been monitored. As shown in Fig. 3b, the device remained stable during the whole period. Interestingly enough, as can be noticed in Fig. 3c, d, the OCMFET turned out to be able to reliably monitor both the basal and the drug-mediated activity of such a culture, thus demonstrating the possibility of using the proposed device as a neuropharmacological tool.

Among the various interesting parameters when dealing with cell cultures, one of the most studied in the past 15 years is the metabolic activity. In fact, this aspect of cells behavior is particularly prone to change in response to various external stimuli and drugs, making it a particularly accurate way of assessing cellular viability. One possible method to monitor the cellular metabolism is measuring the
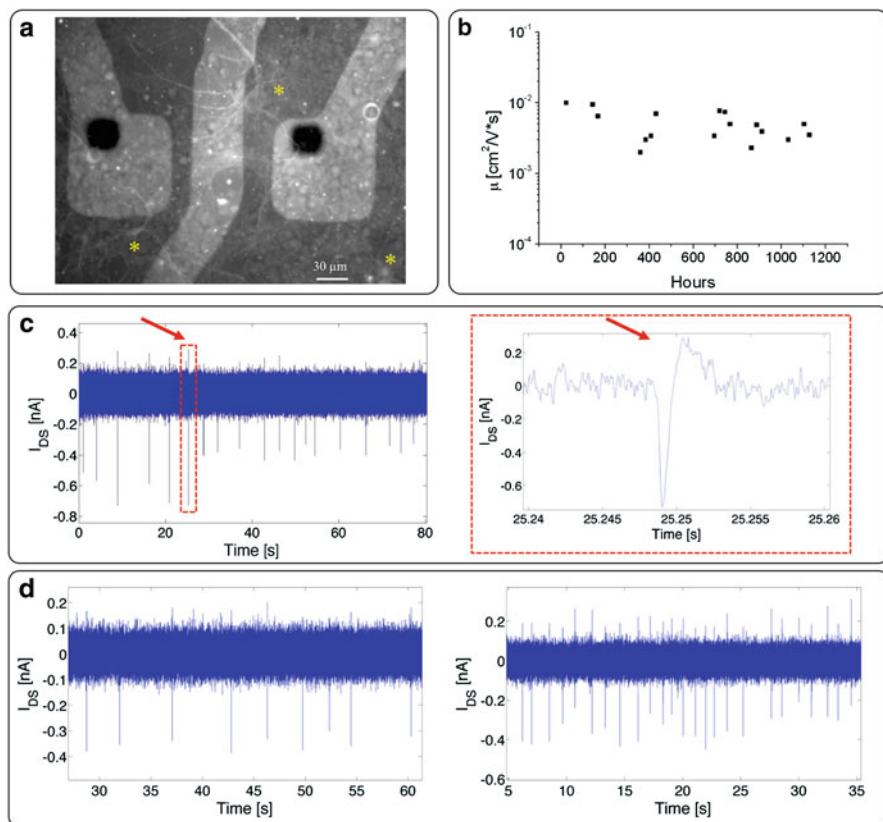
Fig. 3 (**a**) A healthy neuronal culture (hippocampal neurons, 21 DIV), fixed after the recording session. (**b**) Stability assessment of an OCMFET. The device mobility turned out to be stable over a period of 50 days inside an incubator (37 °C, 95% of humidity, and 5% of CO_2). (**c**) Example of hippocampal basal activity (21 DIV) measured with an OCMFET device. (**c**) (inset) Shape of a single hippocampal action potential. (**d**) Chemical modulation of neuronal activity. The basal activity (left) has been modulated by means of the addition of a mixture of drugs (right), namely 25 μM of BIC and 50 μM of 4AP. Copyright 2016, Springer

medium acidification caused by the extracellular accumulation of acidic byproducts (Hynes et al. 2009). Moreover, cells are highly sensitive to local pH variations, which can induce a modification of their physiological state, thus constituting a very important parameter to consider during whatsoever electrophysiological and/or pharmacological experiment.

In the recent past, a number of different approaches have been employed in order to meet the important requirement of reliably monitoring cells metabolism (Hafner 2000; Martinoia et al. 2001; Baumann et al. 1999; Yu et al. 2009). Despite the effort, the goal of having a multisensing platform for such an application is yet to be achieved, and this is mainly due to the complexity and high cost of the existing systems.
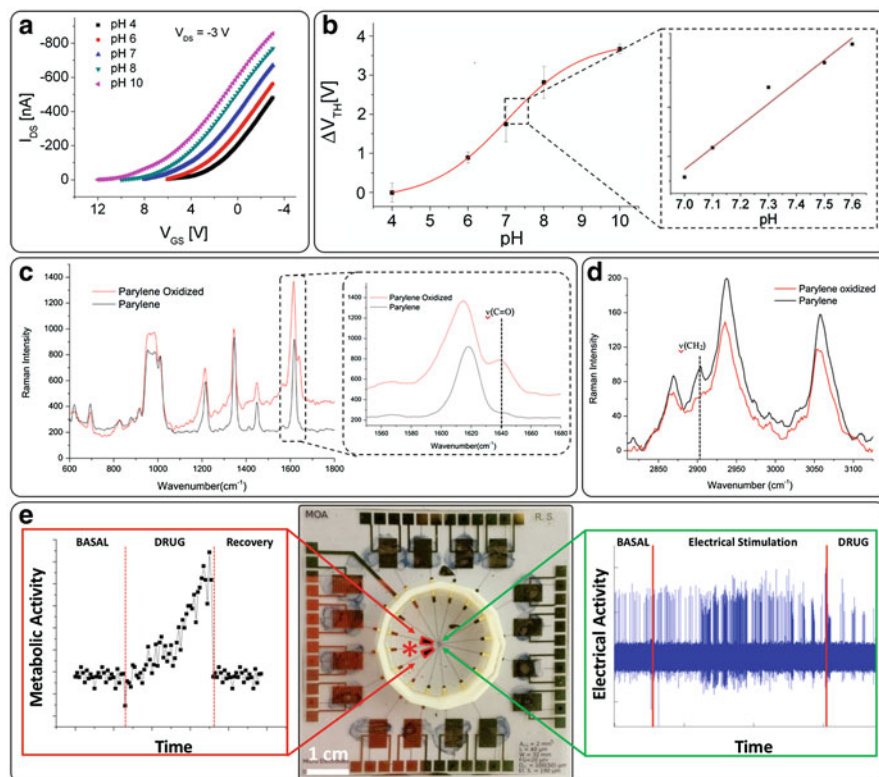
Fig. 4 Characterization of a pH-sensitive OCMFET. (**a**) Transfer characteristics performed while the sensing area is exposed to buffer solutions at different pH values. It is noticeable the gradual shift of the transistor's threshold voltage towards more positive values as the pH increases. (**b**) V_{TH} VS pH calibration curve. The device shows a sigmoidal behavior and has its linear region between pH 6 and pH 8. (**c**) Sensing layer characterization. Raman spectra of pristine Parylene C (black) and of the same Parylene C membrane after oxygen plasma exposure (red). The additional band at 1640 cm^{-1} is related to the vibration of the C=O stretching of the carboxyl group, while the vibration at 2900 cm^{-1} (**d**), which is related to the CH$_2$ stretching, decreased after the oxidation process with the related increase of the band at 1640 cm^{-1} (Spanu et al. 2017). Copyright 2017, Elsevier. (**e**) Example of a possible final design of a multisensing MOA for cellular applications containing pH-sensitive devices for metabolic activity monitoring (red) and channels for the detection of neuronal electrical activity (green)

To the aim of developing a highly efficient and possibly disposable tool for high-throughput in vitro toxicity assays and pharmacology (and thanks to its remarkable versatility), the OCMFET has been turned into an ultrasensitive pH sensor by using a simple sensing area functionalization, being the key element of the proposed approach a simple pH-sensitive membrane, consisting in a Parylene C thin layer exposed to oxygen plasma. As shown in Fig. 4a, b, such an OCMFET turned out to be a very sensitive pH sensor, thanks to the intrinsic charge amplification

given by the peculiar double-gated structure of the device (Spanu et al. 2017). As demonstrated by the Raman spectra shown in Fig. 4c, d, the plasma-activated Parylene C membrane undergoes a surface modification consisting in the exposure of superficial groups (mainly carboxyl groups), which can be protonated or deprotonated depending on the pH. The transduction principle, as previously explained, is related to a variation of the transistor threshold voltage induced by the (pH-dependent) charge immobilized onto the sensing area.

As proposed in Fig. 4e, these super-Nernstian and referenceless pH sensors can be easily integrated in a MOA device together with the OCMFETs for cell electrical activity monitoring, thus opening up the interesting possibilities for the fabrication of innovative low-cost and referenceless multisensing devices that could be able to monitor not only the electrical activity but also the metabolism of cell aggregates in vitro.

4 Conclusions and Future Prospects

The concept of OCMFET unfolded a whole set of new possible solutions in the sensing and biosensing fields, as it offers the unprecedented possibility to obtain a wide range of low-cost, referenceless, and ultrasensitive devices using the same technological approach. The potentials in network electrophysiology and (neuro)pharmacology of such a versatile device have been preliminarily explored, and the proposed approach turned out to be suitable for both the detection of the electrical activity of living cells and the monitoring of small pH variations, the latter application being possible thanks to the super-Nernstian sensitivity of the sensor given by the peculiar double-gated structure of the device itself. Further exciting developments are foreseen by the combination of different sensing capability into the same platform, thus paving the way to the development of low-cost and easy-to-fabricate multisensing tools for cellular applications. However, the possibility of implementing disposable smart-petri dishes with a specific substrate functionalization and containing a multiparametric sensor array based on OCMFET is only one of the possible applications of this system. In fact, precoated and sterile MOA petri dishes can be foreseen as standard tools for neurophysiological studies as well as neuropharmacological and neurotoxicity assays. Moreover, the use of such devices in combination with stem-cell technology for developing new brain-on-a-chip methods for applications in precision medicine (i.e., patient specific studies-therapies) is an additional future application of this organic transistor-based technology.

On a more long-term perspective, thanks to the conformability flexibilities of the substrates on which these devices can be fabricated, possible applications can be foreseen in the field of in vivo brain interfaces and neuroprosthetics. In fact, as recently demonstrated (Viola et al. 2018) OCMFET devices can be easily fabricated onto sub-micrometer substrates, this feature not only allowing the device to conformably cover basically any surface but also conferring on it an incredible
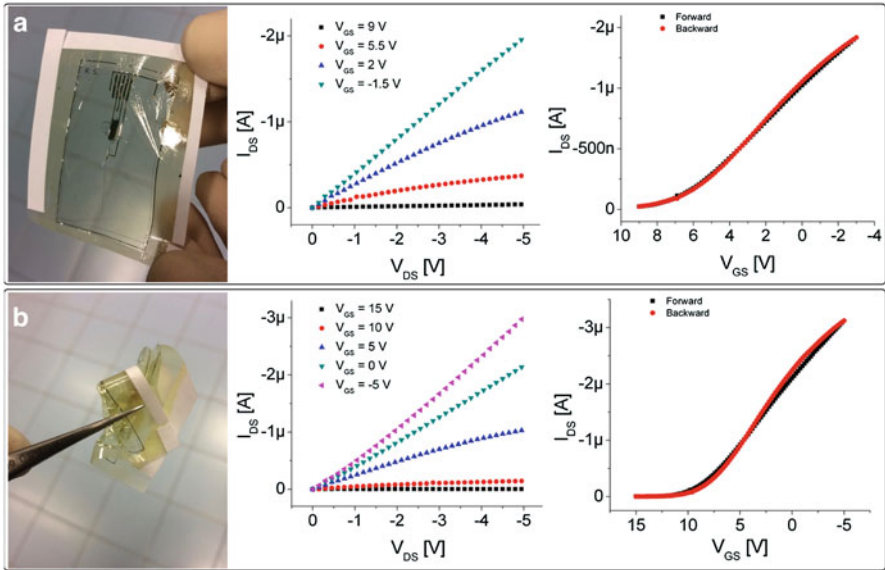
Fig. 5 Characterization of an ultraflexible OCMFET before (**a**) and after (**b**) the exertion of a mechanical stress. The device, thanks to the submicrometer substrate, showed an excellent retention of its electrical characteristics

resistance to mechanical stress (as presented in Fig. 5). In conclusion, although other organic transistor-based devices have been already used for in vivo measurements (Khodagholy et al. 2013, 2015), the OCMFET, thanks to its unique structure and its referenceless nature, represents a very promising and interesting alternative for both acute and chronic clinical neural applications.

References

Barbaro, M., Bonfiglio, A., & Raffo, L. (2006). A charge-modulated FET for detection of biomolecular processes: Conception, modeling, and simulation. *IEEE Transactions on Electron Devices, 53*, 158–166.

Baumann, W. H., Lehmann, M., Schwinde, A., Ehret, R., Brischwein, M., & Wolf, B. (1999). Microelectronic sensor system for microphysiological application on living cells. *Sensors and Actuators B: Chemical, 55*, 77–89.

Berdondini, L., Imfeld, K., Maccione, A., Tedesco, M., Neukom, S., Koudelka-Hep, M., et al. (2009). Active pixel sensor array for high spatio-temporal resolution electrophysiological recordings from single cell to large scale neuronal networks. *Lab on a Chip, 9*, 2644–2651.

Berdondini, L., van der Wal, P. D., Guenat, O., de Rooij, N. F., Koudelka-Hep, M., Seitz, P., et al. (2005). High-density electrode array for imaging in vitro electrophysiological activity. *Biosensors and Bioelectronics, 21*(1), 167–174.

Bergveld, P. (1970). Development of an ion-sensitive solid-state device for neurophysiological measurements. *IEEE Transactions on Biomedical Engineering, 17*(1), 70.

Bergveld, P. (1972). Development, operation, and application of the tool for electrophysiology. *IEEE Transactions on Biomedical Engineering, 19*(5), 342–351.

Bergveld, P., Wiersma, J., & Meertens, H. (1976). Extracellular potential recordings by means of a field effect transistor without gate metal, called OSFET. *IEEE Transactions on Biomedical Engineering, 2*, 136–144.

Blau, A., Murr, A., Wol, S., Sernagor, E., Medini, P., Iurilli, G., et al. (2011). Flexible, all-polymer microelectrode arrays for the capture of cardiac and neuronal signals. *Biomaterials, 32*(7), 1778–1786.

Caboni, A., Orgiu, E., Barbaro, M., & Bonfiglio, A. (2009). Flexible organic thin-film transistors for pH monitoring. *IEEE Sensors Journal, 9*(12), 1963–1970.

Casalini, S., Leonardi, F., Cramer, T., & Biscarini, F. (2013). Organic field-effect transistor for label-free dopamine sensing. *Organic Electronics, 14*(1), 156–163.

Cosseddu, P., Lai, S., Barbaro, M., & Bonfiglio, A. (2012). Ultra-low voltage, organic thin film transistors fabricated on plastic substrates by a highly reproducible process. *Applied Physics Letters, 100*, 093305.

Ecken, H., Ingebrandt, S., Krause, M., Richter, D., Hara, M., & Offenhäusser, A. (2003). 64-Channel extended gate electrode arrays for extracellular signal recording. *Electrochimica Acta, 48*(20–22), 3355–3362.

Fromherz, P., Offenhausser, A., Vetter, T., & Weis, J. (1991). A neuron-silicon junction: A Retzius cell of the leech on an insulated-gate field-effect transistor. *Science, 252*(5010), 1290–1293.

Gross, G. W., Rieske, E., Kreutzberg, G. W., & Meyer, A. (1977). A new fixed-array multi-microelectrode system designed for long-term monitoring of extracellular single unit neuronal activity in vitro. *Neuroscience Letters, 6*(2–3), 101–105.

Hafner, F. (2000). Cytosensor® microphysiometer: Technology and recent applications. *Biosensors and Bioelectronics, 15*, 149–158.

Hubel, D. H. (1957). Tungsten microelectrode for recording from single units. *Science, 125*(3247), 549–550.

Hynes, J., O'Riordan, T. C., Zhdanov, A. V., Uray, G., Will, Y., & Papkovsky, D. B. (2009). In vitro analysis of cell metabolism using a long-decay pH-sensitive lanthanide probe and extracellular acidification assay. *Analytical Biochemistry, 390*, 21–28.

Kergoat, L., Piro, B., Berggren, M., Pham, M.-C., Yassar, A., & Horowitz, G. (2012). DNA detection with a water-gated organic field-effect transistor. *Organic Electronics, 13*(1), 1–6.

Khodagholy, D., Doublet, T., Quilichini, P., Gurfinkel, M., Leleux, P., Ghestem, A., et al. (2013). In vivo recordings of brain activity using organic transistors. *Nature Communications, 4*, 1575.

Khodagholy, D., Gelinas, J. N., Thesen, T., Doyle, W., Devinsky, O., Malliaras, G. G., et al. (2015). NeuroGrid: Recording action potentials from the surface of the brain. *Nature Neuroscience, 18*(2), 310.

Krause, M. (2000). Extended gate electrode arrays for extracellular signal recordings. *Sensors and Actuators B: Chemical, 70*(1–3), 101–107.

Lai, S., Cosseddu, P., Gazzadi, G. C., Barbaro, M., & Bonfiglio, A. (2013b). Towards high frequency performances of ultra-low voltage OTFTs: Combining self-alignment and hybrid, nanosized dielectrics. *Organic Electronics, 14*, 754–761.

Lai, S., Demelas, M., Casula, G., Cosseddu, P., Barbaro, M., & Bonfiglio, A. (2013a). Ultralow voltage, OTFT-based sensor for label-free DNA detection. *Advanced Materials, 25*, 103–107.

Lopez, C. M., Chun, H. S., Berti, L., Wang, S., Putzeys, J., Van Den Bulcke, C., et al. (2018). A 16384-electrode 1024-channel multimodal CMOS MEA for high-throughput intracellular action potential measurements and impedance spectroscopy in drug-screening applications. In *Solid-State Circuits Conference-(ISSCC), 2018 IEEE International*. San Francisco: IEEE.

Martinoia, S., Rosso, N., Grattarola, M., Lorenzelli, L., Margesin, B., & Zen, M. (2001). Development of ISFET array-based microsystems for bioelectrochemical measurements of cell populations. *Biosensors and Bioelectronics, 16*, 1043–1050.

Meyburg, S., Goryll, M., Moers, J., Ingebrandt, S., Böcker-Meffert, S., Lüth, H., et al. (2006). N-channel field-effect transistors with floating gates for extracellular recordings. *Biosensors and Bioelectronics, 21*(7), 1037–1044.

Robinson, D. A. (1968). The electrical properties of metal microelectrodes. *Proceedings of the IEEE, 56*(6), 1065–1071.

Rousche, P. J., Pellinen, D. S., Pivin, D. P., Williams, J. C., Vetter, R. J., & Kipke, D. R. (2001). Flexible polyimide-based intracortical electrode arrays with bioactive capability. *IEEE Transactions on Biomedical Engineering, 48*(3), 361–371.

Schmoltner, K., Kofler, J., Klug, A., & List-Kratochvil, E. J. W. (2013). Electrolyte-gated organic field-effect transistor for selective reversible ion detection. *Advanced Materials, 25*(47), 6895–6899.

Sessolo, M., Khodagholy, D., Rivnay, J., Maddalena, F., Gleyzes, M., Steidl, E., et al. (2013). Easy-to-fabricate conducting polymer microelectrode arrays. *Advanced Materials, 25*(15), 2135–2139.

Spanu, A. (2016). *Organic transistor devices for in vitro electrophysiological applications*. Bosel: Springer.

Spanu, A., Lai, S., Cosseddu, P., Tedesco, M., Martinoia, S., & Bonfiglio, A. (2015). An organic transistor-based system for reference-less electrophysiological monitoring of excitable cells. *Scientific Reports, 5*, 8807.

Spanu, A., Pinna, L., Viola, F., Seminara, L., Valle, M., Bonfiglio, A., et al. (2016). A high-sensitivity tactile sensor based on piezoelectric polymer PVDF coupled to an ultra-low voltage organic transistor. *Organic Electronics, 36*, 57–60.

Spanu, A., Viola, F., Lai, S., Cosseddu, P., Ricci, P. C., & Bonfiglio, A. (2017). A reference-less pH sensor based on an organic field effect transistor with tunable sensitivity. *Organic Electronics, 48*, 188–193.

Stett, A., Müller, B., & Fromherz, P. (1997). Two-way silicon-neuron interface by electrical induction. *Physical Review E, 55*(2), 1779–1782.

Takeuchi, S., Suzuki, T., Mabuchi, K., & Fujita, H. (2004). 3D flexible multichannel neural probe array. *Journal of Micromechanics and Microengineering, 14*(1), 104–107.

Thomas Jr., C. A., Springer, P. A., Loeb, G. E., Berwald-Netter, Y., & Okun, L. M. (1972). A miniature microelectrode array to monitor the bioelectric activity of cultured cells. *Experimental Cell Research, 74*(1), 61–66.

Vassanelli, S., & Fromherz, P. (1997). Neurons from rat brain coupled to transistors. *Applied Physics A: Materials Science and Processing, 65*(2), 85–88.

Verzeano, M., Negishi, K., & Angeles, L. (1960). Neuronal activity in cortical and thalamic networks. A study with multiple microelectrodes. *Journal of General Physiology, 43*, 177–195.

Viola, F. A., Spanu, A., Ricci, P. C., Bonfiglio, A., & Cosseddu, P. (2018). *Scientific Reports, 8*, 8073.

Viswam, V., Jelena Dragas, Amir Shadmani, Yihui Chen, Alexander Stettler, Jan Müller, et al. (2016). 22.8 Multi-functional microelectrode array system featuring 59,760 electrodes, 2048 electrophysiology channels, impedance and neurotransmitter measurement units. In *Solid-State Circuits Conference (ISSCC), 2016 IEEE International*. San Francisco: IEEE.

Weis, R., Müller, B., & Fromherz, P. (1996). Neuron adhesion on a silicon chip probed by an array of field-effect transistors. *Physical Review Letters, 76*(2), 327–330.

Wise, K. D., Angell, J. B., & Starr, A. (1970). An integrated-circuit approach to extracellular microelectrodes. *IEEE Transactions on Biomedical Engineering, 3*, 238–247.

Yu, H., Cai, H., Zhang, W., Xiao, L., Liu, Q., & Wang, P. (2009). A novel design of multifunctional integrated cell-based biosensors for simultaneously detecting cell acidification and extracellular potential. *Biosensors and Bioelectronics, 24*, 1462–1468.

Zhang, Y., Li, J., Li, R., Sbircea, D. T., Giovannitti, A., Xu, J., et al. (2017). Liquid–solid dual-gate organic transistors with tunable threshold voltage for cell sensing. *ACS Applied Materials and Interfaces, 9*(44), 38687–38694.

Part III
Data Analysis Methods

Scaling Spike Detection and Sorting for Next-Generation Electrophysiology

Matthias H. Hennig, Cole Hurwitz, and Martino Sorbaro

Abstract Reliable spike detection and sorting, the process of assigning each detected spike to its originating neuron, are essential steps in the analysis of extracellular electrical recordings from neurons. The volume and complexity of the data from recently developed large-scale, high-density microelectrode arrays and probes, which allow recording from thousands of channels simultaneously, substantially complicate this task conceptually and computationally. This chapter provides a summary and discussion of recently developed methods to tackle these challenges and discusses the important aspect of algorithm validation, and assessment of detection and sorting quality.

Keywords Extracellular recording · Spike sorting · Multielectrode array · Large-scale recording · Clustering

1 Introduction

Extracellular electrical recording of neural activity is an essential tool in neuroscience. If an electrode is placed sufficiently close to a spiking neuron, the extracellular potential recorded often contains a clear, readily detectable signature of the action potential. As extracellular electrodes do not interfere with neural function, such recordings provide an unbiased and precise record of the functioning of intact neural circuits.

M. H. Hennig (✉) · C. Hurwitz
Institute for Adaptive and Neural Computation, School of Informatics, University of Edinburgh, Edinburgh, UK
e-mail: m.hennig@ed.ac.uk; cole.hurwitz@ed.ac.uk

M. Sorbaro
Institute for Adaptive and Neural Computation, School of Informatics, University of Edinburgh, Edinburgh, UK

Computational Science and Technology, KTH Royal Institute of Technology, Stockholm, Sweden
e-mail: martino.sorbaro@ed.ac.uk

Recent progress in CMOS technology (complementary metal-oxide semiconductor technology for low-power integrated circuits) has provided systems that allow recording from thousands of closely spaced channels simultaneously with ever-increasing density and sampling rates. With this technology, it becomes possible to reliably monitor several thousand neurons simultaneously both in vitro and in vivo (Eversmann et al. 2003; Berdondini et al. 2005; Frey et al. 2010; Ballini et al. 2014; Müller et al. 2015; Yuan et al. 2016; Lopez et al. 2016; Jun et al. 2017b; Dimitriadis et al. 2018). This is a significant advancement as it enables, for the first time, the systematic investigation of interactions between neurons in large circuits. Understanding these interactions will contribute to learning more about how neural circuitry is altered by cellular changes in diseases, injury and during pharmacological interventions.

To appreciate the advantages of recording the activity of many neurons, it is important to emphasise that neural circuits are usually highly diverse and heterogeneous (Hromádka et al. 2008; Buzsáki and Mizuseki 2014; Panas et al. 2015). Not only do they consist of different neuron types, but even within groups of neurons of the same type, the firing rates may differ by orders of magnitude. This observation has been made consistently in vitro and in vivo, and it stands to reason that this has biological relevance. Conventional technologies, which allow simultaneous recording of a handful (rarely more than a hundred) of neurons, severely under-sample highly heterogeneous populations. If the recorded neurons are not representative of the whole population, both experimental accuracy and reproducibility between experiments will be negatively affected. Moreover, dense recording systems increase the fraction of neurons isolated in a local population, to a level that was, so far, only accessible with calcium imaging.

A further advantage of recording many neurons at once is that it can be an effective way of probing neural excitability and connectivity, using functional interactions as a proxy measure for the effects of synaptic interactions. In vitro assays are particularly suited for investigation of functional interactions, as they can be augmented with stimulation, fluorescent labelling and targeted optogenetic stimulation (Zhang et al. 2009; Obien et al. 2015). A combination of dense multielectrode arrays and imaging technologies could allow phenotyping at the level of single cells, potentially in combination with further modalities such as gene expression profiling. The high yield of such approaches thus provides entirely new possibilities for systematic assessment of the roles of different genotypes and of drug effects.

The analysis of single-neuron activity requires the correct assignment of each detected spike to the originating neuron, a process called *spike sorting*. In this chapter, we will provide an overview of the most frequently employed methods for the spike sorting for large-scale, dense multielectrode arrays. While many of the issues discussed will also apply to dense in vivo probes, the focus is on in vitro arrays, because they typically provide a large surface area evenly covered with recording channels, which is advantageous for spike sorting. A major additional challenge in in vivo recordings is tissue movement, which causes the signals of neurons to drift over time. For an excellent review of the challenges encountered in

vivo, and of methodology for conventional recording devices with fewer channels, the reader may consult Rey et al. (2015).

In the first section, we will discuss in more detail the technical and practical issues that are introduced when moving from conventional devices with tens of channels to larger, more dense systems. Next, we will introduce the main components of modern spike sorting pipelines, and then discuss each component and existing algorithms in detail. Finally, we will provide an overview of approaches for validation of the quality of these algorithms.

2 Challenges for Large-Scale Spike Sorting

On both conventional and high-density recording devices, electrodes will usually pick up the activity of multiple neurons. While it is possible to directly analyse the multi-unit activity (MUA) from each channel, spike sorting is required to resolve single-unit activity (SUA). Spike sorting resembles the classic "cocktail party" problem: to isolate the voice of a single speaker in a crowd of people. Since the recorded spike waveforms differ in shape and amplitude among neurons, the resulting signal can be de-mixed using either dimensionality reduction paired with clustering or spike templates along with template matching. These approaches have been successfully employed on conventional devices with few, spatially well-separated channels. On large-scale, dense arrays, however, these traditional methods become more difficult both computationally and algorithmically. Instead of finding a single voice in a crowd, the challenge is to isolate the voices of thousands of speakers in a room equipped with thousands of microphones. Overcoming this challenge is imperative as wrong assignments can severely bias subsequent analysis of neuronal populations (Ventura and Gerkin 2012).

Spike sorting is a tractable problem for conventional extracellular recordings as it is commonly done for each recording channel separately. In this case, only a small number of neurons are expected to contribute to the signal on each channel, which allows the use of precise, but computationally more costly algorithms. Also, most existing algorithms for spike sorting still include an element of manual intervention to adjust or improve sorting results. These traditional algorithms struggle when faced with large-scale, dense arrays.

On dense arrays, a single action potential from a neuron is visible on multiple, nearby channels. As a result, spike sorting on single channels is no longer appropriate. Removing duplicate events is feasible in principle, but becomes challenging when nearby neurons are firing with high synchrony. Poor treatment of duplicate removal can lead to false exclusions of action potentials or retention of multiple spikes from the same action potential.

Conventional spike sorting algorithms also struggle with the sheer volume of data that large-scale arrays produce. For instance, a recording from 4096 channels with 18-kHz sampling rate yields about 140 MB per second, or over 8 GB per minute. Simply reading this data volume from hard disk into memory for analysis

can be a severe bottleneck in any spike sorting pipeline. In addition, the massive data volume prevents extensive manual curation of spike sorting results. Highly automated pipelines with minimal need for intervention are needed to overcome these challenges and to fully exploit the capabilities of dense arrays.

3 From Raw Data to Single-Neuron Activity

A typical spike sorting pipeline begins with the detection of candidate events followed by some method of assigning these events to specific neurons (Lewicki 1998; Rey et al. 2015). On large-scale arrays, two approaches have emerged as particularly suitable. One method is based on creating spike templates and then performing template matching. The other method relies on feature extraction and clustering, using both the spike shape and estimated location of the event. A summary of the steps required to obtain sorted spikes from raw data is shown in Fig. 1. Each of these steps is discussed in more detail below.

3.1 Spike Detection

Spikes in the raw signal take the form of biphasic deflections from a baseline level. They can be found through detection of threshold crossings and by using additional shape parameters such as the presence of a biphasic shape as acceptance criteria. As the noise levels may vary among channels and over time, the threshold is usually defined relative to the noise level, which is estimated from portions of the raw signal that do not contain spikes. It is worth noting that signal fluctuations in extracellular data are typically highly non-Gaussian. As a result, a noise estimate based on percentiles is more accurate and also easier to obtain, as opposed to computing the signal variance (Fee et al. 1996; Muthmann et al. 2015).

The choice of the detection threshold determines which events are retained for further analysis. Spikes from well-detected neurons are easily identifiable, but deflections with amplitudes closer to the background noise level are harder to isolate. Since there is typically no clear-cut separation between spikes and noise, events detected close to the threshold may originate from neurons for which only an incomplete activity record can be obtained. The magnitude of electrical noise, which can be estimated when recording from an empty array, is usually much smaller than the magnitude of the fluctuations recorded in the absence of clearly visible spiking activity (Muthmann et al. 2015). This indicates that a large component of the recorded signal fluctuations are due to neural activity, such as neurons located further away from the electrode, or smaller events such as currents during synaptic transmission. The analysis of recordings from the retina shows that even very small detected signals may reflect activity that is typical of stimulus-evoked responses
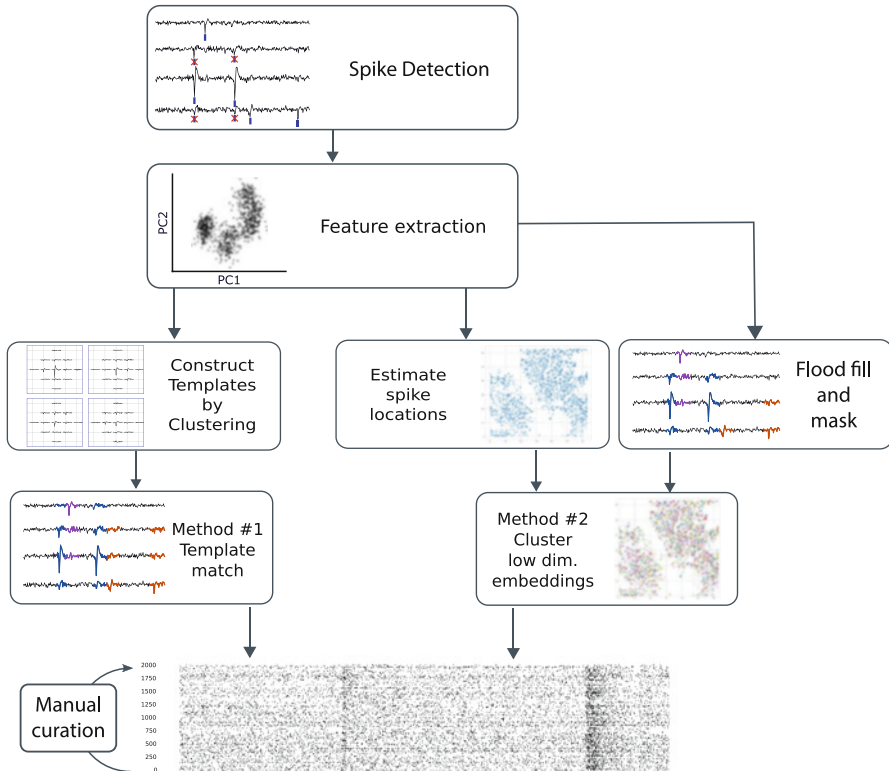
Fig. 1 Schematic overview of existing spike sorting pipelines for high-density microelectrode arrays. Following detection, either neuron templates are formed based on the spatio-temporal event footprints and then used to detect these units in a second pass, or current sources are estimated and clustered together with waveform features, or a mask is created to restrict clustering to channels with a detectable signal. The output consists of a list of spike time stamps for each identified neuron, which often has to be corrected in a final manual curation step

from retinal ganglion cells, hence carries signatures of neural activity rather than noise (Fig. 2).

As a result, the detection step significantly affects the subsequent isolation of single-neuron activity. Choosing a high detection threshold is not an ideal solution as this will potentially leave valid spikes undetected. In contrast, a low threshold guarantees reliable detection of neurons with stronger signals, but also increases the fraction of false positives. As a good compromise, a strategy can be adopted to detect events with a low threshold, and to subsequently discard unreliable units. This can either be done after detection, for instance by using a classifier trained on true spikes and noise events obtained from channels not reporting neural activity (Hilgen et al. 2017), or by removing sorted units with a small number of spikes or poor clustering metric scores after spike sorting (Hill et al. 2011).
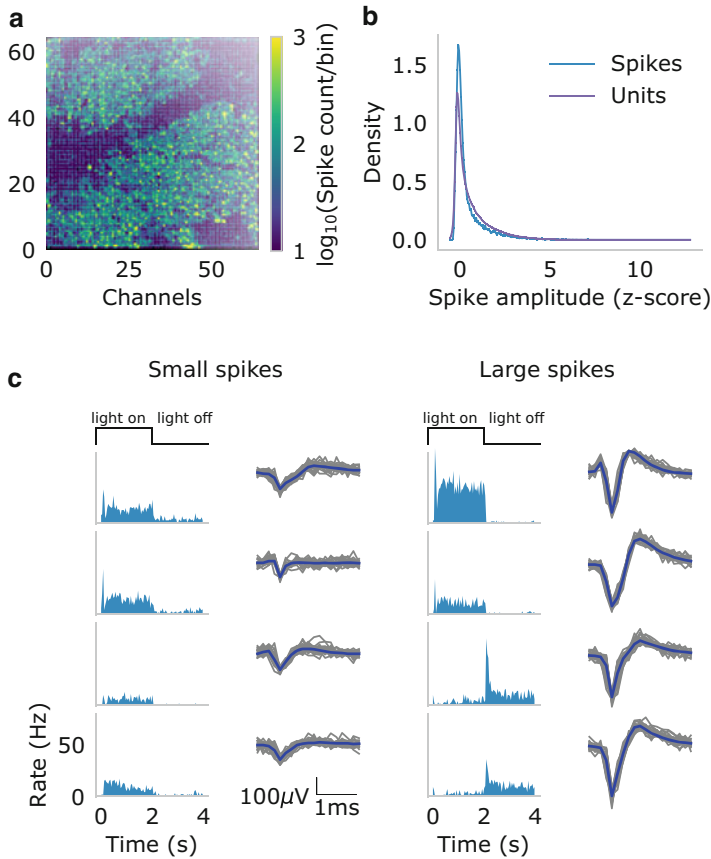
Fig. 2 Even small events detected on a high-density array contain signatures of neural activity. (**a**) Density plot of spatially binned spike counts, estimated from detected and spatially localised spikes using the method described by Hilgen et al. (2017). Spikes were recorded from a light-stimulated mouse retina. Spike detection was performed with a low threshold, and hence false positives were registered in areas where no neural activity was recorded, such as the optic disk on the centre left. (**b**) No clear separation between spikes and noise is seen for recorded amplitudes, or for average amplitudes of units following spike sorting. (**c**) Individual, randomly selected units with small (left) and large amplitudes (right) both show signatures of light stimulation during presentation of full field flashes. For each unit, the light-evoked peri-stimulus time histogram (left), and examples and the average of spike waveforms (right) are shown. The recording was contributed by Gerrit Hilgen and Evelyne Sernagor, University of Newcastle

Recently, a new method for spike detection using a pre-trained neural network was introduced by Lee et al. (2017). This method was shown to outperform conventional threshold-based methods on simulated ground truth data, in particular by achieving a lower false-positive rate. When run on a modern GPU, a neural network-based method is also much faster. This is a very promising avenue, although the considerations regarding detection thresholds outlined above still remain relevant.

3.2 Dealing with Duplicate Spikes

Unlike in conventional recordings, on dense arrays, spikes are detectable on multiple channels. These duplicate spikes pose two significant problems for traditional spike sorting algorithms. First, the amount of computation and memory used for processing each detected event increases with the number of duplicates. Second, the rate of misclassification in spike sorting potentially increases since each duplicate spike must be sorted into the same event.

To avoid the pitfalls associated with duplicate spikes, it is suggested to identify and remove duplicates during detection. One naive method for duplicate removal is to remove all but the largest amplitude spike in a radius that encompasses the spatial footprint of the event. This method will remove almost every duplicate event, but as the radius of duplicate removal increases, so does the number of spikes removed that are not associated with the original event. A more rigorous method for duplicate removal involves keeping the largest amplitude spikes and removing all spikes in a radius that have *decayed in amplitude*. This method allows for the separating of near-synchronous events that are in the same spatial area of the array. Its success, however, relies on the assumption that the timing of spikes from the same event on nearby electrodes is almost identical and only weakly influenced by noise and that the signal spatially decays away from its current source (Hagen et al. 2015).

3.3 Feature Extraction

The relevant signal a spike causes in extracellular recordings lasts around 3 ms, which, depending on the acquisition rate, may correspond to up to 90 data points per event. However, spike shapes are highly redundant and can be efficiently represented in a low-dimensional space. Thus, an appropriate projection method can be used to compute a small number of features for each event, which can be more efficiently clustered than raw waveforms.

The most common feature extraction method for extracellular spikes is principal component analysis (PCA), performed on whitened and peak-aligned spike waveforms. PCA finds principal components, or orthogonal basis vectors, whose directions maximise the variance in the data. Extracellular spikes can be summarised well by just 3–4 principal components, a manageable dimensionality for most clustering algorithms (Adamos et al. 2008). Other less frequently used methods include independent component analysis (ICA) (Hermle et al. 2004) and wavelet decomposition (Quiroga et al. 2004). A comparison of these methods showed that the performance of sorting algorithms depends not only on the feature extraction method employed but also on the clustering algorithm (Quiroga et al. 2004). In practice, the comparably low computational cost and relative effectiveness of PCA in discriminating between different neurons and neuron types makes it particularly suitable for large-scale recordings (Adamos et al. 2008). To reduce memory load, the

PCA decomposition can be evaluated for a subset of events from a large recording and all events can be projected along the chosen dimensions efficiently in batches (Hilgen et al. 2017).

3.4 Clustering Spatio-Temporal Event Footprints

There are five fundamental problems with the clustering phase. The first problem is that the extracellular waveform of neurons are known to change amplitude and shape during bursting (Fee et al. 1996). The second problem is that some recorded waveforms are distorted by overlapping action potentials from synchronous, spatially local events. This occurs frequently in dense arrays and usually exist as outliers in the chosen feature space. The third problem is that electrodes can drift in the extracellular medium, changing the relative position of each neuron to the electrodes. Drift distorts waveform shapes over the duration of the recording. The fourth problem is that the duplication of spikes over neighbouring channels can lead to refractory period violations or misclassifications. The fifth and final problem is that the number of observed neurons is unknown, which requires the use of nonparametric clustering algorithms or requires the user to estimate the number of neurons for a parametric clustering algorithm.

The choice of the clustering algorithm will be determined by the speed and scalability considerations, by hypotheses over the typical shape of a cluster in this space, and by how well the algorithm can deal with the previously listed problems. Many spike sorting methods cluster by fitting Gaussian Mixture Models (GMMs), modelling the feature density profiles as a sum of Gaussians (Harris et al. 2000; Rossant et al. 2016), or by fitting a mixture of t-distributions (Shoham et al. 2003). The unknown number of actual neurons can be introduced as a latent variable, and the inference problem be solved with the expectation–maximisation (EM) algorithm. Bayesian approaches, which also quantify parameter uncertainty, have also been introduced (Wood and Black 2008). These approaches, however, only perform well for single channels and are conceptually and computationally hard to scale up to large, full-chip datasets.

More recent clustering algorithms for spike sorting are density-based. Densitybased algorithms generally detect peaks or high-density regions in the feature space that are separated by low-density regions. These algorithms are non-parametric, allowing the classification pipeline to be fully automatic; however, the number of clusters found can depend heavily on both hyper-parameters and the chosen feature space. Density-based clustering algorithms have been implemented for spike sorting with promising results (Hilgen et al. 2017; Chung et al. 2017).

For dense arrays, an added complication arises since the information contained in event footprints cannot be used directly for sorting spikes, since it is unknown which channels contain responses of a single neuron and how many neurons cause the observed responses. The resulting combinatorial explosion can be dealt with in three ways that are detailed as follows.

3.4.1 Masked Clustering

A straight-forward way to reduce the dimensionality of the clustering problem is to include only channels with detectable responses for each event. Classical expectation maximisation on a mixture model is then possible when the irrelevant parts of the data are masked out and replaced with a tractable noise model (Kadir et al. 2014). This strategy produces excellent results with the help of a semi-automated refinement step (Rossant et al. 2016). A main limitation is, however, a super-linear scaling with the number of recordings channels, which makes it less suitable for the latest generations of large-scale arrays.

3.4.2 Template Matching

Since the raw recorded signal can be linearly decomposed into a mixture of footprints from different neurons (Segev et al. 2004), template matching has been a successful strategy for spike sorting, and implementations are available that scale up to thousands of channels (Pachitariu et al. 2016; Lee et al. 2017; Yger et al. 2018). This approach has two steps. First, a collection of spatio-temporal footprints is obtained in a single pass over the data, and dimensionality reduction and clustering is used to build templates for single neurons. In a second pass, all events are assigned to the most likely template or combination of templates in the case of temporally overlapping events.

A major advantage of template matching is that temporally overlapping spikes are naturally accounted for through addition of two relevant templates. This makes it very suitable for recordings with high firing rates and correlations between nearby neurons. A potential limitation is that neurons spiking at very low rates may remain undiscovered as no reliable template can be built through averaging. Moreover, current implementations require a final manual curation step. This is, however, simplified by correcting the assignment based on templates, which can be merged or split, rather than based on single events.

3.4.3 Spike Localisation

As explained above, the spatial spike footprint allows event localisation through an estimation of the barycentre from the peak event amplitudes in nearby channels. This produces density maps with clear, isolated peaks in event density, which represent spikes from single or multiple, nearby neurons (see Fig. 2 for an example). A two-dimensional density map can be clustered very efficiently, and the combination of locations and waveform features obtained through dimensionality reduction allows successful separation of nearby neurons. Density-based clustering algorithms have been successfully employed to solve this task: DPCLUS, based on the identification of density peaks (Jun et al. 2017a), ISO-SPLIT to grow uni-modal

clusters from small seeds (Chung et al. 2017) and Mean Shift, which herds data points towards high-density areas (Hilgen et al. 2017).

Of all methods discussed here, spike localisation and clustering potentially has the best computational performance, since the actual computation is performed on a data set with much lower dimensionality than the original data (Hilgen et al. 2017; Jun et al. 2017a). Because the number of dimensions in the clustering step has to be kept small, it also discards useful information. However, usually locations and spatio-temporal waveform features exhibit substantial redundancy (Hilgen et al. 2017), making this approach the most suitable for very large arrays.

4   Evaluation

The evaluation of spike detection and sorting quality is complicated by data volume and complexity, which makes both manual and automated curation challenging. It is however possible to assess the quality of an algorithm using data with ground truth annotation. Moreover, methods for post-hoc quality assessment of desirable properties of single units can be used to accept or reject units found through spike sorting.

Specifically, the desired result of a spike sorting pipeline to minimise the false detection of noise as spikes (false positives in detection), and the number of real spikes left undetected (false negatives in detection). Moreover, it should not assign spikes to the wrong neuron, hence it should minimise false positives and negatives in a cluster assignment.

When ground truth annotations are available, false positives and false negatives can be easily counted. A direct, but technically challenging method to obtain ground truth information, is the simultaneous recording of a single neuron, together with an array recording, which will then be analysed using the spike sorting algorithm in question. Three such data sets recorded with dense arrays are currently available, two from the rat cortex recorded in vivo (Neto et al. 2016; Marques-Smith et al. 2018), and one from the mouse retina recorded in vitro (Yger et al. 2018). In both cases, a single juxtacellular electrode placed very closely to the array reliably recorded all spikes from a single neuron. A systematic analysis of spike sorting has shown a clear relationship between measured spike amplitude and classification accuracy with errors strongly increasing for events smaller than 50 mV (Yger et al. 2018). This important result can help motivate exclusion of units with weaker signals.

Ground truth for spike sorting can also be produced by simulations. Recently, it has become possible to simulate a complete biophysical forward model for recorded extracellular potentials in neural tissue (Hagen et al. 2015). This has produced several data sets that are now used to benchmark spike sorting algorithms (see e.g. Lee et al. 2017). In another study, ground truth data was generated by superimposing synthetic spikes onto a recording from an empty array. This data was used to evaluate the effect of noise on event localisation accuracy and to

discover that localisation is inevitably a trade-off between position uncertainty and bias (Muthmann et al. 2015). It is an open question, however, how well results collected from simulated data generalise, since the precise noise model, which may differ between recording systems, impacts spike sorting algorithm performance (Muthmann et al. 2015).

Finally, for cases where no ground truth data is available, Hill et al. (2011) proposed a set of metrics that should accompany all spike sorting methods as an evaluation of their reliability. Their metrics, applied a posteriori, are based on different features of the sorted dataset, which can be summarised as follows:

- The **waveforms** in each cluster. The average waveform can present non-biological features, hinting that the cluster may be a collection of wrongly detected events. Additionally, if properties of the typical waveform change over time, this may be a sign of neurons drifting away from their initial position on the chip. Finally, anomalous variability of each feature above the noise level may be a sign that multiple neurons contributed to the same cluster.
- The **times** of all spikes in a cluster. Violations of the refractory period show that the cluster contains false positives: these can be studied via the autocorrelation function or inter-spike histogram of each cluster.
- The **amplitudes** of action potentials. A sharp drop in the amplitude distribution, caused by the detection threshold, signifies that the latter has introduced an artificial bias.
- The **separation** between pairs of clusters. Ample, sharp interfaces between clusters mean the properties of each neuron's spikes overlap in the selected feature space. If this occurs, there will be a theoretical minimum of false positives and negatives due to the incorrect assignment of events to the wrong cluster.

The last point can be evaluated by re-examining a group of clustered neurons with a mixture model (usually Gaussian), which can be fit using more features than the original algorithm. Assuming that this fit is at least as reliable as the original sorting, a comparison of the two assignments is informative regarding the reliability of each unit. A statistic summarising all these tests can then be used to exclude events and units post hoc. Using this method, detection and clustering parameters do not have to be adjusted carefully prior to each analysis.

5 Outlook

In this chapter, we discussed the existing methodology for recovering single-neuron activity from high-density recordings and the challenges and problems that each approach faces. Six freely available spike sorting pipelines for large-scale extracellular arrays and the methods they use are summarised in Table 1. For more information on their unique advantages and disadvantages, please review their associated references.

Table 1 Summary of the most recent spike sorting methods developed for large, dense arrays

Name and reference	Method	Notes
Kilosort (Pachitariu et al. 2016): https://github.com/cortex-lab/KiloSort	TM	GPU support; MATLAB-based; semi-automated final curation
YASS (Lee et al. 2017): https://yass.readthedocs.io	TM	Neural network-based detection (GPU); outlier triaging; template matching; clustering
Herding Spikes (Hilgen et al. 2017): https://github.com/mhhennig/HS2	SL+D	Fast and scalable; tested on multiple array geometries
MountainSort (Chung et al. 2017): https://github.com/flatironinstitute/mountainsort	D	Fully automatic; scalable; graphical user interface; unique clustering method
JRCLUST (Jun et al. 2017a): www.jrclust.org	SL+D	Probe drift correction; GPU support
SpyKING CIRCUS (Yger et al. 2018): https://spyking-circus.rtfd.org	TM	GPU support; tested on many datasets; robust to overlapping spikes; graphical user interface

For a summary of older algorithms—mostly for smaller, sparser arrays—see Bestel et al. (2012)
TM Template Matching, *SL* Spike Localisation, *D* Density-based clustering (see Sect. 3.4)

Since inaccurate detection and sorting can influence subsequent analysis of neural populations (Ventura and Gerkin 2012), manual curation steps are often still required to guarantee good data quality. However, the recent methods we summarised in this chapter take significant steps in increasing the speed, automatisation and accuracy of the spike sorting pipeline. Looking forward, it may be possible to apply novel machine learning techniques to improving spike sorting. This has already been put into practice with a recent spike sorting algorithm where a neural network is used to improve detection of neural events (Lee et al. 2017). Although neural networks are showing promising results in detection, it may be possible to find new breakthroughs in both feature extraction and in classification using these methods. Moreover, a neural network approach may have the potential of encompassing all of the spike sorting steps within a single model. A challenge when using these machine learning algorithms, however, is the difficulty of obtaining ground truth data, which is poorly available and usually under specific experimental conditions that may not generalise to other data sets.

Increased automation also means that more work is needed in developing reliable methods for validation and quality control of spike sorting results. The introduction of synthetic (Hagen et al. 2015) and experimental ground truth datasets (Neto et al. 2016; Yger et al. 2018) is an important step forward in this direction. A standardisation, both of the sorting pipeline and of its evaluation, should be considered among the next objectives of the spike sorting community. A joint effort should be made in order to guarantee that methods are intuitive to use and results are easy to compare.

References

Adamos, D. A., Kosmidis, E. K., & Theophilidis, G. (2008). Performance evaluation of PCA-based spike sorting algorithms. *Computer Methods and Programs in Biomedicine, 91*(3), 232–244.

Ballini, M., Muller, J., Livi, P., Chen, Y., Frey, U., Stettler, A., et al. (2014). A 1024-channel CMOS microelectrode array with 26,400 electrodes for recording and stimulation of electrogenic cells in vitro. *IEEE Journal of Solid-State Circuits, 49*(11), 2705–2719.

Berdondini, L., van der Wal, P. D., Guenat, O., de Rooij, N. F., Koudelka-Hep, M., Seitz, P., et al. (2005). High-density electrode array for imaging in vitro electrophysiological activity. *Biosensors and Bioelectronics, 21*(1), 167–74.

Bestel, R., Daus, A. W., & Thielemann, C. (2012). A novel automated spike sorting algorithm with adaptable feature extraction. *Journal of Neuroscience Methods, 211*(1), 168–178.

Buzsáki, G., & Mizuseki, K. (2014). The log-dynamic brain: How skewed distributions affect network operations. *Nature Reviews Neuroscience, 15*(4), 264.

Chung, J. E., Magland, J. F., Barnett, A. H., Tolosa, V. M., Tooker, A. C., Lee, K. Y., et al. (2017). A fully automated approach to spike sorting. *Neuron, 95*(6), 1381–1394.

Dimitriadis, G., Neto, J. P., Aarts, A., Alexandru, A., Ballini, M., Battaglia, F., et al. (2018). Why not record from every channel with a CMOS scanning probe? *bioRxiv*, 275818. https://doi.org/10.1101/275818

Eversmann, B., Jenkner, M., Hofmann, F., Paulus, C., Brederlow, R., Holzapfl, B., et al. (2003). A 128×128 CMOS biosensor array for extracellular recording of neural activity. *IEEE Journal of Solid-State Circuits, 38*(12), 2306–2317.

Fee, M. S., Mitra, P. P., & Kleinfeld, D. (1996). Variability of extracellular spike waveforms of cortical neurons. *Journal of Neurophysiology, 76*(6), 3823–3833.

Frey, U., Sedivy, J., Heer, F., Pedron, R., Ballini, M., Mueller, J., et al. (2010). Switch-matrix-based high-density microelectrode array in CMOS technology. *IEEE Journal of Solid-State Circuits, 45*(2), 467–482.

Hagen, E., Ness, T. V., Khosrowshahi, A., Sørensen, C., Fyhn, M., Hafting, T., et al. (2015). ViSAPy: A Python tool for biophysics-based generation of virtual spiking activity for evaluation of spike-sorting algorithms. *Journal of Neuroscience Methods, 245*, 182–204.

Harris, K. D., Henze, D. A., Csicsvari, J., Hirase, H., & Buzsáki, G. (2000). Accuracy of tetrode spike separation as determined by simultaneous intracellular and extracellular measurements. *Journal of Neurophysiololgy, 84*(1), 401–414.

Hermle, T., Schwarz, C., & Bogdan, M. (2004). Employing ICA and SOM for spike sorting of multielectrode recordings from CNS. *Journal of Physiology-Paris, 98*(4–6), 349–356.

Hilgen, G., Sorbaro, M., Pirmoradian, S., Muthmann, J.-O., Kepiro, I. E., Ullo, S., et al. (2017). Unsupervised spike sorting for large-scale, high-density multielectrode arrays. *Cell Reports, 18*(10), 2521–2532.

Hill, D. N., Mehta, S. B., & Kleinfeld, D. (2011). Quality metrics to accompany spike sorting of extracellular signals. *Journal of Neuroscience, 31*(24), 8699–705.

Hromádka, T., Deweese, M. R., & Zador, A. M. (2008). Sparse representation of sounds in the unanesthetized auditory cortex. *PLoS Biology, 6*(1), e16.

Jun, J. J., Mitelut, C., Lai, C., Gratiy, S., Anastassiou, C., & Harris, T. D. (2017a). Real-time spike sorting platform for high-density extracellular probes with ground-truth validation and drift correction. *bioRxiv*, 101030. https://doi.org/10.1101/101030

Jun, J. J., Steinmetz, N. A., Siegle, J. H., Denman, D. J., Bauza, M., Barbarits, B., et al. (2017b). Fully integrated silicon probes for high-density recording of neural activity. *Nature, 551*(7679), 232.

Kadir, S. N., Goodman, D. F., & Harris, K. D. (2014). High-dimensional cluster analysis with the masked EM algorithm. *Neural Computation, 26*(11), 2379–2394.

Lee, J. H., Carlson, D. E., Razaghi, H. S., Yao, W., Goetz, G. A., Hagen, E., et al. (2017). Yass: Yet another spike sorter. In *Advances in neural information processing systems* (pp. 4005–4015).

Lewicki, M. S. (1998, January). A review of methods for spike sorting: The detection and classification of neural action potentials. *Network, 9*, R53–R78.

Lopez, C. M., Mitra, S., Putzeys, J., Raducanu, B., Ballini, M., Andrei, A., et al. (2016). 22.7 a 966-electrode neural probe with 384 configurable channels in 0.13 μm SOI CMOS. In *2016 IEEE International Solid-State Circuits Conference (ISSCC)* (pp. 392–393). San Fransisco, CA: IEEE.

Marques-Smith, A., Neto, J. P., Lopes, G., Nogueira, J., Calcaterra, L., Frazo, J., (2018). Recording from the same neuron with high-density CMOS probes and patch-clamp: A ground-truth dataset and an experiment in collaboration. *bioRxiv*, 370080. https://doi.org/10.1101/370080

Müller, J., Ballini, M., Livi, P., Chen, Y., Radivojevic, M., Shadmani, A., et al. (2015). High-resolution CMOS MEA platform to study neurons at subcellular, cellular, and network levels. *Lab on a Chip, 15*(13), 2767–2780.

Muthmann, J.-O., Amin, H., Sernagor, E., Maccione, A., Panas, D., Berdondini, L., et al. (2015, December). Spike detection for large neural populations using high density multielectrode arrays. *Frontiers in Neuroinformatics, 9*, 1–21.

Neto, J. P., Lopes, G., Frazão, J., Nogueira, J., Lacerda, P., Baião, P., et al. (2016). Validating silicon polytrodes with paired juxtacellular recordings: Method and dataset. *Journal of Neurophysiology, 116*(2), 892–903.

Obien, M. E. J., Deligkaris, K., Bullmann, T., Bakkum, D. J., & Frey, U. (2015, January). Revealing neuronal function through microelectrode array recordings. *Frontiers in Neuroscience, 9*, 423.

Pachitariu, M., Steinmetz, N. A., Kadir, S. N., Carandini, M., & Harris, K. D. (2016). Fast and accurate spike sorting of high-channel count probes with KiloSort. In *Advances in neural information processing systems* (pp. 4448–4456).

Panas, D., Amin, H., Maccione, A., Muthmann, O., van Rossum, M., Berdondini, L., et al. (2015). Sloppiness in spontaneously active neuronal networks. *Journal of Neuroscience, 35*(22), 8480–8492.

Quiroga, R. Q., Nadasdy, Z., & Ben-Shaul, Y. (2004). Unsupervised spike detection and sorting with wavelets and superparamagnetic clustering. *Neural Computation, 16*(8), 1661–87.

Rey, H. G., Pedreira, C., & Quian Quiroga, R. (2015). Past, present and future of spike sorting techniques. *Brain Research Bulletin, 119*, 106–117.

Rossant, C., Kadir, S. N., Goodman, D. F. M., Schulman, J., Hunter, M. L. D., Saleem, A. B., et al. (2016). Spike sorting for large, dense electrode arrays. *Nature Neuroscience, 19*(4), 634–641.

Segev, R., Goodhouse, J., Puchalla, J., & Berry II, M. J. (2004). Recording spikes from a large fraction of the ganglion cells in a retinal patch. *Nature Neuroscience, 7*(10), 1155.

Shoham, S., Fellows, M. R., & Normann, R. A. (2003). Robust, automatic spike sorting using mixtures of multivariate t-distributions. *Journal of Neuroscience Methods, 127*(2), 111–122.

Ventura, V., & Gerkin, R. C. (2012). Accurately estimating neuronal correlation requires a new spike-sorting paradigm. *Proceedings of the National Academy of Sciences, 109*(19), 7230–7235.

Wood, F., & Black, M. J. (2008). A nonparametric Bayesian alternative to spike sorting. *Journal of Neuroscience Methods, 173*(1), 1–12.

Yger, P., Spampinato, G. L., Esposito, E., Lefebvre, B., Deny, S., Gardella, C., et al. (2018). A spike sorting toolbox for up to thousands of electrodes validated with ground truth recordings in vitro and in vivo. *eLife, 7*, e34518.

Yuan, X., Kim, S., Juyon, J., D'Urbino, M., Bullmann, T., Chen, Y., et al. (2016). A microelectrode array with 8,640 electrodes enabling simultaneous full-frame readout at 6.5 kfps and 112-channel switch-matrix readout at 20 ks/s. In *2016 IEEE Symposium on VLSI Circuits (VLSI-Circuits)* (pp. 1–2). Honolulu, HI: IEEE.

Zhang, J., Laiwalla, F., Kim, J. A., Urabe, H., Van Wagenen, R., Song, Y.-K., et al. (2009). Integrated device for optical stimulation and spatiotemporal electrical recording of neural activity in light-sensitized brain tissue. *Journal of neural engineering, 6*(5), 055007.

Burst Detection Methods

Ellese Cotterill and Stephen J. Eglen

Abstract 'Bursting', defined as periods of high-frequency firing of a neuron separated by periods of quiescence, has been observed in various neuronal systems, both in vitro and in vivo. It has been associated with a range of neuronal processes, including efficient information transfer and the formation of functional networks during development, and has been shown to be sensitive to genetic and pharmacological manipulations. Accurate detection of periods of bursting activity is thus an important aspect of characterising both spontaneous and evoked neuronal network activity. A wide variety of computational methods have been developed to detect periods of bursting in spike trains recorded from neuronal networks. In this chapter, we review several of the most popular and successful of these methods.

Keywords Burst detection · Spike train analysis · Multielectrode arrays

Abbreviations

CMA	Cumulative Moving Average
IQR	Inter-Quartile Range
IRT	ISI Rank Threshold
ISI	InterSpike Interval
LTD	Long-Term Depression
LTP	Long-Term Potentiation
MEA	MultiElectrode Array
MI	Max Interval
PS	Poisson Surprise
RS	Rank Surprise
RGS	Robust Gaussian Surprise

E. Cotterill · S. J. Eglen (✉)
Department of Applied Mathematics and Theoretical Physics, University of Cambridge, Cambridge, UK
e-mail: sje30@cam.ac.uk

1 Introduction

Neuronal bursting, observed as intermittent periods of elevated spiking rate of a neuron (see Fig. 1), has been observed extensively in both in vitro and in vivo neuronal networks across various network types and species (Weyand et al. 2001; Chiappalone et al. 2005; Pasquale et al. 2010). These bursts can be isolated to a single neuron or, commonly, occur simultaneously across many neurons, in the form of 'network bursts' (Van Pelt et al. 2004b; Wagenaar et al. 2006; Pasquale et al. 2008; Bakkum et al. 2013).

Bursting activity is believed to play a role in a range of physiological processes, including synapse formation (Maeda et al. 1995) and long-term potentiation (Lisman 1997). Analysis of patterns of bursting activity can thus be used as a proxy for studying the underlying physiological processes and structural features of neuronal networks. A common method of studying bursting activity in vitro involves the use of MEA recordings of spontaneous or evoked neuronal network activity (Lonardoni et al. 2015; Charlesworth et al. 2015; Pimashkin et al. 2011; Van Pelt et al. 2004b). This approach has been employed to study changes in spontaneous network activity over development (Wagenaar et al. 2006), and the effect of pharmacological or genetic manipulations (Eisenman et al. 2015; Charlesworth et al. 2016).

Despite the importance of bursting and its prevalence as a feature used to analyse neuronal network activity, there remains a lack of agreement in the field about the definitive formal definition of a burst (Cocatre-Zilgien and Delcomyn 1992; Gourévitch and Eggermont 2007). There is also no single technique that has been widely adopted for identifying the location of bursts in spike trains. Instead, a large variety of burst detection methods have been proposed, many of which have been developed and assessed using specific data sets and single experimental conditions. As most studies of bursting activity have been performed on experimental data from recordings of rodent neuronal networks (Charlesworth et al. 2015; Mazzoni et al. 2007), this type of data has most often been used to assess the performance of burst detection techniques (Chiappalone et al. 2005; Mazzoni et al. 2007; Gourévitch and Eggermont 2007).

Recently, it has been shown that networks of neurons derived from human stem cells can be grown successfully on MEAs and exhibit spontaneous electrical activity, including bursting (Illes et al. 2007; Heikkilä et al. 2009). Human stem cell-derived

Fig. 1 Example of bursting activity in a spike train recorded from mouse retinal ganglion cells. Horizontal blue lines show the location of bursts. Scale bar represents 1 s

MOUSE   **HUMAN**

Fig. 2 Examples of spike trains from mouse and human neuronal networks. Each row represents the spikes recorded from one electrode and the scale bar represents 30 s. Recordings from human neuronal networks often exhibit more variable and complex spontaneous activity patterns

neuronal cultures have also been demonstrated to be a suitable alternative to rodent neuronal networks in applications such as neurotoxicity testing (Ylä-Outinen et al. 2010). This has led to a demand for a robust method of analysing bursting in these networks, which commonly exhibit more variable and complex patterns of bursting activity than rodent neuronal networks (Kapucu et al. 2012) (see Fig. 2). Recently, some burst detection methods have been developed which specifically focus on analysing bursting activity in these types of variable networks (Kapucu et al. 2012; Välkki et al. 2017).

2 Physiological Significance of Neuronal Bursting

Neuronal bursting is a frequently observed phenomenon in MEA recordings of cultures of dissociated neurons, as well as in numerous in vitro systems (Wagenaar et al. 2006; Pasquale et al. 2008; Weyand et al. 2001; Legéndy and Salcman 1985). In cultured rodent cortical networks, bursts, and in particular, synchronised 'network bursts' generally arise as a feature of the spontaneous network activity after around 1 week in vitro (Kamioka et al. 1996). Most studies observe that these network bursts then increase in frequency and size before reaching a peak around 3 weeks in vitro (Van Pelt et al. 2004a,b; Chiappalone et al. 2006). This peak in network bursting activity generally corresponds to the period in which the synaptic density of the network reaches its maximum (Van Huizen et al. 1985; Kamioka et al. 1996; Van Pelt et al. 2004a). This is followed by a period of shortening of network bursts, which coincides with a stage of 'pruning' or reduction in dendritic spine synapses and maturation of excitatory connections between neurons (Chiappalone et al. 2006; Illes et al. 2007; Ichikawa et al. 1993; Van Pelt et al. 2005). As well as being correlated with neuronal network development and maturation, bursting patterns of

spontaneous activity are also believed to play an important role in regulating cell survival. High-frequency bursting has been shown to increase neuronal survival in cortical cultures, while suppression of spontaneous activity has been observed to greatly increase the rates of programmed cell death (Golbs et al. 2011; Heck et al. 2008).

Bursting has also been observed to be involved in a range of physiological processes in mature neuronal networks. For example, bursting is believed to be a more efficient method of information transfer between neurons than single spikes. Central synapses in various brain regions have been shown to exhibit low probabilities of neurotransmitter release in response to single presynaptic spikes, making information transfer by single spikes unreliable (Borst 2010; Branco and Staras 2009; Allen and Stevens 1994). However, bursts of spikes can lead to 'facilitation', a process in which a rapid succession of spikes leads to a build-up of intracellular Ca^{2+} in the presynaptic terminal. This increases the probability of neurotransmitter release and resultant production of EPSPs with subsequent spikes (Thomson 1997; Krahe and Gabbiani 2004). In addition to being involved in these mechanisms of short-term plasticity, bursting has also been implicated in long-term potentiation (LTP) and depression (LTD). For example, in the hippocampus, postsynaptic bursting at temporally relevant intervals could produce long-term synaptic changes (Pike et al. 2004; Froemke et al. 2006; Thomas et al. 1998).

It has also been suggested that bursts of spikes transmit information with a higher signal-to-noise ratio than single spikes (Sherman 2001). Evidence of this has been seen in a variety of brain regions, such as the hippocampus, where place fields have been shown to be more accurately defined by bursts than individual spikes (Otto et al. 1991). Bursting has also been shown to produce sharper sensory tuning curves (Cattaneo et al. 1981; Krahe and Gabbiani 2004) and more reliable feature extraction than single spikes (Gabbiani et al. 1996; Sherman 2001; Krahe et al. 2002).

The importance of neuronal bursting has also been demonstrated through its association with a variety of behaviours in vivo, including visual processing, reward and goal-directed behaviour and sleep and resting conditions (Cattaneo et al. 1981; Krahe and Gabbiani 2004; Tobler et al. 2003; Schultz et al. 1997; Schultz 1998; Evarts 1964; Barrionuevo et al. 1981; McCarley et al. 1983; Weyand et al. 2001; Steriade et al. 2001). Bursting of hippocampal place cells has also been observed during exploration of new environments (O'Keefe and Recce 1993; Epsztein et al. 2011). The presence of bursting in these, as well as other memory-related behaviours (Burgos-Robles et al. 2007; Xu et al. 2012), suggests that bursting plays a specific role in memory and learning in the adult brain (Paulsen and Sejnowski 2000).

Additionally, bursting activity has been seen to be altered in certain pathological conditions (Walker et al. 2008; Jackson et al. 2004; Miller et al. 2011; Singh et al. 2016). For example, increased bursting activity has been observed in the basal ganglia of Parkinson's patients, with correlations between the level of bursting activity and the progression of the disease (Lobb 2014; Ni et al. 2001). This suggests that the study of bursting activity could not only reveal important features of normal brain function but also how this is altered in diseased states.

3 Previous Approaches to Burst Detection

Since the development of the first methods to identify bursting in neuronal networks more than three decades ago, many techniques have been proposed. These methods take a variety of approaches.

3.1 Fixed Threshold-Based Methods

The simplest approaches involve imposing thresholds on values such as the minimum firing rate or maximum allowed interspike interval (ISI) within a burst, and classifying any sequence of consecutive spikes satisfying these thresholds as a burst. In well-ordered spike trains, these thresholds can be set as fixed values by visual inspection (Weyand et al. 2001; Chiappalone et al. 2005). Other methods also incorporate additional thresholds on relevant parameters such as the minimum interval between two bursts and the minimum duration of a burst, to restrict detected bursts to those with biologically realistic properties (Nex Technologies 2014).

3.2 Adaptive Threshold-Based Methods

As opposed to having fixed threshold parameters that are chosen by the user, other burst detection algorithms derive the values of their threshold parameters adaptively from properties of the data, such as the mean ISI (Chen et al. 2009) or total spiking rate (Pimashkin et al. 2011). Commonly, this involves the use of some form of the distribution of ISIs on a spike train. For spike trains containing bursting activity, the smoothed histogram of ISIs on the train should have a peak in the region of short ISIs, which represents within-burst ISIs, and one or more peaks at higher ISI values, representing intraburst intervals. A threshold for the maximum ISI allowed within a burst can be set at the ISI value representing the turning point in the histogram (Cocatre-Zilgien and Delcomyn 1992).

Several other adaptive burst detection algorithms also use distributions related to the ISI histogram to calculate the thresholds for burst detection. Selinger et al. (2007) and Pasquale et al. (2010) argue that the histogram of log(ISI)s provides a better separation of within- and between-burst intervals, and use this histogram to set the threshold for the maximum within-burst ISI at the minimum between the first two well-separated peaks. Kaneoke and Vitek (1996) use the histogram of discharge density rather than ISIs for burst detection, while Kapucu et al. (2012) derive the threshold parameters for detecting bursts in their algorithm from the cumulative moving average of the ISI histogram.

3.3   Surprise-Based Methods

Another category of burst detection techniques are the surprise-based methods, which use statistical techniques to distinguish periods of bursting from baseline neuronal firing. The earliest of such methods was developed by Legéndy and Salcman (1985), and detects bursts as periods of deviation from an assumed underlying Poisson process of neuronal firing. This method critically assumes Poisson-distributed spike trains, which has been shown to be inappropriate for many common spike trains, in particular because of the refractory period between spikes (Câteau and Reyes 2006). Despite this, the Poisson Surprise method has been one of the most widely used burst detection methods since its development over 30 years ago (398 citations as of June 2018) and is still commonly used for analysing bursting activity in experimental studies of numerous neuronal network types (Singh et al. 2016; Pluta et al. 2015; Senn et al. 2014). More recently, other surprise-based burst detectors have been developed that replace the assumption that baseline firing follows a Poisson process with other assumptions about the underlying distribution of spikes (Ko et al. 2012; Gourévitch and Eggermont 2007).

3.4   Other Methods

Other burst detectors take alternative approaches to separate bursting from background spiking activity. Turnbull et al. (2005) examine the slope of the plot of spike time against spike number to detect bursts as periods of high instantaneous slope. Martinson et al. (1997) require bursts to be separated by intervals at least two standard deviations greater than their average within-burst ISIs, while Tam (2002) proposes a parameter-free burst detection method, in which sequences of spikes are classified as bursts if the sum of their within-bursts ISIs is less than the ISIs immediately before and after the burst.

Numerous studies have also used various forms of hidden Markov models to analyse neuronal activity patterns (Radons et al. 1994; Chen and Brown 2009; Abeles et al. 1995). These methods assume that a neuron stochastically alternates between two or more states, characterised by differences in their levels of activity. Tokdar et al. (2010) apply this idea to burst detection by modelling neuronal activity using hidden semi-Markov models.

3.5   Burst Detection Methods

In this section, we will outline a number of key existing burst detection algorithms. Given the vast number of available burst detection techniques, the following have been chosen for their relevance and popularity in the existing literature, and represent examples of each of the approaches to burst detection outlined above (Table 1).

Table 1 Burst detectors classified by their approach to burst detection

Abbreviation	Method	Reference
Fixed threshold-based methods		
MI	MaxInterval	Nex Technologies (2014)
Adaptive threshold-based methods		
logISI	LogISI	Pasquale et al. (2010)
CMA	Cumulative Moving Average	Kapucu et al. (2012)
IRT	ISI Rank Threshold	Hennig et al. (2011)
Surprise-based methods		
PS	Poisson Surprise	Legéndy and Salcman (1985)
RS	Rank Surprise	Gourévitch and Eggermont (2007)
RGS	Robust Gaussian Surprise	Ko et al. (2012)
Other methods		
HSMM	Hidden Semi-Markov Model	Tokdar et al. (2010)
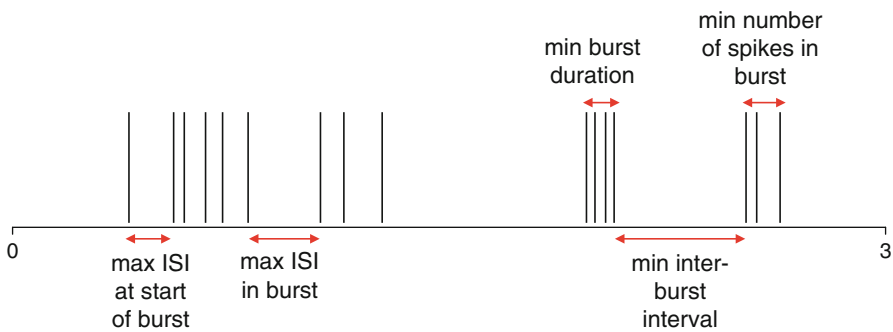
Fig. 3 Illustration of the parameters used by the MaxInterval method

MaxInterval Method (Nex Technologies 2014)
Bursts are defined using five fixed threshold parameters, shown in Fig. 3. The value of these parameters is chosen a priori, and any series of spikes that satisfy these thresholds is classified as a burst.

LogISI Method (Pasquale et al. 2010)
The histogram of log(ISI)s on a spike train is computed, using a bin size of 0.1 in log(ISI) units. Let C_k denote the ISI count in the kth bin of this histogram, which corresponds to an ISI size of ISI_k, and MCV denote a pre-specified threshold value, known as the maximum cut-off value. The location of the peaks of this histogram is found using a custom peak finding algorithm described in Pasquale et al. (2010). The largest peak of the histogram corresponding to an ISI less than or equal to MCV is set as the intraburst peak, C_{IBP}. If no peak is found in the histogram with $ISI_k \leq$ MCV, the spike train is classified as containing no bursts.

In the case that an intraburst peak is present, the minimum value of the histogram between the intraburst peak and each of the following peaks, C_{p_i} ($i = 1, \ldots, N$), is

found. For each minimum, a void parameter is calculated that represents how well the corresponding peak is separated from the intraburst peak, as

$$void(i) = 1 - \frac{C_{min_i}}{\sqrt{C_{IBP} \cdot C_{p_i}}}$$

where C_{min_i} is the minimum value of C_k for $IBP < k < p_i$.

The smallest ISI_{min_i} for which $void(i) > 0.7$ is set as the threshold for the maximum ISI in a burst, $maxISI$ (see Fig. 4). Any series of at least three spikes separated by ISIs less than $maxISI$ are classified as bursts. If no point with a void value above 0.7 is found, or if $maxISI >$ MCV, bursts are detected using MCV as the threshold for the maximum ISI in a burst and then extended to include spikes within $maxISI$ of the beginning or end of each of these bursts.

Cumulative Moving Average (CMA) Method (Kapucu et al. 2012)

This method also uses the histogram of ISIs on a spike train. The cumulative moving average (CMA) at each ISI bin of the histogram is calculated. The CMA of the Nth ISI bin is defined as:

$$CMA_N = \frac{1}{N} \sum_{k=1}^{N} C_k,$$
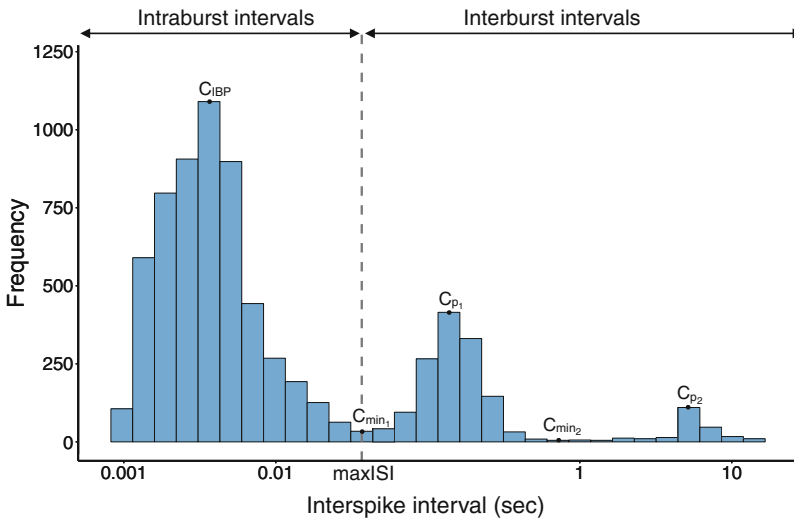
Fig. 4 Example of log-adjusted ISI histogram with the threshold for intra- and interburst intervals found using the logISI method
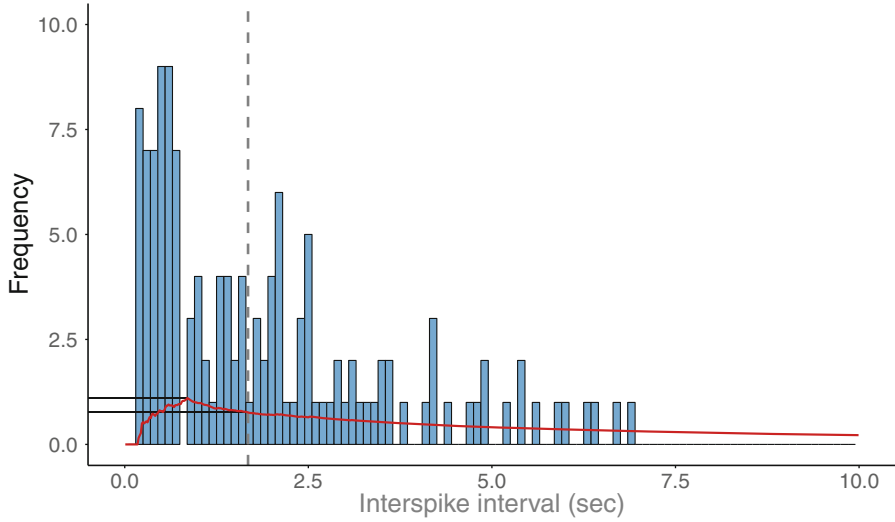
Fig. 5 Example of ISI histogram with the threshold for intra- and interburst intervals found using the CMA method. Red line shows the cumulative moving average of the ISI histogram

where C_k is the ISI count in the kth bin. The skewness of the CMA distribution is used to determine the values of two threshold parameters, α_1 and α_2, based on the scale given in Kapucu et al. (2012). The maximum of the CMA distribution, CMA_{max}, is found and the value of $maxISI$ is set at the ISI bin at which the CMA is closest in value to $\alpha_1 \cdot CMA_{max}$ (see Fig. 5). Burst cores are then found as any sequences of at least three spikes separated by ISIs less than $maxISI$.

Kapucu et al. (2012) suggest extending these burst cores to include burst-related spikes. These are found using a second cut-off, set at the value of the ISI bin at which the CMA is closest to $\alpha_2 \cdot CMA_{max}$. Spikes within this cut-off distance from the beginning or end of the existing burst cores are classified as burst-related spikes. For this study, only the burst cores detected by this method were examined, omitting any burst-related spikes.

ISI Rank Threshold Method (Hennig et al. 2011)

In the ISI rank threshold (IRT) method, the rank of each ISI on a spike train relative to the largest ISI on the train is calculated, with $R(t)$ denoting the rank of the ISI beginning at time t. The probability distribution, $P(C)$, of spike counts in one-second time bins over the spike train is also found. A rank threshold, θ_R, is set to a fixed value, and a spike count threshold, θ_C, is calculated from $P(C)$. A burst is then defined to begin at a spike at time t if the rank of the proceeding ISI satisfies $R(t) < \theta_R$ and the spike count in the following second, $C(t, t+1)$, exceeds θ_C. The burst continues until a spike is found for which $C(t, t+1) < \frac{\theta_C}{2}$.

Poisson Surprise Method (Legéndy and Salcman 1985)

The average firing rate, λ, on a spike train is calculated, and the underlying activity on this spike train is assumed to follow a Poisson process with rate λ. The Poisson surprise (PS) statistic for any period of length T containing N spikes is calculated as:

$$S = -\log P$$

where

$$P = \exp\left(-\lambda T \sum_{n=N}^{\infty} \frac{(\lambda T)^n}{n!}\right)$$

is the probability that N or more spikes occur randomly in a period of length T.

A surprise maximisation algorithm described in Legéndy and Salcman (1985) is then used to find the set of bursts that maximises the PS statistic across the entire spike train. This involves initially identifying bursts as any sequence of three consecutive spikes separated by ISIs which are less than half of the mean ISI on the spike train. Spikes are then added to the end and removed from the beginning of each of these initial bursts until the sequence of spikes with the maximum PS statistic is found. Finally, any bursts which have a PS statistic below a pre-defined threshold level are discarded.

Rank Surprise Method (Gourévitch and Eggermont 2007)

The rank surprise (RS) burst detection algorithm is a non-parametric adaptation of the Poisson surprise approach. To implement this method, all ISIs on a spike train are ranked by size, with the smallest ISI given a rank of one. In the absence of any bursting activity, the ISI ranks should be independently and uniformly distributed. For any period containing N spikes separated by $N-1$ ISIs with ranks r_n, ..., r_{n+N-1}, the rank surprise statistic is defined as:

$$RS = -\log(P(D_N \leq r_n + \ldots + r_{n+N-1}))$$

where D_N is the discrete uniform sum distribution between 1 and N and r_n is the rank of the nth ISI on the spike train.

Bursts are then chosen to maximise the RS statistic across the entire spike train using an exhaustive surprise maximisation algorithm, outlined in Gourévitch and Eggermont (2007). A fixed threshold for $maxISI$ is first calculated from the distribution of ISIs on the spike train. The first sequence of at least three spikes with ISIs less than $maxISI$ are found, and an exhaustive search of all of the subsequences of ISIs within this period is performed to find the subsequence with the highest RS value. If this value is above a fixed minimum significance threshold, chosen a priori, it is labelled as a burst. This process is repeated on the remaining ISI subsequences within the period of interest until all significant bursts are found. Following this, the next sequence of spikes with ISIs below $maxISI$ is examined in a similar fashion, and this process is continued until the end of the spike train.

Robust Gaussian Surprise Method (Ko et al. 2012)

In the robust Gaussian surprise (RGS) method, the distribution of log(ISI)s on each spike train is found and centred around zero. The normalised log(ISI)s from each spike train in the study are then pooled and the central distribution of this joint data set is found using a procedure outlined in Ko et al. (2012). A burst detection threshold for $maxISI$ is set at the 0.5 percentile of this central distribution, which is estimated as 2.58 times the median absolute deviation of the distribution.

The Gaussian burst surprise value in any interval on a spike train is defined as:

$$GS_B = -\log(P)$$

where P is the probability that the sum of normalised log(ISI)s in the interval is greater than or equal to the sum of an equal number of i.i.d. Gaussian random variables with mean and variance equal to that of the central distribution.

Any consecutive sequence of spikes separated by intervals less than $maxISI$ are classified as burst cores. These burst cores are then extended by adding intervals to the beginning and end of the burst cores until the sequence with the maximum value of GS_B is found. In the case of overlapping bursts, the burst with the largest GS_B value is retained. Finally, any detected bursts with GS_B below a pre-defined threshold value are discarded. Ko et al. (2012) also propose a similar method for identifying pauses in spike trains.

Hidden Semi-Markov Model Method (Tokdar et al. 2010)

This method is based on the assumption that neurons switch stochastically between two states: 'non-bursting' (state 0) and 'bursting' (state 1), which can be modelled using a hidden semi-Markov model. The transition times between the two states are modelled using two Gamma distributions, f_0^{ITI} and f_1^{ITI}. Within each of the states, the ISI times are modelled using two additional gamma distributions, f_0^{ISI} and f_1^{ISI}. The parameters of these four distributions are learned from the data. A custom Markov chain Monte Carlo algorithm described in Tokdar et al. (2010) is then used to compute the posterior probability that a neuron is in a bursting state at any given time. A fixed threshold value is chosen a priori, and any periods during which the posterior probability exceeds this value are classified as bursts.

3.6 Evaluation of Burst Detection Techniques

In Cotterill et al. (2016), we performed a thorough evaluation of the burst detection methods outlined above. This involved first assessing the methods against a list of desirable properties that we deemed an ideal burst detector should possess (see Table 2). This was achieved by generating synthetic spike trains with specific properties of interest to represent each desirable property. The output of each burst detector when used to analyse each set of spike trains was then compared to the 'ground truth' bursting activity. Figure 6 shows the performance of the chosen burst

Table 2 Desirable properties for a burst detector

Desirable properties	
D1	Deterministic: the method should detect the same bursts over repeated runs on the same data, to ensure consistency and reproducibility of results
D2	No assumption of spike train distribution: the method should not assume that ISIs follow a standard statistical distribution, to ensure wide applicability to a variety of spike trains
D3	Number of parameters: the method should have few parameters, to reduce the variability inherently introduced through parameter choice
D4	Computational time: the method should run in a reasonable amount of time using standard personal computers
D5	Non-bursting trains: the method should detect few spikes as being within bursts in spike trains containing no obvious bursting behaviour
D6	Non-stationary trains: the method should detect few spikes as being within bursts in spike trains with non-stationary firing rates that contain no obvious bursting behaviour
D7	Regular short bursts: the method should detect a high proportion of spikes in bursts in spike trains containing short well-separated bursts
D8	Non-stationary bursts: the method should detect a high proportion of spikes in bursts in spike trains containing bursts with variable durations and number of spikes per burst
D8	Regular long bursts: the method should detect a high proportion of spikes in bursts and accurate number of bursts in spike trains containing long bursts with low within-burst firing rates
D10	High-frequency bursts: the method should detect a high proportion of spikes in bursts and accurate number of bursts in spike trains containing a large number of short bursts
D11	Noisy train: the method should classify a high number of within-burst spikes as bursting and a low number of interburst spikes as bursting in spike trains containing both bursts and noise spikes

Table reproduced from Cotterill et al. (2016)

detectors on a sample of these properties. Most burst detectors can accurately detect a small amount of bursting activity in spike trains simulated to contain no bursting behaviour (Fig. 6a), with the exception of the HSMM and CMA methods, which detect a significant amount of erroneous bursting. Conversely, most burst detectors accurately identified most bursting activity in spike trains containing only regular short bursts (Fig. 6c). However, the RS, IRT and RGS methods performed poorly here, only detecting a small proportion of the bursting activity.

This approach of assessing the performance of each burst detection method against desirable properties allowed us to determine a ranking for each of the burst detectors, in which the rank surprise, robust gaussian surprise and ISI rank threshold methods ranked particularly poorly (see Table 3). Further assessment of the burst detectors was then achieved by examining the coherence of the bursts detected by each method with visually annotated bursts in experimental recordings of mouse retinal ganglion cells (RGCs). This allowed us to analyse the specificity and sensitivity of the burst detectors as their input parameters were varied. This analysis reinforced the low levels of adaptability of the RS, RGS and IRT methods at analysing this type of data. The HSMM method was also seen to have a consistently high false-positive rate compared to other burst detectors used to analyse this data.
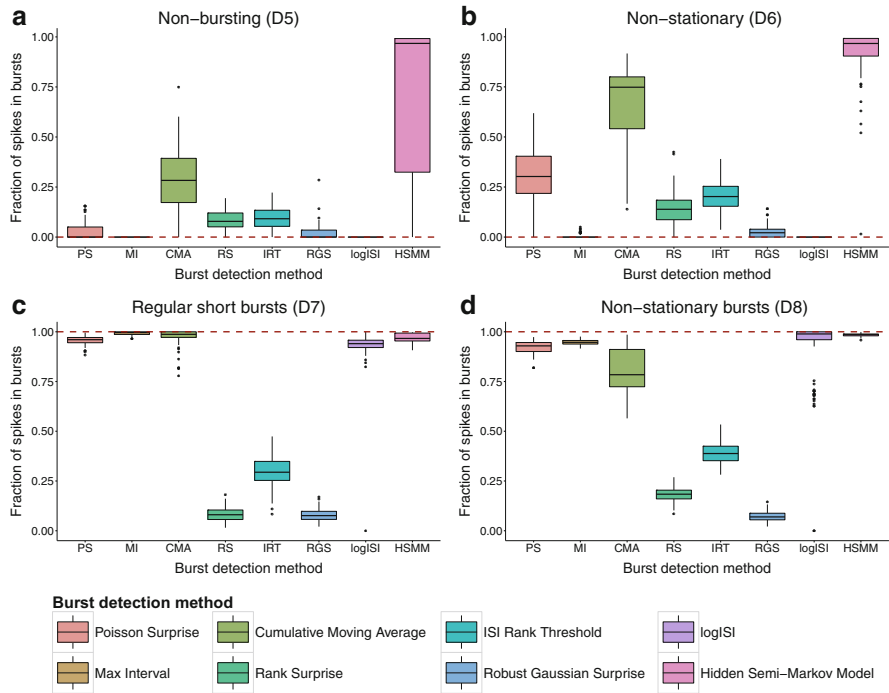
Fig. 6 Fraction of spikes in bursts found by each burst detector in 100 synthetic trains with (**a**) no bursting (D5), (**b**) no bursting and non-stationary firing rate (D6), (**c**) short regular bursts (D7) and (**d**) bursts with non-stationary burst lengths and durations (D8). Dotted line shows desired result from an ideal burst detector; methods close to this line are deemed to work well. In each 'box-and-whisker' plot, boxes show the median $\pm$ inter-quartile range (IQR), and whiskers extend to median $\pm$ 1.5$\times$ IQR. Outliers are represented as points. Figure reproduced with permission from Cotterill et al. (2016)

Based on these assessments, four burst detectors, namely the MI, logISI, PS and CMA methods, were chosen as the best performing burst detection methods, and used to analyse bursting activity in novel recordings of networks of human induced pluripotent stem cell (hiPSC)-derived neuronal networks over several months of development. This analysis showed a slight increase in the proportion of bursting activity observed in these networks as they mature, although this increase was far lower than that which has been observed in developing rodent neuronal networks (Charlesworth et al. 2015; Chiappalone et al. 2005; Wagenaar et al. 2006).

From this analysis, we concluded that no existing burst detector possesses all of the desirable properties required for 'perfect' identification of bursting periods in highly variable networks. The CMA and PS methods possessed many of the desirable properties, but had limitations such as their tendency to overestimate bursting activity in spike trains containing sparse or no bursting activity, particularly those with a non-stationary firing rate.

Table 3 The performance of each method on the desirable properties specified in Table 2

Desirable property	Burst detection method							
	PS	MI	CMA	RS	IRT	RGS	logISI	HSMM
D1 Deterministic	✓	✓	✓	✓	✓	✓	✓	×
D2 Distribution assumption	×	✓	✓	✓	✓	×	✓	×
D3 Number of parameters	✓	×	✓	✓	✓	✓	✓	×
D4 Computational time	✓	✓	✓	✓	✓	✓	✓	×
D5 Non-bursting	4	1	7	5	6	3	1	8
D6 Non-stationary	6	2	7	4	5	3	1	8
D7 Regular bursting	4	1	2	7	6	7	5	3
D8 Non-stat bursts	4	3	5	7	6	8	2	1
D9 Long bursts	2	4	3	8	5	7	6	1
D10 High frequency	5	1	4	7	6	8	2	3
D11 Noisy bursts	5	1	2	7	6	8	4	2
Total (Relative rank)	30 (4)	13 (1)	30 (4)	45 (8)	40 (6)	44 (7)	21 (2)	26 (3)

For binary properties, D1–D4, each method was judged to either possess the property or not, while for properties D5–D11, the performance of each method was ranked against the other methods (1 = best, 8 = worst) and summed to produce an overall ranking. Table adapted from Cotterill et al. (2016)

Overall, the MI and logISI methods showed the most promise for achieving robust burst analysis in a range of contexts. These methods possessed most properties we deemed desirable for a burst detection method and were generally able to achieve high coherence with visually detected bursts in experimental MEA recordings. These methods, however, still had limitations. The MI method requires the choice of five parameters, the optimal values of which can be challenging to determine, particularly when analysing recordings from a variety of experimental conditions (Cotterill et al. 2016). The logISI method had a tendency to underestimate bursting in some spike trains, particularly those with non-standard bursting activity.

The overall recommendation from this analysis was to choose a burst detector from the several high-performing methods outlined above based on the number of freedom the user wishes to control. The MI method is a good first choice for these purposes, and despite the large number of parameters this method requires, these parameters are easy to interpret biologically and adjust to achieve the desired burst detection results for the specific situations in which it is utilised. If appropriate parameters cannot be found for the MI method, a high-performing alternative is the logISI method, which can be implemented without choosing any input parameters. This method is most effective when there is a clear distinction between the size of within- and between-burst intervals on a spike train. In cases when this distinction is not apparent, the PS and CMA methods are reasonably effective alternative burst detection methods; however, post hoc screening for outliers in terms of burst duration is advisable when using either of these methods.

One robust approach to burst detection would be to use several burst detectors to analyse the data of interest and compare the results of each method. If the burst detectors are largely in agreement, this provides confidence in the nature of the bursting activity identified in the experimental data. Any major discrepancies between the results from the methods can also be used to identify areas where one or more burst detectors may be performing poorly, which can be further investigated through inspection of the specific spike trains of interest.

3.7 Network-Wide Burst Detection

As well as single-neuron bursts, synchronous bursting of networks of neurons, termed 'network bursts', are a ubiquitous feature of various neuronal networks. In rat cortical cultures, these network bursts have been observed to arise from around 1 week in vitro, and comprise the dominant form of spontaneous network activity at this age (Chiappalone et al. 2005; Van Pelt et al. 2004a). Network bursts increase in frequency and size before reaching a peak at around 3 weeks in vitro, corresponding to the period in which synaptic density in the network reaches its maximum (Van Pelt et al. 2004a,b; Chiappalone et al. 2006).

As well as in rat cortical cultures, the presence of network bursting activity has also been observed in a variety of other brain regions and species in vitro (Van Den Pol et al. 1996; Ben-Ari 2001; Rhoades and Gross 1994; Harris et al. 2002; Meister et al. 1991) and in vivo (Chiu and Weliky 2001; Leinekugel et al. 2002; Weliky and Katz 1999). Recently, synchronous bursting resembling that in rat cortical cultures has also been observed in networks produced from human embryonic or induced pluripotent stem cell-derived neurons, generally arising 8–12 weeks after differentiation and increasing in frequency over development (Heikkilä et al. 2009; Odawara et al. 2016; Amin et al. 2016).

3.7.1 Existing Network Burst Detection Techniques

A variety of techniques have been developed to detect these network-wide bursts. Several of these methods identify bursts as increases in the network-wide firing rate (Mazzoni et al. 2007; Raichman and Ben-Jacob 2008). These periods, however, do not necessarily consist of single-neuron bursts across multiple electrodes. Other methods define network bursts only when single-neuron bursts occur simultaneously across numerous recorded electrodes (Wagenaar et al. 2006; Pasquale et al. 2010). For example, Bakkum et al. (2013) combine the spikes detected on all channels of an MEA into a single spike train and employ the ISI histogram between every nth spike in this network-wide spike train to determine an appropriate threshold for the maximum ISI within a network burst. Wagenaar et al. (2005), on the other hand, detect 'burstlets' on each electrode individually using an adaptive threshold based

on the electrode's average firing rate. A network burst is then defined as any period in which burstlets on multiple electrodes overlap.

Network-wide information can also be incorporated into single-neuron burst detection techniques to improve their performance. Martens et al. (2014) showed that the peaks corresponding to intra- and interburst spikes in an ISI histogram were better separated when pooled ISIs from multiple electrodes of an MEA were included, rather than simply those from a single spike train. They also proposed a pre-processing technique designed to improve the detection of bursts, particularly on noisy data. This involves creating a return map, which plots the ISI immediately preceding each spike (ISI_{pre}) against the ISI following the spike (ISI_{post}). Background spikes lie in the region of this graph with both high ISI_{pre} and ISI_{post}, and are removed from consideration by the burst detection method. The performance of various single-channel burst detection techniques was shown to be significantly improved when applied to data pre-processed in this way, compared to the original data (Martens et al. 2014).

Additionally, Välkki et al. (2017) adapted the CMA method of Kapucu et al. (2012) to incorporate information from multiple MEA electrodes. In this multi-CMA method, instead of individual histograms for each spike train, the ISI histogram from the combined ISIs from multiple electrodes is used to calculate the threshold for burst detection in an identical method to the original CMA method. This threshold is then used to detect bursts on each electrode individually. The electrodes that are used for combined analysis by this method can be chosen from a variety of options, including analysing all electrodes in a single MEA simultaneously, analysing the spike trains from a single electrode over several experimental time points, or analysing all electrodes over all time points in the experiment. This adaptation has been shown to reduce the number of excessively long sparse bursts identified by the original CMA method, improving its performance at analysing highly variable spike trains.

3.8 Summary and Future Directions

In this chapter, we have summarised the main techniques of burst detection. Moving from an informal definition ("bursts are groups of spikes that are close to each other in time") to a formal mathematical definition has proved challenging. Our experience is that when the datasets are relatively clean, there is good agreement between methods. However, when the data are noisy, not only do different methods disagree, different human observers will also disagree. Here, we have outlined several of the methods that we believe work relatively well, but are fallible when presented with noisy data. Future work in this area might be centred around developing methods that are more robust to noisy data. Possible steps towards this may involve generating more realistic synthetic datasets to train and assess burst detection techniques, or the incorporation of noise-reducing pre-processing steps prior to burst detection, such as those developed by Martens et al. (2014).

Outside of neuroscience, the detection of 'bursty' events is also a more general problem in time series analysis. For example, identifying bursts of gamma rays can aid in the detection of black holes, and the detection of periods of high trading volume of a stock is of relevance to regulators looking for insider trading (Zhu and Shasha 2003). Various techniques have been developed for detecting bursting periods in these and other data types, including sliding window and infinite state automaton-based models (Zhu and Shasha 2003; Zhang and Shasha 2006; Kleinberg 2002; Boyack et al. 2004; Kumar et al. 2003). Ideas from these burst detectors developed in other domains may be useful for informing future approaches to burst detection in a neuroscience context.

The increasing use of high-density MEAs, which contain up to several thousand electrodes (Maccione et al. 2014; Lonardoni et al. 2015), to record in vitro neuronal activity as well as the prevalence of multi-well MEAs in applications such as high-throughput neurotoxicity screening (Valdivia et al. 2014; Nicolas et al. 2014) and drug safety testing (Gilchrist et al. 2015) also has implications for burst detection. In particular, the computational complexity of burst detection methods becomes increasingly relevant in these high-throughput situations, as does the importance of minimising the manual intervention required to run the burst detectors, such as through autonomous parameter selection. The development of online burst detection techniques that can detect bursting activity in real time is also necessary to facilitate areas such as the study of real-time learning in embodied cultured networks, and applications involving bidirectional communication between biological tissue and computer interfaces (Wagenaar et al. 2005; Bakkum et al. 2004). This is another area in which ideas adopted from burst detectors developed outside of neuroscience may benefit the field.

In conclusion, years of study of bursting activity in cultured neuronal networks has led to the development of many promising burst detection methods. However, a 'perfect' method for analysing bursting activity remains elusive. In the future, the development of improved burst detection methods will be essential to keep up with the advances in experimental techniques used to record bursting activity, such as the use of higher density arrays and availability of recordings from human stem cell-derived networks.

Appendix: Other Resources

- Open source R code for the burst detection methods outlined in this chapter are available at https://github.com/ellesec/burstanalysis and archived at https://doi.org/10.5281/zenodo.1284064.

References

Abeles, M., Bergman, H., Gat, I., Meilijson, I., Seidemann, E., Tishby, N., et al. (1995). Cortical activity flips among quasi-stationary states. *Proceedings of the National Academy of Sciences of the United States of America, 92*, 8616–8620.

Allen, C., & Stevens, C. F. (1994). An evaluation of causes for unreliability of synaptic transmission. *Proceedings of the National Academy of Sciences of the United States of America, 91*, 10380–10383.

Amin, H., Maccione, A., Marinaro, F., Zordan, S., Nieus, T., & Berdondini, L. (2016). Electrical responses and spontaneous activity of human iPS-derived neuronal networks characterized for 3-month culture with 4096-electrode arrays. *Frontiers in Neuroscience, 10*, 1–15.

Bakkum, D. J., Radivojevic, M., Frey, U., Franke, F., Hierlemann, A., & Takahashi, H. (2013). Parameters for burst detection. *Frontiers in Computational Neuroscience, 7*, 193.

Bakkum, D. J., Shkolnik, A. C., Ben-Ary, G., Gamblen, P., DeMarse, B., & Potter, S. M. (2004). Removing some 'A' from AI: Embodied cultured networks. In F. Iida, R. Pfeifer, L. Steels, & Y. Kuniyoshi (Eds.), *Embodied artificial intelligence* (pp. 130–146). Berlin: Springer.

Barrionuevo, G., Benoit, O., & Tempier, P. (1981). Evidence for two types of firing pattern during the sleep-waking cycle in the reticular thalamic nucleus of the cat. *Experimental Neurology, 72*, 486–501.

Ben-Ari, Y. (2001). Developing networks play a similar melody. *Trends in Neurosciences, 24*, 353–360.

Borst, J. G. G. (2010). The low synaptic release probability in vivo. *Trends in Neurosciences, 33*, 259–266.

Boyack, K. W., Mane, K., & Börner, K. (2004). Mapping Medline papers, genes and proteins related to melanoma research. In *Proceedings Eighth IEEE International Conference on Computer Vision* (pp. 965–971).

Branco, T., & Staras, K. (2009). The probability of neurotransmitter release: Variability and feedback control at single synapses. *Nature Reviews Neuroscience, 10*, 373–383.

Burgos-Robles, A., Vidal-Gonzalez, I., Santini, E., & Quirk, G. J. (2007). Consolidation of fear extinction requires NMDA receptor-dependent bursting in the ventromedial prefrontal cortex. *Neuron, 53*, 871–880.

Câteau, H., & Reyes, A. D. (2006). Relation between single neuron and population spiking statistics and effects on network activity. *Physical Review Letters, 96*, 058101.

Cattaneo, A., Maffei, L., & Morrone, C. (1981). Two firing patterns in the discharge of complex cells encoding different attributes of the visual stimulus. *Experimental Brain Research, 43*, 115–118.

Charlesworth, P., Cotterill, E., Morton, A., Grant, S. G., & Eglen, S. J. (2015). Quantitative differences in developmental profiles of spontaneous activity in cortical and hippocampal cultures. *Neural Development, 10*, 1–10.

Charlesworth, P., Morton, A., Eglen, S. J., Komiyama, N. H., & Grant, S. G. N. (2016). Canalization of genetic and pharmacological perturbations in developing primary neuronal activity patterns. Neuropharmacology, 100, 47–55.

Chen, L., Deng, Y., Luo, W., Wang, Z., & Zeng, S. (2009). Detection of bursts in neuronal spike trains by the mean inter-spike interval method. *Progress in Natural Science, 19*(2), 229–235.

Chen, Z., & Brown, E. N. (2009). Discrete- and continuous-time probabilistic models and algorithms for inferring neuronal UP and DOWN states. *Neural Computation, 21*(7), 1797–1862.

Chiappalone, M., Bove, M., Vato, A., Tedesco, M., & Martinoia, S. (2006). Dissociated cortical networks show spontaneously correlated activity patterns during in vitro development. *Brain Research, 1093*, 41–53.

Chiappalone, M., Novellino, A., Vajda, I., Vato, A., Martinoia, S., & van Pelt, J. (2005). Burst detection algorithms for the analysis of spatio-temporal patterns in cortical networks of neurons. *Neurocomputing, 65–66*, 653–662.

Chiu, C., & Weliky, M. (2001). Spontaneous activity in developing ferret visual cortex in vivo. *Journal of Neuroscience, 21*, 8906–8914.

Cocatre-Zilgien, J. H., & Delcomyn, F. (1992). Identification of bursts in spike trains. *Journal of Neuroscience Methods, 41*(1), 19–30.

Cotterill, E., Charlesworth, P., Thomas, C. W., Paulsen, O., & Eglen, S. J. (2016). A comparison of computational methods for detecting bursts in neuronal spike trains and their application to human stem cell-derived neuronal networks. *Journal of Neurophysiology, 116*, 306–321.

Eisenman, L. N., Emnett, C. M., Mohan, J., Zorumski, C. F., & Mennerick, S. (2015). Quantification of bursting and synchrony in cultured hippocampal neurons. *Journal of Neurophysiology, 114*, 1059–1071.

Epsztein, J., Brecht, M., & Lee, A. K. (2011). Intracellular determinants of hippocampal CA1 place and silent cell activity in a novel environment. *Neuron, 70*, 109–120.

Evarts, E. V. (1964). Temporal patterns of discharge of pyramidal tract neurons during sleep and waking in the monkey. *Journal of Neurophysiology, 27*, 152–171.

Froemke, R. C., Tsay, I. A., Raad, M., Long, J. D., & Dan, Y. (2006). Contribution of individual spikes in burst-induced long-term synaptic modification. *Journal of Neurophysiology, 95*, 1620–1629.

Gabbiani, F., Metzner, W., Wessel, R., & Koch, C. (1996). From stimulus encoding to feature extraction in weakly electric fish. *Nature, 384*, 563–567.

Gilchrist, K. H., Lewis, G. F., Gay, E. A., Sellgren, K. L., & Grego, S. (2015). High-throughput cardiac safety evaluation and multi-parameter arrhythmia profiling of cardiomyocytes using microelectrode arrays. *Toxicology and Applied Pharmacology, 288*, 249–257.

Golbs, A., Nimmervoll, B., Sun, J.-J., Sava, I. E., & Luhmann, H. J. (2011). Control of programmed cell death by distinct electrical activity patterns. *Cerebral Cortex, 21*, 1192–1202.

Gourévitch, B., & Eggermont, J. J. (2007). A nonparametric approach for detection of bursts in spike trains. *Journal of Neuroscience Methods, 160*(2), 349–358.

Harris, R. E., Coulombe, M. G., & Feller, M. B. (2002). Dissociated retinal neurons form periodically active synaptic circuits. *Journal of Neurophysiology, 88*, 188–195.

Heck, N., Golbs, A., Riedemann, T., Sun, J.-J., Lessmann, V., & Luhmann, H. J. (2008) Activity-dependent regulation of neuronal apoptosis in neonatal mouse cerebral cortex. *Cerebral Cortex, 18*, 1335–1349.

Heikkilä, T. J., Ylä-Outinen, L., Tanskanen, J. M. A., Lappalainen, R. S., Skottman, H., Suuronen, R., et al. (2009). Human embryonic stem cell-derived neuronal cells form spontaneously active neuronal networks in vitro. *Experimental Neurology, 218*(1), 109–116.

Hennig, M. H., Grady, J., van Coppenhagen, J., & Sernagor, E. (2011). Age-dependent homeostatic plasticity of GABAergic signaling in developing retinal networks. *Journal of Neuroscience, 31*(34), 12159–12164.

Ichikawa, M., Muramoto, K., Kobayashi, K., Kawahara, M., & Kuroda, Y. (1993). Formation and maturation of synapses in primary cultures of rat cerebral cortical cells: An electron microscopic study. *Neuroscience Research, 16*, 95–103.

Illes, S., Fleischer, W., Siebler, M., Hartung, H.-P., & Dihné, M. (2007). Development and pharmacological modulation of embryonic stem cell-derived neuronal network activity. *Experimental Neurology, 207*, 171–176.

Jackson, M. E., Homayoun, H., & Moghaddam, B. (2004). NMDA receptor hypofunction produces concomitant firing rate potentiation and burst activity reduction in the prefrontal cortex. *Proceedings of the National Academy of Sciences of the United States of America, 101*, 8467–8472.

Kamioka, H., Maeda, E., Jimbo, Y., Robinson, H. P. C., & Kawana, A. (1996) Spontaneous periodic synchronized bursting during formation of mature patterns of connections in cortical cultures. *Neuroscience Letters, 206*, 109–112.

Kaneoke, Y., & Vitek, J. L. (1996). Burst and oscillation as disparate neuronal properties. *Journal of Neuroscience Methods, 68*(2), 211–223.

Kapucu, F. E., Tanskanen, J. M. A., Mikkonen, J. E., Ylä-Outinen, L., Narkilahti, S., & Hyttinen, J. A. K. (2012). Burst analysis tool for developing neuronal networks exhibiting highly varying action potential dynamics. *Frontiers in Computational Neuroscience, 6*, 38.

Kleinberg, J. (2002). Bursty and hierarchical structure in streams. In *Proceedings of 8th ACM SIGKDD International Conference on Knowledge Discovery and Data Mining* (pp. 91–101).

Ko, D., Wilson, C. J., Lobb, C. J., & Paladini, C. A. (2012). Detection of bursts and pauses in spike trains. *Journal of Neuroscience Methods, 211*(1), 145–158.

Krahe, R., & Gabbiani, F. (2004). Burst firing in sensory systems. *Nature Reviews Neuroscience, 5*, 13–23.

Krahe, R., Kreiman, G., Gabbiani, F., Koch, C., & Metzner, W. (2002). Stimulus encoding and feature extraction by multiple sensory neurons. *Journal of Neuroscience, 22*, 2374–2382.

Kumar, R., Road, H., Jose, S., Road, H., Jose, S., Drive, R., et al. (2003). On the bursty evolution of blogspace. In *International World Wide Web Conference* (pp. 568–576).

Legéndy C. R., & Salcman, M. (1985). Bursts and recurrences of bursts in the spike trains of spontaneously active striate cortex neurons. *Journal of Neurophysiology, 53*(4), 926–939.

Leinekugel, X., Khazipov, R., Cannon, R., Hirase, H., Ben-Ari, Y., & Buzsáki, G. (2002). Correlated bursts of activity in the neonatal hippocampus in vivo. *Science, 296*, 2049–2052.

Lisman, J. E. (1997). Bursts as a unit of neural information: Making unreliable synapses reliable. *Trends Neuroscience, 20*(1), 38–43.

Lobb, C. J. (2014). Abnormal bursting as a pathophysiological mechanism in Parkinson's disease. *Basal Ganglia, 3*, 187–195.

Lonardoni, D., Di Marco, S., Amin, H., Maccione, A., Berdondini, L., & Nieus, T. (2015). High-density MEA recordings unveil the dynamics of bursting events in cell cultures. *Conference Proceedings: Annual International Conference of the IEEE Engineering in Medicine and Biology Society, 2015*, 3763–3766.

Maccione, A., Hennig, M. H., Gandolfo, M., Muthmann, O., van Coppenhagen, J., Eglen, S. J., et al. (2014). Following the ontogeny of retinal waves: Pan-retinal recordings of population dynamics in the neonatal mouse. *The Journal of Physiology, 592*(7), 1545–1563.

Maeda, E., Robinson, H. P., & Kawana, A. (1995). The mechanisms of generation and propagation of synchronized bursting in developing networks of cortical neurons. *The Journal of Neuroscience, 15*(10), 6834–6845.

Martens, M. B., Chiappalone, M., Schubert, D., & Tiesinga, P. H. E. (2014). Separating burst from background spikes in multichannel neuronal recordings using return map analysis. *International Journal of Neural Systems, 24*(04), 1450012.

Martinson, J., Webster, H. H., Myasnikov, A. A., & Dykes, R. W. (1997). Recognition of temporally structured activity in spontaneously discharging neurons in the somatosensory cortex in waking cats. *Brain Research, 750*, 129–140.

Mazzoni, A., Broccard, F. D., Garcia-Perez, E., Bonifazi, P., Ruaro, M. E., & Torre, V. (2007) On the dynamics of the spontaneous activity in neuronal networks. *PLoS One, 2*, e439.

McCarley, R. W., Benoit, O., & Barrionuevo, G. (1983). Lateral geniculate nucleus unitary discharge in sleep and waking: State- and rate-specific aspects. *Journal of Neurophysiology, 50*, 798–818.

Meister, M., Wong, R. O. L., Baylor, D. A., & Shatz, C. J. (1991). Synchronous bursts of action potentials in ganglion cells of the developing mammalian retina. *Science, 252*, 939–943.

Miller, B. R., Walker, A. G., Barton, S. J., & Rebec, G. V. (2011). Dysregulated neuronal activity patterns implicate corticostriatal circuit dysfunction in multiple rodent models of Huntington's disease. *Frontiers in Systems Neuroscience, 5*, 26.

Nex Technologies. (2014). *NeuroExplorer Manual*. Nex Technologies.

Ni, Z. G., Bouali-Benazzouz, R., Gao, D. M., Benabid, A. L., & Benazzouz, A. (2001). Time-course of changes in firing rates and firing patterns of subthalamic nucleus neuronal activity after 6-OHDA-induced dopamine depletion in rats. *Brain Research, 899*, 142–147.

Nicolas, J., Hendriksen, P. J. M., van Kleef, R. G. D. M., de Groot, A., Bovee, T. F. H., Rietjens, I. M. C. M., et al. (2014). Detection of marine neurotoxins in food safety testing using a multielectrode array. *Molecular Nutrition and Food Research, 58*, 2369–2378.

Odawara, A., Katoh, H., Matsuda, N., & Suzuki, I. (2016). Physiological maturation and drug responses of human induced pluripotent stem cell-derived cortical neuronal networks in long-term culture. *Science Reports, 6*, 1–14.

O'Keefe, J., & Recce, M. L. (1993). Phase relationship between hippocampal place units and the EEG theta rhythm. *Hippocampus, 3*, 317–330.

Otto, T., Eichenbaum, H., Wible, C. G., & Wiener, S. I. (1991). Learning-related patterns of CA1 spike trains parallel stimulation parameters optimal for inducing hippocampal longterm potentiation. *Hippocampus, 1*, 181–192.

Pasquale, V., Martinoia, S., & Chiappalone, M. (2010). A self-adapting approach for the detection of bursts and network bursts in neuronal cultures. *Journal of Computational Neuroscience, 29*(1–2), 213–229.

Pasquale, V., Massobrio, P., Bologna, L. L., Chiappalone, M., & Martinoia, S. (2008). Self-organization and neuronal avalanches in networks of dissociated cortical neurons. *Neuroscience, 153*, 1354–1369.

Paulsen, O., & Sejnowski, T. J. (2000). Natural patterns of activity and long-term synaptic plasticity. *Current Opinion in Neurobiology, 10*, 172–179.

Pike, F. G., Meredith, R. M., Olding, A. W. A., & Paulsen, O. (2004). Postsynaptic bursting is essential for 'Hebbian' induction of associative long-term potentiation at excitatory synapses in rat hippocampus. *The Journal of Physiology, 518*, 571–576.

Pimashkin, A., Kastalskiy, I., Simonov, A., Koryagina, E., Mukhina, I., & Kazantsev, V. (2011). Spiking signatures of spontaneous activity bursts in hippocampal cultures. *Frontiers in Computational Neuroscience, 5*, 1–12.

Pluta, S., Naka, A., Veit, J., Telian, G., Yao, L., Hakim, R., et al. (2015). A direct translaminar inhibitory circuit tunes cortical output. *Nature Neuroscience, 18*, 1631–1640.

Radons, G., Becker, J. D., Dülfer, B., & Krüger, J. (1994). Analysis, classification, and coding of multielectrode spike trains with hidden Markov models. *Biological Cybernetics, 71*, 359–373.

Raichman, N., & Ben-Jacob, E. (2008). Identifying repeating motifs in the activation of synchronized bursts in cultured neuronal networks. *Journal of Neuroscience Methods, 170*, 96–110.

Rhoades, B. K., & Gross, G. W. (1994). Potassium and calcium channel dependence of bursting in cultured neuronal networks. *Brain Research, 643*, 310–318.

Schultz, W. (1998). Predictive reward signal of dopamine neurons. *Journal of Neurophysiology, 80*, 1–27.

Schultz, W., Dayan, P., & Montague, P. R. (1997). A neural substrate of prediction and reward. *Science, 275*, 1593–1599.

Selinger, J. V., Kulagina, N. V., O'Shaughnessy, T. J., Ma, W., & Pancrazio, J. J. (2007). Methods for characterizing interspike intervals and identifying bursts in neuronal activity. *Journal of Neuroscience Methods, 162*(1–2), 64–71.

Senn, V., Wolff, S. B. E., Herry, C., Grenier, F., Ehrlich, I., Gründemann, J., et al. (2014). Long-range connectivity defines behavioral specificity of amygdala neurons. *Neuron, 81*, 428–437.

Sherman, S. M. (2001). Tonic and burst firing: Dual modes of thalamocortical relay. *Trends in Neurosciences, 24*, 122–126.

Singh, A., Mewes, K., Gross, R. E., DeLong, M. R., Obeso, J. A., & Papa, S. M. (2016). Human striatal recordings reveal abnormal discharge of projection neurons in Parkinson's disease. *Proceedings of the National Academy of Sciences of the United States of America, 113*, 9629–9634.

Steriade, M., Timofeev, I., & Grenier, F. (2001). Natural waking and sleep states: A view from inside neocortical neurons. *Journal of Neurophysiology, 85*, 1969–1985.

Tam, D. (2002). An alternate burst analysis for detecting intra-burst firings based on inter-burst periods. *Neurocomputing, 46*, 1155–1159.

Thomas, M. J., Watabe, A. M., Moody, T. D., Makhinson, M., & O'Dell, T. J. (1998). Postsynaptic complex spike bursting enables the induction of LTP by theta frequency synaptic stimulation. *The Journal of Neuroscience, 18*, 7118–7126.

Thomson, A. M. (1997). Activity-dependent properties of synaptic transmission at two classes of connections made by rat neocortical pyramidal axons in vitro. *The Journal of Physiology, 502*, 131–147.

Tobler, P. N., Dickinson, A., & Schultz, W. (2003). Coding of predicted reward omission by dopamine neurons in a conditioned inhibition paradigm. *The Journal of Neuroscience, 23*, 10402–10410.

Tokdar, S., Xi, P., Kelly, R. C., & Kass, R. E. (2010). Detection of bursts in extracellular spike trains using hidden semi-Markov point process models. *Journal of Computational Neuroscience, 29*(1–2), 203–212.

Turnbull, L., Dian, E., & Gross, G. (2005) The string method of burst identification in neuronal spike trains. *Journal of Neuroscience Methods, 145*(1–2), 23–35.

Valdivia, P., Martin, M., LeFew, W. R., Ross, J., Houck, K. A., & Shafer, T. J. (2014). Multi-well microelectrode array recordings detect neuroactivity of ToxCast compounds. *Neurotoxicology, 44*, 204–217.

Välkki, I. A., Lenk, K., Mikkonen, J. E., & Kapucu, F. E. (2017). Network-wide adaptive burst detection depicts neuronal activity with improved accuracy. *Frontiers in Computational Neuroscience, 11*, 40.

Van Den Pol, A. N., Obrietan, K., & Belousov, A. (1996). Glutamate hyperexcitability and seizure-like activity throughout the brain and spinal cord upon relief from chronic glutamate receptor blockage in culture. *Neuroscience, 74*, 653–674.

Van Huizen, F., Romijn, H. J., & Habets, A. M. M. C. (1985). Synaptogenesis in rat cerebral cortex cultures is affected during chronic blockade of spontaneous bioelectric activity by tetrodotoxin. *Developmental Brain Research, 19*, 67–80.

Van Pelt, J., Corner, M. A., Wolters, P. S., Rutten, W. L. C., & Ramakers, G. J. A. (2004). Longterm stability and developmental changes in spontaneous network burst firing patterns in dissociated rat cerebral cortex cell cultures on multielectrode arrays. *Neuroscience Letters, 361*, 86–89.

Van Pelt, J., Vajda, I., Wolters, P. S., Corner, M. A., & Ramakers, G. J. A. (2005). Dynamics and plasticity in developing neuronal networks in vitro. *Progress in Brain Research, 147*, 173–188.

Van Pelt, J., Wolters, P. S., Corner, M. A., Rutten, W. L. C., & Ramakers, G. J. A. (2004). Long-term characterization of firing dynamics of spontaneous bursts in cultured neural networks. *IEEE Transactions on Biomedical Engineering, 51*, 2051–2062.

Wagenaar, D., Demarse, T. B., & Potter, S. M. (2005). MeaBench: A toolset for multi-electrode data acquisition and on-line analysis. In *Proceedings of 2nd International IEEE EMBS Conference on Neural Engineering* (pp. 518–521)

Wagenaar, D. A., Pine, J., & Potter, S. M. (2006). An extremely rich repertoire of bursting patterns during the development of cortical cultures. *BMC Neuroscience, 7*, 11.

Walker, A. G., Miller, B. R., Fritsch, J. N., Barton, S. J., & Rebec, G. V. (2008). Altered information processing in the prefrontal cortex of Huntington's disease mouse models. *The Journal of Neuroscience, 28*, 8973–8982.

Weliky, M., & Katz, L. C. (1999). Correlational structure of spontaneous neuronal activity in the developing lateral geniculate nucleus in vivo. *Science, 285*, 599–604.

Weyand, T. G., Boudreaux, M., & Guido, W. (2001). Burst and tonic response modes in thalamic neurons during sleep and wakefulness. *Journal of Neurophysiology, 85*(3), 1107–1118.

Xu, W., Morishita, W., Buckmaster, P. S., Pang, Z. P., Malenka, R. C., & Südhof, T. C. (2012). Distinct neuronal coding schemes in memory revealed by selective erasure of fast synchronous synaptic transmission. *Neuron, 73*, 990–1001.

Ylä-Outinen, L., Heikkilä, J., Skottman, H., Suuronen, R., Aänismaa, R., & Narkilahti, S. (2010). Human cell-based micro electrode array platform for studying neurotoxicity. *Frontiers in Neuroengineering, 3*, 1–9.

Zhang, X., & Shasha, D. (2006). Better burst detection. In *Proceedings of the 22nd International Conference on Data Engineering* (p. 146).

Zhu, Y., & Shasha, D. (2003). Efficient elastic burst detection in data streams. In *Proceedings of Ninth ACM SIGKDD International Conference on Knowledge Discovery and Data Mining* (pp. 336–345).

Reconstruction of Functional Connectivity from Multielectrode Recordings and Calcium Imaging

Paolo Bonifazi and Paolo Massobrio

Abstract In the last two decades, increasing research efforts in neuroscience have been focused on determining both structural and functional connectivity of brain circuits, with the main goal of relating the wiring diagram of neuronal systems to their emerging properties, from the microscale to the macroscale. While combining multisite parallel recordings with structural circuits' reconstruction in vivo is still very challenging, the reductionist in vitro approach based on neuronal cultures offers lower technical difficulties and is much more stable under control conditions. In this chapter, we present different approaches to infer the connectivity of cultured neuronal networks using multielectrode array or calcium imaging recordings. We first formally introduce the used methods, and then we will describe into details how those methods were applied in case studies. Since multielectrode array and calcium imaging recordings provide distinct and complementary spatiotemporal features of neuronal activity, in this chapter we present the strategies implemented with the two different methodologies in distinct sections.

Keywords Cross-correlation · Functional connectivity · Calcium imaging · Spontaneous activity · Spike trains

1 Introduction

In this chapter, we will present how microelectrode array (MEA) and calcium imaging (abbreviated as "CaIm" in what follows within this chapter) recordings can be used to study the connectivity of cultured neuronal networks. From a

P. Bonifazi (✉)
Biocruces Health Research Institute, Barakaldo, Spain

IKERBASQUE, Basque Foundation for Science, Bilbao, Spain

P. Massobrio
Department of Informatics, Bioengineering, Robotics, System Engineering (DIBRIS), University of Genova, Genoa, Italy
e-mail: paolo.massobrio@unige.it

wider perspective, understanding the relationships between the structural and functional connectivity in neuronal circuits is one of the big challenges of modern neurosciences (Friston 2011). This is a multiscale problem where the dynamics of the circuits is shaped by the cellular types composing them and the way cells connect (microscale), and scales up to circuits forming large-scale brain networks (macroscale). Brain functions arise synergistically from the neural dynamics emerging on the multiscale neural connectivity substrate, in a sort of loop where structure shapes dynamics and dynamics reshape structure. The complexity of the neural connections and the difficulties of combining multisite parallel recordings with structural circuits' reconstruction in in vivo experimental models hampered the systematic study of the emergent properties of neuronal circuitries. To this end, the reductionist in vitro approach based on dissociated cultures or slices where the activity of multiple neurons can be monitored has been extensively used to extract the topological properties of neuronal circuits (Bonifazi et al. 2009, 2013; Feldt et al. 2011; Poli et al. 2015). Thanks to the recent advances in multichannel and imaging recording techniques (cf., Chapters "Large Scale, High-Resolution Microelectrode Arrays for Interrogation of Neurons and Networks" and "Active High-Density Electrode Arrays: Technology and Applications in Neuronal Cell Cultures"), it is nowadays possible to record the activities of thousands of neurons simultaneously making more detailed the reconstruction of the topological properties of the network.

1.1 Functional Versus Structural Connectivity

When we talk about the topology of neural circuits/networks, we can mostly distinguish two forms: the structural and functional topology. While the neural units define the nodes of the networks (i.e., neurons in the microscale and brain regions/circuits in the macroscale), the links between the nodes can represent *structural connections* (i.e., synapses or myelinated fibers depending on the scale) or *functional connections* (Feldt et al. 2011). *Functional connections* are defined as statistical dependencies between the neurophysiological events of the nodes, and they are inferred on the basis of pairwise correlations among the neuronal activity, by means of different approaches ranging from correlation-based to model-based methods. Similar to functional connectivity, *effective connectivity* is a further class of connectivity estimated from the activity of the neuronal systems, and it is aimed at revealing causal relationships between the activity of the neural elements. In the following, to keep a simplified approach, we will just refer to structural and functional connections as those arising respectively from the anatomical connectivity and the statistics of the activity of the neural nodes.

   If structural connectivity is responsible for the physical architecture of the synaptic connections within a neuronal assembly, functional networks give an indication about how peculiar dynamics is sustained by the network connectivity. However, the persistence of functional networks, directly estimated by the spontaneous activity of

neuronal ensembles, is influenced by the underlying structural connectivity: current evidence suggests that structural connections are predictive of functional ones (and vice versa), and that, more relevantly, the topological properties of a structural network are maintained in a functional one (Bullmore and Sporns 2009). Thus, if a strong interplay between functional and structural networks exists, estimation of functional connectivity may be a useful way to infer structural connectivity (Stetter et al. 2012). When a structural morphological reference is not available, it is crucial to have reliable methods that can identify functional links that partly reconstruct the network architecture and therefore the topological features.

Before entering into the details of the methodologies used to infer the network topology based on MEAs and CaIm recordings (i.e., on the dynamics of the neuronal activity), it is important to remind the reader that when such methodologies are applied to reconstruct directed functional connectivity, they identify statistically resolved temporal relationships between the activity of the neurons. The further attempt to link directed functional connections to structural connections, and to quantify the match between functional and structural connections, does not relate directly to the existence or not of well-defined temporal relationship. The existence of time-lagged activity between neuronal pairs do not necessarily go through monosynaptic paths but could emerge by more complex dynamics (such as synchronization). Therefore, identifying functional connections and studying the match between functional and structural connections are two distinct problems although related. And this also means that functional connections not matched by structural connections are not mistaken, by simply display statistical features in the neuronal firing not related to a direct anatomical connection.

1.2   Spatiotemporal Resolution Constraints for Inferring Connectivity: Differences Between Multielectrode and Calcium Imaging Recordings

Before entering into the details of the different analyses implemented and proposed in the few works studying connectivity in neuronal cultures, it is worth pointing out the few main features characterizing the difference between MEAs and CaIm recordings, since they constrain the reconstruction of the network topology.

Although the recent application of high-density MEAs partially changed the scenario (Eversmann et al. 2003) (cf., also Section II "Large scale, high-resolution microelectrode arrays for interrogation of neurons and networks"), historically, MEAs and CaIm recordings were characterized by opposite spatiotemporal resolutions (Weisenburger and Vaziri 2018) having MEAs high temporal and low spatial resolution, while vice versa applied for CaIm.

Standard low-density MEA recordings (i.e., the first MEA generation with a few dozen electrodes (Fejtl et al. 2006)) typically capture the activity of one or more "unknown" neuron per electrode, the so-called multiunit activity (Bonifazi et al. 2005). Single neuron resolution can be achieved only classifying subsets of spikes

through spike sorting which allows to identify the activity of the single neurons displaying sufficiently high signal-to-noise ratio in the extracellular recordings (Lefebvre et al. 2016; Rey et al. 2015). More challenging remains to distinguish the cellular type of the recorded cell (e.g., inhibitory versus excitatory cells (Becchetti et al. 2012)). Cell type sorting has been proposed for specific cellular types (such as fast spiking cells, which are putative inhibitory cells), and using metrics to quantify the variability of the spiking activity such as the Fano Factor (Becchetti et al. 2012). On the contrary, CaIm allows to image the activity of dozen or thousands of cells (depending on the culture density and objective magnification (Weisenburger and Vaziri 2018)) with single cell resolution, and the cellular type of each imaged neuron can be revealed by post hoc immunostaining (see below Fig. 8) or online by genetically encoded fluorescent markers (such as GFP and RFP (Bonifazi et al. 2009)).

The high spatial resolution achieved by CaIm is mostly harmed by artefacts due to the light scattering and by contamination of signals generated by overlapping cellular processes (Lichtman and Denk 2011). In fact, only mono-layered neuronal networks in culture can be easily imaged with single cell resolution (using wide field imaging), while 3D cultured networks require more advanced (and often more expensive) imaging methodologies to achieve similar resolution (Marom et al. 2017).

While CaIm has better spatial resolution compared to the one of MEAs, the opposite applies for the temporal resolution, since the high sampling frequency of MEAs drastically overcome the slow dynamics and limited dynamical range of calcium indicators (Herzog et al. 2011). MEAs offer the possibility to reconstruct neuronal firing within the network at submillisecond precision, that is, with single action potential resolution. On the contrary, also when using very fast optical signal detectors (such as latest generation CMOS cameras reaching a maximum of few kHz acquisition rate (Weisenburger and Vaziri 2018)), the dynamics of the calcium indicators and the calcium binding process, either limit the possibility to resolve action potential trains at single spike resolution or to detect isolated single spikes (due to low signal to noise (Bovetti et al. 2017)). Typically, calcium signals from cultured networks performed with a magnification between $4\times$ to $20\times$ on large fields of view (spanning in size from several hundreds of micrometers to few millimeters (Tibau et al. 2013)) originate from the spontaneous synchronized bursting activity of the neurons, in an ON-OFF fashion, mostly reflecting if a neuron participate or not in an event which recruit several or all neurons in the network (Kanner et al. 2018). At higher magnifications (such as $40\times$ (Herzog et al. 2011)), also isolated spikes or intrinsic spontaneous firing of neurons could be resolved, although the number of recorded cells would be limited to a few units (Herzog et al. 2011). Therefore, in a large field imaging ($4\times$ to $20\times$ magnification) the temporal information offered by CaIm signals is mostly related to the firing burst onset.

The estimation of functional connections in in vitro neuronal circuits follows two different approaches: the first one relies on the analysis of the acquired raw signals (such as in Figs. 1a and 8a), while the second one deals with point processes (e.g., spike trains). Specifically, a spike train is a binary time series where 1's mark
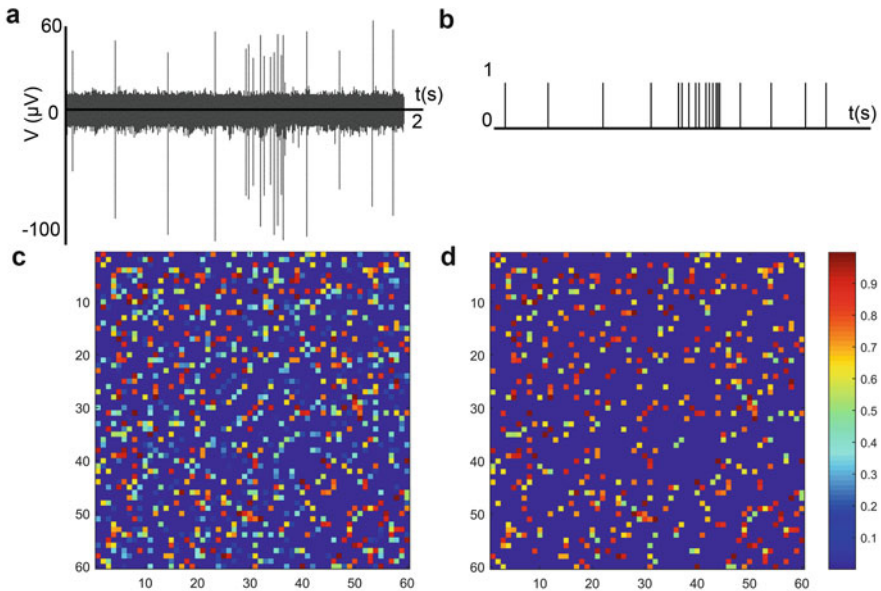
Fig. 1 (**a**) Typical pattern of electrophysiological activity displayed by a mature cortical culture, where a mix of spiking and bursting activity appears. (**b**) By means of spike detection algorithms is possible to translate the time series (raw data) into a point process (spike train). (**c**) Connectivity Matrix (CM) computed by applying cross-correlation to a MEA with 60 recording sites. (**d**) Applying a thresholding procedure, in the CM only the most significant links are preserved

the timing where spikes are detected (i.e., action potentials in the case of MEA recordings and calcium events in the case of CaIm; see Figs. 1b and 7b1).

Given the abovementioned distinctions between the CaIm and MEA recordings which necessarily determine the algorithmic implementation of correlation-based and information theory-based metrics, in the following, we will present in separated sections the methodologies and results about the inference of functional connections in neuronal cultures using MEAs, and CaIm.

2 Connectivity Inference from MEA Recording

2.1 Correlation-Based Methods for Inferring Functional Connectivity

Inferring the functional connectivity of a neuronal network from spike data is not straightforward (Van Bussel et al. 2011). Statistical analysis of spike train data was pioneered in 1969 by Perkel et al. (1967) and followed by more than four decades of methodology development in this area. Cross-correlation-based

methods remain the main statistics to evaluate interactions among the elements in a neuronal network, and produce a weighted assessment of the connections' strength. Correlation-based techniques include independent components analysis and various measures of synchrony (Ventura et al. 2005), cross-correlation (Salinas and Sejnowski 2001), correlation coefficient (Bedenbaugh and Gerstein 1997), and partial correlation (Eichler et al. 2003).

Generally, correlation-based algorithms produce as output a symmetric connectivity matrix (CM), often represented as false color map (Fig. 1c). This matrix is symmetric since correlation functions are symmetric by definition (cf., Sects. 2.1 and 2.2). The (i, j) element of the CM contains the peak value (i.e., the maximum) of the cross-correlation function evaluated around zero time lag: thus, CM comprises both weak and strong connections. However, weak and nonsignificant connections tend to obscure the relevant network topology made up of strong and significant links, and therefore they are often discarded by applying thresholding methods. Different thresholding procedures with different levels of complexity can be found in the literature. There are complex thresholding methods based on shuffling procedures (Grun and Rotter 2010) which destroy the possible correlation between pairs of electrodes, obtaining independent data (i.e., surrogate data). The simplest thresholding procedure makes use of a hard threshold, defined in function of the CM values (Poli et al. 2016). This thresholding procedure is strongly dependent on the distribution of the CM's values. Shuffling techniques are more precise and less heuristic, but they are computationally expensive. At the end of the thresholding procedure the achieved thresholded connectivity matrix (TCM) contains the statistically significant links (Fig. 1d) and can be used to characterize the functional topological properties of the network.

Nonetheless, correlation-based methods allow to recognize the directionality and the strength of the connections by observing the peak latency from zero and the peak value of the cross-correlogram, respectively. If the peak falls in the negative portion of the correlation window, the connection is directed from j to i (meaning that the electrode j is presynaptic for the electrode i). An opposite situation corresponds to the peak found in the correlation window's positive portion. If the peak falls in the central bin, no indications can be obtained about the direction of the detected connection.

In the next two sections, we will present and describe cross-correlation and partial correlation methods to infer functional connectivity in dissociated cultures coupled to MEAs. Afterwards, some applications and recent results will be presented and discussed.

2.2 Cross-Correlation

Cross-correlation (CC) measures the frequency at which one particular neuron or electrode fires ("target") as a function of time, relative to the firing of an event in another one ("reference"). Mathematically, the correlation function represents the

average value of the product of two spike trains. Given a reference electrode x and a target electrode y, the correlation function reduces to a simple probability $C_{xy}(\tau)$ of observing a spike in one train y at time $(t + \tau)$, given that there was a spike in a second train x at time t; τ is called the time shift or the time lag. We define the cross-correlation as follows:

$$C_{xy}(\tau) = \frac{1}{\sqrt{NxNy}} \sum_{s=1}^{Nx} x(t_s) y(t_s - \tau) \tag{1}$$

where t_s indicates the timing of a spike in the x train, N_x is the total number of spikes in the x train, and N_y is the total number of spikes in the y train. Cross-correlation is limited to the interval [0,1] and symmetric $C_{xy}(\tau) = C_{yx}(-\tau)$. The cross-correlogram is then defined as the correlation function computed over a chosen correlation window (W, $\tau = [-W/2, W/2]$). The factor $\frac{1}{\sqrt{NxNy}}$ is the normalization factor.

Different shapes of cross-correlograms can be obtained from pairs of analyzed spike trains. The occurrence of significant departures from a flat background in the cross-correlogram (i.e., a peak or a trough) is an indication of a functional connection (Aertsen and Gerstein 1985). In particular, a peak corresponds to an excitatory connection and a trough to an inhibitory link. The different amplitude of the peaks can be related to the existence of different levels of synchronization between neural spike trains.

Starting from Eq. (1), the extraction of negative peaks (rather than troughs) obtained through a simple filtering operation and followed by distinct thresholding operations for excitatory and inhibitory connections, permits to identify a significant percentage of inhibitory connections with a high level of accuracy. Theoretically, cross-correlation is able to detect both an increase and a decrease of the synchrony between spike trains related to putative interconnected neurons. However, in real experimental data, the cross-correlogram is very jagged making difficult the detection of small peaks and troughs, and, apart from specific conditions (i.e., high and tonic firing rate), hindering the detection of inhibition. A recently devised approach (Pastore et al. 2018) consists in a simple postprocessing of the cross-correlation histogram, obtaining what it has been called filtered and normalized cross-correlation histogram (FNCCH, in curly brackets of Eq. (2)). Given a reference neuron x and a target neuron y, Eq. (2) provides the mathematical definition of the absolute peak of the FNCCH.

$$\text{FNCCH}_{xy_{peak}} = C_{xy}(\tau) \mid \tau = \underset{t}{\arg\max} \left\{ \left| C_{xy}(t) - \frac{1}{W} \sum_{v=-\frac{W}{2}}^{v=\frac{W}{2}} C_{xy}(v) \right| \right\} \tag{2}$$

where W is the time window where FNCCH is evaluated. The filtering procedure consists to subtract the mean value of the cross-correlogram (in the time window W) to the values of the normalized cross-correlogram $C_{xy}(v)$, $v \in [-W/2, W/2]$.
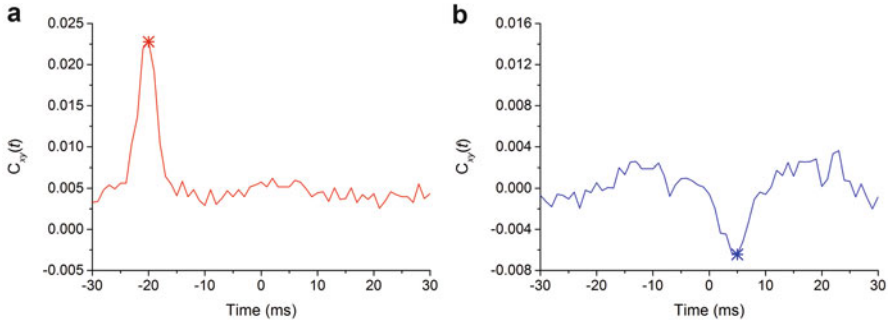
Fig. 2 Example of two cross-correlograms relative to a functional (**a**) excitatory and (**b**) inhibitory connection identified by the FNCCH. Adapted from Pastore et al. (2018)

The subsequent peaks extraction operation is performed by considering the absolute values to compute the highest peak. In this way, it is possible to distinguish between peaks and troughs by taking into account the original sign, being a positive value referred to an excitatory link and, conversely, being a negative value referred to an inhibitory one. Figure 2 shows an application of the FNCCH applied to two examples of synthetic (i.e., simulated) spike trains. Panel A refers to an excitatory connection, while panel B refers to an inhibitory one. The two correlograms show clearly different shapes (highlighted by the normalization procedure) which allow to distinguish between excitatory and inhibitory links.

2.3 Partial Correlation

Although several versions of cross-correlation have been developed in the last years (cf., Sect. 2.2) this approach has the intrinsic limitation not to distinguish between direct and indirect connections. To overcome such a limitation, in 1976, Brillinger et al. introduced the concept of partial coherence (Brillinger et al. 1976) in which the effects of the activity of all other spike trains (assumed to be additive) could be removed. After a long period where the partialization process disappears in the computational studies, in 2003, Eichler and coworkers developed a new partialization method in the time domain, based on a scaled version of the partial covariance density, known as *scaled partial covariance density* (SPCD) (Eichler et al. 2003). SPCD combines the advantages of cross-correlation histograms and of partialization analysis in the frequency domain. Practically, the method reads peaks and troughs in the same way as cross-correlation histograms, as excitatory and inhibitory connections respectively, and then it allows to discriminate direct and indirect connections and common inputs. Here below, we will present the mathematical derivation of the partial correlograms.

Let x, y be two neurons belonging to a population V. Let $R_{xy}(\tau)$ be their correlation, and $R_{xx}(\tau)$ and $R_{yy}(\tau)$ the autocorrelation of x and y, respectively. The Fourier transform of $R_{xy}(\tau)$, that is, the cross-spectral density $S_{xy}(\omega)$, defines the spectral coherence $SCh_{xy}(\omega)$ that can be written as follows:

$$SCh_{xy}(\omega) = \frac{S_{xy}(\omega)}{\sqrt{S_{xx}(\omega)\, S_{yy}(\omega)}} \tag{3}$$

where $S_{xx}(\omega)$ and $S_{yy}(\omega)$ are the Fourier transform of $R_{xx}(\tau)$ and $R_{yy}(\tau)$, respectively.

The partialization process introduced by Brillinger et al. (1976) removes from $S_{xy}(\omega)$ the effect Z of all other (possibly multivariate) spike trains of the population V in the following way:

$$Z = V - [x, y] \tag{4}$$

$$S_{xy|Z}(\omega) = S_{xy}(\omega) - S_{xZ}(\omega)\, S_{ZZ}^{-1}(\omega)\, S_{Zy}(\omega) \tag{5}$$

where $S_{ZZ}(\omega)$ is autocorrelation of Z in the frequency domain and the inverse Fourier transform of $S_{xy \mid Z}(\omega)$, $R_{xy \mid Z}(t)$, is the partial covariance density. $|C_{xy \mid Z}(\omega)|^2$ corresponds to the partial coherence function, while the partial spectral coherence can be defined by the inversion of the spectral matrix $S(\omega)$ of the whole set of nodes (Dahlhaus et al. 1997; Eichler et al. 2003). Thus, if $G(\omega) = S(\omega)^{-1}$, we can write:

$$S_{xx|V\setminus\{x\}}(\omega) = \frac{1}{G_{xx}(\omega)} \tag{6}$$

$$S_{yy|V\setminus\{y\}}(\omega) = \frac{1}{G_{yy}(\omega)} \tag{7}$$

$$C_{xy|Z}(\omega) = -\frac{G_{xy}(\omega)}{\sqrt{G_{xx}(\omega)\, G_{yy}(\omega)}} \tag{8}$$

$$S_{xy|Z}(\omega) = \frac{C_{xy|Z}(\omega)}{1 - \left|C_{xy|Z}(\omega)\right|^2} \tag{9}$$

$$S_{xy|Z}(\omega) = -\frac{G_{xy}(\omega)}{\sqrt{G_{xx}(\omega)\, G_{yy}(\omega)}} \frac{C_{xy|Z}(\omega)}{1 - \left|C_{xy|Z}(\omega)\right|^2} \sqrt{S_{xx|V\setminus\{x\}}(\omega)\, S_{yy|V\setminus\{y\}}(\omega)} \tag{10}$$
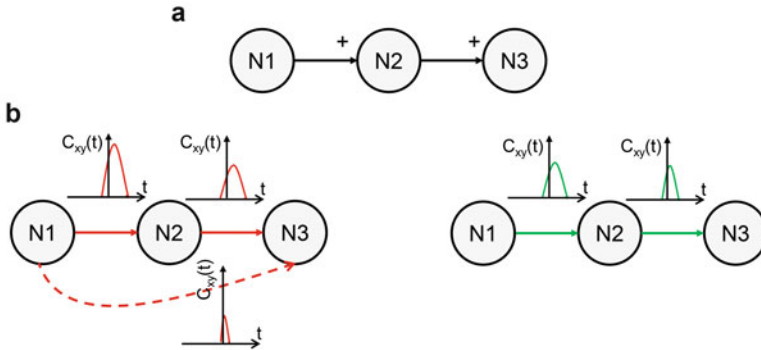
Fig. 3 Sketch showing the working principle of the partial correlation. (**a**) Three neurons are structurally connected by means of excitatory synapses in a feed-forward configuration. (**b**) Cross-correlation (left) allows to infer the correct functional links between neurons, but it also adds an indirect connection (false positive) between neuron N1 and N3 (dashed red line). Partial correlation (right) discharges the indirect connection and the so achieved functional network (green lines) is predictive of the structural one. In the panel B cross-correlograms (red) and partial (green) correlograms are reported above every detected link

To assess functional connectivity we consider the aforementioned SPCD, a scaled version of $R_{xy \mid Z}(t)$ defined as:

$$s_{xy|Z}(t) = \frac{R_{xy|Z}(t)}{\sqrt{r_x r_y}} \tag{11}$$

where r_x and r_y are the maximum peak values of the autocorrelation function.

The sketch depicted in Fig. 3 shows the effect of the partialization process compared to the classical cross-correlation in the simple case of three excitatory neurons arranged in a cascade fashion. Cross-correlation (Fig. 3b left) individuates the structural or morphological connections of the neuronal network (Fig. 3a), but it adds also the indirect link between neuron N1 and N3 (dashed red line). On the other hand, the partialization process embedded in the partial correlation algorithm allows to discharge the indirect link and thus to achieve a functional network (Fig. 3b right) that resembles the morphological connections. In this sense, partial correlation is one of the best methods to infer structural connectivity from functional one (Poli et al. 2016).

2.4 Applications of Correlation-Based Methods

In the next two sections, we will present some applications of the aforementioned methods of correlation used to infer topological properties of large-scale neuronal networks coupled to MEAs.
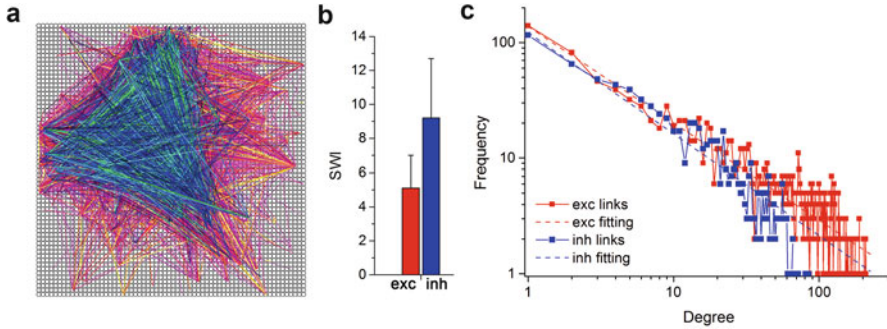
Fig. 4 Cortical networks coupled to MEAs display a complex functional topology characterized by both small-world and scale-free properties. (**a**) Example of functional connectivity map inferred by means of the FNCCH. The excitatory and inhibitory populations are easily recognizable. (**b**) SWI for excitatory (red) and inhibitory (blue) populations. (**c**, **d**) Degree distributions of excitatory (red) and inhibitory (blue) links. Adapted from Pastore et al. (2018)

2.4.1 Network Topologies of Large-Scale In Vitro Cortical Networks

The normalized cross-correlation algorithm described in Sect. 2.1 has been used to extract the topological properties of cortical networks coupled to last-generation MEAs with thousands of microelectrodes (Berdondini et al. 2009). Figure 4a shows a connectivity graphs of a cortical network during its mature stage of development coupled to a MEA with 4096 microelectrodes (Berdondini et al. 2009). Cortical networks coupled to MEA with thousands of recording sites show a clear small-world topology, as the Small-World Index (SWI) of Fig. 4b shows. Nonetheless, this topological configuration is found both in the excitatory and inhibitory subnetworks: in fact, the inhibitory functional links had a SWI equal to 9.2 ± 3.5, while the excitatory links 5.1 ± 1.9. Although these *segregation* properties are typical of small-world networks, in vitro cortical networks present also both inhibitory and excitatory long connections contributing to *integrate* the information. The simultaneous existence of both segregation and integration properties suggests the presence of possible scale-free attributes which have been evaluated by computing the link degree distribution of the excitatory (Fig. 4c) and, inhibitory (Fig. 4d) populations. As Fig. 4 shows, the presence of robust power-law distributions ($R_{exc}^2 = 0.94$, $R_{inh}^2 = 0.92$) demonstrates how cortical networks display a functional organization where both scale-free and small-world properties coexist simultaneously. This result reinforces theoretical predictions which speculate the necessity to have complex topologies to originate the spiking/bursting spatiotemporal patterns of activity which mature cortical cultures display (Massobrio et al. 2015).

The detectability of excitatory and inhibitory connections depends on the firing conditions of the network: it was demonstrated that the detectability of the functional inhibitory links is preserved if the firing rate of the network is more than 5–6 spikes/s (Pastore et al. 2018); if such a condition is not met, a significant
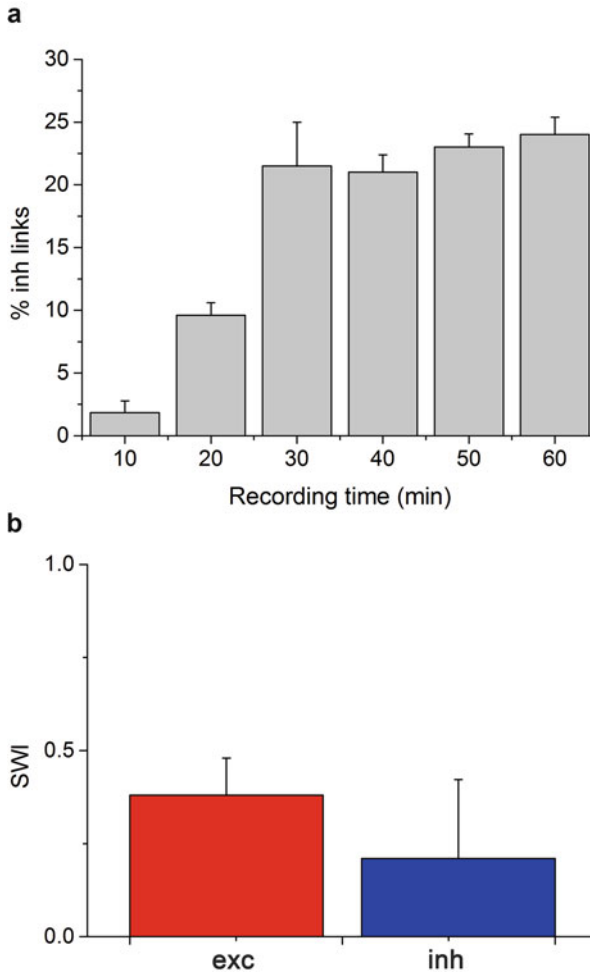
Fig. 5 The detection and identification of links strongly depends on the experimental design. (**a**) Percentage of the inhibitory links revealed by the FNCCH at the varying of the recording time length; (**b**) SWI evaluation in the case of MEA with few recording electrodes. The topological properties cannot be correctly solved

decrease of the performances emerges. Nonetheless, another important condition regards the experimental design. Figure 5a shows the effect of the recording time on the detectability of the inhibitory conditions. Starting from 1 h of data stream, the recording time has been decreased (10 min steps). Below 30 min, the detection of inhibitory links becomes difficult.

The good performances of the cross-correlation algorithm to infer the functional topological properties of a neuronal network are sustained by the technology of the microtransducer devices used to record the electrophysiological activity.

Unlike recently presented findings (Schroeter et al. 2015), we demonstrated that the emergence of small-worldness, cannot be reliably derived or observed in a neuronal population probed by a reduced number (<100) of recording sites. To characterize connectivity properties, besides the importance of well-defined statistical tools used for the analysis, it is fundamental to probe network activity by using large-scale MEAs (i.e., with at least 200 electrodes). As Fig. 5b shows, the apparent random organizations of cortical networks coupled to MEAs with tens of microelectrodes are due to the low number of recording sites; in fact, it is worth to remember that the SWI is computed by comparing cluster coefficient (CC) and average shortest path length (PL) of the analyzed networks to the corresponding values for surrogate random equivalent networks (same number of nodes and links).

2.4.2 From Functional to Structural Connectivity Using Partial Correlation

To evaluate the goodness of partial correlation to infer structural connectivity from functional one, we considered data coming from segregated yet structurally and functionally connected neuronal populations. The rationale was to investigate whether the partialization approach is capable of clearly identify the two segregated populations by means of the modularity index MI[1] (Newman 2006; Sporns 2013). Such an index is extracted by applying the CC and PC algorithms to the spontaneous activity of a dataset of mature cortical assemblies grown in vitro by using a dual-compartment experimental setup (Kanagasabapathi et al. 2012). We quantified whether and to what extent the methods identified the segregation effects. Figure 6a, b shows two examples of functional connectivity graphs, obtained by means of PC applied to the two experimental setups (i.e., the standard MEA device Fig. 6a) and the dual compartment system (Fig. 6b: the black lines indicate the functional connections that cross the physical barrier between the compartments). The compartmentalization effect was identified by all connectivity methods (Fig. 6c); however, the modularity detected by PC was much higher and more significantly different than CC and one-delay TE; PC modularity $\sim$0.63 $\pm$ 0.04, $p < 0.001$; CC and one-delay TE modularity <0.5 $\pm$ 0.03, $p < 0.01$ and $p < 0.05$ respectively). This is a clear proof about the actual performance of the connectivity methods used in these experimental conditions. Therefore, this result confirms the idea that PC can be conveniently applied to estimate the structural topology of the network.

---

[1]Modularity Index (MI) quantifies the degree to which a network can be clustered into small groups (modules). It measures the strength of the division of a network into modules. Networks with high modularity have dense connections between the nodes within modules but sparse connections between nodes in different modules.
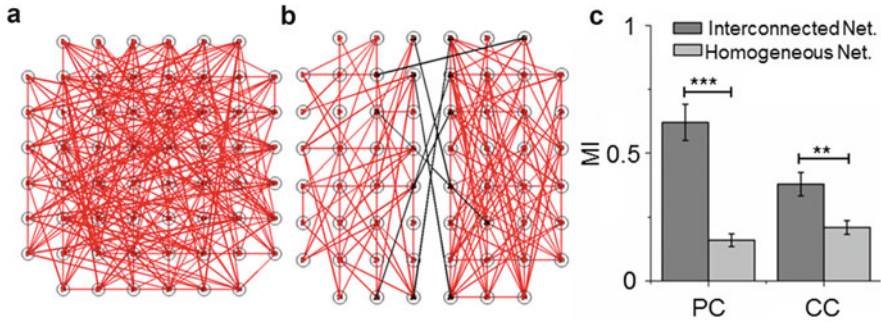
Fig. 6 (**a**) Example of functional connectivity map obtained by applying the PC algorithm to a homogeneous cortical network. (**b**) Connectivity map obtained by applying the PC algorithm to a dual compartment network. (**c**) Modularity index (MI) obtained by applying PC, CC to the experimental data (homogeneous (grey) and interconnected (dark grey) networks). Adapted from Poli et al. (2016)

3 Connectivity Inference from Calcium Imaging Recordings

Contrary to the vast literature reporting different methodologies and results on in vitro neuronal networks' connectivity reconstructed from multielectrode recordings, much less studies have been trying to infer topological network properties in cultures using CaIm. In the last 10 years a vast literature was devoted to the analysis of calcium signals, in order to reliably reconstruct underlying neuronal firing and the emerging functional connections, mostly due to the accumulating dataset from in vivo experimental studies (Weisenburger and Vaziri 2018). Indeed, it is important to note that, the electrical patterns and the dynamics generated by different circuits in different experimental conditions (such slices vs. in vivo intact circuits, adulthood vs development, anesthetized vs awake, etc.) can be very different (Buzsaki 2006), for example the highly synchronous events generated in in vitro developmental hippocampal circuits compared to the sparse activity observed in the cortical circuits in adult mice during behavior (Bonifazi et al. 2009; Spanne and Jörntell 2015). In this context, the activity of neuronal cultures is characterized by spontaneous and highly synchronous events, similarly to circuits during development or in absence of stimuli (such as anaesthesia or in resting conditions) (Marom and Shahaf 2002). So when we try to reconstruct functional connectivity using CaIm in neuronal cultures, we have to think about the constraints imposed on this analysis by the intrinsic emergent activity patterns of this neuronal system, where network-wise synchronized calcium spikes are generated, as we will discuss more in detail below (see Figs. 7 and 8). The above constraint and characteristics in the dynamics of cultured circuits, explain why only a limited body of the literature of CaIm and connectivity has been focused on neuronal cultures.

Given the above introductory notions, we will next introduce the two main methodologies reported in literature to reconstruct the connectivity of the cultured
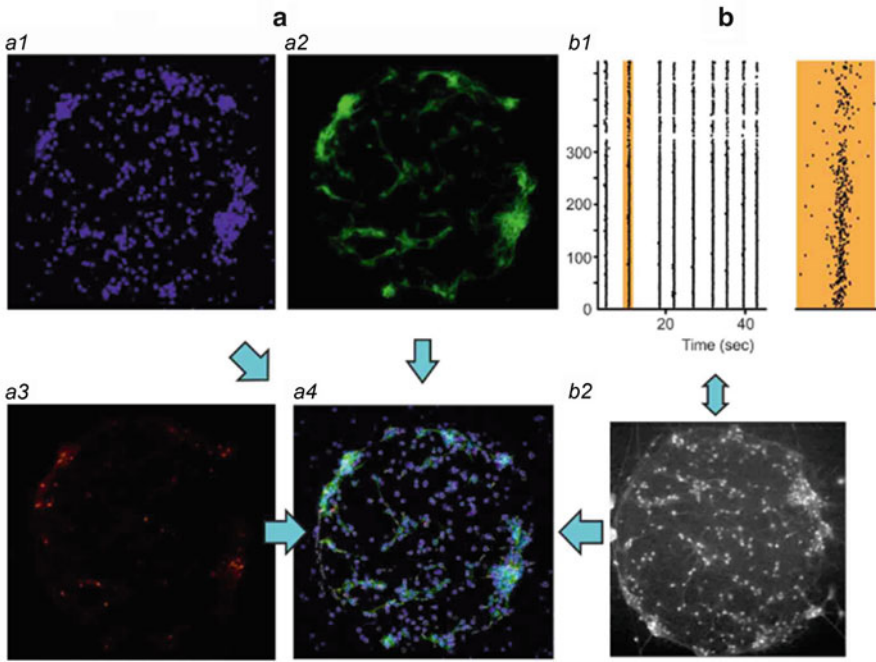
Fig. 7 Linking single neuron dynamics to cellular type by immunocytochemistry and calcium imaging. (**a**) Immunocytochemical staining revealing cellular nuclei (blue, DAPI, *a1*), neuronal cells (green, MAP 2, *a2*), GABAergic neurons from a primary cortical culture (red, GAD67, *a3*). In panel (*a4*), the contours of the cells monitored through calcium imaging (white) are superimposed to the merged immunocytochemical pictures. (**b**) Monitoring the dynamics of the neuronal circuit through calcium imaging. Raster plot (*b1* left plot) of the activity of the circuit (shown in panel *a*) displaying stereotyped spontaneous network synchronizations (broken vertical lines). The activity of a representative network synchronization (marked in orange) is shown with higher temporal resolution on the right orange plot (bottom scale bar 0.5 s). The cells loaded with the calcium indicator OGB are shown in the panel (*b2*) (objective magnification 10×, field of view 800 × 800 μm). Figure and legend adapted from Bonifazi et al. (2013)

networks using CaIm, mostly arising from (Bonifazi et al. 2009, 2013; Orlandi et al. 2014; Stetter et al. 2012). The two methodologies use two complementary approaches: while in one case (Orlandi et al. 2014; Stetter et al. 2012) the whole raw signals are used to assess the functional connectivity using generalized transfer entropy (GTE, a more elaborated version of the original "transfer entropy" introduced by Schreiber (2000)), in the other case (Bonifazi et al. 2009, 2013) solely the timing of the firing onset of neurons (i.e., the onsets of calcium spikes) is used for reconstructing the network connectivity. We will describe these two methodologies separately in the next two sections.
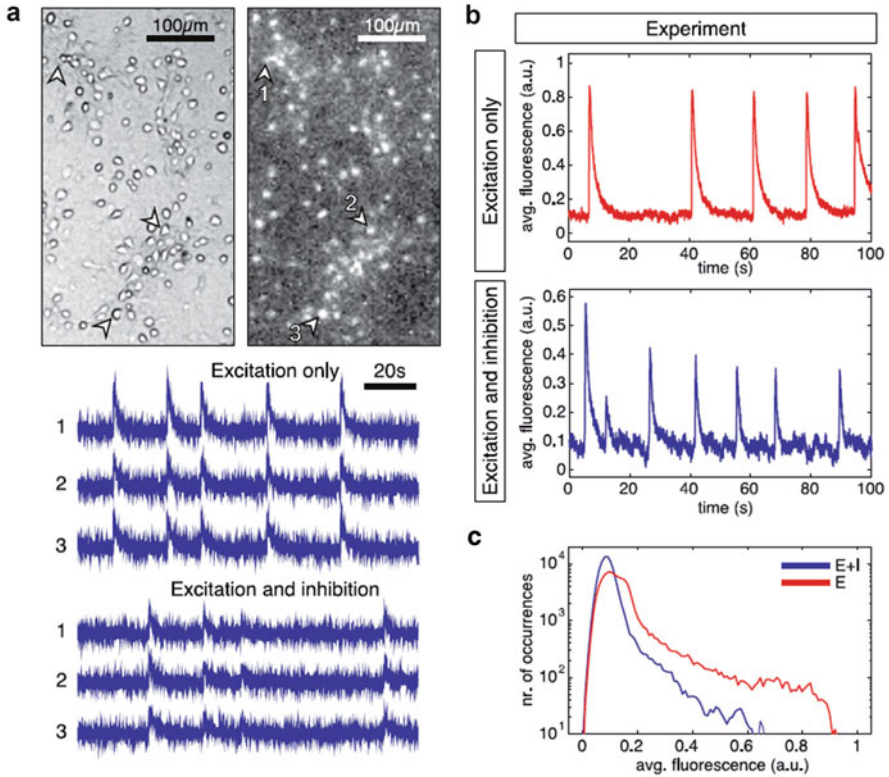
Fig. 8 Neuronal network dynamics. (**a**) Top: Bright field and fluorescence images of a small region of a neuronal culture at day in vitro 12. Bright spots correspond to firing neurons. Bottom: Representative time traces of recorded fluorescence signals of three individual neurons. The numbers beside each trace identify the neurons on the images. Data shows, for the same neurons, the signal in recordings with only excitation active ("E") and the signal with both excitation and inhibition active ("E + I"). (**b**) Population-averaged fluorescence signals for: a disinhibited network ("E–only" data; inhibition was silenced through application of saturating concentrations of bicuculline) and for a network in presence of excitation and inhibition ("E + I" data). Network bursts appear as a fast increase of the fluorescence signal followed by a slow decay. Bursts are more frequent and display lower and more heterogeneous amplitudes in the presence of inhibitory connections. (**c**) Histogram of population-averaged fluorescence intensity for a 1 h recordings. Data is shown in semilogarithmic scale for clarity. Red curves correspond to the "E–only" condition, and the blue curves to the "E + I" one. Figure and legend adapted from Orlandi et al. (2014) and Stetter et al. (2012)

3.1 Inferring Networks' Connectivity Using Generalized Transfer Entropy

Transfer entropy (Schreiber 2000) is a metric derived from information theory to quantify the transfer of information between two processes (Beckenbach 1956;

Granger 1969) and it has been extensively applied to identify directed functional connections between neurons. Deeper in the neuronal firing context, TE is a directed pairwise metric quantifying "causal influence" or "improved predictability" (Pereda et al. 2005) between two neurons, that is, it provides an estimation of how much the past activity (or state, we will use these words as synonymous here) of a source neuron (n_S) predict the future state of a target neuron (n_T) after having removed any contribution in n_T originating from its own past activity. When applied to the time series of the CaIm signals, TE is calculated across consecutive image frames and therefore the slow temporal resolution of the CaIm (typically in the order of few dozens of milliseconds (Lichtman and Denk 2011)) opposite to the fast dynamics of neurons and synaptic transmission (few milliseconds), represents a clear bottleneck in the information flow reconstruction, being a significant portion of it (such as those mediated by monosynaptic connections) hidden within the same time (i.e., camera) frame. Since in this context the use of TE would be missing important temporal features, Stetter and colleagues (Orlandi et al. 2014; Stetter et al. 2012) proposed, and validated in silico, the use of an extended definition of the TE, called generalized transfer entropy (GTE), which also incorporate the predictability of the state of the n_T based the state of the n_s at the same time frame. Note that in (Stetter et al. 2012), the GTE is applied not directly to the calcium traces but to the first derivative time series of the neurons, that is, after a minimal preprocessing step that also allow to improve the signal-to-noise ratio of the raw signal.

Before proceeding to the details of the application of the GTE to raw calcium signals data, another important factor has also to be considered about the CaIm time series arising from neuronal cultures.

As already pointed out above, the synchronized bursting dynamics of the neuronal cultures and the limited temporal resolution of the CaIm, result in very stereotyped neuronal calcium signals across cells, as those shown in the left panel in Fig. 8. Therefore, in order to more finely dissect directed functional connections, it is also important to separate the major dynamical regimes emerging from the same topological organization, that is, the synchronous bursts or network-wise events (corresponding to the peaks in Fig. 8b), and the interburst activity mostly shaped by pairwise dynamics (Stetter et al. 2012). Conditioning the analysis to different level of network activity as reflected by the average value of calcium signal in the whole network (Stetter et al. 2012) (Fig. 9a), can provide access at different functional regimes in the network.

Figure 9 show the reconstructed directed functional connections in a simulated network composed of excitatory neurons when the GTE analysis is limited to distinct network regimes (seven network regimes are marked, refer to the Fig. 9 legend for the definition). Clearly different dynamical states of the network correspond to different functional connectivity maps, with the best match between functional and structural topology obtained when the activity in between network synchronizations is considered (regime II and III).

Figure 10a quantifies with a receiver operating characteristic (ROC) curve the clear advantage of using same bin interaction and network regime selection
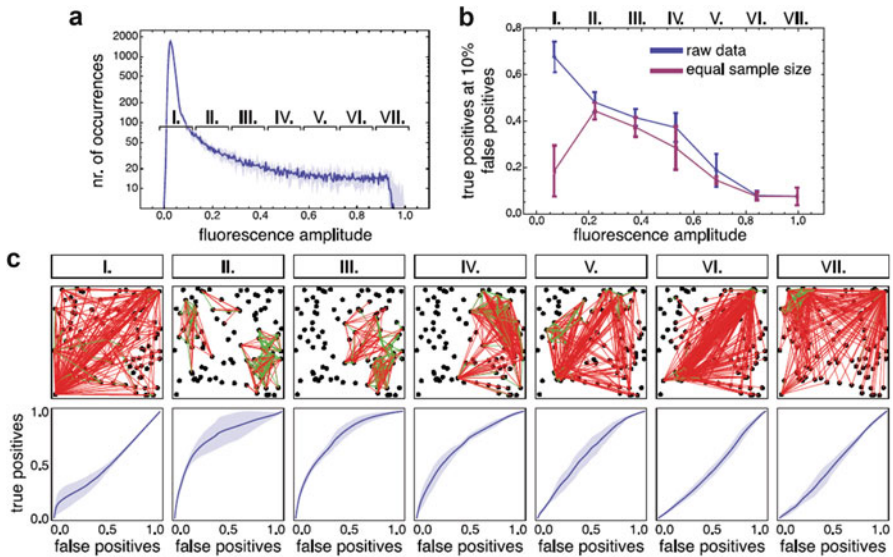
Fig. 9 Dependence of the directed functional connectivity on the dynamical state. (**a**) The distribution of averaged fluorescence amplitudes is divided into seven fluorescence amplitude ranges. The functional connectivity associated to different dynamical regimes is then assessed by focusing the analysis on specific amplitude ranges. (**b**) Quality of reconstruction as a function of the average fluorescence amplitude of each range. The blue line corresponds to an analysis carried out using the entire data sampled within each interval, while the red line corresponds to an identical number of data points per interval. (**c**) Visual representation of the reconstructed network topology (top 10% of the links only), together with the corresponding ROC curves, for the seven dynamical regimes studied. Edges marked in green are present in both the reconstructed and the real topology, while edges marked in red do not match any actual structural link. Reconstructions are based on an equal number of data points in each interval, therefore reflecting the equal sample size performance (red curve) in panel B. Interval I corresponds to a noise-dominated regime; intervals II to IV correspond to interburst intervals with intermediate firing rate and provide the best reconstruction; and intervals V–VII correspond to network bursts with highly synchronized neuronal activity. Simulations were carried out on a network with local topology (l∼0:25 mm) and light scattering in the fluorescence dynamics. The results were averaged over six network realizations, with the error bars in B and the shaded regions in C indicating a 95% confidence interval. Figure and legend adapted from Stetter et al. (2012)

(conditioning) on the match between structural and functional connections. With a 10% level of false positives, 75% true positive connections are achieved.

When focusing on the connection type, GTE is not capable to discriminate inhibitory from excitatory connections (Fig. 10c). However, in the case the cell types are known, the identification of inhibitory connections drastically improves (Fig. 10b) although never reaching the performance of excitatory connection identification. Since post hoc staining of neuronal cultures do allow the identification of GABAergic neurons (Bonifazi et al. 2013) (Fig. 7), using GTE in such conditions would allow to obtain good reconstruction of inhibitory and excitatory connection maps.
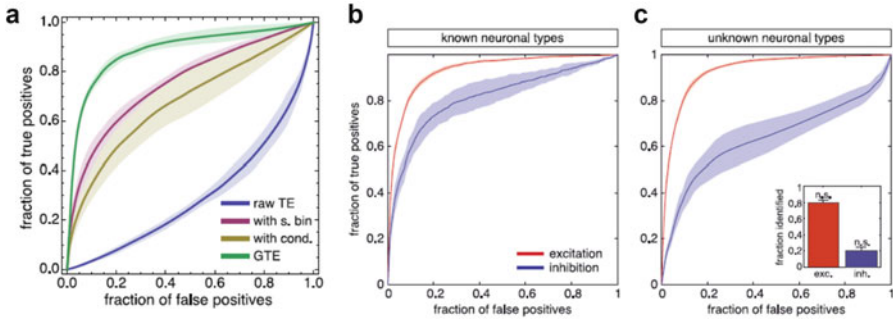
Fig. 10 (**a**) ROC curves for network topology reconstruction based on three TE formulations: conventional TE (blue), generalized TE with same bin interactions only (red) or also including optimal conditioning (yellow). Note that a remarkable boost in performance is obtained only when the inclusion of same-bin interactions and optimal conditioning are combined together (green color curves). (**b**) ROC curves for the GTE reconstruction of a network with both excitatory and inhibitory connections active, supposing to know a priori information about neuronal type. (**c**) same as panel B but for identification of excitatory and inhibitory connections, when information on neuronal type is inaccessible. Figure and legend adapted from Orlandi et al. (2014) and Stetter et al. (2012)

3.2 Reconstructing Functional Connectivity Maps Using Calcium Signal Onsets

A different approach to analyze the CaIm traces, originally developed for the analysis of developing hippocampal circuits imaged using two-photon microscopy, and later applied also to neuronal cultures, has been described by Bonifazi et al. (2009, 2013). In this approach, the calcium traces of each neuron are converted into binary time series where the ones mark the times of neuronal firing onset, that is, the onset of calcium signals. Analysis between time series based on cross-correlations (Bonifazi et al. 2009, 2013; Feldt et al. 2011) is used to identify directed functional connections, that is, repeatedly and statistically significant time lagged activations between neurons. Essentially, given the firing onset time series f of neuron a, the distribution of events occurring in neuron b at different time lags is calculated according to:

$$D_{ab}(\tau) = \sum_{t=|\tau|}^{T-|\tau|} f_a(t) \cdot f_b(t + \tau)$$ (12)

where t is the index of the time frames and T the total number of frames and τ the time lag. The quantification of the distribution of time-lagged occurrences is typically calculated in the frames covering the interval of half second so, for a camera acquisition rate of F, the range is $-F/2 < \tau < F/2$.

Statistical tests like Kolmogorov–Smirnov and Student's *t-test* are used to quantify the significant distinction of the distribution D_{ab} respectively from (1)

a uniform distribution corresponding to neurons with totally uncorrelated firing onsets and (2) a Gaussian with zero mean, corresponding to neurons activating simultaneously with time lag zero. When these two conditions are fulfilled, a link is directed either from *a* to *b*, if the average time lag was lower than zero, or from *b* to *a* if it was higher than zero.

Since most of the spontaneous activity in neuronal cultures (such as in developing neuronal circuits) is characterized by network-wise events recruiting most of the cells in a few dozens or hundreds of milliseconds, the main rationale of this approach is to avoid to include functional connections characterized by zero delay correlations which arise due both to the low temporal resolution of the imaging system, and to the calcium indicator not capable to resolve the fast network synchronization process, as discussed above.

Once directed functional connections are identified, metrics derived from complex networks can be calculated to highlight network properties, such as input and output node degree. Using such an approach it has been demonstrated the existence of GABAergic hub neurons in the developing hippocampal circuits (Bonifazi et al. 2009), that is, highly developed cells combining a high degree of output functional connectivity, effective connectivity, and structural connectivity. In addition, directed functional connectivity has been used in neuronal cultures to describe the functional reorganization induced after lesion (Bonifazi et al. 2013) (Fig. 11).

A temporal analysis of the firing onset time series related to the directed functional connectivity description is also provided by computing the "time-correlation graph" (Bonifazi et al. 2009, 2013; Marissal et al. 2012). In this case the cross-correlation between firing onsets time series of individual neurons is used to estimate the average correlation and average time of activation of each neuron relative to all others. Specifically, given any neuronal pair *(a,b)* and the cross-correlation $CC_{ab}(\tau)$ of the firing onsets time series f_a and f_b, the maximum cross-correlation value ($CC_{ab}^{\max}$) and the time lag of its occurrence ($\tau^{\max}_{ab}$) are first computed. Finally, for each given neuron *i*, the average maximum cross-correlation and time occurrence are calculated according to the formulas:

$$\langle CC_i^{\max} \rangle = \frac{1}{N} \sum_{i \neq j} CC_{ij}^{\max} \tag{13}$$

$$\langle \tau_i^{\max} \rangle = \frac{1}{N} \sum_{i \neq j} \tau_{ij}^{\max} \tag{14}$$

where *N* is the total number of neurons and $1 \leq i \leq N$. In this way the signature of the firing of each neuron to the rest of the network can be summarized by these two scalars which can be plotted in the time-correlation graph. Figure 12 shows the time-correlation graph for the cultured cortical network shown in Fig. 7, highlighting in red also the GABAergic cells (identified from post hoc immunochemical staining). The time-correlation graph allows to separate the neuronal populations early and late activated in the network events respectively plotted on the left (i.e., with a time lag <0), and on the right (i.e., with a time lag >0) sides of the graph. Top left dots in the time-correlation graph represent the neurons with highest reliable activation
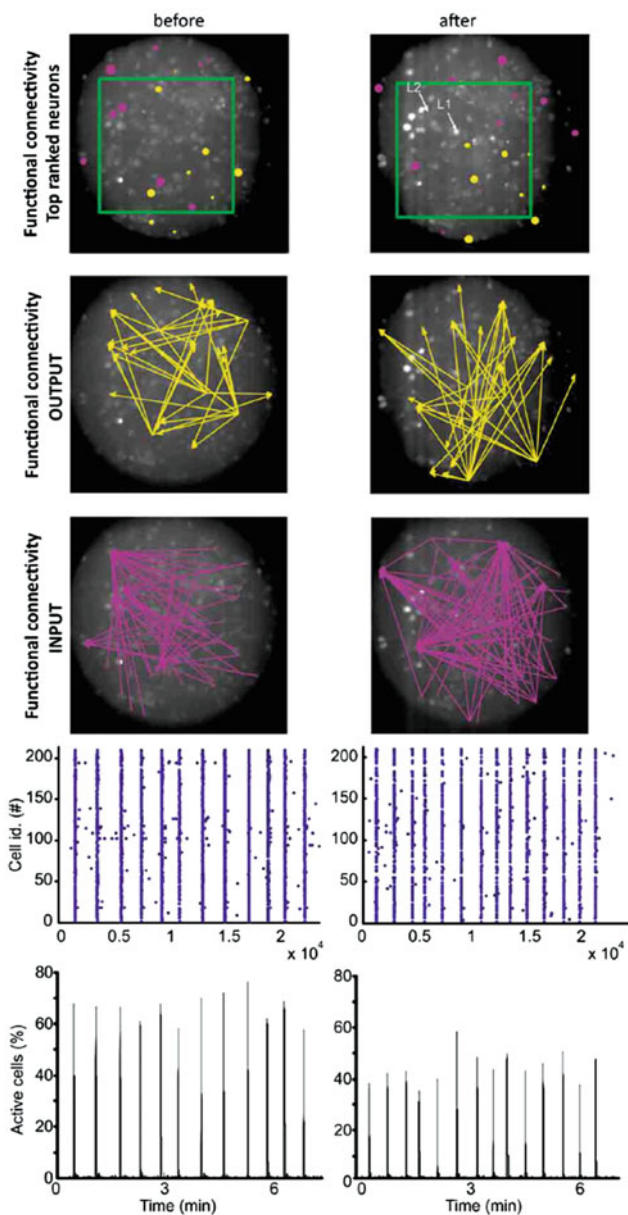
Fig. 11 Directed functional connectivity before (left) and after (right) circuit's lesion. The number of OUTPUT and INPUT functional connections has been calculated for all the imaged neurons based on the temporal correlation between the firing onsets of the neurons. The ten top ranked cells, that is, the cells with the largest number of functional OUTPUT (yellow) and INPUT connections (pink), are represented in the top row. For graphic clarity, the connectivity graphs shown in the second and third rows (respectively INPUT and OUTPUT connections) include only the five top ranked cells. The locations of the two lesions (L1 and L2) are marked by the white arrows. The field of view is a circular region of 244 μm diameter. The raster plot (representing the firing onsets) and the fraction of activated cells are shown respectively in the fourth and fifth row. Figure and legend adapted from Bonifazi et al. (2013)
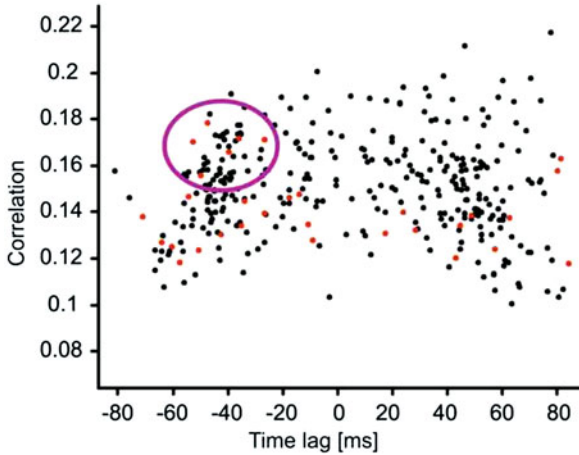
Fig. 12 Time-correlation graph for the circuit shown in Fig. 8 plotting for each imaged neuron the average correlation and average time of activation relative to all other cells. Red dots indicate GABAergic cells. The violet circle highlights GABAergic cells reliably activated at the synchronization build up possibly playing a key role in the orchestration of network synchrony similarly to what previously documented for the developing hippocampal circuits (Bonifazi et al. 2009). Figure and legend adapted from Bonifazi et al. (2013)

preceding the activation of the other neurons. Interestingly, the existence of a characteristic, early-activated neuronal population within the network synchronizations has been already documented in developing hippocampal circuits (Bonifazi et al. 2009) even in absence of GABAergic transmission (Marissal et al. 2012).

4   Conclusions

The main methodologies presented in this chapter to infer network topology in neuronal cultures are correlation based and information theory based. In the case of calcium imaging, correlation-based analysis was applied on the firing onset of the neurons (point processes), mostly generated by the synchronized neuronal bursts, and allowed to identify neurons early activated in network synchronizations. On the other side, GTE, an information theory-based metric, allowed to identify functional connections with highest match to structural connections when limited to the interburst activity, the latter identified using a conditional methodology on the calcium signal amplitude. Differently from the MEA analysis, the neuronal firing measured with calcium imaging does not allow to reveal inhibitory transmission. Therefore, the extraction of directed functional connectivity using calcium imaging can be related to the transmission type (inhibitory or excitatory) using genetically encoded fluorescent markers or post hoc immunostaining to identify the cell type of each neuron.

On the other hand, the described correlation-based algorithms (namely filtered cross-correlation and partial correlation) applied to the electrophysiological activity of large-scale neuronal assemblies allow to solve two intricate problems: the identification of the inhibitory links as well as the detection of polysynaptic connections that are interneuron mediated.

References

Aertsen, A., & Gerstein, G. L. (1985, August). Evaluation of neuronal connectivity: Sensitivity of crosscorrelation. *Brain Research, 340*, 341–354.

Becchetti, A., Gullo, F., Bruno, G., Dossi, E., Lecchi, M., & Wanke, E. (2012). Exact distinction of excitatory and inhibitory neurons in neural networks: A study with GFP-GAD67 neurons optically and electrophysiologically recognized on multielectrode arrays. *Frontiers in Neural Circuits, 6*, 63.

Beckenbach, E. F. (1956). *Modern mathematics for the engineer*. New York: McGraw-Hill.

Bedenbaugh, P., & Gerstein, G. L. (1997, Auguest 15). Multiunit normalized cross correlation differs from the average single-unit normalized correlation. *Neural Computation, 9*, 1265–1275.

Berdondini, L., Imfeld, K., Maccione, A., Tedesco, M., Neukom, S., Koudelka-Hep, M., et al. (2009). Active pixel sensor array for high spatio-temporal resolution electrophysiological recordings from single cell to large scale neuronal networks. *Lab on a Chip, 9*, 2644–2651.

Bonifazi, P., Difato, F., Massobrio, P., Breschi, G. L., Pasquale, V., Levi, T., et al. (2013). In vitro large-scale experimental and theoretical studies for the realization of bi-directional brain-prostheses. *Frontiers in Neural Circuits, 7*, 40.

Bonifazi, P., Goldin, M., Picardo, M. A., Jorquera, I., Cattani, A., Bianconi, G., et al. (2009, December 4). GABAergic hub neurons orchestrate synchrony in developing hippocampal networks. *Science, 326*, 1419.

Bonifazi, P., Ruaro, M. E., & Torre, V. (2005, December 1). Statistical properties of information processing in neuronal networks. *European Journal of Neuroscience, 22*, 2953–2964.

Bovetti, S., Moretti, C., Zucca, S., Dal Maschio, M., Bonifazi, P., & Fellin, T. (2017, January 5). Simultaneous high-speed imaging and optogenetic inhibition in the intact mouse brain. *Scientific Reports, 7*, 40041.

Brillinger, D. R., Bryant, H. L., & Segundo, J. P. (1976). Identification of synaptic interactions. *Biological Cybernetics, 22*, 213–228.

Bullmore, E., & Sporns, O. (2009, March). Complex brain networks: Graph theoretical analysis of structural and functional systems. *Nature Reviews Neuroscience, 10*, 186–198.

Buzsaki, G. (2006). *Rhythms of the brain*. New York: Oxford University Press.

Dahlhaus, R., Eichler, M., & Sandkuhler, J. (1997, November 7). Identification of synaptic connections in neural ensembles by graphical models. *Journal of Neuroscience Methods, 77*, 93–107.

Eichler, M., Dahlhaus, R., & Sandkuhler, J. (2003). Partial correlation analysis for the identification of synaptic connections. *Biological Cybernetics, 89*, 289–302.

Eversmann, B., Jenkner, M., Paulus, C., Hofmann, F., Brederlow, R., Holzapfl, B., et al. (2003). A 128/spl times/128 CMOS bio-sensor array for extracellular recording of neural activity. In *2003 IEEE international solid-state circuits conference, 2003. Digest of technical papers. ISSCC* (Vol. 1, pp. 222–489).

Fejtl, M., Stett, A., Nisch, W., Boven, K. H., & Möller, A. (2006). *Advances in network electrophysiology: Using multi-electrode arrays*. New York: Springer.

Feldt, S., Bonifazi, P., & Cossart, R. (2011, May). Dissecting functional connectivity of neuronal microcircuits: Experimental and theoretical insights. *Trends in Neuroscience, 34*, 225–236.

Friston, K. J. (2011, January 1). Functional and effective connectivity: A review. *Brain Connectivity, 1*, 13–36.

Granger, C. W. J. (1969). Investigating causal relations by econometric models and cross-spectral methods. *Econometrica, 37*, 424–438.

Grun, S., & Rotter, S. (Eds.) (2010). *Analysis of parallel spike trains* (Series in computational neuroscience). New York: Springer.

Herzog, N., Shein-Idelson, M., & Hanein, Y. (2011, October). Optical validation of in vitro extracellular neuronal recordings. *Journal of Neural Engineering, 8*, 056008.

Kanagasabapathi, T. T., Massobrio, P., Barone, R. A., Tedesco, M., Martinoia, S., Wadman, W. J., et al. (2012). Functional connectivity and dynamics of cortical-thalamic networks co-cultured in a dual compartment device. *Journal of Neural Engineering, 9*, 036010.

Kanner, S., Goldin, M., Galron, R., Ben Jacob, E., Bonifazi, P., & Barzilai, A. (2018, July 31). Astrocytes restore connectivity and synchronization in dysfunctional cerebellar networks. *Proceedings of the National Academy of Sciences of the United States of America, 115*, 8025–8030.

Lefebvre, B., Yger, P., & Marre, O. (2016, November). Recent progress in multi-electrode spike sorting methods. *Journal of Physiology, Paris, 110*, 327–335.

Lichtman, J. W., & Denk, W. (2011, November 4). The big and the small: Challenges of imaging the brain's circuits. *Science, 334*, 618–623.

Marissal, T., Bonifazi, P., Picardo, M. A., Nardou, R., Petit, L. F., Baude, A., et al. (2012). Pioneer glutamatergic cells develop into a morpho-functionally distinct population in the juvenile CA3 hippocampus. *Nature Communications, 3*, 1316.

Marom, A., Shor, E., Levenberg, S., & Shoham, S. (2017). Spontaneous activity characteristics of 3D "optonets". *Frontiers in Neuroscience, 10*, 602.

Marom, S., & Shahaf, G. (2002, February). Development, learning and memory in large random networks of cortical neurons: Lessons beyond anatomy. *Quarterly Reviews of Biophysics, 35*, 63–87.

Massobrio, P., Pasquale, V., & Martinoia, S. (2015). Self-organized criticality in cortical assemblies occurs in concurrent scale-free and small-world networks. *Scientific Reports, 5*, 10578.

Newman, M. E. J. (2006). Modularity and community structure in networks. *Proceedings of the National Academy of Sciences of the United States of America, 103*, 8577–8582.

Orlandi, J. G., Stetter, O., Soriano, J., Geisel, T., & Battaglia, D. (2014). Transfer entropy reconstruction and labeling of neuronal connections from simulated calcium imaging. *PLoS One, 9*, e98842.

Pastore, V. P., Massobrio, P., Godjoski, A., & Martinoia, S. (2018). Identification of excitatory-inhibitory links and network topology in large scale neuronal assemblies from multi-electrode recordings. *PLoS Computational Biology, 14*, e1006381.

Pereda, E., Quiroga, R. Q., & Bhattacharya, J. (2005, September 1). Nonlinear multivariate analysis of neurophysiological signals. *Progress in Neurobiology, 77*, 1–37.

Perkel, D. H., Gerstein, G. L., & Moore, G. P. (1967). Neuronal spike train and stochastic point processes I. the single spike train. *Biophysical Journal, 7*, 391–418.

Poli, D., Pastore, V. P., Martinoia, S., & Massobrio, P. (2016). From functional to structural connectivity using partial correlation in neuronal assemblies. *Journal of Neural Engineering, 13*, 026023.

Poli, D., Pastore, V. P., & Massobrio, P. (2015). Functional connectivity in *in vitro* neuronal assemblies. *Frontiers in Neural Circuits, 9*, 57.

Rey, H. G., Pedreira, C., & Quian Quiroga, R. (2015, October 1). Past, present and future of spike sorting techniques. *Brain Research Bulletin, 119*, 106–117.

Salinas, E., & Sejnowski, T. J. (2001). Correlated neuronal activity and the flow of neural information. *Nature Reviews Neuroscience, 2*, 539–550.

Schreiber, T. (2000, July 10). Measuring information transfer. *Physical Review Letters, 85*, 461–464.

Schroeter, M. S., Charlesworth, P., Kitzbichler, M. G., Paulsen, O., & Bullmore, E. T. (2015). Emergence of Rich-Club topology and coordinated dynamics in development of hippocampal functional networks *in vitro*. *The Journal of Neuroscience, 35*, 5459–5470.

Spanne, A., & Jörntell, H. (2015, July 1). Questioning the role of sparse coding in the brain. *Trends in Neurosciences, 38*, 417–427.

Sporns, O. (2013). Structure and function of complex brain networks. *Dialogues in Clinical Neuroscience, 15*, 247–262.

Stetter, O., Battaglia, D., Soriano, J., & Geisel, T. (2012). Model-free reconstruction of excitatory neuronal connectivity from calcium imaging signals. *PLoS Computational Biology, 8*, e1002653.

Tibau, E., Valencia, M., & Soriano, J. (2013). Identification of neuronal network properties from the spectral analysis of calcium imaging signals in neuronal cultures. *Frontiers in Neural Circuits, 7*, 199.

Van Bussel, F., Kriener, B., & Timme, M. (2011, February 1). Inferring synaptic connectivity from spatio-temporal spike patterns. *Frontiers in Computational Neuroscience, 5*, 3.

Ventura, V., Cai, C., & Kass, R. E. (2005). Statistical assessment of time-varying dependency between two neurons. *Journal of Neurophysiology, 94*, 2940.

Weisenburger, S., & Vaziri, A. (2018). A guide to emerging technologies for large-scale and whole-brain optical imaging of neuronal activity. *Annual Review of Neuroscience, 41*, 431–452.

Open-Source Tools for Processing and Analysis of In Vitro Extracellular Neuronal Signals

Mufti Mahmud and Stefano Vassanelli

Abstract The recent years have seen unprecedented growth in the manufacturing of neurotechnological tools. The latest technological advancements presented the neuroscientific community with neuronal probes containing thousands of recording sites. These next-generation probes are capable of simultaneously recording neuronal signals from a large number of channels. Numerically, a simple 128-channel neuronal data acquisition system equipped with a 16 bits A/D converter digitizing the acquired analog waveforms at a sampling frequency of 20 kHz will generate approximately 17 GB uncompressed data per hour. Today's biggest challenge is to mine this staggering amount of data and find useful information which can later be used in decoding brain functions, diagnosing diseases, and devising treatments. To this goal, many automated processing and analysis tools have been developed and reported in the literature. A good amount of them are also available as open source for others to adapt them to individual needs. Focusing on extracellularly recorded neuronal signals in vitro, this chapter provides an overview of the popular open-source tools applicable on these signals for spike trains and local field potentials analysis, and spike sorting. Towards the end, several future research directions have also been outlined.

Keywords Neuroengineering · Neuronal activity · Neuronal spikes · Local field potentials · Neuronal signal processing and analysis

M. Mahmud (✉)
Computing and Technology, School of Science and Technology, Nottingham Trent University, Nottingham, UK
e-mail: mufti.mahmud@ntu.ac.uk

S. Vassanelli
NeuroChip Lab, Department of Biomedical Sciences, University of Padova, Padova, Italy

233

1 Introduction

Recent technological advancements allowed scientists to have unprecedented access to biological data. These data come from different organs in the body and have been effectively utilized in screening and diagnosis of diseases and their treatment (Mahmud et al. 2018). Brain is the most complex organ in the mammals. Though it is analog, its capability in decision-making and pattern recognition is higher than any existing computing machines (Mahmud et al. 2017). To understand brain's functionality, diagnose disease, and devise treatments, scientists have been investigating it using different approaches (Mahmud and Vassanelli 2016). In last two decades, micro- and nanotechnology underwent an exponential growth in terms of developing novel miniaturized devices and this allowed neuroscientists to target large populations of neurons and record from them to decode the activities of the brain cells (Mahmud et al. 2017; Vassanelli 2011; Vassanelli et al. 2012b,a; Vassanelli 2014; Schröder et al. 2015; Thewes et al. 2016; Jun et al. 2017). However, these novel techniques to acquire neuronal signals generate huge amount of data. And, analyzing this data and mining relevant information is a big challenge. To this goal, individual research groups have contributed towards the development of automated, efficient, and intelligent processing methods and disseminated them to the neuroscientific community (Mahmud and Vassanelli 2016). The interdisciplinary "Neuroengineering" community (Vassanelli and Mahmud 2016) used these tools to mine useful information from these large datasets (Mahmud and Vassanelli 2016). Targeting different applications and needs, these methods deal with processing and analysis of data coming from single or multiple channels. However, with today's increasing number of recording sites accommodated in a single probe, many of these methods are difficult to rescale and fit to analyze these data. Therefore, the community is still in need of novel analysis tools targeting multichannel neurophysiological data coming from high-resolution neuronal probes. This chapter aims in introducing the reader with available open-source toolboxes capable of performing processing and analysis of multichannel extracellular neuronal signals recorded in vitro.

2 State of the Art of Extracellular Neuronal Signal Analysis

Modern neuroscience research has emerged as a data-driven discipline where both experimental and computational approaches go hand-in-hand (see Fig. 1) (Mahmud et al. 2018). The two approaches of neuroscience research are bridged through a relatively new discipline, called data science, which mainly deals with the analytics of the acquired data, and interpretation of the simulated results and design novel experiments suggested by the obtained results.
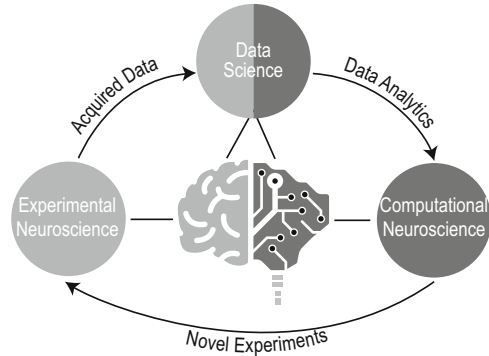
Focusing on the extracellular neuronal signals acquired in vitro, this chapter is going to deal with the data analytics part, and provide an overview of the available open-source data analytics resources which can be exploited to process and analyze the recorded signals. Using the in vitro experimental paradigm (see Fig. 2), mainly two types of signals can be recorded: (1) neuronal spikes and their trains, and (2) field potentials. Therefore, the following subsections will contain the state-of-the-art open-source resources categorized by signal types, e.g., field potentials, and spikes. Despite that the majority of the available resources are application and signal specific, there exist a few toolboxes which provide methods applicable on multiple types of signals. For the sake of simplicity, the tools are divided into following two categories:

- Toolboxes for spike trains and field potentials analysis and
- Toolboxes for spike sorting

It is also worthy to note that majority of the available toolboxes are developed using MATLAB (Mathworks Inc., Natick, USA; www.mathworks.com) and python (www.python.org) programming languages due to their diffused usage in the neuroscience community. In addition, popular programming languages including C, C++, C#, Delphi7, Java, and R have also been employed in some of the toolboxes.

2.1   Toolboxes for Spike Trains and Field Potentials Analysis

With the growing amount data acquired via simultaneously recorded channels from an increasing number of neurons, the neuroengineering community has developed automated toolboxes addressing the required processing and analyses. The following subsections describe—in alphabetical order—popular publicly available toolboxes. Table 1 summarizes the different packages with their representative features.
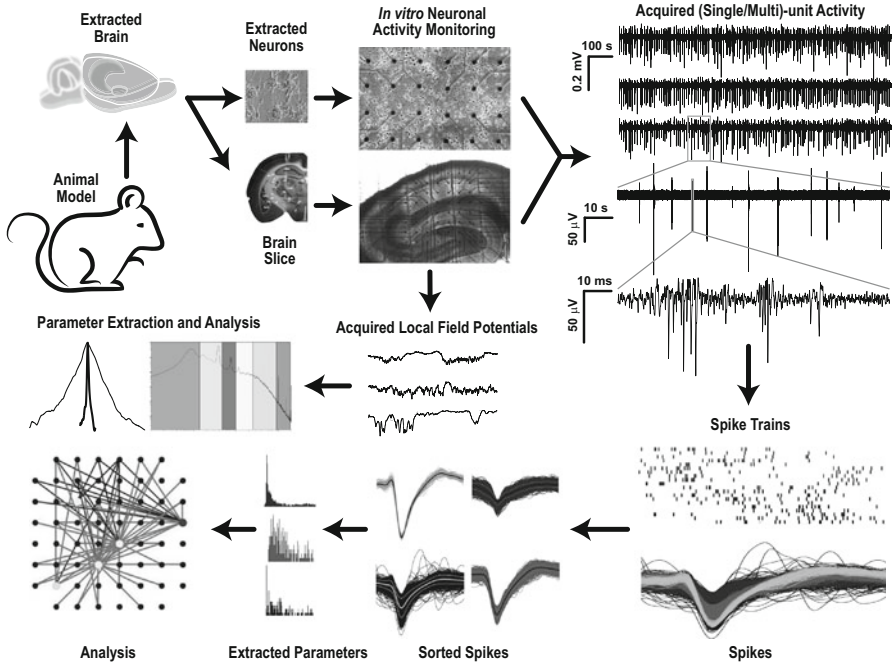
Fig. 2 Exemplary overview of the in vitro neuronal signal acquisition and analysis paradigm

2.1.1 Brain System for Multivariate AutoRegressive Time Series (BSMART)

"BSMART" toolbox is written in MATLAB/C for spectral analysis of neurophysiological signals (Cui et al. 2008). It provides multi- or bivariate AutoRegressive modeling, spectral analysis through coherence and Granger causality, and network analysis. The main analyses include: adaptive (bi-/multi-)variate autoregressive model, fast Fourier transform, Granger causality (Granger 1969), coherence, coherent network analysis, and Granger causality network analysis. Available at http://www.brain-smart.org/.

2.1.2 Chronux

"Chronux" toolbox is developed in MATLAB for the analysis of both point process and continuous data (Bokil et al. 2010). It provides spike sorting, and local regression and multitaper spectral analysis of neural signals. The main analyses include: hierarchical clustering method (Fee et al. 1996), locally weighted sum of squares (Cleveland 1979), local regression fitting and density estimation (Loader 1999), multitaping method (Thomson 1982), coherence, and spike field coherence. Available at http://chronux.org/.

Table 1 Popular spike train and field potential processing and analysis toolboxes with their representative features

Toolbox	Features					
	Lang	PF	GUI DV	DIE	AR	PDP
BSMART	Matlab/C	OSML	Yes	Yes	No	No
Chronux	Matlab	LMW	Yes	No	No	No
DATA-MEAns	Delphi7	W	Yes	No	No	No
FIND	Matlab	OSML	Yes	Yes	No	No
ibTB	Matlab	LMW	No	No	No	No
KNSNDM	C++	LMW	Yes	Yes	Yes	No
MeaBench	C++/Matlab	L	Yes	No	Yes	No
MVGC	Matlab	OSML	No	No	No	No
nSTAT	Matlab	OSML	No	No	No	No
PANDORA	Matlab	LMW	No	Yes	No	EMP
QSpikeTools	Matlab	ML	No	No	Yes	EMP
SigMate	Matlab	OSML	Yes	Yes	Yes	No
sigTOOL	Matlab	OSML	Yes	Yes	No	No
SpiCoDyn	C#	W	Yes	Yes	No	No
SPKTool	Matlab	OSML	Yes	Yes	No	No
STAToolkit	Matlab/C	LMW	Yes	No	No	Yes
ToolConnect	C#	W	Yes	Yes	No	No

Lang Language; *PF* Platform; *GUI DV* GUI and data visualization; *DIE* Data import/export; *AR* Artifact removal; *PDP* Parallel data processing; *KNSNDM* Klusters, NeuroScope, NDManager; *L* Linux; *U* Unix; *M* Mac; *W* Windows; *OSML* Operating system supported by Matlab; *EMP* Embarrassingly parallel

2.1.3   DATA-MEAns

"DATA-MEAns" is a toolbox developed in Borland Delphi 7 (Embarcadero Technologies Inc., Austin, USA) and MATLAB (Bonomini et al. 2005). It provides data visualization, basic analysis (i.e., autocorrelations, perievent histograms, rate curves, PSTHs, ISIs, etc.), and nearest neighbor or k-means clustering. The analyses include: poststimulus time and perievent histogram estimation, auto- and cross-correlation, Fano factor and coherence calculation, event synchrony (Quian Quiroga et al. 2002), and nearest neighbor (Cover and Hart 1967) and K-means (MacQueen 1967) clustering. Available at http://cortivis.umh.es/.

2.1.4   Finding Information in Neural Data (FIND)

"FIND" is a platform-independent framework for the analysis of neuronal data based on MATLAB (Meier et al. 2008). It provides a unified data import function from various proprietary formats simplifying standardized interfacing with analysis tools and provides means for analysis of discrete series of spike events, continuous

time series, and imaging data. Also, it allows simulating multielectrode activity using point-process-based stochastic model. The analyses include: co-variance estimation, point process modeling, pair-wise cross-correlation, asymmetric Savitzky–Golay filter calculation (Savitzky and Golay 1964), response latency differences estimation (Nawrot et al. 2003), and spike detection. Available at http://find.bccn.uni-freiburg.de/.

2.1.5 Information Breakdown ToolBox (ibTB)

"ibTB" is a Matlab-based toolbox which implements information theory methods for spike, LFP, and EEG analysis (Magri et al. 2009). It provides information breakdown technique to decode the encoding of sensory stimuli by different groups of neurons. The major supported analyses include: direct method, quadratic extrapolation (Strong et al. 1998), Panzeri and Treves method (Panzeri and Treves 1996) for bias correction, shuffling procedure (Montemurro et al. 2007), bootstrap bias correction (Optican et al. 1991), and Gaussian method (Misra et al. 2005). The source code can be obtained from the publisher's website (http://static-content.springer.com/esm/art%3A10.1186%2F1471-2202-10-81/MediaObjects/1471-2202-10-81-S1.zip).

2.1.6 Klusters, NeuroScope, and NDManager

"Klusters," "NeuroScope," and "NDManager" are three integrated modules bundled together for processing and analysis of spike and field potential signals (Hazan et al. 2006). Klusters performs spike sorting using KlustaKwik (see Sect. 2.2.3) and displays 2D projection of features, spike traces, correlograms, and error matrix view. NeuroScope allows inspection, selection, and event editing of spike signals as well as local field potentials (LFPs). NDManager facilitates experimental and preprocessing parameter management. The major analyses include: auto- and cross-correlation estimation, spike detection and sorting, and classification expectation–maximization (Celeux and Govaert 1992). Available at http://neurosuite.sourceforge.net/.

2.1.7 MeaBench

"MeaBench" is a toolbox written mainly in C++ with certain parts written in Perl[1] and Matlab. It is intended for data acquisition and online analysis of commercial multielectrode array recordings from Multichannel Systems GmbH (Reutlingen, Germany) (Wagenaar et al. 2005). It allows real-time data visualization, line and

---

[1]https://www.perl.org/.

stimulus artifact suppression, and spike and burst detection and validation. Available at www.danielwagenaar.net/res/software/meabench/.

2.1.8 Multivariate Granger Causality Toolbox (MVGC)

"MVGC" is a toolbox written in MATLAB that implements Wiener–Granger causality (G-causality) on multiple equivalent representations of a vector autoregressive model in both time and frequency domains (Barnett and Seth 2014). The main analyses supported by the toolbox include: ordinary least squares estimation, Wiener (root mean square) method (Levinson 1946), vector autoregressive maximum likelihood estimator method, cross-power spectral density, multitaper method, fast Fourier transform, and unconditional Granger causality. It can be applied to neuroelectric, neuromagnetic, and fMRI signals and can be obtained from http://www.sussex.ac.uk/sackler/mvgc/.

2.1.9 nSTAT

"nSTAT" toolbox is coded in MATLAB and performs spike train analysis in time domain (e.g., Kalman Filtering), frequency domain (e.g., multitaper spectral estimation), and mixed time–frequency domain (e.g., spectrogram) (Cajigas et al. 2012). The supported analyses include: point process generalized linear model (Paninski et al. 2007), generalized linear model-based peristimulus time histogram estimation, Akaike's and Bayesian information criteria, state-space generalized linear model, Kalman filtering, multitaper method, and spectrogram. Available at www.neurostat.mit.edu/nstat/.

2.1.10 PANDORA

"PANDORA" is a MATLAB-based toolbox that extracts user-defined characteristics from spike train signals and creates numerical database tables from them (Gunay et al. 2009). Further analyses (e.g., drug and parameter effects, spike shape characterization, histogramming and comparison of distributions, cross-correlation, etc.) can then be performed on these tables. However, spike detection and feature extraction can also be performed. The supported analyses include: rational database creation from datasets, extraction of spike shape characteristics, Kullback–Leibler divergence measure (Kullback and Leibler 1951) estimation, and resistor-average distance (Johnson et al. 2001) estimation. It is available at https://github.com/cengique/pandora-matlab.

2.1.11 QSpike Tools

"QSpike Tools" is a Linux/Unix-based cloud-computing framework, modeled using client–server architecture and developed in MATLAB/Bash scripts,[2] for processing and analysis of extracellular spike trains (Mahmud et al. 2014). It performs batch preprocessing of CPU-intensive operations for each channel (e.g., filtering, multiunit activity detection, spike sorting, etc.), in parallel, by delegating them to a multicore computer or to a computers cluster. The main analyses include: spike detection and validation, poststimulus time and perievent histogram estimation, burst detection and validation, and spike sorting through Wave_Clus package (see Sect. 2.2.11). It can be obtained from https://sites.google.com/site/qspiketool/.

2.1.12 SigMate

"SigMate" is a MATLAB-based comprehensive framework that allows preprocessing and analysis of EEG, LFPs, and spike signals (Mahmud et al. 2012a). Its main contribution is in the analysis of LFPs which includes data display, file operations, baseline correction, artifact removal, noise characterization, current source density (CSD) analysis, latency estimation from LFPs and CSDs, determination of cortical layer activation order using LFPs and CSDs, and single LFP clustering. The main processing and analyses include: various file operations (e.g., file splitting, concatenation, and column rearranging), latency calculation (Mahmud et al. 2016), detection of cortical layer activation order (Mahmud et al. 2010), current source density analysis (Mahmud et al. 2011), classification of single-trial LFPs (Mahmud et al. 2012c), and spike analysis. The spike analyses are provided through Wave_Clus (see Sect. 2.2.11) toolbox. It can be obtained from https://sites.google.com/site/muftimahmud/codes.

2.1.13 sigTOOL

"sigTOOL" toolbox is written in MATLAB and allows direct loading of a wide range of proprietary file formats (Lidierth 2009). The usable data file formats originate from various hardware vendors such as Alpha Omega, Axon Instruments, Blackrock Microsystems, Cambridge Electronic Design, Heka, MultiChannel Systems, NeuroExplorer, NeuroShare native, and Plexon. The major analyses supported by the toolbox include: auto- or cross-correlation, power spectral analysis, and coherence estimation in addition to usual spike train analysis (i.e., ISI, event auto- and cross-

---

[2]https://en.wikipedia.org/wiki/Bash_(Unix_shell).

correlations, spike-triggered averaging, perievent time histograms, frequencygrams, etc.). Available at http://sigtool.sourceforge.net/.

2.1.14   SpiCoDyn

"SpiCoDyn" is an open-source windows-only graphical user interface-based toolbox focusing on functional-effective connectivity analysis and spiking and bursting dynamics analysis (Pastore et al. 2018). Developed in C#, under the Microsoft .NET platform, it supports HDF5,[3] level 5 MAT files[4] and text files. The toolbox provides optimized implementations of two main transfer entropy algorithms (i.e., delayed transfer entropy and high-order transfer entropy) and provides analysis platform for multiple spike trains originating from large number of electrodes. Available at https://www.nitrc.org/projects/spicodyn/.

2.1.15   Spike Train Analysis Toolkit (STAToolkit)

"STAToolkit" is a MATLAB/C-hybrid toolbox implementing information theoretic methods to quantify how well the stimuli can be distinguished based on the timing of neuronal firing patterns in a spike train (Goldberg et al. 2009). The main analyses include: direct method (Strong et al. 1998), metric space method (Victor and Purpura 1997), binless method (Victor 2002), asymptotically debiased method (Treves and Panzeri 1995), Jackknife debiased method (Thomson and Chave 1991), debiased Ma bound method (Ma 1981), best upper bound method (Paninski 2003), coverage-adjusted method (Chao and Shen 2003), and Bayesian with Dirichlet prior (Wolpert and Wolf 1995). Available at http://neuroanalysis.org.

2.1.16   SPKTool

"SPKTool" is coded in MATLAB for the detection and analysis of neural spiking activity (Liu et al. 2011). It performs spike detection, feature extraction, and manual and semiautomatic clustering of spike trains. Spike detection by thresholding and raw and nonlinear energy of signal, extraction of various spike features (e.g., principal components, peaks, valleys, energy, timestamps, slice of waveforms, etc.), implementation of popular spike-sorting techniques (e.g., K-means, template matching, EM of Gaussian mixed model, valley seeking, manual contour based method, etc.), ISI, Poincare maps, correlation, firing rate histograms, and perievent rasters and histograms. Available at http://spktool.sourceforge.net/.

---

[3] https://support.hdfgroup.org/HDF5/.

[4] https://www.mathworks.com/help/pdf_doc/matlab/matfile_format.pdf.

2.1.17 ToolConnect

"ToolConnect" is a standalone windows-only tool, developed in C#, targeting to infer functional connectivity from spike trains data (Pastore et al. 2016). This toolbox has been optimized for in vitro networks grown on high-density multielectrode arrays. The implemented analyses include: cross- and partial correlation, and joint and transfer entropy. Additionally, it contains several add-ons for the visualization of the functional connectivity graphs as well as extraction of topological features of the network. Available at https://www.nitrc.org/projects/toolconnect/.

2.2 Toolboxes for Spike Sorting

A great amount of efforts have been put towards the development of sophisticated tools capable of accurate spike sorting and analysis. Rey et al. (2015), in their review, outline the primary concepts of spike sorting, the requirements for applying specific techniques, and most importantly, the shortcomings of currently available algorithms. Due to the vast amount of methods and tools available for the purpose, we restrict our discussion only to the popular open-source toolboxes.

2.2.1 EToS

"EToS" or Efficient Technology of Spike sorting is a spike-sorting toolbox aimed mainly at heterogeneous neural population recordings (Takekawa et al. 2012). It is written in C++ implementing multimodality-weighted PCA for feature extraction and variational Bayes for student's t mixture model for clustering. The spike-sorting code is parallelized through OpenMP (www.openmp.org) and available at http://etos.sourceforge.net/.

2.2.2 KiloSort

"KiloSort" is a spike-sorting package developed in MATLAB for handling data coming from MEAs with large number of recording electrodes (Pachitariu et al. 2016). The package uses template matching for detection and clustering of spikes and can handle batch processing using both GPUs and CPUs. The source code can be downloaded from https://github.com/cortex-lab/KiloSort.

2.2.3 KlustaKwik

"KlustaKwik" is a standalone program written in C++ for automatic clustering analysis (Harris et al. 2000) of high-dimensional spiking data by fitting a mixture

of Gaussians and hard expectation–maximization algorithm with unconstrained covariance matrices (Kadir et al. 2014; Rossant et al. 2016). The package can be downloaded from https://github.com/klusta-team/klustakwik.

2.2.4   MClust

"MClust" is a spike-sorting toolbox developed in MATLAB. It supports both manual and automated clustering with possibility to manual feature selection (Redish 2014) on data recorded from single electrode, stereotrode, and tetrode. It allows manual corrections to automated clustering results and can be obtained from http://redishlab. neuroscience.umn.edu/MClust/MClust.html.

2.2.5   NEV2lkit

"NEV2lKit" is a package written in C++ with routines for analysis, visualization, and classification of spikes (Bongard et al. 2014). It is a preprocessor for the analysis of intra- and extracellular spiking neuronal signals. The main purposes served by the toolbox includes: loading ASCII files as well as neural event files (NEV) and extract spike events from them, PCA-based sorting of spikes based on the spike waveform, and saving of spike timestamps, unit information, and the spike signals into ASCII or NEV files. It provides accurate, efficient, and consistency across experiments. Available at http://nev2lkit.sourceforge.net/.

2.2.6   OSort

"OSort" is a template-based, unsupervised, online spike-sorting algorithm written in MATLAB (Rutishauser et al. 2006). It uses residual-sum-of-squares-based distance method and custom thresholds to on-the-fly sort of the recorded spikes. As the algorithm is online, the tool uses a technique where the clusters are built and adapted iteratively over the course of the recording. Available at http://www.urut.ch/new/ serendipity/index.php?/pages/osort.html.

2.2.7   SpikeOMatic

"SpikeOMatic" is a spike-sorting package developed in R (Pouzat and Chaffiol 2009). It implements two sophisticated data generation models, namely Gaussian mixture model (GMM) and dynamic hidden Markov model (DHMM). For statistical inference for the abovementioned models, the tool makes use of expectation–maximization for GMM and Markov chain Monte Carlo method for DHMM. The package can be downloaded from http://www.biomedicale.univ-paris5.fr/ SpikeOMatic/.

2.2.8 Spyke

"Spyke" is a python toolbox for visualizing, navigating, and spike sorting of high-density multichannel extracellular spikes (Spacek et al. 2009). It uses PCA for dimensionality reduction and modified gradient ascent clustering algorithm (Fukunaga and Hostetler 1975; Swindale and Spacek 2014) to classify the features. The sorting method initially assigns each event to a channel and then these channel-based clusters are subdivided into possible distinguished clusters. Available at http://spyke.github.io/.

2.2.9 SpyKING CIRCUS

"SpyKING CIRCUS" is a python toolbox aiming to provide spike sorting for high-density multichannel extracellular spikes (Yger et al. 2018). This semiautomatic spike-sorting package performs highly parallel code execution to handle large number of recording electrodes. Based on a greedy template matching approach and with the help of a smart clustering technique, the package can efficiently sort spikes from up to 4225 channels. The code is available at https://github.com/spyking-circus/spyking-circus with a ground truth dataset at https://zenodo.org/record/1205233/export/hx#.WrORP3XwaV4.

2.2.10 UltraMegaSort2000

"UltraMegaSort2000" is a MATLAB-based toolbox for spike detection and clustering which implements a hierarchical clustering scheme using similarities of spike shape and spike timing statistics, and provides false-positive and false-negative errors as quality evaluation metrics (Fee et al. 1996; Hill et al. 2011). The toolbox also provides the users with tools to manually correct the automatically generated clusters. Available at http://physics.ucsd.edu/neurophysics/software.php.

2.2.11 Wave_Clus

"Wave_Clus" is probably the most popular spike-sorting package to date. Developed in MATLAB, it uses sophisticated wavelet transformation-based time–frequency analysis for feature selection and a "temperature"-based superparamagnetic clustering (Blatt et al. 1996) method to sort the features into different clusters (Quian Quiroga et al. 2004). It is available for downloading at https://github.com/csn-le/wave_clus.

3 Future Perspectives

In terms of offline processing and analysis of extracellular neuronal signals, the neuroscientific community has seen active participation and contribution from diverse disciplines where individual laboratories developed novel tools and techniques and shared them with the community. As a result of these great efforts, now it has been possible to establish some standardized analyses from these available tools. However, it is noteworthy that, to date, only a few tools are available to the community which are capable of doing the extracellular neuronal signal processing and analysis online which is huge bottleneck for future generation closed-loop real-time systems (Mahmud and Vassanelli 2016).

Also, keeping pace with the technological advancements and speed of the Internet, next-generation online distributed processing and analysis tools are becoming increasingly essential. Exploiting the existing institutional infrastructures, it might be possible to transform the interinstitutional competition into multi-institutional collaboration. In such scenario, a vital requirement is to have secure infrastructures where multi-institutional neuronal signal analysis facilities shall be capable of integrating their data and tools seamlessly (Mahmud et al. 2012b) with the option to protect individual institute's proprietary data. Additionally, these infrastructures should support user-friendly interfaces allowing even experimentalists with minimal information technology skills to explore, navigate, and use provided scientific data and services. Towards these goals, cloud computing and service-oriented architectures might be utilized through the distributed infrastructure. These approaches allow better representation of responsibilities taken by the different users in accordance to their granted privileges. As an early example of such systems, the Spike-Sorting Evaluation Project initiative (http://spike.g-node.org/) aims to lay a platform for evaluating the performance of spike-sorting algorithms through sharing benchmark data and receiving spike-sorting results for comparison.

Furthermore, considering the growing usage of in vitro MEA technology in applications contributing to improved quality of life for patients, such as pharmacological screening and stem-cell-derived neuronal cultures (Tanskanen et al. 2018), it is becoming increasingly important to standardize experimental protocols and analysis procedures, and data and code sharing to foster experimental reproducibility and validation of obtained results for a combined and accelerated maturation of ground-breaking discoveries.

In our opinion, the development is expected towards:

– Development of novel tools capable of performing online analyses,
– Design and implementation of secure and protected systems,
– Advance on cloud-based web applications,
– Facilitate easy deployment of data,
– Reusability and sharing of tools with adaptability to changing requirements, and
– Empower researchers to share data and functionalities that they want to publish.

4   Conclusion

With the tremendous growth of neurotechnologies, scientists can acquire data from multiple levels and multiple sources. This poses a great challenge to the neuroscientific community to automatically process and analyze those data in order to find meaningful conclusions towards understanding brain's functioning and to devise translatable technologies towards autonomous diagnosis and treatment strategies for treating brain diseases. This chapter introduced the reader to the popular opensource automated methods for processing and analysis of extracellularly recorded neuronal signals from in vitro devices. Towards the end, some perspective research lines—where future developments are expected—have also been outlined.

References

Barnett, L., & Seth, A. K. (2014). The MVGC multivariate Granger causality toolbox: A new approach to Granger-causal inference. *Journal of Neuroscience Methods, 223*, 50–68.

Blatt, M., Wiseman, S., & Domany, E. (1996 April). Superparamagnetic clustering of data. *Physical Review Letters, 76*, 3251–3254.

Bokil, H., Andrews, P., Kulkarni, J. E., Mehta, S., & Mitra, P. P. (2010). Chronux: A platform for analyzing neural signals. *Journal of Neuroscience Methods, 192*(1), 146–151.

Bongard, M., Micol, D., & Fernandez, E. (2014). NEV2lkit: A new open source tool for handling neuronal event files from multi-electrode recordings. *International Journal of Neural Systems, 24*(4), 1450009.

Bonomini, M. P., Ferrandez, J. M., Bolea, J. A., & Fernandez, E. (2005). DATA-MEAns: An open source tool for the classification and management of neural ensemble recordings. *Journal of Neuroscience Methods, 148*(2):137–146.

Cajigas, I., Malik, W. Q., & Brown, E. N. (2012). nSTAT: Open-source neural spike train analysis toolbox for Matlab. *Journal of Neuroscience Methods, 211*(2), 245–264.

Celeux, G., & Govaert, G. (1992). A classification EM algorithm for clustering and two stochastic versions. *Computational Statistics and Data Analysis, 14*(3), 315–332.

Chao, A., & Shen, T. J. (2003). Nonparametric estimation of Shannon's index of diversity when there are unseen species in sample. *Environmental and Ecological Statistics, 10*(4), 429–443.

Cleveland, W. S. (1979), Robust locally weighted regression and smoothing scatterplots. *Journal of the American Statistical Association, 74*(368), 829–836.

Cover, T., & Hart, P. (1967). Nearest neighbor pattern classification. *IEEE Transactions on Information Theory, 13*(1), 21–27.

Cui, J., Xu, L., Bressler, S. L., Ding, M., & Liang, H. (2008). BSMART: A Matlab/C toolbox for analysis of multichannel neural time series. *Neural Networks, 21*(8), 1094–1104.

Fee, M. S., Mitra, P. P., & Kleinfeld, D. (1996). Automatic sorting of multiple unit neuronal signals in the presence of anisotropic and non-Gaussian variability. *Journal of Neuroscience Methods, 69*(2), 175–188.

Fukunaga, K., & Hostetler, L. (1975). The estimation of the gradient of a density function, with applications in pattern recognition. *IEEE Transactions on Information Theory, 21*(1), 32–40.

Goldberg, D., Victor, J., Gardner, E., & Gardner, D. (2009). Spike train analysis toolkit: Enabling wider application of information–theoretic techniques to neurophysiology. *Neuroinformatics, 7*, 165–178.

Granger, C. W. J. (1969). Investigating causal relations by econometric models and cross-spectral methods. *Econometrica, 37*(3), 424–438.

Gunay, C., Edgerton, J., Li, S., Sangrey, T., Prinz, A., & Jaeger, D. (2009). Database analysis of simulated and recorded electrophysiological datasets with PANDORA's toolbox. *Neuroinformatics, 7*, 93–111.

Harris, K. D., Henze, D. A., Csicsvari, J., Hirase, H., & Buzsaki, G. (2000). Accuracy of tetrode spike separation as determined by simultaneous intracellular and extracellular measurements. *Journal of Neurophysiology, 84*(1), 401–414.

Hazan, L., Zugaro, M., & Buzsaki, G. (2006). Klusters, NeuroScope, NDManager: A free software suite for neurophysiological data processing and visualization. *Journal of Neuroscience Methods 155*, 207–316.

Hill, D. N., Mehta, S. B., & Kleinfeld, D. (2011). Quality metrics to accompany spike sorting of extracellular signals. *The Journal of Neuroscience, 31*(24), 8699–8705.

Johnson, D. H., & Sinanovic, S. (2001). *Symmetrizing the Kullback-Leibler distance*. Available from: http://www.ece.rice.edu/~dhj/resistor.pdf. Accessed 15 April 2016.

Jun, J. J., Steinmetz, N. A., Siegle, J. H., Denman, D. J., Bauza, M., Barbarits, B., et al. (2017 November). Fully integrated silicon probes for high-density recording of neural activity. *Nature, 551*(7679), 232–236.

Kadir, S. N., Goodman, D. F., & Harris, K. D. (2014). High-dimensional cluster analysis with the masked EM algorithm. *Neural Computation, 26*(11), 2379–2394.

Kullback, S., & Leibler, R. A. (1951). On information and sufficiency. *Annals of Mathematical Statistics, 22*(1), 79–86. Available from: http://www.jstor.org/stable/2236703.

Levinson, N. (1946). The wiener (root mean square) error criterion in filter design and prediction. *Journal of Mathematical Physics, 25*(1–4), 261–278.

Lidierth, M. (2009). sigTOOL: A MATLAB-based environment for sharing laboratory-developed software to analyze biological signals. *Journal of Neuroscience Methods, 178*, 188–196.

Liu, X. Q., Wu, X., & Liu, C. (2011). SPKtool: An open source toolbox for electrophysiological data processing. In *International Conference on Biomedical Engineering and Informatics, BMEI 2011* (Vol. 2, pp. 854–857).

Loader, C. (1999). *Local regression and likelihood*. New York: Springer.

Ma, S. k. (1981). Calculation of entropy from data of motion. *Journal of Statistical Physics, 26*(2), 221–240.

MacQueen, J. (1967). Some methods for classification and analysis of multivariate observations. In *Proceedings of the Fifth Berkeley Symposium on Mathematical Statistics and Probability, 1965/66*(1), 281–297.

Magri, C., Whittingstall, K., Singh, V., Logothetis, N., & Panzeri, S. (2009). A toolbox for the fast information analysis of multiple-site LFP, EEG and spike train recordings. *BMC Neuroscience, 10*(1), 81.

Mahmud, M., Bertoldo, A., Girardi, S., Maschietto, M., & Vassanelli, S. (2012a). SigMate: A Matlab-based automated tool for extracellular neuronal signal processing and analysis. *Journal of Neuroscience Methods, 207*(1), 97–112.

Mahmud, M., Bertoldo, A., Maschietto, M., Girardi, S., & Vassanelli, S. (2010). Automatic detection of layer activation order in information processing pathways of rat barrel cortex under mechanical whisker stimulation. In *Conference Proceedings: Annual International Conference of the IEEE Engineering in Medicine and Biology Society, 2010* (6095–6098).

Mahmud, M., Cecchetto, C., Maschietto, M., Thewes, R., & Vassanelli, S. (2017). Towards high-resolution brain-chip interface and automated analysis of multichannel neuronal signals. In *2017 IEEE Region 10 Humanitarian Technology Conference (R10-HTC)* (pp. 868–872).

Mahmud, M., Cecchetto, C., & Vassanelli, S. (2016). An automated method for characterization of evoked single-trial local field potentials recorded from rat barrel cortex under mechanical whisker stimulation. *Cognitive Computation, 8*(5), 935–945.

Mahmud, M., Kaiser, M. S., Hussain, A., & Vassanelli, S. (2018). Applications of deep learning and reinforcement learning to biological data. *IEEE Transactions on Neural Networks Learning Systems, 29*(6), 1–17. [Epub ahead of print].

Mahmud, M., Kaiser, M. S., Rahman, M. M., Rahman, M. A., Shabut, A., Al-Mamun, S., et al. (2018). A brain-inspired trust management model to assure security in a cloud based IoT framework for neuroscience applications. *Cognitive Computation, 10*(5), 864–873. [Epub ahead of print].

Mahmud, M., Pasqualotto, E., Bertoldo, A., Girardi, S., Maschietto, M., & Vassanelli, S. (2011). An automated method for detection of layer activation order in information processing pathway of rat barrel cortex under mechanical whisker stimulation. *Journal of Neuroscience Methods, 196*(1), 141–150.

Mahmud, M., Pulizzi, R., Vasilaki, E., & Giugliano, M. (2014). QSpike tools: A generic framework for parallel batch preprocessing of extracellular neuronal signals recorded by substrate microelectrode arrays. *Frontiers in Neuroinformatics, 8*, 26.

Mahmud, M., Rahman, M. M., Travalin, D., Raif, P., & Hussain, A. (2012b). Service oriented architecture based web application model for collaborative biomedical signal analysis. *Biomedizinische Technik. Biomedical Engineering, 57*(Suppl 1), 780–783.

Mahmud, M., Travalin, D., Bertoldo, A., Girardi, S., Maschietto, M., & Vassanelli, S. (2012c). An automated classification method for single sweep local field potentials recorded from rat barrel cortex under mechanical whisker stimulation. *Journal of Medical and Biological Engineering, 32*(6), 397–404.

Mahmud, M., & Vassanelli, S. (2016). Processing and analysis of multichannel extracellular neuronal signals: State-of-the-art and challenges. *Frontiers in Neuroscience, 10*(Jun), 248.

Meier, R., Egert, U., Aertsen, A., & Nawrot, M. P. (2008). FIND – A unified framework for neural data analysis. *Neural Networks, 21*(8):1085–1093.

Misra, N., Singh, H., & Demchuk, E. (2005). Estimation of the entropy of a multivariate normal distribution. *Journal of Multivariate Analysis, 92*(2), 324–342.

Montemurro, M. A., Senatore, R., & Panzeri, S. (2007). Tight data-robust bounds to mutual information combining shuffling and model selection techniques. *Neural Computation, 19*(11), 2913–2957.

Nawrot, P. M., Aertsen, A., & Rotter, S. (2003). Elimination of response latency variability in neuronal spike trains. *Biological Cybernetics, 88*(5), 321–334.

Optican, L. M., Gawne, T. J., Richmond, B. J., & Joseph, P. J. (1991). Unbiased measures of transmitted information and channel capacity from multivariate neuronal data. *Biological Cybernetics, 65*(5), 305–310.

Pachitariu, M., Steinmetz, N. A., Kadir, S. N., Carandini, M., & Harris, K. D. (2016). Fast and accurate spike sorting of high-channel count probes with KiloSort. In D. D. Lee, M. Sugiyama, U. V. Luxburg, I. Guyon, & R. Garnett (Eds.), *Advances in Neural Information Processing Systems 29* (pp. 4448–4456). Red Hook: Curran Associates, Inc.

Paninski, L. (2003). Estimation of entropy and mutual information. *Neural Computation, 15*(6), 1191–1253.

Paninski, L., Pillow, J., & Lewi, J. (2007). Statistical models for neural encoding, decoding, and optimal stimulus design. *Progress in Brain Research, 165*, 493–507.

Panzeri, S., & Treves, A. (1996). Analytical estimates of limited sampling biases in different information measures. *Network: Computation in Neural Systems, 7*(1), 87–107.

Pastore, V. P., Godjoski, A., Martinoia, S., & Massobrio, P. (2018). SpiCoDyn: A toolbox for the analysis of neuronal network dynamics and connectivity from multi-site spike signal recordings. *Neuroinform, 16*(1), 15–30.

Pastore, V. P., Poli, D., Godjoski, A., Martinoia, S., & Massobrio, P. (2016). ToolConnect: A functional connectivity toolbox for in vitro networks. *Frontiers in Neuroinformatics, 10*, 13.

Pouzat, C., & Chaffiol, A. (2009). Automatic spike train analysis and report generation. An implementation with R, R2HTML and STAR. *Journal of Neuroscience Methods, 181*(1), 119–144.

Quian Quiroga, R., Kreuz, T., & Grassberger, P. (2002 October). Event synchronization: A simple and fast method to measure synchronicity and time delay patterns. *Physical Review E, 66*, 041904.

Quian Quiroga, R., Nadasdy, Z., & Ben-Shaul, Y. (2004). Unsupervised spike detection and sorting with wavelets and superparamagnetic clustering. *Neural Computation, 16*(8), 1661–1687.

Redish, A. D. (2014). *MClust Free-ware spike sorting*. Available from: http://redishlab. neuroscience.umn.edu/MClust/MClust.html. Accessed 07 January 2016.

Rey, H. G., Pedreira, C., & Quian Quiroga, R. (2015). Past, present and future of spike sorting techniques. *Brain Research Bulletin, 119*(Pt B), 106–117.

Rossant, C., Kadir, S. N., Goodman, D. F., Schulman, J., Hunter, M. L., Saleem, A. B., et al. (2016). Spike sorting for large, dense electrode arrays. *Nature Neuroscience, 19*(4), 634–641.

Rutishauser, U., Schuman, E. M., & Mamelak, A. N. (2006). Online detection and sorting of extracellularly recorded action potentials in human medial temporal lobe recordings, in vivo. *Journal of Neuroscience Methods, 154*(1–2), 204–224.

Savitzky, A., & Golay, M. J. E. (1964 July). Smoothing and differentiation of data by simplified least squares procedures. *Analytical Chemistry, 36*(8), 1627–1639.

Schröder, S., Cecchetto, C., Keil, S., Mahmud, M., Brose, E., Dogan, O., et al. (2015). CMOS-compatible purely capacitive interfaces for high-density in-vivo recording from neural tissue. In *Proceedings of 2015 IEEE Biomedical Circuits and Systems Conference (BioCAS)* (pp. 1–4).

Spacek, M., Blanche, T., & Swindale, N. (2009). Python for large-scale electrophysiology. *Front Neuroinform, 2*, 9.

Strong, S. P., Koberle, R., de Ruyter van Steveninck, R. R., & Bialek, W. (1998 Janaury). Entropy and information in neural spike trains. *Physical Review Letters, 80*, 197–200.

Swindale, N. V., & Spacek, M. A. (2014). Spike sorting for polytrodes: A divide and conquer approach. *Frontiers in Systems Neuroscience, 8*(6).

Takekawa, T., Isomura, Y., & Fukai, T. (2012). Spike sorting of heterogeneous neuron types by multimodality-weighted PCA and explicit robust variational Bayes. *Frontiers in Neuroinformatics, 6*, 5.

Tanskanen, J. M. A., Kapucu, F. E., & Hyttinen, J. A. K. (2018). A line of MEA signal analysis methods for human stem cell-derived and other dynamic neuronal cultures. *Frontiers in Cellular Neuroscience, 20*. https://doi.org/10.3389/conf.fncel.2018.38.00020.

Thewes, R., Bertotti, G., Dodel, N., Keil, S., Schroder, S., Boven, K. H., et al. (2016). Neural tissue and brain interfacing CMOS devices – An introduction to state-of-the-art, current and future challenges. In *Proceedings of the IEEE International Symposium on Circuits and Systems* (Vol. 2016-July, pp. 1826–1829).

Thomson, D. J. (1982). Spectrum estimation and harmonic analysis. *Proceedings of the IEEE, 70*(9), 1055–1096.

Thomson, D. J., & Chave, A. D. (1991). Jackknifed error estimates for spectra, coherences, and transfer functions. In *Advances in Spectrum Analysis and Array Processing* (pp. 58–113), Upper Saddle River, NJ: Prentice-Hall.

Treves, A., & Panzeri, S. (1995). The upward bias in measures of information derived from limited data samples. *Neural Computation, 7*(2), 399–407.

Vassanelli, S. (2011). Brain-chip interfaces: The present and the future. *Procedia Computer Science, 7*, 61–64.

Vassanelli, S. (2014). Multielectrode and multitransistor arrays for in vivo recording. In M. De Vittorio, L. Martiradonna, & J. Assad (Eds.), *Nanotechnology and Neuroscience: Nanoelectronic, Photonic and Mechanical Neuronal Interfacing* (pp. 239–267). Springer: New York.

Vassanelli, S., Felderer, F., Mahmud, M., Maschietto, M., & Girardi, S. (2012a). CyberRat probes: High-resolution biohybrid devices for probing the brain. In *Living Machines 2012: Biomimetic and Biohybrid Systems*. LNAI (Vol. 7375, pp. 274–285).

Vassanelli, S., & Mahmud, M. (2016). Trends and challenges in neuroengineering: Toward "intelligent" neuroprostheses through brain-"brain inspired systems" communication. *Frontiers in Neuroscience, 10*(Sep), 438.

Vassanelli, S., Mahmud, M., Girardi, S., & Maschietto, M. (2012b). On the way to large-scale and high-resolution brain-chip interfacing. *Cognitive Computation, 4*(1), 71–81.

Victor, J. D. (2002 November). Binless strategies for estimation of information from neural data. *Physical Review E, 66*, 051903.

Victor, J. D., & Purpura, K. P. (1997). Metric-space analysis of spike trains: Theory, algorithms and application. *Network: Computation in Neural Systems, 8*(2), 127–164.

Wagenaar, D., DeMarse, T. B., & Potter, S. M. (2005). MeaBench: A toolset for multi-electrode data acquisition and on-line analysis. In *Proceedings of the 2nd International IEEE EMBS Conference on Neural Engineering* (pp. v–viii).

Wolpert, D. H., & Wolf, D. R. (1995 December). Estimating functions of probability distributions from a finite set of samples. *Physical Review E, 52*, 6841–6854.

Yger, P., Spampinato, G. L., Esposito, E., Lefebvre, B., Deny, S., Gardella, C., et al. (2018). A spike sorting toolbox for up to thousands of electrodes validated with ground truth recordings in vitro and in vivo. *eLIFE, 7*, e34518.

Part IV
Applications

Active High-Density Electrode Arrays: Technology and Applications in Neuronal Cell Cultures

Davide Lonardoni, Hayder Amin, Stefano Zordan, Fabio Boi, Aziliz Lecomte, Gian Nicola Angotzi, and Luca Berdondini

Abstract Active high-density electrode arrays realized with complementary metal–oxide–semiconductor (CMOS) technology provide electrophysiological recordings from several thousands of closely spaced microelectrodes. This has drastically advanced the spatiotemporal recording resolution of conventional multielectrode arrays (MEAs). Thus, today's electrophysiology in neuronal cultures can exploit label-free electrical readouts from a large number of single neurons within the same network. This provides advanced capabilities to investigate the properties of self-assembling neuronal networks, to advance studies on neurotoxicity and neurodevelopmental alterations associated with human brain diseases, and to develop cell culture models for testing drug- or cell-based strategies for therapies.

Here, after introducing the reader to this neurotechnology, we summarize the results of different recent studies demonstrating the potential of active high-density electrode arrays for experimental applications. We also discuss ongoing and possible future research directions that might allow for moving these platforms forward for screening applications.

Keywords CMOS-MEAs · Dense recordings · Network electrophysiology · Disease modelling · Electrical readouts · Neuronal cultures

D. Lonardoni · S. Zordan · F. Boi · A. Lecomte · G. N. Angotzi · L. Berdondini (✉)
Istituto Italiano di Tecnologia (IIT), Genova, Italy
e-mail: luca.berdondini@iit.it

H. Amin
Istituto Italiano di Tecnologia (IIT), Genova, Italy

Plasticity Models for Aging & Neurodegeneration Group, Deutsches Zentrum für Neurodegenerative Erkrankungen e.V. (DZNE), Dresden, Germany

1 Neuroelectronic Principles of Substrate-Integrated Electrodes

The aim of this section is to provide a concise introduction on the main neuroelectronic interfacing principles used in substrate-integrated electrode array devices for sensing and actuating neuronal signals. As a general premise, as stated by Fromherz (2003), it is interesting to note that both computers and brains operate with electrical charges, but the carriers of these charges and the architecture on which these systems process information are radically different. For instance, while electronics exploits electrons and their high mobility in solid substrates (e.g., mobility of electrons in Si $\sim 10^2$ cm/Vs), biological processing of information in the brain involves ions in a polar fluid and shows a much lower mobility (e.g., mobility of ions in water $\sim 10^{-3}$ cm/Vs). These differences have significant implications on the implementation and performances of these "computing" systems, but also govern the interface between neurons and transducers of neuronal activity.

A widely used methodology to transduce bioelectrical neuronal signals is the one based on metal electrodes. Electrodes can establish bidirectional neuroelectronic interfaces between a side governed by electrons (i.e., metal electrode) and the cellular environment governed by ions. This allows for label-free sensing (i.e., without the use of fluorescence reporters such as in Ca^{2+} imaging) of neuronal activity as well as to deliver electrical stimuli that can evoke neuronal responses. Action potentials, or spikes, are bioelectrical signals generated by single neurons and used for their intercellular communication in the nervous system. These signals emerge from the cellular transmembrane ionic activity, that finely regulates the inlet and outlet in the cell of specific ions (such as Na^+ and K^+), with the consequence of modifying at submillisecond timescale the content of ionic charges both inside a cell and near it, in the intracellular and extracellular environments, respectively. The resulting potential across the cellular membrane (or transmembrane potential) can be directly measured in single neurons with intracellularly positioned electrodes (i.e., "patch-clamp," Sakmann and Neher 1984). These electrodes measure the voltage changes induced by the ionic cellular activity with respect to a reference electrode located in the extracellular environment. Intracellular electrodes can sense large-amplitude single-neuron action potentials (e.g., several mV_{p-p} in cultured rodent neurons) but also, uniquely, subthreshold synaptic and ion-channel signals. However, conventional patch-clamp electrodes need to be individually micro-positioned at the target cell and loss of cellular viability over time preclude long-lasting recordings. An alternative strategy to overcome these limitations exploits the transient alteration of the extracellular content of ions near cells due to the ionic membrane activity of spiking neurons. Thus, extracellular potentials induced by neuronal activity can be measured with extracellular microelectrodes positioned near the cell, with respect to a far, unperturbed, reference electrode. Extracellular electrodes do not break the cellular membrane and can, therefore, record for a longer time, but at the cost of a smaller signal amplitude (e.g., ~ 80–100 μV_{p-p} spikes in rodent neurons) and of a lack of sensitivity for subthreshold signals. Additionally,

it is worth mentioning that extracellular signals sensed by microelectrodes are not necessarily single-neuron signals. Rather, extracellular signals can consist of the collective contribution of multiple cells, or even entire circuits, depending on the experimental model. In other words, extracellular electrodes are capable of sensing a rich repertoire of signals ranging from high-frequency spiking activity from single or multiple neurons at the microscale of a brain circuit, to low-frequency field potentials reflecting the macroscopic activity of brain circuits (Schwartz et al. 2006). Hence, the analysis of extracellular neuronal signals requires an adapted signal preprocessing chain depending on the experimental model (such as cell cultures, ex vivo brain tissues, or living animals). Typically, this may include filtering of high- and low-frequency signals, detection of activity events, and sorting them to allocate spikes to individual neurons (Rey et al. 2015).

The peculiar features of extracellular electrodes together with the advent of thin-film fabrication processes motivated already in the 1970s the development of substrate-integrated multielectrode arrays (for a review see Pine 2006). In particular, by establishing neuronal interfaces at multiple sites with microelectrodes realized with reproducible micrometer precision, these devices become a powerful tool to study the functional properties of neuronal networks and brain circuits. Over the last decades, many studies have contributed to advance the technology of substrate-integrated electrode arrays. Shortly, these conventional multielectrode array devices (MEAs) are realized using thin-film technology and integrate on single substrates (made of glass, silicon, or polymers) a few tens of microelectrodes. Because the transducing performances of extracellular electrodes mainly depend on the electrochemical properties of the electrode–electrolyte interface in the physiological environment and on the neuron–electrode coupling, many studies have evaluated different electrode's materials and morphologies as well as surface functionalization methods. Indeed, as opposed to many electrochemical techniques (e.g., cyclic voltammetry, amperometry, impedance spectroscopy), electrodes used for sensing bioelectrical activity are operated unpolarized. A metal electrode in contact with an electrolyte assumes an equilibrium potential while, given the high mobility of charges (i.e., electrons) in the metal, a distribution of ions is established on the electrolyte side of the interface. This ionic distribution, also modelled as a double, or multiple layer capacitance, plays a major role in determining the electrode performances (Grattarola and Massobrio 1998). These interfacing properties can be characterized by impedance spectroscopy and need to be optimized by tuning the properties of the electrode sites. However, the performances of extracellular electrodes in transducing bioelectric cellular signals are not only the result of the engineered electrode properties. Rather, these performances also depend on the biological response of cells in establishing a tight coupling with substrate-integrated electrodes. A tight neuron–electrode coupling (i.e., high sealing resistance) is fundamental to minimize fast charge leakages that can drastically reduce the extracellular voltage amplitude. Thus, before seeding cells on substrate-integrated electrode arrays, these devices need surface coatings to promote cell-adhesion. These coatings need to be optimized depending on the target application and cell types. Adhesion-promoting coatings such as single layer coatings of polylysine or

polyethylenimine (PEI), double layers of polylysine and laminin, or poly-D-lysine–ornithine (PDLO) were used for culturing networks of rodents (mice or rats) or human-derived neurons on multielectrode array devices (Malerba et al. 2018).

2 Active High-Density Electrode Array Devices

In the previous section, we have pointed out a major advantage of electrodes that is their capability of resolving with submillisecond temporal precision the spiking activity of single neurons. Multielectrode arrays (MEAs) exploit this feature to sample neuronal activity from multiple substrate-integrated electrode sites, thus overcoming the need of manually positioning individual electrodes. However, while much progress has been made to improve the neurointerfacing performances of microelectrodes, until the early 2000s, little improvement was brought to increase even further the spatial resolution of these devices. This is because increasing the number and density of substrate-integrated electrode sites of devices realized using thin-film technology is severely limited by spatial constraints in routing each microelectrode to a dedicated contact pad (Berdondini et al. 2005). Because of these constraints, this technology allowed the realization of passive MEAs with only a few tens of microelectrodes and electrode separations in the range of hundreds of micrometers. Therefore, in order to conceive MEAs that could resolve single-neuron spiking activity within neuronal networks covering areas of several square millimeters required the development of an alternative technological approach to overcome the issue of electrode connectivity (Fig. 1). Solutions to realize large-area MEAs with closely spaced electrodes, possibly down to cellular and subcellular scales, were developed by exploiting CMOS technology and by adopting concepts that were previously established for light imaging sensors. Referred to as active high-density MEAs (or CMOS-MEAs) (Berdondini et al. 2001; Imfeld et al. 2008; Hafizovic et al. 2007), these devices integrate on the same substrate an array of microelectrodes together with on-chip analogue and digital microelectronic circuits. By exploiting these circuits to address a large number of closely spaced microelectrodes, bioelectrical signals from several thousands of microelectrodes can be read out upon on-chip amplification, filtering, and multiplexing on a few output channels. Thus, differently than for conventional passive MEAs, active high-density MEAs do not individually wire each microelectrode to specific contact pads. Rather, each microelectrode is addressed through on-chip digital logic circuits and is therefore connected to the external world when needed.

Following this strategy, there have been two major and substantially different concepts to realize active high-density MEAs providing large and dense arrays of substrate-integrated metal microelectrodes. These differences rely on their circuit architectures, with consequent differences in performances with respect to the number of simultaneous recording electrodes, spatial resolution, and signal-to-noise ratio. A first type of CMOS-MEAs was implemented using a circuit architecture
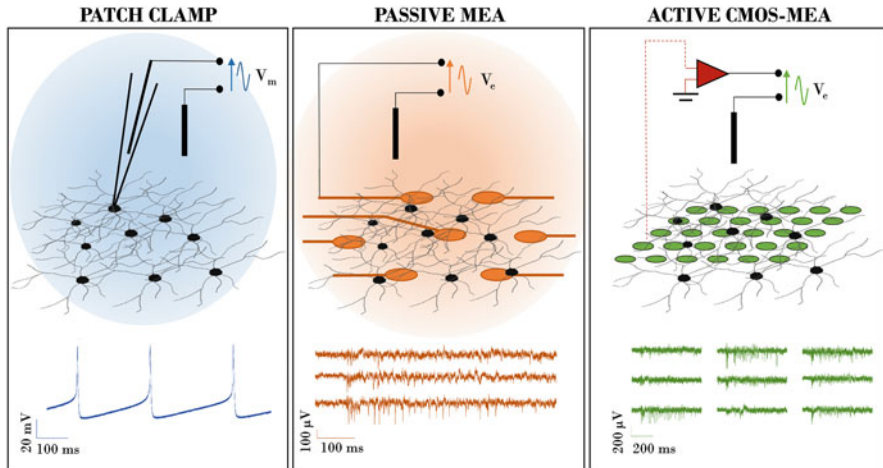
Fig. 1 Schematic diagram depicting the main current methods for in vitro electrical recordings from neural cultures and their representative recorded traces. Active CMOS-MEAs provide large-scale recordings of extracellular neuronal signals in neuronal cultures, thus increasing the spatiotemporal resolution of conventional passive MEAs

based on the use of active matrices to select the recording electrodes and to connect them to on-chip amplifiers located outside of the electrode array area (Frey et al. 2010). By using this switch-matrix (SM) scheme, it is possible to integrate very large electrode arrays consisting of several thousands of selectable microelectrodes and having very small interelectrode separations (Hierlemann et al. 2011). Remarkably, these devices available from MaxWell Biosystems AG (Switzerland) can track bioelectrical signal in neuronal networks with subcellular resolutions (Müller et al. 2015). Additionally, the location of the front-end circuits outside of the electrode array allows for integrating large circuits, relaxing noise issues that in CMOS circuits are typically inversely proportional with the circuit area. However, because the simultaneous acquisition of electrode requires the integration of an amplifier on the side of the chip, these devices typically provide recordings from only a subset of the available electrodes in the array.

A second type of CMOS-MEAs with a different circuit architecture was proposed for whole-array readouts. These devices (nowadays commercially available from 3Brain AG, Switzerland) rely on the Active Pixel Sensor concept used in CMOS light imaging sensors (Fossum 1997). In order to integrate arrays with electrode pitches of a few tens of micrometers, this approach required scaling down the size of the first-stage front-end circuit. Indeed, by placing this circuit underneath each microelectrode this approach uses electrode-pixel components that can be digitally addressed at sufficiently high frequency to read out, on a few multiplexed output channels, the whole array with submillisecond temporal resolution. In our work we have demonstrated a 4096 electrode CMOS-MEA having electrode-pixel sizes of

$42 \times 42 \ \mu m^2$, electrode pitches (center–center) of 42 μm and a full-frame readout frequency of 7.8 kHz (Berdondini et al. 2005, 2009). To do so, a small area, low-noise in-pixel circuit was designed using a DC-coupled low-pass circuit solution that regularly samples the DC potential of each electrode and subtracts it to the input of the in-pixel circuit. This autozeroing circuit avoids saturation of the high-gain (>40 dB) first-stage amplifier resulting from the fluctuating DC electrode potential. While these devices do not reach the spatial resolution of the first type of CMOS-MEAs, they enable to literally image extracellular bioelectrical signals from large active areas of several square millimeters at submillisecond temporal resolution. Notably, the scalability of the APS approach up to 19,584 simultaneously recording electrodes on planar devices was recently presented (Yuan et al. 2018).

So far, we have described how high-resolution recording capabilities are implemented in CMOS-MEAs. However, as pointed out in the first section of this chapter, microelectrodes are bidirectional transducers of bioelectrical activity and are therefore capable of delivering electrical stimuli. Conventional passive MEAs allow the user to exploit each microelectrode for both recording and stimulation by connecting them to a recording or a stimulation device, respectively. Yet providing this capability on CMOS-MEAs is challenging due to the very dense circuit integration and difficulties in managing in the small area allocated to in-pixel circuits the cross talk artifacts that might arise from large amplitude stimulation signals on the recording circuit. To overcome this limitation, a first solution consists in interleaving microelectrodes dedicated to electrical stimulation within the high-density recording electrode array. As recently shown (Amin et al. 2016; Nieus et al. 2018) this simple, yet effective solution allows to spatially and temporally resolve electrically evoked responses in neuronal networks since their initiation. Indeed, the electrical artifact induced by the stimuli is confined in a restricted area (<100 μm in diameter) near the electrode delivering the stimuli and short latency evoked spiking responses (<4 ms) after electrical stimuli can be recorded. Alternatively, an advanced dual mode circuit architecture (SM & APS) was recently presented (Yuan et al. 2018). Further, by exploiting notions from compressive sensing, the laboratory of K. L. Shepard (Tsai et al. 2017) recently proposed an APS-based circuit architecture integrating a different in-pixel circuit of $25.5 \times 25.5 \ \mu m^2$ in size. Remarkably, this planar CMOS-MEA provides 65,536 simultaneously recording and stimulating microelectrodes. To achieve this, authors proposed to minimize even further the size of the recording in-pixel circuit by exploiting knowledge on the nature of the electrophysiological recording noise and to use the saved in-pixel area to integrate an isolated switchable circuit for electrical stimulation. Briefly, rather than consuming in-pixel silicon area to integrate low-pass filters needed to avoid aliasing in traditional implementations, this approach uses signal post-processing algorithms to remove the contribution of thermal noise in microelectrode recordings, that is typically uniformly distributed in the frequency domain and has a Gaussian amplitude distribution in the time domain.

3   Applications of High-Resolution Recordings in Neuronal Cultures

Active high-density MEAs offer an unprecedented spatiotemporal resolution for large-area electrophysiological recordings in neuronal networks in vitro. This capability of imaging bioelectrical activity in neural cultures with resolutions down to cellular/subcellular details has several implications for the study of the network dynamics as well as for the development of applied electrical readouts on in vitro models of brain diseases (Fig. 2).

As known from studies performed with conventional MEAs, neuronal cultures respond to electrical stimuli (Jimbo and Kawana 1992; Amin et al. 2016) and express spontaneous spiking patterns that develop over time during cell culture (Pasquale et al. 2008; Wagenaar et al. 2006). These spiking patterns culminate in the spontaneous generation of network bursting events (NBs). These events are network-wide transient activation of neurons occurring over a few hundreds of milliseconds timescale (Kamioka et al. 1996; Segev and Ben-Jacob 2001). Whether the recurrent generation of NBs has a functional role beyond neuronal maturation (Corner et al. 2002) or whether they represent a pathological state, is still a matter of debate. However, since all healthy neuronal cultures eventually enter in the NBs firing regime (Vassallo et al. 2017; Van Pelt et al. 2004) and express both sparse and coordinated spontaneous spiking firing regimes, these neuronal systems offer an ideal substrate to investigate the effects of chemical compounds (Suresh et al. 2016), exogenous stimulation (Jimbo and Kawana 1992; Pulizzi et al. 2016), or structural confinement (Bisio et al. 2014; Alagapan et al. 2016; Soloperto et al. 2016) in modulating the spontaneous spiking activity of a neuronal population.
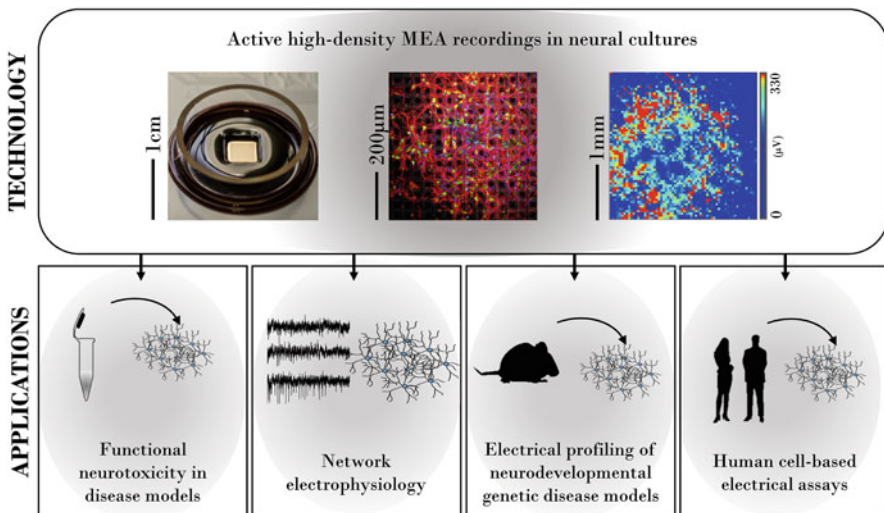

Fig. 2 Schematic diagram of the broad range of applications emerging from active high-density MEA recordings in neural cultures

Active high-density electrode arrays can follow the application fields developed with passive MEAs, both on cell cultures models prepared form rodent or human-derived neurons (Amin et al. 2016). However, by taking advantage of these active devices these applications can exploit large-scale electrophysiological recordings to precisely quantify mean activity parameters in each cell culture (Maccione et al. 2010), to track and classify spatiotemporal activity patterns (Gandolfo et al. 2010) and to resolve spiking activity in the network down to subcellular resolution (Müller et al. 2015). Interestingly, by optimizing the on-chip cell culture conditions, it was shown that the analysis of high-resolution recordings provided by active high-density MEAs can characterize neural cell culture networks exhibiting remarkably similar statistics (Amin et al. 2015). In the next sections, we review a few recent studies of our laboratory that, in our opinion, demonstrate the application potential to different R&D fields of an active high-density MEA device providing an array of 4096 simultaneously recording electrodes.

3.1 Network Electrophysiology Studies with Active High-Density MEAs

A first application field of active high-density MEAs takes advantage of the enhanced spatiotemporal sampling of neuronal activity provided by active high-density MEAs to study the electrophysiological properties of self-organizing neuronal cell culture networks.

A few recent studies used high-resolution recordings of spontaneous activity to unveil subtle spiking dynamics in neuronal cultures, specifically concerning the internal spatiotemporal structure of NBs. In detail, high-density extracellular recordings, and also Ca^{2+} imaging recordings, revealed that NBs consist of a spatiotemporal propagation of spiking activity in the network rather than a mere network-wide synchronization (Gandolfo et al. 2010; Orlandi et al. 2013; Lonardoni et al. 2015). Further, the enhanced spatial sampling capabilities of CMOS-MEAs allowed for classifying NBs of any given cell culture in a few groups according to their trajectory of propagation (Gandolfo et al. 2010; Nieus et al. 2015; Lonardoni et al. 2017). Interestingly, the limited alphabet of trajectories expressed by each neuronal culture highlighted that NBs are recurrently generated in dedicated and spatially localized regions of the neuronal network. As a result, computational (Lonardoni et al. 2017; Luccioli et al. 2014; Masquelier and Deco 2013; Brunel et al. 2000) and experimental works (Orlandi et al. 2013; Pasquale et al. 2017; Eckmann et al. 2008) focused on studying the generation of NBs to elucidate how they might be spontaneously initiated. Besides single neuronal and synaptic properties, an initiation mechanism based on amplification of spontaneous coincident spiking activities in localized microcircuits of the network (Luczak and MacLean 2012) has been pushed forward by many recent works (Orlandi et al. 2013; Lonardoni et al. 2017; Pasquale et al. 2017; Effenberger et al. 2015). In simulations, dedicated and
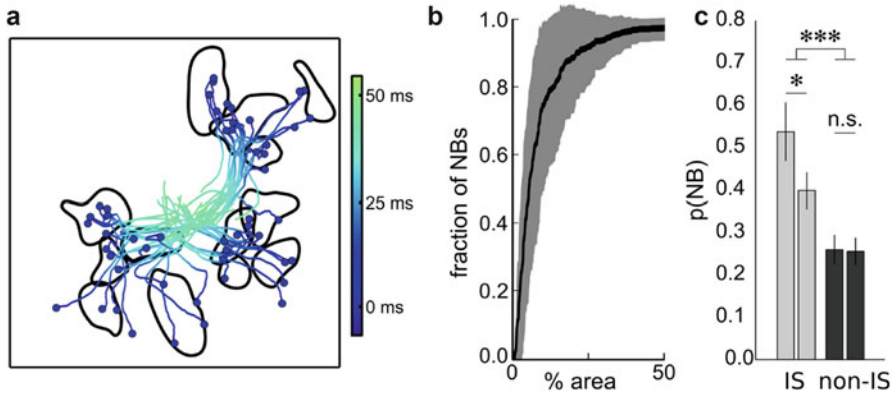
Fig. 3 High-resolution data-driven modelling and studies on network bursts initiation. (**a**) Spatial maps of NB trajectories illustrating the regions dedicated to their initiation (black). The ignition sites (ISs, blue dots) of the NBs and their propagations (color-coded line) are depicted up to 50 ms for clarity. (**b**) Fraction of NBs with ISs within one of the detected regions as a function of the area covered by the regions (black: $n = 20$ simulations, mean value: solid line, standard deviation: shaded area). (**c**) In simulations, a mild stimulation delivered to regions associated to NB initiation evokes NBs with a higher probability than other regions in the network. Adapted from Lonardoni et al. (2017)

localized regions devoted to NB initiation were shown to emerge by simple and biologically plausible rules of connectivity (Lonardoni et al. 2017). Functionally, these regions exhibited the following properties: (1) the spiking activity among neurons within these regions was one order of magnitude more correlated than the one displayed by any other equivalent group of neurons; (2) nearly all the NBs initiated within the borders, or in the close neighborhood, of these regions (Fig. 3a, b); (3) a mild subthreshold stimulation of neurons in these regions gave rise to NBs twice as likely as the same stimulation delivered to any other equivalent group of neurons in the network (Fig. 3c). Additionally (Pasquale et al. 2017), localized electrical stimulation evoked NBs whose spatiotemporal patterns were remarkably similar to the ones observed during spontaneous activity, independently from the stimulation location. Therefore, all these results strengthen the hypothesis of the existence of preferential microcircuits underlying the emergence of NBs (Luczak and MacLean 2012). Moreover, a local circuitry initiating the NBs by amplifying a few asynchronous spikes can also explain the consistently similar spatiotemporal spiking pattern observed in the activation phase of NBs associated to a particular class of propagations (Pimashkin et al. 2011; Lonardoni et al. 2017). These findings pinpoint a relevant role for the structural, and consequently functional, connectivity in regulating the spiking activity in neuronal culture networks at the microcircuit scale, which is different in each culture. Nevertheless, different neuronal cultures eventually converge to a remarkably similar firing regime suggesting that such microcircuit might be a consequence of a spatially invariant mechanism of neuronal wiring.

A sufficient condition for the generation of such microcircuits is a structural connectivity based on the relative position among neurons, in which closer neurons are more likely to be connected. This simple rule has been proven to reliably reproduce in computational models the overall spiking activity of 2D (Lonardoni et al. 2017) or 3D (Bosi et al. 2015) neuronal cultures at a mature stage (>21DIVs). At the early stage, however, other connectivity rules recapitulate the most salient firing features (Luccioli et al. 2014). A potential biophysical candidate mechanism to bridge early and mature stage connectivity is represented by the spike-timing-dependent plasticity (STDP). After synaptic formation, STDP drives the network's dynamic by strengthening the connections of neurons (Vasilaki and Giugliano 2014). Such synaptic remodelling yield to local micro-circuits that provide an efficient substrate for the NBs initiation if coincidently activated (Effenberger et al. 2015; Lonardoni et al. 2017). In this view, NBs might initiate and propagate little by little during cell culture development, strengthening an increasing subset of connections. The spontaneous self-organization of neurons into networks equipped with local microcircuit that are susceptible to coincident spiking activities in vitro suggest that similar mechanisms might provide an essential substrate for sensory information processing in vivo (Womelsdorf et al. 2007).

Other interesting properties of neuronal cell culture networks were recently reported by studying their state-dependent representation of stimulus-evoked activity on active high-density electrode arrays equipped with on-chip electrodes designed for delivering electrical stimuli (Nieus et al. 2018). In different brain circuits in vivo, it was shown that neuronal circuit responses to external stimuli depend, except for the stimuli itself, on some internal neuronal and network variables, denoted as the "state" of the circuit (Buonomano and Maass 2009; Ritter et al. 2015). Indeed, state changes in single cells or small populations of neurons (Safaai et al. 2015; Kayser et al. 2015; Huang et al. 2016) can modulate their spontaneous activity and eventually affect their stimulus-response representations. By using information-theoretic analysis (Borst and Theunissen 1999; Kermany et al. 2010) and high-resolution recordings of ongoing and electrically evoked spiking responses in hippocampal neuronal cultures grown for 24 days in vitro, we have recently shown that also these large and isolated neuronal networks show state-dependent responses (Nieus et al. 2018). Indeed, equal electrical stimuli evoked NBs whose response magnitude increased according to the amount of time passed from the last spontaneous NB. Specifically, the time between stimulation and the last spontaneous NB was found to be the most informative network state variable in these networks in explaining intertrial response variability, see Fig. 4a. Thus, this study extends previous works that revealed the existence of a relationship between responses to electrical stimuli of cultured networks and the stimulus latency relative to the previous NB (Dranias et al. 2013; Jun et al. 2017; Weihberger et al. 2013; Kumar et al. 2016). In particular, using linear models (Kayser et al. 2015; Lin et al. 2015; Panzeri et al. 2016), we demonstrated that the time delay from the last NB accounted for multiplicative stimulus-response gain, rather than additive. In addition, we found that small subsets of electrodes with a well-organized spatial
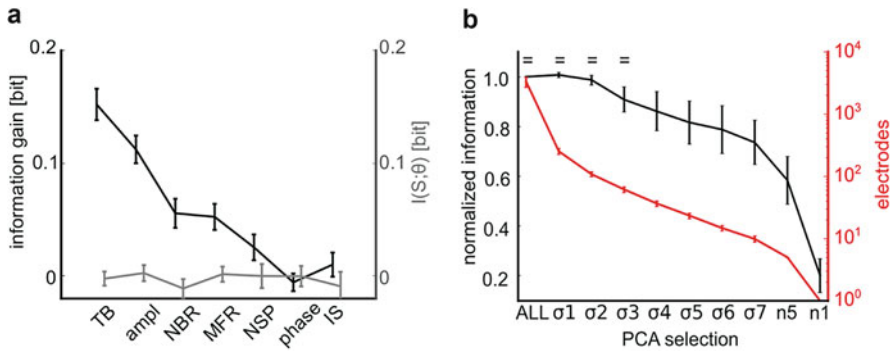
Fig. 4 Investigating the state-dependent representation of stimulus-evoked activity in neural cultures with active high-density electrode arrays. (**a**) The timing from last spontaneous network burst (TB) carries most information about the response to electrically evoked NBs respect to other features such as amplitude (ampl) and phase (phase) of low frequency fluctuations, network burst rate (NBR), mean firing rate (MFR), number of spikes in the last NB (NSP), and ignition site (IS). Note that all these features are not providing any information per se (gray) but only take into account the information of the network response (black curve). (**b**) The mean information of a subset of electrodes selected based on the deviation from the mean principal component value ($\sigma1-\sigma7$) is comparable to the information of the entire electrode array (ALL) up to $\sigma3$, that corresponds to ~61 selected electrodes. Adapted from Nieus et al. (2018)

organization carry most of the stimulus information and of its state information gain, see Fig. 4b.

Overall, these findings together with those on NB initiation, show how the analysis and computational modelling of high-resolution recordings in neuronal cultures can support advancing the investigation of the network electrophysiological properties of these in vitro neuronal systems. It is particularly interesting to note that both studies (Lonardoni et al. 2017; Nieus et al. 2018) suggest that even if these networks are formed by homogeneously planted neurons, these cells can self-organize to generate non-arbitrary spatially and functionally organized subnetworks at the cellular level.

3.2 Electrical Readouts in In Vitro Brain Disease Models Exploiting High-Resolution Recordings

A second range of recent studies demonstrated the potential of applying active high-density electrode array devices to implement neurotoxicity studies, to test different rescue strategies for therapeutic development and to investigate the electrophysiological network developmental profile associated with genetic brain diseases. Together with the growing R&D effort focused on the development of in vitro models relevant to human diseases, these application fields can nowadays take advantage of electrical readouts exploiting the spatiotemporal resolution provided

by active high-density electrode arrays. For instance, high-resolution electrical read-outs might include quantifications of network-wide averaged activity parameters (Wagenaar et al. 2006; Lonardoni et al. 2015), estimations of functional connectivity metrics (Schroeter et al. 2015; Pastore et al. 2018), or characterizations of single-cell population's activity (Maccione et al. 2012). It is important to highlight that an emerging strategy to exploit neuronal cell culture models for these applications consists in combining the use of active high-density electrode arrays platforms with other electrophysiological, microscopy, and biomolecular techniques, including intracellular patch-clamp recordings, immunofluorescence imaging, and qPCR. Put together, these multimodal approaches offer the opportunity to quantify at multiple scales subcellular, neuronal, and network features involved in neurodegenerative and neurodevelopmental disease processes. With the aim of illustrating the potential of high-resolution electrical recordings in neuronal cell culture models, here we shortly summarize some of the main findings observed in a few proof-of-concept studies performed in our laboratory.

As described in the previous sections, conventional multielectrode arrays (MEAs) provide multisite, label-free, noninvasive, and long-term measurements of spontaneous spiking activity in neuronal cultures. This allows to detect induced toxicity responses and to characterize the effects of potential therapeutics (Keefer et al. 2001; Stett et al. 2003; Robinette et al. 2011; Novellino et al. 2011; Charkhkar et al. 2015). However, the few tenths of electrodes integrated on conventional MEAs preclude the characterization of changes in the network dynamics at the cellular level and affect the quantification of mean activity parameters upon activity-dependent changes induced by toxins or drugs. Recently (Amin et al. 2017a, b) we have demonstrated the application of a 4096-electrodes active high-density MEA to quantify early activity-dependent changes induced by toxic oligomers associated with Alzheimer disease in neuronal cell culture networks. In this study, neurotoxicity was induced in 24-day in vitro rat hippocampal neuronal cultures by adding in the cell culture media Aβ-oligomers solutions (tetramers) prepared from a synthesized Aβ(1-42) peptide. The network spiking activity was recorded at multiple time-points for 26 h in cultures treated with a low concentration (0.1 μM) of Aβ-oligomers as well as in three cell culture control groups, that is, untreated, scrambled-amyloid-β, and vehicle. A first outcome of these experiments shows that large-scale electrode array recordings and optimized cell culture conditions can provide a very low interculture and interanimal variability, see Fig. 5a. Further, average activity parameters (e.g., mean firing rate, mean bursting rate) computed from these recordings achieve a remarkably high statistical significance for each group of cell cultures. Indeed, the same analysis performed on these experimental data by scaling down the electrode density to a similar layout as conventional 60 electrodes MEAs (Fig. 5b) does not achieve the same statistical significance (see Supplementary Fig. 2c–e in Amin et al. 2017a, b).

Secondly, these electrical readouts show that samples treated with Aβ-oligomers had a progressive network dysfunction and c-fos immunofluorescence (i.e., a marker of neuronal activity) confirmed that this disrupted network-wide activity recorded with active high-density MEAs originated from cellular dysfunctions. However, at
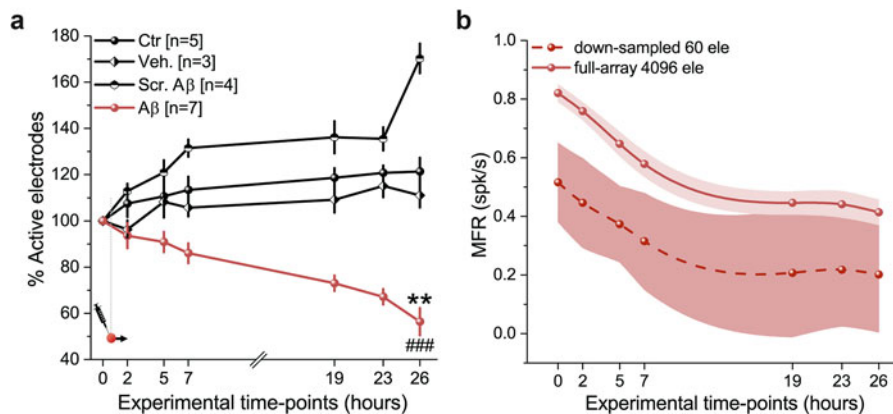
Fig. 5 Example of high-resolution electrical readouts in neuronal cell culture networks applied to the quantification of activity-dependent changes induced by early Aβ-neurotoxicity. (**a**) Large-scale array electrical readouts (mean-firing-rate, MFR) of control groups (black lines) versus the 0.1 μM Aβ-induced toxicity group (red line). ***$p < 0.001$, ANOVA. (**b**) Quantification of the MFR for the Aβ-treated group computed based on recordings that were down-sampled to a 60-electrode array layout (19 ele/mm^2) show higher variability compared to the same quantification computed for high-resolution (1849 ele/mm^2) recordings obtained from 4096 electrodes CMOS-MEAs. For comparison, we considered only electrodes from a recording area of 1.67×1.67 mm^2 as in passive MEAs from Multi Channel Systems Gmbh (MCS, Germany). The MFRs quantifications for both groups are significantly different over seven phases of recordings. $p < 0.001$, Kolmogorov–Smirnov test. Adapted from Amin et al. (2017a, b)

a low concentration (0.1 μM) of Aβ-oligomers and until 26 h after having induced neurotoxicity, caspase-3 immunofluorescence and MTT-colorimetric assays showed that these dysregulated responses of cellular and network-wide activities were not caused by cell death. It has to be noted that cell death was observed for higher concentrations of Aβ-oligomers or for longer times of exposure. Therefore, this cell culture model allows, under well-controlled conditions, to study with extended acuteness the early neurotoxicity effects associated with Aβ-oligomers as well as to test different hypothesis of neurotoxicity mechanisms. Importantly, access to such an early time window since the onset of neurotoxicity is typically unavailable in vivo in animal models. Consequently, as developed in our study, this in vitro cell culture model together with high-resolution electrical readouts allows to evaluate the effects of potential drug-/cell-based neuroprotective strategies during the very early phase after neurotoxicity induction.

Moreover, the methodology demonstrated in this study is not restricted to the neurotoxicity effects of Aβ-oligomers but can be applied to studies and screenings in neuronal cultures involving the use of different disease-relevant pathways of neurotoxicity. Furthermore, statistically significant quantifications of average activity parameters obtained from high-resolution recordings in neuronal cultures, can advance the application of MEA platforms for evaluating the effects of chemical compounds or nanoparticles. In particular, inorganic nanoparticles are considered

as new tools to develop treatments for brain diseases (Kotov et al. 2009; Nel et al. 2009; Carvalho-de-Souza et al. 2015). In Dante et al. (2017) we took advantage of these readouts together with intracellular patch-clamp recordings and immunofluorescence imaging to reveal the key role of nanoparticles surface charge in interaction with electrically excitable neurons. Interestingly, we have shown that the nanoparticle–cell interaction for negative surface charges was selectively restricted to excitable neurons, while no interaction was observed with non-excitable glial cells. Thus, this study suggests that high-resolution electrical readouts in neuronal cultures are an efficient methodology for the optimization of nanoparticles targeting therapeutic strategies on brain cells.

Finally, in another study (Amin et al. 2017a, b) we demonstrated the application of active high-density electrode arrays to characterize the spontaneous electrical developmental profile of neuronal cell cultures prepared from a Di George Syndrome mouse model (Lgdel+/−, 22q11.2 microdeletion, Merscher et al. 2001). By comparing the analysis of high-resolution electrical recordings from neuronal cultures prepared from wild-type mice, we found that networks formed by neurons from this genetic mouse model showed an altered development of network activity and altered homeostatic responses. We have further shown that these alterations are due to embryonic-premature alterations in the neuronal chloride cotransporters (NKCC1 and KCC2). Indeed, the application of bumetanide, an inhibitor of NKCC1, significantly decreased the hyper-excitable action of GABAA receptor signalling and restored network homeostatic plasticity in these Lgdel+/− networks. Thus, these results on in vitro neuronal networks suggest that a delayed embryonic development might contribute to the heterogeneous pathological phenotypes of the Di George syndrome, which includes cognitive and behavioural dysfunctions, developmental delays in childhood, schizophrenia, and autism.

Overall, these studies performed on in vitro networks of neurons prepared from animal models demonstrate the potential of exploiting active high-density electrode arrays and neuronal cell culture models. In particular, a unique opportunity available nowadays consists in the development and study of disease-relevant on CMOS models based on human iPSC-derived neurons. As a first step in this direction, (Amin et al. 2016) we have demonstrated the feasibility of growing on active high-density electrode arrays human iPSC-derived neuronal cultures and the capability of monitoring up to three months their spontaneous and electrically evoked activities at high temporal and spatial resolution.

4 Challenges and Perspectives of Active High-Density MEAs

Since the advent of substrate-integrated electrode arrays in the 1970s, this neurotechnology has raised the interests and contributions of a very broad cross-disciplinary research community. As described in this chapter, in the 1980s–1990s, this research was mainly focused on tackling challenges inherent to advance device fabrication processes, to establish stable and performing neuroelectronic interfaces

as well as to develop computational data analysis tools and models for detecting and interpreting network dynamics in neuronal cultures. While these research fields are of fundamental relevance, the advent of active high-density electrode arrays capable of recording neuronal activity from more than an order of magnitude larger number of electrode sites than conventional passive devices has even broadened this research community and introduced additional challenges for their application.

In particular, these devices can easily generate several tens of MB/s. Therefore, a relevant challenge resides in the development of data processing solutions capable of providing rapid readouts upon the analysis of large-scale electrophysiological recordings (Maccione et al. 2015). Promising approaches rely on the design of innovative processing algorithms that can take advantage from closely spaced recording microelectrodes, as recently proposed for spike detection (Muthmann et al. 2015) and sorting (Hilgen et al. 2017), as well as the implementation of hardware-embedded solutions (Seu et al. 2018). It is also important to note that an alternative way to exploit large-scale recording might be to identify specific neurons of interest and then restrict data acquisition and analysis to the monitoring of these specific cells. For instance, in (Nieus et al. 2018) we exploited high-resolution recordings to investigate how the ongoing activity expressed by neuronal cultures affects the information that neuronal responses carry about the location of electrical stimuli, and we have found that large-scale recordings can actually be used to individuate small subsets of neurons that carry most information.

An additional challenge is to advance this neurotechnology to answer stringent needs in screening applications in vitro. Nowadays, these applications can take advantage from the availability of human-derived neurons (see also Chapters "Past, Present and Future of Neuronal Models In Vitro" and "Advances in Human Stem Cell-Derived Neuronal Cell Culturing and Analysis" of this book). Thus, they have a high potential in neurotoxicity studies, R&D on neurodegeneration and neurodevelopmental human brain diseases as well as in the development of platforms for precision medicine. To do so, commercially available active high-density electrode arrays are rapidly shifting from single-well to multiwell formats and might soon integrate neurointerfacing solutions capable of intracellular-like action potential recordings. Indeed, by exploiting spontaneous poration, electroporation, surface functionalization, or, more recently, plasmonic poration of microstructures/nanostructures (Duan et al. 2012; Xie et al. 2012; Robinson et al. 2012; Spira and Hai 2013; Dipalo et al. 2017, and Chapter "In Vitro Neuronal Networks: From Culturing Methods to Neuro-technological Applications" of this book), different laboratories have demonstrated the opportunity to improve signal quality of conventional extracellular single-cell recordings. However, in addition to the need for adapted data management and analysis approaches, these directions introduce issues in seeding and maintaining neuronal cell cultures in small wells, such as those of 96-/384-well plates. Possible solutions based on microfluidics are under development (e.g., Pauwelyn et al. 2018), but future generations of active high-density electrode array platforms shall take into consideration these requirements. Integrated lab-on-chip platforms could for instance present with features for multimodal readouts based on optical, electrical, and biomolecular

methods. Such readouts may provide unique capabilities to study the complex dynamics involved in neuronal networks at multiple scales, that is, from molecules, individual cells, up to whole networks.

Finally, we also have to consider that 2D neuronal cultures might be insufficient physiological models for many applications. Indeed, 3D models such as spheroids and brain organoids have been suggested to better account for physiological properties observed in vivo. Existing planar electrode array devices are not currently able of sampling the activity of a large number of single-neurons in 3D models. Thus, an additional technological advance is required. The recent development of implantable active high-density electrode array probes for large-scale recordings in vivo (Jun et al. 2017; Raducanu et al. 2016; Angotzi et al. 2018) may give rise to novel opportunities in this direction.

References

Alagapan, S., Franca, E., Pan, L., Leondopulos, S., Wheeler, B. C., & DeMarse, T. B. (2016). Structure, function, and propagation of information across living two, four, and eight node degree topologies. *Frontiers in Bioengineering and Biotechnology, 4*, 15.

Amin, H., Maccione, A., Marinaro, F., Zordan, S., Nieus, T., & Berdondini, L. (2016). Electrical responses and spontaneous activity of human iPS-derived neuronal networks characterized for 3-month culture with 4096-electrode arrays. *Frontiers in Neuroscience, 10*, 121.

Amin, H., Maccione, A., Zordan, S., Nieus, T., & Berdondini, L. (2015). High-density MEAs reveal lognormal firing patterns in neuronal networks for short and long term recordings. In *2015 7th international IEEE/EMBS conference on neural engineering (NER)*, pp. 1000–1003.

Amin, H., Marinaro, F., De Pietri Tonelli, D., & Berdondini, L. (2017a). Developmental excitatory-to-inhibitory GABA-polarity switch is disrupted in 22q11.2 deletion syndrome: A potential target for clinical therapeutics. *Scientific Reports, 7*, 15752.

Amin, H., Nieus, T., Lonardoni, D., Maccione, A., & Berdondini, L. (2017b). High-resolution bioelectrical imaging of Aβ-induced network dysfunction on CMOS-MEAs for neurotoxicity and rescue studies. *Scientific Reports, 7*, 2460.

Angotzi, G. N., Malerba, M., Boi, F., Miele, E., Maccione, A., Amin, H., et al. (2018). A synchronous neural recording platform for multiple high-resolution CMOS probes and passive electrode arrays. *IEEE Transactions on Biomedical Circuits and Systems, 12*, 532–542.

Berdondini, L., Imfeld, K., Maccione, A., Tedesco, M., Neukom, S., Koudelka-Hep, M., et al. (2009). Active pixel sensor array for high spatio-temporal resolution electrophysiological recordings from single cell to large scale neuronal networks. *Lab on a Chip, 9*, 2644–2651.

Berdondini, L., Overstolz, T., de Rooij, N. F., Koudelka-Hep, M., Wany, M., Seitz, P. (2001). High-density microelectrode arrays for electrophysiological activity imaging of neuronal networks. In *ICECS 2001. 8th IEEE international conference on electronics, circuits and systems (Cat. No.01EX483)*, pp. 1239–1242.

Berdondini, L., van der Wal, P. D., Guenat, O., de Rooij, N. F., Koudelka-Hep, M., Seitz, P., et al. (2005). High-density electrode array for imaging in vitro electrophysiological activity. *Biosensors & Bioelectronics, 21*, 167–174.

Bisio, M., Bosca, A., Pasquale, V., Berdondini, L., & Chiappalone, M. (2014). Emergence of bursting activity in connected neuronal sub-populations. *PLoS One, 9*, e107400.

Borst, A., & Theunissen, F. E. (1999). Information theory and neural coding. *Nature Neuroscience, 2*, 947–957.

Bosi, S., Rauti, R., Laishram, J., Turco, A., Lonardoni, D., Nieus, T., et al. (2015). From 2D to 3D: Novel nanostructured scaffolds to investigate signalling in reconstructed neuronal networks. *Scientific Reports, 5*, 9562.

Brunel, N. (2000). Phase diagrams of sparsely connected networks of excitatory and inhibitory spiking neurons. *Neurocomputing, 32–33*, 307–312.

Buonomano, D. V., & Maass, W. (2009). State-dependent computations: Spatiotemporal processing in cortical networks. *Nature Reviews Neuroscience, 10*, 113–125.

Carvalho-de-Souza, J. L., Treger, J. S., Dang, B., Kent, S. B. H., Pepperberg, D. R., & Bezanilla, F. (2015). Photosensitivity of neurons enabled by cell-targeted gold nanoparticles. *Neuron, 86*, 207–217.

Charkhkar, H., Meyyappan, S., Matveeva, E., Moll, J. R., McHail, D. G., Peixoto, N., et al. (2015). Amyloid beta modulation of neuronal network activity in vitro. *Brain Research, 1629*, 1–9.

Corner, M. A., van Pelt, J., Wolters, P. S., Baker, R. E., & Nuytinck, R. H. (2002). Physiological effects of sustained blockade of excitatory synaptic transmission on spontaneously active developing neuronal networks—an inquiry into the reciprocal linkage between intrinsic biorhythms and neuroplasticity in early ontogeny. *Neuroscience and Biobehavioral Reviews, 26*, 127–185.

Dante, S., Petrelli, A., Petrini, E. M., Marotta, R., Maccione, A., Alabastri, A., et al. (2017). Selective targeting of neurons with inorganic nanoparticles: Revealing the crucial role of nanoparticle surface charge. *ACS Nano, 11*, 6630–6640.

Dipalo, M., Amin, H., Lovato, L., Moia, F., Caprettini, V., Messina, G. C., et al. (2017). Intracellular and extracellular recording of spontaneous action potentials in mammalian neurons and cardiac cells with 3D plasmonic nanoelectrodes. *Nano Letters, 17*, 3932–3939.

Dranias, M. R., Ju, H., Rajaram, E., & VanDongen, A. M. J. (2013). Short-term memory in networks of dissociated cortical neurons. *The Journal of Neuroscience, 33*, 1940–1953.

Duan, X., Gao, R., Xie, P., Cohen-Karni, T., Qing, Q., Choe, H. S., et al. (2012). Intracellular recordings of action potentials by an extracellular nanoscale field-effect transistor. *Nature Nanotechnology, 7*, 174–179.

Eckmann, J.-P., Jacobi, S., Marom, S., Moses, E., & Zbinden, C. (2008). Leader neurons in population bursts of 2D living neural networks. *New Journal of Physics, 10*, 015011.

Effenberger, F., Jost, J., & Levina, A. (2015). Self-organization in balanced state networks by STDP and homeostatic plasticity. *PLoS Computational Biology, 11*, e1004420.

Fossum, E. R. (1997). CMOS image sensors: Electronic camera-on-a-chip. *IEEE Transactions on Electron Devices, 44*, 1689–1698.

Frey, U., Sedivy, J., Heer, F., Pedron, R., Ballini, M., Mueller, J., et al. (2010). Switch-matrix-based high-density microelectrode array in CMOS technology. *IEEE Journal of Solid-State Circuits, 45*, 467–482.

Fromherz, P. (2003). Semiconductor chips with ion channels, nerve cells and brain. *Physica E: Low-Dimensional Systems and Nanostructures, 16*, 24–34.

Gandolfo, M., Maccione, A., Tedesco, M., Martinoia, S., & Berdondini, L. (2010). Tracking burst patterns in hippocampal cultures with high-density CMOS-MEAs. *Journal of Neural Engineering, 7*, 056001.

Grattarola, M., & Massobrio, G. (1998). *Bioelectronics handbook : MOSFETs, biosensors, and neurons*. New York: McGraw-Hill.

Hafizovic, S., Heer, F., Ugniwenko, T., Frey, U., Blau, A., Ziegler, C., et al. (2007). A CMOS-based microelectrode array for interaction with neuronal cultures. *Journal of Neuroscience Methods, 164*, 93–106.

Hierlemann, A., Frey, U., Hafizovic, S., & Heer, F. (2011). Growing cells atop microelectronic chips: Interfacing electrogenic cells in vitro with CMOS-based microelectrode arrays. *Proceedings of the IEEE, 99*, 252–284.

Hilgen, G., Sorbaro, M., Pirmoradian, S., Muthmann, J.-O., Kepiro, I. E., Ullo, S., et al. (2017). Unsupervised spike sorting for large-scale, high-density multielectrode arrays. *Cell Reports, 18*, 2521–2532.

Huang, C., Resnik, A., Celikel, T., & Englitz, B. (2016). Adaptive spike threshold enables robust and temporally precise neuronal encoding. *PLoS Computational Biology, 12*, e1004984.

Imfeld, K., Neukom, S., Maccione, A., Bornat, Y., Martinoia, S., Farine, P.-A., et al. (2008). Large-scale, high-resolution data acquisition system for extracellular recording of electrophysiological activity. *IEEE Transactions on Biomedical Engineering, 55*, 2064–2073.

Jimbo, Y., & Kawana, A. (1992). Electrical stimulation and recording from cultured neurons using a planar electrode array. *Bioelectrochemistry and Bioenergetics, 29*, 193–204.

Jun, J. J., Steinmetz, N. A., Siegle, J. H., Denman, D. J., Bauza, M., Barbarits, B., et al. (2017). Fully integrated silicon probes for high-density recording of neural activity. *Nature, 551*, 232–236. https://doi.org/10.1038/nature24636

Kamioka, H., Maeda, E., Jimbo, Y., Robinson, H. P., & Kawana, A. (1996). Spontaneous periodic synchronized bursting during formation of mature patterns of connections in cortical cultures. *Neuroscience Letters, 206*, 109–112.

Kayser, C., Wilson, C., Safaai, H., Sakata, S., & Panzeri, S. (2015). Rhythmic auditory cortex activity at multiple timescales shapes stimulus-response gain and background firing. *The Journal of Neuroscience, 35*, 7750–7762.

Keefer, E. W., Norton, S. J., Boyle, N. A. J., Talesa, V., & Gross, G. W. (2001). Acute toxicity screening of novel AChE inhibitors using neuronal networks on microelectrode arrays. *Neurotoxicology, 22*, 3–12.

Kermany, E., Gal, A., Lyakhov, V., Meir, R., Marom, S., & Eytan, D. (2010). Tradeoffs and constraints on neural representation in networks of cortical neurons. *The Journal of Neuroscience, 30*, 9588–9596.

Kotov, N. A., Winter, J. O., Clements, I. P., Jan, E., Timko, B. P., Campidelli, S., et al. (2009). Nanomaterials for neural interfaces. *Advanced Materials, 21*, 3970–4004.

Kumar, S. S., Wülfing, J., Okujeni, S., Boedecker, J., Riedmiller, M., & Egert, U. (2016). Autonomous optimization of targeted stimulation of neuronal networks. *PLoS Computational Biology, 12*, e1005054.

Lin, I.-C., Okun, M., Carandini, M., & Harris, K. D. (2015). The nature of shared cortical variability. *Neuron, 87*, 644–656. https://doi.org/10.1016/j.neuron.2015.06.035

Lonardoni, D., Amin, H., Di Marco, S., Maccione, A., Berdondini, L., & Nieus, T. (2017). Recurrently connected and localized neuronal communities initiate coordinated spontaneous activity in neuronal networks. *PLoS Computational Biology, 13*, e1005672.

Lonardoni, D., Di Marco, S., Amin, H., Maccione, A., Berdondini, L., Nieus, T. (2015). High-density MEA recordings unveil the dynamics of bursting events in cell cultures. In *2015 37th annual international conference of the IEEE engineering in medicine and biology society (EMBC)*, pp. 3763–3766.

Luccioli, S., Ben-Jacob, E., Barzilai, A., Bonifazi, P., & Torcini, A. (2014). Clique of functional hubs orchestrates population bursts in developmentally regulated neural networks. *PLoS Computational Biology, 10*, e1003823.

Luczak, A., & MacLean, J. N. (2012). Default activity patterns at the neocortical microcircuit level. *Frontiers in Integrative Neuroscience, 6*, 30.

Maccione, A., Gandolfo, M., Tedesco, M., Nieus, T., Imfeld, K., Martinoia, S., et al. (2010). Experimental investigation on spontaneously active hippocampal cultures recorded by means of high-density MEAs: Analysis of the spatial resolution effects. *Frontiers in Neuroengineering, 3*, 4.

Maccione, A., Gandolfo, M., Zordan, S., Amin, H., Di Marco, S., Nieus, T., et al. (2015). Microelectronics, bioinformatics and neurocomputation for massive neuronal recordings in brain circuits with large scale multielectrode array probes. *Brain Research Bulletin, 119*, 118–126.

Maccione, A., Garofalo, M., Nieus, T., Tedesco, M., Berdondini, L., & Martinoia, S. (2012). Multiscale functional connectivity estimation on low-density neuronal cultures recorded by high-density CMOS micro electrode arrays. *Journal of Neuroscience Methods, 207*, 161–171.

Malerba, M., Amin, H., Angotzi, G. N., Maccione, A., & Berdondini, L. (2018). Fabrication of multielectrode arrays for neurobiology applications. *Methods in Molecular Biology, 1771*, 147–157.

Masquelier, T., & Deco, G. (2013). Network bursting dynamics in excitatory cortical neuron cultures results from the combination of different adaptive mechanism. *PLoS One, 8*, e75824.

Merscher, S., Funke, B., Epstein, J. A., Heyer, J., Puech, A., Lu, M. M., et al. (2001). TBX1 is responsible for cardiovascular defects in velo-cardio-facial/DiGeorge syndrome. *Cell, 104*, 619–629.

Müller, J., Ballini, M., Livi, P., Chen, Y., Radivojevic, M., Shadmani, A., et al. (2015). High-resolution CMOS MEA platform to study neurons at subcellular, cellular, and network levels. *Lab on a Chip, 15*, 2767–2780.

Muthmann, J.-O., Amin, H., Sernagor, E., Maccione, A., Panas, D., Berdondini, L., et al. (2015). Spike detection for large neural populations using high density multielectrode arrays. *Frontiers in Neuroinformatics, 9*, 28.

Nel, A. E., Mädler, L., Velegol, D., Xia, T., Hoek, E. M. V., Somasundaran, P., et al. (2009). Understanding biophysicochemical interactions at the nano-bio interface. *Nature Materials, 8*, 543–557.

Nieus, T., D'Andrea, V., Amin, H., Di Marco, S., Safaai, H., Maccione, A., et al. (2018). State-dependent representation of stimulus-evoked activity in high-density recordings of neural cultures. *Scientific Reports, 8*, 5578.

Nieus, T., Di Marco, S., Maccione, A., Amin, H., Berdondini, L. (2015). Investigating cell culture dynamics combining high density recordings with dimensional reduction techniques. In *2015 37th annual international conference of the IEEE engineering in medicine and biology society (EMBC)*, pp. 3759–3762.

Novellino, A., Scelfo, B., Palosaari, T., Price, A., Sobanski, T., Shafer, T. J., et al. (2011). Development of micro-electrode array based tests for neurotoxicity: Assessment of interlaboratory reproducibility with neuroactive chemicals. *Frontiers in Neuroengineering, 4*, 4.

Orlandi, J. G., Soriano, J., Alvarez-Lacalle, E., Teller, S., & Casademunt, J. (2013). Noise focusing and the emergence of coherent activity in neuronal cultures. *Nature Physics, 9*, 582–590.

Panzeri, S., Safaai, H., De Feo, V., & Vato, A. (2016). Implications of the dependence of neuronal activity on neural network states for the design of brain-machine interfaces. *Frontiers in Neuroscience, 10*, 165. https://doi.org/10.3389/fnins.2016.00165

Pasquale, V., Martinoia, S., & Chiappalone, M. (2017). Stimulation triggers endogenous activity patterns in cultured cortical networks. *Scientific Reports, 7*, 9080.

Pasquale, V., Massobrio, P., Bologna, L. L., Chiappalone, M., & Martinoia, S. (2008). Self-organization and neuronal avalanches in networks of dissociated cortical neurons. *Neuroscience, 153*, 1354–1369.

Pastore, V. P., Massobrio, P., Godjoski, A., & Martinoia, S. (2018). Identification of excitatory-inhibitory links and network topology in large-scale neuronal assemblies from multi-electrode recordings. *PLoS Computational Biology, 14*, e1006381.

Pauwelyn, T., Miccoli, B., Velnayagam, A., Jan Boom, R., Skolimowski, M., Vrouwe, E., et al. (2018). High-throughput CMOS MEA system with integrated microfluidics for cardiotoxicity studies. *Frontiers in Cellular Neuroscience*. https://doi.org/10.3389/conf.fncel.2018.38.00009

Pimashkin, A., Kastalskiy, I., Simonov, A., Koryagina, E., Mukhina, I., & Kazantsev, V. (2011). Spiking signatures of spontaneous activity bursts in hippocampal cultures. *Frontiers in Computational Neuroscience, 5*, 46.

Pine, J. (2006). A history of MEA development. In *Advances in network electrophysiology* (pp. 3–23). New York: Springer.

Pulizzi, R., Musumeci, G., Van den Haute, C., Van De Vijver, S., Baekelandt, V., & Giugliano, M. (2016). Brief wide-field photostimuli evoke and modulate oscillatory reverberating activity in cortical networks. *Scientific Reports, 6*, 24701.

Raducanu, B. C., Yazicioglu. R. F., Lopez, C. M., Ballini, M., Putzeys, J., & Wang, S., et al. (2016). Time multiplexed active neural probe with 678 parallel recording sites. In *2016 46th European solid-state device research conference (ESSDERC)*, pp. 385–388.

Rey, H. G., Pedreira, C., & Quian Quiroga, R. (2015). Past, present and future of spike sorting techniques. *Brain Research Bulletin, 119*, 106–117.

Ritter, P., Born, J., Brecht, M., Dinse, H. R., Heinemann, U., Pleger, B., et al. (2015). State-dependencies of learning across brain scales. *Frontiers in Computational Neuroscience, 9*, 1.

Robinette, B. L., Harrill, J. A., Mundy, W. R., & Shafer, T. J. (2011). In vitro assessment of developmental neurotoxicity: Use of microelectrode arrays to measure functional changes in neuronal network ontogeny. *Frontiers in Neuroengineering, 4*, 1.

Robinson, J. T., Jorgolli, M., Shalek, A. K., Yoon, M.-H., Gertner, R. S., & Park, H. (2012). Vertical nanowire electrode arrays as a scalable platform for intracellular interfacing to neuronal circuits. *Nature Nanotechnology, 7*, 180–184.

Safaai, H., Neves, R., Eschenko, O., Logothetis, N. K., & Panzeri, S. (2015). Modeling the effect of locus coeruleus firing on cortical state dynamics and single-trial sensory processing. *Proceedings of the National Academy of Sciences, 112*, 12834–12839.

Sakmann, B., & Neher, E. (1984). Patch clamp techniques for studying ionic channels in excitable membranes. *Annual Review of Physiology*. https://doi.org/10.1146/annurev.ph.46.030184.002323

Schroeter, M. S., Charlesworth, P., Kitzbichler, M. G., Paulsen, O., & Bullmore, E. T. (2015). Emergence of rich-club topology and coordinated dynamics in development of hippocampal functional networks in vitro. *The Journal of Neuroscience, 35*, 5459–5470.

Schwartz, A. B., Cui, X. T., Weber, D. J., & Moran, D. W. (2006). Brain-controlled interfaces: Movement restoration with neural prosthetics. *Neuron, 52*, 205–220.

Segev, R., & Ben-Jacob, E. (2001). Spontaneous synchronized bursting in 2D neural networks. *Physica A: Statistical Mechanics and its Applications, 302*, 64–69.

Seu, G. P., Angotzi, G. N., Boi, F., Raffo, L., Berdondini, L., & Meloni, P. (2018). Exploiting all programmable SoCs in neural signal analysis: A closed-loop control for large-scale CMOS multielectrode arrays. *IEEE Transactions on Biomedical Circuits and Systems, 12*, 839–850.

Soloperto, A., Bisio, M., Palazzolo, G., Chiappalone, M., Bonifazi, P., & Difato, F. (2016). Modulation of neural network activity through single cell ablation: An in vitro model of minimally invasive neurosurgery. *Molecules, 21*, 1018.

Spira, M. E., & Hai, A. (2013). Multi-electrode array technologies for neuroscience and cardiology. *Nature Nanotechnology, 8*, 83–94.

Stett, A., Egert, U., Guenther, E., Hofmann, F., Meyer, T., Nisch, W., et al. (2003). Biological application of microelectrode arrays in drug discovery and basic research. *Analytical and Bioanalytical Chemistry, 377*, 486–495.

Suresh, J., Radojicic, M., Pesce, L. L., Bhansali, A., Wang, J., Tryba, A. K., et al. (2016). Network burst activity in hippocampal neuronal cultures: The role of synaptic and intrinsic currents. *Journal of Neurophysiology, 115*, 3073–3089.

Tsai, D., Sawyer, D., Bradd, A., Yuste, R., & Shepard, K. L. (2017). A very large-scale microelectrode array for cellular-resolution electrophysiology. *Nature Communications, 8*, 1802.

Van Pelt, J., Wolters, P. S., Corner, M. A., Rutten, W. L. C., & Ramakers, G. J. A. (2004). Long-term characterization of firing dynamics of spontaneous bursts in cultured neural networks. *IEEE Transactions on Biomedical Engineering, 51*, 2051–2062.

Vasilaki, E., & Giugliano, M. (2014). Emergence of connectivity motifs in networks of model neurons with short- and long-term plastic synapses. *PLoS One, 9*, e84626.

Vassallo, A., Chiappalone, M., De Camargos Lopes, R., Scelfo, B., Novellino, A., Defranchi, E., et al. (2017). A multi-laboratory evaluation of microelectrode array-based measurements of neural network activity for acute neurotoxicity testing. *Neurotoxicology, 60*, 280–292.

Wagenaar, D., Pine, J., & Potter, S. (2006). An extremely rich repertoire of bursting patterns during the development of cortical cultures. *BMC Neuroscience, 7*, 11.

Weihberger, O., Okujeni, S., Mikkonen, J. E., & Egert, U. (2013). Quantitative examination of stimulus-response relations in cortical networks in vitro. *Journal of Neurophysiology, 109*, 1764–1774.

Womelsdorf, T., Schoffelen, J.-M., Oostenveld, R., Singer, W., Desimone, R., Engel, A. K., et al. (2007). Modulation of neuronal interactions through neuronal synchronization. *Science, 316*, 1609–1612.

Xie, C., Lin, Z., Hanson, L., Cui, Y., & Cui, B. (2012). Intracellular recording of action potentials by nanopillar electroporation. *Nature Nanotechnology, 7*, 185–190.

Yuan, X., Hierlemann, A., & Frey, U. (2018). Dual-mode microelectrode array with 20k-electrodes and high SNR for high-throughput extracellular recording and stimulation. *Frontiers in Cellular Neuroscience*. https://doi.org/10.3389/conf.fncel.2018.38.00088

Application of Microelectrode Array Approaches to Neurotoxicity Testing and Screening

Timothy J. Shafer

Abstract Neurotoxicity can be defined by the ability of a drug or chemical to alter the physiology, biochemistry, or structure of the nervous system in a manner that may negatively impact the health or function of the individual. Electrophysiological approaches have been utilized to study the mechanisms underlying neurotoxic actions of drugs and chemicals for over 50 years, and in more recent decades, high-throughput patch-clamp approaches have been utilized by the pharmaceutical industry for drug development. The use of microelectrode array recordings to study neural network electrophysiology is a relatively newer approach, with commercially available systems becoming available only in the early 2000s. However, MEAs have been rapidly adopted as a useful approach for neurotoxicity testing. In this chapter, I will review the use of MEA approaches as they have been applied to the field of neurotoxicity testing, especially as they have been applied to the need to screen large numbers of chemicals for neurotoxicity and developmental neurotoxicity. In addition, I will also identify challenges for the field that when addressed will improve the utility of MEA approaches for toxicity testing.

Keywords Developmental neurotoxicity · Neurotoxicity · Screening

T. J. Shafer (✉)
Integrated Systems Toxicology Division, National Health and Environmental Effects Research Laboratory (NHEERL), US EPA, Research Triangle Park, NC, USA
e-mail: shafer.tim@epa.gov

275

1 Introduction

The nervous system, and especially the developing nervous system, is uniquely sensitive to perturbation by a wide variety of natural toxins, drugs, and a wide range of environmental chemicals (metals, pesticides, solvents, etc.). The nervous system is unique from other organ systems (such as the liver, kidney, and lungs) due to the nature of its function; it must receive input from the environment, rapidly transmit that information over long distances, integrate information from multiple sources, store it and generate appropriate responses. This is accomplished through the rapid transition of biochemical to electrical signals (and vice versa) and through spatio-temporal patterns of electrical signals to encode and convey information within networks of interconnected neurons and to target tissues (e.g., smooth and skeletal muscle, endocrine glands).

Because of the complexity of the nervous system, there are a wide variety of approaches used to study how its function is perturbed. At the whole animal level, the fields of behavioral pharmacology and toxicology have been important to identifying how different toxicants alter function of the nervous system (Weiss and Laties 1975), as have the fields of neuroimaging and neuropathology. Neurochemical approaches have also been widely utilized to understand mechanisms underlying toxicant actions on the nervous system. However, because of the electrical excitability of the nervous system, neurophysiological approaches have been critical to both identifying and understanding which, and how, compounds alter nervous system function. At the whole animal level, neurophysiological approaches such as visual, auditory, and somatosensory evoked potential recordings (Otto et al. 1988; Boyes 1993, 1994) helped to identify the neurotoxicity of solvents and pesticides. By contrast, at the cellular and sub-cellular level, patch-clamp and sharp electrode recordings helped to identify the mechanisms by which metals disrupted neurotransmission at the neuromuscular junction and by which pyrethroids produced acute neurotoxicity by altering voltage-gated sodium channel kinetics in neurons (Shafer and Atchison 1995; Narahashi 2002).

Small networks of interconnected neurons are critical to nervous system function. These networks often exhibit synchronous and oscillatory behavior (Uhlhaas et al. 2009; Salinas and Sejnowski 2001), which when disrupted are associated with pathological disease, including schizophrenia, epilepsy, autism, and neurodegenerative diseases (Uhlhaas and Singer 2006). Because the field of microelectrode array recording evolved later than other electrophysiological approaches, much less is known about how neurotoxicants alter function at the level of neuronal networks. However, MEAs have a unique niche in the neurotoxicologist's toolbox, as they alone facilitate the evaluation of how chemicals alter the function of small networks of interconnected neurons. One way that this approach is contributing to our knowledge is by providing additional mechanistic information on the actions of compounds on neural networks. A second, and perhaps more important way that MEA approaches are impacting the field of neurotoxicity is in the screening of compounds for their potential to cause neurotoxicity or developmental neurotox-

icity. The lack of information on these endpoints for thousands of chemicals has resulted in an urgent need for rapid and economical approaches to address this data gap, which can in part be filled by MEA approaches. As such, the role of MEAs in neurotoxicity screening has been an area of considerable growth in the last decade and will be further addressed below.

In this chapter, I will present an overview of how neural networks cultured on MEAs have been used to address both mechanistic questions and screening approaches related to neurotoxicity testing. I will discuss some important methodological considerations of using MEAs for this purpose, as my experience has been that good methodology is critical to obtaining usable screening data. Finally, I will also present some challenges for the future, better utilization of the rich information in MEA recordings and better incorporation of neural networks derived from humans into neurotoxicity studies with MEAs.

2 Platforms and Methodological Considerations

Standard MEA formats usually consist of a grid of planar microelectrodes (typically 8–64 electrodes/MEA) that are 10–50 µm in diameter and are spaced from 150–300 µm apart, such that they will detect signals from separate portions of the network. These differ from the high-density MEAs, which can contain thousands of CMOS-based electrodes that are closely spaced ($\sim$20 µm) such that multiple points can be recorded from the same neuron. More information on these systems can be found in chapters "Large Scale, High-Resolution Microelectrode Arrays for Interrogation of Neurons and Networks" and "Active High-Density Electrode Arrays: Technology and Applications in Neuronal Cell Cultures" of this book. Although they have not yet been utilized in toxicological studies, they offer the opportunity to evaluate chemical effects on action-potential generation and propagation, and associate electrical changes with structural features at the level of the individual cell. However, since CMOS-based MEAs have not been widely utilized in neurotoxicological studies, the rest of this chapter will focus on the conventional format MEAs. In the last decade or so, MEA recording approaches have become much more available to the scientific community as MEA systems have been commercialized and software has been improved to facilitate the execution of experiments and analysis of the resultant data. The throughput of MEA systems has also increased, from single well systems with (typically) 60–64 electrodes/MEA chip to multi-well plate formats that may have as many as 96 wells each with 8 electrodes. Typically, an MEA system will consist of the following components: MEA chips or plates; amplifier, computer; data collection and analysis software. In terms of laboratory space, MEA systems have a small footprint (a few square feet) and are easy to accommodate. Detailed information on systems and requirements can be found on the websites of the manufacturers of MEA equipment, provided

Table 1 Manufacturers of MEA equipment

Company	Format	Website
Axion Biosystems	Single and multi-well	www.axionbiosystems.com
MED64	Single and multi-well	www.med64.com
Multichannel Systems	Single and multi-well	www.multichannelsystems.com
Maxwell Biosystems	Single and multi-well (CMOS-based systems)	www.mxwbio.com/

in Table 1. Other laboratory requirements will be a cell culture facility including a laminar flow hood, incubator and associated equipment. One consideration of importance, especially for multi-well systems, is data storage space; a single 1 h raw recording from a 48 well plate on the Axion system can be as large as 50 GB. Thus, an active laboratory can easily produce several terabytes of data in a few months. Having adequate space to store and back up this data is crucial, especially if the data are to be used for regulatory purposes, where there may be specific requirements for data storage and handling.

Good quality MEA data, especially in higher-throughput systems, starts with good and consistent laboratory tissue culture techniques. In part, this is driven by having experienced hands preparing the plates and the cultures. However, even those less experienced with tissue culture techniques can prepare high quality cultures by following established protocols closely and consistently. There are several publications that address good cell culture practices related for toxicology studies (Pamies et al. 2017, 2018; Pamies and Hartung 2017; Eskes et al. 2017). Successful MEA recordings can be made from a wide variety of different tissue types, including primary cultures of rodent cortex (Xiang et al. 2007), hippocampus (Arnold et al. 2005), brain stem (Su and Jiang 2006), auditory cortex (Gopal and Gross 1996), and dorsal root ganglion (Newberry et al. 2016). Active cultures can be prepared from either fresh tissue, or from frozen cells, which gives researchers some options for tissue sources. There has been tremendous progress in the availability of human-derived tissues for MEA recordings in the past decade. Several different vendors now supply human embryonic or inducible pluripotent stem cell-derived models that result in neural networks that exhibit robust spiking, bursting, and coordinated bursting, similar to their rodent counterparts (Fig. 1). For these commercially available human models, the vendors often have worked out and provide detailed protocols for the use of their cells on different MEA systems. Following these protocols as written will result in successful recordings and make the best use of these cells, which are not inexpensive.

Another important methodological consideration is attention to detail during the execution of experiments. Network activity is sensitive to and influenced by temperature, pH, osmolarity, and physical disruptions. Most MEA systems have built-in temperature control, and some newer systems also have environmental controls for humidity and CO_2 that help to mitigate against evaporation of the media and pH changes that may occur over time with longer recordings. Mechanical
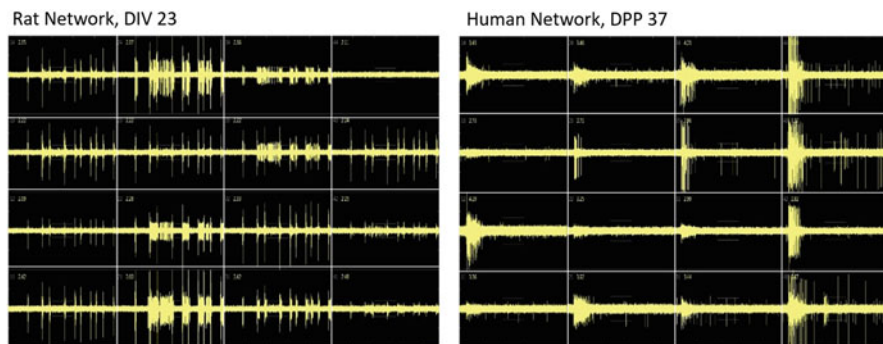
Fig. 1 Comparison of rodent vs human neural networks. Screenshots of spiking and bursting activity in a rat (left) and human (right) cortical network grown in 48 well plates for 23 and 37 days, respectively. Human networks of direct differentiated neurons (1.4×10^5 excitatory cells, 0.6×10^5 inhibitory cells), and glia (0.7×10^5) astroglial cells/well recorded at 37 days post-plating (DPP) show similar spiking and bursting patterns when compared to rat cells plated at 150,000 cells/well from post-natal day 0 cortex (as described in Valdivia et al. 2014) recorded at 23 days in vitro (DIV). Human cells provided by J. Davila and D. Haag, Stanford University

disturbances can temporarily change network activity, so typically a period of time (10–30 min) is needed for activity to stabilize again following transfer of cultures from the incubator into the amplifier or the addition of test compounds. Thus, each laboratory needs to establish the appropriate amount of time for both based on their experience, and dosing needs to be done carefully in order to minimize the disturbance.

With respect to evaluating the potential neurotoxicity of compounds using MEAs, it is important to consider whether network activity is being disrupted due to effects on the neurophysiology or concomitantly with alterations in cell health. This is important whether acute or longer term (e.g., developmental or delayed/"chronic") effects are being examined. Most single-well MEA formats are made from glass or other clear substrates, making morphological evaluation possible. Further, the low throughput of these formats is also amenable to the more time-consuming evaluation of morphological alterations on each network treated with a compound. The increased availability of multi-well format MEAs has complicated evaluation of cell health for two reasons; the number of networks to evaluate is dramatically increased and not all multi-well formats are transparent, which prevents visual and/or morphological assessments. Consider an experiment where triplicate measurements are made across three 48 well plates. Even if visual inspection is possible, there are 144 wells to inspect. Thus, other methods are required to examine cell health following treatment with potentially neurotoxic compounds. One can use "sister plates" to examine cell health in parallel with MEA experiments. However, this increases both time and materials required for tissue culture and maintenance of cells. Wallace et al. (2015) demonstrated that multiplexed measurements of network activity and cell viability could be made

by using lactate dehydrogenase (LDH) and alamar blue (AB) assays immediately following recordings (detailed protocols are available in Brown et al. 2017). Caveats regarding any cell viability assays should be kept in mind. For example, the assays above reflect the health of all cells in the culture, whether neurons or glia. Thus, effects on a specific population might be blunted or missed, if for example a compound was only cytotoxic to neurons. Thus, the lack of a response in these assays does not necessarily indicate that a compound had no adverse effects on cell health. By contrast, a decreased signal also does not necessarily indicate cell death, especially following developmental or longer term exposures. For example, a compound might decrease glial proliferation, resulting in lower total LDH as well as reduced metabolic activity (AB), even though no cell death has occurred. Even with these caveats, having some information on cell health can be useful in screening, and more mechanistic assessments can always be conducted as a follow-up to hits (chemicals that alter network function).

The availability of multi-well MEA formats has made possible screening large numbers of compounds for potential effects on network activity and development of network activity. There are several experimental design issues that must be considered when conducting screening experiments using multi-well plates, including how many replicates are needed, whether to place those replicates on the same plate or different plates, and whether or not there are differences between wells along the edge of the plate compared to those in the interior. Each laboratory will have to determine empirically what works best in its hands. However, our experience with 48 well MEA plates has been that well-to-well variability is as high or higher than plate-to-plate variability, and that culture-to-culture variability is higher than either of these. This is likely due to our use of primary cultures as each culture is made from a different litter of animals every week. When screening for neurotoxicity or developmental neurotoxicity, we typically test compounds in triplicates across three different plates within the same culture (Fig. 2). This is a common approach for screening of compounds (Malo et al. 2006) as it reduces biological variability due to day-to-day and culture-to-culture differences. For higher throughput, a single high concentration of a compound can be screened to identify "hits" (e.g., Strickland et al. 2018). This allows more compounds to be tested on a plate, and hits can then be followed up with concentration-response characterization. A concern when screening with multi-well plates is that the microenvironment of the wells along the edge of the plate differs from the middle wells, giving rise to differences in cellular responses. Therefore, we analyzed historical data for potential differences between edge and interior wells, and did find that some parameters were statistically different. However, the mean differences between edge and interior wells were very small (Table 2) and were only detected as statistically different due to the large sample size. As such, they were not considered biologically relevant. However, to prevent all of the control data coming from edge wells, we commonly distribute our control wells on each plate between both edge and control wells (Fig. 2).
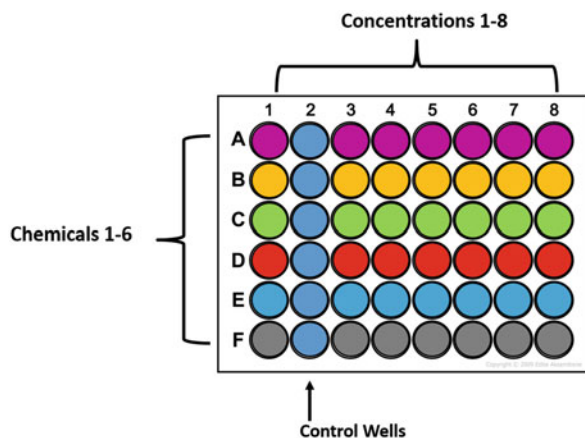
Fig. 2 Example plate layout for screening chemicals. A typical arrangement of chemicals on MEA plates for a screening experiment. Six chemicals are tested over seven different concentrations on triplicate plates. One row on each plate is used for each chemical (represented by different colors, while different concentrations (typically increasing) are arranged across columns 1–8). The blue wells represent control wells, which are always located so that both edge and interior wells are included. Each plate contains six control wells; if needed, some wells can be used for positive control (e.g., bicuculline or tetrodotoxin) treatments, or as control wells for viability assays (see Brown et al. 2017 for additional details)

Table 2 Comparison of edge and inner wells on 48 well MEA plates

Endpoint	p-value from paired t-test	Mean difference[a]	DF (# of averaged recordings -1)
Mean firing rate	NS	NA	199
Burst/min	NS	NA	199
% of spikes in burst	2.739×10^{-9}	-5.369	199
# active electrodes	0.02963	-0.28667	199
# actively bursting electrodes	0.01117	-0.352	199
# of network spikes	1.418×10^{-7}	20.18396	199
% spikes in network spike	0.02814	0.8132	199
r	0.003842	-0.01311	199

50 total plates (each with four DIVs (5, 7, 9, and 12) resulting in recordings from 200 edge well and 200 inner well values for paired t-test)
[a]Differences were calculated by subtracting the inner well values from the edge wells and taking the mean of the result. Mean (Edge well $-$ Inner well)

3 Data and Data Analysis for MEA Recordings

As mentioned above and shown in Fig. 1, neural activity as measured by MEAs is complex and results in spatially and temporally rich patterns of activity. Initially, toxicological studies using MEAs focused primarily on the mean firing rate (MFR) of the network (although some studies examined multiple parameters). The focus

on MFR was driven by the fact that it is both a sensitive measure and the one that is easily extracted from the data, which facilitated rapid evaluation of whether or not a compound disrupted activity. However, other parameters can be extracted from the recordings that describe the characteristics of bursting, synchrony, oscillations of network activity and mutual information (Ball et al. 2017) contained in the network. These and other network parameters are described in Table 3. As discussed in Sect. 6, a more complete description of the pattern of network parameter disruption caused by a potential toxicant might be useful to identify the class of compound or predict in vivo activities (e.g., seizures).

Typically, the ability of a compound to disrupt network activity is reported in one of two ways, alteration of activity beyond a preset threshold (e.g., McConnell et al. 2012; Valdivia et al. 2014; Strickland et al. 2018) or by reporting the potency of the compound for altering a particular parameter (e.g., Defranchi et al. 2011; Brown et al. 2016; Frank et al. 2017; Zwartsen et al. 2018). The former is typically employed when testing only a single concentration of a compound for effects on network activity. Typically, the change in one or more parameters is compared to the change resulting from treating sister wells with the vehicle used for dissolving the compounds, such as DMSO, ethanol, or water. Often, the test compound is not considered active (or a hit) unless the change it causes lies beyond one or (more typically) two times the change caused by the vehicle. The latter approach, in which potency is determined, can be used when networks are exposed to multiple concentrations of the same compound, either in a cumulative manner (the concentration of compound is increased in the same well and compared to pre-exposure values) or a "multi-well" approach, where each well receives one concentration of a compound and the effects are compared to pre-exposure values and/or wells treated with vehicle. In either case, potency is usually determined by calculating an EC_{50} (Effective Concentration that changes the response by 50%, compared to control) by fitting the data to a non-linear relationship such as a sigmoidal dose-response curve.

While the above approaches work for single timepoint measurements, they fail to take advantage of the ability of MEAs to make repeated measures of network function over time. However, analysis of such data is more complex, as the overall effects is a function of both time- and concentration-parameters. To address this issue, we have used the area under the curve, which captures both time and concentration-dependent effects (Fig. 3). We first calculate the trapezoidal area under the curve (AUC) for each concentration and timepoint, and then determine the EC_{50} values by fitting the AUC values at each concentration to a sigmoidal dose-response relationship.

4 Use of MEAs for Acute Neurotoxicity Screening

MEAs have been used to understand the actions of neuroactive and neurotoxic substances since they were introduced in the late 1990s. In 2010, Andrew Johnstone, myself, and others (Johnstone et al. 2010) reviewed the use of MEAs for this purpose

Table 3 Examples of different parameters of network function that can be evaluated by MEA recordings

| Type of measure	Parameter	Description
General activity	Mean firing rate or mean spike rate	The mean firing (spiking) rate. Typically measured on each electrode, with the value the mean across all electrodes in the well and reported in spikes/min or in Hz
	Burst rate	The number of bursts per unit time; typically reported in bursts/min
	Number of active electrodes	Number of electrodes firing at or above a pre-defined spike rate
	Number of actively bursting electrodes	Number of electrodes with burst rates at or above a pre-defined burst rate
Bursting activity	Interspike Interval (ISI) within a burst	Time interval between spikes within a burst. Typically reported in milliseconds
	Percentage of spikes in burst	The number of spikes that occur within a burst as a percentage of the total spikes. Recorded at the electrode level but often reported as a well-wide average
	Mean burst duration	Mean duration of a burst. Typically reported in milliseconds (ms)
	Mean interburst interval (IBI)	Mean time interval between bursts. Typically reported in seconds (s)
Network connectivity	Number of network spikes (also called network bursts)	A network spike (or burst) is activity that co-occurs simultaneously across a set minimum number of electrodes (see Eytan and Marom 2006)
	Network spike peak	The number of electrodes active at peak of network spike
	Network spike duration (NSD)	The average duration (ms) of a network spike
	SD of network spike duration	Standard deviation of network spike duration. Describes how consistent the network spike is
	ISI in network spike	Mean interspike interval for spikes in network spikes
	Mean number of spikes in network spikes	Number of spikes in network spike
	% spikes in network spike	Number of spikes that occur within a network spike over the total number of spikes
	Mean correlation (r)	The average of all pairwise correlation between all electrodes
	Normalized mutual information	A measure of complexity and synchrony in a network that is robust with respect to changes in the size of the network (see Ball et al. 2017)
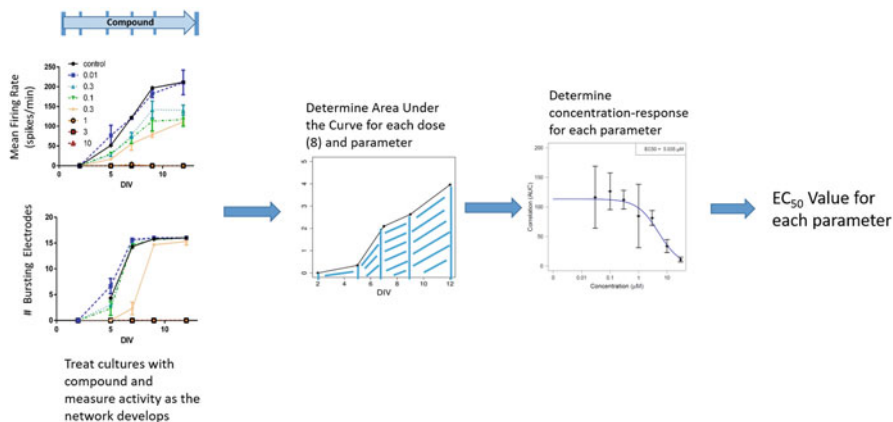
Fig. 3 Determining EC_{50} values based on Area Under the Curve (AUC) measurements. In the example above, networks were exposed to compound and activity was recorded on days in vitro (DIV) 5, 7, 9, and 12. On the far left, examples are shown for two parameters, mean firing rate and number of bursting electrodes, but the approach can be expanded to multiple parameters. In the middle panel, an example is shown illustrating how the trapezoidal area under the curve is determined for each concentration (8 in this case) and parameter. Once AUC values are determined for each parameter, they can be fit to sigmoidal concentration-response relationships (right panel)

and further proposed that MEAs could be a useful tool for screening larger numbers of compounds for potential neurotoxicity. As part of the review, we included a table that summarized the use of MEAs for toxicity studies, and therefore I will not present that same information here. Since then, neural networks grown on MEAs have been used to determine the activity of a large number of different types and classes of compounds, including agrochemicals (Alloisio et al. 2015), pyrethroid insecticides (Shafer et al. 2008; Meyer et al. 2008; Mohana Krishnan and Prakhya 2016; Baskar and Murthy 2018) and mixtures of pyrethroids (Scelfo et al. 2012; Johnstone et al. 2017), nanoparticles (Gramowski et al. 2010; Strickland et al. 2016a, b), tricresyl phosphate (Duarte et al. 2017), illicit drugs (Hondebrink et al. 2016), glufosinate (Lantz et al. 2014), antiepileptic drugs (Colombi et al. 2013), excitotoxicants (Frega et al. 2012), components of harmful algae (Alloisio et al. 2016), neuroactive toxins (Pancrazio et al. 2014; Kasteel and Westerink 2017), and metals (Dingemans et al. 2016; Huang et al. 2016).

In addition to these studies directed at understanding specific types of compounds, tremendous progress has been made in the last 8 years towards demonstrating that neural networks grown on MEAs are indeed useful for acute neurotoxicity screening. This has in part been driven by the availability of commercially available multi-well MEA formats that have substantially increased throughput of MEA testing as well as the publication of the report from the NRC on *Toxicity testing in the 21st Century* (NRC 2007), which called for increased development of predictive, in vitro approaches for toxicity hazard characterization.

Two of the earlier studies demonstrating proof-of-principle for using MEAs for neurotoxicity screening were published by Defranchi et al. (2011) and McConnell et al. (2012). In both cases, the authors selected a small number of compounds (20 and 30, respectively) that had well-established effects on nervous system function or lack thereof (negative controls). Neural networks grown on MEAs were shown to have high sensitivity (correct identification of active compounds), with these studies reporting that 77–87% of the neurotoxic/neuroactive substances altered mean firing rates of networks. Specificity (correct identification of non-neuroactive compounds) was also high, ranging from 86 to 100%. In an additional study, Nicolas and co-workers demonstrated 88% sensitivity of rat cortical cultures grown on MEAs to detect 15 known neuroactive compounds, including marine neurotoxins found in seafood (Nicolas et al. 2014). These initial studies indicate that neural networks grown on MEAs could be useful for screening compounds where potential for neurotoxicity had not yet been evaluated, and in the case of marine toxins, may be a less expensive, faster and more ethical approach than current animal-based approaches (Nicolas et al. 2014). There is also evidence that results across different laboratories and platforms are also quite replicable. Two different studies involving multiple laboratories have demonstrated consistency in results in response to neuroactive drugs (Novellino et al. 2011) as well as positive and negative control neurotoxicants (Vassallo et al. 2017). While only a small number of chemicals were tested in each of these studies, the collective high sensitivity and cross-laboratory reproducibility indicates that MEAs offer potential for neurotoxicity screening. Nevertheless, additional evaluation of the approach, including testing larger numbers of chemicals, was needed.

As a follow-up to the study by McConnell, my laboratory obtained 93 compounds from the ToxCast library (Richard et al. 2016) and tested these in primary cortical networks grown on MEAs. These compounds had all been tested in the ToxCast program, which examines the effects of compounds in a battery or over 800 assays. A sub-set of 20 ToxCast assays measure activity towards voltage- and ligand-gated ion channels. Again, MEAs were quite specific, detecting approximately 73% of compounds that were recognized to be neurotoxic/neuroactive. In addition, MEAs also detected classes of compounds that were not identified as active in the ToxCast ion channel assays, including GABAergic and pyrethroid compounds (Valdivia et al. 2014). Interestingly and importantly, this study also indicated that combining the MEA assay with ToxCast assays may improve screening for neurotoxicity overall, as the cortical culture used in this study appears to be relatively insensitive to nicotinic compounds (McConnell et al. 2012; Valdivia et al. 2014), which were well detected by alpha-bungarotoxin binding assays in ToxCast. Combining the MEA and ToxCast assays resulted in 85% sensitivity. Thus, MEAs also appear to be complimentary to other screening approaches, increasing their value as part of an integrated testing approach.

These initial studies provided the justification to screen the entire Phase I and II libraries of the ToxCast chemical space in rat primary cortical neurons grown on MEAs. The goal here was not to evaluate sensitivity or specificity of MEAs, but rather to demonstrate that they could be used to screen a large set

of chemicals (Crofton et al. 2011); the Phase I and II library consists of 1055 unique substances. Greater than 85% of the active compounds (326 total) fell into five broad chemical categories: pesticides, pharmaceuticals, chemical intermediates, microbiocides/fungicides and herbicides (Strickland et al. 2018). Since the chemical space covered by ToxCast includes broad categories such as fragrances, "green chemicals," food flavors and additives, and surfactants (Richard et al. 2016), these results indicated that compounds which disrupt network activity may be largely comprised of those that were specifically designed to be biologically active (e.g., pharmaceuticals, pesticides, etc.). Testing of additional compounds will help to confirm this observation. The entire set of compounds was screened at a single concentration in less than a year (Strickland et al. 2018). While this may not on the surface appear to be very remarkable, consider that this was done without the assistance of automation (plating or dosing robots, for example), and that the single largest limiting factor was the ability of our tissue culture facility to generate cultures. In this case, the use of fresh primary cultures, due to requirements for timed pregnant animals, reduced the number of cultures that could be made to one per week. Additional considerations related to screening are discussed below.

5 Use of MEAs to Screen Compounds for Developmental Neurotoxicity

In the last 20–30 years, there have been world-wide reports of increasing rates of neurodevelopmental disorders (Grandjean and Landrigan 2006, 2014; Hertz-Picciotto et al. 2006; Karr 2012; Polańska et al. 2012) such as autism and attention-deficit hyperactivity disorder (ADHD). While increased diagnostic awareness does contribute to this, it is unlikely to completely account for these increases. There is concern that developmental exposure to environmental chemicals may contribute to the etiology of these diseases (Grandjean and Landrigan 2006, 2014). Testing chemicals for potential developmental neurotoxicity (DNT) is time-consuming, expensive, and animal-intensive (Crofton et al. 2012), and as a result, only slightly more than 100 (Makris et al. 2009) of the tens of thousands of compounds present in the environment (Judson et al. 2009) have been evaluated for DNT using formalized guideline studies. To address this data gap, considerable effort has been directed over the last decade towards development of rapid, cost-effective in vitro screens capable of testing large numbers of compounds for the potential to cause DNT. The proposed assays cover different biological processes important to development of the nervous system, such as proliferation and differentiation of neuroprogenitor cells, synapse and network formation, among others. Furthermore, a wide variety of approaches ranging from genomic/transcriptomic profiling, morphological assessment using high-content imaging, and behavioral assessments in alternative species (e.g., zebrafish) have been proposed. Recently, a comprehensive review and proposal for development of a tiered screening strategy for DNT testing

has been published (Bal-Price et al. 2018); assessment of compound effects on neural network development using MEA approaches is a critical component of this approach.

The use of MEAs for DNT screening offers three clear benefits to a battery of assays. First, and foremost, it provides for a functional assessment of compound effects on network development. Many of the other assays are based on structural changes or alterations in the expression of genomic or transcriptomic signals. A general feature of neurons grown on MEAs is a clear ontogeny of spontaneous activity reflecting network development (Fig. 4). Spontaneous network activity initially consists of sporadic, unorganized single action potential "spikes" that over time transitions to an organized network that exhibits synchronous bursting activity (Biffi et al. 2013; Charlesworth et al. 2015; Chiappalone et al. 2006; Cotterill et al. 2016; van Pelt et al. 2005; Wagenaar et al. 2006a). A second important feature of MEAs for DNT screening is that they are non-invasive, and thus allow for repeated measurement from the same network on multiple occasions during network development. Thus, effects of environmental compounds on neural network development can easily be evaluated in MEAs; most of the other assays that would comprise a DNT screening battery rely on assessment of compound effect at a single timepoint following exposure. Finally, network development is a more apical process than many of the other processes that are proposed in the battery (e.g., proliferation, neurite outgrowth). Thus, it incorporates aspects of neuronal differentiation and neurite outgrowth, synaptogenesis, interactions between neurons and glia, potentially making network formation assays using MEAs a more "broadband" endpoint that may be capable of catching compounds that other assays miss. However, this possibility cannot be explored fully until more chemicals have been tested across several assays in the proposed battery.

Two early studies established the proof-of-concept that MEAs could be utilized to screen compounds for potential developmental neurotoxicity. We demonstrated that the protein kinase C inhibitor bisindolylmaleimide (Bis-1) caused decreases in the firing and bursting rates of the networks following exposure during the first 2 weeks in vitro (Robinette et al. 2011). Furthermore, these changes in network development occurred at concentrations that decreased neurite outgrowth (Harrill et al. 2011). Our colleagues working at the European Commission's Joint Research Center showed that exposure to low concentrations of domoic acid during network development and maturation increased network activity and altered the pharmacological responsiveness of the network to bicuculline (Hogberg et al. 2011). An important limitation highlighted by these studies was that they relied on single-well MEA devices, and thus lacked the throughput necessary to be useful for screening purposes. This was addressed by the advent of multi-well MEA formats that appeared on the market around the time these studies were published. A second limitation of these studies was that while they included untreated controls, they evaluated only one compound each and did not include a "negative" control compound.
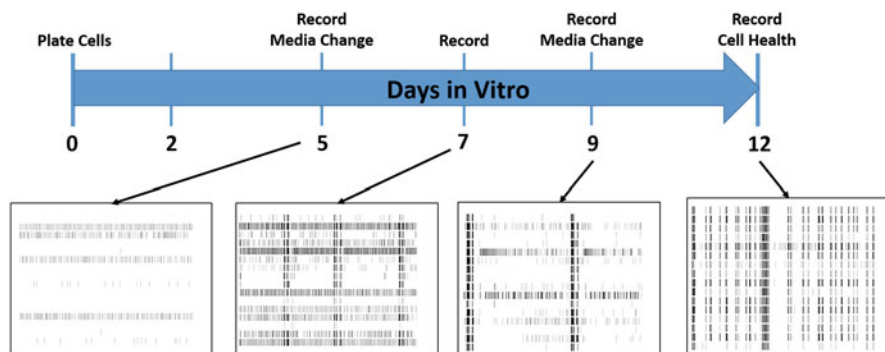
Fig. 4 Experimental design for the Network Formation Assay (NFA) using MEAs. To screen compound for the potential to cause developmental neurotoxicity, primary cortical cultures are treated with compounds 2 h after plating, so that the compound is present throughout development of the network. Recordings are made (15 min) on days in vitro (DIV) 5, 7, 9, and 12, and media is changed (with refresh of chemical) on DIVs 5 and 9. Following recording on DIV 12, cell health is assessed using lactate dehydrogenase and alamar blue assays. The raster plots illustrate network activity from untreated networks on DIVs 5, 7, 9, and 12. As the culture matures, activity increases across the electrodes in a well and becomes more organized

The availability of multi-well MEA formats has accelerated development of a network formation assay on MEAs that could be used for DNT screening. Brown and colleagues demonstrated that assay positive controls (Crofton et al. 2011) altered network formation as expected, and that the negative control compound acetaminophen was without effects (Brown et al. 2016). The general protocol for this assay is illustrated in Fig. 4. Following this, the approach was used to screen a set of 86 compounds which consisted of compounds where there was evidence in the literature that they caused developmental neurotoxicity in vivo, compounds that were putative "negative" compounds, and compounds with unknown effects on nervous system development in vivo (Frank et al. 2017). In Table 4, an analysis of the sensitivity and specificity of this data is presented, similar to that presented in Harrill et al. (2018) for data from high-content imaging assays. The network formation assay using MEAs has both high sensitivity (correct identification of in vivo DNT compounds) and specificity (correct identification of compounds without evidence of DNT in vivo). When results are filtered to include only those where the effect on the network activity parameter was at least threefold more potent than the effect on viability, the sensitivity of the assay decreases. However, consider that not all compounds that cause DNT in vivo will alter network formation, as well as the fact that sensitivity for this assay is higher than for any of the other assays evaluated in Harrill et al. (2018).

The ability of MEAs to make multiple assessments over time was utilized for a subsequent analysis of the data in Frank et al. (2018) that determined "tipping points" for chemical effects on network development. Tipping points represent the critical concentration above which perturbations in function can no longer

Table 4 Sensitivity and specificity of the network formation assay for developmental neurotoxicants

Measure	# compounds	Correct classification[a]	% correct	Correct selective classification[b]	% correct selective classification
Sensitivity	60	49	82	35	58
Specificity	23	21	91	21	91

Sensitivity = number of correctly identified compounds with evidence of in vivo DNT that had effects in the network formation assay in vitro

Specificity = number of correctly identified negative compounds; those that are without effects on DNT in vivo and were without effects in the network formation assay in vitro

[a]Considers effects on network activity endpoints and cell viability

[b]Considers only specific effects wherein there was at least a threefold difference between the EC_{50} value for network activity endpoints compared to the EC_{50} for viability

be compensated for using homeostatic mechanisms. Of the 64 compounds that altered some aspect of network activity in Frank et al. (2017), tipping points could be determined for 42 of them (Frank et al. 2018). Further, for a small number of compounds where sufficient data were available for estimation of in vivo concentrations, the tipping point could be related to in vivo levels that were associated with developmental neurotoxicity. Although the number of chemicals that have been assessed is small, the results indicate that effects of some of these compounds to disrupt network development are comparable to in vivo levels that are associated with developmental neurotoxicity.

6 Future Directions

While tremendous progress has been made in the last decade towards using MEAs for neurotoxicity and developmental neurotoxicity screening, there are several areas where improvements could be made that would increase the acceptance and utilization of MEA data for regulatory decision-making. The first area is to have larger numbers of chemicals tested by more laboratories, including chemicals in common across laboratories. While it might not seem like the most effective use of resources to re-test the same chemicals, it will provide the data needed to increase confidence that MEA data are replicable and reliable for screening and decision-making purposes. In addition, it will help to define the "fit-for-purpose" of the assay, by demonstrating classes of chemicals or particular pharmacological responses that may not be detected by MEA assays. For example, work related to whether or not neural networks on MEAs are capable of detecting nicotinic compounds has been inconsistent. Previous studies in my laboratory (McConnell et al. 2012; Valdivia et al. 2014) with nicotine and neonicotinoid insecticides (with the exceptions of clothianidin and thiamethoxam) indicated a lack of sensitivity to nicotinic compounds or a false negative response (e.g., due to dose selection). By contrast, reports from other laboratories indicate varying effects of nicotine on mean

firing rate (MFR) of cortical cultures on MEAs, including slight increases at 100 μM (Defranchi et al. 2011; Hondebrink et al. 2016), lack of statistically significant effects (≤500 μM; Mack et al. 2014) or significant inhibition (300–1000 μM; Hondebrink et al. 2016). Effects of the nAChR-selective antagonist mecamylamine were limited to changes in burst duration and the percentage of spikes occurring in a burst (Hammond et al. 2013). These parameters were not evaluated in the current or previous (Defranchi et al. 2011; McConnell et al. 2012; Valdivia et al. 2014; Hondebrink et al. 2016) studies. Thus, it may be that there is a better metric than MFR to detect nicotinic effects in neural networks.

Better use of the rich spatial and temporal data provided by MEA recordings is a second area where advancements could increase the acceptance and utilization of MEA data for regulatory decisions. More information on burst detection methodologies is available in the chapter by Cotterill and Eglen (this volume), so the focus here will be on how characterization of bursting and other metrics of network activity have been applied to toxicity assessments using MEAs. To date, the majority of studies of effects of neuroactive or neurotoxic compounds have focused primarily on their actions on the MFR of networks, despite the fact that many other parameters of activity regarding the spike train can be evaluated. In part, this is because the MFR has traditionally been a very sensitive metric and is easily extractable from the data. However, vendor supplied software for some systems now routinely analyze multiple aspects of network activity, facilitating examination of multiple endpoints, and scripts for such analyses are also increasingly freely available through sources such as GitHub. The small number of overall studies that consider multiple endpoints have universally demonstrated its added value. In 2014, Mack and co-workers demonstrated that a group of different classes of neurotoxicants could be separated by considering multiple bursting endpoints and conducting a principle components analysis of the data. This approach clearly separated GABA$_A$ antagonists from other classes of compounds (Mack et al. 2014). Using a similar multiparametric approach, Alloisio et al. (2015) were able to demonstrate different patterns of activity that separated 11 pesticides into four groups producing different phenotypic changes in activity (Alloisio et al. 2015). A more recent study (Bradley et al. 2018) has demonstrated that a group of 16 seizuragenic compounds could be distinguished and assigned to different groups based on 12 parameters of firing, bursting, and synchrony from MEA recordings while similar approaches were used by Bader et al. (2017) to characterize phenotypically different responses mediated by different GABA$_A$ and GABA$_B$ receptor-active pharmacological agents (Bader et al. 2017). Consideration of bursting characteristics as well as measures of network connectivity (e.g., correlated activity across electrodes) is also an efficient approach for identification of compounds that alter neural network development (Brown et al. 2016; Frank et al. 2017). Using random forest analysis, these studies demonstrated that as a network matures in vitro, network parameters besides MFR, such as mutual information (Ball et al. 2017), correlation (r), burst rate, and number of network spikes/bursts, become increasingly more important to correct identification of treatments that alter activity in neural networks grown on MEAs. From the standpoint of screening

unknown compounds for potential neuroactivity/neurotoxicity, developing methods to characterize "fingerprints" would be exceptionally valuable, as the fingerprints of unknown compounds could be compared to a database of known compounds to classify an unknown into a particular mode of action (e.g., compound A resembles a pyrethroid, while compound B resembles an opioid). Such information could be used for a number of purposes, to choose between safer drugs/chemicals during the development process, to rank compounds within a particular class with respect to potency or to design focused in vivo studies that would require fewer animals. In the example of the compounds above, one might evaluate compound A for stereotypical signs of pyrethroid poisoning (choreoathetosis, salivation, hyperactivity, tremor), while compound B would be evaluated for sedation. However, more widespread use of multiparametric evaluation is needed, including the testing of many more chemicals from different classes of compounds.

The use of human-derived, rather than rodent, neurons is also important to advancing toxicity testing with MEAs. Chapter 6 (Narkilahti and co-workers) of this book is devoted to use of human models in MEAs, so the comments here will focus on the use of these models in toxicity testing and screening. To date, there have been small numbers of publications that have examined effects of neurotoxic compounds on network activity using neurons derived from human embryonic or inducible pluripotent stem (iPS) cells. In terms of ethical considerations, inducible pluripotent-derived neurons may be preferable and are becoming widely available through a number of vendors. In one of the earliest studies, sub-micromolar levels of methylmercury dramatically inhibited network activity in human embryonic stem cell-derived neural networks (Ylä-Outinen et al. 2010). More recently, iCell neurons from CDI were used to evaluate the effects of glutamate, GABA, endosulfan, and amphetamine on network activity (Tukker et al. 2016). While there were differences in the activity of the iCell neurons and rat primary cortical cultures, the former responded to these four treatments appropriately. Hondebrink et al. (2017) have recently characterized the actions of the psychoactive substance methoxetamine on network activity in both cortical (glutamatergic and gabaergic) and midbrain (dopaminerginic) iPS-derived neurons, with and without glia. In the presence of glia, the concentration-response was left-shifted compared to recordings in the absence of glia. In addition, the midbrain culture was less sensitive than the cortical culture to inhibition of activity by methoxetamine (Hondebrink et al. 2017). In one of the few studies where direct comparisons of neurotoxic effects have been made in human and rodent networks, the potency of the marine neurotoxin tetrodotoxin was equipotent in human and rodent networks (10 and 7 nM, respectively; Kasteel and Westerink 2017). Additional studies comparing concentration-response between human and rodent networks are needed to understand better species differences and to facilitate cross-species comparisons between in vitro and in vivo rodent data and in vitro human data that will allow extrapolation to in vivo exposures in humans. To date, the studies above have focused mostly on exposures following establishment of robust network activity. While it would be desirable to use human stem cell-derived networks for screening compounds for potential developmental neurotoxicity, this may be challenging. In general, neural networks derived from

human models tend to take longer (~3–5 weeks) to develop robust, coordinated spiking and bursting activity that is typically observed in rodent cultures (2–3 weeks; Odawara et al. 2014). This more prolonged developmental profile is less useful for higher-throughput screening because an assay would be longer and require more time and resources to test a compound compared to rodent cultures. However, with currently available human models, it should be possible to confirm activity observed in rodent models, when such data are required.

A unique feature of the nervous system is its plasticity. At the whole animal level, this is exhibited in the form of learning and memory, while at the circuit level, processes such as long-term potentiation (LTP) and long-term depression (LTD) are possible mechanisms that may mediate some forms of learning and memory. Plasticity is also sensitive to disruption by chemical neurotoxicants (Gilbert 2000; Ogiue-Ikeda et al. 2008; Holahan and Smith 2015). LTP and LTD are easily measured in recordings from preparations such as hippocampal slices, and there are well-established protocols for inducing these that can be carried out by any competent laboratory in the world. Although numerous protocols to induce plasticity changes in dissociated neurons grown on MEAs have been published (Arnold et al. 2005; Chiappalone et al. 2008; Massobrio et al. 2015; Odawara et al. 2016), none has been established to date as a ubiquitous protocol (see Wagenaar et al. 2006b for further discussion). The establishment of a protocol for examining plasticity in dissociated neural networks should be a high priority among neurobiologists working in this area. Current methods that could be used to screen compounds for effects on plasticity are either hippocampal slices from rodents or non-mammalian preparations such as *C. elegans* or Drosophila. These models either lack throughput or relevance to humans, whereas a dissociated culture model using human neurons grown on MEAs (e.g., Odawara et al. 2016) could dramatically increase throughput and provide human relevance for testing of drugs that enhance or chemicals that perturb plasticity.

Summary Since their first uses in the late 1990s, MEA approaches have evolved from a niche neurophysiological application into commercially available, high-throughput and high-content platforms. During this time, their use to address neurotoxicological questions has increased steadily. At present, these platforms are being utilized to address mechanistic issues and screen compounds for neurotoxicity and developmental neurotoxicity. The more recent greater availability of human neural models has only served to increase both the possibilities and the relevance of this approach to toxicity testing, and the promises of future improvements mean that MEAs will be a relevant and well-utilized approach that will provide meaningful data to both scientists and regulators.

References

Alloisio, S., Giussani, V., Nobile, M., Chiantore, M., & Novellino, A. (2016). Microelectrode array (MEA) platform as a sensitive tool to detect and evaluate Ostreopsis cf. ovata toxicity. *Harmful Algae, 55*, 230–237.

Alloisio, S., Nobile, M., & Novellino, A. (2015). Multiparametric characterisation of neuronal network activity for in vitro agrochemical neurotoxicity assessment. *Neurotoxicology, 48*, 152–165.

Arnold, F. J., Hofmann, F., Bengtson, C. P., Wittmann, M., Vanhoutte, P., & Bading, H. (2005). Microelectrode array recordings of cultured hippocampal networks reveal a simple model for transcription and protein synthesis-dependent plasticity. *The Journal of Physiology, 564*(Pt 1), 3–19.

Bader, B. M., Steder,A., Klein, A. B., Frølund, B., Schroeder. O. H. U., Jensen, A. A. (2017). Functional characterization of GABAA receptor-mediated modulation of cortical neuron network activity in microelectrode array recordings. PLoS One. 2017. 12(10):e0186147.

Ball, K. R., Grant, C., Mundy, W. R., & Shafer, T. J. (2017). A multivariate extension of mutual information for growing neural networks. *Neural Networks, 95*, 29–43.

Bal-Price, A., Hogberg, H. T., Crofton, K., Mardas Daneshian, M., FitzGerald, R. E., Fritsche, E., et al. (2018). Recommendation and application of in vitro alternative test readiness criteria: exemplified for developmental neurotoxicity (DNT). Accepted in ALTEX on February 23, 2018.

Baskar, M. K., & Murthy, P. B. (2018). Acute in vitro neurotoxicity of some pyrethroids using microelectrode arrays. *Toxicology In Vitro, 47*, 165–177.

Biffi, E., Regalia, G., Menegon, A., Ferrigno, G., & Pedrocchi, A. (2013). The influence of neuronal density and maturation on network activity of hippocampal cell cultures: A methodological study. *PLoS One, 8*, e83899.

Boyes, W. K. (1993). Sensory-evoked potentials: Measures of neurotoxicity. *NIDA Research Monograph, 136*, 63–98.

Boyes, W. K. (1994). Rat and human sensory evoked potentials and the predictability of human neurotoxicity from rat data. *Neurotoxicology, 15*, 569–578.

Bradley, J. A., Luithardt, H. H., Metea, M. R., & Strock, C. J. (2018). In vitro screening for seizure liability using microelectrode array technology. *Toxicological Sciences, 163*, 240.

Brown, J., Hall, D., Frank, C., Wallace, K., Mundy, W. R., & Shafer, T. J. (2016). Evaluation of a microelectrode array-based assay for neural network ontogeny using training set chemicals. *Toxicological Sciences, 154*, 126–139.

Brown, J. P., Lynch, B., Curry-Chisolm, I., Shafer, T. J., & Strickland, J. D. (2017). Assaying spontaneous network activity and cellular viability using multi-well microelectrode arrays. *Methods in Molecular Biology, 1601*, 153–170.

Charlesworth, P., Cotterill, E., Morton, A., Grant, S. G. N., & Eglen, S. J. (2015). Quantitative differences in developmental profiles of spontaneous activity in cortical and hippocampal cultures. *Neural Development, 10*, 1.

Chiappalone, M., Bove, M., Vato, A., Tedesco, M., & Martinoia, S. (2006). Dissociated cortical networks show spontaneously correlated activity patterns during in vitro development. *Brain Research, 1093*, 41–53.

Chiappalone, M., Massobrio, P., & Martinoia, S. (2008). Network plasticity in cortical assemblies. *The European Journal of Neuroscience, 28*, 221–237.

Colombi, I, Mahajani, S., Frega, M., Gasparini, L., & Chiappalone, M. (2013). Effects of antiepileptic drugs on hippocampal neurons coupled to micro-electrode arrays. *Frontiers in Neuroengineering, 6*, 10.

Cotterill, E., Hall, D., Wallace, K., Mundy, W. R., Eglen, S., & Shafer, T. J. (2016). Characterization of early cortical neural network development in multiwell microelectrode array plates. *Journal of Biomolecular Screening, 21*, 510–519.

Crofton, K. M., Mundy, W. R., Lein, P. J., Bal-Price, A., Coecke, S., Seiler, A. E., et al. (2011). Developmental neurotoxicity testing: Recommendations for developing alternative methods for the screening and prioritization of chemicals. *ALTEX, 28*(1), 9–15.

Crofton, K. M., Mundy, W. R., & Shafer, T. J. (2012). Developmental neurotoxicity testing: A path forward. *Congenital Anomalies, 52*(3), 140–146.

Defranchi, E., Novellino, A., Whelan, M., Vogel, S., Ramirez, T., van Ravenzwaay, B., et al. (2011). Feasibility assessment of micro-electrode chip assay as a method of detecting neurotoxicity in vitro. *Frontiers in Neuroengineering, 4*, 1–12.

Dingemans, M. M., Schütte, M. G., Wiersma, D. M., de Groot, A., van Kleef, R. G., Wijnolts, F. M., et al. (2016). Chronic 14-day exposure to insecticides or methylmercury modulates neuronal activity in primary rat cortical cultures. *Neurotoxicology, 57*, 194–202.

Duarte, D. J., Rutten, J. M., van den Berg, M., & Westerink, R. H. (2017). In vitro neurotoxic hazard characterization of different tricresyl phosphate (TCP) isomers and mixtures. *Neurotoxicology, 59*, 222–230.

Eskes, C., Boström, A. C., Bowe, G., Coecke, S., Hartung, T., Hendriks, G., et al. (2017). Good cell culture practices and in vitro toxicology. *Toxicology In Vitro, 45*, 272–277.

Eytan, D., & Marom, S. (2006). Dynamics and effective topology underlying synchronization in networks of cortical neurons. *The Journal of Neuroscience, 26*, 8465–8476.

Frank, C. L., Brown, J. P., Wallace, K., Mundy, W. R., & Shafer, T. J. (2017). Screening 86 compounds in the neural network formation assay: Developmental neurotoxicants disrupt formation of cortical networks on microelectrode arrays. *Toxicological Sciences, 160*, 121–135.

Frank, C. L., Brown, J. P., Wallace, K., Wambaugh, J. F., Shah, I., & Shafer, T. J. (2018). Defining toxicological tipping points in neuronal network development. *Toxicology and Applied Pharmacology, 354*, 81.

Frega, M., Pasquale, V., Tedesco, M., Marcoli, M., Contestabile, A., Nanni, M., et al. (2012). Cortical cultures coupled to micro-electrode arrays: A novel approach to perform in vitro excitotoxicity testing. *Neurotoxicology and Teratology, 34*, 116–127.

Gilbert, M. E. (2000). In vitro systems as simulations of in vivo conditions: The study of cognition and synaptic plasticity in neurotoxicology. *Annals of the New York Academy of Sciences, 919*, 119–132.

Gopal, K. V., & Gross, G. W. (1996). Auditory cortical neurons in vitro: Cell culture and multichannel extracellular recording. *Acta Oto-Laryngologica, 116*, 690–696.

Gramowski, A., Flossdorf, J., Bhattacharya, K., Jonas, L., Lantow, M., Rahman, Q., et al. (2010). Nanoparticles induce changes of the electrical activity of neuronal networks on microelectrode array neurochips. *Environmental Health Perspectives, 118*, 1363–1369.

Grandjean, P., & Landrigan, P. J. (2006). Developmental neurotoxicity of industrial chemicals. *Lancet, 368*, 2167–2178.

Grandjean, P., & Landrigan, P. J. (2014). Neurobehavioural effects of developmental toxicity. *Lancet Neurology, 13*, 330–338.

Hammond, M. W., Xydas, D., Downes, J. H., Bucci, G., Becerra, V., Warwick, K., et al. (2013). Endogenous cholinergic tone modulates spontaneous network level neuronal activity in primary cortical cultures grown on multi-electrode arrays. *BMC Neuroscience, 14*, 38.

Harrill, J. A., Freudenrich, T. F., Wallace, K., Ball, K., Shafer, T. J., & Mundy, W. R. (2018). Testing for developmental neurotoxicity using a battery of in vitro assays for key cellular events in neurodevelopment. *Toxicology and Applied Pharmacology, 354*, 24–39.

Harrill, J. A., Freudenrich, T. M., Robinette, B. L., & Mundy, W. R. (2011). Comparative sensitivity of human and rat neural cultures to chemical-induced inhibition of neurite outgrowth. *Toxicology and Applied Pharmacology, 256*, 268–280.

Hertz-Picciotto, I., Croen, L. A., Hansen, R., Jones, C. R., van de Water, J., & Pessah, I. N. (2006). The CHARGE study: An epidemiologic investigation of genetic and environmental factors contributing to autism. *Environmental Health Perspectives, 114*, 1119–1125.

Hogberg, H. T., Sobanski, T., Novellino, A., Whelan, M., Weiss, D. G., & Bal-Price, A. K. (2011). Application of micro-electrode arrays (MEAs) as an emerging technology for developmental neurotoxicity: Evaluation of domoic acid-induced effects in primary cultures of rat cortical neurons. *Neurotoxicology, 32*, 158–168.

Holahan, M. R., & Smith, C. A. (2015). Phthalates and neurotoxic effects on hippocampal network plasticity. *Neurotoxicology, 48*, 21–34.

Hondebrink, L., Kasteel, E. E. J., Tukker, A. M., Wijnolts, F. M. J., Verboven, A. H. A., & Westerink, R. H. S. (2017). Neuropharmacological characterization of the new psychoactive substance methoxetamine. *Neuropharmacology, 123*, 1–9.

Hondebrink, L., Verboven, A. H., Drega, W. S., Schmeink, S., de Groot, M. W., van Kleef, R. G., et al. (2016). Neurotoxicity screening of (illicit) drugs using novel methods for analysis of microelectrode array (MEA) recordings. *Neurotoxicology, 55*, 1–9.

Huang, T., Wang, Z., Wei, L., Kindy, M., Zheng, Y., Xi, T., et al. (2016). Microelectrode Array-evaluation of neurotoxic effects of magnesium as an implantable biomaterial. *Journal of Materials Science and Technology, 32*, 89–96.

Johnstone, A. F., Gross, G. W., Weiss, D. G., Schroeder, O. H., Gramowski, A., & Shafer, T. J. (2010). Microelectrode arrays: A physiologically based neurotoxicity testing platform for the 21st century. *Neurotoxicology, 31*, 331–350.

Johnstone, A. F. M., Strickland, J. D., Crofton, K. M., Gennings, C., & Shafer, T. J. (2017). Effects of an environmentally-relevant mixture of pyrethroid insecticides on spontaneous activity in primary cortical networks on microelectrode arrays. *Neurotoxicology, 60*, 234–239.

Judson, R. S., Richard, A., Dix, D. J., Houck, K., Martin, M., Kavlock, R., et al. (2009). The toxicity data landscape for environmental chemicals. *Environmental Health Perspectives, 117*, 685–695.

Karr, C. (2012). Children's environmental health in agricultural settings. *Journal of Agromedicine, 17*, 127–139.

Kasteel, E. E., & Westerink, R. H. (2017). Comparison of the acute inhibitory effects of tetrodotoxin (TTX) in rat and human neuronal networks for risk assessment purposes. *Toxicology Letters, 270*, 12–16.

Lantz, S. R., Mack, C. M., Wallace, K., Keys, E. F., Shafer, T. J., & Casida, J. E. (2014). Glufosinate excitotoxicity mediated in part by N-methyl-D-aspartate receptor activation. *Neurotoxicology, 45*, 38–47.

Mack, C. M., Lin, B., Turner, J., Johnstone, A. F. M., Burgoon, L., & Shafer, T. J. (2014). Burst and principal components analysis of MEA data separates chemicals by class. *Neurotoxicology, 40*, 75–85.

Makris, S. L., Raffaele, K., Allen, S., Bowers, W. J., Haas, U., Alleva, E., et al. (2009). A retrospective performance assessment of the developmental neurotoxicity study in support of OECD Test Guideline 426. *Environmental Health Perspectives, 117*, 17–25.

Malo, N., Hanley, J. A., Cerquozzi, S., Pelletier, J., & Nadon, R. (2006). Statistical practice in high-throughput screening data analysis. *Nature Biotechnology, 24*, 167–175.

Massobrio, P., Tessadori, J., Chiappalone, M., & Ghirardi, M. (2015). In vitro studies of neuronal networks and synaptic plasticity in invertebrates and in mammals using multielectrode arrays. *Neural Plasticity, 2015*, 196195.

McConnell, E. R., McClain, M. A., Ross, J., Lefew, W. R., & Shafer, T. J. (2012). Evaluation of multi-well microelectrode arrays for neurotoxicity screening using a chemical training set. *Neurotoxicology, 33*, 1048–1057.

Meyer, D. A., Carter, J. M., Johnstone, A. F., & Shafer, T. J. (2008). Pyrethroid modulation of spontaneous neuronal excitability and neurotransmission in hippocampal neurons in culture. *Neurotoxicology, 29*, 213–225.

Mohana Krishnan, B., & Prakhya, B. M. (2016). In vitro evaluation of pyrethroid-mediated changes on neuronal burst parameters using microelectrode arrays. *Neurotoxicology, 57*, 270–281.

Narahashi, T. (2002). Nerve membrane ion channels as the target site of insecticides. *Mini Reviews in Medicinal Chemistry, 2*, 419–432.

Newberry, K., Wang, S., Hoque, N., Kiss, L., Ahlijanian, M. K., Herrington, J., et al. (2016). Development of a spontaneously active dorsal root ganglia assay using multiwell multielectrode arrays. *Journal of Neurophysiology, 115*, 3217–3228.

Nicolas, J., Hendriksen, P. J. M., van Kleef, R. G. D. M., de Groot, A., Bovee, T. F. H., Rietjens, I. M. C. M., et al. (2014). Detection of marine neurotoxins in food safety testing using a multielectrode array. *Molecular Nutrition & Food Research, 58*, 2369–2378.

Novellino, A., Scelfo, B., Palosaari, T., Price, A., Sobanski, T., Shafer, T., et al. (2011). Development of micro-electrode array based tests for neurotoxicity: Assessment of interlaboratory reproducibility with neuroactive chemicals. *Frontiers in Neuroengineering, 4*, 4.

NRC. (2007). *Toxicity testing in the twenty-first century: A vision and a strategy*. Washington, DC: The National Academies Press.

Odawara, A., Katoh, H., Matsuda, N., & Suzuki, I. (2016). Induction of long-term potentiation and depression phenomena in human induced pluripotent stem cell-derived cortical neurons. *Biochemical and Biophysical Research Communications, 469*(4), 856–862.

Odawara, A., Saitoh, Y., Alhebshi, A. H., Gotoh, M., & Suzuki, I. (2014). Long-term electrophysiological activity and pharmacological response of a human induced pluripotent stem cell-derived neuron and astrocyte co-culture. *Biochemical and Biophysical Research Communications, 443*, 1176–1181.

Ogiue-Ikeda, M., Tanabe, N., Mukai, H., Hojo, Y., Murakami, G., Tsurugizawa, T., et al. (2008). Rapid modulation of synaptic plasticity by estrogens as well as endocrine disrupters in hippocampal neurons. *Brain Research Reviews, 57*, 363–375.

Otto, D., Hudnell, K., Boyes, W., Janssen, R., & Dyer, R. (1988). Electrophysiological measures of visual and auditory function as indices of neurotoxicity. *Toxicology, 49*, 205–218.

Pamies, D., Bal-Price, A., Chesné, C., Coecke, S., Dinnyes, A., Eskes, C., et al. (2018). Advanced good cell culture practice for human primary, stem cell-derived and organoid models as well as microphysiological systems. *ALTEX, 35*(3), 353–378.

Pamies, D., Bal-Price, A., Simeonov, A., Tagle, D., Allen, D., Gerhold, D., et al. (2017). Good cell culture practice for stem cells and stem-cell-derived models. *ALTEX, 34*, 95–132.

Pamies, D., & Hartung, T. (2017). 21st century cell culture for 21st century toxicology. *Chemical Research in Toxicology, 30*, 43–52.

Pancrazio, J. J., Gopal, K., Keefer, E. W., & Gross, G. W. (2014). Botulinum toxin suppression of CNS network activity in vitro. *Journal of Toxicology, 2014*, 732913.

Polańska, K., Jurewicz, J., & Hanke, W. (2012). Exposure to environmental and lifestyle factors and attention-deficit / hyperactivity disorder in children - a review of epidemiological studies. *International Journal of Occupational Medicine and Environmental Health, 25*, 330–355.

Richard, A. M., Judson, R. S., Houck, K. A., Grulke, C. M., Volarath, P., Thillainadarajah, I., et al. (2016). The ToxCast chemical landscape: Paving the road to 21st century toxicology. *Chemical Research in Toxicology, 29*, 1225–1251.

Robinette, B., Harrill, J., Mundy, W. R., & Shafer, T. J. (2011). In vitro assessment of developmental neurotoxicity: Use of microelectrode arrays to measure functional changes in neuronal network ontogeny. *Frontiers in Neuroengineering, 4*, 1.

Salinas, E., & Sejnowski, T. J. (2001). Correlated neuronal activity and the flow of neural information. *Nature Reviews. Neuroscience, 2*, 539–550.

Scelfo, B., Politi, M., Reniero, F., Palosaari, T., Whelan, M., & Zaldívar, J. M. (2012). Application of multielectrode array (MEA) chips for the evaluation of mixtures neurotoxicity. *Toxicology, 299*, 172–183.

Shafer, T. J., & Atchison, W. D. (1995). Methods for analysis of effects of neurotoxicants on synaptic transmission. In L. W. Chang & W. Slikker Jr. (Eds.), *Neurotoxicology: Approaches and methodologies* (pp. 157–181). New York: Academic Press.

Shafer, T. J., Rijal, S. O., & Gross, G. W. (2008). Complete inhibition of spontaneous activity in neuronal networks in vitro by deltamethrin and permethrin. *Neurotoxicology, 29*, 203–212.

Strickland, J. D., LeFew, W. R., Crooks, J., Hall, D., Ortenzio, J. N., Dreher, K., et al. (2016a). In vitro screening of silver nanoparticles and ionic silver using neural networks yields differential effects on spontaneous activity and pharmacological responses. *Toxicology, 355–356*, 1–8.

Strickland, J. D., Lefew, W. R., Crooks, J., Hall, D., Ortenzio, J. N., Dreher, K., et al. (2016b). In vitro screening of metal oxide nanoparticles for effects on neural function using cortical networks on microelectrode arrays. *Nanotoxicology, 10*, 619–628.

Strickland, J. D., Martin, M. T., Richard, A. M., Houck, K. A., & Shafer, T. J. (2018). Screening the ToxCast phase II libraries for alterations in network function using cortical neurons grown on multi-well microelectrode array (mwMEA) plates. *Archives of Toxicology, 92*, 487–500.

Su, J., & Jiang, C. (2006). Multicellular recordings of cultured brainstem neurons in microelectrode arrays. *Cell and Tissue Research, 326*, 25–33.

Tukker, A. M., de Groot, M. W., Wijnolts, F. M., Kasteel, E. E., Hondebrink, L., & Westerink, R. H. (2016). Is the time right for in vitro neurotoxicity testing using human iPSC-derived neurons? *ALTEX, 33*(3), 261–271.

Uhlhaas, P. J., Pipa, G., Lima, B., Melloni, L., Neuenschwander, S., Nikolić, D., et al. (2009). Neural synchrony in cortical networks: History, concept and current status. *Frontiers in Integrative Neuroscience, 3*, 17.

Uhlhaas, P. J., & Singer, W. (2006). Neural synchrony in brain disorders: Relevance for cognitive dysfunctions and pathophysiology. *Neuron, 52*, 155–168.

Valdivia, P., Martin, M. T., Houck, K., Lefew, W. R., Ross, J., & Shafer, T. J. (2014). Multi-well microelectrode array recordings detect neuroactivity of ToxCast compounds. *Neurotoxicology, 44*, 204–217.

van Pelt, J., Vajda, I., Wolters, P. S., Corner, M. A., & Ramakers, G. J. A. (2005). Dynamics and plasticity in developing neuronal networks in vitro. In J. van Pelt, M. Kamermans, C. N. Levelt, A. van Ooyen, G. J. A. Ramakers, & P. R. Roelfsema (Eds.), *Development, dynamics and pathology of neuronal networks: From molecules to functional circuits* (Vol. 147, pp. 171–188). Amsterdam: Elsevier.

Vassallo, A., Michela Chiappalone, M., De Camargo Lopes, R., Scelfo, B., Novellino, A., Defranchi, E., et al. (2017). A multi-laboratory evaluation of microelectrode array-based measurements of neural network activity for acute neurotoxicity testing. *Neurotoxicology, 60*, 280–292.

Wagenaar, D. A., Pine, J., & Potter, S. M. (2006a). An extremely rich repertoire of bursting patterns during the development of cortical cultures. *BMC Neuroscience, 7*, 11.

Wagenaar, D. A., Pine, J., & Potter, S. M. (2006b). Searching for plasticity in dissociated cortical cultures on multi-electrode arrays. *Journal of Negative Results in Biomedicine, 5*, 16.

Wallace, K., Strickland, J. D., Valdivia, P., Mundy, W. R., & Shafer, T. J. (2015). A multiplexed assay for determination of neurotoxicant effects on spontaneous network activity and viability from microelectrode arrays. *Neurotoxicology, 49*, 79–85.

Weiss, B., & Laties, V. C. (Eds.). (1975). *Behavioral toxicology*. New York: Springer. 469 pp.

Xiang, G., Pan, L., Huang, L., Yu, Z., Song, X., Cheng, J., et al. (2007). Microelectrode array-based system for neuropharmacological applications with cortical neurons cultured in vitro. *Biosensors & Bioelectronics, 22*, 2478–2484.

Ylä-Outinen, L., Heikkilä, J., Skottman, H., Suuronen, R., Aänismaa, R., & Narkilahti, S. (2010). Human cell-based micro electrode array platform for studying neurotoxicity. *Frontiers in Neuroengineering, 3*, 1–9.

Zwartsen, A., Hondebrink, L., & Westerink, R. H. (2018). Neurotoxicity screening of new psychoactive substances (NPS): Effects on neuronal activity in rat cortical cultures using microelectrode arrays (MEA). *Neurotoxicology, 66*, 87–87.

Advances in Human Stem Cell-Derived Neuronal Cell Culturing and Analysis

Laura Ylä-Outinen, Jarno M. A. Tanskanen, Fikret E. Kapucu, Anu Hyysalo, Jari A. K. Hyttinen, and Susanna Narkilahti

Abstract This chapter provides an overview of the current stage of human in vitro functional neuronal cultures, their biological application areas, and modalities to analyze their behavior. During the last 10 years, this research area has changed from being practically non-existent to one that is facing high expectations. Here, we present a case study as a comprehensive short history of this process based on extensive studies conducted at NeuroGroup (University of Tampere) and Computational Biophysics and Imaging Group (Tampere University of Technology), ranging from the differentiation and culturing of human pluripotent stem cell (hPSC)-derived neuronal networks to their electrophysiological analysis. After an introduction to neuronal differentiation in hPSCs, we review our work on their functionality and approaches for extending cultures from 2D to 3D systems. Thereafter, we discuss our target applications in neuronal developmental modeling, toxicology, drug screening, and disease modeling. The development of signal analysis methods was required due to the unique functional and developmental properties of hPSC-derived neuronal cells and networks, which separate them from their much-used rodent counterparts. Accordingly, a line of microelectrode array (MEA) signal analysis methods was developed. This work included the development of action potential spike detection methods, entropy-based methods and additional methods for burst detection and quantification, joint analysis of spikes and bursts to analyze the spike waveform compositions of bursts, assessment methods for network synchronization, and computational simulations of synapses and neuronal networks.

L. Ylä-Outinen · A. Hyysalo · S. Narkilahti (✉)
NeuroGroup, Faculty of Medicine and Health Technology, Tampere University, Tampere, Finland
e-mail: susanna.narkilahti@tuni.fi

J. M. A. Tanskanen · J. A. K. Hyttinen
Computational Biophysics and Imaging Group, Faculty of Medicine and Health Technology, Tampere University, Tampere, Finland

F. E. Kapucu
Danish Research Institute of Translational Neuroscience - DANDRITE, Aarhus University, Aarhus, Denmark

Department of Biomedicine, Aarhus University, Aarhus, Denmark

1 Introduction to Human Stem Cells and Neuronal Differentiation

Human pluripotent stem cells (hPSCs) are defined by their capacity to self-renew and differentiate into derivatives of all three germ layers: the endoderm, mesoderm, and ectoderm. These cells also follow in vivo developmental principles and can be directed to differentiate into all cell types in the human body. hPSCs are divided into human embryonic stem cells (hESCs) and human induced pluripotent stem cells (hIPSCs). hESCs are derived from the inner cell mass of blastocyst-stage embryos (Thomson et al. 1998), whereas hIPSCs are derived from somatic cells using specific transcription factors, such as *Oct4*, *Sox2*, *klf4*, *c-myc*, *Nanog*, and *lin28*, to induce the pluripotent state (Takahashi et al. 2007; Yu et al. 2007). Thus, hIPSCs enable the generation of a variety of cell types that represent an individual's unique genetic background, including known genetic cause(s) of disease(s).

Neural differentiation of hPSCs was first described in 2001 (Carpenter et al. 2001; Reubinoff et al. 2001). These protocols were based on the embryoid body (EB) formation step prior to adherent cell culturing in neural differentiation-inducing media. Since then, a vast number of differentiation protocols directing neural development from hPSCs have been published, many of which use the principle of EB formation (Erceg et al. 2009; Zirra et al. 2016). EBs are 3D cell aggregates that produce a mixed population of differentiating cells, including neural cells. In adherent culture conditions, the cells differentiating towards neural lineage (i.e., neural precursor cells (NPCs)) produce radially arranged structures called rosettes, mimicking neural tube formation in vivo (Fig. 1). Rosettes can be selectively isolated for further culturing in order to enhance the purity of the produced neural population (Muratore et al. 2014). The 3D aggregates can also be formed directly in neural induction media. In this case, the aggregates are considered to produce mostly cells committed to the neural lineage and are thus termed neurospheres (Nat et al. 2007). Lately, culturing methods for the creation of human brain organoids, which at least partially mimic human brain tissue, have been developed (Kawada et al. 2017; Kelava and Lancaster 2016). Further development of differentiation methods has enabled capturing of cells in the neuroepithelial or NPC stage, where they are committed to neural lineage but can be still efficiently expanded and further differentiated into a variety of different neural cells (Brafman et al. 2013; Falk et al. 2012). In 2009, an efficient neuronal differentiation method, fully based on adherent cell culture conditions, was introduced (Chambers et al. 2009). The key element in this protocol was the inhibition of BMP signaling with Noggin and Activin/Nodal/transforming growth factor beta (TGFβ) signaling by small molecule SB431542. The aim was to inhibit the formation of endodermal and mesodermal derivatives in the early stage of differentiation. This principle,
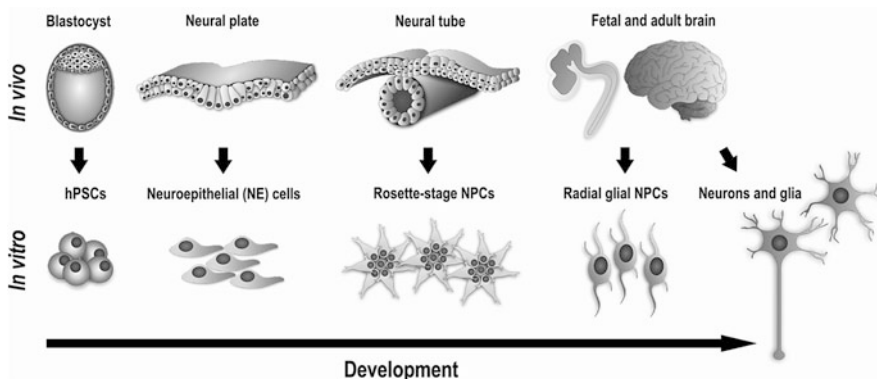
Fig. 1 Neural development in vivo and in vitro. Neural tube formation induces the transition of neuroepithelial cells into NPCs. NPCs further acquire the phenotype of radial glial precursor cells and give rise to differentiating neurons in the central nervous system through asymmetric cell division. They also form long radial processes to the outer surface of the neural tube, guiding the migration of newly born NPCs and neurons (Martynoga et al. 2012). Although all the developmental stages are often not separated in vitro, neural differentiation typically proceeds from neuroepithelial cells to NPCs, which is followed by final maturation into neurons and glial cells. (Reprinted from Hyysalo 2017; adapted from Mertens et al. 2016) with permission from academic dissertation)

termed "dual-SMAD inhibition," has since become extensively utilized in neuronal differentiation protocols. Current neuronal differentiation protocols often combine different culturing methods with temporally defined combinations of patterning factors and growth factors, aiming for the production of increasingly specified neuronal populations (Kirkeby et al. 2012; Maury et al. 2015; Paşca et al. 2015). Prolonged neural differentiation of hPSCs induces a neuroglial switch in the population (Lappalainen et al. 2010; Paavilainen et al. 2018). The differentiation capacity of radial glial NPCs shifts towards astrocytes and oligodendrocytes, representing in vivo development, where the generation of glial cells is initiated later than that of neurons (Martynoga et al. 2012) (Fig. 1). Initially, hPSC-derived glial cells (especially astrocytes) were mainly generated as side products of neuronal differentiation, but later, targeted differentiation protocols were developed for also glial cell types (Douvaras et al. 2014; Krencik et al. 2011; Pawlowski et al. 2017; Roybon et al. 2013). Latest development in neural differentiation protocols utilizes induced overexpression of transcription factors, which enables production of hPSC-derived neurons even as rapidly as 7 days (Busskamp et al. 2014; Goparaju et al. 2017; Frega et al. 2017). However, these induced overexpression methods have been associated with the potential problem of host genome modifications and the fact that the cells pass the in vivo—mimicking developmental stages, which makes them unsuitable for some research applications.

Recently, hPSC-derived neural cells in vitro have been exploited in developmental and toxicological studies, drug discovery, and disease modeling. Traditionally, these studies have been performed using animal models or primary cell cultures

due to the inaccessibility and technical limitations concerning the use of primary human cells and tissues (Markou et al. 2009). Although models based on animals (mainly rodents) are important and vastly utilized tools, these models have some drawbacks, and fundamental species-specific differences hinder the extrapolation of results from rodents to humans. At the genomic level, for example, despite the large number of orthologous genes between human and mouse, there are human-specific genes or functions of genes associated with various diseases (Miller et al. 2010). At the cellular level, differences between human and mouse brains are found in, for example, glial cell populations, as characteristics such as the astrocyte to neuron ratio and astrocyte complexity are both distinctly higher in the human brain (Nedergaard et al. 2003). The species also vary in several aspects of embryonic development, and human neurons require considerably longer morphological and electrophysiological maturation times than their mouse counterparts, both in vivo and in vitro (Suzuki and Vanderhaeghen 2015). Thus, as increasing amount of studies are performed with hPSC-derived neuronal cultures, these results are often compared to rodent primary neuronal cultures (Odawara et al. 2014). In these cases, it should be considered that in addition to species-dependent differences, the developmental stage of the cells is also very different (Fig. 2). Furthermore, although many neurodegenerative diseases can be modeled in rodents, pharmacological responses can be strikingly different between humans and rodents (Athauda and Foltynie 2015). The polygenic and multifactorial nature of many diseases also prevents the replication of an entire disease phenotype in animal models.

While hPSC-based in vitro models avoid the problems caused by species-specific differences, some challenges still exist. These include, for example, a lack of understanding of comprehensive maturation processes of differentiated cells and thus relevant modeling of late-onset neurodegenerative diseases (Avior et al. 2016). Furthermore, complex interactions between different cell types or tissues are not simple to replicate in vitro. In practice, hPSC-differentiation methods, which do not include genetic modifications, are often lengthy and may vary in differentiation efficiency both between passages and individual hPSC lines. During the past decade, hIPSCs have been increasingly utilized beside hESCs in the stem cell research. hIPSCs provide ethically less controversial cell source, which is also easier to obtain (Pappas and Yang 2008). hIPSC-based disease modeling facilitates the understanding of precise genotype–phenotype relationships and high-throughput drug discovery. On the other hand, hESCs are considered as more natural cell source, with the lack of essential genetic modifications and potential epigenetic modulators related to hIPSCs (Pappas and Yang 2008).

2   Functionality of hPSC-Derived Neuronal Networks

Typically, in vitro cell cultures are studied with various highly advanced techniques, ranging from genetic screenings to metabolomics. In addition, functional analysis is a specific requirement in neuronal cell culture studies, although this requirement has been addressed less frequently than other characteristics. Recently, the importance
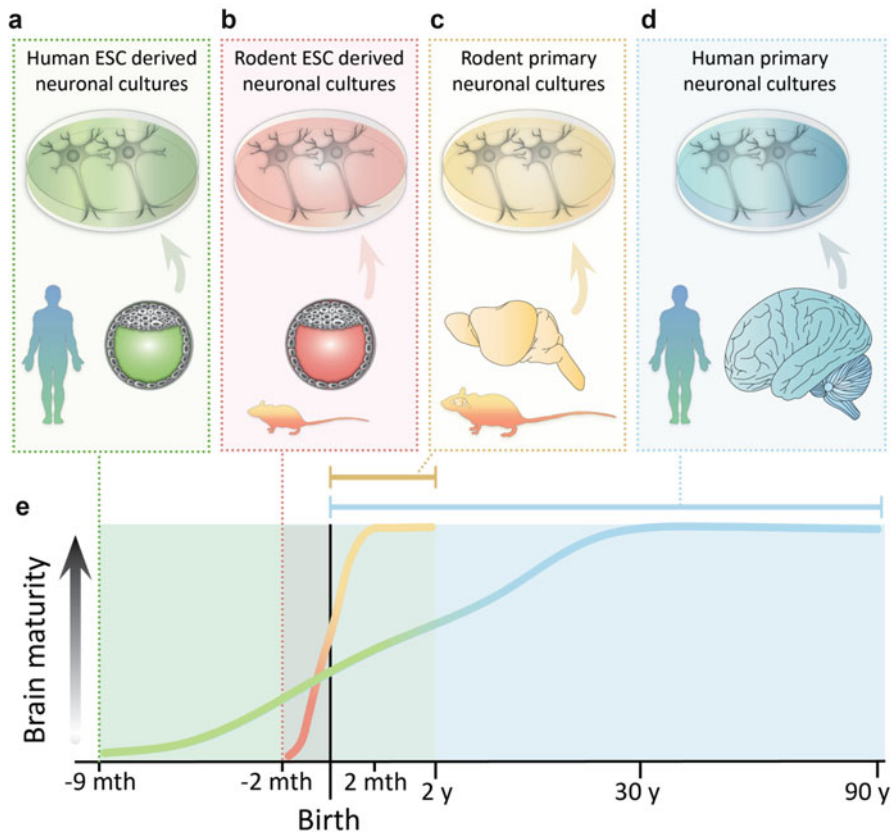
Fig. 2 Neuronal in vitro cultures. Traditionally, neuronal in vitro cultures have been created from rodent (typically mouse or rat) (**c**) embryonic or post-natal brain tissue and are called primary cultures, which are the most vastly used and explored cultures. (**b**) Mouse embryonic stem cells (mESCs) have also been used to create rodent neuronal cultures. (**d**) Human neuronal cultures have been created from aborted human fetal brain tissue, adult human brain after surgical operations, or postmortem tissue. (**a**) Since 2001, human neuronal cultures have been established from hESCs. More recently, similar type of human neuronal cultures have been established from hIPSCs. In (**e**), time dependent human brain development and maturation is shown with green to blue line whereas for rat it is shown with red to orange line. Expected lifespan is shown with blue line for humans and with orange line for rat. Time line (x-axis) is not in scale

of functional analysis has been better recognized. Functional characterization includes a variety of methods, such as patch clamp, fast calcium imaging, and microelectrode arrays (MEAs). Of these methods, MEAs are an interesting tool as they provide repeatable, non-invasive, network-level assays that can be performed in high throughput. Since 2009, hPSC-derived neuronal networks have been shown to develop spontaneous activity in MEAs (Heikkilä et al. 2009). Thereafter, these cells have been proven to be suitable for functional neurotoxicity studies (Ylä-Outinen et al. 2010). Importantly, hIPSC-derived neuronal cells are able to develop into

spontaneously active networks that are similar to their hESC counterparts (Hyysalo et al. 2017b; Schutte et al. 2018; Toivanen et al. 2017). Recent studies, however, have shown that hPSC-derived networks develop and express unique functionalities that are not directly comparable to those in rodent primary cultures. This include for example temporal network activity development, development of GABAergic system, role of astrocytes in network development (Mäkinen et al. 2018; Paavilainen et al. 2018).

3 Human Stem Cell-Derived Neuronal Networks: From 2D to 3D Cultures

Typically neuronal network is cultured in 2D in various cell culture well formats (Fig. 3a). Traditional 2D cultures are easy to use since, for example, cell density is standardized for multiple analysis methods, high-throughput screening platforms are available, handling of cultures can be automatized, and used cells amount is typically less than in more complex culturing conditions. This approach is also practical for functional studies, since MEAs can be easily embedded on the well bottom, and cells are easy to observe in monolayer or thin cultures. In addition, in 2D cultures, neurons are randomly oriented and form free connections between each other. Thus, forming networks are freely organized. This method has been regarded as a standard approach in rodent primary cultures and in hPSC-derived neuronal cells (Heikkilä et al. 2009; Lappalainen et al. 2010; Odawara et al. 2014; Ylä-Outinen et al. 2010). However, both repeatability and complexity of more in vivo-like neuronal networks are lacking.

During brain development, neuronal cells are guided by chemical and structural cues and form highly organized 3D structures in vivo. To mimic better this situation in vitro, both structural and 3D support might need to be provided (Hopkins et al. 2015). These goals can be achieved by structural guidance devices that provide cues and limited growth areas for the cells (Fig. 3b) or by 3D cell culture scaffolds (Fig. 4c). Structural guidance devices (Fig. 3b, more closely described in Sect. 4) can be fabricated in many ways, e.g., they can be microfluidistic devices, oriented nano/micro-scale fibers, grooves, or chemical patterns. All these devices can guide cell or neurite migration or limit cell growth area, providing more organized and structured 2D neuronal networks. For example, these devices can guide unidirectional axonal growth, providing a model for axon bundles (Hyysalo et al. 2017a; Park et al. 2006). In addition to these guidance devices, models that more closely resemble in vivo structures can be created with 3D culture systems (Fig. 3c, more closely described in Sect. 5). These models include organoids, hydrogel scaffolds, and engineered structural 3D scaffolds (Hopkins et al. 2015; Kawada et al. 2017; Kelava and Lancaster 2016; Shuler and Hickman 2014). Organoids or spheroids are cell aggregates that are formed spontaneously from stem cell-derived cell masses during differentiation. Cells, cell-to-cell interactions,
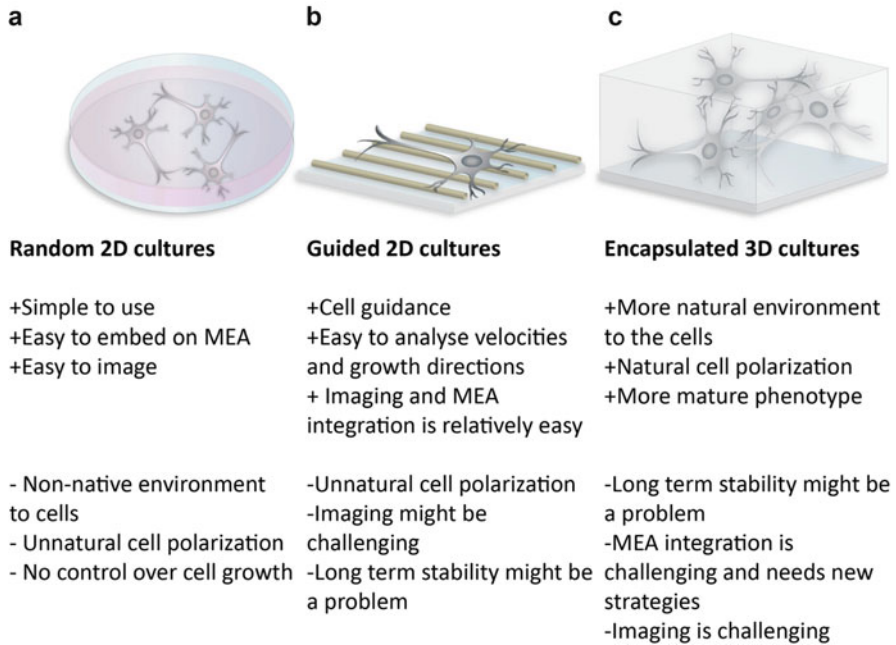
Fig. 3 Different strategies in the formation of stem cell-derived neuronal cultures. The pros (+) and cons (−) of each culture type are listed below. (**a**) Normal random 2D cultures are the most commonly used culture format and are suitable for many applications. (**b**) Guided 2D devices are proposed for cell or axon guidance and allow different analysis strategies since cells are unidirectional and cells or cell parts (like axons) can possibly be restricted. (**c**) Encapsulated 3D cell cultures, where cells are growing inside a biomaterial scaffold or form organoids, provide a more natural environment for the cells, but at the same time, they lead to more challenges in functional and imaging analyses

and cell-to-extracellular matrix (ECM) interactions thus form 3D structures. So far, the most advanced brain organoids have been shown to contain cortical structures, mimicking the human cortex. However, the uncontrolled growth of brain organoids creates a challenge for their use in studies and standard analysis (Kelava and Lancaster 2016). Hydrogel scaffolds provide practical scaffolds for hPSC-derived neuronal cells since their elastic and mechanical properties mimic native brain ECM. Another way to produce 3D structures is to mimic guidance cues in 3D. With 3D printing, molding or additive method structures, which are made of harder material than hydrogel scaffolds, can be engineered (Hopkins et al. 2015). These scaffolds provide growth cues but usually lack cell–ECM interactions.
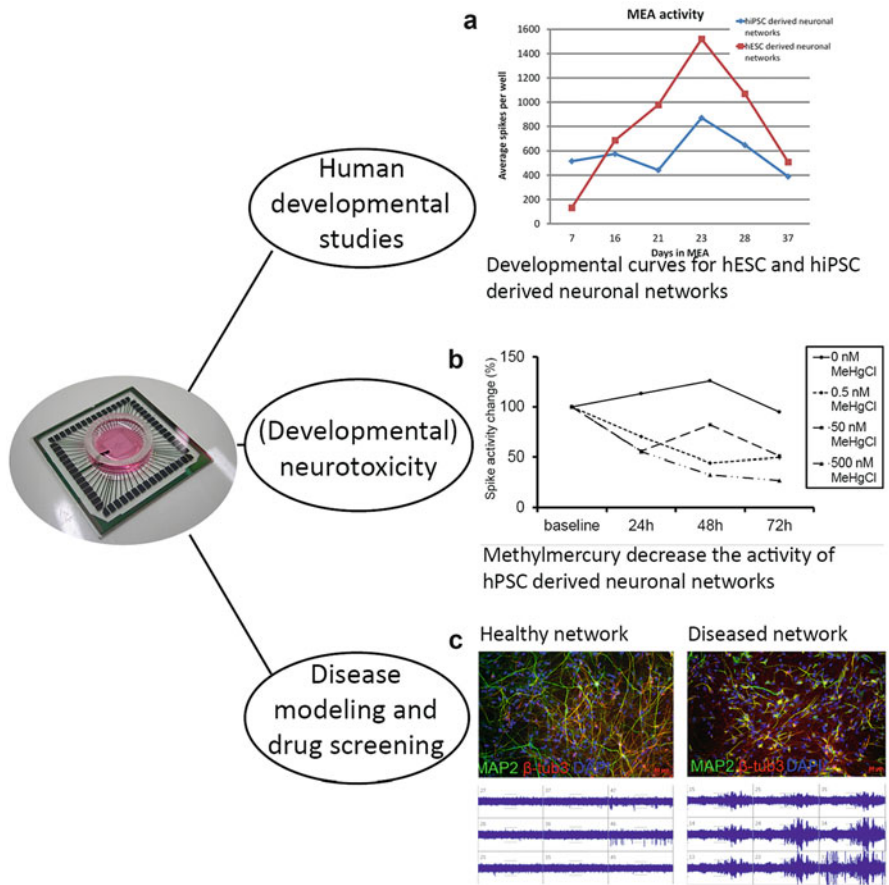
Fig. 4 Application areas for human pluripotent stem cell (hPSC)-derived neuronal networks on MEA. (**a**) hPSCs offer a tool to study species-specific development while also providing new important basic research information about human cells. Activity in MEA is shown for hESC and hIPSC-derived neuronal networks from culturing days 7–37. The red line represents hESC-derived neuronal networks, and the blue line represents hIPSC-derived neuronal networks. (**b**) Neurotoxicological platforms offer human cell-based methods to study toxicity at a functional level. An activity curve from hPSC-derived neuronal networks exposed to low doses of methyl mercury is shown. Even at low concentrations, a clear effect on activity is seen in MEA. (Reprinted from Ylä-Outinen et al. 2010 with permission.) (**c**) Disease modeling in dish and in vitro drug screening has experienced a new era with hIPSC technology. hIPSCs can be used to reproduce the diseased phenotype in dish. Healthy neuronal network (left side) and diseased cells (right side, from patient suffering from epilepsy with genetic background) are cultured in MEA. Both networks express normal neuronal markers in immunostaining, but clearly, abnormal MEA activity is seen in the diseased networks. (Unpublished data courtesy of Meeri Mäkinen (NeuroGroup, BioMediTech, and Faculty of Medicine and Life Sciences, University of Tampere) and Riikka Äänismaa (Research Programs Unit, Molecular Neurology, Biomedicum-Helsinki, University of Helsinki, Helsinki))

4 Applications of 2D Human Stem Cell-Derived Neuronal Networks

Currently, human neuronal networks are increasingly used as in vitro models and their functional measurements give unique information about human neural development, how their properties compare to animal cells, and human diseases and disorders (Canals et al. 2015; Odawara et al. 2014, Seidel et al. 2017; Ylä-Outinen et al. 2010). Particularly, their usability has been recognized in the areas of (developmental) neurotoxicity, disease modeling, and drug screening (Canals et al. 2015; Hopkins et al. 2015; Johnstone et al. 2010; Pamies et al. 2016; Tukker et al. 2016). Lately, their usability for studying very early human neuronal network development has been proven (Mäkinen et al. 2018).

4.1 Developmental Modeling

Human neuronal development can be studied in vitro using hPSC-derived neuronal networks and using MEA as a continuous, network-level functionality measurement tool (Broccoli et al. 2014) (Fig. 4a). Human cell-based in vitro models provide unique data on human early development, which is otherwise impossible to study in detail. It has been found that human neuronal networks form similar networks to rodent derivatives (Heikkilä et al. 2009) but still possess unique properties (Mäkinen et al. 2018). The development and maturation of human neuronal networks takes much longer time than that of rodent cultures as mature network activity development can take months up to a year contrast to few weeks needed with rodent networks. This also requires use of long culturing protocols (Odawara et al. 2016b; Paavilainen et al. 2018). In addition, human networks have some prominent features. One of these features is network variability (Mäkinen et al. 2018; Paavilainen et al. 2018; Ylä-Outinen et al. 2010). Human PSC-derived neuronal networks show cell-to-cell variability at their differentiation stage, specifically in GABA system development or cell composition (Mäkinen et al. 2018). Additionally, batch-to-batch and cell-line-to-cell-line variations influence the "neutrality" or purity of the produced cultures (Toivonen et al. 2013). This variability naturally influences functionality, causing differences in activity patterns such as the number of active electrodes, the time scale of functional maturation, and burst parameters, which prevents their direct comparison to primary rodent cultures (Mäkinen et al. 2018; Paavilainen et al. 2018). These variations cause new challenges to MEA analysis (discussed more closely later). All in all, human neuronal networks develop into bursting phase networks (Heikkilä et al. 2009; Paavilainen et al. 2018) and also develop network bursting activity at later time points (Odawara et al. 2016b). They respond to basic pharmacological treatments mostly as expected according to rodent data (Heikkilä et al. 2009; Odawara et al. 2016a; Paavilainen et al. 2018) but still possess specific characteristics, such as varying response to bicuculline

(Mäkinen et al. 2018). In these cultures, bicuculline can have no effect, a silencing effect, or an activating effect (Heikkilä et al. 2009; Odawara et al. 2016b; Paavilainen et al. 2018). Most likely, this difference in effects is caused by immaturity and different maturation stages, which are even found in the same populations (Mäkinen et al. 2018).

4.2 Neurodevelopmental Toxicity and Neurotoxicological Applications

Human neuronal tissue is unique, e.g., drug responses can differ from those seen in animal tissues, and thus, there is a huge need for toxicological platforms built on human neuronal cells (Fritsche et al. 2018; Johnstone et al. 2010; Kasteel and Westerink 2017; Tukker et al. 2016). hPSC-derived neuronal networks on MEA platforms are an excellent approach for these studies. In particular, human developmental neurotoxicity is an area that is otherwise challenging to study (Bal-Price et al. 2010; Fritsche et al. 2018). Nevertheless, the stabilization of neuronal networks and minimization of variations are requirements for reliable testing platforms; however, in the case of human cultures, these goals have been challenging to achieve. As previously mentioned, hPSC-derived cells are commonly more immature than primary rodent cortical cells (Kasteel and Westerink 2017), which leads to differences in typical MEA signaling, and in some cases, in drug responses (Heikkilä et al. 2009; Kasteel and Westerink 2017; Odawara et al. 2014). Thus, both experimental setups (including analysis time points) and analysis (for example, burst detection) need to be optimized (Kapucu et al. 2012; Ylä-Outinen et al. 2010). In simplest terms, this means an optimized culture period that is much longer than that of primary rodent cells (Heikkilä et al. 2009; Odawara et al. 2016b; Ylä-Outinen et al. 2010). Moreover, cell culture medium supplements, growth factors, cell density, and culturing conditions might also need to be considered (Kreutzer et al. 2012, 2017; Paavilainen et al. 2018). These variabilities also increase the need for special requirements and solutions in MEA analysis, which we will discuss later in this chapter.

Despite all these challenges, human neural cell-based MEA platforms have already been applied for testing the known toxicity of methylmercury (Ylä-Outinen et al. 2010). We demonstrated that MEA is a sensitive method, showing sub-acute toxic effects prior to phenotypical changes (Fig. 4b). In addition, the effect of well-known sodium channel blocker tetrodotoxin (TTX) was compared between human and rodent cultures on MEA (Kasteel and Westerink 2017). This study showed that interspecies differences are low in the case of TTX and that this information can be used for risk assessment purposes. Typically, responses for APV and CNQX are similar between human and rodent networks. These rare cases prove that human networks on MEA are applicable to toxicological studies, but there is a long way to go for robust, high-throughput human cell-based platforms in this field.

4.3   Disease Modeling and Drug Screening

hIPSCs provide a new way to study diseases in vitro. Cells carrying the genetic mutation that causes symptoms in the patient can be first induced into stem cells and then further differentiated into neuronal cells and cultured on MEA plates (Canals et al. 2015; Avior et al. 2016; Odawara et al. 2014). Using this strategy, it is possible to identify abnormal signaling in patient cells. For example, cells from patients who are suffering from severe epilepsy with a genetic background can be cultured in an MEA dish, and the signaling of these cells shows abnormal, seizure-like activity (Fig. 4c).

There is also a great need for drug screening platforms. hPSC-derived cells, especially induced pluripotent derivatives, create new possibilities for patient- and disease-specific drug screening in vitro (Avior et al. 2016). With hIPSC technology, cell lines from patients with various neurological diseases (including amyotrophic lateral sclerosis, Alzheimer disease, and Parkinson disease) have been established, differentiated towards neuronal cells, and studied for drug screening purposes (Kasteel and Westerink 2017; Lee et al. 2017; Xie et al. 2017; Zirra et al. 2016). Still, only a limited number of these cells have been cultured on MEA platforms and studied at a functional network level. Odawara et al. (2014) demonstrated the usability of human neuronal networks on MEA as suitable for this purpose. However, cell maturation took several months, thus decreasing the usability and increasing the costs of human cell-based platforms for drug screening purposes. There is still an unmet need for higher throughput, more standardized platforms, and overall better quality of drug screening and toxicity platforms (Johnstone et al. 2010; Kasteel and Westerink 2017).

5   Applications and Advances of Guidance Devices for Human Stem Cell-Derived Neuronal Networks

As discussed earlier, in vivo brain tissue is highly organized, and for some in vitro platform purposes, it is important to try to mimic this organization. The organization and alignment of neuronal cell growth can be achieved with chemical or mechanical cues, patterns, or topographical cues (Fig. 5). Axonal guidance or separation of somas and neuronal cell processes can be achieved with these cues. MEA analysis usually benefits from guidance, since signaling is more organized and homogenous than in freely formed networks (Toivanen et al. 2017). This characteristic is important, especially in a human neuronal network context, where signaling might be variable and only some of the cells are participating in detectable MEA signaling.

Specifically, for example, axonal velocity experiments need some structural guidance. Microfluidic devices provide a means to guide, restrict, and isolate the growth of neuronal cells or cell parts, such as somas or axons. With these devices, a
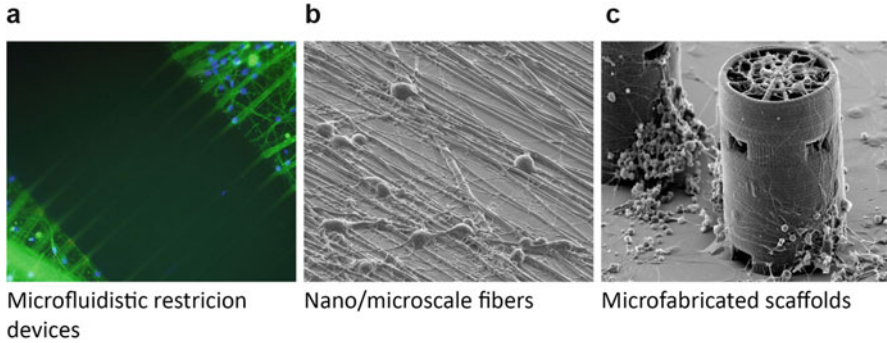
Fig. 5 Strategies to guide neuronal cells or axons. (**a**) Microfluidistic restriction devices are widely used to limit cell growth or restrict the axons from cell somas. Here, microfluidistic tunnels are used to separate two neuronal networks (labeled against MAP-2 in green and DAPI in blue) from each other, allowing only axons to migrate through tunnels. (Image courtesy of Anssi Pelkonen (NeuroGroup, BioMediTech, and Faculty of Medicine and Life Sciences, University of Tampere).) (**b**) Fibers and topographical cues are used to guide and orientate cell growth. Here, hPSC-derived neuronal cells are growing along submicron-scale electrospun fibers. (**c**) Different microfabrication techniques can be used to build guidance scaffolds for neurons. Here, two-photon polymerized structures are used as a growth scaffold for hPSC-derived neuronal networks. (Image courtesy of Sanna Turunen (BioMediTech and Faculty of Biomedical Sciences and Engineering, Tampere University of Technology) and Tiina Joki (NeuroGroup, BioMediTech, and Faculty of Medicine and Life Sciences, University of Tampere))

variety of different in vitro models can be created, for example, to study myelination, schizophrenia, or epilepsy in the future in a way that better mimics in vivo structures. It has also been shown that a limited growth area increases hPSC-derived neuronal network activity (Kreutzer et al. 2012; Toivanen et al. 2017). A limited growth area increases the success rate of network formation and detected signaling (Kreutzer et al. 2012), whereas a limited cell culture liquid volume seems to increase the chances of detecting activity in neuronal networks (Toivanen et al. 2017). Various 2D guidance devices have been used with rodent neuronal cells, but there are fewer reports on utilizing them with human cells, indicating that there may be species-related challenges in using human neuronal cells with these devices.

6   Applications and Advances of 3D Human Stem Cell-Derived Neuronal Networks

Neuronal cells are shown to mature into a more in vivo-like morphology in hydrogel scaffolds (Ylä-Outinen et al. 2014) or in brain organoids (Kelava and Lancaster 2016). Thus, 3D cultures might be beneficial when the aim is to create mature cells and in vivo mimicking platforms (Hopkins et al. 2015). Plenty of different materials have been tested for the 3D growth of human neuronal networks (Edgar et al. 2017;
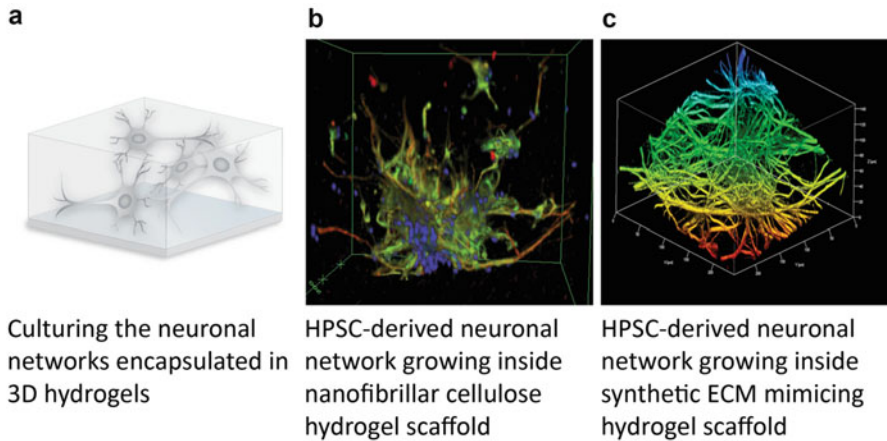
a

Culturing the neuronal networks encapsulated in 3D hydrogels

b

HPSC-derived neuronal network growing inside nanofibrillar cellulose hydrogel scaffold

c

HPSC-derived neuronal network growing inside synthetic ECM mimicking hydrogel scaffold

Fig. 6 3D culturing of neuronal cells. (**a**) Concept of 3D culture. Network formation of hPSC-derived neuronal cells (**b**) on the nanofibrous cellulose material Growdex® (Image courtesy of Tiina Joki, Laura Ylä-Outinen, Lauri Paasonen, Susanna Narkilahti, and UPM Biochemicals.) and (**c**) on synthetic ECM mimicking PuraMatrix® (Image courtesy of Tiina Joki)

Karvinen et al. 2018; Koivisto et al. 2017; Ylä-Outinen et al. 2014) (Fig. 6). The first challenge in 3D cultures is choosing the right materials. A suitable 3D scaffold material for in vitro models should be cytocompatible, should offer structural and chemical support so that the neuronal cells can spread and form networks, and should be stable enough to give cells sufficient time to mature (Hopkins et al. 2015; Ylä-Outinen et al. 2014). Studies have shown that with good supportive materials, human neuronal cells can form dense interconnected networks in 3D (Koivisto et al. 2017; Ylä-Outinen et al. 2014) (Fig. 6). The needed cell amount is, however, huge (on average 10 times more) for 3D cultures compared to traditional 2D cultures, making it a limiting factor in some cases. Another important limiting factor is challenges in the analysis of 3D networks. Imaging of 3D networks is more difficult, requires specific equipment, and is much slower than 2D imaging. Further, 3D functional measurements have not yet been reported.

Little is known about the electrophysiological characteristics of 3D cultured human neuronal networks. Functional activity has been detected with planar 2D MEAs beneath 3D encapsulated networks (Ylä-Outinen et al. 2014). There is a clear need for electrophysiological measurements in 3D environments for more complex, in vivo-like developmental, toxicity, and disease modeling (Hopkins et al. 2015). This goal is, however, very challenging; how do we stabilize the network in 3D? How do we realize MEA electrodes in 3D? What is sufficient spatial resolution in 3D cultures and how do we ensure sufficient neuron density in 3D so that most electrodes can detect signals? In Table 1, some potential modalities are listed to overcome these challenges. For electrophysiological measurements, MEA electrodes used in in vivo measurements can be applied in vitro to obtain

Table 1 Potential modalities for functional electrophysiological measurements in 3D

	3D flexi-MEA	3D Utah/Michigan array type MEAs	Calcium imaging	Patch clamp
Scale	Network level	Network level	Single cell/network level	Single cell level
Time-scalability	Can be placed after cell seeding and immobilized during the whole culturing period	Can be placed after cell seeding and immobilized during the whole culturing period	Only used for one time point	Only used for one time point
	Allows long term measurements	Allows long term measurements	End-point analysis	End-point analysis
Sensitivity	Low detection rate	Low detection rate	High detection rate	High detection rate
Spatial resolution	Limited spatial access	Good spatial access	Good spatial access (depending on microscope)	Very limited spatial access
	Low/mid spatial resolution	Low/mid spatial resolution	Good spatial resolution	Good spatial resolution
Temporal resolution	Very good temporal resolution	Very good temporal resolution	Low temporal resolution	Good temporal resolution

data within hydrogel scaffolds. So far it has been only conducted with rodent 3D networks (Pautot et al. 2008; Frega et al. 2014). Calcium imaging has already been applied in 3D imaging but has only been used for rodent networks (Broguiere et al. 2016). Additionally, patch clamping from 3D neuronal networks is possible but challenging (Simão et al. 2015; Xu et al. 2009). All of these strategies are applicable to human neuronal networks, and with intensive optimization, these strategies could be the basis of new, powerful human cell in vitro platforms.

7 Electrophysiological Signal Analysis and Computational Modeling

The maturation process of hPSCs to neuronal cells has many degrees of freedom. As was seen in Fig. 2, during normal cell experiments, the developmental stage of hPSC-derived neuronal cells and networks is completely different from that in rodent cell cultures. At the time point when rodent cells have matured, hPSC-derived cultures may still be very much in progress towards their mature cell types. hPSC-derived neuronal cells and networks develop and evolve during culturing, and their spiking statistics vary greatly during this time from single apparently random spikes via spike trains to bursts, which finally may achieve spatial synchronization over several MEA electrodes (Heikkilä et al. 2009). Thusly, MEA signal characteristics encountered with hPSC-derived cultures often differ from those measured from acute brain slices or dissociated cultures of rodent neuronal cells. The differences

are in general so large that signal analysis methods developed for primary cell measurements are unsuitable for the analysis of MEA measurements from the hPSC-derived cells. The main differences are in the spiking statistics and their variability in time during maturation and networking, and the statistics may also vary over different parallel cultures at any given time point. For example, visually evident bursts in hPSC-derived networks can be missed by traditional burst detection methods that are based on a priori set burst parameters. The differences call for the development of new, more adaptive signal-based electrophysiological signal analysis methods. Furthermore, many previous methods rely on operator experience and on the analysis parameters set by the operators. To overcome these matters, the main philosophy of our work has been to develop methods that tune themselves based on the measured signals, i.e., according to neuronal activity, and rely minimally (or preferably not at all) on parameters set a priori by the operator, i.e., the methods should be as objective as possible.

A hypothesis in our work has been that MEA field potential measurements of neuronal activity carry more information than what can be assessed by the commonly used spike and burst analysis methods alone. With this need and hypothesis in mind, the following signal analysis tasks have been investigated and advanced:

1. Neuronal action potential detection
2. Adaptive burst detection and analysis
3. Joint analysis of bursts and sorted spikes
4. Network connectivity/synchronization analysis

These MEA signal analysis approaches and the resulting new information are collected in Fig. 7 and described in the sequel. Figure 7 illustrates also data flow in one possible MEA signal analysis system to characterize the measured signals and the underlying neuronal network function, as seen based on MEA measurements.

7.1 Adaptive Thresholding-Based Spike Detection

Neuronal action potential spike detection is the basis of all analysis methods operating on spikes. Spike detection (Lewicki 1998; Wilson and Emerson 2002) is still often performed by mere thresholding: any signal reaching above a threshold is interpreted as a spike. Thresholding is computationally very efficient and can be performed online during measurement. Commonly, the standard deviation (STD) of measurement noise or STD of a measured signal is estimated, and the threshold is set to a multiple (e.g., 4–8 times) of the STD. Some thresholding methods use only either negative or positive thresholds, and thus detect only negative or positive spikes, whereas other methods utilize symmetric positive and negative thresholds to capture spikes of both polarities. In general, thresholds are set by convention by an expert operator, assessing measurements visually and aiming to maximize the number of detected real neuronal spikes while minimizing the number of spurious,
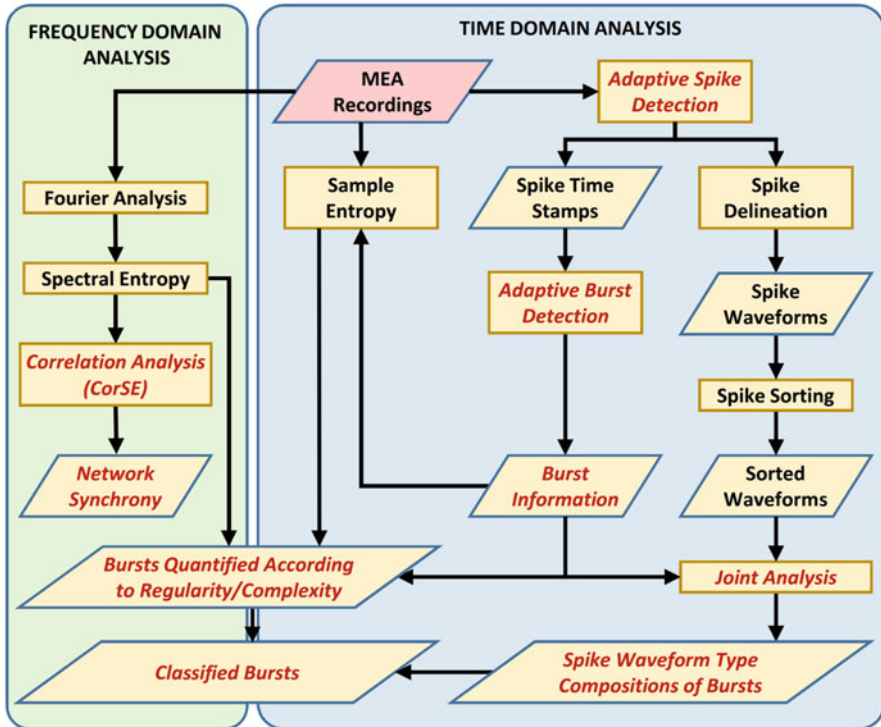
Fig. 7 MEA recording analysis methods (rectangles) and data (parallelograms) considered here and their relations. Only the most important data are shown. The developed methods and novel data are indicated by red text. (Adapted from Kapucu 2016b)

i.e., false spikes detected due to noise. During a measurement, the actual number of spurious spikes remains unknown. Spuriousness is not considered in the analysis, but all detected spikes are taken as true spikes. Spike waveform analysis might reveal spurious spikes, but it is usually not utilized. Additionally, thresholds set this way are always subjective.

To facilitate spike detection for different cell cultures and noise conditions, we developed a signal analysis-based thresholding method that automatically finds the thresholds based on the signals themselves. Neuronal action potential spike detection is the basis of all analysis methods operating on spikes. To facilitate cell culture- and noise condition-optimized spike detection, we developed a signal analysis-based thresholding method that automatically finds the thresholds based on the signals themselves. Thus, our method is objective, i.e., independent of the human operator and does not require preset parameters that would directly affect the threshold levels.

We developed a simple objective measure for this approach. The working hypothesis of the developed spike detection method is that contributions from

noise and spikes should be identifiable in spike count histograms, given that there is a sufficient number of spikes reaching sufficiently beyond the noise and that there exist sufficient periods of time when only background noise is measured. In practice, at least the latter requirement is always fulfilled. The algorithm illustrated in Fig. 8a realizes this principle (Tanskanen et al. 2016). First, a spike count histogram is formed. To enhance the potentially useful features of the histogram, a smoothed gradient of the histogram is calculated. Next, the extrema of the smoothed gradient are found. The local minimum closest to the global maximum, appearing at an amplitude smaller than that of the global maximum, is taken as the negative threshold for spike detection. The positive threshold is found at the local maximum closest to global minimum appearing at an amplitude larger than that of the global maximum (Fig. 8a).

As evident from Fig. 8a, the a priori set parameters of the algorithm are the number of thresholding levels between the global extrema, the filter coefficients to calculate the smoothed gradient of the histogram, and the final threshold validity check limits. Thus, the method is objective, i.e., the operator and the programmer cannot directly affect the thresholds. Finding the thresholds for an in vitro measurement from human brain tissue samples (Roopun et al. 2010) is shown in Fig. 8b, and the signal with the found thresholds is shown in Fig. 8c.

Matlab (MathWorks, Natick, MA) implementation of the basic method is freely available (Tanskanen 2017). Planned future updates include adaptive threshold setting in a running window and baseline drift suppression. Traditional thresholding methods fail if the spiking is too dense compared to the signal sampling frequency: dense spiking results in the thresholds being set too high. The proposed method may also be beneficial in these cases, although the biological relevance of the spike detection results is yet to be demonstrated.

7.2 Adaptive Burst Detection and Burst Analysis

For conventional rodent brain slices and primary neuronal cultures, in general, spike statistics remain quite stable during experiments. Traditional spike signal analysis methods with a priori set (often ad hoc selected) parameters tend to work fine with such cultures. Interspike interval (ISI) is a simple and computationally efficient metric. Bursts are typically detected (Chiappalone et al. 2005; Wagenaar et al. 2006; Mazzoni et al. 2007) by the fulfillment of at least two conditions: a fixed minimum number of spikes and a fixed maximum ISI in a burst. ISI histograms have been employed to assess general firing characteristics, e.g., by Christodoulou and Bugmann (2001). Since ISI histograms are challenging to read in their raw form, logarithmic scale ISI histograms have been used. Sometimes, they can reveal the differences between firing characteristics of individual and burst spikes (Selinger et al. 2007; Pasquale et al. 2010). In addition, several adaptive methods have been proposed for burst detection, such as the method by Pasquale et al. (2010), and they can also be applicable in analyzing measurements from hPSC-derived neuronal
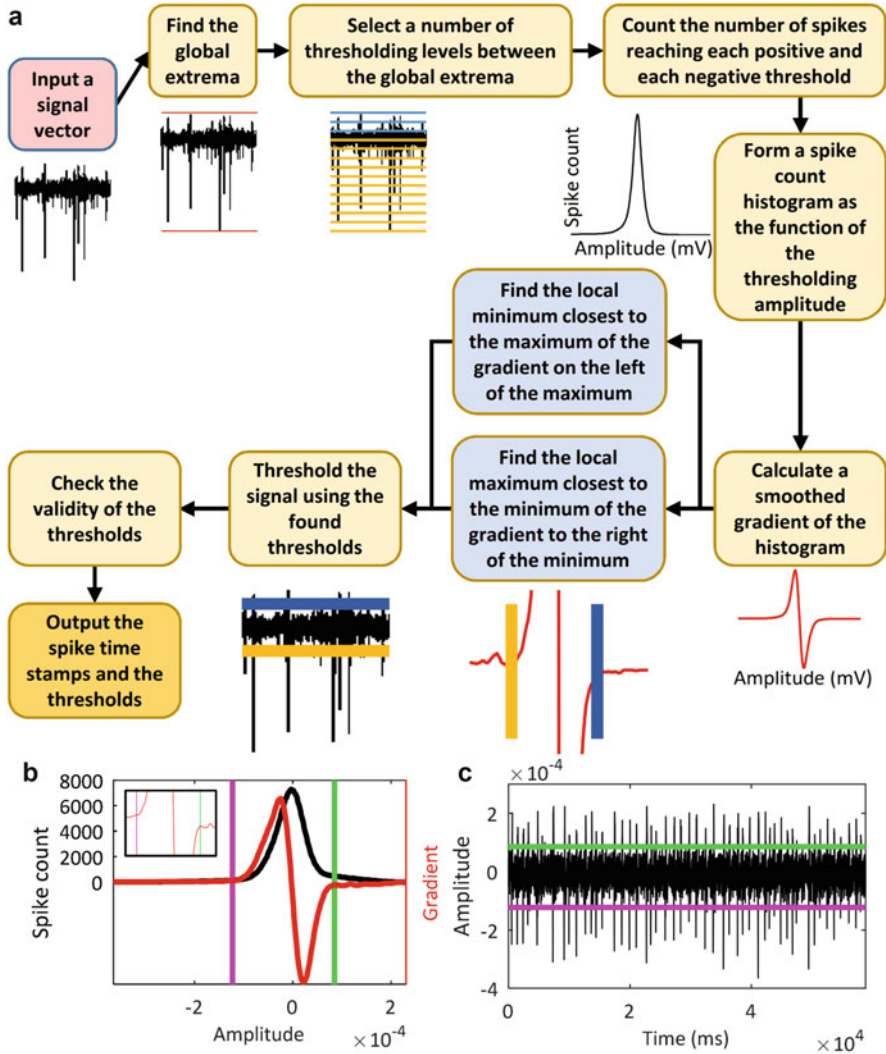
Fig. 8 (**a**) The proposed thresholding algorithm. (**b**) Spike count histogram (black), smoothed gradient of the histogram (red), and the found negative (magenta) and positive thresholds (green), with a detailed view of the gradient features and the found thresholds in the inset. The gradient axis spans from −200 to 200. (**c**) An exemplary measurement from in vitro human brain tissue (black), and the automatically found thresholds. (©2016 IEEE. Reprinted, with permission, from Tanskanen et al. 2016. Adaptations for clarity only)

cultures. Recently, eight adaptive methods were thoroughly reviewed and compared by Cotterill et al. (2016). Adaptive methods are crucially important for detecting bursts recorded from dynamic cultures.
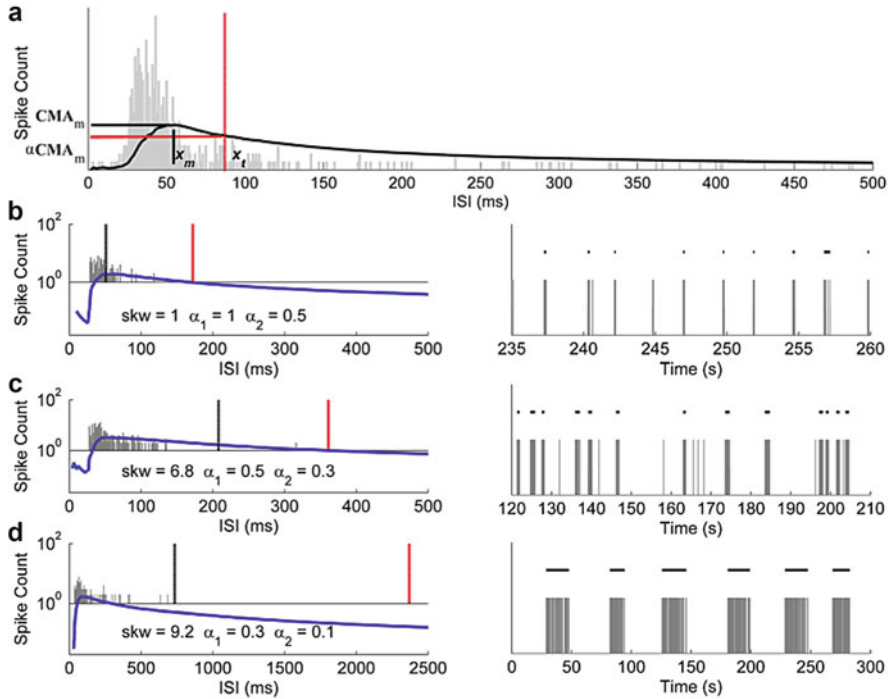
Fig. 9 Selecting the ISI threshold for burst detection using a CMA curve, along with exemplary bursts and their ISI characteristics. (**a**) The ISI histogram (gray vertical bars), and the corresponding CMA curve (black). The maximum of the CMA curve (CMA_m) is reached at the ISI x_m, and the ISI threshold x_t for burst detection is set at the ISI corresponding to the CMA value closest to $\alpha \cdot CMA_m$. The ISI threshold for burst detection is marked with the red vertical line. (**b–d**) Setting burst detection ISI thresholds (left panels) for MEA measurements from three differently behaving hESC-derived neuronal networks, and the detected spikes and bursts (right panels). Left panels: ISI histograms (gray vertical bars), CMA curves (blue), skewness values (skw), and the corresponding α_1 and α_2 for calculating burst and burst related spike detection ISI thresholds, respectively. Also shown are the burst and burst related spike detection ISI thresholds (black and red vertical lines, respectively). Right panels: the detected spikes (vertical lines) and bursts (horizontal lines/dots above the spike indicators). (Reprinted from Kapucu et al. 2012 under CC BY-NC 3.0 license)

Some studies have shown that hPSC-derived neuronal cultures exhibit not only very dynamic firing statistics but also highly varying bursting behavior (Heikkilä et al. 2009), with bursts lasting from milliseconds to seconds. In addition, bursts formed by a few or tens of spikes are seen frequently in these networks (Heikkilä et al. 2009; Kapucu et al. 2012) (see Fig. 9). Thus, in the analysis, methods based on a priori fixed parameters may fail, and burst detection should be done based on the signals themselves.

To overcome the limitations of previous burst detection methods and to detect successfully bursts under dynamic firing statistics, we proposed a general analysis framework based on the cumulative moving average (CMA) of ISI histograms

(Kapucu et al. 2012) (Fig. 9). The general characteristics of bursting activity can be observed as a peak and followed by a gradual decay in the ISI histogram, which can be associated with a Poisson distribution with a signal dependent mean (Christodoulou and Bugmann 2001; Chen et al. 2009). Skewness is a measure of the asymmetry of a distribution. Skewness is an important feature of ISI histograms and can be utilized to detect bursts with different ISI distributions. The CMA of an ISI histogram shows the overall trend of the ISI histogram and allows the definition of an ISI value that marks a critical point in the histogram. In our CMA-based method, the maximum of the CMA curve is found, and the skewness of the ISI histogram is estimated. The ISI threshold for burst detection is set at the ISI corresponding to α times the maximum of the CMA curve (Fig. 9a). See (Kapucu et al. 2012) for a possible mapping between α and skewness. Similarly, an ISI threshold can be defined for burst related spikes (Fig. 9b–d), i.e., for the pre-burst spikes and the spikes in the burst tails, by defining another fraction (α_2) of the maximum CMA value.

The CMA-based burst detection method can be applied on single channel recordings (Kapucu et al. 2012) or tuned to network-wide spiking characteristics, which can provide more stable and comparable measures, e.g., for long term studies (Välkki et al. 2017). After delineating the bursts, burst cut-outs and burst statistics can be obtained for further analysis. The detected bursts can be quantified, e.g., by conventional parameters and metrics, such as burst duration and frequency and the number of spikes in bursts, by the developed entropy-based algorithms (Kapucu et al. 2015), and by assessing the spike type compositions of the bursts (Kapucu et al. 2016b) (Fig. 10). Recently, the CMA method has been validated in hPSC works (Hyysalo et al. 2017b; Toivanen et al. 2017; Paavilainen et al. 2018; Mäkinen et al. 2018) and thus is routinely used in the analysis of hPSC-derived networks.

7.3 Joint Burst and Spike Analysis: Spike Type Compositions of Bursts

Burst detection and waveform-based spike sorting are often used in MEA signal analysis. By associating each burst spike with a spike type given by spike sorting, it was possible to obtain the spike type compositions of the bursts. This observation resulted in a new method: joint analysis of bursts and spike waveforms (Kapucu et al. 2016b), which is schematically presented in Fig. 10a. In the joint analysis, each spike in a burst is associated with a spike type according to the sorting results of the spike in question. During an experimental paradigm, the results of joint analysis provide the spike type compositions of bursts, which is a different type of information than what mere burst detection or spike sorting-based analysis alone can provide. This finding by Kapucu et al. (2016b) also proves our original working hypothesis that MEA field potential measurements of neuronal activity carry more information than what can be assessed by the commonly used spike and burst analysis methods alone.
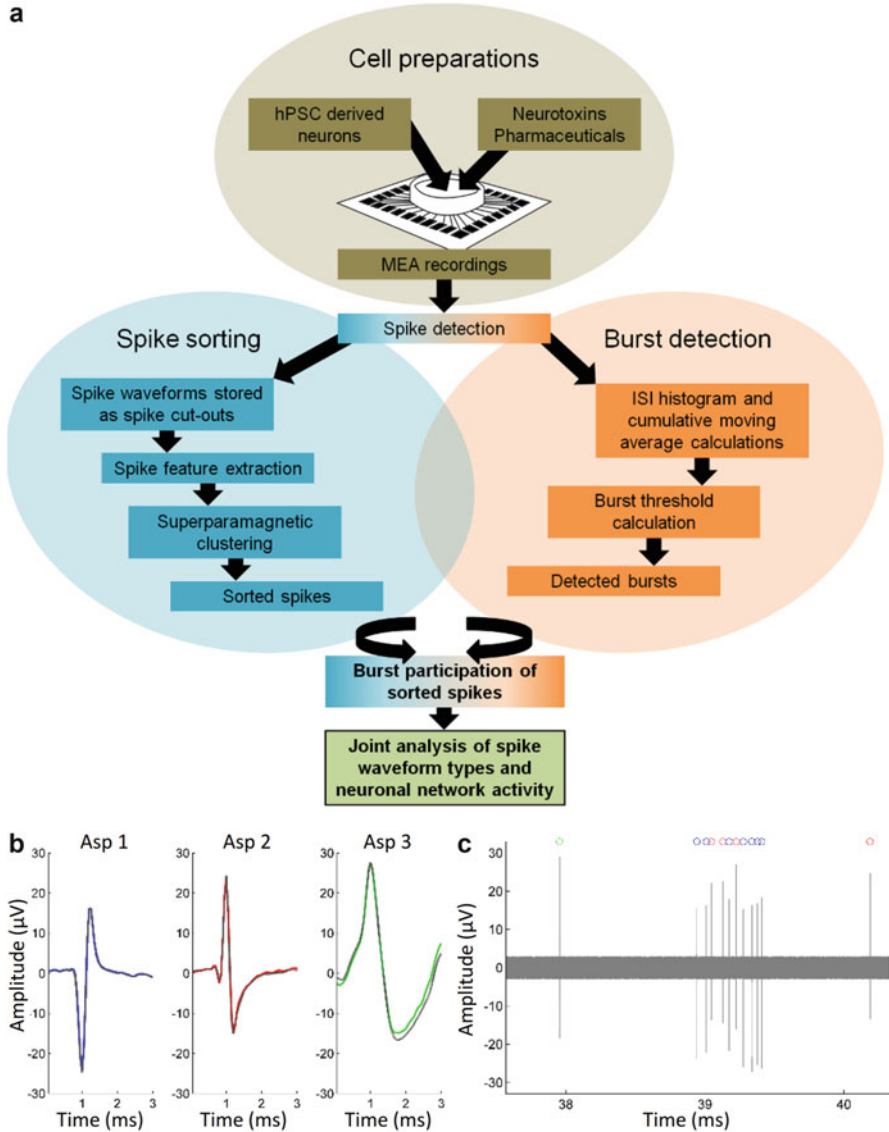
Fig. 10 (**a**) A schematic presentation of the joint analysis. The joint analysis framework consists of spike sorting and burst detection, followed by analysis of the participation of spikes of different types in bursts. (**b**) Simulated spike sorting results with three spike waveforms, ASp 1 (blue), ASp 2 (red), and ASp 3 (green), along with the corresponding average waveform (gray). (**c**) Joint analysis result: a sample of the simulated signal with the sorted spikes indicated by circles with colors corresponding to the particular spike type (**b**). (Reprinted from Kapucu et al. 2016b with permission from Elsevier)

Sample simulation results are shown in Fig. 10 (Kapucu et al. 2016b), where spike waveforms resulting from spike sorting are shown (Fig. 10b), along with a burst and its spikes associated with the spike waveforms (Fig. 10c). The joint analysis of bursts and spikes can be implemented with any waveform-based spike sorting and burst detection methods that are suitable to analyze the signal at hand.

A change in the spike type composition of bursts during an experimental paradigm indicates that something changed in the neuronal cells or in the functional networks participating in the burst generation. Such experimental paradigms include those with multiple pharmacological applications or other chemical alterations, electrical stimulation, or network maturation. Any experiments in which bursts can be observed before and after an alteration or at different time points can be subject to joint analysis. Joint analysis may reveal changes in bursts even though there might have been no observable changes in the traditional burst metrics, such as the number of spikes in the bursts or the number or duration of the bursts. For the advancement of neuroscience, it would be preferable that methods capable of extracting more information from the measurements, such as joint analysis, were utilized more extensively. However, these new methods need to be validated, the biological relevance of the new information must be shown, and the methods must be adopted in everyday use. For joint analysis, these tasks are the next steps to be taken. A Matlab implementation of the method is freely available (Kapucu 2015).

7.4 Entropy-Based Burst Assessment and Network Analysis

Entropy is a measure of disorder or uncertainty, and it has been widely employed in signal analysis in many fields. In neuroscience, entropy-based methods have been used to study, for example, complex physiological systems or the uncertainty of neuronal behavior at the brain level (Burggren and Monticino 2005) and information transfer between different neuronal populations or locations in a neuronal system (Garofalo et al. 2009; Ito et al. 2011). Complex system analysis methods have also been used to detect events of neuronal origin in epilepsy or even in complex decision tasks (Subramaniyam and Hyttinen 2015; Subramaniyam et al. 2015; Subramaniyam 2016). Here, entropy was found to be lucrative for assessing neuronal networks and their function based on MEA measurements. Entropy can be calculated to produce one single entropy value either for an entire MEA signal or for a section of it (such as an MEA signal during a burst). Alternatively, entropy can be calculated in a running window (with the window length a small fraction of the length of the MEA signal of interest), producing an entropy signal for the entire MEA signal or, for example, for only the duration of a previously detected burst. Entropy-based methods were proposed for three different uses: (1) to detect bursts based on changes in the entropy signal of an MEA recording, (2) to evaluate the information content of bursts and thus to classify or quantify bursts, and (3) to assess functional connectivity, i.e., spatial network relations.

Entropy-based burst detection methods can be employed on measured signals as such, and thus differ fundamentally from the burst detection methods that rely on detected spikes. For any MEA measurement with active neuronal cells distributed spatially on an MEA, some neuronal cells will be located so far from a microelectrode that their action potential amplitudes at the microelectrode are lower than the MEA measurement baseline noise amplitude level. Such action potentials cannot be detected by thresholding. Consequently, since bursts are usually detected based on spike time stamp signals, no bursts composed of such spikes can be found. However, entropy-based methods do not depend on detected spikes, but on signal complexity (or on the complexity of signal spectrum). Temporally dense spiking, even if buried in noise, will change the signal complexity (and the complexity of signal spectrum) compared to mere measurement noise, and the bursts may be detected. Naturally, this phenomenon does not depend on the neuronal cell source.

The applicability of entropy measures for burst detection was demonstrated with bursts detected in MEA measurements from dissociated rat cortical cell cultures (Fig. 11a, b) (Kapucu et al. 2015). An exemplary result is shown in Fig. 11, where an MEA signal is shown with bursts detected by the automatized burst detection method (Fig. 11a), along with the corresponding sample entropy (SmE) and spectral entropy (SE) signals (Fig. 11b). In the case seen in Fig. 11a, b, the bursts are obvious and easily detectable, and SmE and SE could be used to quantify them. Self-similarity, quantified by SmE, and spectral uniformity, quantified by SE, were found to be promising metrics for quantifying bursts for further classification (Kapucu et al. 2015). For the data at hand, both entropy measures were good at detecting changes in neuronal recordings during bursts. SmE was found more sensitive to the burst duration and number of spikes in bursts for the signals at hand. SmE also showed more potential for classifying presumably different kinds of bursts than SE (Kapucu et al. 2015).

In our further experiments with hPSC-derived neurons, it was demonstrated that SE also has the potential to detect bursts with burst spikes that are buried in noise. An MEA signal measured from hPSC-derived neurons with clearly observable bursts and the corresponding SE signal are shown in Fig. 11c, e, respectively, whereas a signal with no visually detectable bursts is shown in Fig. 11d with the corresponding SE signal in Fig. 11f, which clearly indicates probable bursts buried in noise. While entropy-based methods have shown clear potential for burst detection and quantification, their biological relevance in these applications should still be stringently validated.

Entropy-based measures can also be employed to reveal spatial network relations (Kapucu et al. 2016a, c, 2017a, b). Kapucu et al. (2016c) showed that spatial network relations can be revealed by time-variant SE signals, and the correlated spectral entropy method (CorSE) was developed for this application. SE quantifies the uniformity, or complexity, of the frequency spectrum distribution of a signal, such as an MEA measurement. In CorSE, an SE signal is formed for each MEA signal measured via an electrode. Next, correlations between all SE signal pairs are calculated. Correlation between two SE signals quantifies how similarly the uniformities of the frequency spectra of the two MEA signals change in time. If the
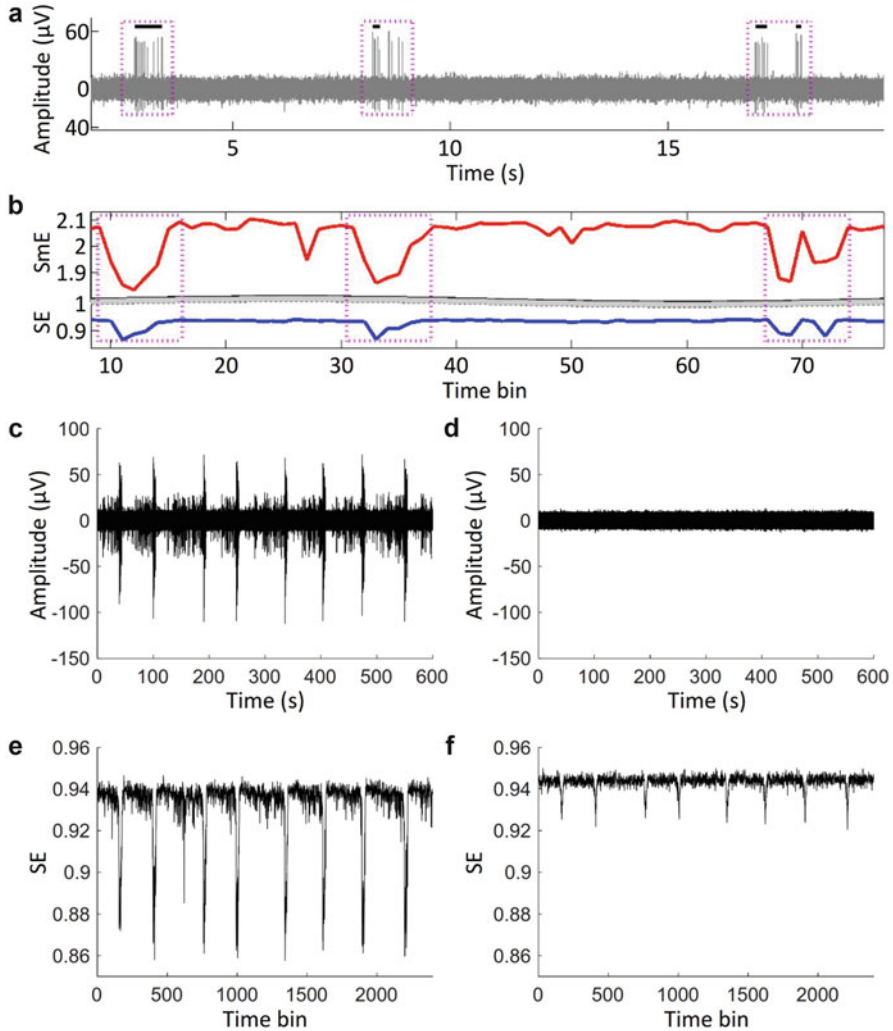
Fig. 11 (**a**) A signal with bursts detected with the automatized burst detection algorithm. Detected bursts are labeled with black horizontal lines above the signal. (**b**) SmE (red) and SE (blue) signals calculated for the signal seen in (**a**). The purple boxes delineate the changes in the SmE values. The boxes in (**b**) correspond to the boxes in (**a**) over time. (**c**) and (**e**) Exemplary MEA signals measured from hPSC-derived neurons (Data courtesy of Tanja Hyvärinen (NeuroGroup, BioMediTech and Faculty of Medicine and Life Sciences, University of Tampere)). (**d**) and (**f**) The SE signals for the MEA signals in (**c**) and (**e**), correspondingly. ((**a**) and (**b**) ©2015 IEEE. Reprinted, with permission, from Kapucu et al. 2015)

correlation between the two SE signals is sufficiently high, the network locations at the electrodes are considered to be functionally connected. A benefit of this method is that it is independent of spike detection and spike timings at the two considered network locations; to observe functional connectivity, it is sufficient that

the complexities of the two signals change similarly as the network functions. CorSE could be particularly beneficial in tracking the development of maturing neuronal networks. Work using CorSE in analysis of the functional networking dynamics of hPSC-derived neuronal networks during maturation is ongoing (Tanja Hyvärinen, Emre F. Kapucu, et al. unpublished). This work is expected to demonstrate the biological relevance of the results of CorSE. A Matlab implementation of CorSE is freely available (Kapucu 2016a).

8 Conclusions and Discussion

hPSCs have changed and opened up new research and application areas that in the long run can have a significant impact on many fields, ranging from basic developmental science to an understanding of human tissue development, valid in vitro testing platforms for toxicology and drug screening, and finally, disease modeling and even regenerative medicine. Especially for neuroscience, these cells provide an invaluable source for producing neural cells, the building blocks of our brains, in a dish, and thus provide a tool to study the most complex organ closer than ever before. During the last few years, the use of hPSC-derived neuronal cells has received much interest, particularly in neurodevelopmental toxicity and disease modeling. At the same time, we have started to realize that in vitro cultured human neuronal cells and networks, and especially network functionality, are different from their rodent counterparts, which are considered the gold standard. Taking species specificity into account, the differences between rodent and human cultures should not be very surprising. This finding does, however, increase our challenge beyond the difficulties encountered with traditional culturing and analysis methods. In this chapter, we provided an overview of the current state of the art of culturing hPSC-derived neuronal cells from traditional 2D to evolving 3D systems and noted specific needs that require novel approaches and the development of new analysis methods. As the demand to utilize these cells in numerous applications is continually increasing, we hope that our work identifies ways to further extend this research area.

In conclusion, hPSC-derived, neural cell-based in vitro models hold remarkable potential for extending our knowledge of the developmental bases of human evolution and disease and developing therapeutic applications in the future has been cut off. Not necessary though.

References

Athauda, D., & Foltynie, T. (2015). The ongoing pursuit of neuroprotective therapies in Parkinson disease. *Nature Reviews. Neurology, 11*(1), 25–40.

Avior, Y., Sagi, I., & Benvenisty, N. (2016). Pluripotent stem cells in disease modelling and drug discovery. *Nature Reviews. Molecular Cell Biology, 17*(3), 170–182.

Bal-Price, A. K., Hogberg, H. T., Buzanska, L., Lenas, P., van Vliet, E., & Hartung, T. (2010). In vitro developmental neurotoxicity (DNT) testing: Relevant models and endpoints. *Neurotoxicology, 31*(5), 545–554. https://doi.org/10.1016/j.neuro.2009.11.006

Brafman, D. A., Moya, N., Allen-Soltero, S., Fellner, T., Robinson, M., McMillen, Z. L., et al. (2013). Analysis of SOX2-expressing cell populations derived from human pluripotent stem cells. *Stem Cell Reports, 1*(5), 464–478.

Broccoli, V., Giannelli, S. G., & Mazzara, P. G. (2014). Modeling physiological and pathological human neurogenesis in the dish. *Frontiers in Neuroscience, 8*, 183.

Broguiere, N., Isenmann, L., & Zenobi-Wong, M. (2016). Novel enzymatically cross-linked hyaluronan hydrogels support the formation of 3D neuronal networks. *Biomaterials, 99*, 47–55.

Burggren, W. W., & Monticino, M. G. (2005). Assessing physiological complexity. *The Journal of Experimental Biology, 208*, 3221–3232.

Busskamp, V., Lewis, N. E., Guye, P., Ng, A. H. M., Shipman, S. L., Byrne, S. M., et al. (2014). Rapid neurogenesis through transcriptional activation in human stem cells. *Molecular Systems Biology, 10*, 760.

Canals, I., Soriano, J., Orlandi, J. G., Torrent, R., Richaud-Patin, Y., Jiménez-Delgado, S., et al. (2015). Activity and high-order effective connectivity alterations in sanfilippo C patient-specific neuronal networks. *Stem Cell Reports, 5*(4), 546–557.

Carpenter, M. K., Inokuma, M. S., Denham, J., Mujtaba, T., Chiu, C.-P., & Rao, M. S. (2001). Enrichment of neurons and neural precursors from human embryonic stem cells. *Experimental Neurology, 172*(2), 383–397.

Chambers, S. M., Fasano, C. A., Papapetrou, E. P., Tomishima, M., Sadelain, M., & Studer, L. (2009). Highly efficient neural conversion of human ES and iPS cells by dual inhibition of SMAD signaling. *Nature Biotechnology, 27*(3), 275–280.

Chen, L., Deng, Y., Luo, W., Wang, Z., & Zeng, S. (2009). Detection of bursts in neuronal spike trains by the mean inter-spike interval method. *Progress in Natural Science, 19*(2), 229–235.

Chiappalone, M., Novellino, A., Vajda, I., Vato, A., Martinoia, S., & van Pelt, J. (2005). Burst detection algorithms for the analysis of spatio-temporal patterns in cortical networks of neurons. *Neurocomputing, 65–66*, 653–662.

Christodoulou, C., & Bugmann, G. (2001). Coefficient of variation vs. mean interspike interval curves: What do they tell us about the brain? *Neurocomputing, 38-40*, 1141–1149.

Cotterill, E., Charlesworth, P., Thomas, C. W., Paulsen, O., & Eglen, S. J. (2016). A comparison of computational methods for detecting bursts in neuronal spike trains and their application to human stem cell-derived neuronal networks. *Journal of Neurophysiology, 116*(2), 306–321.

Douvaras, P., Wang, J., Zimmer, M., Hanchuk, S., O'Bara, M. A., Sadiq, S., et al. (2014). Efficient generation of myelinating oligodendrocytes from primary progressive multiple sclerosis patients by induced pluripotent stem cells. *Stem Cell Reports, 3*(2), 250–259.

Edgar, J. M., Robinson, M., & Willerth, S. M. (2017). Fibrin hydrogels induce mixed dorsal/ventral spinal neuron identities during differentiation of human induced pluripotent stem cells. *Acta Biomaterialia, 51*, 237–245.

Erceg, S., Ronaghi, M., & Stojković, M. (2009). Human embryonic stem cell differentiation toward regional specific neural precursors. *Stem Cells, 27*(1), 78–87.

Falk, A., Koch, P., Kesavan, J., Takashima, Y., Ladewig, J., Alexander, M., et al. (2012). Capture of neuroepithelial-like stem cells from pluripotent stem cells provides a versatile system for in vitro production of human neurons. *PLoS One, 7*(1), e29597.

Frega, M., Tedesco, M., Massobrio, P., Pesce, M., & Martinoia, S. (2014). Network dynamics of 3D engineered neuronal cultures: A new experimental model for in-vitro electrophysiology. *Scientific Reports, 4*, 5489.

Frega, M., van Gestel, S. H. C., Linda, K., van der Raadt, J., Keller, J., Van Rhijn, J.-R., et al. (2017). Rapid neuronal differentiation of induced pluripotent stem cells for measuring network activity on micro-electrode arrays. *Journal of Visualized Experiments*, 119. https://doi.org/10.3791/54900

Fritsche, E., Grandjean, P., Crofton, K. M., Aschner, M., Goldberg, A., Heinonen, T., et al. (2018). Consensus statement on the need for innovation, transition and implementation of developmental neurotoxicity (DNT) testing for regulatory purposes. *Toxicology and Applied Pharmacology*. https://doi.org/10.1016/j.taap.2018.02.004

Garofalo, M., Nieus, T., Massobrio, P., & Martinoia, S. (2009). Evaluation of the performance of information theory-based methods and cross-correlation to estimate the functional connectivity in cortical networks. *PLoS One, 4*(8), e 6482.

Goparaju, S. K., Kohda, K., Ibata, K., Soma, A., Nakatake, Y., Akiyama, T., et al. (2017). Rapid differentiation of human pluripotent stem cells into functional neurons by mRNAs encoding transcription factors. *Scientific Reports, 7*, 42367.

Heikkilä, T. J., Ylä-Outinen, L., Tanskanen, J. M. A., Lappalainen, R. S., Skottman, H., Suuronen, R., et al. (2009). Human embryonic stem cell-derived neuronal cells form spontaneously active neuronal networks in vitro. *Experimental Neurology, 218*(1), 109–116.

Hopkins, A. M., DeSimone, E., Chwalek, K., & Kaplan, D. L. (2015). 3D in vitro modeling of the central nervous system. *Progress in Neurobiology, 125*, 1–25.

Hyysalo, A. (2017). *In vitro culturing conditions for human pluripotent stem cell-derived neural cells: Tissue engineering applications for spinal cord injury repair* (Dissertation, Tampere University Press, 2017).

Hyysalo, A., Ristola, M., Joki, T., Honkanen, M., Vippola, M., & Narkilahti, S. (2017a). Aligned poly(ε-caprolactone) nanofibers guide the orientation and migration of human pluripotent stem cell-derived neurons, astrocytes, and oligodendrocyte precursor cells in vitro. *Macromolecular Bioscience, 17*(7), 1600517.

Hyysalo, A., Ristola, M., Mäkinen, M. E.-L., Häyrynen, S., Nykter, M., & Narkilahti, S. (2017b). Laminin α5 substrates promote survival, network formation and functional development of human pluripotent stem cell-derived neurons in vitro. *Stem Cell Research, 24*, 118–127.

Ito, S., Hansen, M. E., Heiland, R., Lumsdaine, A., Litke, A. M., & Beggs, J. M. (2011). Extending transfer entropy improves identification of effective connectivity in a spiking cortical network model. *PLoS One, 6*(11), e27431.

Johnstone, A. F. M., Gross, G. W., Weiss, D. G., Schroeder, O. H.-U., Gramowski, A., & Shafer, T. J. (2010). Microelectrode arrays: A physiologically based neurotoxicity testing platform for the 21st century. *Neurotoxicology, 31*(4), 331–350.

Kapucu, F. E. (2015). *Joint analysis of extracellular spike waveforms and neuronal network bursts*. [Software] Available via MATLAB Central File Exchange, The MathWorks, Inc. Accessed March 5, 2018, from https://se.mathworks.com/matlabcentral/fileexchange/54277

Kapucu, F. E. (2016a). *Spectral entropy based neuronal network synchronization analysis: CorSE*. [Software] Available via MATLAB Central File Exchange, The MathWorks, Inc. Accessed March 5, 2018, from https://se.mathworks.com/matlabcentral/fileexchange/59626

Kapucu, F. E. (2016b). *Methods to enhance information extraction from microelectrode array measurements of neuronal networks* (Dissertation, Tampere University of Technology, vol. 1438, 2016).

Kapucu, F. E., Mäkinen, M. E.-L., Tanskanen, J. M. A., Ylä-Outinen, L., Narkilahti, S., & Hyttinen, J. A. K. (2016b). Joint analysis of extracellular spike waveforms and neuronal network bursts. *Journal of Neuroscience Methods, 259*, 143–155.

Kapucu, F. E., Mikkonen, J. E., Tanskanen, J. M. A., & Hyttinen J. A. K.. (2015). Quantification and automatized adaptive detection of in vivo and in vitro neuronal bursts based on signal complexity. In *Proceedings of 2015 37th annual international conference of the engineering in medicine and biology society (EMBC), Milan, Italy* (pp. 4729–4732).

Kapucu, F. E., Mikkonen, J. E., Tanskanen, J. M. A., & Hyttinen J. A. K.. (2016a). Analyzing the feasibility of time correlated spectral entropy for the assessment of neuronal synchrony. In *2016 IEEE 38th annual international conference of the engineering in medicine and biology society (EMBC), Orlando* (pp. 1595–1598).

Kapucu, F. E., Tanskanen, J. M. A., Christophe, F., Mikkonen, T., & Hyttinen, J. A. K.. (2017a). Evaluation of the effective and functional connectivity estimators for microelectrode array recordings during in vitro neuronal network maturation. In H. Eskola, O. Väisänen, J. Viik, et al. (Eds.), *European medical and biological engineering conference, Nordic-Baltic conference on biomedical engineering and medical physics (EMBEC & NBC 2017), Tampere, Finland, June 2017. IFMBE proceedings* (Vol. 65, pp. 1105–1108). Singapore: Springer.

Kapucu, F. E., Tanskanen, J. M. A., Mikkonen, J. E., Ylä-Outinen, L., Narkilahti, S., & Hyttinen, J. A. K. (2012). Burst analysis tool for developing neuronal networks exhibiting highly varying action potential dynamics. *Frontiers in Computational Neuroscience, 6*, 38.

Kapucu, F. E., Välkki, I., Christophe, F., Tanskanen, J. M. A., Johansson, J., Mikkonen, T., et al.. (2017b). On electrophysiological signal complexity during biological neuronal network development and maturation. In *2017 39th annual international conference of the IEEE engineering in medicine and biology society (EMBC), Seogwipo, South Korea* (pp. 3333–3338).

Kapucu, F. E., Välkki, I., Mikkonen, J. E., Leone, C., Lenk, K., Tanskanen, J. M. A., et al. (2016c). Spectral entropy based neuronal network synchronization analysis based on microelectrode array measurements. *Frontiers in Computational Neuroscience, 10*, 112.

Karvinen, J., Joki, T., Ylä-Outinen, L., Koivisto, J. T., Narkilahti, S., & Kellomäki, M. (2018). Soft hydrazone crosslinked hyaluronan- and alginate-based hydrogels as 3D supportive matrices for human pluripotent stem cell-derived neuronal cells. *Reactive and Functional Polymers, 124*, 29–39.

Kasteel, E. E. J., & Westerink, R. H. S. (2017). Comparison of the acute inhibitory effects of tetrodotoxin (TTX) in rat and human neuronal networks for risk assessment purposes. *Toxicology Letters, 270*, 12–16.

Kawada, J., Kaneda, S., Kirihara, T., Maroof, A., Levi, T., Eggan, K., et al. (2017). Generation of a motor nerve organoid with human stem cell-derived neurons. *Stem Cell Reports, 9*(5), 1441–1449.

Kelava, I., & Lancaster, M. A. (2016). Dishing out mini-brains: Current progress and future prospects in brain organoid research. *Developmental Biology, 420*(2), 199–209.

Kirkeby, A., Grealish, S., Wolf, D. A., Nelander, J., Wood, J., Lundblad, M., et al. (2012). Generation of regionally specified neural progenitors and functional neurons from human embryonic stem cells under defined conditions. *Cell Reports, 1*(6), 703–714.

Koivisto, J. T., Joki, T., Parraga, J. E., Pääkkönen, R., Ylä-Outinen, R., Salonen, L., et al. (2017). Bioamine-crosslinked gellan gum hydrogel for neural tissue engineering. *Biomedical Materials, 12*(2), 025014.

Krencik, R., Weick, J. P., Liu, Y., Zhang, Z.-J., & Zhang, S.-C. (2011). Specification of transplantable astroglial subtypes from human pluripotent stem cells. *Nature Biotechnology, 29*(6), 528–534.

Kreutzer, J., Ylä-Outinen, L., Kärnä, P., Kaarela, T., Mikkonen, J., Skottman, H., et al. (2012). Structured PDMS chambers for enhanced human neuronal cell activity on MEA platforms. *Journal of Bionic Engineering, 9*(1), 1–10.

Kreutzer, J., Ylä-Outinen, L., Mäki, A.-J., Ristola, M., Narkilahti, S., & Kallio, P. (2017). Cell culture chamber with gas supply for prolonged recording of human neuronal cells on microelectrode array. *Journal of Neuroscience Methods, 280*, 27–35.

Lappalainen, R. S., Salomäki, M., Ylä-Outinen, L., Heikkilä, T. J., Hyttinen, J. A. K., Pihlajamäki, H., et al. (2010). Similarly derived and cultured hESC lines show variation in their developmental potential towards neuronal cells in long-term culture. *Regenerative Medicine, 5*(5), 749–762.

Lee, J., Woo, D.-H., Park, H.-J., Park, K., Ko, D. S., & Kim, J.-H. (2017). Human induced pluripotent stem cell line with cytochrome P450 enzyme polymorphism (CYP2C19*2/CYP3A5*3C) generated from lymphoblastoid cells. *Stem Cell Research, 27*, 34–37.

Lewicki, M. S. (1998). A review of methods for spike sorting: The detection and classification of neural action potentials. *Network: Computation in Neural Systems, 9*(4), R53–R78.

Mäkinen, M. E.-L., Ylä-Outinen, L., & Narkilahti, S. (2018). GABA and gap junctions in the development of synchronized activity in human pluripotent stem cell-derived neural networks. *Frontiers in Cellular Neuroscience, 12*, 56.

Markou, A., Chiamulera, C., Geyer, M. A., Tricklebank, M., & Steckler, T. (2009). Removing obstacles in neuroscience drug discovery: The future path for animal models. *Neuropsychopharmacology, 34*(1), 74–89.

Martynoga, B., Drechsel, D., & Guillemot, F. (2012). Molecular control of neurogenesis: A view from the mammalian cerebral cortex. *Cold Spring Harbor Perspectives in Biology, 4*, a008359.

Maury, Y., Côme, J., Piskorowski, R. A., Salah-Mohellibi, N., Chevaleyre, V., Peschanski, M., et al. (2015). Combinatorial analysis of developmental cues efficiently converts human pluripotent stem cells into multiple neuronal subtypes. *Nature Biotechnology, 33*(1), 89–96.

Mazzoni, A., Broccard, F. D., Garcia-Perez, E., Bonifazi, P., Ruaro, M. E., & Torre, V. (2007). On the dynamics of the spontaneous activity in neuronal networks. *PLoS One, 2*(5), e439.

Mertens, J., Marchetto, M. C., Bardy, C., & Gage, F. H. (2016). Evaluating cell reprogramming, differentiation and conversion technologies in neuroscience. *Nature Reviews. Neuroscience, 17*(7), 424–437.

Miller, J. A., Horvath, S., & Geschwind, D. H. (2010). Divergence of human and mouse brain transcriptome highlights Alzheimer disease pathways. *Proceedings of the National Academy of Sciences of the United States of America, 107*(28), 12698–12703.

Muratore, C. R., Srikanth, P., Callahan, D. G., & Young-Pearse, T. L. (2014). Comparison and optimization of hiPSC forebrain cortical differentiation protocols. *PLoS One, 9*(8), e105807.

Nat, R., Nilbratt, M., Narkilahti, S., Winblad, B., Hovatta, O., & Nordberg, A. (2007). Neurogenic neuroepithelial and radial glial cells generated from six human embryonic stem cell lines in serum-free suspension and adherent cultures. *Glia, 55*(4), 385–399.

Nedergaard, M., Ransom, B., & Goldman, S. A. (2003). New roles for astrocytes: Redefining the functional architecture of the brain. *Trends in Neurosciences, 26*(10), 523–530.

Odawara, A., Katoh, H., Matsuda, N., & Suzuki, I. (2016a). Induction of long-term potentiation and depression phenomena in human induced pluripotent stem cell-derived cortical neurons. *Biochemical and Biophysical Research Communications, 469*(4), 856–862.

Odawara, A., Katoh, H., Matsuda, N., & Suzuki, I. (2016b). Physiological maturation and drug responses of human induced pluripotent stem cell-derived cortical neuronal networks in long-term culture. *Scientific Reports, 6*, 26181.

Odawara, A., Saitoh, Y., Alhebshi, A. H., Gotoh, M., & Suzuki, I. (2014). Long-term electrophysiological activity and pharmacological response of a human induced pluripotent stem cell-derived neuron and astrocyte co-culture. *Biochemical and Biophysical Research Communications, 443*(4), 1176–1181.

Paavilainen, T., Pelkonen, A., Mäkinen, M. E.-L., Peltola, M., Huhtala, H., Fayuk, D., et al. (2018). Effect of prolonged differentiation on functional maturation of human pluripotent stem cell-derived neuronal cultures. *Stem Cell Research, 27*, 151–161.

Pamies, D., Barreras, P., Block, K., Makri, G., Kumar, A., Wiersma, D., et al. (2016). A human brain microphysiological system derived from induced pluripotent stem cells to study neurological diseases and toxicity. *ALTEX, 34*(3), 362–337.

Pappas, J. J., & Yang, P. C. (2008). Human ESC vs. iPSC—Pros and cons. *Journal of Cardiovascular Translational Research, 1*(2), 96–99.

Park, J. W., Vahidi, B., Taylor, A. M., Rhee, S. W., & Jeon, N. L. (2006). Microfluidic culture platform for neuroscience research. *Nature Protocols, 1*(4), 2128–2136.

Paşca, A. M., Sloan, S. A., Clarke, L. E., Tian, Y., Makinson, C. D., Huber, N., et al. (2015). Functional cortical neurons and astrocytes from human pluripotent stem cells in 3D culture. *Nature Methods, 12*(7), 671–678.

Pasquale, V., Martinoia, S., & Chiappalone, M. (2010). A self-adapting approach for the detection of bursts and network bursts in neuronal cultures. *Journal of Computational Neuroscience, 29*(1–2), 213–229.

Pautot, S., Wyart, C., & Isacoff, E. Y. (2008). Colloid-guided assembly of oriented 3D neuronal networks. *Nature Methods, 5*(8), 735–740.

Pawlowski, M., Ortmann, D., Bertero, A., Tavares, J. M., Pedersen, R. A., Vallier, L., et al. (2017). Inducible and deterministic forward programming of human pluripotent stem cells into neurons, skeletal myocytes, and oligodendrocytes. *Stem Cell Reports, 8*(4), 803–812.

Reubinoff, B. E., Itsykson, P., Turetsky, T., Pera, M. F., Reinhartz, E., Itzik, A., et al. (2001). Neural progenitors from human embryonic stem cells. *Nature Biotechnology, 19*(12), 1134–1140.

Roopun, A. K., Simonotto, J. D., Pierce, M. L., Jenkins, A., Nicholson, C., Schofield, I. S., et al. (2010). A nonsynaptic mechanism underlying interictal discharges in human epileptic neocortex. *Proceedings of the National Academy of Sciences of the United States of America, 107*(1), 338–343.

Roybon, L., Lamas, N. J., Garcia-Diaz, A., Yang, E. J., Sattler, R., Jackson-Lewis, V., et al. (2013). Human stem cell-derived spinal cord astrocytes with defined mature or reactive phenotypes. *Cell Reports, 4*(5), 1035–1048.

Schutte, R. J., Xie, Y., Ng, N. N., Figueroa, P., Pham, A. T., & O'Dowd, D. K. (2018). Astrocyte-enriched feeder layers from cryopreserved cells support differentiation of spontaneously active networks of human iPSC-derived neurons. *Journal of Neuroscience Methods, 294*, 91–101.

Seidel, D., Jahnke, H.-G., Englich, B., Girard, M., & Robitzki, A. A. (2017). In vitro field potential monitoring on a multi-microelectrode array for the electrophysiological long-term screening of neural stem cell maturation. *Analyst, 142*(11), 1929–1937.

Selinger, J. V., Kulagina, N. V., O'Shaughnessy, T. J., Ma, W., & Pancrazio, J. J. (2007). Methods for characterizing interspike intervals and identifying bursts in neuronal activity. *Journal of Neuroscience Methods, 162*(1–2), 64–71.

Shuler, M. L., & Hickman, J. J. (2014). Toward in vitro models of brain structure and function. *Proceedings of the National Academy of Sciences of the United States of America, 111*(38), 13682–13683.

Simão, D., Pinto, C., Piersanti, S., Weston, A., Peddie, C. J., Bastos, A. E. P., et al. (2015). Modeling human neural functionality in vitro: Three-dimensional culture for dopaminergic differentiation. *Tissue Engineering. Part A, 21*(3–4), 654–668.

Subramaniyam, N. P. (2016). *Recurrence network analysis of EEG signals: A geometric approach* (Dissertation, Tampere University of Technology, Vol. 1364, 2016).

Subramaniyam, N. P., & Hyttinen, J. (2015). Dynamics of intracranial electroencephalographic recordings from epilepsy patients using univariate and bivariate recurrence networks. *Physical Review E, 91*(2), 022927.

Subramaniyam, N. P., Hyttinen, J., Hatsopoulos, N. G., & Takahashi, K.. (2015). Recurrence network analysis of wide band oscillations of local field potentials from the primary motor cortex reveals rich dynamics. In *2015 7th international IEEE/EMBS conference on neural engineering (NER), Montpellier, France* (pp. 960–963).

Suzuki, I. K., & Vanderhaeghen, P. (2015). Is this a brain which I see before me? Modeling human neural development with pluripotent stem cells. *Development, 142*(18), 3138–3150.

Takahashi, K., Tanabe, K., Ohnuki, M., Narita, M., Ichisaka, T., Tomoda, K., et al. (2007). Induction of pluripotent stem cells from adult human fibroblasts by defined factors. *Cell, 131*(5), 861–872.

Tanskanen, J. (2017). *Automatic objective neuronal spike detection*. Available via MATLAB Central File Exchange, The MathWorks, Inc. Accessed March 5, 2018, from https://se.mathworks.com/matlabcentral/fileexchange/55227

Tanskanen, J. M. A., Kapucu, F. E., Vornanen, I., & Hyttinen, J. A. K.. (2016). Automatic objective thresholding to detect neuronal action potentials. In *2016 24th European signal processing conference (EUSIPCO), Budapest, Hungary, August–September 2016* (pp. 662–666).

Thomson, J. A., Itskovitz-Eldor, J., Shapiro, S. S., Waknitz, M. A., Swiergiel, J. J., Marshall, V. S., et al. (1998). Embryonic stem cell lines derived from human blastocysts. *Science, 282*(5391), 1145–1147.

Toivanen, M., Pelkonen, A., Mäkinen, M., Ylä-Outinen, L., Sukki, L., Kallio, P., et al. (2017). Optimised PDMS tunnel devices on MEAs increase the probability of detecting electrical activity from human stem cell-derived neuronal networks. *Frontiers in Neuroscience, 11*, 606.

Toivonen, S., Ojala, M., Hyysalo, A., Ilmarinen, T., Rajala, K., Pekkanen-Mattila, M., et al. (2013). Comparative analysis of targeted differentiation of human induced pluripotent stem cells (hiPSCs) and human embryonic stem cells reveals variability associated with incomplete transgene silencing in retrovirally derived hiPSC lines. *Stem Cells Translational Medicine, 2*(2), 83–93.

Tukker, A. M., de Groot, M. W. G. D. M., Wijnolts, F. M. J., Kasteel, E. E. J., Hondebrink, L., & Westerink, R. (2016). Is the time right for in vitro neurotoxicity testing using human iPSC-derived neurons? *ALTEX, 33*(3), 261–271.

Välkki, I. A., Lenk, K., Mikkonen, J. E., Kapucu, F. E., & Hyttinen, J. A. K. (2017). Network-wide adaptive burst detection depicts neuronal activity with improved accuracy. *Frontiers in Computational Neuroscience, 11*, 40.

Wagenaar, D. A., Pine, J., & Potter, S. M. (2006). An extremely rich repertoire of bursting patterns during the development of cortical cultures. *BMC Neuroscience, 7*, 11.

Wilson, S. B., & Emerson, R. (2002). Spike detection: A review and comparison of algorithms. *Clinical Neurophysiology, 113*(12), 1873–1881.

Xie, Y., Schutte, R. J., Ng, N. N., Ess, K. C., Schwartz, P. H., & O'Dowd, D. K. (2017). Reproducible and efficient generation of functionally active neurons from human hiPSCs for preclinical disease modeling. *Stem Cell Research, 26*, 84–94.

Xu, T., Molnar, P., Gregory, C., Das, M., Boland, T., & Hickman, J. J. (2009). Electrophysiological characterization of embryonic hippocampal neurons cultured in a 3D collagen hydrogel. *Biomaterials, 30*(26), 4377–4383.

Ylä-Outinen, L., Heikkilä, J., Skottman, H., Suuronen, R., Äänismaa, R., & Narkilahti, S. (2010). Human cell-based micro electrode array platform for studying neurotoxicity. *Frontiers in Neuroengineering, 3*, 111.

Ylä-Outinen, L., Joki, T., Varjola, M., Skottman, H., & Narkilahti, S. (2014). Three-dimensional growth matrix for human embryonic stem cell-derived neuronal cells. *Journal of Tissue Engineering and Regenerative Medicine, 8*(3), 186–194.

Yu, J., Vodyanik, M. A., Smuga-Otto, K., Antosiewicz-Bourget, J., Frane, J. L., Tian, S., et al. (2007). Induced pluripotent stem cell lines derived from human somatic cells. *Science, 318*(5858), 1917–1920.

Zirra, A., Wiethoff, S., & Patani, R. (2016). Neural conversion and patterning of human pluripotent stem cells: A developmental perspective. *Stem Cells International, 2016*, 8291260.

Long-Term Activity Dynamics of Single Neurons and Networks

Sebastian Reinartz

Abstract The firing rate of neuronal spiking in vitro and in vivo significantly varies over extended timescales, characterized by long-memory processes and complex statistics, and appears in spontaneous as well as evoked activity upon repeated stimulus presentation. These variations in response features and their statistics, in face of repeated instances of a given physical input, are ubiquitous in all levels of brain-behavior organization. They are expressed in single neuron and network response variability but even appear in variations of subjective percepts or psychophysical choices and have been described as stemming from history-dependent, stochastic, or rate-determined processes.

But what are the sources underlying these temporally rich variations in firing rate? Are they determined by interactions of the nervous system as a whole, or do isolated, single neurons or neuronal networks already express these fluctuations independent of higher levels? These questions motivated the application of a method that allows for controlled and specific long-term activation of a single neuron or neuronal network, isolated from higher levels of cortical organization.

This chapter highlights the research done in cultured cortical networks to study (1) the inherent non-stationarity of neuronal network activity, (2) single neuron response fluctuations and underlying processes, and (3) the interface layer between network and single cell, the non-stationary efficacy of the ensemble of synapses impinging onto the observed neuron.

Keywords Response fluctuations · Long-memory processes · Self-organized criticality · Single neuron · Direct response · Synaptic dynamics

S. Reinartz (✉)
Tactile Perception and Learning Lab, International School for Advanced Studies (SISSA), Trieste, Italy

1 Activity Dynamics (Variability) in Neuronal Systems

The principle of variation that we propose states that biological organisms are specific objects and, thereby, fundamentally different from the objects defined in physical theories. The principle, which draws directly on Darwin's insights on biological variation, embeds a specific notion of randomness, which corresponds to unpredictable changes of the mathematical structure required to describe biological objects. In this framework, biological objects are inherently variable, historical and contextual (Montévil et al. 2016).

Unexplained variability exists at all levels of brain-behavior organization and can appear in spontaneous activity fluctuations, as well as trial-to-trial variability in response to repeated presentation of an identical stimulus. Next to noise, defined as random unpredictable disturbances to trial-to-trial variability due to measurement inaccuracies or biological random processes at all levels of organization (Faisal et al. 2008), there are fluctuations characterized by temporal structure (e.g., sequential correlations). The temporal structure of these fluctuations, often measured in terms of reliability and precision (Tiesinga et al. 2008; Masquelier 2013), is highly complex (Marom 2010).

Wherever data is sufficiently long to enable proper temporally extended analyses, the overall picture that emerges is characterized by complex statistics with the flavor of long-memory processes (defined in Baillie 1996), reflected in long-range correlations and quasi-stable response patterns (Teich 1989; Lowen and Teich 1996; Gal et al. 2010). Spectral analysis of spike time series often reveals a spectral power continuously decaying at low frequencies, and appears to follow a 1/frequency behavior. This could imply a phenomenon, found in many natural processes, known in physics as "one-over-*f*" noise (Beran 1994). In theoretical controversies, this was interpreted either as stemming from general system principles, or through a proliferation of individual mechanisms (Milotti 2002) as of superposition of several underlying relaxation processes. As discussed in Marom (2010), these underlying processes could either possess discrete timescales or be scale invariant in itself.

There are countless behavioral phenomena that show timescale-free fluctuations such as somatosensory stimulus detection (Monto et al. 2008), in two-alternative-forced choice discrimination tasks (discussed in Gilden 2001), and adaptation to sensory percepts (e.g., Rose and Lowe 1982) and in reproduction tasks (e.g., Gilden et al. 1995). Behavioral performances, EEG or FMRI signals of individuals show correlations over extended timescales when responding to identical near-threshold stimuli in psychophysical experiments (Werthheimer 1953; Nir et al. 2007; Monto et al. 2008; Marom and Wallach 2011). Recordings of neuronal networks in vitro also show temporally complex characteristics (Segev et al. 2002; Mazzoni et al. 2007; Esposti et al. 2009). Even at the level of single ionic channels, temporal complexity is preserved (Liebovitch et al. 1987; Toib et al. 1998; Ellerkmann et al. 2001).

On the contrary, in other experiments high reliability and precision can be seen in cortex (e.g., Tiesinga et al. 2008; Kayser et al. 2010; Panzeri and Diamond 2010); for this reason, Masquelier (2013) argued that the lack of control over all parameters,

input from higher levels or neuronal states are responsible for trial-to-trial variability in vivo rather than neuron intrinsic mechanisms. However, firstly these possibilities are not necessarily mutually exclusive, they are even interdependent; different neuronal states can be caused by channel/synaptic dynamics or the inverse. Secondly, as described below, long-term single neuron response fluctuations can even be found in synaptically isolated neurons in vitro that are independent of the network or higher order cortical areas (see Sect. 4).

The concept of self-organized criticality (SOC) may provide a possible interpretation of this coexistence of variability and precision in neuronal performance. Applying this theoretical framework, used for describing complex systems, to neuroscience (Jensen 1998; Plenz and Niebur 2014 and references therein), the excitable system (e.g., network) is suggested to be composed of many weakly and nonlinearly coupled subsystems (e.g., neurons). A critical system operates at or near phase transition, for instance between a disordered, noisy state and an ordered but fixed state. Fluctuating along this critical point enables the system to generate coherent function, while allowing some degree of flexibility. The specific characteristic of a SOC system is the insensitivity of its behavior to outer physical parameters, as the system positions itself near to a critical point (dynamic attractor). Scale-invariant behavior and long-range correlations are seen as a characteristic feature emerging SOC systems (Bak 1997).

From human behavioral performance down to neuronal membrane excitability, irrespective of the level of organization that expresses temporal variability, determinants can be generalized to three main factors: (1) processes that are dependent on the context in which the current stimulus is presented, meaning the input to which the system has been exposed to before the stimulus (e.g., adaptation or perceptual stimulus history effects) (Laughlin 1981; Brenner et al. 2000; Fritsche et al. 2017); (2) processes dependent on the history of the output of the system (Gal et al. 2010; Fründ et al. 2014; Braun et al. 2018); and (3) stochastic processes that are independent of input or output (Faisal et al. 2008).

Various strategies have been adopted to isolate these factors, one of them being the subject of this book: the experimental model of cultured cortical networks that enables studies of isolated neuronal networks or single neurons and control over various parameters. An experimental method that allows for controlling the output of a neuronal system to potentially isolate possible sources of variability is called the Response clamp method (reviewed in Wallach 2013). Adopting strategies from the voltage clamp approach, the output of a neuronal system—for example the response spike probability—is clamped by adjusting the stimulus intensity with negative feedback control. In this way, a closed-loop feedback can be used for system identification and characterization. Stimulation intensities (e.g., electrical, pharmacological, and optogenetic) and their fluctuations, being the output of a controller (e.g., PID) necessary to clamp the neuronal systems output, can be analyzed with respect to threshold and its variability. So far, it has been successfully applied on single neurons (Wallach et al. 2011; Wallach and Marom 2012), neuronal

networks (Keren and Marom 2014; Kaufman et al. 2014), thalamic neurons of anesthetized rats (Newman et al. 2015) and in a human visual detection task (Marom and Wallach 2011).

2 Cultured Cortical Networks as a Model to Study Activity Dynamics

As a precondition to study general questions on long-term neuronal activity dynamics, independent of cell type or brain area, it is advantageous to make use of a (1) generic model, lacking predefined anatomical structures and input from remote modules (Eytan and Marom 2006) that provides (2) stable access to neuronal activity over extended timescales in a (3) highly controllable system.

In this section, I briefly give an overview of the advantages of using cortical neurons derived from newborn rats, cultured on substrate integrated micro-electrode arrays (MEA), for long-term electrophysiological recording (up to several months) and electrical stimulation.

Generic Model During the first hours after seeding the enzymatically and mechanically dissociated cortical tissue (neuron, glial cells) on the pretreated (e.g., polyethylene-imine and poly-D-lysine) substrate, neurons start to extend processes, developing a densely connected mature-phase monolayer with axodendritic branches extending over 1 mm and high numbers of functional synapses (Marom and Shahaf 2002 and references therein). Comparisons of the distributions of types of neurons were made by immunohistochemistry to show the similarities between ex-vivo and in-vivo developing cortical networks. Similar to cerebral cortex, the broad majority of neurons were found to be excitatory glutamatergic, while consisting of 10–25% inhibitory GABAergic (γ-Aminobutyric-acid) cells and 2–3% of cells that synthesize acetylcholine (Neale et al. 1983; Huettner and Baughman 1986; Bonifazi et al. 2005).

Cultured cortical networks exhibit rich spontaneous activity dynamics (Marom and Shahaf 2002; van Pelt et al. 2004; Wagenaar et al. 2006) characterized by Network Bursts (NB), synchronized neuronal bursting events that are alternated by phases of low firing probability. Comparable spontaneous activity characteristics can be found in some stages of the developing neocortex (Katz and Shatz 1996; Golshani et al. 2009) and in sleeping states of adult neocortex (Steriade et al. 1993; Destexhe et al. 1999; Volgushev et al. 2006). On a single neuron level, the depolarization and hyperpolarization occurring during the course of such a network burst exhibit considerable similarities to "up" and "down" states recorded in vivo (Harris and Thiele 2011; Kaufman et al. 2014).

Systematic changes of activity patterns were described during the development of cortical cell cultures (van Pelt et al. 2005; Wagenaar et al. 2006; Chiappalone et al. 2006). First, uncorrelated single neuron firing during the end of the first week in vitro is followed by synchronous regular bursting between ∼9–22 days.

After approximately three weeks, the cultures exhibited more complicated activity patterns, such as non-periodically occurring NBs with fluctuations in the firing probability, which do not change prominently over two months (Kamioka et al. 1996).

In parallel to the developmental changes in network firing, the primarily homogenously distributed neurons spontaneously aggregate to form densely populated neuronal clusters connected by fasciculated neurites (Kriegstein and Dichter 1983; Segev et al. 2003). The high accessibility to the different processes occurring in parallel has been appealing for studying the relationships between structural and functional properties in neuronal network development (e.g., Soriano et al. 2008; Okujeni et al. 2017). The spontaneous activity of the network, whether sporadic or synchronized, is correlated with the development of synaptic connections. An increase in the NB frequency, for example, was correlated to the number of synapses (Van Huizen et al. 1985; Muramoto et al. 1993). Furthermore, nonperiodic, complex network bursting was accompanied with a decline in the number of synapses starting in the fourth week, resembling synaptic pruning processes (van Huizen et al. 1985; van Pelt et al. 2004).

Long-Term Stable Interaction Long-term electrophysiological recordings and stimulation of single neurons and neuronal networks can be performed by growing cortical cell cultures on substrate-integrated arrays with usually 60, sometimes even up to >1000 (Berdondini et al. 2005; Frey et al. 2010; see also Obien and Frey in Chapter 4), micro electrodes (MEA). MEA glass substrates allow for parallel patch-clamp recordings or access with optical methods (e.g., Robinson et al. 1993; Minerbi et al. 2009; El Hady et al. 2013; Pulizzi et al. 2016).

Field electrical stimulation of cortical networks growing on microelectrode arrays (MEAs) evokes a range of neuronal response features (Jimbo et al. 2000; Marom and Shahaf 2002; Wagenaar et al. 2004): An early component, due to local activation of proximate areas, and a late component designated as "reverberating wave" and identical to spontaneous Network Bursts. The NB evokes synaptically mediated reverberating activity, strong enough to amplify, propagate and maintain itself for hundreds of milliseconds (Jimbo et al. 2000; Marom and Shahaf 2002; Eytan and Marom 2006). Interestingly, almost comparable bimodal response dynamics with a precise early response (<50 ms) followed by a late response (50–400 ms) was found in barrel cortex neurons in a tactile detection task, with the early part being predictive of stimulus features and the late part more to perceptual report (Sachidhanandam, et al. 2013).

A "direct response" in this framework corresponds to a neuronal spike, insensitive to the presence of synaptic blockers (Fig. 1a–d), elicited by direct somatic, or antidromic stimulation of an axon (Fig. 1e, *blue*). Especially axon initial segments or other accessible axon positions are widely seen as sites for direct neuronal activation (Gustafsson and Jankowska 1976; Tehovnik et al. 2006; Bakkum et al. 2008). Direct responses are early (<20 ms after stimulus) and extremely reliable spikes, with high temporal precision (Bakkum et al. 2008; Wallach et al. 2011) and allow direct access to neuronal excitability and its variability.
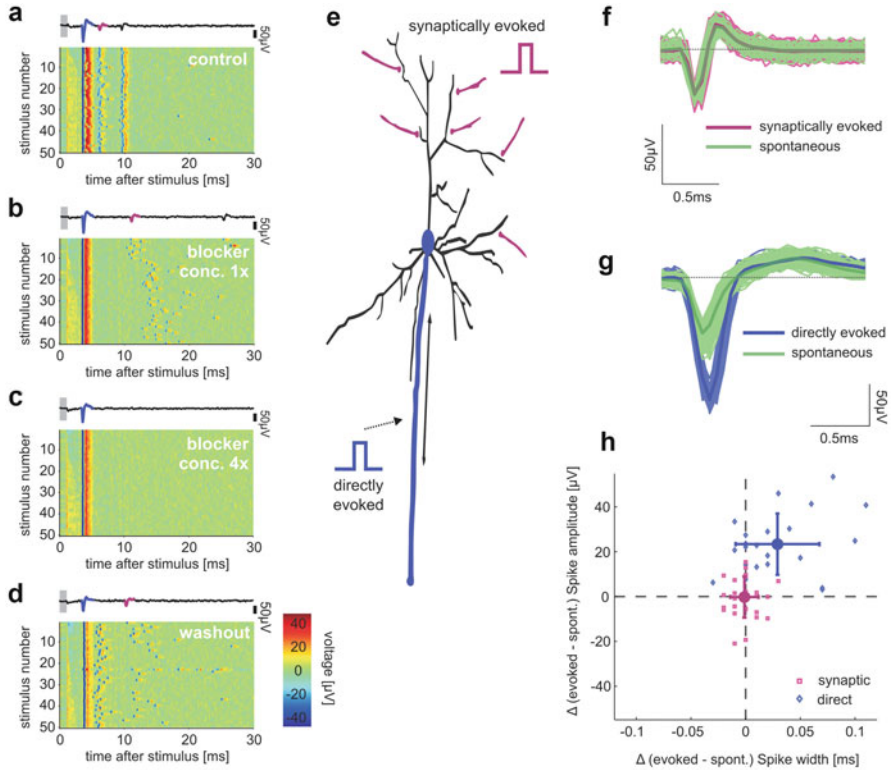
Fig. 1 Direct and synaptically mediated response spikes. Pseudo-color plots (**a–d**) show voltage traces detected by an electrode that records both directly evoked and synaptically mediated spikes, in different concentrations of synaptic blockers: (**a**) Control solution with no blockers; (**b**) Added blockers (8 μM APV, 4 μM CNQX, 2 μM BIC); (**c**) Four-fold concentrations compared to (**b**); and (**d**) Back to control solution after washing out the blockers. Single voltage traces above each panel depict direct (blue) and synaptic (magenta) mediated spikes in the first trace of each condition. Focusing on the immediate synaptically evoked responses, we did not consider secondary spikes of the synaptically activated neuron. Gray bars mark blanking period. Color bar in (**d**) indicates voltage-color correspondence, identical in (**a–d**). (**e**) Conceptual scheme of the two local responses to direct (blue) and synaptic (magenta) activation. Sketches of stimulation signal illustrate potential locations of stimulation electrode for each of the two response types. (**f**) Shapes of spikes generated spontaneously by the network (green) or by synaptic stimulation (magenta); average traces are depicted with bold lines. (**g**) Shapes of spikes of another neuron that was directly stimulated (blue) and activated by the network (green). (**h**) Synaptic mediated response spike waveforms resemble spontaneous network-mediated spike shapes. Each dot represents the difference in mean amplitudes and half-widths, between evoked and spontaneous spikes in one single neuron. Mean and σ of the distributions are depicted (big markers, error bars). Spike half-width was determined as the width at half maximum amplitude, using an extrapolation between the two points closest to the half maximum amplitude. Figure and caption reproduced from Reinartz et al. (2014) under the terms of the Creative Commons Attribution License (CC BY)

Another type of early response, a "synaptically evoked spike", was briefly mentioned by Wagenaar et al. (2004) and further described by Bonifazi et al. (2005) as glutamatergic dependent, precise (temporal jitter <0.25 ms) and highly reliable (Fig. 1a–d). Systematic comparisons of direct and synaptically evoked early responses in cortical cell cultures and acute slices (Reinartz et al. 2014), suggested that synaptic responses are generated by an orthodromic activation of synaptic input pathways to the recorded neuron., termed *synaptic envelope* (Fig. 1e, *magenta*). In contrast to direct, synaptically activated neurons exhibit spike waveforms resembling unstimulated, network mediated spikes (Fig. 1f–h) and therefore appear as a more physiological way of single neuron activation.

Maintaining the stability of the system allowed for studying long-term response dynamics (>24 h electrical stimulation) of phenomena in each of the above-mentioned response regimes (Gal et al. 2010; Reinartz et al. 2014; Haroush and Marom 2015).

Controllable System Firstly, maintenance of near steady-state conditions over several days can be ensured by temperature control, CO_2 buffering, and slow but continuous exchange of culturing medium (e.g., Potter and Demarse 2001; Eytan and Marom 2006). Secondly, in order to isolate single neuron response fluctuations from synaptic input of the network, all synaptic transmission can be blocked pharmacologically. In order to further dissect the system, pharmacological treatment can also be applied by individually blocking particular synaptic receptors or channel types or by changing concentrations of relevant ions (Robinson et al. 1993; Jimbo et al. 2000; Pasquale et al. 2008). Further, neuronal network synchronization can be manipulated by pharmacological intervention (Canepari et al. 1997; Kaufman et al. 2012, 2014). Even network clustering can be manipulated mechanically (Chiappalone et al. 2006, 2007) or pharmacologically (Okujeni et al. 2017).

3 Long-Term Non-stationarities in Neuronal Networks

Ongoing network activity contributes to trial-to-trial variability in vivo (Arieli et al. 1996; Azouz and Gray 1999) and in vitro (Harsch and Robinson 2000; Wallach and Marom 2012; Weihberger et al. 2013) and thus, possibly determines temporal complexity of single neuron firing. This section provides an overview about research done on long-term activity dynamics of neuronal networks and possible underlying processes, using cultured cortical or hippocampal networks.

Next to the developmental changes in the long-term statistics of Network Bursts during the course of cultured network maturation mentioned previously, long-term activity dynamics in NBs can be studied in recordings prolonged over several hours. After binning and summarizing the spiking activity across all electrodes, a threshold in array-wide firing rate can be defined for detection of NB events.

Segev et al. (2002) showed scale invariance and long-range correlations in cultured networks of different sizes, by identifying power-law decays at low

frequencies of NB event sequences and non-Gaussian heavy-tail distributions of inter-event intervals. Interestingly, these statistics were found in both single neuron and network activity, with a separation of timescales. This can be interpreted as reflecting self-organization at two excitable systems—networks and neurons—each composed of nonlinearly coupled subsystems (here, for example, neurons and ionic channels respectively). In a similar analysis, using data from developing cultured networks (Wagenaar et al. 2006), (Esposti et al. (2009) and colleagues), found long-term non-stationarities throughout the development of the network starting after approximately 17 days in vitro, probably related to a further clustering of the network observed at these ages.

Comparable long-term correlations and 1/f behaviors were found both, in random hippocampal and hierarchical leech ganglion networks (Mazzoni et al. 2007). These global dynamical properties were attenuated when the balance between inhibition and excitation was altered by pharmacologic attenuation of one of them. Indeed, another study suggested a dynamic excitation-inhibition ratio to be reflected in long-term network response variations (Haroush and Marom 2015). Pharmacological manipulations of inhibitory and excitatory synaptic strengths and systematic assessment of network response dynamics to repeated field electric stimulation revealed instantaneous observables to fluctuating inhibition and excitation strengths.

Next to scale-free statistics in the purely temporal domain of neuronal network activity, there is an entire branch of research that studies scale invariance and SOC at the spatiotemporal dimension. A theoretical principle of information transmission in neuronal networks, called *synfire chains* (Abeles 1991), suggested sequential activation of neuronal ensembles like in a wave, just without necessary spatial ordering of the activated ensembles. Beggs and Plenz (2003) were showing this kind of cascading activity in cortical networks of cultured slices and firstly demonstrated that these cascades, termed *neuronal avalanches* reflect critical dynamics. Simulations demonstrated the requirements for criticality in cascade formation to enhance information transmission: When a neuronal group engages a smaller group (subcritical), the activity is likely to die out due to propagation of this decrement of number of cells activated. And reversely, when the group size increases, the entire network can be activated in a nonselective manner (supercritical). The distribution of cascade sizes identifies spontaneous activity as neuronal avalanches, if it follows a power-law and if the scaling exponent (often close to 1.5) does not change with size of the recorded area (given a constant ratio of spatial/temporal resolution). As the underlying network of neuronal interactions is able to balance these cascades at criticality (given various structures, densities and sizes) it is seen as an evidence for self-organized critical dynamics (Beggs and Plenz 2003; Plenz and Thiagarajan 2007; Chialvo 2010). Spatiotemporal dynamics of spontaneous activity in developing cortical cultures also exhibited self-organized criticality (Pasquale et al. 2008; Tetzlaff et al. 2010). The previously defined and well-described developmental stages and the opportunity of selective pharmacological manipulation allowed to further assess under which conditions these networks can develop into a critical state.

4 Single Neuron Excitability Dynamics

When a single neuron is recorded in the brain that responds to an ongoing stimulus, usually variability can be seen at the level of neuronal responses. This is relevant, as these fluctuations are characterized by long-memory processes across behaviorally relevant timescales. Ongoing network activity contributes to single neuron trial-to-trial variability; therefore, it has been unclear if variability is generated inherently to the single neuron, independent of higher levels (Lowen et al. 1999; Gilboa et al. 2005). Two methodological requirements had to be overcome in order to address this question: (1) functional isolation of the neuron from higher level influence and (2) a stable interaction for stimulation across extended timescales. "Direct" responses (see also Sect. 2) to field electric stimulation of neurons that are embedded in, but synaptically decoupled from cultured cortical networks, offer a unique setting for investigating long-term (>24 h) excitability dynamics (see below, as described in Gal et al. 2010).

When main synaptic receptors (glutamatergic and GABAergic) are blocked pharmacologically, spontaneous activity, synaptic responses and inter-neuron correlations are abolished. Continuous, low frequency (1 Hz) electric stimulation evokes early, highly precise and reliable direct response spikes ("*1:1 response mode*", see Fig. 1a–d). When stimulation frequency is raised, following a "*transient*" phase of increasing response latencies but reliable spiking, a new steady state with stabilized responses can be established (Fig. 2a, b). In case the stimulation frequency is raised above a critical value (>7 Hz), after responses reached a certain critical latency, neuronal spiking enters a highly variable, "*intermittent*" response mode (Fig. 2a–c). Experimental instability can be hereby excluded as a source to response variability, by elimination of neurons with trends in spike shape and verifying a lack of neuron-to-neuron cross-correlations. Response latencies and firing rates start to strongly fluctuate around a steady-state value that is independent of input frequency (Fig. 2d–f). This could reflect an intrinsic limit to firing rate, when activated over prolonged periods. Considering rates of activation measured in different settings in vivo, Gal and colleagues (Gal et al. 2010) suggested that neurons residing in an awake brain operate in the intermittent regime, for being constantly exposed to synaptic inputs at those elevated rates.

When stimulation is prolonged for many hours, it is possible to study the temporal statistics of response rate and latency, for example, by applying periodogram or Fano factor analysis. In the latter, a count sequence $A_T(n)$ is generated using logarithmically spaced bin sizes. For each count sequence, the Fano factor (variance-to-mean ratio) can be plotted as a function of bin size [i.e., $FF(T) = \frac{\text{var}(A_T)}{\text{mean}(A_T)}$]. Variability over several timescales and power-law behavior were illustrated with those and several alternative measures (e.g., Fig. 2g–i). Taken together with observed quasi-stable response patterns, neuronal firing at these regimes revealed
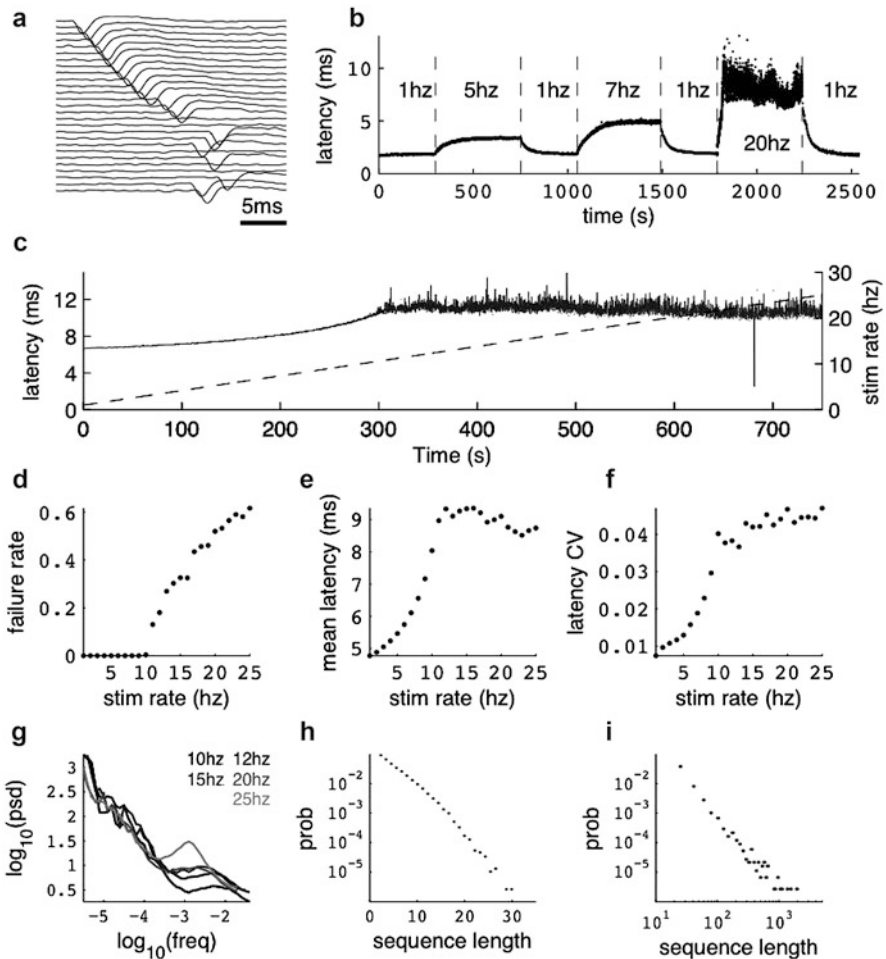
Fig. 2 Experimental observation of excitability dynamics. (**a**) The response of a single isolated neuron to sequences of pulse stimuli delivered at 20 Hz. The responses are ordered top to bottom, every 20th response is shown for clarity. The delaying of the AP can be observed, as well as response failures when excitability is below threshold. (**b**) The AP latency plotted as a function of time in an experiment where the stimulation rate is changed. For low stimulation rate, the excitability stabilizes at a fixed, supra threshold value. For high stimulation rate (20 Hz), excitability decreases below threshold, and the neuron responds intermittently. (**c**) response latencies (solid line) in response to a stimulation sequence with slowly increasing stimulation rate (dashed line). (**d**) Failure (no spike) probability as a function of stimulation rate. A critical stimulation rate is clearly evident. (**e**) Mean response latency as a function of stimulation rate. The increase of the latency accelerates as the stimulation rate approaches the critical point. (**f**) The jitter (coefficient of variation) of the latency as a function of stimulation rate. (**g**) Scale free fluctuations in the intermittent mode. Periodograms of the failure rate fluctuations, at five different stimulation rates above r0. (**h**) Length distribution of spike-response sequences, on a semilogarithmic plot, demonstrating an exponential behavior. Example from one neuron stimulated at 20 Hz for 24 h. (**i**) Length distribution of no-spike response sequences from the same neuron, on a double logarithmic plot, demonstrating a power-law-like behavior. Reprinted figure and caption with permission from [Gal A, Marom S; Self-organized criticality in single-neuron excitability. Phys Rev E 88; 062717; 2013.] Copyright (2018) by the American Physical Society

complex dynamics and pointed to a multitude of underlying activity-dependent processes that fluctuate at different timescales (see also Liebovitch et al. 1987; Toib et al. 1998; Ellerkmann et al. 2001). Therefore, the above observations were further interpreted in the framework of self-organized criticality (Gal and Marom 2013a). Neuronal excitability as a biophysical property of a membrane, here observed as response rate or latency had been described long before, to result from collective interaction of membrane-embedded ion channels (Hodgkin and Huxley 1952). The main observation hereby was an ongoing transition between the *excitable state*, when the neuron responds at elevated activation rates, and the *unexcitable state* characterized by power-law distributed sequences of failure trials for restoring excitability (Fig. 2i). These complex dynamics appear at response latencies and scaling exponents of the failure rate periodogram, independent to stimulation frequency. A model was suggested, related to adaptive transition rates of ion channels (Marom 2009), as a possible underlying mechanism.

Another experiment was designed to study the entrainment of single neuron response dynamics in cultured cortical networks. On a shorter timescale, single neuron variability in response to constant input has been quenched by introducing variation in the input itself (Mainen and Sejnowski 1995; Churchland et al. 2010). This entrainment to input fluctuations at a timescale of seconds was reproduced in a Hodgkin-Huxley model when relating it to the properties of underlying ion channels (Schneidman et al. 1998). Furthermore, natural sensory input, often characterized by scale-free temporal structure (e.g., Simoncelli 2003), has been shown to reduce neuronal response variability (Aertsen and Johannesma 1981; Yu et al. 2005; Garcia-Lazaro et al. 2006). Inspired by this, Gal and Marom (2013b) measured the impacts of temporal input structure to response variability over extended timescales. Comparing response dynamics at intermittency to three statistically different stimulation sequences (constant interval times, white noise modulated, scale-free modulated), no significant differences were found in the global statistical properties of the responses, all exhibiting scale-free dynamics. However, at extended timescales, the correlation between input and response as well as the response repeatability has been significantly improved for scale-free stimulation statistics. Results were congruent when extending the stimulation protocol to the complete (unblocked) network level (Scarsi et al. 2017). Cross-correlations between input and output (network responses) were maximal, when stimulation sequences followed 1/f statistics. Furthermore, network response rates were independent to average stimulation frequency only under scale free stimulus regimes.

An interpretation consistent with the above findings on single neuron and network response dynamics can be formulated, imagining weakly coupled processes (oscillators) underlying the neural systems excitability that can be entrained at different frequencies. The intrinsic dynamics are rather matched by a complex and temporally rich than with a constant, or noisy but memory-less input.

5 Synaptic Envelope Contributes to Single Neuron Response Fluctuations

One concern regarding studies of long-term single neuron response fluctuations and neuronal excitability in general is that many experiments reveal these processes by direct electrical stimulation of single neurons, either intracellularly or extracellularly. In natural situations however, the aforementioned activity-dependent processes are not instantaneously activated by an electric field, their activation is rather integrating excitatory postsynaptic potentials (EPSPs) mediated via a synaptic envelope. The synaptic envelope can be defined as the subset of synapses impinging on a neuron, which collectively become active and release neurotransmitter, either in response to a unique stimulus or as part of ongoing network activity (Jia et al. 2010; Scholl et al. 2010; Chen et al. 2013). This ensemble of synapses constitutes an interface between the network and a given cell, and might significantly modulate the statistical structure of network input to the cell.

The study described below (Reinartz et al. 2014) was performed in order to investigate this issue, and specifically motivated by the following three main aspects: first, to examine neuronal excitability dynamics under more physiological conditions (see Fig. 1f–h); second, to study the long-term synaptic filtering properties that might manipulate the temporal input statistics to which the neuronal excitability machinery is exposed to, shown on shorter timescales so far (Thomson 1997; Markram et al. 1998; Fortune and Rose 2001); and third, since the dynamics of synaptic transmission might be complex in itself (e.g., Lowen et al. 1997; Levina et al. 2007; Turrigiano 2008; Minerbi et al. 2009), to study whether they could become a potential source of long-memory processes and complex statistics of neuronal activity.

Therefore, a method was developed that caters to long-term activation of "isolated" cortical neurons in vitro via their synaptic envelope. Specifically, the "receptive" area of a neuron was stimulated so that synaptic population input could depolarize dendrites, sufficiently to evoke an action potential at the soma (as illustrated in Fig. 1e). The experimental separation between those early and precise synaptic and direct responses, can be performed by comparing input/output characteristics to varying stimulation amplitudes. While directly activated neurons start responding with almost 100% reliability with a fixed latency once a certain threshold stimulation amplitude is reached, synaptically activated neurons are characterized by a graded input-output curve and significantly changing response latencies close to the threshold. This method has been validated, considering the intact microcircuits of cortical tissue, in intracellular neuronal recordings in acute cortical slices. Hence it serves as a fast classification method preceding each experiment. At experimental termination, pharmacological blockage of excitatory synapses (Fig. 1a–d) allow a final confirmation of the previously attributed response

type. While being independent to NMDA receptor antagonists on short as well as long timescales, early synaptic responses are mediated by AMPA receptors. In order to isolate synaptically mediated single neuron response characteristics, spontaneous and evoked NBs can be suppressed by pharmacological blockage of NMDA channels (Robinson et al. 1993; Kamioka et al. 1996; Jimbo et al. 2000; Bonifazi et al. 2005).

Prolonged electrical stimulation allows comparing response statics and dynamics of direct responses, mainly determined by membrane excitability, and responses that are determined by transmission via a synaptic population. In direct responses, from a certain critical stimulation frequency on (>4 Hz), the long-term output rate saturates and remains relatively constant independent of the input frequency, reflecting neuronal excitability processes (Figs. 2 and 3b). In synaptic mediated responses, in contrast, the synaptic envelope imposes a bottleneck to long-term input, being characterized by an "optimal" input frequency that maximizes output rate (Fig. 3a, b). That means that the underlying neuronal membrane can only be activated by a certain synaptically determined frequency band (<4 Hz). Further, the neuronal activation rates observed when obtaining long-memory and complex statistics in neuronal output (e.g., power spectral density in Fig. 3c), when the neuron is activated via its synaptic envelope (over periods of minutes), may be as low as 2 Hz. Such low stimulation rates evoke 1:1 responsiveness in directly stimulated neurons and thereby are unlikely to give rise to long-term threshold fluctuations in the underlying membrane excitability of synaptically activated neurons.

Therefore, within the range of physiological activation frequencies, long-memory processes in neuronal response spike time series are significantly impacted by synaptic dynamics. This conclusion is further supported by the following observation: spike amplitude, which indirectly reflects neuronal excitability (e.g., Henze and Buzsaki 2001; de Polavieja et al. 2005), correlates with latency in direct but not synaptic response fluctuations. Most importantly, it does not decrease with increasing stimulation frequencies (raising failure rates) in synaptically mediated spikes, while it does in directly evoked responses (Fig. 3b, d). Hence, while spike amplitudes fluctuate and decay with increasing stimulation frequency in direct responses, reflecting excitability dynamics, they are insensitive to input frequency in synaptic responses, as synaptic filtering prevents the excitability machinery to reach intermittent response modes. This suggests that failure rates, giving rise to complex response dynamics in single neuron firing, are not determined by membrane excitability but synaptic processes, when neurons are activated via a synaptic envelope.

The described synaptic dominance, however, can hold for the case of a single synaptic envelope, representing a single activation source of the neuron, assuming a relative stable reactivation of an identical synaptic population (Jia et al. 2010; Scholl et al. 2010; Chen et al. 2013). On the other hand, it is well possible that a neuron is activated via several input paths (representing different network states, or sensory
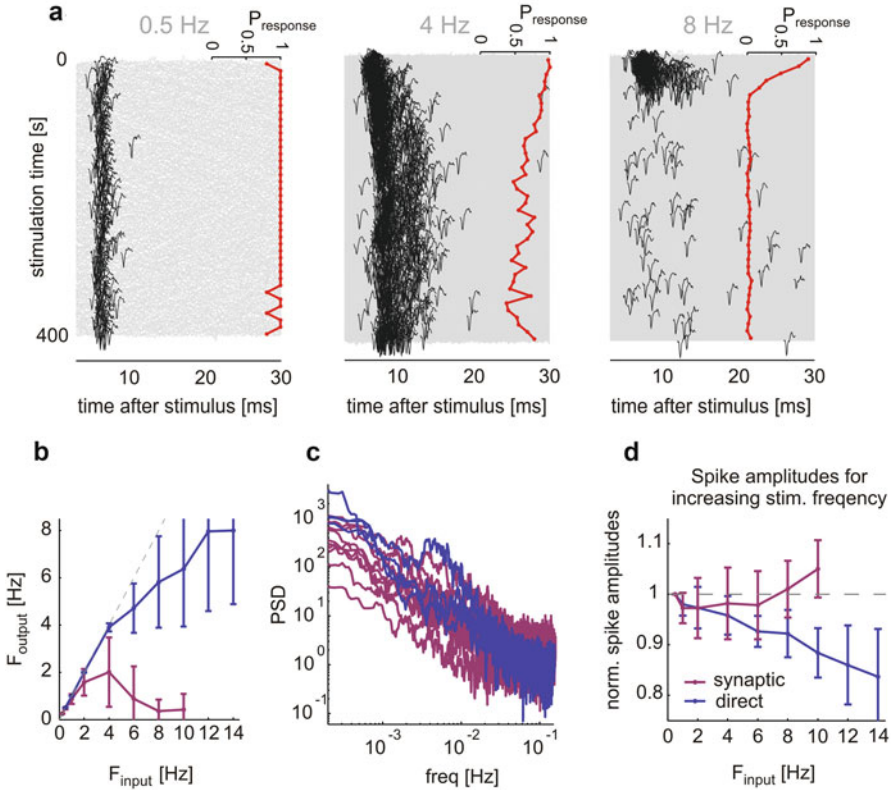
Fig. 3 Long-memory processes in neuronal response spike time series are determined by synaptic dynamics. (**a**) Response transients at different stimulation frequencies in a synaptically stimulated neuron. All response traces within a 400 s stimulation session are plotted (gray), first spikes (black) indicated by using identical voltage scales. Binned response probabilities (bin size = 10 s), are plotted at right side of each panel. At 4 Hz, the neuron exhibits rich firing dynamics in contrast to almost steady rates at higher and lower frequencies. (**b**) Mean and SD of the Input-Output curves display the response rate of the neuron. (calculated over the last 200 s of each stimulation epoch), plotted as a function of the stimulation rate. Direct responses only reach sporadic firing modes at input rates above 4 Hz, significantly higher frequencies than synaptic response output rate. (**c**) Long-term response rate and latency dynamics in direct and synaptic responses. Firing rate periodogram, comparing synaptic (magenta) to direct (blue) response fluctuation statistics plotted on a log-log scale. (**d**) In contrast to synaptic, the directly mediated spike amplitudes decrease significantly with increasing stimulation frequencies. Means and SDs of spike amplitudes belonging to the same neurons, shown in (**b**) and therefore contain different counts of data points for each stimulation frequency. Figure and caption reproduced from Reinartz et al. (2014) under the terms of the Creative Commons Attribution License (CC BY)

pathways for instance), allowing for higher activation rates of the membrane. In such a scenario, temporal complexity can be generated in each synaptic envelope, as well as in the intrinsic membrane excitability of the neurons involved.

6 Concluding Remarks

Neuronal activity dynamics are characterized by long-term non-stationarities and correlations across behaviorally relevant timescales. This chapter creates an overview of the ubiquity of these processes throughout brain-behavior organization and focuses on the scientific contributions offered by employing cultured cortical networks. Prolonged electrical stimulation of cultured networks allowed to overcome limitations in the understanding of neuronal response dynamics existing so far, by stably accessing single neuron and network responses over extended timescales, omitting higher level influences. The emerging long-memory processes in single neuron and network activity in this reduced experimental setting, allowed to discuss possible mechanisms underlying dynamics in excitable systems and physical approximations like SOC. Studying long-term filtering properties of the synaptic envelope, a synaptic population activating a neuron in response to a given stimulus, allowed to observe single neuron response dynamics under more physiological conditions. While membrane excitability dynamics as a possible mechanism underlying long-term neuronal response dynamics could not be excluded, possible transformations to the neuronal input statistics could be described, that is, the transmission variability of a synaptic population over repeated activation of a constant stimulus, an additional process contributing to complex response statistics.

References

Abeles, M. (1991). *Corticonics: Neural circuits of cerebral cortex*. Cambridge: Cambridge University Press.

Aertsen, A. M., & Johannesma, P. I. (1981). A comparison of the spectro-temporal sensitivity of auditory neurons to tonal and natural stimuli. *Biological Cybernetics, 42*, 145–156.

Arieli, A., Sterkin, A., Grinvald, A., & Aertsen, A. (1996). Dynamics of ongoing activity: Explanation of the large variability in evoked cortical responses. *Science, 273*, 1868–1871.

Azouz, R., & Gray, C. M. (1999). Cellular mechanism contributing to response variability of cortical neurons in vivo. *The Journal of Neuroscience, 19*, 2209–2223.

Baillie, R. T. (1996). Long memory processes and fractional integration in econometrics. *Journal of Econometrics, 73*, 5–59.

Bak, P. (1997). *How nature works*. Oxford: Oxford University Press.

Bakkum, D. J., Chao, Z. C., & Potter, S. M. (2008). Long-term activity-dependent plasticity of action potential propagation delay and amplitude in cortical networks. *PLoS One, 3*, e2088.

Beggs, J. M., & Plenz, D. (2003). Neuronal avalanches in neocortical circuits. *The Journal of Neuroscience, 23*, 11167–11177.

Beran, J. (1994). *Statistics for long-memory processes*. New York: Chapman & Hall/CRC.

Berdondini, L., van der Wal, P. D., Guenat, O., de Rooij, N. F., Koudelka-Hep, M., Seitz, P., et al. (2005). High-density electrode array for imaging in vitro electrophysiological activity. *Biosensors and Bioelectronics, 21*, 167–174.

Bonifazi, P., Ruaro, M. E., & Torre, V. (2005). Statistical properties of information processing in neuronal networks. *The European Journal of Neuroscience, 22*, 2953–2964.

Braun, A., Urai, A. E., & Donner, T. H. (2018). Adaptive history biases result from confidence-weighted accumulation of past choices. *The Journal of Neuroscience, 38*, 2418–2429.

Brenner, N., Bialek, W., & de Ruyter van Steveninck, R. R. (2000). Adaptive rescaling maximizes information transmission. *Neuron, 26*, 695–702.

Canepari, M., Bove, M., Maeda, E., Cappello, M., & Kawana, A. (1997). Experimental analysis of neuronal dynamics in cultured cortical networks and transitions between different patterns of activity. *Biological Cybernetics, 77*, 153–162.

Chen, X., Rochefort, N. L., Sakmann, B., & Konnerth, A. (2013). Reactivation of the same synapses during spontaneous up states and sensory stimuli. *Cell Reports, 4*, 31–39.

Chialvo, D. (2010). Emergent complex neural dynamics. *Nature Physics, 6*(10), 744–750.

Chiappalone, M., Bove, M., Vato, A., Tedesco, M., & Martinoia, S. (2006). Dissociated cortical networks show spontaneously correlated activity patterns during in vitro development. *Brain Research, 1093*, 41–53.

Chiappalone, M., Vato, A., Berdondini, L., Koudelka-Hep, M., & Martinoia, S. (2007). Network dynamics and synchronous activity in cultured cortical neurons. *International Journal of Neural Systems, 17*, 87–103.

Churchland, M. M., Yu, B. M., Cunningham, J. P., Sugrue, L. P., Cohen, M. R., Corrado, G. S., et al. (2010). Stimulus onset quenches neural variability: A widespread cortical phenomenon. *Nature Neuroscience, 13*, 369–378.

de Polavieja, G. G., Harsch, A., Kleppe, I., Robinson, H. P. C., & Juusola, M. (2005). Stimulus history reliably shapes action potential waveforms of cortical neurons. *The Journal of Neuroscience, 25*, 5657–5665.

Destexhe, A., Contreras, D., & Steriade, M. (1999). Spatiotemporal analysis of local field potentials and unit discharges in cat cerebral cortex during natural wake and sleep states. *The Journal of Neuroscience, 19*, 4595–4608.

El Hady, A., Afshar, G., Bröking, K., Schlüter, O. M., Geisel, T., Stühmer, W., et al. (2013). Optogenetic stimulation effectively enhances intrinsically generated network synchrony. *Front Neural Circuits, 7*, 167.

Ellerkmann, R. K., Riazanski, V., Elger, C. E., Urban, B. W., & Beck, H. (2001). Slow recovery from inactivation regulates the availability of voltage-dependent sodium channels in hippocampal granule cells, hilar neurons and basket cells. *The Journal of Physiology, 532*, 385–397.

Esposti, F., Signorini, M. G., Potter, S. M., & Cerutti, S. (2009). Statistical long-term correlations in dissociated cortical neuron recordings. *IEEE Transactions on Neural Systems and Rehabilitation Engineering, 17*, 364–369.

Eytan, D., & Marom, S. (2006). Dynamics and effective topology underlying synchronization in networks of cortical neurons. *The Journal of Neuroscience, 26*, 8465–8476.

Faisal, A. A., Selen, L. P. J., & Wolpert, D. M. (2008). Noise in the nervous system. *Nature Reviews. Neuroscience, 9*, 292–303.

Fortune, E. S., & Rose, G. J. (2001). Short-term synaptic plasticity as a temporal filter. *Trends in Neurosciences, 24*, 381–385.

Frey, U., Sedivy, J., Heer, F., Pedron, R., Ballini, M., Mueller, J., et al. (2010). Switch-matrix-based high-density microelectrode array in CMOS technology. *IEEE Journal of Solid-State Circuits, 45*, 467–482.

Fritsche, M., Mostert, P., & de Lange, F. P. (2017). Opposite effects of recent history on perception and decision. *Current Biology, 27*(4), 590–595.

Fründ, I., Wichmann, F. A., & Macke, J. H. (2014). Quantifying the effect of intertrial dependence on perceptual decisions. *Journal of Vision, 14*(7), 9.

Gal, A., Eytan, D., Wallach, A., Sandler, M., Schiller, J., & Marom, S. (2010). Dynamics of excitability over extended timescales in cultured cortical neurons. *The Journal of Neuroscience, 30*, 16332–16342.

Gal, A., & Marom, S. (2013a). Self-organized criticality in single-neuron excitability. *Physical Review E, 88*, 062717.

Gal, A., & Marom, S. (2013b). Entrainment of the intrinsic dynamics of single isolated neurons by natural-like input. *The Journal of Neuroscience, 33*(18), 7912–7918.

Garcia-Lazaro, J. A., Ahmed, B., & Schnupp, J. W. (2006). Tuning to natural stimulus dynamics in primary auditory cortex. *Current Biology, 16*, 264–271.

Gilboa, G., Chen, R., & Brenner, N. (2005). History-dependent multiple-timescale dynamics in a single-neuron model. *The Journal of Neuroscience, 25*, 6479–6489.

Gilden, D. (2001). Cognitive emissions of 1/f noise. *Psychological Review, 108*(1), 33–56.

Gilden, D., Thornton, T., & Mallon, M. (1995). 1/f noise in human cognition. *Science, 267*(5205), 1837.

Golshani, P., Gonçalves, J. T., Khoshkhoo, S., Mostany, R., Smirnakis, S., & Portera-Cailliau, C. (2009). Internally mediated developmental desynchronization of neocortical network activity. *The Journal of Neuroscience, 29*, 10890–10899.

Gustafsson, B., & Jankowska, E. (1976). Direct and indirect activation of nerve cells by electrical pulses applied extracellularly. *The Journal of Physiology, 258*(1), 33–61.

Haroush, N., & Marom, S. (2015). Slow dynamics in features of synchronized neural network responses. *Frontiers in Computational Neuroscience, 9*, 40.

Harris, K. D., & Thiele, A. (2011). Cortical state and attention. *Nature Reviews. Neuroscience, 12*, 509–523.

Harsch, A., & Robinson, H. P. (2000). Postsynaptic variability of firing in rat cortical neurons: The roles of input synchronization and synaptic nmda receptor conductance. *The Journal of Neuroscience, 20*, 6181–6192.

Henze, D. A., & Buzsaki, G. (2001). Action potential threshold of hippocampal pyramidal cells in vivo is increased by recent spiking activity. *Neuroscience, 105*, 121–130.

Hodgkin, A., & Huxley, A. (1952). A quantitative description of membrane current and its application to conduction and excitation in nerve. *The Journal of Physiology, 117*, 500–544.

Huettner, J. E., & Baughman, R. W. (1986). Primary culture of identified neurons from the visual cortex of postnatal rats. *The Journal of Neuroscience, 6*(10), 3044–3060.

Jensen, H. J. (1998). *Self-organized criticality*. Cambridge: Cambridge University Press.

Jia, A., Rochefort, N. L., Chen, X., & Konnerth, A. (2010). Dendritic organization of sensory input to cortical neurons in vivo. *Nature, 464*, 1307–1312.

Jimbo, Y., Kawana, A., Parodi, P., & Torre, V. (2000). The dynamics of a neuronal culture of dissociated cortical neurons of neonatal rats. *Biological Cybernetics, 83*, 1–20.

Kamioka, H., Maeda, E., Jimbo, Y., Robinson, H. P., & Kawana, A. (1996). Spontaneous periodic synchronized bursting during formation of mature patterns of connections in cortical cultures. *Neuroscience Letters, 206*, 109–112.

Katz, L. C., & Shatz, C. J. (1996). Synaptic activity and the construction of cortical circuits. *Science, 274*, 1133–1138.

Kaufman, M., Corner, M. A., & Ziv, N. E. (2012). Long-term relationships between cholinergic tone, synchronous bursting and synaptic remodeling. *PLoS ONE, 7*, e40980.

Kaufman, M., Reinartz, S., & Ziv, N. E. (2014). Adaptation to prolonged neuromodulation in cortical cultures: An invariable return to network synchrony. *BMC Biology, 12*, 83.

Kayser, C., Logothetis, N. K., & Panzeri, S. (2010). Millisecond encoding precision of auditory cortex neurons. *Proceedings of the National Academy of Sciences of the United States of America, 107*, 16976–16981.

Keren, H., & Marom, S. (2014). Controlling neural network responsiveness: Tradeoffs and constraints. *Frontiers Neuroengineering, 7*, 11.

Kriegstein, A. R., & Dichter, M. A. (1983). Morphological classification of rat cortical neurons in cell culture. *The Journal of Neuroscience, 3*, 1634–1647.

Laughlin, S. B. (1981). A simple coding procedure enhances a neuron's information capacity. *Zeitschrift für Naturforschung, 36*, 910–912.

Levina, A., Herrmann, J. M., & Geisel, T. (2007). Dynamical synapses causing self-organized criticality in neural networks. *Nature Physics, 3*(12), 857–860.

Liebovitch, L. S., Fischbarg, J., Koniarek, J. P., Todorova, I., & Wang, M. (1987). Fractal model of ion-channel kinetics. *Biochimica et Biophysica Acta, 896*, 173–180.

Lowen, S., Liebovitch, L., & White, J. (1999). Fractal ion-channel behavior generates fractal firing patterns in neuronal models. *Physical Review E, 59*, 5970–5980.

Lowen, S. B., Cash, S. S., Poo, M., & Teich, M. C. (1997). Quantal neurotransmitter secretion rate exhibits fractal behavior. *The Journal of Neuroscience, 17*, 5666–5677.

Lowen, S. B., & Teich, M. C. (1996). The periodogram and allan variance reveal fractal exponents greater than unity in auditory-nerve spike trains. *The Journal of the Acoustical Society of America, 99*, 3585–3591.

Mainen, Z. F., & Sejnowski, T. J. (1995). Reliability of spike timing in neocortical neurons. *Science, 268*, 1503–1506.

Markram, H., Gupta, A., Uziel, A., Wang, Y., & Tsodyks, M. (1998). Information processing with frequency-dependent synaptic connections. *Neurobiology of Learning and Memory, 70*(1-2), 101–112.

Marom, S. (2009). Adaptive transition rates in excitable membranes. *Frontiers in Computational Neuroscience, 3*, 2.

Marom, S. (2010). Neural timescales or lack thereof. *Progress in Neurobiology, 90*, 16–28.

Marom, S., & Shahaf, G. (2002). Development, learning and memory in large random networks of cortical neurons: Lessons beyond anatomy. *Quarterly Reviews of Biophysics, 35*, 63–87.

Marom, S., & Wallach, A. (2011). Relational dynamics in perception: Impacts on trial-to-trial variation. *Frontiers in Computational Neuroscience, 5*, 16.

Masquelier, T. (2013). Neural variability, or lack thereof. *Frontiers in Computational Neuroscience, 7*, 7.

Mazzoni, A., Broccard, F. D., Garcia-Perez, E., Bonifazi, P., Ruaro, M. E., & Torre, V. (2007). On the dynamics of the spontaneous activity in neuronal networks. *PLoS One, 2*, e439.

Milotti, E. (2002). 1/f noise: A pedagogical review. Arxiv: Physics 0204033v1.

Minerbi, A., Kahana, R., Goldfeld, L., Kaufman, M., Marom, S., & Ziv, N. E. (2009). Long-term relationships between synaptic tenacity, synaptic remodeling, and network activity. *PLoS Biology, 7*, e1000136.

Montévil, M., Mossio, M., Pocheville, A., & Longo, G. (2016). Theoretical principles for biology: Variation. *Progress in Biophysics and Molecular Biology, 122*(1), 36–50.

Monto, S., Palva, S., Voipio, J., & Palva, J. (2008). Very slow EEG fluctuations predict the dynamics of stimulus detection and oscillation amplitudes in humans. *The Journal of Neuroscience, 28*(33), 8268.

Muramoto, K., Ichikawa, M., Kawahara, M., Kobayashi, K., & Kuroda, Y. (1993). Frequency of synchronous oscillations of neuronal activity increases during development and is correlated to the number of synapses in cultured cortical neuron networks. *Neuroscience Letters, 163*(2), 163–165.

Neale, E. A., Oertel, W. H., Bowers, L. M., & Weise, V. K. (1983). Glutamate decarboxylase immunoreactivity and gamma-[3H] aminobutyric acid accumulation within the same neurons in dissociated cell cultures of cerebral cortex. *The Journal of Neuroscience, 3*(2), 376–382.

Newman, J. P., Fong, M. F., Millard, D. C., Whitmire, C. J., Stanley, G. B., & Potter, S. M. (2015). Optogenetic feedback control of neural activity. *eLife, 4*, e07192.

Nir, Y., Fisch, L., Mukamel, R., Gelbard-Sagiv, H., Arieli, A., Fried, I., et al. (2007). Coupling between neuronal firing rate, gamma LFP, and BOLD fMRI is related to interneuronal correlations. *Current Biology, 17*(15), 1275–1285.

Okujeni, S., Kandler, S., & Egert, U. (2017). Mesoscale architecture shapes initiation and richness of spontaneous network activity. *The Journal of Neuroscience, 37*, 3972–3987.

Panzeri, S., & Diamond, M. E. (2010). Information carried by population spike times in the whisker sensory cortex can be decoded without knowledge of stimulus time. *Front Synaptic Neuroscience, 2*, 17.

Pasquale, V., Massobrio, P., Bologna, L. L., Chiappalone, M., & Martinoia, S. (2008). Self-organization and neuronal avalanches in networks of dissociated cortical neurons. *Neuroscience, 153*, 1354–1369.

Plenz, D., & Niebur, E. (Eds.). (2014). *Criticality in neural systems*. New York: Wiley.

Plenz, D., & Thiagarajan, T. (2007). The organizing principles of neuronal avalanches: Cell assemblies in the cortex. *Trends in Neurosciences, 30*, 101–110.

Potter, S. M., & Demarse, T. B. (2001). A new approach to neural cell culture for long-term studies. *Journal of Neuroscience Methods, 110*, 17–24.

Pulizzi, R., Musumeci, G., Van den Haute, C., Van De Vijver, S., Baekelandt, V., & Giugliano, M. (2016). Brief wide-field photostimuli evoke and modulate oscillatory reverberating activity in cortical networks. *Scientific Reports, 6*, e24701.

Reinartz, S., Biro, I., Gal, A., Giugliano, M., & Marom, S. (2014). Synaptic dynamics contribute to long-term single neuron response fluctuations. *Front Neural Circuits, 8*, 71.

Robinson, H. P., Kawahara, M., Jimbo, Y., Torimitsu, K., Kuroda, Y., & Kawana, A. (1993). Periodic synchronized bursting and intracellular calcium transients elicited by low magnesium in cultured cortical neurons. *Journal of Neurophysiology, 70*, 1606–1616.

Rose, D., & Lowe, I. (1982). Dynamics of adaptation to contrast. *Perception, 11*(5), 505–528.

Sachidhanandam, S., Sreenivasan, V., Kyriakatos, A., Kremer, Y., & Petersen, C. C. H. (2013). Membrane potential correlates of sensory perception in mouse barrel cortex. *Nature Neuroscience, 16*, 1671–1677.

Scarsi, F., Tessadori, J., Chiappalone, M., & Pasquale, V. (2017). Investigating the impact of electrical stimulation temporal distribution on cortical network responses. *BMC Neuroscience, 18*, 49.

Schneidman, E., Freedman, B., & Segev, I. (1998). Ion channel stochasticity may be critical in determining the reliability and precision of spike timing. *Neural Computation, 10*, 1679–1703.

Scholl, B., Gao, X., & Wehr, M. (2010). Nonoverlapping sets of synapses drive on responses and off responses in auditory cortex. *Neuron, 65*(3), 412–421.

Segev, R., Benveniste, M., Hulata, E., Cohen, N., Palevski, A., Kapon, E., et al. (2002). Long term behavior of lithographically prepared in vitro neuronal networks. *Physical Review Letters, 88*, 118102.

Segev, R., Benveniste, M., Shapira, Y., & Ben-Jacob, E. (2003). Formation of electrically active clusterized neural networks. *Physical Review Letters, 90*, 168101.

Simoncelli, E. P. (2003). Vision and the statistics of the visual environment. *Current Opinion in Neurobiology, 13*, 144–149.

Soriano, J., Rodríguez Martínez, M., Tlusty, T., & Moses, E. (2008). Development of input connections in neural cultures. *Proceedings of the National Academy of Sciences of the United States of America, 105*, 13758–13763.

Steriade, M., Nuñez, A., & Amzica, F. (1993). Intracellular analysis of relations between the slow (<1 Hz) neocortical oscillation and other sleep rhythms of the electroencephalogram. *The Journal of Neuroscience, 13*, 3266–3283.

Tehovnik, E. J., Tolias, A. S., Sultan, F., Slocum, W. M., & Logothetis, N. K. (2006). Direct and indirect activation of cortical neurons by electrical microstimulation. *Journal of Neurophysiology, 96*(2), 512–521.

Teich, M. (1989). Fractal character of the auditory neural spike train. *IEEE Transactions on Biomedical Engineering, 36*(1), 150–160.

Tetzlaff, C., Okujeni, S., Egert, U., Worgotter, F., & Butz, M. (2010). Self-organized criticality in developing neuronal networks. *PLoS Computational Biology, 6*, e1001013.

Thomson, A. M. (1997). Activity-dependent properties of synaptic transmission at two classes of connections made by rat neocortical pyramidal axons in vitro. *The Journal of Physiology, 502*(Pt 1), 131–147.

Tiesinga, P., Fellous, J. M., & Sejnowski, T. J. (2008). Regulation of spike timing in visual cortical circuits. *Nature Reviews. Neuroscience, 9*, 97–107.

Toib, A., Lyakhov, V., & Marom, S. (1998). Interaction between duration of activity and time course of recovery from slow inactivation in mammalian brain Na channels. *The Journal of Neuroscience, 18*, 1893–1903.

Turrigiano, G. G. (2008). The self-tuning neuron: Synaptic scaling of excitatory synapses. *Cell, 135*(3), 422–435.

van Huizen, F., Romijn, H. J., & Habets, A. M. (1985). Synaptogenesis in rat cerebral cortex cultures is affected during chronic blockade of spontaneous bioelectric activity by tetrodotoxin. *Brain Research, 351*(1), 67–80.

van Pelt, J., Vajda, I., Wolters, P. S., Corner, M. A., & Ramakers, G. J. A. (2005). Dynamics and plasticity in developing neural networks in vitro. *Progress in Brain Research, 147*, 171–188.

van Pelt, J., Wolters, P. S., Corner, M. A., Rutten, W. L., & Ramakers, G. J. (2004). Long-term characterization of firing dynamics of spontaneous bursts in cultured neural networks. *IEEE Transactions on Biomedical Engineering, 51*, 2051–2062.

Volgushev, M., Chauvette, S., Mukovski, M., & Timofeev, I. (2006). Precise long-range synchronization of activity and silence in neocortical neurons during slow-wave oscillations. *The Journal of Neuroscience, 26*, 5665–5672.

Wagenaar, D. A., Pine, J., & Potter, S. M. (2004). Effective parameters for stimulation of dissociated cultures using multi-electrode arrays. *Journal of Neuroscience Methods, 138*, 27–37.

Wagenaar, D. A., Pine, J., & Potter, S. M. (2006). An extremely rich repertoire of bursting patterns during the development of cortical cultures. *BMC Neuroscience, 7*, 11.

Wallach, A. (2013). The response clamp: Functional characterization of neural systems using closed-loop control. *Frontiers in Neural Circuits, 7*, 5.

Wallach, A., Eytan, D., Gal, A., Zrenner, C., & Marom, S. (2011). Neuronal response clamp. *Front Neuroeng, 4*, 3.

Wallach, A., & Marom, S. (2012). Interactions between network synchrony and the dynamics of neuronal threshold. *Journal of Neurophysiology, 107*, 2926–2936.

Weihberger, O., Okujeni, S., Mikkonen, J. E., & Egert, U. (2013). Quantitative examination of stimulus-response relations in cortical networks in vitro. *Journal of Neurophysiology, 109*, 1764–1774.

Werthheimer, M. (1953). An investigation of the randomness of threshold measurements. *Journal of Experimental Psychology, 45*, 294–303.

Yu, Y., Romero, R., & Lee, T. S. (2005). Preference of sensory neural coding for 1/f signals. *Physical Review Letters, 94*, 108103.

Closed-Loop Systems and In Vitro Neuronal Cultures: Overview and Applications

Marta Bisio, Alexey Pimashkin, Stefano Buccelli, Jacopo Tessadori, Marianna Semprini, Timothée Levi, Ilaria Colombi, Arseniy Gladkov, Irina Mukhina, Alberto Averna, Victor Kazantsev, Valentina Pasquale, and Michela Chiappalone

Abstract One of the main limitations preventing the realization of a successful dialogue between the brain and a putative enabling device is the intricacy of brain signals. In this perspective, closed-loop in vitro systems can be used to investigate the interactions between a network of neurons and an external system,

M. Bisio
Department of Neurosciences, University of Padova, Padova, Italy

A. Pimashkin · V. Kazantsev
Department of Neurotechnologies, Lobachevsky State University of Nizhni Novgorod, Nizhnij Novgorod, Russia

S. Buccelli · I. Colombi · M. Chiappalone (✉)
Rehab Technologies IIT-INAIL Lab, Istituto Italiano di Tecnologia, Genova, Italy

Department of Neuroscience and Brain Technologies, Istituto Italiano di Tecnologia, Genova, Italy
e-mail: michela.chiappalone@iit.it

J. Tessadori
Department of Advanced Robotics, Istituto Italiano di Tecnologia, Genova, Italy

M. Semprini · A. Averna
Rehab Technologies IIT-INAIL Lab, Istituto Italiano di Tecnologia, Genova, Italy

T. Levi
Institute of Industrial Science, IIS, The University of Tokyo, Tokyo, Japan

IMS Lab, University of Bordeaux, Talence, France

A. Gladkov · I. Mukhina
Department of Neurotechnologies, Lobachevsky State University of Nizhni Novgorod, Nizhnij Novgorod, Russia

Central Research Laboratory, Privolzhsky Research Medical University, Nizhnij Novgorod, Russia

V. Pasquale
Department of Neuroscience and Brain Technologies, Istituto Italiano di Tecnologia, Genova, Italy

such as an interacting environment or an artificial device. In this chapter, we provide an overview of closed-loop in vitro systems, which have been developed for investigating potential neuroprosthetic applications. In particular, we first explore how to modify or set a target dynamical behavior in a network of neurons. We then analyze the behavior of in vitro systems connected to artificial devices, such as robots. Finally, we provide an overview of biological neuronal networks interacting with artificial neuronal networks, a configuration currently offering a promising solution for clinical applications.

Keywords Neuroprosthetics · Neurorobotics · Neurodynamics · Neuromorphic engineering · Stimulation

1 Introduction

Brain disorders and their disabling effects on patients represent one of the biggest public health challenges for the twenty-first century (Gustavsson et al. 2011). Over the years, the global health impact of neurological disorders had been underestimated (Murray 1996) despite the extension of life expectancy and the suffering caused by diseases (Sartorius and Henderson 1992; Gwatkin et al. 1999). Indeed, several neurological disorders may be nonfatal but still cause severe disability at the level of the neural pathways, muscle control, or the muscles themselves, thus making patients still experiencing the world around them but losing any ability to interact with it. Unfortunately, only a minority of disabled patients can achieve independence in simple daily living activities; thus the impossibility to reach a complete recovery leads to the necessity of developing innovative technologies integrating multidisciplinary approaches.

Humans have long been fascinated by the possibility of interfacing and controlling artificial devices with biological signals, and nowadays the combination of brains and machines is becoming a reality for treating diseases or even enhancing humans' capabilities (Panuccio et al. 2018; Silva 2018).

In the last decades, several scientific and technological efforts have been made to develop hybrid systems that link, via neural interfaces, the human nervous system with electronic and/or robotic prostheses for restoring motor and sensory functions in patients with spinal cord injuries, brain injuries, or degenerative diseases (Wolpaw et al. 2002; Navarro et al. 2005; Daly and Wolpaw 2008; Mak and Wolpaw 2009). In particular, brain-machine interfaces (BMIs) and neuroprostheses constitute a fascinating approach whose adoption has demonstrated to allow non-self-sufficient patients to interact with the surrounding environment (Millan et al. 2010; Hochberg et al. 2012; Moxon and Foffani 2015; Downey et al. 2016; Schwartz 2016; Zeng et al. 2017).

However, modern neural interfaces are mainly devoted to restoring lost motor functions acting only in one direction, i.e., from the brain to the body (Abdulkader et al. 2015) or from the body to the brain (Flesher et al. 2016), so the great challenge is represented by the implementation of complex and specific neural interfaces

for guarantying a bidirectional communication (i.e., closed-loop). Although these technological advancements have proven to be effective in enhancing patients' life quality, it is important to highlight that this approach is associated with some degree of invasiveness, making it difficult for the system to be tested and validated (Morgante et al. 2007). Furthermore, the development of these inherent complex and low controllable systems needs to overcome issues related to replicability of in vivo models and experiments.

In the future, sensory, motor, and modulatory BMIs are likely to take advantage of a continuous dialogue between the nervous system and artificial computational devices. However, bridging the large chasm between the present and the future neural interfaces will certainly require much basic research using reduced preparations, as pointed out by S. Potter (Potter 2010). Indeed, simple experimental preparations such as in vitro neuronal cultures can be easily controlled and manipulated, reducing the experimental variability and thus facilitating the interpretation of results. Furthermore, hybrid systems based on in vitro cultures constantly dialoguing with an external agent are particularly desirable for investigating basic electrophysiological properties and plastic changes induced in a neuronal network. This "closed-loop" experimental framework can provide the experimenter with the possibility to test interesting scientific questions related to coding and decoding of information while the neuronal network is constantly subjected to different type of environmental/artificial stimuli.

In this chapter we will present an overview of the closed-loop hybrid systems composed of in vitro neuronal cultures coupled to microelectrode arrays (MEAs) interfaced with external agents (e.g., small robots, processors, neuromorphic systems), and we will discuss the perspectives related to the use of such an experimental approach for the development of next-generation BMIs and neuroprostheses to be adopted in the clinical practice.

2 An Historical Overview on Closed-Loop Neural Interfaces

In order to interact with the nervous system, it is necessary to develop a bidirectional communication, channel able to extract and inject information in both directions. To extract information from the nervous system, several decoding techniques can be used, depending on the specific application (Panzeri et al. 2014; Rey et al. 2015; Zeng et al. 2017). The first pioneering application of decoding techniques for brain interfacing dates back to 1999, when Chapin and colleagues (Chapin et al. 1999) showed that rats could move a robotic arm by modulating the activity of their motor cortical neurons. These innovative experiments suggested the possibility of creating a new generation of neural interfaces based on the decoding of brain signals in order to operate an end effector.

On the other hand, in order to inject information into the nervous system, it is necessary to modulate its activity and this is typically accomplished with electrical stimulation. The use of electrical stimulation of the nervous tissue began with the Italian physician and scientist Luigi Galvani (Galvani and Aldini 1792),

when he discovered that nerves and muscles are electrically excitable (Grahn et al. 2014). In more recent years, intraspinal stimulation has been extensively used to study the effects of electrical stimulation on the central nervous system (Renshaw 1946; Jankowska and Roberts 1972a, b; Gustafsson and Jankowska 1976) and, in particular, to investigate restoration of motor functions in spinalized and anesthetized rodents (van den Brand et al. 2012) and cats (Mushahwar et al. 2002; Bamford et al. 2005; Pikov et al. 2007; Yakovenko et al. 2007; Holinski et al. 2011; Kasten et al. 2013; Sunshine et al. 2013; Grahn et al. 2014). In the last decades, electrical stimulation was adopted for the development of neuroprostheses. Indeed, neuroprosthetic systems are devices interfacing with the CNS and supplementing or substituting specific functionalities in a subject's body (Wright et al. 2016), and they often rely on electrical stimulation for enhancing functional responses (Ethier et al. 2012; Nishimura et al. 2013; Bouton et al. 2016; Ajiboye et al. 2017). In 2006 the group of Fetz (Jackson et al. 2006) showed that cortical reorganization can be induced by activity-dependent plasticity achieved by implementing a causal relationship between presynaptic and postsynaptic activities. Some years later, the group led by Nudo (Guggenmos et al. 2013) applied these findings to the treatment of stroke and demonstrated the very first example of a neural bridge aimed at promoting functional re-connection between two cortical areas (i.e., the premotor cortex and the somatosensory cortex) in a rat model of traumatic brain injury (TBI). The artificial bridge was based on an activity-dependent stimulation protocol implemented through a custom, wireless chip interconnecting the two far away cortical areas via closed-loop interaction.

Neuroprosthetic systems can be implemented with different configurations [for a review see (Greenwald et al. 2016)], depending on the modality used to interface the brain with the external device. The first distinction should be made between open-loop and closed-loop architectures, both involving the two systems—a device (D) and a brain or neural preparation (B)—characterized by their specific I/O functions (I_D/O_D for the device and I_B/O_B for the brain) (Panuccio et al. 2018). In open-loop systems (Fig. 1a), the output of the device (O_D) consists of a stimulus (e.g., electrical pulse) which is directly delivered to the brain ($I_B = O_D$). The brain processes the incoming information (I_B) and produces an output response (O_B). The input to the device (I_D) can be any function determining the features of the stimulation sequence; however, it is not modulated by any feedback from the brain. Closed-loop devices are based on feedback (Fig. 1b): the output of the brain (O_B), consisting in the ongoing brain activity or its processed version, serves as the input for the device ($I_D = O_B$), which triggers the device operation. The output of the device (O_D) is the input to the brain ($I_B = O_D$). This system generates an I/O loop, which continues indefinitely.

Many neuroprosthetic systems present an open-loop configuration (Moro et al. 1999; Molinuevo et al. 2000), which does not respond to unexpected internal or external perturbations (Blaha and Phillips 1996; Lee et al. 2006). Indeed, in open-loop neuroprosthetics, the system output has no effect upon the input to the nervous system (Vassileva et al. 2018), while in closed-loop configurations, the feedback signal can be used to both control and adjust the whole system behavior (Berenyi et al. 2012; Xu et al. 2014; Miao and Koomson 2018; Sisterson et al. 2019). Recently,
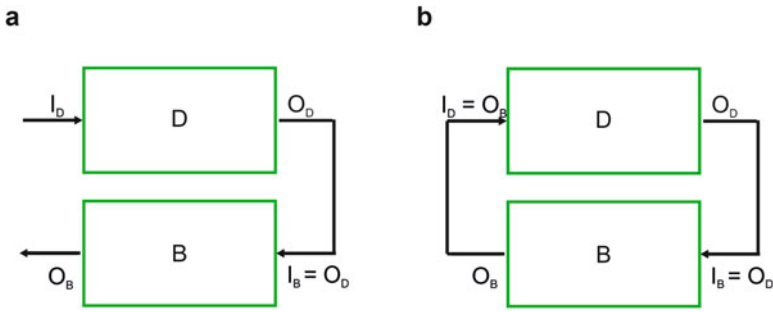
Fig. 1 Schematic representation of open- and closed-loop architectures. (**a**) Open-loop configuration: the output of the device (O_D) becomes the input of the biological counterpart (I_B). (**b**) Closed-loop configuration: the output of each block is the input for the other block. *B* biological counterpart, *D* artificial device, I_i input of block *i*, $O_i =$ output of block *i*. Modified from Panuccio et al. (2018)
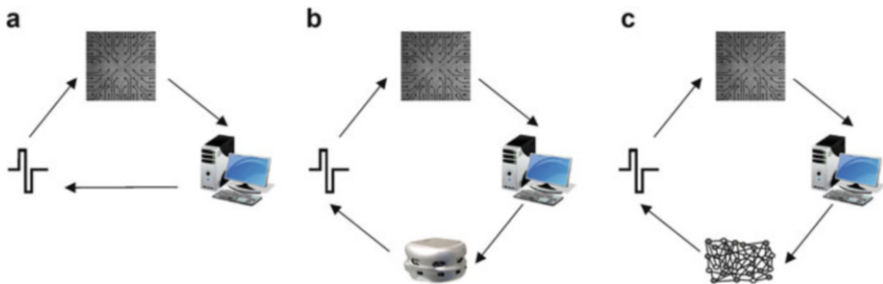

Fig. 2 Three different types of closed-loop paradigms. (**a**) Signals from an in vitro neuronal network (top) are recorded and processed by a signal processing unit (here represented by a personal computer but can also be a stand-alone device). The processing unit detects an event and triggers an electrical stimulus that closes the loop. (**b**) A neurorobotic closed-loop system. In this case the processing unit drives a robot that explores the surrounding environment, according to specific coding/decoding policies. (**c**) Closed-loop hybrid system for brain interaction and repair. This class of closed-loop systems involves the use of an artificial spiking neural network (SNN) in the loop aimed at substituting a part of an injured brain

closed-loop stimulation strategies have been successfully introduced also for deep brain stimulation (DBS) systems (Rosin et al. 2011; Little et al. 2013; Cagnan et al. 2017; Arlotti et al. 2018).

In the following paragraphs we have grouped the various modes of in vitro closed-loop systems into three categories. The first paragraph describes closed-loop systems aimed at controlling dynamics of in vitro neuronal networks (Fig. 2a) by means of activity-dependent stimulation protocols (*cf.* "Closed-loop control of neuronal network dynamics in vitro"). The second one describes the neurorobotic research field, involving the use of a robotic system interacting with a cell culture (Fig. 2b) (*cf.* "Neurorobotic systems: connecting neurons with robots"). The third

paragraph describes a novel class of experiments involving the use of an artificial neural network dialoguing with a cell culture (Fig. 2c) aimed at interacting and/or repairing the brain following an injury (*cf.* "Hybrid interaction and hybrid systems for brain repair").

3 Closed-Loop Control of Neuronal Network Dynamics In Vitro

During the last two decades, closed-loop technologies have been applied to control dynamics of in vitro neuronal networks, with the aim of understanding information processing, network-level adaptation, and learning. Indeed, feedback based on activity-dependent stimulation induced functional reorganization of the network.

3.1 Closed-Loop Implementation

During the last two decades, several open-source solutions were proposed to implement closed-loop architectures involving multichannel electrophysiological in vitro systems. Each solution showed its own balance between development cost, setup difficulty, and closed-loop timing, which limited the timescale of the dynamics of interest. One of the first systems, *MEABench*, was developed in the lab of Potter (Wagenaar et al. 2005a), which implemented the closed-loop for a commercial acquisition system, based on the Multichannel Systems (MCS, Reutlingen, Germany) data acquisition cards. Then, the same lab introduced *NeuroRighter*, a system for a broad range of closed-loop applications with online spike-sorting, data visualization, and optical stimulation (Rolston et al. 2009; Newman et al. 2013). One of the least expensive and easy to implement systems was recently presented in the literature and it was based on Windows platform and additional DAQ board (Hazan and Ziv 2017). Details of other developed systems can be found in several reviews (Siegle et al. 2015; Hazan and Ziv 2017). It should be noted that the previously described closed-loop architectures for in vitro applications often do not require a real-time feedback in millisecond timescale. Several experimental designs presented in the literature, such as learning protocols, response clamp, and closed-loop bursting control, can be implemented using a stimulation frequency lower than 1 Hz. Those systems can be replicated by using an entirely software-based architecture with a closed-loop duration 1 s timescale using Labview(R) and .NET libraries for the most commonly used commercial hardware from MCS (Reutlingen, Germany) MEA1060 system (Pimashkin et al. 2013) and Matlab for MEA2100 system.

3.2 Electrical Closed-Loop

The first implementation of a closed-loop system employing in vitro cultures was introduced by the group of Marom (Shahaf and Marom 2001; Marom and Shahaf 2002) to study learning mechanisms (Fig. 3a). Their closed-loop stimulation was designed with the purpose of driving network activity towards a specific state: electrical stimulation was used to provide a reinforcement signal whenever the network spontaneously displayed the desired behavior.

In particular, the closed-loop protocol consisted of low-frequency stimulation (0.3–1 Hz) with continuous monitoring of each stimulus response as number of evoked spikes appearing in a window of 50 ± 10 ms post-stimulus interval. Stimuli were applied to a pair of close electrodes (input) and recording was performed from a selected electrode (output). A response-to-stimulus ratio (R/S) for selected electrodes was defined as the number of spikes over ten preceding responses and it was used to characterize slow changes in synaptic pathways between stimulating and recording neurons (input-output). Initially, an electrode with relatively weak connectivity (R/S = 0.1) was selected, which had a potential for strengthening during learning process and reach the desired threshold R/S = 0.2. During the stimulation, when the response spontaneously reached the threshold, a reinforcement was introduced as a 5-min period of no stimulation (Fig. 3b). Then the cycle was repeated several times. Time interval to reach the R/S threshold in each cycle decreased over time indicating the learning (Fig. 3c). Low-frequency stimulation in conditions without the reinforcement (open-loop) did not induce the learning effect (Fig. 3c).

Changes in the response were observed only at selected electrodes, whereas such an effect was not found in other electrodes. Such learning in ex vivo conditions may be referred to instrumental conditioning as a learning through error avoidance by reward. The discussion of such learning paradigm in biology can be found in a review by Marom (Marom and Eytan 2005).

The results were replicated by several groups (Li et al. 2007; le Feber et al. 2010; Pimashkin et al. 2013; Sinapayen et al. 2017) and some constraints on the learning and its relations to spontaneous activity were defined. After the learning, the profiles of spontaneous bursts were changed and spiking synchrony increased (Li et al. 2007; Stegenga et al. 2009).

Importantly, synaptic plasticity effects, obtained by delivering a tetanic (i.e., high frequency) stimulation, were better revealed by patterns of activity in the whole network than by individual stimulus responses (Jimbo et al. 1998; Bonifazi et al. 2005; Chiappalone et al. 2008); for a comprehensive review on neuroplasticity in vitro, see also Massobrio et al. (2015). Le Feber et al. proposed that the neuronal network develops an overall "balance between connectivity and activity," which should be monitored in the whole network instead of just one connection (le Feber et al. 2007). Le Feber et al. then estimated a functional connectivity of the network before and after the learning with conditional firing probability (CFP) based on cross-correlation between all electrode pairs (le Feber et al. 2010).
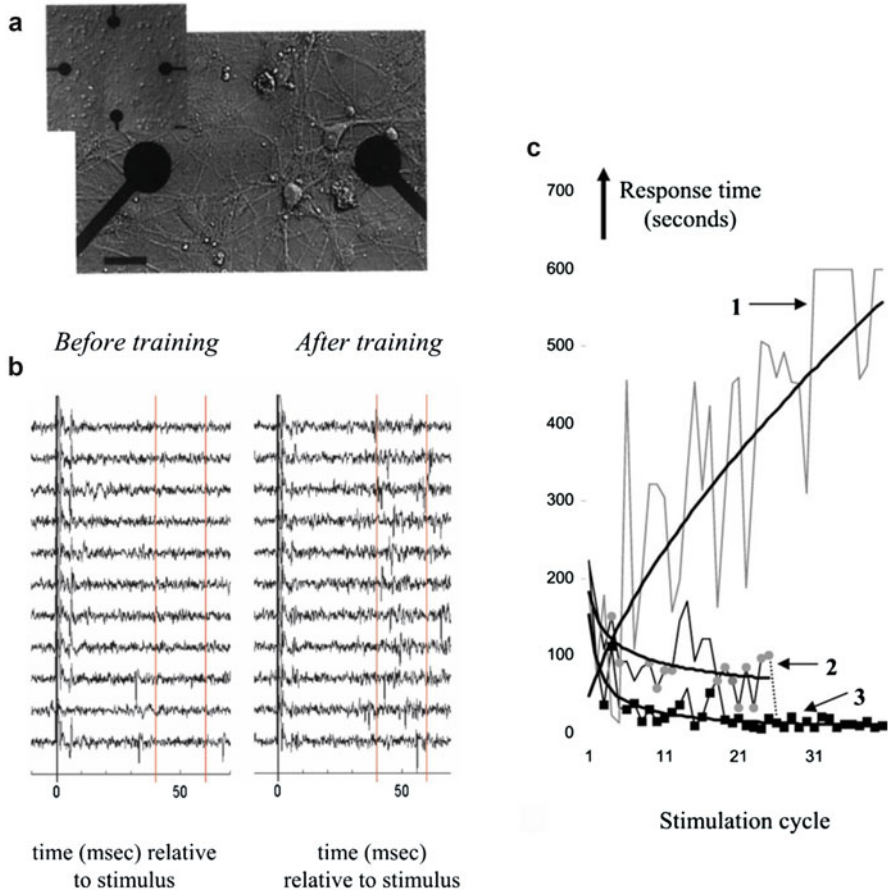
Fig. 3 Signals and learning curves in the experiment presented by the group of Marom. (**a**) Large random cortical networks cultured on substrate-embedded multielectrode arrays. Scale bar, 30 μm. (**b**) Example of learning in a cultured network of cortical neurons. Each trace within a panel shows recordings obtained 10 ms before the stimulus to 60 ms after the stimulus, before (left) and after (right) the training procedure. (**c**) Average control (curve 1), average response over all non-control trials (curve 2), and average learning curve (curve 3). Each point depicts the average time (in seconds) to accomplish the task in one cycle. Filled gray circles (in curve 2) and filled black squares (in curve 3) depict points that are significantly different from averaged control (curve 1; F test, $p < 0.05$). From Shahaf and Marom (2001)

Closed-loop stimulation induced significantly higher connectivity reorganization than the spontaneous changes in the whole network (Fig. 4). The learning protocol enhanced certain connections and reduced the others, while an average strength of all connections remained unchanged. Because activity patterns arise from certain connectivity, and activity, in turn, influences connectivity, the finding that networks develop stable activity patterns may be interpreted as an established balance between activity and connectivity (van Pelt et al. 2004; le Feber et al. 2007). It
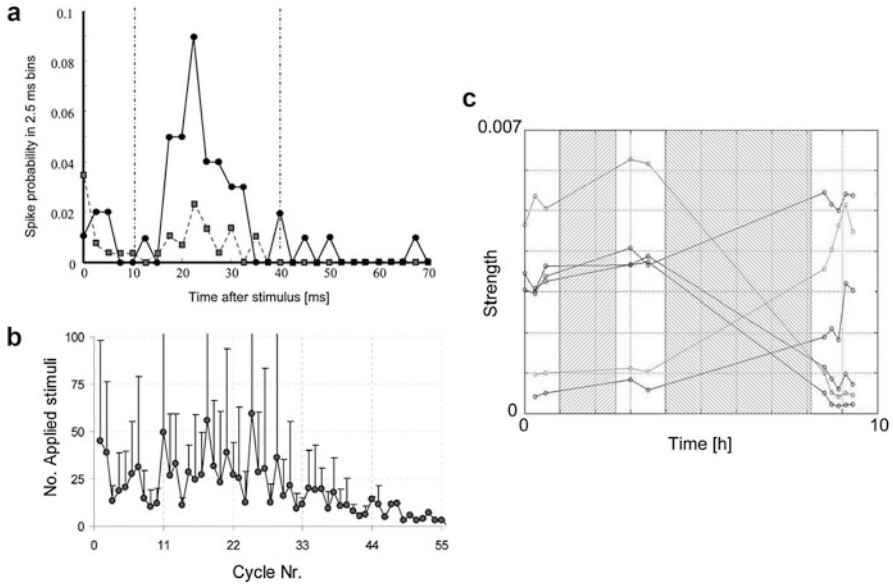
Fig. 4 Closed-loop stimulation induces complex functional connectivity changes in the network. (**a**) Effect of training protocol on the post-stimulus time histogram (responsiveness) of the evaluation electrode. Dashed (gray) line shows the probability to record an action potential at a selected evaluation electrode during the first ten stimuli of the training protocol. The time interval to determine the "responsiveness" (the fraction of stimuli that yielded at least one action potential in this interval) was set at 10–40 ms (dash-dotted lines), such that the summed probability before training was about 0.1. Solid (black, N) line: same probability during the last ten stimuli of the training protocol. (**b**) Average development (N, mean 6 SD) of all ten experiments. On average the number of applied stimuli decreases significantly with trial Nr. (Kendall's tau: Correlation coefficient: −0.33; $P < 0.01$). (**c**) Strengths of persisting connections during one experiment. There were only six persisting functional connections and the development of their strengths is represented by the six lines. The experiments had five phases. White areas: spontaneous activity recordings. Left hatched area: random stimulation. Right hatched area: training protocol. The graph illustrates that the strength of most individual connections was affected by the protocol. In total, the strength of 64% of all persisting connections was significantly changed. The figure also suggests that global parameters like mean strength may not be affected by the protocol. Presented example was rather exceptional, and used mainly to illustrate the conclusion that was drawn from all data with many more persisting connections. From le Feber et al. (2010)

was proposed that slow electrical stimulation evoked complex bursting activity which pushed the network out of balance between activity and connectivity, until the desired state was achieved.

In summary, a relatively low and early synaptic response (40–60 ms) between input-output neurons can be enhanced only by closed-loop stimulation of specifically selected electrodes, while the functional connectivity, measured by CFP, changed the whole network in open-loop and closed-loop conditions.

Further studies introduced adaptive and activity-dependent reinforcement condition defined by the R/S threshold value calculated from the statistics of control

stimulation (e.g., the open-loop). Such an approach enhanced relatively strong synaptic input-output pathways (0.1 < R/S < 1) (Pimashkin et al. 2013). The increase in the response involved higher number of the electrodes inducing target R/S, indicating that stronger spontaneously developed pathways required higher R/S threshold for learning which resulted in stronger network changes.

All research groups observed a successful learning (examples shown in Figs. 3c and 4b), while in 20–50% of the cultures such effect was not found. Indeed previous attempts to study plasticity phenomena at whole network level were not successful (Wagenaar et al. 2006b). Various factors can influence the final results. On the cellular level: different cell types, cell density, neuro-glia ratio, and the neuron spiking rate. On the network level: network size, spontaneous fluctuations of bursting activity, and random network connectivity. In terms of the dynamics, the stimulation affected the connectivity to unpredicted direction depending on initial functional and morphological state. Such changes might fail to develop the desired response (R/S threshold of the selected electrode), which led to unsuccessful learning (le Feber et al. 2010).

Ikegami's group proposed that the mechanisms of such network-level learning are based on STDP plasticity (Sinapayen et al. 2017). It was also shown with mathematical modeling that unsuccessful learning can be caused by asymmetric-STDP plasticity, in which long-term depression (LTD) component of synaptic weight function was higher than long-term potentiation (LTP) (coefficient 0.12 vs. 0.1). The response to the stimulation was gradually suppressed by such form of plasticity, weakening the connection strength and "isolating the input neurons" (Masumori et al. 2018).

Needless to say that low-frequency stimulation of multiple electrodes in open-loop induced "memory traces," unique to each stimulation site (le Feber et al. 2015). The stimulation lasting several hours significantly changed the bursting response pattern, which then was induced multiple times from different electrodes. As previously proposed (le Feber et al. 2010), the stimulation disturbed the activity-connectivity balance of the network and induced a new dynamical equilibrium. The results opened a new area in the study of network-wide memory formation and information processing. Note that such stimulation changed the stimulus response to unpredicted pattern, in contrast to "desired" response in the closed-loop experiment.

3.3   Controlling Bursting with Closed-Loop

Self-organized complex bursting activity is highly variable across different cultures and dramatically changes during culture development (Wagenaar et al. 2006a). It was hypothesized that high excitability and high network synchronization developed due to lack of external afferent activity and complex homeostatic processes (Turrigiano and Nelson 2000; Turrigiano 2012). Wagenaar et al. introduced a method to control bursting at population level. The method permitted to change a spiking rate of the responses depending on the stimulation frequency: low frequency enhanced

the bursting activity of the responses, while high frequency significantly reduced it (Wagenaar et al. 2005b). Also, the closed-loop stimulation applied to multiple electrodes was found to be optimal to suppress bursting and achieve dispersed spiking similar to in vivo conditions.

Another experiment exploiting the closed-loop technology, the "response clamp," was developed for studying basic mechanisms of neural response threshold in neuronal cultures in vitro (Wallach et al. 2011). Similar to patch-clamp and current-clamp, the neuronal responses of the selected electrode can be controlled to achieve stable spiking response with desired characteristics, e.g., the spiking rate or precise spike timing. The method was performed with a PID controller in closed-loop conditions which continuously monitored and compared each response with the desired one to minimize error by adapting the stimulus amplitude. Such an approach provided stable control over the probability to obtain desired number of the spikes in short post-stimulus interval (10–40 ms) and the spiking timing delay. In general, the response clamp might be implemented at any level of organization of neural systems in order to control its dynamical parameters and uncover input–output relationships in macroscopic scale.

Desired response features of the neural network can be also achieved with reinforcement learning using phenomenological model based on Markov decision process. The group of Egert (Kumar et al. 2016) developed a controller which autonomously optimized low-frequency stimulation settings and evaluated control strategy in real time. Statistics of the burst magnitudes and spontaneous events were used to predict and to optimize an optimal inter-stimulus intervals maximizing the response efficacy for each individual network. In addition to the previous approach (Keren and Marom 2014), the presented study controls also a magnitude of network responses as a number of spikes within 500 ms. Such studies bring promising strategy to intervene in the dynamics of pathological networks while adapting to ongoing activity.

Recent breakthrough in high-density microelectrode arrays (HD MEAs) allowed to process a single neuron in the network in real time. Closed-loop system with submillisecond feedback was recently developed for such HD MEA which can be used to uncover information processing mechanisms on the network level (Muller et al. 2013). In order to optimize the performance of such system, advanced signal processing techniques need to be used, able to rapidly and reliably compute and extract useful information from the recorded signals. In this context, machine learning algorithms and information theoretic quantities are rapidly taking ground respectively for autonomously adjusting system parameters (Kumar et al. 2016) and for extracting relevant features from neural signals (Panzeri et al. 2017).

3.4   Optical Closed-Loop

The possibility of selectively control (i.e., excite or inhibit) single neuronal cells at the millisecond timescale has become a reality since the advent of optogenetics

(Boyden et al. 2005). Optogenetic stimulation has offered several advantages over electrical stimulation and paved new ways towards the achievement of temporally precise, noninvasive control of activity in well-defined neuronal populations (Zhang et al. 2007). With electrical stimulation, all neurons in a given volume are stimulated, both excitatory and inhibitory, thus reducing its overall efficacy. Moreover, only excitation can be provided using electrical stimulation. In contrast, optogenetics overcomes many of those disadvantages, by using (1) proteins that directly elicit electrical currents across cellular membranes in response to light (Zhang et al. 2011), (2) genetic methods for targeting specific opsin gene expression to selected cellular elements of the brain (Madisen et al. 2012; Mattis et al. 2012), and (3) advanced optical methods for guiding sufficiently strong and precisely timed light to specific brain regions, cells, or parts of cells (Bovetti and Fellin 2015).

The ability to perturb single cells at precise time resolution offered unprecedented possibilities for the implementation of closed-loop systems aimed at controlling the activity of neuronal networks, and several studies have presented closed-loop optogenetic stimulation architectures (Armstrong et al. 2013; O'connor et al. 2013; Zhang et al. 2018). In those systems optogenetic stimulation can be triggered by the readout of neuronal activity monitored either with electrophysiological or optical methods, or by behavioral events. In case of activity-dependent stimulation, the goal was either to suppress pathological activations (Krook-Magnuson et al. 2013; Paz et al. 2013) or to study the causal relationship between neuronal activity and behavior by imposing specific patterns of activations (Zhang et al. 2018).

In neuronal cultures plated on MEAs, optogenetic stimulation has been coupled with multi-unit electrophysiological recording, by investigating the effects of either wide-field (Pulizzi et al. 2016) or 2D patterned illumination (Ju et al. 2015) at the network level. In 2015, Newman and colleagues presented a closed-loop system allowing continuous, bidirectional, control of neuronal networks' firing rate by delivering wide-field optogenetic stimulation, and tested it both in vitro and in vivo across a wide range of stimulation and feedback control parameters (i.e., Optoclamp). The use of in vitro neuronal networks plated on MEAs allowed to demonstrate that population firing levels could be controlled in real time over timescales ranging from seconds to days, due to the noninvasiveness of both recording and stimulation techniques. They also used optogenetics in combination with chronic pharmacological blockade of either excitatory or inhibitory transmission, allowing for instance to decouple network firing levels from neurotransmission in the study of different forms of plasticity, like homeostatic plasticity (Fong et al. 2015). Further developments, such as the combination of spatial light modulators to shape light (Bovetti and Fellin 2015) with feedback control techniques, would finally allow to fully exploit the spatio-temporal flexibility of closed-loop optogenetic stimulation.

As in many other contexts, in vitro neuronal networks could be exploited as a test-bed system for investigating the efficacy of closed-loop optogenetic stimulation paradigms, for example to suppress pathological activity regimes (e.g., epilepsy) using inhibitory opsins, or to rescue normal activity levels in case of neural injuries.

4   Neurorobotic Systems: Connecting Neurons with Robots

The neurorobotic field aims at integrating recent breakthroughs in brain neuroscience, robotics, and artificial intelligence. In particular, closed-loop electrophysiology allows the realization of hybrid systems, in which a biological brain can control an artificial body. The main advantage of such a system is the high degree of accessibility of relevant variables, as typically a significant number of neurons are available for recording/stimulation, while both the environment and the robot itself are fully defined by experimenters. These setups allow therefore testing hypotheses on coding, decoding, and memory properties of neural preparation with a unique degree of control.

Since the beginning of the twenty-first century, several pioneering projects have been undertaken within this field, linking in vitro neural systems with either artificial external devices (Novellino et al. 2007; Tessadori et al. 2012; Li et al. 2016; Lobov et al. 2017) or virtual environments (Demarse et al. 2001; Kositsky et al. 2009). They are schematically depicted in Fig. 5.

The first remarkable example of bidirectional in vitro biohybrid system is reported thanks to Mussa-Ivaldi's and coworkers' work. In their study, a closed-loop hybrid neurorobotic system was implemented to establish a two-way communication between the dissected brain of a lamprey and a small mobile robot, with the purpose of investigating the behavioral, computational, and neurobiological mechanisms of sensory-motor learning (Reger et al. 2000; Karniel et al. 2005; Kositsky et al. 2009). Potter's group implemented several different systems in which biological neurons acted as controllers for simulated agents, e.g., an animal in a virtual world (Demarse et al. 2001) or a plane in a flight simulator (DeMarse and Dockendorf 2005). Similarly, the European project NeuroBIT aimed at developing algorithms and techniques for establishing a bidirectional connection between in vitro neurons, plated on a microelectrode array, and an external robot, thus allowing real-time closed-loop interaction (Martinoia et al. 2004b; Novellino et al. 2007).

Another relevant example is represented by another neurorobotic project, a merging of art and science, called MEART (i.e., the semi-living artist). It consisted of a pneumatically actuated robotic arm to create drawings, controlled by a living network of neurons grown on a MEA (Bakkum et al. 2007).

In most of these systems, "sensory" information was coded as a low-frequency electrical stimulation delivered from multiple sites, whereas multiple algorithms were proposed for decoding neural activity. For instance, precise spike timing (Shahaf et al. 2008), spiking rate (Tessadori et al. 2012; Pimashkin et al. 2016; Poli et al. 2017), or spiking patterns (Demarse et al. 2001) were investigated as possible decoding paradigms.

To summarize, in recent years, several different biohybrid model systems have been developed (Mussa-Ivaldi et al. 2010; Warwick et al. 2010; Kudoh et al. 2011) that allow the use of an artificial body whose dynamics can be easily and completely modeled while the exchange of information between the "brain" and the environment can be limited to the desired level of complexity, as opposed to the case of even the simplest animals.
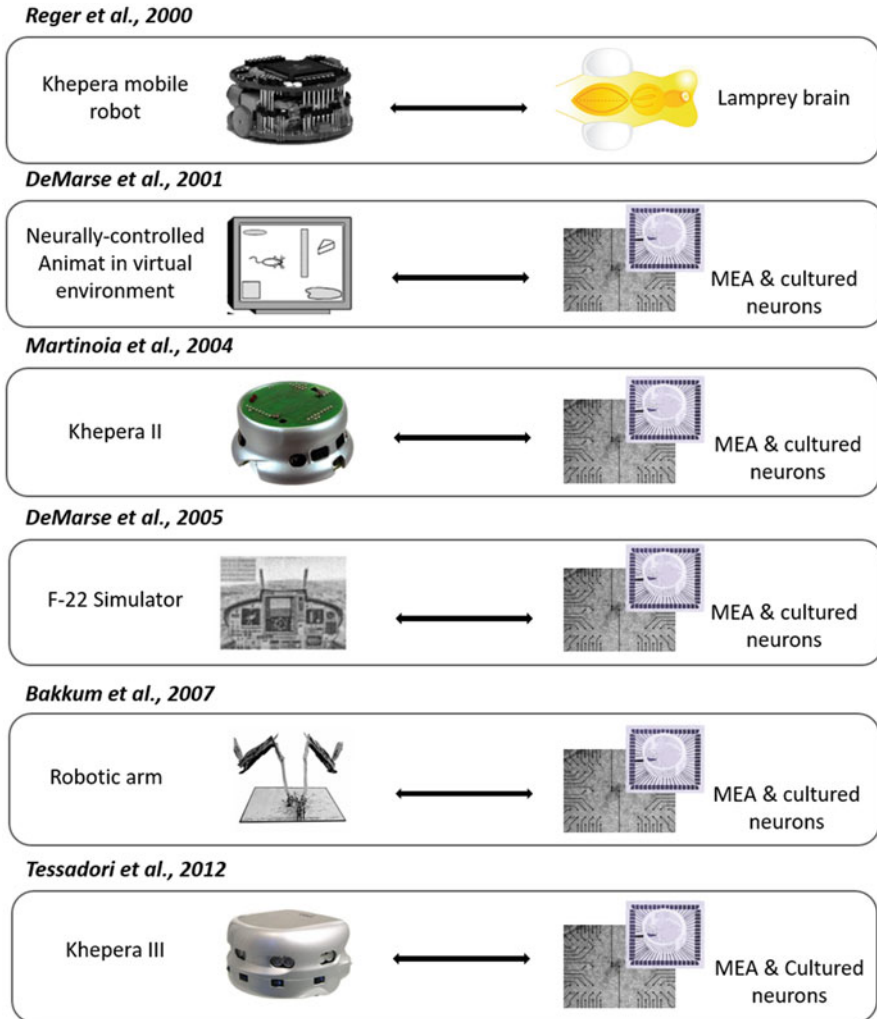
Fig. 5 Temporal scheme of some examples of in vitro neurorobotic closed-loop system published starting from the beginning of the twenty-first century

4.1 Focus on a Neurorobotic System: Hybrain

The Hybrain project is a clear example of merging of two different disciplines, i.e., biology and engineering, aiming at finding a way to naturally drive an external device in performing a specific task. In particular, a hybrid neurorobotic architecture is presented, based on a neural controller bidirectionally connected to a physical/virtual robot (Tessadori et al. 2012). Indeed, it is known that behaviors, from simple to most complex, require a two-way interaction with the environment.

   The proposed paradigm represents an innovative, simplified, and controllable closed-loop system where it is possible to investigate the dynamic and adaptive properties of a neural population interacting with an external environment by means of an artificial body (i.e., the mobile robot). The main innovations of this experimental setup are (1) the flexible software architecture at the base of the closed-loop experiments and (2) the introduction of a modular network design.

   This paradigm offers a framework for studying, in simplified model systems, neuro-artificial bidirectional interfaces for the development of new strategies for brain-machine interaction. It is worth pointing out that the final objective is not to achieve the best possible control of the robot; indeed, excluding any biological component would easily provide better performance and more reliable results. What is being developed here is groundwork for the integration of electronic systems and neural networks, with the twofold long-term objectives of taking advantage of neural plasticity in more complex control systems and performing closed-loop experiments to gauge the computational and learning properties of relatively simple neural models.

   The adopted robot is characterized by proximity sensors and wheels (Fig. 6a, *top*), allowing it to navigate into a circular arena with obstacles of different sizes. For our experiments, we actually used a virtual implementation of both the robot and the arena (Fig. 6a, *bottom*). As neural controller, two different types of experimental preparations have been exploited: in vitro uniform (Fig. 6b, *top*) and bimodular neuronal networks (Fig. 6b, *bottom*), dissociated from rat embryos brains and cultured over MEAs surface.
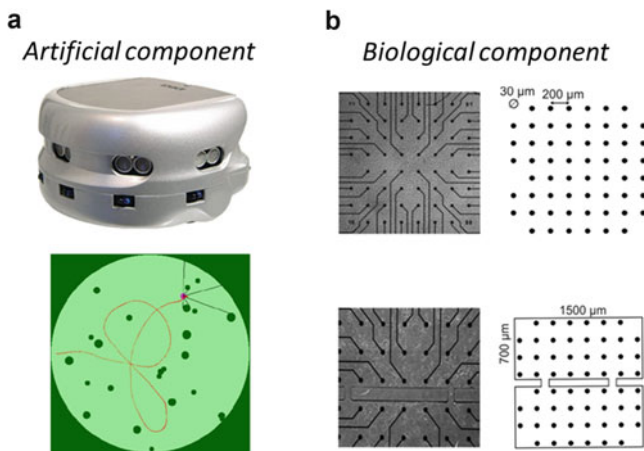

Fig. 6 Artificial and biological components of the closed-loop system. (**a**) Robot with two wheels and two sensors per each side (*top*); virtual implementation of the circular arena in which the robot (pink dot) is free to move (pink trajectory over light green area). Physical obstacles of different sizes are displayed as dark green circles in the virtual arena (*bottom*). (**b**) Optical image of a uniform neuronal network (*top left*) and geometrical organization of the electrodes over the MEA surface (*top right*). Optical image of a bimodular neuronal network (*bottom left*) and dimensions of the physical constraint positioned over the MEA surface (*bottom right*)

Uniform networks are characterized by randomly connected neurons, i.e., no physical constraints have been adopted; instead, in order to mimic the high degree of modularity present in the brain, the choice of using modular networks was introduced. Indeed, the modularity property has been pointed out by different studies as having a profound impact on neural activity (Hubel et al. 1977; Sporns et al. 2000; Derdikman et al. 2003; Kumar et al. 2010; Pan et al. 2010; Boucsein et al. 2011). For this reason, "bimodular" neuronal networks have been adopted, i.e., realized using a physical constraint to guide neuronal growth along specific pathways in order to obtain two partially separated neuronal populations interacting through microchannels.

The initial experiments have been performed using uniform networks and have proved that neuronal networks can be successfully interfaced to an artificial device. The decision to start using bimodular networks came from the need to improve the robot's performances, since uniform networks showed the tendency to spontaneously evolve towards a degenerate state where mostly network-wide synchronous activity can be observed (Fig. 7a), while modularity qualitatively changed the behavior of the network, preventing or at least strongly reducing the appearance of synchronized network bursts (Fig. 7b).

As previously mentioned, modulation of the activity of neuronal networks typically occurs by means of electrical stimulation and the typical response can be evaluated through the so-called post-stimulus time histogram (PSTH, Fig. 8a1, b1). The PSTH is usually characterized by an "early response," lasting 20–40 ms,
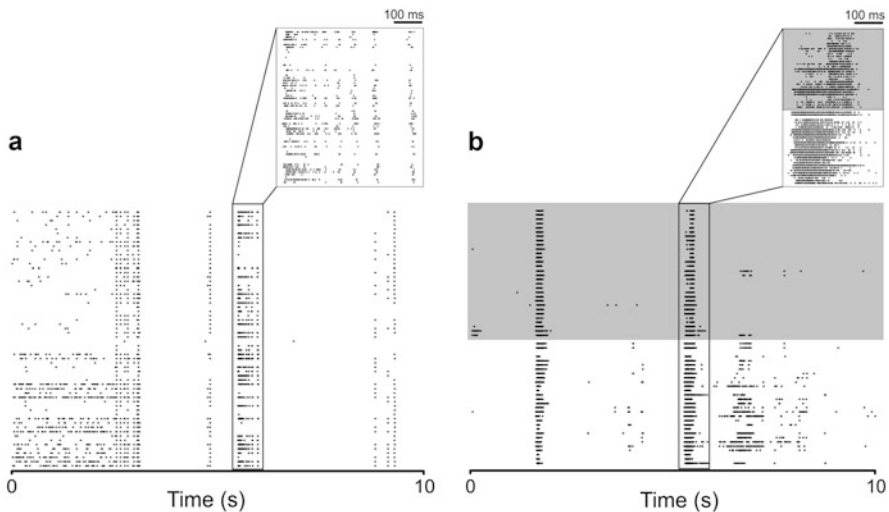

Fig. 7 Dynamical activity patterns observed within a 10-s window in a mature uniform (**a**) and bimodular neuronal network (**b**), i.e., aged 16–25 days in vitro (DIVs). The insets show a zoom (i.e., 100 ms) of a single burst of activity. The gray rectangle indicates the upper compartment of the bimodular network. Adapted from Bisio et al. (2014)
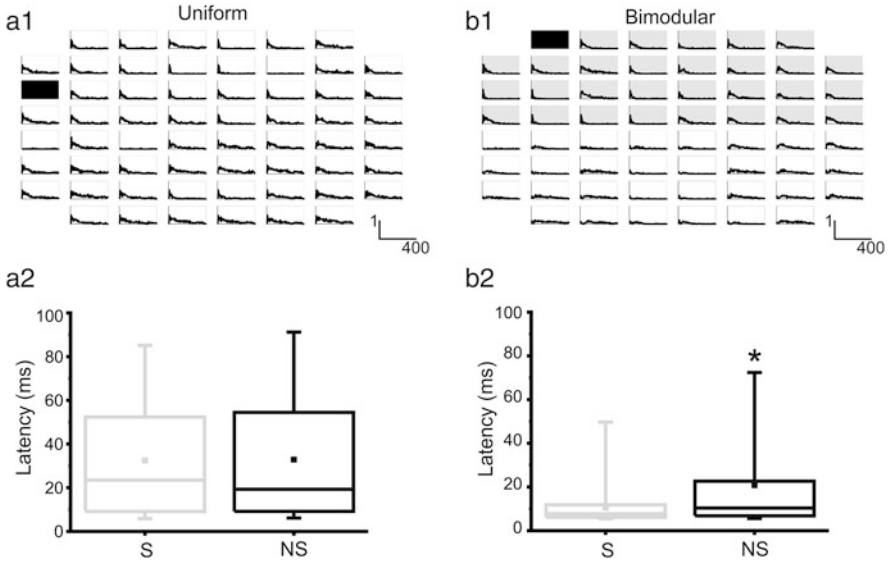
Fig. 8 Evoked activity in random and bimodular networks. (**a1**) PSTH map obtained from 59 electrodes as a consequence of the stimulation from electrode 13 (black rectangle) in a uniform network. *X*-axis: time [0, 400] ms, bin 4 ms; *Y*-axis: probability of evoking a spike. (**b1**) PSTH map obtained from 59 electrodes as a consequence of the stimulation from electrode 21 (black rectangle) belonging to the top compartment of a bimodular network. Shaded area indicates the top compartment. *X*-axis: time [0, 400] ms, bin 4 ms; *Y*-axis: probability of evoking a spike. (**a2**) Box plots of the latency observed in the stimulated (S) and non-stimulated (NS) compartment. $N = 11$ uniform networks. (**b2**) Box plots of the latency observed in the stimulated (S) and non-stimulated (NS) compartment. $N = 6$ bimodular cultures. Box range: percentile 25–75; Box whiskers: percentile 5–95; Line: median; Square: mean. Mann-Whitney test for not-normal data, significance level $= *p < 0.05$. Modified from Tessadori et al. (2012)

and by a late response, lasting more than 100–200 ms, due to the generation of an evoked burst synchronized over the whole network (Warwick et al. 2010). The sum over the PSTH profile represents the average number of evoked spikes at a specific site and it is used for quantifying the strength of the connection between a specific stimulation site and all the recording ones (Chiappalone et al. 2008).

This parameter is used to choose the input-output connections necessary for neurorobotic applications. Figure 8 reports the PSTH maps obtained both in a uniform (a) and in a modular network (b). The black rectangles indicate the sites stimulation has been delivered from. The advantage of bimodular networks can be observed in Fig. 8b1, in which the confinement of responses to electrical stimulation to a single compartment can be clearly observed.

To further test the actual bounds of evoked responses, the mean latencies distribution has been analyzed (i.e., the temporal distance between the stimulus and the first evoked spike) for each couple of stimulation-recording electrodes (Jimbo et al. 1998; Kudoh et al. 2011).

Figure 8a2, b2 compares the average time elapsed between stimulation and the first recorded spike observed in the same and opposite compartments (respectively, labeled as S and NS): while there is no effect on response latency for the uniform case, in the bimodular one neural activity requires a significant amount of time to cross between subcultures, hence the difference in response times between the S and NS channels. It is worth pointing out that compartments are physically separated only in the bimodular case, while, for uniform networks, the grouping of channels in compartments is only nominal, in order to relate channel groups with comparable distances in both uniform and bimodular cultures.

The protocol of a typical Hybrain experiment consists of a four-step procedure: (1) monitoring of the network's spontaneous activity in order to determine which electrodes are the most likely candidate as sites which stimulation must be delivered from; (2) stimulation test from a set of electrodes for quantifying the strength of connection between each stimulation site and the recording ones (Chiappalone et al. 2008) in order to choose the I/O of the network (Gal et al. 2010); (3) 20-min run; (4) evaluation of the robot's performances on the basis of specific navigation's parameters.

Although many different decoding schemes are possible, the one implemented here is a frequency rate-based algorithm (Adrian 1928; Rieke et al. 1997; Martinoia et al. 2004a), i.e., the spikes' frequency computed at each electrode is the key feature. Furthermore, in the current architecture, a linear relation is implemented between wheels' speed and motor signal, and a low-pass filtering effect is added to smooth robot movements.

Likewise, the coding scheme is linear and rate-based, i.e., two groups of electrodes are defined as "input areas" and assigned to the sensors on the left and right side of the robot body. Each sensor provides a reading of the distance between the robot and the closest obstacle, and a fixed stimulus is delivered at the sensory area at a frequency directly proportional to the sensor readings.

Figure 9 shows that controlling the robot by a bimodular network enhances its capabilities in avoiding obstacles. Indeed, robot collisions against obstacles are a frequent occurrence when using uniform networks as neural controller. Instead, the introduction of a physical confinement shows a marked separation in the responses evoked by the stimulation leading to a reduction in the amount of "cross talk" between input and output electrodes, with a consequent increase in the navigation performance of the robot. Specifically, Fig. 9a shows the comparison between performances evaluated as the average distance traveled by the robot between consecutive collisions, while Fig. 9b displays the same performances evaluated through a different parameter, i.e., the average number of hits per second. While results are statistically significant only in the case of average distance between hits, the wide discrepancy in variability observed in the number of hits between modular and random cultures suggests a qualitative difference between the two conditions.

In conclusion, within the Hybrain project, a network of neurons has been successfully interfaced, bidirectionally, with a robot performing a collision-avoidance task in a static arena with obstacles.
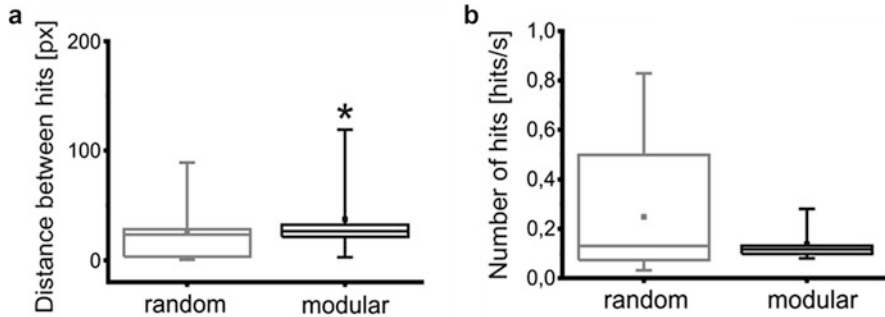
Fig. 9 Performance of the neuro-controlled robot during an obstacle-avoidance task. (**a**) Average distance traveled by the robot between consecutive hits, calculated in pixels, both if controlled by uniform and by bimodular neuronal networks. (**b**) Number of hits per second computed when the robot is controlled both by uniform and by bimodular networks. $N = 11$ experiments with uniform networks; $N = 6$ experiments with bimodular networks. Box range: percentile 25–75; Box whiskers: percentile 5–95; Line: median; Square: mean. Statistical analysis was carried out by using Mann-Whitney test for not-normal data, significance level = *$p < 0.05$. Adapted from Tessadori et al. (2012)

The behavior of the robot during the closed-loop experiments resulted significantly better than that in open-loop (i.e., without any sensory feedback), proving that the activity driving the robot is actually neural based. In general, these results prove that an in vitro network of biological neurons can control an external device. Furthermore, bimodularity is introduced in the networks' topology for the first time in the context of closed-loop interfaces and its impact is shown to be relevant for the performance of the embodied agent. Once more, it is important to highlight that the final goal of this project was to facilitate progress in testing communication schemes of neural structures, in order to better understand neural pathologies, design neural prosthetics, and create fundamentally different types of artificial or hybrid intelligence.

5 Hybrid Interaction and Hybrid Systems for Brain Repair

Within the field of neuroprostheses, the long-term goal of replacing damaged brain areas with artificial devices requires the development of neuronal network models which faithfully reproduce the network dynamics of the cell assemblies in the brain. Specifically, they should not only fit the recorded electrophysiological patterns, but also reproduce the correct stimulation patterns for the brain to recover the desired function. To reach this ambitious goal, biomimetic spiking neural networks (SNNs) can be a convenient solution as interfacing system with biological neural networks (Mahowald and Douglas 1991; Levi et al. 2008; Indiveri et al. 2011). A biomimetic SNN is a neuromorphic system composed of a network of

artificial neurons connected via silicon synapses and implementing plasticity rules. We will briefly overview the use of SNNs for performing hybrid experiments between biological cells and artificial neurons, with the final goal of developing new generation neuroprostheses.

5.1 State of the Art of SNN

SNN can be simulated through appropriate simulation software (Hines and Carnevale 2001; Gewaltig and Diesmann 2007; Goodman and Brette 2009) and/or neuromorphic hardware (Broccard et al. 2017). The time and the energy required to simulate neuronal behavior are becoming relevant as neuroscientists turn to supercomputers to simulate brain-scale neural networks at cellular resolution. Today's supercomputers require several minutes to simulate one second of biological time and consume lots of kilowatts of power (Kunkel et al. 2014; Jordan et al. 2018). This means that any studies on processes like plasticity, learning, and development exhibited over hours and days of biological time are currently out of our reach. Hardware implementations of smaller networks can realize simulations in a time comparable or shorter than biological time and with low power consumption. For biohybrid experiments, the choice of hardware systems is then more relevant.

Hardware implementations of SNN are divided into two major categories: analog implementation (based on dedicated chips) and digital implementation (based on FPGA, microprocessors, microcontrollers, or neurochips). The very first platforms appeared more than twenty years ago (Mahowald and Douglas 1991; Jung et al. 2001; Le Masson et al. 2002).

In case of analog implementations, some systems implement multi-compartmental models (Hasler et al. 2007; George et al. 2013), conductance models (Binczak et al. 2006; Renaud et al. 2007; Grassia et al. 2011; Levi et al. 2018b; Natarajan and Hasler 2018), or threshold models such as Izhikevich model (Liu and Douglas 2004; Vogelstein et al. 2004; Indiveri and Fusi 2007; Schemmel et al. 2007; Qiao et al. 2015; Kohno et al. 2016). All these platforms start from an analog computing core, usually an ASIC, which describes the activity of the neuron. The architecture of the different platforms results from a compromise between the computational cost and the complexity of the model (directly correlated to biological plausibility). The integration of plasticity and synapses is usually done by a digital map that makes the link between the different analog chips.

On the digital implementation side, SNN implementations on FPGAs are generally used for engineering task like image or signal processing (Rice et al. 2009; Sabarad et al. 2012; Wang et al. 2013a; Nanami and Kohno 2016; Levi et al. 2018c). The number of implementations on the FPGA platform has been steadily increasing since 1997. Cassidy (Cassidy et al. 2011) proposed the implementation of one million LIF neurons in FPGA for accelerated time simulations, Wang (Wang et al. 2013b) the implementation of 4000 neurons and 1.15 million synapses with STDP and axonal delay, and Bonabi (Bonabi et al. 2012) the implementation of

120 simplified HH neurons. Simulating large-scale networks implies to perform accelerated neural network calculations or to increase the time step of computations. We describe here two platforms, one digital and one analog which are used for the Human Brain Project (Markram 2012).

- The *SpiNNaker* (Furber et al. 2013; van Albada et al. 2018) platform is a digital system with a multiprocessor architecture (made of ARM processors), running software neuron models, and performing the calculations instead of physical silicon neurons. SpiNNaker system achieves real-time performance for an integration time step of 1 ms which is sufficient for applications in robotics and artificial neural networks; however a time step of at least 0.1 ms is typical for neuroscience applications.
- The *BrainScale* system is a stack of modules composed of a wafer integrating 448 analog neuromorphic chips and a routing system. Each module emulates the activity of 512 neurons and 115,000 synapses, performing calculations 104 times faster than biological time (Rast et al. 2013).

Another line of research is focused on the integration of artificial neural networks based on memristors (memory resistors), which is a passive electronic component whose resistance varies according to the applied current and electrical circuits (Boyn et al. 2017; Chiolerio et al. 2017). The goal is to use memristors to simulate the behavior of a synapse and its learning. The great advantage is the very low power consumption (Budiman et al. 2018).

5.2 Hybrid Experiments

With the emergence of real-time neuromorphic platforms, the desire to connect artificial neural networks with biological neural networks has emerged (Broccard et al. 2017). The features needed for these systems are biological real-time simulation, complex neuron models, and implementation of plasticity rules that reproduce temporal neuronal dynamics. Extracellular multielectrode arrays (MEAs) are used to record from and stimulate populations of neurons, providing an effective bidirectional interface at the network level between neural populations and electronic circuits. In the literature (Potter et al. 2014; Levi et al. 2018a) different works regarding closed-loop hybrid experiments, characterized by the interconnection between biological neural networks and their artificial counterparts, have been presented. In their editorial article, Potter et al. (2014) show the latest innovations in the field, such as closed-loop hybrid experiments using MEAs (Bareket-Keren and Hanein 2012; Robinson et al. 2013), in vitro experiments (Bonifazi et al. 2013; Pimashkin et al. 2013), in vivo experiments (Opris et al. 2012; Nishimura et al. 2013), and clinical trials (Walter et al. 2012; Fernandez-Vargas et al. 2013). Vassanelli and Mahmud (2016) introduced the term "neurobiohybrid" for one system formed by at least living neurons and at least one artificial entity that establish a uni- or bidirectional communication between them.

5.3   Examples of Hybrid Interaction in In Vitro Systems

As anticipated in Sect. 1 of this chapter, stimulation provided through neuroprosthetics offers promising prospects for restoring function in the damaged central nervous system. They require the identification of appropriate stimulation sites and the coordination of their activation to achieve the restoration of functional activity. In the long term, one perspective is to control stimulation by biomimetic SNN hybridized with living tissue. The main objective is to produce an adequate stimulation in order to restore the desired neural function. Regarding spinal cord injury, the role of a SNN could be to emulate the activity of CPGs (Central Pattern Generator), at the origin of the locomotion. The SNN activity should trigger a biological-like series of stimulations on an injured spinal cord, thus helping recreating healthy locomotion. Capogrosso et al. (2016) presented a promising work on primates; however simple oscillators have been used. A perspective of this work is to use more complex behaviors created by SNN. The first hybrid experiments with a population of neurons and SNN have been made by Jung et al. (1996) and Joucla et al. (2016). In this first study, CPGs from isolated lamprey spinal cord were coupled with a CPG model implemented in analog VLSI neuromorphic hardware (Jung et al. 2001). Jung and colleagues used a computational model with realistic connectivity and three populations of conductance-based neurons. Joucla et al. (2016) presented a hybrid approach to intraspinal microstimulation control using biomimetic SNN. Microelectrode arrays were inserted into the lumbar region to determine the appropriate stimulation sites. Biomimetic SNN creates CPG to generate a rhythmic activity and which was hybridized to the living spinal cord to generate electrical microstimulations at the two identified sites. Using this strategy, locomotor activities can be generated either in the intact spinal cord or in the severed spinal cord. These results are a first step towards hybrid artificial/biological solutions for the restoration of lost function in the damaged central nervous system. When dealing with spinal cord injuries researchers are forced to work on in vivo models because they need a body to prove the efficacy of the stimulation protocol. Other pathologies (like traumatic brain injuries and stroke) can be studied, in a first place at the electrophysiological level only. In this context, in vitro cultures coupled to microelectrode arrays (MEAs) constitute a valuable and accessible model to understand the possibilities and limits of a hybrid interaction. In contrast to an in vivo system, cultures of neurons do not have efferent motor outputs and afferent sensory inputs but show electrophysiological patterns of activity comparable to those recorded in developing brains (Ben-Ari 2001). Starting from these considerations, the European Project BrainBow was aimed at the realization of neural prostheses capable of replacing a lesioned neuronal circuit. The general idea of the BrainBow project, described in Bonifazi et al. (2013), was based on a multidisciplinary approach. From the biological side an innovative plating method (Shein-Idelson et al. 2011; Bisio et al. 2014) was used to reproduce the modular topology of the brain (Fig. 10). From the engineering side they built a powerful and reliable digital device (based on field-programmable gate arrays,
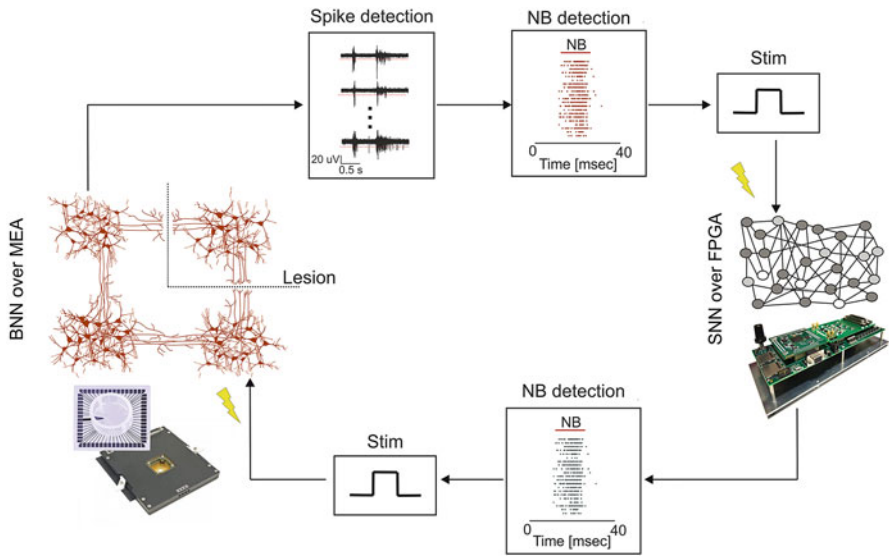
Fig. 10 Schematic of the BrainBow project hybrid interaction after lesion. On the left: a schematic representation of a patterned culture (with 4 modules) plated over a 60-electrodes MEA after a focal lesion aimed at isolating the top right module. Proceeding clockwise, a real-time spike detection (red lines representing thresholds) and a real-time network burst (NB) detection are applied to the recorded BNN. If a spike count in a time window exceeds a certain threshold a stimulation pulse is delivered to the SNN model implemented on the neuroprosthetic device. Another NB detector, applied to the SNN, triggers an electrical stimulation to the BNN thus closing the loop. The aim of the SNN is to interact with the rest of the BNN and behave like the isolated module

FPGA) to reach hard real-time performances and accurate spiking neural network (SNN) real-time simulations. The ultimate goal was to develop a hybrid interaction as similar as possible to what occurs between biological neural networks (BNNs).

In the last few decades, experimental and theoretical evidences supported the possibility that the brain operates through coordinated activation of cell assemblies (Berdondini et al. 2006; Buzsaki 2010; Meunier et al. 2010; Levy et al. 2012; Bisio et al. 2014). While homogeneous networks tend to display bursts which spread to most of the connected cells (van Pelt et al. 2004; Chiappalone et al. 2006; Eytan and Marom 2006), networks composed of smaller subnetworks with sparse connections usually present non-repetitive patterns of sparse spiking and local bursts (Macis et al. 2007; Idelson et al. 2010). BNN activity patterns are strongly dependent on the complexity of their geometry (Shein-Idelson et al. 2011). Bonifazi and coauthors (Bonifazi et al. 2013) showed that individual cell populations varied between a few dozen up to a few hundred. They also demonstrated that after 2 weeks in culture it is possible to record spontaneous synchronized events (called network bursts, NB) occurring with a frequency linearly correlated with the number of cells present in the circuit. The use of patterned cultures is particularly useful for two reasons: first, it's a simplified model that resembles the modular topology of intact brains; second,

it is possible to perform controlled lesions (by means of a custom-made laser setup) and study the effect of a therapeutic stimulation with a reduced complexity with respect to in vivo models.

Once the characteristics of the biological networks have been analyzed, and before proceeding with the hybrid interaction, it is necessary to recreate a digital version of the BNN electrophysiological activity. The digital side of interaction (i.e., the spiking neural network, SNN) was implemented on both software [NEST (Gewaltig and Diesmann 2007)] and hardware (on FPGA) in order to mimic as much as possible the main features of the BNN (e.g., number of neurons, spiking rate, network burst rate, connectivity). An Izhikevich model (Izhikevich 2003) was used to create a database of SNNs with a range of variability, in terms of spiking and bursting rate, similar to its biological counterpart. One of the typical characteristics of cell cultures is the presence of NBs; thus the NB detection can be crucial for the transfer of information between the digital and the biological module. A NB detector, based on spike count (Fig. 10), was implemented on the FPGA in order to detect this kind of activity on both SNN and BNN in real time.

In order to realize a useful interaction (i.e., a mutual action or influence), there is the need to create hybrid communication between biological and digital neurons. From digital to biological neurons the communication is achieved through electrical stimulation (every time a network burst is detected on the SNN an electric pulse is delivered to one of the 60 electrodes of the MEA). From biological to digital neurons the communication is achieved through digital stimulation (i.e., a digital current is delivered to a settable number of neurons of the SNN model).

As reported in literature (Wagenaar et al. 2005b) during slow single-electrode stimulation (0.05 stim/s), most or all stimuli entrained bursts. At higher frequencies (from 1 to 5 stim/s) most stimuli did not elicit bursts and the burstiness began to drop below spontaneous levels. During a hybrid interaction, the digital part of the system must behave similarly to the BNN. Figure 11 depicts a series of representative hybrid interactions during unidirectional and bidirectional communication. During unidirectional interaction from SNN to BNN, if two NBs are detected on the SNN within a short time window the second stimulus will be less effective than the first one in evoking a NB (Fig. 11a). The behavior of the SNN when the stimuli are triggered from the BNN and delivered to ten excitatory neurons of the SNN is similar to the previous one (Fig. 11b). This aspect is particularly important when the interaction is bidirectional. During bidirectional interaction, it can happen that the BNN starts communicating through a stimulus delivered to the SNN (i.e., a NB is detected first on the BNN). This stimulus can elicit a NB on the SNN thus causing a response in the form of an electrical pulse delivered to the BNN. The interaction is so fast that the effect of the responding pulse is weak (Fig. 11c). When communication started from the SNN (i.e., a NB is detected first on the BNN), the responding stimulus to the SNN cannot elicit a strong response because of the short time passed from the last NB (Fig. 11d). This feature can prevent the sending of an excessive number of stimulations in a short time interval.
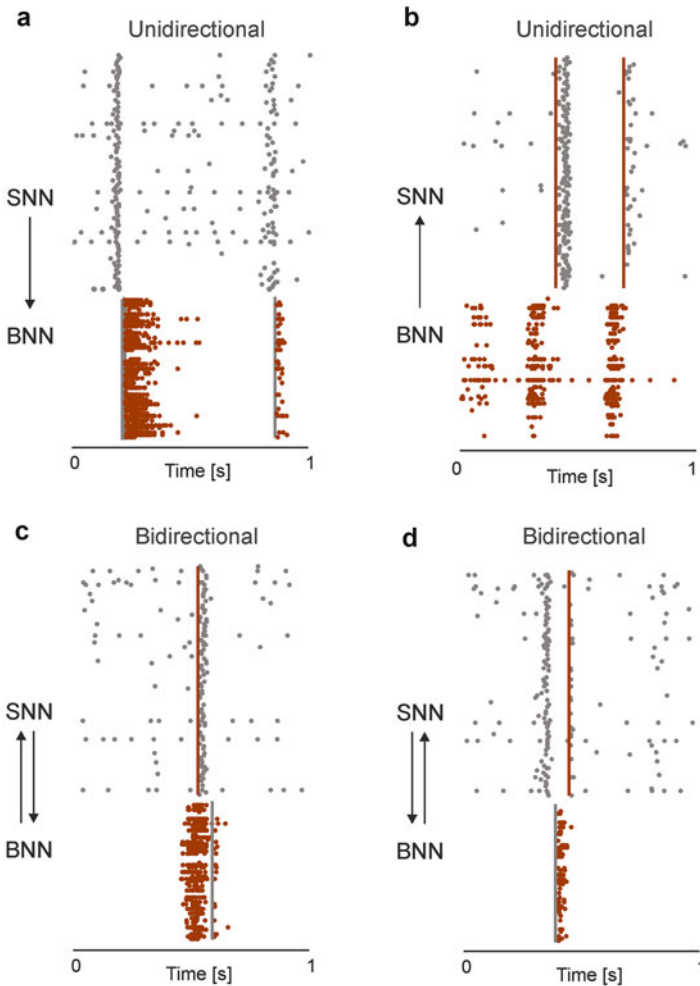
Fig. 11 Representative phases of unidirectional and bidirectional hybrid interaction. Panel (**a**), rasterplot depicting two unidirectional stimulations (gray vertical lines) from SNN (gray dots) to BNN (brown dots). The second stimulus was not as effective as the first one because of the short time since the last NB. Panel (**b**), rasterplot depicting two unidirectional stimulations (brown vertical lines) from BNN (brown dots) to SNN (gray dots). The second stimulus was not as effective as the first one because of the short time since the last NB. Panel (**c**), rasterplot depicting a bidirectional hybrid interaction. A NB was detected on the BNN thus triggering a stimulus (brown vertical line) to the SNN. Few tens of milliseconds after, a NB was detected on the SNN thus triggering a stimulus back to the BNN (gray vertical line). The effect of the second stimulus was weak because of the short time passed from the last NB. Panel (**d**), rasterplot depicting a bidirectional hybrid interaction. A NB was detected on the SNN thus triggering a stimulus (gray vertical line) to the BNN. Few tens of milliseconds after, a NB was detected on the BNN thus triggering a stimulus back to the SNN (brown vertical line). The effect of the second stimulus was weak because of the short time passed from the last NB
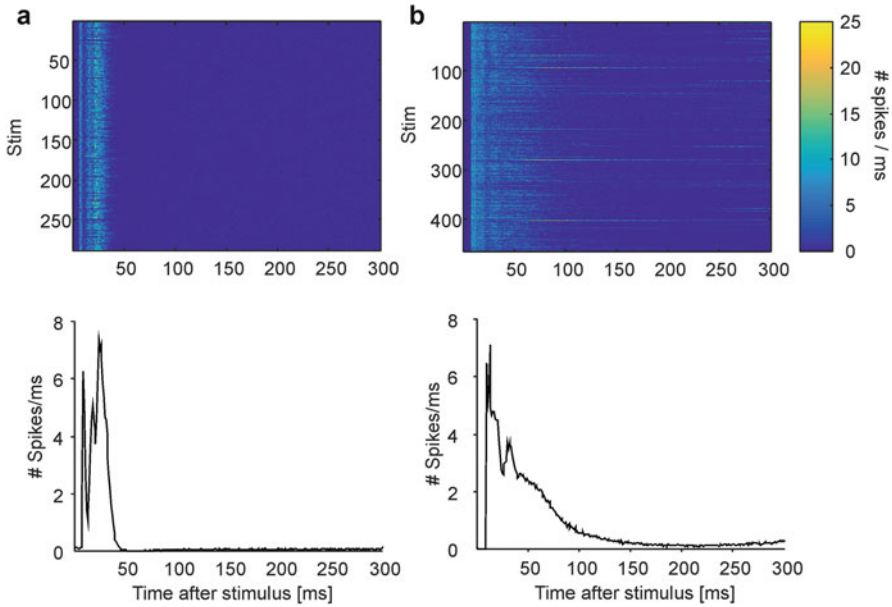
Fig. 12 Comparison between evoked responses on a representative SNN and BNN. (**a**) Top, spike count depicted in false colors represents a sequence of 289 stimuli delivered to ten excitatory neurons of one SNN (color bar from 0 to 25). Bottom, post-stimulus time histogram (PSTH) of the same sequence of stimuli in which it is possible to see a short response time (lower than 50 ms). (**b**) Top, false color representation of a sequence of 466 stimuli delivered to one electrode of a cell culture plated over a 60-channel MEA. Bottom, post-stimulus time histogram (PSTH) of the same sequence of stimuli in which it is possible to see a longer response time (with respect to SNN)

Figure 12 compares the different evoked responses on two representative SNN (panel A) and BNN (panel B). The response, in terms of spikes recorded over the entire network, is shorter on the SNN but the number of spikes is overall similar. For the BrainBow project, only NBs were considered relevant for the communication and thus only that feature was targeted. However, all the other features (spike rate, burst duration, etc.) can be tuned depending on the task.

Hybrid systems with in vitro BNNs coupled to SNNs have not been so common. Few studies focused on unidirectional or bidirectional influence of the two networks, investigating dynamics of interaction between the BNN and SNN, in which case the SNN played a role of an artificial counterpart of its biological original (Bruzzone et al. 2015; Chou et al. 2015). In Bruzzone et al. (2015) only unidirectional connectivity was considered, with input from the SNN (simulated beforehand through software) to the BNN. The same year, Chou et al. (2015) presented a bidirectional interface between a SNN and a retinal slice obtained from an adult rat and recorded by means of a MEA. They recorded 1 s of activity on BNN and

only at the end of this period, they delivered 1 s of stimulation to the SNN. Only at the end of the next second, once they obtained the results from SNN, they delivered stimulation back to BNN using the spike count as trigger feature. This huge delay means that, as they said, the effects of the SNN to BNN stimulation cannot be seen in the same time window of the BNN to SNN stimulation.

In conclusion, in order to perform a hybrid interaction between a biological and artificial neural network, at least two features are mandatory: SNN behavior, in terms of electrophysiological activity, must resemble its biological counterpart and the device that interacts with the BNN must simulate the SNN and perform all computations in real time.

6 Conclusions

This chapter aimed at describing why and how new biohybrid systems made their way into the research field with the final goal of producing results and respond to basic scientific questions which can be exploited for innovative clinical applications, in particular, for patients affected by neurological deficits.

In vitro systems and, specifically, dissociated neuronal cultures grown over MEAs' surface avoid all the drawbacks related to the use of other experimental models, thanks to their high controllability, manipulation, and replicability (Pasquale et al. 2017). In the chapter we presented three types of closed-loop hybrid systems involving MEA-cultured networks: (1) closed-loop systems to control the dynamics of biological networks; (2) neurorobotic systems constituted by neuronal cultures driving an external actuator/robot, and (3) hybrid systems composed of artificial networks used to "replace" a nonfunctioning biological network.

Therefore, all the presented neurohybrid systems have an important role in paving the way for future applications, which are even more challenging for those patients with irreversible deficits.

From now on, new technologies should be exploited in order to make them more versatile and even more easily usable by individuals (miniaturization processes, wi-fi communication, etc.), thus realizing an increasingly energy-efficient, i.e., "high-level," communication between natural and artificial neuronal networks in vivo. *This* will allow the development of "intelligent" neuroprostheses for augmentation of brain function, offering novel therapeutic perspectives for a high number of diseases (Vassanelli and Mahmud 2016).

References

Abdulkader, S. N., Atia, A., & Mostafa, M. S. M. (2015). Brain computer interfacing: Applications and challenges. *Egyptian Informatics Journal, 16*, 213–230.

Adrian, E. D. (1928). *The basis of sensation*. New York: W W Norton & Co.

Ajiboye, A. B., Willett, F. R., Young, D. R., Memberg, W. D., Murphy, B. A., Miller, J. P., et al. (2017). Restoration of reaching and grasping movements through brain-controlled muscle stimulation in a person with tetraplegia: A proof-of-concept demonstration. *Lancet, 389*, 1821–1830.

Arlotti, M., Marceglia, S., Foffani, G., Volkmann, J., Lozano, A. M., Moro, E., et al. (2018). Eight-hours adaptive deep brain stimulation in patients with Parkinson disease. *Neurology, 90*, e971–e976.

Armstrong, C., Krook-Magnuson, E., Oijala, M., & Soltesz, I. (2013). Closed-loop optogenetic intervention in mice. *Nature Protocols, 8*, 1475.

Bakkum, D. J., Gamblen, P. M., Ben-Ary, G., Chao, Z. C., & Potter, S. M. (2007). MEART: The semi-living artist. *Frontiers in Neurorobotics, 1*, 5.

Bamford, J. A., Putman, C. T., & Mushahwar, V. K. (2005). Intraspinal microstimulation preferentially recruits fatigue-resistant muscle fibres and generates gradual force in rat. *The Journal of Physiology, 569*, 873–884.

Bareket-Keren, L., & Hanein, Y. (2012). Carbon nanotube-based multi electrode arrays for neuronal interfacing: Progress and prospects. *Front Neural Circuits, 6*, 122.

Ben-Ari, Y. (2001). Developing networks play a similar melody. *Trends in Neurosciences, 24*, 353–360.

Berdondini, L., Chiappalone, M., Van Der Wal, P., Imfeld, K., de Rooij, N. F., Koudelka-Hep, M., et al. (2006). A microelectrode array (MEA) integrated with clustering structures for investigating in vitro neurodynamics in confined interconnected sub-populations of neurons. *Sensors and Actuators B: Chemical, 114*, 530–541.

Berenyi, A., Belluscio, M., Mao, D., & Buzsaki, G. (2012). Closed-loop control of epilepsy by transcranial electrical stimulation. *Science, 337*, 735–737.

Binczak, S., Jacquir, S., Bilbault, J. M., Kazantsev, V. B., & Nekorkin, V. I. (2006). Experimental study of electrical FitzHugh-Nagumo neurons with modified excitability. *Neural Networks, 19*, 684–693.

Bisio, M., Bosca, A., Pasquale, V., Berdondini, L., & Chiappalone, M. (2014). Emergence of bursting activity in connected neuronal sub-populations. *PLoS One, 9*, e107400.

Blaha, C. D., & Phillips, A. G. (1996). A critical assessment of electrochemical procedures applied to the measurement of dopamine and its metabolites during drug-induced and species-typical behaviours. *Behavioural Pharmacology, 7*, 675–708.

Bonabi, S. Y., Asgharian, H., Bakhtiari, R., Safari, S. & Ahmadabadi, M. N. (2012). FPGA implementation of a cortical network based on the Hodgkin-Huxley neuron model. *International Conference on Neural Information Processing* (pp. 243–250). Berlin: Springer.

Bonifazi, P., Difato, F., Massobrio, P., Breschi, G. L., Pasquale, V., Levi, T., et al. (2013). In vitro large-scale experimental and theoretical studies for the realization of bi-directional brain-prostheses. *Front Neural Circuits, 7*, 40.

Bonifazi, P., Ruaro, M. E., & Torre, V. (2005). Statistical properties of information processing in neuronal networks. *European Journal of Neuroscience, 22*, 2953–2964.

Boucsein, C., Nawrot, M., Schnepel, P., & Aertsen, A. (2011). Beyond the cortical column: Abundance and physiology of horizontal connections imply a strong role for inputs from the surround. *Frontiers in Neuroscience, 5*, 32.

Bouton, C. E., Shaikhouni, A., Annetta, N. V., Bockbrader, M. A., Friedenberg, D. A., Nielson, D. M., et al. (2016). Restoring cortical control of functional movement in a human with quadriplegia. *Nature, 533*, 247–250.

Bovetti, S., & Fellin, T. (2015). Optical dissection of brain circuits with patterned illumination through the phase modulation of light. *Journal of Neuroscience Methods, 241*, 66–77.

Boyden, E. S., Zhang, F., Bamberg, E., Nagel, G., & Deisseroth, K. (2005). Millisecond-timescale, genetically targeted optical control of neural activity. *Nature Neuroscience, 8*, 1263.

Boyn, S., Grollier, J., Lecerf, G., Xu, B., Locatelli, N., Fusil, S., et al. (2017). Learning through ferroelectric domain dynamics in solid-state synapses. *Nature Communications, 8*, 14736.

Broccard, F. D., Joshi, S., Wang, J., & Cauwenberghs, G. (2017). Neuromorphic neural interfaces: From neurophysiological inspiration to biohybrid coupling with nervous systems. *Journal of Neural Engineering, 14*, 041002.

Bruzzone, A., Pasquale, V., Nowak, P., Tessadori, J., Massobrio, P., & Chiappalone, M. (2015). Interfacing in silico and in vitro neuronal networks. *Engineering in Medicine and Biology Society (EMBC), 37th Annual International Conference of the IEEE* (pp. 3391–3394). IEEE.

Budiman, F., Hernowo, D. G. O., Pandey, R. R., & Tanaka, H. (2018). Recent progress on fabrication of memristor and transistor-based neuromorphic devices for high signal processing speed with low power consumption. *Japanese Journal of Applied Physics, 57*, 03EA06.

Buzsaki, G. (2010). Neural syntax: Cell assemblies, synapsembles, and readers. *Neuron, 68*, 362–385.

Cagnan, H., Pedrosa, D., Little, S., Pogosyan, A., Cheeran, B., Aziz, T., et al. (2017). Stimulating at the right time: Phase-specific deep brain stimulation. *Brain, 140*, 132–145.

Capogrosso, M., Milekovic, T., Borton, D., Wagner, F., Moraud, E. M., Mignardot, J.-B., et al. (2016). A brain–spine interface alleviating gait deficits after spinal cord injury in primates. *Nature, 539*, 284.

Cassidy, A., Andreou, A. G. & Georgiou, J. (2011) Design of a one million neuron single FPGA neuromorphic system for real-time multimodal scene analysis. *Information Sciences and Systems (CISS), 45th Annual Conference on.* (pp. 1–6). IEEE.

Chapin, J. K., Moxon, K. A., Markowitz, R. S., & Nicolelis, M. A. L. (1999). Real-time control of a robot arm using simultaneously recorded neurons in the motor cortex. *Nature Neuroscience, 2*, 664–670.

Chiappalone, M., Bove, M., Vato, A., Tedesco, M., & Martinoia, S. (2006). Dissociated cortical networks show spontaneously correlated activity patterns during in vitro development. *Brain Research, 1093*, 41–53.

Chiappalone, M., Massobrio, P., & Martinoia, S. (2008). Network plasticity in cortical assemblies. *The European Journal of Neuroscience, 28*, 221–237.

Chiolerio, A., Chiappalone, M., Ariano, P., & Bocchini, S. (2017). Coupling resistive switching devices with neurons: State of the art and perspectives. *Frontiers in Neuroscience, 11*, 70.

Chou, Z., Lim, J., Brown, S., Keller, M., Bugbee, J., Broccard, F. D., et al. (2015). Bidirectional neural interface: Closed-loop feedback control for hybrid neural systems. *Engineering in Medicine and Biology Society (EMBC), 37th Annual International Conference of the IEEE* (pp. 3949–3952). IEEE.

Daly, J. J., & Wolpaw, J. R. (2008). Brain-computer interfaces in neurological rehabilitation. *Lancet Neurology, 7*, 1032–1043.

DeMarse, T. B. & Dockendorf, K. P. (2005). Adaptive flight control with living neuronal networks on microelectrode arrays. *Neural Networks. IJCNN'05. Proceedings. 2005 IEEE International Joint Conference on.* (Vol. 3, pp. 1548–1551). IEEE.

Demarse, T. B., Wagenaar, D. A., Blau, A. W., & Potter, S. M. (2001). The neurally controlled animat: Biological brains acting with simulated bodies. *Autonomous Robots, 11*, 305–310.

Derdikman, D., Hildesheim, R., Ahissar, E., Arieli, A., & Grinvald, A. (2003). Imaging spatiotemporal dynamics of surround inhibition in the barrels somatosensory cortex. *The Journal of Neuroscience, 23*, 3100–3105.

Downey, J. E., Weiss, J. M., Muelling, K., Venkatraman, A., Valois, J. S., Hebert, M., et al. (2016). Blending of brain-machine interface and vision-guided autonomous robotics improves neuroprosthetic arm performance during grasping. *Journal of Neuroengineering and Rehabilitation, 13*, 28.

Ethier, C., Oby, E. R., Bauman, M. J., & Miller, L. E. (2012). Restoration of grasp following paralysis through brain-controlled stimulation of muscles. *Nature, 485*, 368–371.

Eytan, D., & Marom, S. (2006). Dynamics and effective topology underlying synchronization in networks of cortical neurons. *Journal of Neuroscience, 26*, 8465–8476.

Fernandez-Vargas, J., Pfaff, H. U., Rodriguez, F. B., & Varona, P. (2013). Assisted closed-loop optimization of SSVEP-BCI efficiency. *Front Neural Circuits, 7*, 27.

Flesher, S. N., Collinger, J. L., Foldes, S. T., Weiss, J. M., Downey, J. E., Tyler-Kabara, E. C., et al. (2016). Intracortical microstimulation of human somatosensory cortex. *Science Translational Medicine, 8*(361), 361ra141.

Fong, M.-F., Newman, J. P., Potter, S. M., & Wenner, P. (2015). Upward synaptic scaling is dependent on neurotransmission rather than spiking. *Nature Communications, 6*, 6339.

Furber, S. B., Lester, D. R., Plana, L. A., Garside, J. D., Painkras, E., Temple, S., et al. (2013). Overview of the SpiNNaker system architecture. *IEEE Transactions on Computers, 62*, 2454–2467.

Gal, A., Eytan, D., Wallach, A., Sandler, M., Schiller, J., & Marom, S. (2010). Dynamics of excitability over extended timescales in cultured cortical neurons. *The Journal of Neuroscience, 30*, 16332–16342.

Galvani, L., & Aldini, G. (1792). *De viribus electricitatis in motu musculari comentarius cum joannis aldini dissertatione et notis; accesserunt epistolae ad animalis electricitatis theoriam pertinentes*. Apud Societatem Typographicam.

George, S., Hasler, J., Koziol, S., Nease, S., & Ramakrishnan, S. (2013). Low power dendritic computation for wordspotting. *Journal of Low Power Electronics Applications, 3*, 73–98.

Gewaltig, M.-O., & Diesmann, M. (2007). Nest (neural simulation tool). *Scholarpedia, 2*, 1430.

Goodman, D. F., & Brette, R. (2009). The brian simulator. *Frontiers in Neuroscience, 3*, 192–197.

Grahn, P. J., Mallory, G. W., Berry, B. M., Hachmann, J. T., Lobel, D. A., & Lujan, J. L. (2014). Restoration of motor function following spinal cord injury via optimal control of intraspinal microstimulation: Toward a next generation closed-loop neural prosthesis. *Frontiers in Neuroscience, 8*, 296.

Grassia, F., Buhry, L., Levi, T., Tomas, J., Destexhe, A., & Saighi, S. (2011). Tunable neuromimetic integrated system for emulating cortical neuron models. *Frontiers in Neuroscience, 5*, 134.

Greenwald, E., Masters, M. R., & Thakor, N. V. (2016). Implantable neurotechnologies: Bidirectional neural interfaces—applications and VLSI circuit implementations. *Medical & Biological Engineering & Computing, 54*, 1–17.

Guggenmos, D. J., Azin, M., Barbay, S., Mahnken, J. D., Dunham, C., Mohseni, P., et al. (2013). Restoration of function after brain damage using a neural prosthesis. *Proceedings of the National Academy of Sciences of the United States of America, 110*, 21177–21182.

Gustafsson, B., & Jankowska, E. (1976). Direct and indirect activation of nerve cells by electrical pulses applied extracellularly. *The Journal of Physiology, 258*, 33–61.

Gustavsson, A., Svensson, M., Jacobi, F., Allgulander, C., Alonso, J., Beghi, E., et al. (2011). Cost of disorders of the brain in Europe 2010. *European Neuropsychopharmacology, 21*, 718–779.

Gwatkin, D. R., Guillot, M., & Heuveline, P. (1999). The burden of disease among the global poor. *Lancet, 354*, 586–589.

Hasler, P., Kozoil, S., Farquhar, E. & Basu, A. (2007). Transistor channel dendrites implementing HMM classifiers. *2007 IEEE International Symposium on Circuits and Systems* (vols. 1–11, p. 3359).

Hazan, H., & Ziv, N. E. (2017). Closed Loop Experiment Manager (CLEM)—an open and inexpensive solution for multichannel electrophysiological recordings and closed loop experiments. *Frontiers in Neuroscience, 11*, 579.

Hines, M. L., & Carnevale, N. T. (2001). NEURON: A tool for neuroscientists. *The Neuroscientist, 7*, 123–135.

Hochberg, L. R., Bacher, D., Jarosiewicz, B., Masse, N. Y., Simeral, J. D., Vogel, J., et al. (2012). Reach and grasp by people with tetraplegia using a neurally controlled robotic arm. *Nature, 485*, 372–375.

Holinski, B. J., Mazurek, K. A., Everaert, D. G., Stein, R. B., & Mushahwar, V. K. (2011). Restoring stepping after spinal cord injury using intraspinal microstimulation and novel control

strategies. *Annual International Conference of the IEEE Engineering in Medicine and Biology Society (Embc), 2011*, 5798–5801.

Hubel, D. H., Wiesel, T. N., & LeVay, S. (1977). Plasticity of ocular dominance columns in monkey striate cortex. *Philosophical Transactions of the Royal Society of London. Series B, Biological Sciences, 278*, 377–409.

Idelson, M. S., Ben-Jacob, E., & Hanein, Y. (2010). Innate synchronous oscillations in freely-organized small neuronal circuits. *PLoS One, 5*, e14443.

Indiveri, G., & Fusi, S. (2007). Spike-based learning in VLSI networks of integrate- and-fire neurons. *IEEE International Symposium on Circuits and Systems, 1–11*, 3371–3374.

Indiveri, G., Linares-Barranco, B., Hamilton, T. J., Van Schaik, A., Etienne-Cummings, R., Delbruck, T., et al. (2011). Neuromorphic silicon neuron circuits. *Frontiers in Neuroscience, 5*, 73.

Izhikevich, E. M. (2003). Simple model of spiking neurons. *IEEE Transactions on Neural Networks, 14*, 1569–1572.

Jackson, A., Mavoori, J., & Fetz, E. E. (2006). Long-term motor cortex plasticity induced by an electronic neural implant. *Nature, 444*, 56–60.

Jankowska, E., & Roberts, W. J. (1972a). An electrophysiological demonstration of the axonal projections of single spinal interneurones in the cat. *The Journal of Physiology, 222*, 597–622.

Jankowska, E., & Roberts, W. J. (1972b). Synaptic actions of single interneurones mediating reciprocal Ia inhibition of motoneurones. *The Journal of Physiology, 222*, 623–642.

Jimbo, Y., Robinson, H. P. C., & Kawana, A. (1998). Strengthening of synchronized activity by tetanic stimulation in cortical cultures: Application of planar electrode arrays. *IEEE Transactions on Biomedical Engineering, 45*, 1297–1304.

Jordan, J., Ippen, T., Helias, M., Kitayama, I., Sato, M., Igarashi, J., et al. (2018). Extremely scalable spiking neuronal network simulation code: From laptops to exascale computers. *Frontiers in Neuroinformatics, 12*, 2.

Joucla, S., Ambroise, M., Levi, T., Lafon, T., Chauvet, P., Saighi, S., et al. (2016). Generation of locomotor-like activity in the isolated rat spinal cord using intraspinal electrical microstimulation driven by a digital neuromorphic CPG. *Frontiers in Neuroscience, 10*, 67.

Ju, H., Dranias, M. R., Banumurthy, G., & VanDongen, A. M. (2015). Spatiotemporal memory is an intrinsic property of networks of dissociated cortical neurons. *Journal of Neuroscience, 35*, 4040–4051.

Jung, R., Brauer, E. J., & Abbas, J. J. (2001). Real-time interaction between a neuromorphic electronic circuit and the spinal cord. *IEEE Transactions on Neural Systems and Rehabilitation Engineering, 9*, 319–326.

Jung, R., Kiemel, T., & Cohen, A. H. (1996). Dynamic behavior of a neural network model of locomotor control in the lamprey. *Journal of Neurophysiology, 75*, 1074–1086.

Karniel, A., Kositsky, M., Fleming, K. M., Chiappalone, M., Sanguineti, V., Alford, S. T., et al. (2005). Computational analysis in vitro: Dynamics and plasticity of a neuro-robotic system. *Journal of Neural Engineering, 2*, S250.

Kasten, M. R., Sunshine, M. D., Secrist, E. S., Horner, P. J., & Moritz, C. T. (2013). Therapeutic intraspinal microstimulation improves forelimb function after cervical contusion injury. *Journal of Neural Engineering, 10*, 044001.

Keren, H., & Marom, S. (2014). Controlling neural network responsiveness: Tradeoffs and constraints. *Frontiers in Neuroengineering, 7*, 11.

Kohno, T., Sekikawa, M., Li, J., Nanami, T., & Aihara, K. (2016). Qualitative-modeling-based silicon neurons and their networks. *Frontiers in Neuroscience, 10*, 273.

Kositsky, M., Chiappalone, M., Alford, S. T., & Mussa-Ivaldi, F. A. (2009). Brain-machine interactions for assessing the dynamics of neural systems. *Frontiers in Neurorobotics, 3*, 1.

Krook-Magnuson, E., Armstrong, C., Oijala, M., & Soltesz, I. (2013). On-demand optogenetic control of spontaneous seizures in temporal lobe epilepsy. *Nature Communications, 4*, 1376.

Kudoh, S. N., Tokuda, M., Kiyohara, A., Hosokawa, C., Taguchi, T., & Hayashi, I. (2011). Vitroid—the robot system with an interface between a living neuronal network and outer world. *International Journal of Mechatronics and Manufacturing Systems, 4*, 135–149.

Kumar, A., Rotter, S., & Aertsen, A. (2010). Spiking activity propagation in neuronal networks: Reconciling different perspectives on neural coding. *Nature Reviews. Neuroscience, 11*, 615–627.

Kumar, S. S., Wulfing, J., Okujeni, S., Boedecker, J., Riedmiller, M., & Egert, U. (2016). Autonomous optimization of targeted stimulation of neuronal networks. *PLoS Computational Biology, 12*, e1005054.

Kunkel, S., Schmidt, M., Eppler, J. M., Plesser, H. E., Masumoto, G., Igarashi, J., et al. (2014). Spiking network simulation code for petascale computers. *Frontiers in Neuroinformatics, 8*, 78.

le Feber, J., Stegenga, J., & Rutten, W. L. (2010). The effect of slow electrical stimuli to achieve learning in cultured networks of rat cortical neurons. *PLoS One, 5*, e8871.

le Feber, J., van Pelt, J., & Rutten, W. (2007). Latency dependent development of related firing patterns of cultured cortical neurons. *Conference Proceedings: Annual International Conference of the IEEE Engineering in Medicine and Biology Society, 2007*, 3000–3003.

le Feber, J., Witteveen, T., van Veenendaal, T. M., & Dijkstra, J. (2015). Repeated stimulation of cultured networks of rat cortical neurons induces parallel memory traces. *Learning & Memory, 22*, 594–603.

Le Masson, G., Renaud-Le Masson, S., Debay, D., & Bal, T. (2002). Feedback inhibition controls spike transfer in hybrid thalamic circuits. *Nature, 417*, 854–858.

Lee, K. J., Jang, K. S., & Shon, Y. M. (2006). Chronic deep brain stimulation of subthalamic and anterior thalamic nuclei for controlling refractory partial epilepsy. *Acta Neurochirurgica. Supplement, 99*, 87–91.

Levi, T., Bonifazi, P., Massobrio, P., & Chiappalone, M. (2018a). Editorial: Closed-loop systems for next-generation neuroprostheses. *Frontiers in Neuroscience, 12*, 26.

Levi, T., Khoyratee, F., Saïghi, S., & Ikeuchi, Y. (2018b). Digital implementation of Hodgkin–Huxley neuron model for neurological diseases studies. *Artificial Life Robotics, 23*, 10–14.

Levi, T., Lewis, N., Saïghi, S., Tomas, J., Bornat, Y. & Renaud, S. (2008). Neuromimetic integrated circuits. In Iniewski, K. (ed) *VLSI Circuits for Biomedical Applications*. Artech House, 241–264.

Levi, T., Nanami, T., Tange, A., Aihara, K., & Kohno, T. (2018). Development and applications of biomimetic neuronal networks toward brainmorphic artificial intelligence. *IEEE Transactions on Circuits and Systems II: Express Briefs, 65*, 577–581.

Levy, O., Ziv, N. E., & Marom, S. (2012). Enhancement of neural representation capacity by modular architecture in networks of cortical neurons. *European Journal of Neuroscience, 35*, 1753–1760.

Li, Y., Sun, R., Wang, Y., Li, H., & Zheng, X. (2016). A novel robot system integrating biological and mechanical intelligence based on dissociated neural network-controlled closed-loop environment. *PLoS One, 11*, e0165600.

Li, Y. L., Zhou, W., Li, X. N., Zeng, S. Q., Liu, M., & Luo, Q. M. (2007). Characterization of synchronized bursts in cultured hippocampal neuronal networks with learning training on microelectrode arrays. *Biosensors and Bioelectronics, 22*, 2976–2982.

Little, S., Pogosyan, A., Neal, S., Zavala, B., Zrinzo, L., Hariz, M., et al. (2013). Adaptive deep brain stimulation in advanced Parkinson disease. *Annals of Neurology, 74*, 449–457.

Liu, S. C., & Douglas, R. (2004). Temporal coding in a silicon network of integrate-and-fire neurons. *IEEE Transactions on Neural Networks, 15*, 1305–1314.

Lobov, S., Balashova, K., Makarov, V., & Kazantsev, V. (2017). Competition of spike-conducting pathways in STDP driven neural networks. *Proceedings of the 5th International Congress on Neurotechnology, Electronics and Informatics (NEUROTECHNIX 2017)*, 15–21. https://doi.org/10.5220/0006497400150021

Macis, E., Tedesco, M., Massobrio, P., Raiteri, R., & Martinoia, S. (2007). An automated microdrop delivery system for neuronal network patterning on microelectrode arrays. *Journal of Neuroscience Methods, 161*, 88–95.

Madisen, L., Mao, T., Koch, H., Zhuo, J.-M., Berenyi, A., Fujisawa, S., et al. (2012). A toolbox of Cre-dependent optogenetic transgenic mice for light-induced activation and silencing. *Nature Neuroscience, 15*, 793.

Mahowald, M., & Douglas, R. (1991). A silicon neuron. *Nature, 354*, 515–518.

Mak, J. N., & Wolpaw, J. R. (2009). Clinical applications of brain-computer interfaces: Current state and future prospects. *IEEE Reviews in Biomedical Engineering, 2*, 187–199.

Markram, H. (2012). The human brain project. *Scientific American, 306*, 50–55.

Marom, S., & Eytan, D. (2005). Learning in ex-vivo developing networks of cortical neurons. *Progress in Brain Research, 147*, 189–199.

Marom, S., & Shahaf, G. (2002). Development, learning and memory in large random networks of cortical neurons: Lessons beyond anatomy. *Quarterly Reviews of Biophysics, 35*, 63–87.

Martinoia, S., Massobrio, P., Bove, M., & Massobrio, G. (2004a). Cultured neurons coupled to microelectrode arrays: Circuit models, simulations and experimental data. *IEEE Transactions on Biomedical Engineering, 51*, 859–863.

Martinoia, S., Sanguineti, V., Cozzi, L., Berdondini, L., Van Pelt, J., Tomas, J., et al. (2004b). Towards an embodied in vitro electrophysiology: The NeuroBIT project. *Neurocomputing, 58*, 1065–1072.

Massobrio, P., Tessadori, J., Chiappalone, M., & Ghirardi, M. (2015). In vitro studies of neuronal networks and synaptic plasticity in invertebrates and in mammals using multielectrode arrays. *Neural Plasticity, 2015*, 196195.

Masumori, A., Sinapayen, L., Maruyama, N., Mita, T., Bakkum, D. J., Frey, U., et al. (2018). Autonomous regulation of self and non-self by stimulation avoidance in embodied neural networks. *Artificial Life Conference Proceedings* (pp. 163–170). Cambridge: MIT Press.

Mattis, J., Tye, K. M., Ferenczi, E. A., Ramakrishnan, C., O'shea, D. J., Prakash, R., et al. (2012). Principles for applying optogenetic tools derived from direct comparative analysis of microbial opsins. *Nature Methods, 9*, 159.

Meunier, D., Lambiotte, R., & Bullmore, E. T. (2010). Modular and hierarchically modular organization of brain networks. *Frontiers in Neuroscience, 4*, 200.

Miao, Y., & Koomson, V. J. (2018). A CMOS-based bidirectional brain machine interface system with integrated fdNIRS and tDCS for closed-loop brain stimulation. *IEEE Transactions on Biomedical Circuits and Systems, 12*, 554–563.

Millan, J. D., Rupp, R., Muller-Putz, G. R., Murray-Smith, R., Giugliemma, C., Tangermann, M., et al. (2010). Combining brain-computer interfaces and assistive technologies: State-of-the-art and challenges. *Frontiers in Neuroscience, 4*, 161.

Molinuevo, J. L., Valldeoriola, F., Tolosa, E., Rumia, J., Valls-Sole, J., Roldan, H., et al. (2000). Levodopa withdrawal after bilateral subthalamic nucleus stimulation in advanced Parkinson disease. *Archives of Neurology, 57*, 983–988.

Morgante, L., Morgante, F., Moro, E., Epifanio, A., Girlanda, P., Ragonese, P., et al. (2007). How many parkinsonian patients are suitable candidates for deep brain stimulation of subthalamic nucleus? Results of a questionnaire. *Parkinsonism & Related Disorders, 13*, 528–531.

Moro, E., Scerrati, M., Romito, L. M., Roselli, R., Tonali, P., & Albanese, A. (1999). Chronic subthalamic nucleus stimulation reduces medication requirements in Parkinson's disease. *Neurology, 53*, 85–90.

Moxon, K. A., & Foffani, G. (2015). Brain-machine interfaces beyond neuroprosthetics. *Neuron, 86*, 55–67.

Muller, J., Bakkum, D. J., & Hierlemann, A. (2013). Sub-millisecond closed-loop feedback stimulation between arbitrary sets of individual neurons. *Frontiers in Neural Circuits, 6*, 121.

Murray, J. B. (1996). Psychophysiological aspects of autistic disorders: Overview. *The Journal of Psychology, 130*, 145–158.

Mushahwar, V. K., Gillard, D. M., Gauthier, M. J., & Prochazka, A. (2002). Intraspinal micro stimulation generates locomotor-like and feedback-controlled movements. *IEEE Transactions on Neural Systems and Rehabilitation Engineering, 10*, 68–81.

Mussa-Ivaldi, S., Alford, S. T., Chiappalone, M., Fadiga, L., Karniel, A., Kositsky, M., et al. (2010). New perspectives on the dialogue between brains and machines. *Frontiers in Neuroscience, 3*, 8.

Nanami, T., & Kohno, T. (2016). Simple cortical and thalamic neuron models for digital arithmetic circuit implementation. *Frontiers in Neuroscience, 10*, 181.

Natarajan, A., & Hasler, J. (2018). Hodgkin-Huxley neuron and FPAA dynamics. *IEEE Transactions on Biomedical Circuits and Systems, 12*, 918–926.

Navarro, X., Krueger, T. B., Lago, N., Micera, S., Stieglitz, T., & Dario, P. (2005). A critical review of interfaces with the peripheral nervous system for the control of neuroprostheses and hybrid bionic systems. *Journal of the Peripheral Nervous System, 10*, 229–258.

Newman, J. P., Zeller-Townson, R., Fong, M. F., Desai, S. A., Gross, R. E., & Potter, S. M. (2013). Closed-loop, multichannel experimentation using the open-source NeuroRighter electrophysiology platform. *Frontiers in Neural Circuits, 6*, 98.

Nishimura, Y., Perlmutter, S. I., & Fetz, E. E. (2013). Restoration of upper limb movement via artificial corticospinal and musculospinal connections in a monkey with spinal cord injury. *Front Neural Circuits, 7*, 57.

Novellino, A., D'Angelo, P., Cozzi, L., Chiappalone, M., Sanguineti, V., & Martinoia, S. (2007). Connecting neurons to a mobile robot: An in vitro bidirectional neural interface. *Computational Intelligence and Neuroscience, 2007*, 12725.

O'connor, D. H., Hires, S. A., Guo, Z. V., Li, N., Yu, J., Sun, Q.-Q., et al. (2013). Neural coding during active somatosensation revealed using illusory touch. *Nature Neuroscience, 16*, 958.

Opris, I., Fuqua, J. L., Huettl, P. F., Gerhardt, G. A., Berger, T. W., Hampson, R. E., et al. (2012). Closing the loop in primate prefrontal cortex: Inter-laminar processing. *Front Neural Circuits, 6*, 88.

Pan, R. K., Chatterjee, N., & Sinha, S. (2010). Mesoscopic organization reveals the constraints governing Caenorhabditis elegans nervous system. *PLoS One, 5*, e9240.

Panuccio, G., Semprini, M., Natale, L., Buccelli, S., Colombi, I. & Chiappalone, M. (2018). Progress in neuroengineering for brain repair: New challenges and open issues. *Brain and Neuroscience Advances*, *2*. https://doi.org/10.1177/2398212818776475.

Panzeri, S., Harvey, C. D., Piasini, E., Latham, P. E., & Fellin, T. (2017). Cracking the neural code for sensory perception by combining statistics, intervention, and behavior. *Neuron, 93*, 491–507.

Panzeri, S., Ince, R. A. A., Diamond, M. E., & Kayser, C. (2014). Reading spike timing without a clock: Intrinsic decoding of spike trains. *Philosophical Transactions of the Royal Society, B: Biological Sciences, 369*, 20120467.

Pasquale, V., Martinoia, S., & Chiappalone, M. (2017). Stimulation triggers endogenous activity patterns in cultured cortical networks. *Scientific Reports, 7*, 9080.

Paz, J. T., Davidson, T. J., Frechette, E. S., Delord, B., Parada, I., Peng, K., et al. (2013). Closed-loop optogenetic control of thalamus as a tool for interrupting seizures after cortical injury. *Nature Neuroscience, 16*, 64.

Pikov, V., Bullara, L., & McCreery, D. B. (2007). Intraspinal stimulation for bladder voiding in cats before and after chronic spinal cord injury. *Journal of Neural Engineering, 4*, 356.

Pimashkin, A., Gladkov, A., Agrba, E., Mukhina, I., & Kazantsev, V. (2016). Selectivity of stimulus induced responses in cultured hippocampal networks on microelectrode arrays. *Cognitive Neurodynamics, 10*, 287–299.

Pimashkin, A., Gladkov, A., Mukhina, I., & Kazantsev, V. (2013). Adaptive enhancement of learning protocol in hippocampal cultured networks grown on multielectrode arrays. *Front Neural Circuits, 7*, 87.

Poli, D., Thiagarajan, S., DeMarse, T. B., Wheeler, B. C., & Brewer, G. J. (2017). Sparse and specific coding during information transmission between co-cultured dentate gyrus and CA3 hippocampal networks. *Frontiers in Neural Circuits, 11*, 13.

Potter, S. M. (2010). Closing the loop between neurons and neurotechnology. *Frontiers in Neuroscience, 4*, 15.

Potter, S. M., El Hady, A., & Fetz, E. E. (2014). Closed-loop neuroscience and neuroengineering. *Frontiers in Neural Circuits, 8*, 115.

Pulizzi, R., Musumeci, G., Van den Haute, C., Van De Vijver, S., Baekelandt, V., & Giugliano, M. (2016). Brief wide-field photostimuli evoke and modulate oscillatory reverberating activity in cortical networks. *Scientific Reports, 6*, 24701.

Qiao, N., Mostafa, H., Corradi, F., Osswald, M., Stefanini, F., Sumislawska, D., et al. (2015). A reconfigurable on-line learning spiking neuromorphic processor comprising 256 neurons and 128K synapses. *Frontiers in Neuroscience, 9*, 141.

Rast, A. D., Partzsch, J., Mayr, C., Schemmel, J., Hartmann, S., Plana, L. A., et al. (2013). A location-independent direct link neuromorphic interface. *2013 International Joint Conference on Neural Networks (Ijcnn).*

Reger, B. D., Fleming, K. M., Sanguineti, V., Alford, S., & Mussa-Ivaldi, F. A. (2000). Connecting brains to robots: An artificial body for studying the computational properties of neural tissues. *Artificial Life, 6*, 307–324.

Renaud, S., Tomas, J., Bornat, Y., Daouzli, A., & Saighi, S. (2007). Neuromimetic ICs with analog cores: An alternative for simulating spiking neural networks. *IEEE International Symposium on Circuits and Systems, 1–11*, 3355–3358.

Renshaw, B. (1946). Observations on interaction of nerve impulses in the gray matter and on the nature of central inhibition. *The American Journal of Physiology, 146*, 443–448.

Rey, H. G., Ahmadi, M., & Quian Quiroga, R. (2015). Single trial analysis of field potentials in perception, learning and memory. *Current Opinion in Neurobiology, 31*, 148–155.

Rice, K. L., Bhuiyan, M. A., Taha, T. M., Vutsinas, C. N. & Smith, M. C. (2009). FPGA implementation of Izhikevich spiking neural networks for character recognition. *2009 International Conference on Reconfigurable Computing and Fpgas* (p. 451).

Rieke, F., Warland, D., de Ruyter van Steveninck, R., & Bialek, W. (1997). *Spikes* (p. 3). Cambridge: Massachusetts Institute of Technology.

Robinson, J. T., Jorgolli, M., & Park, H. (2013). Nanowire electrodes for high-density stimulation and measurement of neural circuits. *Front Neural Circuits, 7*, 38.

Rolston, J. D., Gross, R. E., & Potter, S. M. (2009). NeuroRighter: Closed-loop multielectrode stimulation and recording for freely moving animals and cell cultures. *Conference Proceedings: Annual International Conference of the IEEE Engineering in Medicine and Biology Society, 2009*, 6489–6492.

Rosin, B., Slovik, M., Mitelman, R., Rivlin-Etzion, M., Haber, S. N., Israel, Z., et al. (2011). Closed-loop deep brain stimulation is superior in ameliorating parkinsonism. *Neuron, 72*, 370–384.

Sabarad, J., Kestur, S., Park, M. S., Dantara, D., Narayanan, V., Chen, Y., et al. (2012) A reconfigurable accelerator for neuromorphic object recognition. *2012 17th Asia and South Pacific Design Automation Conference (Asp-Dac)* (pp. 813–818).

Sartorius, N., & Henderson, A. S. (1992). The neglect of prevention in psychiatry. *The Australian and New Zealand Journal of Psychiatry, 26*, 550–553.

Schemmel, J., Bruderle, D., Meier, K., & Ostendorf, B. (2007). Modeling synaptic plasticity within networks of highly accelerated I&F neurons. *IEEE International Symposium on Circuits and Systems, 1–11*, 3367–3370.

Schwartz, A. B. (2016). Movement: How the brain communicates with the world. *Cell, 164*, 1122–1135.

Shahaf, G., Eytan, D., Gal, A., Kermany, E., Lyakhov, V., Zrenner, C., et al. (2008). Order-based representation in random networks of cortical neurons. *PLoS Computational Biology, 4*, e1000228.

Shahaf, G., & Marom, S. (2001). Learning in networks of cortical neurons. *The Journal of Neuroscience, 21*, 8782–8788.

Shein-Idelson, M., Ben-Jacob, E., & Hanein, Y. (2011). Engineered neuronal circuits: A new platform for studying the role of modular topology. *Frontiers in Neuroengineering, 4*, 10.

Siegle, J. H., Hale, G. J., Newman, J. P., & Voigts, J. (2015). Neural ensemble communities: Open-source approaches to hardware for large-scale electrophysiology. *Current Opinion in Neurobiology, 32*, 53–59.

Silva, G. A. (2018). A new frontier: The convergence of nanotechnology, brain machine interfaces, and artificial intelligence. *Frontiers in Neuroscience, 12*, 843.

Sinapayen, L., Masumori, A., & Ikegami, T. (2017). Learning by stimulation avoidance: A principle to control spiking neural networks dynamics. *PLoS One, 12*, e0170388.

Sisterson, N. D., Wozny, T. A., Kokkinos, V., Constantino, A., & Richardson, R. M. (2019). Closed-loop brain stimulation for drug-resistant epilepsy: Towards an evidence-based approach to personalized medicine. *Neurotherapeutics, 16*, 119–127.

Sporns, O., Tononi, G., & Edelman, G. M. (2000). Theoretical neuroanatomy: Relating anatomical and functional connectivity in graphs and cortical connection matrices. *Cerebral Cortex, 10*, 127–141.

Stegenga, J., Le Feber, J., Marani, E., & Rutten, W. L. (2009). The effect of learning on bursting. *IEEE Transactions on Biomedical Engineering, 56*, 1220–1227.

Sunshine, M. D., Cho, F. S., Lockwood, D. R., Fechko, A. S., Kasten, M. R., & Moritz, C. T. (2013). Cervical intraspinal microstimulation evokes robust forelimb movements before and after injury. *Journal of Neural Engineering, 10*(3), 036001.

Tessadori, J., Bisio, M., Martinoia, S., & Chiappalone, M. (2012). Modular neuronal assemblies embodied in a closed-loop environment: Toward future integration of brains and machines. *Front Neural Circuits, 6*, 99.

Turrigiano, G. (2012). Homeostatic synaptic plasticity: Local and global mechanisms for stabilizing neuronal function. *Cold Spring Harbor Perspectives in Biology, 4*, a005736.

Turrigiano, G. G., & Nelson, S. B. (2000). Hebb and homeostasis in neuronal plasticity. *Current Opinion in Neurobiology, 10*, 358–364.

van Albada, S. J., Rowley, A. G., Senk, J., Hopkins, M., Schmidt, M., Stokes, A. B., et al. (2018). Performance comparison of the digital neuromorphic hardware SpiNNaker and the neural network simulation software NEST for a full-scale cortical microcircuit model. *Frontiers in Neuroscience, 12*, 291.

van den Brand, R., Heutschi, J., Barraud, Q., DiGiovanna, J., Bartholdi, K., Huerlimann, M., et al. (2012). Restoring voluntary control of locomotion after paralyzing spinal cord injury. *Science, 336*, 1182–1185.

van Pelt, J., Wolters, P. S., Corner, M. A., Rutten, W. L., & Ramakers, G. J. (2004). Long-term characterization of firing dynamics of spontaneous bursts in cultured neural networks. *IEEE Transactions on Biomedical Engineering, 51*, 2051–2062.

Vassanelli, S., & Mahmud, M. (2016). Trends and challenges in neuroengineering: Toward "intelligent" neuroprostheses through brain-"brain inspired systems" communication. *Frontiers in Neuroscience, 10*, 438.

Vassileva, A., van Blooijs, D., Leijten, F., & Huiskamp, G. (2018). Neocortical electrical stimulation for epilepsy: Closed-loop versus open-loop. *Epilepsy Research, 141*, 95–101.

Vogelstein, R. J., Mallik, U. & Cauwenberghs, G. (2004). Silicon spike-based synaptic array and address-event transceiver. *Proceedings of the IEEE International Symposium on Circuits and Systems* (Vol. 5, pp. 385–388).

Wagenaar, D., DeMarse, T. B. & Potter, S. M. (2005a) MeaBench: A toolset for multi-electrode data acquisition and on-line analysis. *Neural Engineering, 2005. Conference Proceedings. 2nd International IEEE EMBS Conference on* (pp. 518–521). IEEE.

Wagenaar, D. A., Madhavan, R., Pine, J., & Potter, S. M. (2005b). Controlling bursting in cortical cultures with closed-loop multi-electrode stimulation. *The Journal of Neuroscience, 25*, 680–688.

Wagenaar, D. A., Pine, J., & Potter, S. M. (2006a). An extremely rich repertoire of bursting patterns during the development of cortical cultures. *BMC Neuroscience, 7*, 11.

Wagenaar, D. A., Pine, J., & Potter, S. M. (2006b). Searching for plasticity in dissociated cortical cultures on multi-electrode arrays. *Journal of Negative Results in Biomedicine, 5*, 16.

Wallach, A., Eytan, D., Gal, A., Zrenner, C., & Marom, S. (2011). Neuronal response clamp. *Frontiers in Neuroengineering, 4*, 3.

Walter, A., Ramos Murguialday, A., Spuler, M., Naros, G., Leao, M. T., Gharabaghi, A., et al. (2012). Coupling BCI and cortical stimulation for brain-state-dependent stimulation: Methods for spectral estimation in the presence of stimulation after-effects. *Front Neural Circuits, 6*, 87.

Wang, R. C., Cohen, G., Stiefel, K. M., Hamilton, T. J., Tapson, J. T., & van Schaik, A. (2013a). An FPGA implementation of a polychronous spiking neural network with delay adaptation. *Frontiers in Neuroscience, 7*, 14.

Wang, R. M., Cohen, G., Stiefel, K. M., Hamilton, T. J., Tapson, J. C., & van Schaik, A. (2013b). An FPGA implementation of a polychronous spiking neural network with delay adaptation. *Frontiers in Neuroscience, 7*, 14.

Warwick, K., Xydas, D., Nasuto, S. J., Becerra, V. M., Hammond, M. W., Downes, J. H., et al. (2010). Controlling a mobile robot with a biological brain. *Defence Science Journal, 60*, 5–14.

Wolpaw, J. R., Birbaumer, N., McFarland, D. J., Pfurtscheller, G., & Vaughan, T. M. (2002). Brain-computer interfaces for communication and control. *Clinical Neurophysiology, 113*, 767–791.

Wright, J., Macefield, V. G., van Schaik, A., & Tapson, J. C. (2016). A review of control strategies in closed-loop neuroprosthetic systems. *Frontiers in Neuroscience, 10*, 312.

Xu, R., Jiang, N., Lin, C., Mrachacz-Kersting, N., Dremstrup, K., & Farina, D. (2014). Enhanced low-latency detection of motor intention from EEG for closed-loop brain-computer interface applications. *IEEE Transactions on Biomedical Engineering, 61*, 288–296.

Yakovenko, S., Kowalczewski, J., & Prochazka, A. (2007). Intraspinal stimulation caudal to spinal cord transections in rats. Testing the propriospinal hypothesis. *Journal of Neurophysiology, 97*, 2570–2574.

Zeng, H., Wang, Y., Wu, C., Song, A., Liu, J., Ji, P., et al. (2017). Closed-loop hybrid gaze brain-machine interface based robotic arm control with augmented reality feedback. *Frontiers in Neurorobotics, 11*, 60.

Zhang, F., Aravanis, A. M., Adamantidis, A., de Lecea, L., & Deisseroth, K. (2007). Circuit-breakers: Optical technologies for probing neural signals and systems. *Nature Reviews Neuroscience, 8*, 577.

Zhang, F., Vierock, J., Yizhar, O., Fenno, L. E., Tsunoda, S., Kianianmomeni, A., et al. (2011). The microbial opsin family of optogenetic tools. *Cell, 147*, 1446–1457.

Zhang, Z., Russell, L. E., Packer, A. M., Gauld, O. M., & Häusser, M. (2018). Closed-loop all-optical interrogation of neural circuits in vivo. *Nature Methods, 15*(12), 1037–1040.